

SAPIENZA
UNIVERSITÀ DI ROMA

Department of Chemistry and Technology of Drugs

PhD Thesis

Metabolomic approach in the study of foods by high-resolution liquid state NMR and HPLC techniques

Presented by

Giacomo Di Matteo

Tutor

Prof. Luisa Mannina

Co-Tutor

Dr. Anatoly P. Sobolev

International PhD course in Molecular design and characterization for the promotion of health and well-being: from drug to food - XXXV cycle

A.A. 2021-2022

LIST OF PUBLICATIONS

Number of publications with first name/co-first name: 5

1. **Di Matteo, G.;** Spano, M.; Grosso, M.; Salvo, A.; Ingallina, C.; Russo, M.; Ritieni, A.; Mannina, L. Food and COVID-19: Preventive/co-therapeutic strategies explored by current clinical trials and in silico studies. *Foods* 2020, 9, doi:10.3390/foods9081036.
2. Ingallina, C.; Maccelli, A.; Spano, M.; Di **Matteo, G.;** Sotto, A. Di; Giusti, A.M.; Vinci, G.; Giacomo, S. Di; Rapa, M.; Ciano, S.; et al. Chemico-biological characterization of torpedino di fondi® tomato fruits: A comparison with san marzano cultivar at two ripeness stages. *Antioxidants* 2020, 9, 1–29, doi:10.3390/antiox9101027.
3. Spano, M.; **Di Matteo, G.;** Rapa, M.; Ciano, S.; Ingallina, C.; Cesa, S.; Menghini, L.; Carradori, S.; Giusti, A.M.; Di Sotto, A.; et al. Commercial hemp seed oils: A multimethodological characterization. *Appl. Sci.* 2020, 10, 1–15, doi:10.3390/app10196933.
4. **Di Matteo, G.;** Spano, M.; Esposito, C.; Santarcangelo, C.; Baldi, A.; Daglia, M.; Mannina, L.; Ingallina, C.; Sobolev, A.P. NMR Characterization of Ten Apple Cultivars from the Piedmont Region. *Foods* 2021, 10, doi:https://doi.org/10.3390/foods10020289.
5. Spano, M.; **Di Matteo, G.;** Ingallina, C.; Botta, B.; Quaglio, D.; Ghirga, F.; Balducci, S.; Cammarone, S.; Campiglia, E.; Giusti, A.M.; et al. A Multimethodological Characterization of Cannabis sativa L . Inflorescences from Seven Dioecious Cultivars Grown in Italy : The Effect of Different Harvesting Stages. *Molecules* 2021, 26, 2912, doi:https://doi.org/10.3390/molecules26102912.
6. **Di Matteo, G.;** Di Matteo P.; Sambucci, M.; Tirill, J.; Giusti, A.M.; Vinci, G.; Gobbi, L.; Prencipe, S.A.; Salvo, A.; Ingallina, C.; et al. Commercial Bio-Packaging to Preserve the Quality and Extend the Shelf-Life of Vegetables :

The Case-Study of Pumpkin Samples Studied by a Multimethodological Approach. *Foods* 2021, 1–24.

7. Spano, M.; Maccelli, A.; **Di Matteo, G.;** Ingallina, C.; Biava, M.; Crestoni, M.E.; Bardaud, J.; Giusti, A.M.; Mariano, A.; Abusco, A.S.D.; et al. Metabolomic Profiling of Fresh Goji (Lycium barbarum L .) A Multi-Methodological Approach. *Molecules* 2021, 1–23.
8. Rotondo, A.; Torre, G.L. La; Gervasi, T.; **Di Matteo, G.;** Spano, M.; Ingallina, C.; Salvo, A. A fast and efficient ultrasound-assisted extraction of tocopherols in cow milk followed by HPLC determination. *Molecules* 2021, 26, 1–12, doi:10.3390/molecules26154645.
9. **Di Matteo, G**.; Spano, M.; Grosso, M.; Salvo, A.; Russo, M.; Pietropaolo, V.A.; Prezioso, C.; Mannina, L.; Ritieni, A. Foods and COVID-19. *World J. Food Nutr.* 2021, 1, 1–2.
10. Farinon, B.; Costantini, L.; Molinari, R.; **Di Matteo, G.;** Garzoli, S.; Ferri, S.; Ceccantoni, B.; Mannina, L.; Merendino, N. Effect of malting on nutritional and antioxidant properties of the seeds of two industrial hemp (Cannabis sativa L.) cultivars. *Food Chem.* 2022, 370, doi:10.1016/j.foodchem.2021.131348.
11. Ullah, H.; Sommella, E.; Santarcangelo, C.; Avino, D.D.; Rossi, A.; Dacrema, M.; Di Minno, A.; **Di Matteo, G.;** Mannina, L.; Campiglia, P.; et al. Hydroethanolic Extract of Prunus domestica L .: Metabolite Profiling and In Vitro Modulation of Molecular Mechanisms Associated to Cardiometabolic Diseases. *Nutrients* 2022, 14, doi:https://doi.org/10.3390/nu14020340.
12. Spano, M.; **Di Matteo, G.;** Ingallina, C.; Ambroselli, D.; Carradori, S.; Gallorini, M.; Giusti, A.M.; Salvo, A.; Grosso, M.; Mannina, L. Modulatory Properties of Food and Nutraceutical Components Targeting NLRP3 Inflammasome Activation. *Nutrient* 2022, 14, 1–44, doi:https://doi.org/10.3390/ nu14030490.

13. Sobolev, A. P., Ingallina, C., Spano, M., & **Di Matteo, G.** NMR-Based Approaches in the Study of Foods. *Molecules* 2022, 27, 7906, doi:https://doi.org/https://doi.org/10.3390/ molecules27227906.
14. Spano, M., **Di Matteo, G.**, Ingallina, C., Sobolev, A. P., Giusti, A. M., Vinci, G., Cammarone, S., Tortora, C., Lamelza, L., Prencipe, S. A., Gobbi, L., Botta, B., Marini, F., Campiglia, E., & Mannina, L. Industrial Hemp (Cannabis sativa L .) Inflorescences as Novel Food : The Effect of Different Agronomical Practices on Chemical Profile. *Foods* 2022, 11, 3658, doi:https://doi.org/https://doi.org/10.3390/ foods11223658.

LIST OF POSTERS/ABSTRACTS

1. G. Di Matteo, M. Spano, M. Grosso, A. Salvo, C. Ingallina, M. Russo, A. Ritieni, L. Mannina. "FISV Symposium on SARS-CoV-2 Biology and COVID-19: Current research and perspectives". Poster presentation. FISV Federazione Italiana Scienze della Vita, **Roma**, Italia, 16 Settembre 2020.
2. G. Di Matteo, C. Ingallina, A. Sobolev, M. Spano, A. Maccelli, M. Crestoni, S. Fornarini, C. Cordeiro, M. Sousa Silva, L. Mannina. "Untargeted methodologies to investigate tomatoes fruits". Abstract presentation. 6th International Conference on Foodomics. **Cesena**, Italy, 14-16 October 2020.
3. G. Di Matteo, A. P. Sobolev, M. Spano, C. Ingallina, L. Mannina. "NMR Methodology in the study of italian local products". Poster presentation. XLIX National Congress on Magnetic Resonance, **online**, 8-10 Settembre 2021.
4. G. Di Matteo, M. Spano, L. Mannina. " NMR characterization of roots, leaves and flowers of Gentiana Lutea L. from Majella National Park". Joint Italian-French meeting on Magnetic Resonance, **Milan**, Italy, 27-30 September 2022.

LIST OF ORAL COMMUNICATIONS

1. "L'influenza di differenti pratiche agronomiche sul profile metabolomico di infiorescenze della cultivar Ferimon". La Canapa industriale: sviluppo e valorizzazione di una nuova filiera agroalimentare ecosostenibile. Sapienza University of Rome, **Rome**, Italy, 22 September 2020.
2. "Profilo NMR metabolomico di campioni di zucca protetti da biofilm". Il packaging per gli alimenti ad alto valore nutrizionale: metodologie avanzate per nuove soluzioni. Sapienza University of Rome, **Rome**, Italy, 16 June 2021.
3. "NMR Methodology in the study of italian local products". XLIX National Congress on Magnetic Resonance, **online**, 8-10 September 2021.
4. "Italian local products characterization by NMR methodologies". MRFOOD2022 – 15th International Conference on the Applications of Magnetic Resonance in Food Science, Aarhus University, **Aarhus**, Denmark, 7-10 June 2022
5. "A multi-methodological approach for the hemp seed oils characterization". SISSG – Oli e grassi alimentari: innovazione e sostenibilità nella produzione e nel controllo, **Perugia**, 15-17 June 2022
6. "NMR methodologies for the valorisation of Italian local products". SYNC2022 – First Symposium for Young Chemists: Innovation and Sustainability. Sapienza University of Rome, **Rome**, Italy, 20-23 June 2022.
7. "Profilo NMR metabolomico di campioni di zucca protetti da biofilm". VII Workshop – Applicazioni della Risonanza Magnetica nella scienza degli alimenti. Sapienza University of Rome, **Rome**, Italy, 23-24 June 2022.
8. "Gentiana Lutea L. : analisi della distribuzione dei metaboliti dalla radice a foglie e fiori". Caratterizzazione multi-metodologica di piante officinali. Sapienza University of Rome, **Rome**, Italy, 9 September 2022.

BOOK CHAPTERS

1. **OLEUM**, Lanfranco Conte and Maurizio Servili, Chapter contribution: "Analisi tramite Risonanza Magnetica Nucleare in oli extra vergini di oliva", Edagricole, ISBN 978-88-506-5617-2.

LIST OF PROJECTS

1. Research project of MIPAAF. "Ortopackhealth". Participant; member of the research team. **2019**.
2. Research project of Sapienza University of Rome. "Innovative bio-packaging to preserve quality and extend the shelf-life of fruits and vegetables". Participant as a member of the research team. **2020**.
3. Research project of Sapienza University of Rome. "Dalla valorizzazione degli scarti agroalimentari del comparto ortofrutticolo alla formulazione di integratori alimentari". Participant as a member of the research team. **2021**.
4. Research project of Sapienza University of Rome. "Dalla valorizzazione degli scarti agroalimentari del comparto ortofrutticolo alla formulazione di integratori alimentari". Principal investigator. Participant as a member of the research team. **2021.**

TABLE OF CONTENTS

Aim 1

Chapter 1: Introduction

1.1. Food definitions and their limits 5

1.2. Food classification and description systems 13

1.2.1. Food classification systems 16

1.2.2. Food description systems 19

1.2.3. Food classification and description systems 21

1.2.4. Food composition databases 22

1.3. Non-conventional foods 26

1.3.1. Functional foods 27

1.3.2. Fortified foods 31

1.3.3. Ultra-processed foods 36

1.3.4. Superfoods 37

1.3.5. Transgenic foods 38

1.3.6. Novel foods 40

1.4. Foodomics 41

1.5. Metabolomics in the study of foods 50

1.6. References 56

Chapter 2: Basics of Nuclear Magnetic Resonance

2.1. Introduction 63

2.2. Classical description of Nuclear Magnetic Resonance 65

2.2.1. Nuclear magnetic moment 65

2.2.2. Nuclear Magnetic Resonance phenomenon 73

2.3. CW-NMR and FT-NMR 80

2.4. The NMR spectrometer 88

2.5. NMR experiments 97

2.6. NMR data processing 99

2.7. References 103

Chapter 3: Basics of High-Performance Liquid Chromatography

3.1. Introduction 109

3.2. Theory of the chromatographic techniques 111

3.2.1. Conventional parameters 111

3.2.2. Chromatographic efficiency: Van Deemter equation 115

3.2.3. Broadening of the chromatographic band due to extra column effects 117

3.2.4. Stationary phases 119

3.2.5. HPLC instrument 121

3.3. Extraction method to study food matrices by means of HPLC 129

3.3.1. Liquid-Liquid extraction (LLE) 130

3.3.2. Solid-Liquid Extraction (SLE) 130

3.3.3. Innovation in the extraction methods for solid foods 131

3.3.4. Innovation in the extraction methods for liquid foods 134

3.4. References 137

Chapter 4: Application of the NMR metabolomics approach in Food Science

4.1. NMR methodology approach for food analysis 143

4.2. NMR metabolomics workflow 149

4.2.1. Experimental design 149

4.2.2. Sampling 150

4.2.3. Sample extraction 152

4.2.4. Sample preparation for NMR analysis 158

4.2.5. Data acquisition, pre-processing and pre-treatment 161

4.2.6. Data statistical analysis 169

4.3. References 180

Chapter 5: NMR metabolomics for the valorization of Italian local products and for the quality preservation of vegetables

5.1. Introduction 191
5.2. Case study 1: Torpedino di Fondi and San Marzano tomato cultivars of Lazio Region 196
5.3. Case study 2: Ten apple cultivars from the Piedmont Region 227
5.4. Case study 3: Goji berries cultivars cultivated in Lazio Region 251
5.5. Case study 4: Metabolomic NMR profile of pumpkin packaged with commercial biofilms 277

Chapter 6: NMR characterization of foodstuff to find potential application for human health

6.1. Introduction 305
6.2. Case study: *Prunus domestica* L. extracts as food supplement ingredients in the prevention of metabolic syndrome 307

Chapter 7: NMR metabolomics and HPLC analysis applied on plant matrices in the perspective of food applications

7.1. Introduction 331
7.1.1. *Cannabis Sativa* L. 331
7.1.2. *Gentiana Lutea* L. 336
7.1.3. References 339
7.2. Case study 1: Multimethodological characterization of seven dioecious cultivars of industrial hemp 347
7.3. Case study 2: Multimethodological characterization of Ferimon monoecious cultivar cultivated with different agronomical practices 369
7.4. Case study 3: Malted hempseeds characterization through HPLC analysis 391
7.5. Case study 4: Hemp seed oils characterization by multimethodological approach 405
7.6. Case study 5: Metabolomic characterization of Gentian Lutea L.: analysis of the distribution of metabolites from root to leaves and flowers 423

Chapter 8: Review articles

8.1. Introduction 447

8.2. Review 1: Role of food in the COVID-19 pandemic 449

8.3. Review 2: Food bioactive compounds as NLRP3 inflammasome modulators 469

8.4. Review 3: NMR based approaches in the study of foods 515

Acknowledgments 541

Aim

Foodstuffs are complex matrices characterized by a large and rich chemical profile, whose qualitative and quantitative composition is affected by a wide number of variables regarding cultivation practices, storage, and treatments. The qualitative and quantitative characteristics of a biological system are very important since they can define the nutritional, biological, and organoleptic properties for a foodstuffs. Therefore, a very exhaustive matrix characterization is strongly needed, and in this context, -omics sciences, and in particular, metabolomics, can represent an important powerful tool for this kind of analysis.

Chapter 1: Introduction

1.1. Food definitions and their limits

"*Foods are materials, in a raw, processed or formulated form, that are consumed orally by humans or animals for growth, health and satisfaction or pleasure*", this is a definition for foodstuffs proposed by M. Shafiur Rahman and Owen J. McCarthy in the 1999 (Rahman & McCarthy, 1999). To date, the main definitions for food for human consumption come from the Regulation (EC) No 178/2002 in Europe; Federal Food, the Drug, and Cosmetic Act (1938) in United States (US) and the Food Sanitation Act (1947) in Japan. As it can be seen in Table 1. 1, there are some differences among definitions. American definition includes animal feed and any substance that migrates from the food articles to the food, while Japanese definition is as not specific as the other ones.

Table 1. 1. Statutory definitions for food by international regulations.

Area/country [Regulation]	**Definition**
Europe [Regulation (EC) No 178/2002]	*"Any substance or product, whether processed, partially processed or unprocessed, intended to be, or reasonably expected to be ingested by humans. Drinks, chewing gum and any substance (including water) that is added to the food voluntarily during the manufacturing, preparation or treatment stages are considered foods. Feed, live animals (unless they are intended for human consumption), plants before harvesting, medicinal products, narcotic or psychotropic substances, cosmetics, tobacco and tobacco products, and residues and contaminants, are not included in this definition".*
US [Federal Food, Drug, and Cosmetic Act (1938)]	*"Articules used for food or drink for man or other animals, chewing gum and articles used for components of any such article'. This term includes human food, substances migrating to food from food-contact articles, pet food and animal feed".*
Japan [Food Sanitation Act (1947)]	*"Food and drink, excluding pharmaceutical products or quasi-pharmaceutical products specified by the Pharmaceutical Affairs Act (1960)".*

In the scientific world there is the well-known tendency to classify, group and label every things, so it is not so strange a definition also for food. In my opinion, a proper manner to explore the food world and to try to understand what are the limits in the food field is to study the current available classification or description system. In fact, to study a field and understanding its extension the better way is to compare the elements in order to find their similarity and differences, obtaining at the end a classification/description of the field.

In the opposite end, *medicine* is a product which has scientifically demonstrated at the recommended doses any pharmacological, immunological or metabolic action, that come from an *active substance* inside the medicine. Apparently, it is clear the difference between medicine (with an immediate health effect) and food (with a more long-term health effect). In fact, in Europe there is an agreement that the recognized therapeutic active level of substances should be viewed as a "cut off point" to make the proper difference. One product containing a substance with a lower recommended daily intake than this cut off point would be under food products regulation.

By contrary, if the recommended daily dosage is higher than this cut off point, the product would be regulated by medicines regulation. However, the appearance of different functional products in the global market such as functional foods, food supplements and nutraceuticals, that are presented as a new potential strategy for reducing the risk and preventing chronic diseases, has strongly increased the difficulty to distinguish between nutrition and pharma (Figure 1. 1) (Domínguez Díaz et al., 2020).

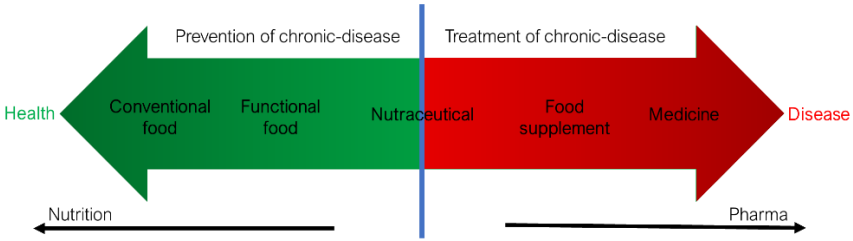


Figure 1. 1. Nutrition-Pharma interface

Regarding the food supplements, that are part of the "pharma world", they are consumed in order to complement the normal diet and ensure the proper intake of specific components (vitamins, minerals…) for a specific period of time.

They may also be capable of reducing the risk of disease. As medicines, food supplements take the pharmaceutical forms (pills, tablets, capsules, sirups, etc.), which results to be the most remarkable difference with functional foods.

While, Nutraceuticals, as a concept, are considered to be in the border among nutrition and pharma. In fact, the term "nutraceutical" is a portmanteau of the words "nutrient" and "pharmaceutical" which was coined in 1989 by Stephen L. DeFelice who defined it as "*a food or parts of food that provide medical or health benefits, including the prevention and/or treatment of disease*". In order to understand the complexity of this concept, people used to associate it with the alleged Hippocratic principle "*let food be thy medicine and medicine be thy food*", which was responsible of the widespread misunderstanding that food was synonymous of medicine. The most recent definition of nutraceuticals is "*the phytocomplex if they derive from a food of vegetal origin, and as the pool of the secondary metabolites if they derive from a food of animal origin, concentrated and administered in the more suitable pharmaceutical form, which are capable of providing beneficial health effects, including the prevention and/or the treatment*

of a disease". However, no specific regulation in Europe, US and Japan provides a statutory definition for nutraceuticals. Thus, the term 'nutraceutical' is incorrectly used to refer to a great number of products, ranging from isolated ingredients, nutrients and food components, to food, processed food, functional foods, herbal products and above all, food supplements. In this scenario, nutraceuticals are commercialized as "food-pharma products" with a non-clear-cut publicity about its capacity to treat or prevent disorders, which creates an atmosphere of ambiguity confusing consumers. Hence, a clear and comprehensive definition as well as an international specific regulation are highly needed (Domínguez Díaz et al., 2020).

While regarding the functional products in the "food world", such as functional foods and the other non-conventional foods an explication is provided in the section 1.3.

Here a summary of the explained differences among these products on the nutrition-pharma interface in European Union countries is reported in Table 1. 2.

Table 1. 2. Differences between the concepts "food", "functional foods", "food supplements", "nutraceuticals" and "medicines" in European Union countries.

Concepts	**Presentations**	**Regularity of consumption**	**Functions**
Food/Foodstuff	Food	Daily	Maintenance of the proper nutrition balance.
Functional foods	Food	As part of the normal and daily diet	Enhancement of human well-being and health. Reduction of the risk of disease.
Nutraceuticals	Pharmaceutical form (pills, tablets, capsules, sirups)	During a specific period of time	Promotion of human well-being. Prevention of diseases. Treatment of diseases.
Food supplements	Pharmaceutical form (pills, tablets, capsules, sirups)	During a specific period of time	Complementing normal and daily diet by ensuring the intake of concrete components (vitamins, minerals, etc.). Possible reduction of the risk of disease.
Medicines	Pharmaceutical form (pills, tablets, capsules, sirups, injectables, etc.)	During a specific period of time (according to medical prescriptions	Treatment and cure of a specific disease.

In conclusion, the ambiguity around them confuses consumers and an harmonized regulation concerning these functional products is needed. In fact, functional products could be able to reduce the risk of chronic disease as well as promote and maintain human health status, well-being and life quality. They could represent another viable option in the management of chronic disease in combination with prescribed medication. Proper communication about nutrition-pharma combinations is highly necessary to prevent food-medicine interactions and the replacement of medicinal therapies by the consumption of these functional products. Further research in the near and long term is essential to establish which of these combinations provide the most favourable benefit-risk and cost-effectiveness ratio for each chronic disease (Domínguez Díaz et al., 2020).

1.2. Food classification and description systems

Inside the "food world" there is a general agreement on the importance of food nomenclature, description and classification. In fact the simple food name can be inadequate or

ambiguous to those who are not closely familiar with the local language and culture. A common name may be misleading when the same name is used for different foods in different regions or when it is used for foods having different scientific names. Similarly, one may not recognize some terms used by people in other parts of the world or maybe even within the same country. The situation is further confused by homonyms, synonyms, identical brand names for different products, and culinary or technological terms. To solve this issue, a lot of food identification systems were created, take into count that an international understanding of standardized food identification could solve many of the problems arising from the mis-identication of foods (Jayne D. Ireland & Møller, 2000). The principal two manner of organize the knowledge about foods used as methods of food identification are the creation of food classification systems, that tend to group or aggregate foods with similar characteristics, and food description systems, that are a tool of the data originator who wants to give a description of the food.

First of all, a noteworthy international and well-known comprehensive collection of food standards is the Codex Alimentarius (FAO, n.d.). It is created by the joint commission between the Food and Agriculture Organization of the United Nations (FAO) and the World Health Organization (WHO) in 1962 to assist in their harmonization and in doing so to facilitate international trade. The Codex Alimentarius includes standards regarding the quality and safety for all the principal foods, whether processed, semi-processed or raw, for distribution to the consumer. Moreover, it includes provisions in respect of food hygiene, food additives, residues of pesticides and veterinary drugs, contaminants, labelling and presentation, methods of analysis and sampling, and import and export inspection and certification. For instance, regarding honey it report the definition "honey is the natural sweet substance produced by honey bees", prohibit the addition of any food ingredient and the processing and heating to alter the composition or quality. So the Codex Alimentarius constrain to sell the honey in the exact manner produced from the honeybees. It clusters the honey in two groups: the nectar honey

and the honeydew honey. Moreover, it report the essential composition, the labelling, the method of analysis, the maximum limits of heavy metals, residues of pesticides and veterinary drugs, the hygiene practices, the quality factors and its method of analysis.

However the Codex Alimentarius Food Standards is not a classification system. Taking into account the existing types of classification systems, historically each country have developed national and regional databases based on national criteria, and the food groups may be very specific. This is clearly mainly due to legal aspects and traditions linked with the cultural and economic importance of foods. For instance, there is a separate group for coconut products in the food composition tables of the Pacific Islands, groups for bananas, maize, and cornbreads in the Central America and Panama database, and a group for edible insects in the Thai food composition database.

1.2.1. Food classification systems

However, the creation of food classification systems depend on the point of view of its creation and are purpose-

specific. An international classification system is the Codex Food Categorization System of the union FAO/WHO. It is hierarchical, applies to all foodstuffs and with the aim to provide a database with all the provisions for food additives that have been adopted by the Codex Alimentarius Commission. Foods are classified in 16 main food categories, then sub-categories, according to additive authorizations. When the use of an additive is permitted in a certain category, it is automatically permitted in all its sub-categories. The entire food category hierarchy is reported in Figure 1. 2, where is expanded the honey section as example. In this system honey is grouped in the section 11.0 of the sweeteners.

GSFA Online

FRANÇAIS | ESPAÑOL

Updated up to the 42nd Session of the Codex Alimentarius Commission (2019)

FOOD CATEGORIES

Food Category	Number
Dairy products and analogues, excluding products of category 02.0	01.0
Fats and oils, and fat emulsions	02.0
Edible ices, including sherbet and sorbet	03.0
Fruits and vegetables (including mushrooms and fungi, roots and tubers, pulses and legumes, and aloe vera), seaweeds, and nuts and seeds	04.0
Confectionery	05.0
Cereals and cereal products, derived from cereal grains, from roots and tubers, pulses, legumes and pith or soft core of palm tree, excluding bakery wares of food category 07.0	06.0
Bakery wares	07.0
Meat and meat products, including poultry and game	08.0
Fish and fish products, including mollusks, crustaceans, and echinoderms	09.0
Eggs and egg products	10.0
Sweeteners, including honey	11.0
Refined and raw sugars	11.1
White sugar, dextrose anhydrous, dextrose monohydrate, fructose	11.1.1
Powdered sugar, powdered dextrose	11.1.2
Soft white sugar, soft brown sugar, glucose syrup, dried glucose syrup, raw cane sugar	11.1.3
Dried glucose syrup used to manufacture sugar confectionery	11.1.3.1
Glucose syrup used to manufacture sugar confectionery	11.1.3.2
Lactose	11.1.4
Plantation or mill white sugar	11.1.5
Brown sugar excluding products of food category 11.1.3	11.2
Sugar solutions and syrups, also (partially) inverted, including treacle and molasses, excluding products of food category 11.1.3	11.3
Other sugars and syrups (e.g. xylose, maple syrup, sugar toppings)	11.4
Honey	11.5
Table-top sweeteners, including those containing high-intensity sweeteners	11.6
Salts, spices, soups, sauces, salads, protein products	12.0
Foodstuffs intended for particular nutritional uses	13.0
Beverages, excluding dairy products	14.0
Ready-to-eat savouries	15.0
Prepared foods	16.0

Figure 1. 2. Food category hierarchy of the Codex Food Categorization System with the honey section expanded (number 11.5) as an example.

Another system is the Codex Classification of Foods and Feeds of the union FAO/WHO, that is a complete list of food commodities in trade designed to promote harmonization pesticide residues limit; Harmonized Commodity Description and Coding System of the World Trade Organization (in Europe it corresponds to the European Combined Nomenclature), that comprises 20 sections, four of which apply to foods, and is used for international trade and to generate trade statistics; Food Balance Sheets of the FAO, that presents a comprehensive picture of a country's food supply during a specific reference period (FAO, n.d.); Eurocode-2 Food Coding System, that is a mono-hierarchical classification of foods according to groups and subgroups that are useful in dietary studies. Instead, the second method of food identification is based on the food description

1.2.2. Food description systems

The food description systems want to give a picture of the food, as precisely as possible, without the necessity of aggregating them, exist many food description systems (Jayne

D. Ireland & Møller, 2000). The two major systems used to describe foods in food composition databases are the LanguaL thesaurus (that is a structure that manages the complexities of terminology and provides conceptual relationships, through classification/ontology), and the INFOODS system. LanguaL™ stands for "Langua aLimentaria" or "language of food" and was started in the late 1970's by the Center for Food Safety and Applied Nutrition (CFSAN) of the United States Food and Drug Administration.. It is an automated method for describing, capturing and retrieving data about food. Regarding the example of honey, it report the following definition: “Honey is a natural sweet substance produced by bees from the nectar of plants or from secretions of living parts of plants or excretions of plant-sucking insects on plants”. The second system, INFOODS, is the International Network of Food Data Systems, established in 1984 and now coordinate by FAO. It is a worldwide network of food composition experts aiming to improve the quality, availability, reliability and use of food composition data.

1.2.3. Food classification and description systems

All the developed systems are fundamental and functional tools for the clear and organization of the *food world* also to avoid food mis-identification at an international level, but now the first need is to link and harmonize the existing systems to produce a reliable and universal food organization system. With this scope, the European Food Safety Authority (EFSA) has create a food classification and description system, the FoodEx2 (J. D. Ireland & Møller, 2015; "The food classification and description system FoodEx 2 (revision 2)," 2017). FoodEx2 consists of a detailed list of individual food items aggregated into 21 food groups and broader food categories (Figure 1. 3). The system includes parallel hierarchies, aggregating food items and food groups in different ways according to the needs of specific food safety domains: general reporting, chemical exposure, pesticide residues, zoonoses, veterinary drugs, and animal feeds. Some descriptors are based on the LanguaL™ thesaurus.



Figure 1. 3 List of the 21 food groups of the FoodEx2 database.

1.2.4. Food composition databases

However these illustrated methods of food identification, the food classification systems and the food description systems, are used in the food composition databases (Pehrsson & Haytowitz, 2015). In fact, chemically foods are composed

mainly of water, macronutrients (lipids, proteins, and carbohydrates) with small proportions of minerals (e.g. calcium, iron, sodium) and organic compounds like vitamins, emulsifiers, acids, antioxidants, pigments, polyphenols, flavours, etc. Hence the food composition databases have the mission to determine and compile what is in the foods we eat, reporting information on all these wide range of components, and is the critical bridge between nutrition, health, and disease prevention and food production. There are a number of different types of food composition databases available. Regional food composition databases are developed in areas where a number of small countries exist with similar climates and cuisines; an example is the West African Food Composition Database developed by the FAO. While, an example of national database is the National Nutrient Database for Standard Reference (SR) of the US Department of Agriculture (USDA) that contains data for up to 150 components for nearly 8600 food items. Moreover, Special interest databases (SIDs) are often developed by database compilers for a number of various compounds or compound class. An example is the Food

Composition Database of EFSA that gives information on the amount of vitamins and minerals contained in different foods to establish dietary reference values (EFSA, n.d.). Another interesting database Europe based is the EuroFIR eSearch facility (EuroFIR, n.d.). The European Food Information Resource Network (EuroFIR) to promote the data exchange about food information throughout Europe allows users, with its facility, to simultaneously search more than 20 national and specialised food composition databases of Europe. Regarding the international databases, a list of food composition tables and databases was compiled and is available on the INFOODS website. These are organized by the regional data centres and many can be viewed online. A number have searchable databases that allow one to look up the composition of foods in the particular database. Another useful food composition database is the freely available and open-access FoodDB created by David S. Wishart of the University of Alberta. Now it is the world's largest and most comprehensive resource on food constituents, chemistry and biology. It provides information on both macronutrients and micronutrients, including many of the

constituents that give foods their flavour, colour, taste, texture and aroma (EuroFIR, n.d.; Functional Food Center Inc., n.d.).

In general, developing a food composition databases, it is important to use good quality data taking into account: the sampling plan, the sample handling, the number of samples, the analytic method, and the analytic quality control. Other important things are: each given component should always be presented in the same units (for instance per 100g of edible portion); the results could be report on a wet-weight basis or on a dry-weight basis. The source of the data should be clearly identified: if from a study sponsored by the database developer, the name of the study and when it was conducted should be given; if data are used from a journal article, a full citation should be provided. If values were calculated, codes indicating how the calculations were performed should be developed and used. Lastly, a database could report different types of data, including the analytic data (that are the values determined by direct analysis of a food sample).

In my opinion, other crucial information's, that impact the amounts of components in foods, have to be reported together

with the analytic data, like the agronomic condition and the method of analysis. Moreover, future upgrade of all the food composition databases could be the addition, for each food, the composition of the food local variety, as a sub-category, to valorise the local products of each country or area.

1.3. Non-conventional foods

Today the food chain, beyond the conventional foods, provide many food types options. In fact in recent year appear many new food classes, namely "functional food", "ultra-processed food", "fortified food", "superfoods", etc. It is often difficult to distinguish due to mis-leading definitions and different countries legislation. This complicated nutritional vocabulary, have confused the consumers during the last decade. To date, consumer requirements in the field of food production have changed considerably: In fact, consumers increasingly believe that food contribute directly to their health. Thus, foods are no more intended to only satisfy hunger and to provide the necessary nutrients, but also and especially to prevent nutrition-related diseases and to improve physical and

mental well-being. In this scenario, the innovations introduced in the food industry in recent years mainly refer to new scientific and technical approaches in food processing, and to the introduction of novel foods

Here, some of the most used innovative food classes were reported trying to make a discrimination and clarification of the different classes in order to understand how each food could be studied with the metabolomic approach. As first, functional foods are discussed. Indeed, functional foods play an outstanding role, as demonstrated by their increasing demand derived from the increasing cost of healthcare, the steady increase in life expectancy, and the desire of older people for an improved quality of life in their later years.

1.3.1. Functional foods

The term "functional food" was first coined in Japan in 1984, defining functional food as "Food products fortified with special constituents that possess advantageous physiological effects". Subsequently countries and scientific organizations have attempted to create their own definitions of functional

food. Functional foods have no universally accepted definition. However, the current definition of functional foods reported by the Functional Food Center (FFC), the leading organization in the world for evaluating functional food products and educating public in Functional Food Science, is the following: "Natural or processed foods that contain biologically-active compounds; which, in defined, effective, non-toxic amounts, provide a clinically proven and documented health benefit utilizing specific biomarkers, to promote optimal health and reduce the risk of chronic/viral diseases and manage their symptoms" (Functional Food Center Inc., n.d.; Gur et al., 2018; Martirosyan & Singh, 2015). Based on this definition, functional foods can be natural or processed (M. S. Arshad, W. Khalid, R. S. Ahmad, M. K. Khan, M. H. Ahmad, S. Safdar, S. Kousar, H. Munir, U. Shabbir, M. Zafarullah, M. Nadeem, Z. Asghar, 2021). By this, we mean that foods in their pure unchanged or changed forms can be functional. A natural unchanged food has not undergone human interference. A changed food has undergone some chemical modification, whether it be the addition, removal, alteration, or increased bioavailability of a chemical

compound within the food. For instance, a natural food may be a pure orange or avocado, while a processed food may be folate-fortified cereal or milk infused with Vitamin C. As for the meaning of food, scientists and governing bodies disagree. Japan includes pills and capsules under functional foods while the EU does not. The FFC defines food as components of a normal diet for optimized nutrition. This includes conventional foods and not pills or capsules. It is clear that also "fortified foods" fall in the functional foods definition. Moreover, bioactive compounds are considered the source of functional food effectiveness, which makes them the central point of this definition. Biologically-active compounds or secondary metabolites are molecules in food, usually in small amounts, that act synergistically to benefit health. The active components of functional foods may be an essential macronutrient (e.g. carbohydrates, proteins, and fats), that must be consumed in large amounts since they make up most of human diet, or an essential micronutrient (e.g. vitamins or minerals), that must be ingested in certain trace amounts.

One general classification of functional food from the review article of (Bigliardi & Galati, 2013) propose the following classification from a product point of view:

- Food fortified with additional nutrients (labelled fortified products), such as fruit juices fortified with vitamin C, vitamin E, folic acid, zinc and calcium;
- Food with additional new nutrients or components not normally found in a particular food (labelled enriched products), like fruit juices with calcium, probiotics or prebiotics;
- Food from which a deleterious component has been removed, reduced or replaced by another with beneficial effects (labelled altered products), for example fibres as fat releasers in meat or ice cream, or milk with oleic acid (replacement of saturated fat);
- Food in which one of the components have been naturally enhanced (labelled enhanced commodities), e.g., eggs with increased omega-3 content or fruits with enhanced content of vitamins.

1.3.2. Fortified foods

The Codex General Principles for the Addition of Essential Nutrients to Foods defines "fortification", or synonymously "enrichment", as "the addition of one or more essential nutrients to a food whether or not it is normally contained in the food, for the purpose of preventing or correcting a demonstrated deficiency of one or more nutrients in the population or specific population groups". In recent years, due to the increasing of diverse set of public health circumstances were developed a range of different types of fortified foods.

A general example of food fortification is the one with micronutrients (Guidelines on food fortification with micronutrients, 2006). The fortification with micronutrient, such as vitamins and minerals (including trace elements), represent a valid technological practise to increase the intake of micronutrients in the control or prevention of the micronutrient malnutrition, that is widespread in the industrialized nations, but even more so in the developing regions, and for sure in the

poorer regions of the world since the undernutrition due to food shortages and the diets lack diversity. Today worldwide, the three most common forms of micronutrient malnutrition are iron, vitamin A and iodine deficiency. Together, these affect at least one third of the world's population, the majority of whom are in developing countries. Of the three, iron deficiency is the most prevalent. It is estimated that just over 2 billion people are anaemic, just under 2 billion have inadequate iodine nutrition and 254 million preschool-aged children are vitamin A deficient. The issue related with the micronutrient malnutrition is also the higher risk factor for many diseases, that can contribute to increase morbidity and even mortality. Other widespread micronutrient malnutrition's are zinc, folate and vitamin D deficiency, but their prevalence are much more difficult to quantify since their adverse effects on health are sometimes non-specific.

In particular, some examples of well-known and effectiveness food fortification are:

- Iodine fortification: Numerous studies, particularly from the developed world, have clearly established that

salt iodization is an effective means of controlling iodine deficiency reducing the prevalence of goitre and deaf mutism.

- Iron fortification: The effectiveness of iron fortification has been demonstrated in several world regions. Examples of iron fortification are the fortification of infant formulas, flours, milk and soy sauce to control the iron deficiency.
- Combined iron and iodine fortification: the dual fortification of salt with iron and iodine can improve both iron and iodine status. Moreover, recent studies demonstrate that the combined fortification maximize the impact of the iodine fortification since iron deficiency reduces the efficacy of iodine prophylaxis (because of iron is required for thyroxine synthesis).
- Vitamine A fortification: fortification of sugar with vitamin A is a strategy that has been used extensively in programmes of Central America to reduce the prevalence of low serum retinol values. In Guatemala this sugar fortification is still ongoing.

- Folic acid fortification: The introduction of the mandatory fortification of wheat flour with folic acid in some national programmes in Unites States, Canada and Chile have showed a significant increase of serum folate and a reduction of serum homocysteine.
- Vitamin D fortification: The addition of vitamin D to milk is a well-known practices used to eliminate the childhood rickets and have also the advantage to reduce the risk of osteoporosis in the elderly, especially in higher latitude regions where levels of incident ultraviolet light are lower during the winter months.

However, in general there are three main types of fortification:

- Mass fortification: fortification of foods that are widely consumed by the general population;
- Targeted fortification: fortification of foods designed for specific population subgroups, such as complementary foods for young children or rations for displaced populations;

- Market-driven fortification: fortification to allow food manufacturers to voluntarily fortify foods available in the market place.

Mass fortification is nearly always mandatory, targeted fortification can be either mandatory or voluntary depending on the public health significance of the problem it is seeking to address, and market-driven fortification is always voluntary, but governed by regulatory limits (Figure 1. 4).

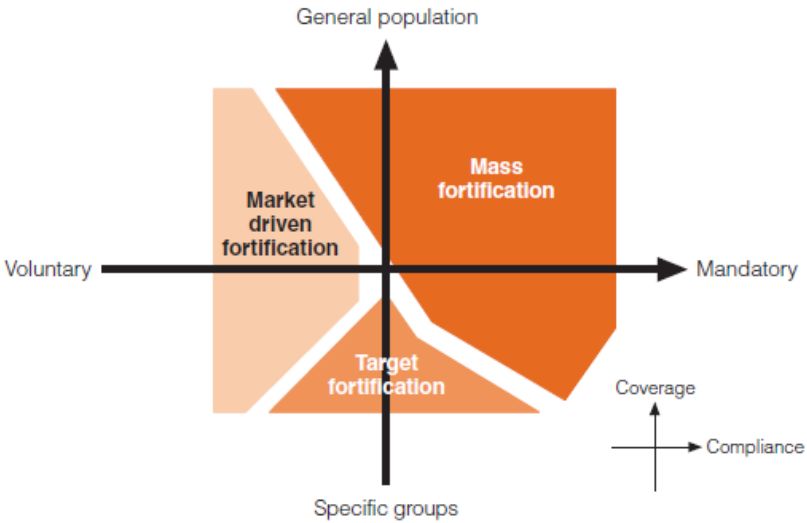


Figure 1. 4. Interrelationships among the levels of coverage and compliance and the types of food fortification (source: (Guidelines on food fortification with micronutrients, 2006)*)*

1.3.3. Ultra-processed foods

Ultra-processed foods are entirely or mostly made not from foods, but from industrial ingredients and additives, are ready-to-consume and are extremely profitable. In fact, ultra-processed products are made from processed substances extracted or refined from whole foods, like oils, hydrogenated oils and fats, flours and starches, variants of sugar, and cheap parts or remnants of animal foods. Products include burgers, frozen pasta, pizza and pasta dishes, nuggets and sticks, crisps, biscuits, confectionery, cereal bars, carbonated and other sugared drinks, and various snack products. They are typically energy dense; have a high glycemic load; are low in dietary fiber, micronutrients, and phytochemicals; and are high in unhealthy types of dietary fat, free sugars, and sodium. The commercial advantages of these kind of foods, respect to the fresh and perishable whole or minimally processed foods, are the durability and the fact that are ready to consume.

When consumed in small amounts and with other healthy sources of calories, ultra-processed products are harmless. However, intense palatability (achieved by high content of fat,

sugar, salt, and cosmetic and other additives), omnipresence, and sophisticated and aggressive marketing strategies, all make modest consumption of ultra-processed products unlikely and displacement of fresh or minimally processed foods very likely. These factors also make ultra-processed products liable to harm endogenous satiety mechanisms and so promote energy over-consumption and thus obesity (Monteiro et al., 2013).

1.3.4. Superfoods

Superfoods is a marketing term and there is no established medical definition. The Oxford English Dictionary defines the term as "a food considered especially nutritious or otherwise beneficial to health and well-being" (Oxford English Dictionary). There are neither guidelines for classifying foods as superfoods, nor is there a comprehensible overview of such a classification available. Chia seeds, quinoa and goji barriers are examples of foods frequently labelled as superfoods. Typically, benefits of superfoods arise from their nutritional profile, including a high content of vitamins, minerals, or antioxidants. However in the current scientific literature there

aren't available article that pay attention at this new term, neither in a legislative manner nor in a chemical understanding, but only survey studies to assess the public's understanding and judgment about superfoods (Kirsch et al., 2022). Hence, the meaning of the term is predominantly shaped by the marketing industry.

1.3.5. Transgenic foods

Transgenic foods are foods that are derived from or contains genetically modified organisms (GMOs). The rapid development of recombinant DNA technology in agriculture has prompted the production of GM crops that include benefits in agronomic productivity and industrial processing. Regarding safety issues of GMOs, the presence of potential unintended changes resulting from genetic transformation represents one of the central issues for debate. A leading accepted strategy, termed substantial equivalence, proposes to start risk assessment of GMOs by comparing them with traditional varieties. Substantial equivalence is based on the assumption that commercialized traditional crops have been

consumed for decades and have gained a history of safe use; consequently, they can be used as comparators for the safety assessment of new GMOs derived from established plant varieties. In comparative safety assessment, comparisons are typically performed on the basis of targeted analysis of predefined compounds that include macronutrients and micronutrients, antinutrients, and natural toxins, following recommendations in the Organization of Economic Cooperation and Development (OECD) consensus documents for individual crops. However, it has been pointed out that this targeted strategy is biased, and that some unforeseen, unintended effects that could result directly or indirectly from the genetic transformation may escape detection. Hence, As an alternative approach to targeted analysis, the European Food Safety Agency (EFSA) has recommended development and use of profiling technologies able to broaden the coverage in comparative analyses of GMOs (Valdés et al., 2013). Thus, foodomics can provide valuable information about molecular profiling, based on genomics, transcriptomics, proteomics

and/or metabolomics analysis, which could be essential for GMO characterization and traceability.

1.3.6. Novel foods

Novel foods means any food that was not used for human consumption to a significant degree within the Union before 15 May 1997 (Regulation (EU) 2015/2283). Any new candidate novel food has to be authorized by the Commission. This category includes new food sources, recently used substances in food as well as new ways and technologies for food production. The EU is also responsible of the novel foods principles: consumer safety, transparent labelling that does not mislead the consumer, and its consumption must not be disadvantageous from a nutritional point of view. To date the novel food category is regulated by (Regulation (EU) 2015/2283), which replaces Regulation (EC) no. 258/97 and Regulation (EC) no. 1852/2001 (which were in force until 31 December 2017). The main contributions of the new Regulation are: the enlargement of the category, the simplification of the food authorization, the creation of a European catalogue of

novel foods, the recognition of EFSA as authority responsible for assessing the food safety of candidate foods and a series of concessions for the recognition of traditional foods from non-EU countries as novel food. Examples of recognized novel foods are some insects. The insects that the European Commission has recognized as novel food are: the mealworm larva (*Tenebrio molitor*) in 2021, the grasshopper (*Locusta migratoria*) in 2021, and the domestic cricket (*Acheta domesticus*) in 2022.

1.4. Foodomics

The term Foodomics is firstly defined in 2009 by Alejandro Cifuentes as "*a discipline that studies the Food and Nutrition domains through the application of omics technologies*" (Alejandro Cifuentes, 2009). Foodomics makes possible to unravel the huge complexity of the Foodome, which has been defined as "*the pool of all compounds present in a food sample and/or in a biological system interacting with the investigated food at a given time*" (Alejandro Cifuentes, 2018). In other hands, the Foodomics is "*a global discipline that includes all the working areas in which food (including nutrition) and advanced omics tools are put*

together" (A Cifuentes, 2013). A representation of this concept is shown in Figure 1. 5. Thus, the use of omics tools such as genomics, epigenomics, transcriptomics, proteomics, and metabolomics is a must in this new discipline. By taking advantage of the newest omics methodologies, foodomics is continuously pushing the research into different hot topics in food science and nutrition. One of the main goals and interests in foodomics is in line with medicine and biosciences toward prevention of future diseases through adequate food intake, and the development of the so-called functional foods and nutraceuticals. Moreover, another goal of foodomics is to understand the bioactivity of food and food ingredients in our body at the molecular level to characterize and identify potential beneficial compounds and investigate the association between dietary exposure and health (Valdés et al., 2017). Furthermore, foodomics can also help to investigate and solve crucial questions in food science and nutrition such as global omics strategies to explore food safety, quality and traceability (Álvarez-Rivera et al., 2021).

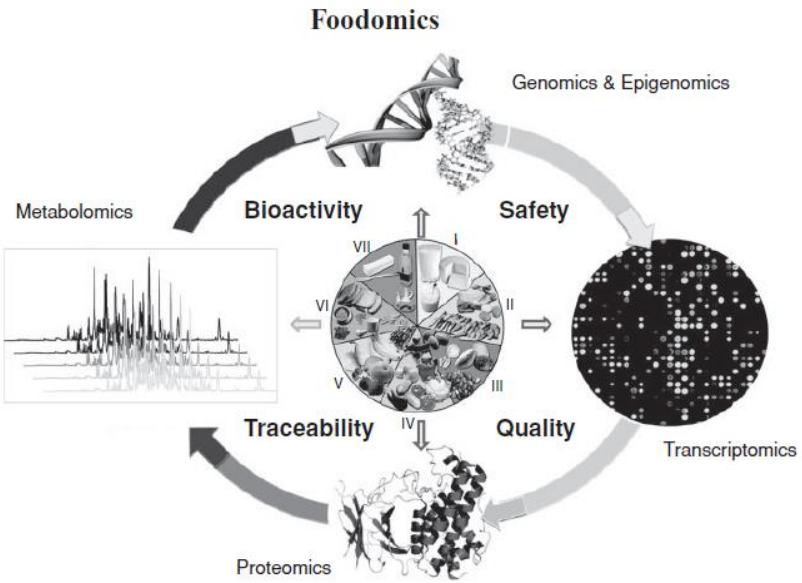


Figure 1. 5. Foodomics: covered areas and tools (Source: (A Cifuentes, 2013)*).*

To face the enormous challenges in different subdisciplines and applications, foodomics involves the use of multiple omics tools capable of providing molecular information on the different expression levels, i.e. gene, transcript, protein, or metabolite.

The terms "Ome" derived from a Greek word and "Omics" are derivations of the suffix -ome which means "whole," "all," or "complete." With the addition of -ome to

cellular molecules, such as gene, transcript, protein, metabolite, it can be referred as genome, transcriptome, proteome, metabolome, respectively. Omics refers to collective and high-throughput analyses including genomics, transcriptomics, proteomics, and metabolomics/lipidomics that integrated through robust systems biology, bioinformatics, and computational tools to study the mechanism, interaction, and function of cell populations' tissues, organs, and the whole organism at the molecular level in a non-targeted and nonbiased manner (Nalbantoglu & Karadag, 2019).

- Genomics: is the systematic study of an organism's entire genome. The human genome is made up of DNA (deoxyribonucleic acid) comprising approximately 3 billion base pairs of four chemical structures (adenine, guanine, cytosine, and thymine), also called nucleotides. DNA contains genetic information required to build and maintain cells. A gene denotes a specific unit of DNA that hold information to make a specific functional unit named protein. It is estimated that the entire human genome contains approximately 21,500 genes. The order

of the nucleotides reveals the meaning of the information encoded in DNA. Emergence of high-throughput sequencing technologies, such as next-generation sequencing, enables analysis of variations between individuals at the genomics level. Combined with appropriate statistical and bioinformatic tools, these methods will permit the identification of all the loci that are epigenetically altered.

- Transcriptomics: Transcriptomics is the study of transcriptome that comprises the entire collection of RNA (ribonucleic acid) sequences, called transcripts, in a cell. It is estimated that a human cell contains about 25,000 transcripts. RNAs are classified into two groups: (1) mRNA is the coding RNA that is translated into protein sequences. (2) Non-coding RNAs are also classified into two subgroups; short non-coding RNAs such as microRNA (miRNA) and long non-coding RNAs (lncRNA). Noncoding RNAs are involved in gene regulation. Next-generation RNA sequencing technologies allow deeply understanding of variations

and gene expression on various types of RNA molecules including miRNA, mRNA, and lncRNA. Two conceptually different analytical approaches have emerged to allow quantitative and comprehensive analysis of changes in mRNA expression levels of hundreds or thousands of genes. One approach is based on microarray technology, and the other group of techniques is based on DNA sequencing. Next, typically real-time PCR is applied to confirm the up- or down-regulation of a selected number of genes.

- Proteomics: Proteomics is the study of proteome, which is defined as the set of all expressed proteins and interacting protein family networks, and biochemical pathways in a cell, tissue, or organism. Although, the exact number of proteins/peptides is still unclear, it is estimated to be around a few hundred thousand. Normally, the analytical protocols for the proteome study, present a first step of separation of the thousands of proteins found in the biological sample by electrophoresis or chromatography, followed by

analysis of the isolated proteins (or peptides) by mass spectrometry (MS) via the so-called "soft ionization" techniques, such as electrospray ionization (ESI) and matrix-assisted laser desorption/ionization (MALDI). Two fundamental analytical strategies can be employed: the bottom-up and the top-down approach. Both methodologies differ on the separation requirements and the type of MS instrumentation. New proteomic approaches based on array technology are also being employed.

- Metabolomics: Metabolomics is the study of metabolome within cells, biofluids, tissues, or organisms. Metabolome can be defined as the small molecules (<1000-1500 Da) and their interactions within a biological system under a given genetic, nutritional, and environmental condition. Since the metabolome is the final downstream product, changes and interactions between gene expression, protein expression, and the environment are directly reflected in metabolome making it more physically and chemically complex than

the other "omes." The metabolome is the closest to the phenotype among other omics approaches. Metabolomics best modulates and represents the molecular phenotype of health and disease. In this regard, metabolomics is a brilliant source for disease-associated biomarkers. A more detailed explication of metabolomics is provided in the next section 1.4.

A growing trend in the scientific community, is the application of a multi-omics approach to obtain a greater depth of knowledge that otherwise would not be achieved through a single "omics"-based study. For instance, combining metagenomic and transcriptomic data with proteomics and metabolomic datasets will provide researchers and clinicians details on the microbial population present and their metabolic functions. In addition, multi-omics research provides a path for self-validating findings through a combined parallel 'omics' approach, and will ultimately result in the accelerated understanding of these complex populations and processes, driving better diagnostic techniques and drug therapies, environmental remediation strategies and the development of

innovative synthetic/engineered biological products. In conclusion, a multi-omics approach can enable a well and depth characterization of biological systems (Beale et al., 2016).

However, regarding the post-analysis part in omics studies, due to the huge amount of data (data sets) usually obtained, it has been necessary to develop strategies of data analysis to convert the complex raw data obtained into useful information. Thus, bioinformatics has become a crucial tool in Foodomics. Statistic and chemometric tools also are usually applied. However, it is important to understand that every data analysis approach reveals only a very restricted aspect of the whole data sets. In fact, each approach return different outputs, that represent aspects of the whole data set, and it is essentially impossible to extract all of the information contained therein. Therefore, all methods return their own outputs, which represent their viewpoints, but lack the viewpoints of other methods. In other words, all of the methods and pipelines have advantages and disadvantages and it is crucial to choose the better interpretation approach for each obtained data set (Yamada et al., 2021).

1.5. Metabolomics in the study of foods

Foods are complex matrices that can take advantage of the metabolomics. In fact, among omics branches, metabolomics represents the "endpoint" of the cascade, being the closest one to food phenotype, so it can give direct signature of the food biochemical activity and a direct view of the food substances that interact with our organisms. Food metabolome originates from biochemical reactions and carries information not only about the biological source of a given foodstuff but also about all treatments during food production. The metabolome of a foodstuff is the result of its history from the origin (genetic background) to the final step when it is ready to be consumed. During this history different factors influence its metabolite composition in a different manner, leaving an imprint at the molecular level. Moreover, it is noteworthy the fact that in the animal bodies exist no more than ten thousand kinds of major metabolites, while the number of proteins is thought to well exceed 100,000. This feature of metabolites is likely to result in more comprehensive features of metabolomics analysis than proteomics analysis. However, exhaustive analysis of

metabolites is in fact fraught with difficulties and usually requires the use of techniques requiring a high skill level, due to the diversity of the chemical properties of metabolites, which is much greater than those of transcripts and proteins. Another difficulty derives from the width of the abundance of metabolites. Despite these difficulties, metabolomics analysis is a powerful tool in food and nutrition science.

There are three basic approaches that can be used in metabolomics:

- Target analysis: involve the quantitative measurement of selected analytes, such as specific biomarkers or reaction products;
- Metabolic profiling: is a untargeted strategy that focuses on the study of a group of related metabolites or a specific metabolic pathway;
- Metabolic fingerprinting: aim to compare the patterns of metabolites that change in response to the cellular environment, without identify all metabolites.

Regarding the analytical platforms, currently two analytical techniques are used for metabolomic analyses: MS-

and NMR-based systems. The MS detection is usually combined with separation techniques, such as High-Performance Liquid Chromatography (HPLC), ultra-HPLC (UHPLC), Gas-Chromatography (GC), Capillary Electrophoresis (CE), and supercritical fluid chromatography (SFC) (Segers et al., 2019). Each of these analytical technique is characterized by both advantages and disadvantages from a preparative, experimental, and post-analysis points of view, see Table 1. 3.

Table 1. 3. Comparison of the analytical techniques in metabolomic profiling (source: (Segers et al., 2019)*).*

Property	Technique					
	NMR	**HPLC-MS**	**UHPLC-MS**	**SFC-MS**	**CE-MS**	**GC-MS**
Sensitivity	-	++	+++	+++	+	+++
Reproducibility	High	Lower than NMR				
Resolution	Low	Higher than NMR				
Quantification	Yes, internal standard needed	Yes, external calibration curve needed				
Time for sample preparation	Low	Medium	Medium	Medium	Medium	Extensive
Sample volume needed	100-500 µL	2-10 µL	2-10 µL	2-10 µL	1-20 nL	1-2 µL
Range of metabolites	Polar and non-polar	RPLC: non-polar HILIC: polar		Polar and non-polar	Polar	Volatile polar and non-polar
Metabolites structure identification	Easy	Difficult (using database)				

HILIC: Hydrophilic-interaction liquid chromatography; RPLC: Reversed-phase liquid chromatography

Among these techniques, high resolution NMR spectroscopy is a powerful tool to perform both quantitative analysis, using an internal standard, and qualitative analysis, realizing structural determination of metabolites in complex mixture in absence of commercial standards, in a single NMR experiment. Moreover, it does not require complicated sample preparation and compounds separation prior to analysis. All these elements make NMR to be recognized as one of the main analytical methodologies giving a complete view of the foodstuffs metabolite profile.

However, due to the low sensibility of the NMR techniques, the combination with MS- based systems can guarantee greater success of the analysis. In fact, these systems offer an higher sensibility while having a lack in the compound structure determination, since their identification is based on large databases, covered by the NMR methodologies.

Moreover, in the case of targeted analysis, if we are interested in the investigation of selected analytes of certain compound classes, the application of targeted methods like chromatographic systems coupled with ultraviolet detection,

such as High-Performance Liquid Chromatography — Photodiode array detection (HPLC-PDA), could be also useful. In fact in this simply analysis, realizing a previous chromatographic separation of the selected analytes, it is possible to clearly identify, using commercial standards, and quantify, by external calibration curve, the interested compounds with an higher sensibility respect to the NMR.

1.6. References

Álvarez-Rivera, G., Valdés, A., León, C., & Cifuentes, A. (2021). Foodomics – Fundamentals, State of the Art and Future Trends. In *Foodomics: Omic Strategies and Applications in Food Science* (pp. 1–53). https://doi.org/10.1039/9781839163005-00001

Beale, D. J., Karpe, A. V., & Ahmed, W. (2016). Beyond Metabolomics: A Review of Multi-Omics-Based Approaches. In *Microbial Metabolomics: Applications in Clinical, Environmental, and Industrial Microbiology* (pp. 1–321). https://doi.org/10.1007/978-3-319-46326-1

Bigliardi, B., & Galati, F. (2013). Innovation trends in the food industry: The case of functional foods. *Trends in Food Science and Technology*, *31*(2), 118–129. https://doi.org/10.1016/j.tifs.2013.03.006

Cifuentes, A. (2013). FOODOMICS: PRINCIPLES AND APPLICATIONS. In *Foodomics: Advanced Mass Spectrometry in Modern Food Science and Nutrition*.

Cifuentes, Alejandro. (2009). Food analysis and foodomics. *Journal of Chromatography A*, *1216*(43), 7109.

https://doi.org/10.1016/j.chroma.2009.09.018

Cifuentes, Alejandro. (2018). Advanced food analysis, foodome and foodomics. *Electrophoresis*, *39*(13), 1525–1526. https://doi.org/10.1002/elps.201870106

Domínguez Díaz, L., Fernández-Ruiz, V., & Cámara, M. (2020). The frontier between nutrition and pharma: The international regulatory framework of functional foods, food supplements and nutraceuticals. *Critical Reviews in Food Science and Nutrition*, *60*(10), 1738–1746. https://doi.org/10.1080/10408398.2019.1592107

EFSA. (n.d.). *Food Composition Database*. Retrieved August 28, 2022, from https://www.efsa.europa.eu/it/data-report/food-composition-data

EuroFIR. (n.d.). *EuroFIR eSearch facility*. Retrieved August 29, 2022, from https://www.eurofir.org/food-information/food-composition-databases/

Guidelines on food fortification with micronutrients, (2006).

FAO. (n.d.). *Food Balance Sheets*. Retrieved August 25, 2022, from https://www.fao.org/faostat/en/#data/FBS

Functional Food Center Inc. (n.d.). *Definition of Functional Food*.

Retrieved September 5, 2022, from https://www.functionalfoodscenter.net/#:~:text=Definition of Functional Food%3A The,specific biomarkers%2C to promote optimal

Gur, J., Mawuntu, M., & Martirosyan, D. (2018). FFC's advancement of functional food definition. *Functional Foods in Health and Disease*, *8*(7), 385–397. https://doi.org/10.31989/ffhd.v8i7.531

Ireland, J. D., & Møller, A. (2015). Food Classification and Description. In *Encyclopedia of Food and Health* (1st ed.). Elsevier Ltd. https://doi.org/10.1016/B978-0-12-384947-2.00307-X

Ireland, Jayne D., & Møller, A. (2000). Review of international food classification and description. *Journal of Food Composition and Analysis*, *13*(4), 529–538. https://doi.org/10.1006/jfca.2000.0921

Kirsch, F., Lohmann, M., & Böl, G. F. (2022). The Public's Understanding of Superfoods. *Sustainability (Switzerland)*, *14*(7). https://doi.org/10.3390/su14073916

M. S. Arshad, W. Khalid, R. S. Ahmad, M. K. Khan, M. H.

Ahmad, S. Safdar, S. Kousar, H. Munir, U. Shabbir, M. Zafarullah, M. Nadeem, Z. Asghar, and H. A. R. S. (2021). Functional Foods and Human Health: An Overview. In *unctional Foods - Phytochemicals and Health Promoting Potential*. IntechOpen. https://www.intechopen.com/chapters/78318 doi: 10.5772/intechopen.99000

Martirosyan, D. M., & Singh, J. (2015). A new definition of functional food by FFC: What makes a new definition unique? *Functional Foods in Health and Disease*, *5*(6), 209–223. https://doi.org/10.31989/ffhd.v5i6.183

Monteiro, C. A., Moubarac, J. C., Cannon, G., Ng, S. W., & Popkin, B. (2013). Ultra-processed products are becoming dominant in the global food system. *Obesity Reviews*, *14*(S2), 21–28. https://doi.org/10.1111/obr.12107

Nalbantoglu, S., & Karadag, A. (2019). Introductory Chapter: Insight into the OMICS Technologies and Molecular Medicine. In *Molecular Medicine*. https://doi.org/10.5772/intechopen.86450

Regulation (EU) 2015/2283.

Oxford English Dictionary. (n.d.). *Superfood*. Retrieved October 8, 2022, from https://www.oed.com/view/Entry/194186?redirectedFrom=superfood#eid69476470

Pehrsson, P. R., & Haytowitz, D. B. (2015). Food Composition Databases. In *Encyclopedia of Food and Health* (1st ed.). us-gov. https://doi.org/10.1016/B978-0-12-384947-2.00308-1

Rahman, M. S., & McCarthy, O. J. (1999). A classification of food properties. *International Journal of Food Properties*, *2*(2), 93–99. https://doi.org/10.1080/10942919909524593

Segers, K., Declerck, S., Mangelings, D., Heyden, Y. Vander, & Eeckhaut, A. Van. (2019). Analytical techniques for metabolomic studies: A review. *Bioanalysis*, *11*(24), 2297–2318. https://doi.org/10.4155/bio-2019-0014

The food classification and description system FoodEx 2 (revision 2). (2017). *EFSA Supporting Publications*, *12*(5), 1–90. https://doi.org/10.2903/sp.efsa.2015.en-804

Valdés, A., Cifuentes, A., & León, C. (2017). Foodomics evaluation of bioactive compounds in foods. *TrAC - Trends in Analytical Chemistry*, *96*, 2–13.

https://doi.org/10.1016/j.trac.2017.06.004

Valdés, A., Simó, C., Ibáñez, C., & García-Cañas, V. (2013). Foodomics strategies for the analysis of transgenic foods. *TrAC - Trends in Analytical Chemistry*, *52*, 2–15. https://doi.org/10.1016/j.trac.2013.05.023

Yamada, R., Okada, D., Wang, J., Basak, T., & Koyama, S. (2021). Interpretation of omics data analyses. *Journal of Human Genetics*, *66*(1), 93–102. https://doi.org/10.1038/s10038-020-0763-5

Chapter 2: Basics of Nuclear Magnetic Resonance

2.1. Introduction

Nuclear Magnetic Resonance in the condensed phase was discovered in 1946 independently by two groups of scientists, Bloch, Hansen and Packard at the University of Stanford (California, USA) (Bloch, F, Hanse W.W, 1946), and Purcell, Torrey and Pound at the University of Cambridge (Massachussets, USA) (Purcell et al., 1946).

Right from the beginning, NMR has been approached from two distinct perspectives. Bloch and coworkers envisioned NMR in classical terms, considering the orientation of microscopic magnetic moments with respect to an external magnetic field, whereas Purcell and coworkers pictured NMR in terms of quantum transitions.

The first conception affords one a rather simple and efficient way to describe the NMR phenomenon, providing insight regarding fundamental issues such as magnetization precession and nuclear relaxation. However, the classical description becomes rapidly limited and the second approach, the so-called spectroscopic description, relying mainly on quantum mechanics, becomes indispensable as soon as a

deeper understanding of the interactions that rule nuclear spins is sought. Both the researchers were awarded with the Nobel Prize in physics for their work in 1952.

In the NMR history, another protagonist was Richard Ernst. His work have transformed the NMR in a basic and indispensable tool in chemistry and also have extended its usefulness to other scientific fields, including physics, biology and medicine. The major contribution of Ernst to the field of NMR spectroscopy were: the creation of the Fourier transformation applied to the received signal, improving the NMR sensibility and allowing to study more types of nuclei and small amounts of material, and the development of 2D experiments, that were the bases of the application of the NMR to determine the 3D structure of organic and inorganic compounds and large complex molecules such as proteins; to study the interaction between biologic molecules and metal ions, water molecules, drug molecules, and other substances; to identify chemical species; and to study the rates of chemical reactions.

However, regarding the Purcell and Bloch theory for the description of the NMR experiment, in this chapter will be reported an indicative description of classical NMR theory. Anyway, in the spectroscopic description, NMR phenomenon is explained in terms of quantum mechanical frameworks such as the theory of stationary perturbations.

2.2. Classical description of Nuclear Magnetic Resonance

This section describes the theoretical bases of NMR focusing on the so-called classical approach due to Bloch. The notion of magnetic moment is explained, and the NMR phenomenon is described.

2.2.1. Nuclear magnetic moment

The NMR phenomenon is related to the existence of nuclear paramagnetism caused by the orientation of the individual nuclear magnetic moments $\vec{\mu}$ in the presence of an external static magnetic field $\vec{B}_0$. The magnetic moment of a nucleus $\vec{\mu}$ is proportional to the nuclear spin angular momentum $\vec{I}$ according to the following equation:

$$\vec{\mu} = \gamma \hbar \vec{I} \qquad (1)$$

where γ is the gyromagnetic ratio of the nucleus and $\hbar$ is Planck's constant divided by 2π.

In contrast with the electron, whose spin number *I* always equals ½, the nuclear spin number *I* of a nucleus ${}^{A}_{Z}X$ depends on the mass number *A* and the atomic number *Z*:

- If A is odd, then I is an half integer (^{1}H, ^{13}C, ^{27}Al, ^{23}Na);
- If A is even and Z is odd, then I is an integer (^{14}N, ^{2}H);
- If both A and Z are even, then I is zero and the nucleus is not active in NMR (^{12}C, ^{16}O).

The application of an external magnetic field B_0, that is supposed to be oriented along the z axis only, leads to a motion of precession of all nuclear magnetic moments around the z axis at the Larmor frequency given by

$$\omega_0 = \gamma B_0 \,(\text{rad s}^{-1}) \quad \text{or} \quad \upsilon_0 = \frac{\gamma B_0}{2\pi} \,(\text{Hz}) \qquad (2)$$

It is noteworthy to explain the real representation of the precession in a number of particles in a magnetic field. Proton nuclei (like whatever particles with spin) have spin polarization

axes (namely the vector that represent the direction of the spin angular momentum of a particle) point in all possible directions (Figure 2. 1).

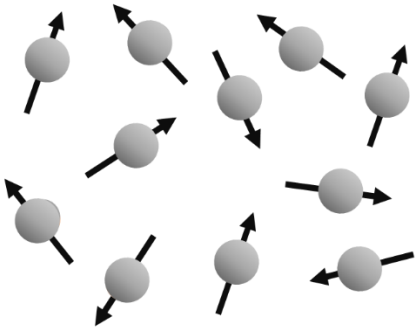


Figure 2. 1. Randomly directed spin polarizations.

Regarding the magnetic moment, if the particle is in a magnetic field, it moves on a cone, keeping a constant angle between the spin magnetic moment and the field (precession). The spin polarization axis goes around and around on the same precession cone, always keeping the same angle between the spin axis and the field, and the angle of the cone depends only on the initial spin polarization (Levitt, 2008). Hence, if the spin is initially polarized exactly along or against the field, then it

simply stays there, corresponding to precession on a cone of zero angle. If the spin is initially polarized exactly perpendicular to the field, then the spin polarization moves on a flat disk. For the majority of spins, the angle is intermediate between these extremes (Figure 2. 2)

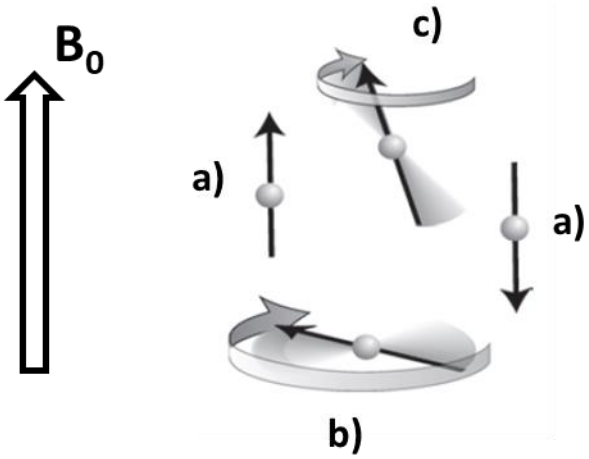


Figure 2. 2. The angle of the precession cone depends on the initial direction of the spin: a) spin polarized with the same direction of the magnetic field; b) spin polarized perpendicular to the magnetic field; c) spin polarized with a certain angle respect to the magnetic field (adapted from: (Levitt, 2008)*)*

In the classical description of NMR, the motion of precession does not affect the isotropic distribution of nuclear magnetic moments, and hence there is no net resulting magnetization. In

contrast, the interaction of the nuclear magnetic moments with their environment (such as the thermal vibrations of the lattice) leads at equilibrium characterized by an anisotropic distribution according to Boltzmann's law and hence gives a net longitudinal magnetization M_z (Figure 2. 3).

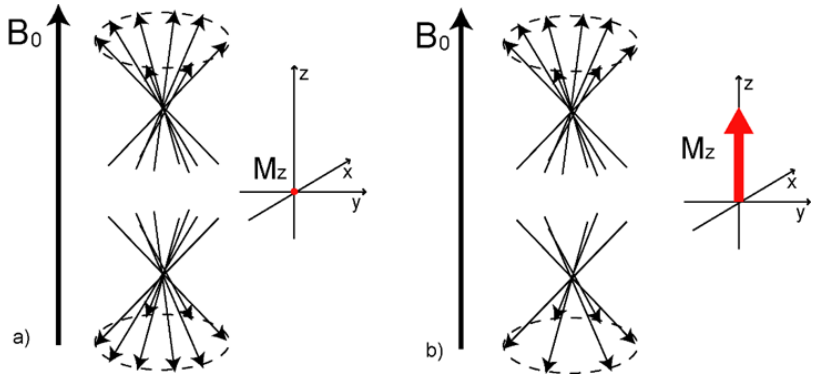


Figure 2. 3. (a) Isotropic distribution of nuclear magnetic moments with no net resulting macroscopic magnetization; (b) Anisotropic distribution of nuclear magnetic moments with resulting net macroscopic magnetization, Mz, aligned the direction of the static magnetic field, $\vec{B}_0$

Also in this case, it is noteworthy to stress the fact that it is often stated that spin 1/2 particles in a magnetic field may only be polarized either "up" or "down", while, like showed before to explain the precession, the reality is that at a microscopic level all the possible spin orientations exist. However, in the

magnetic field, the net distribution of spin orientations, with magnetic moments along the field slightly, became more probable than orientations with magnetic moments opposed to the field. So we can imagine to make a sum of the magnetic moment projection on the z axis of each spin obtaining the resulting net macroscopic magnetization aligned at the direction of the magnetic field (Figure 2. 4).

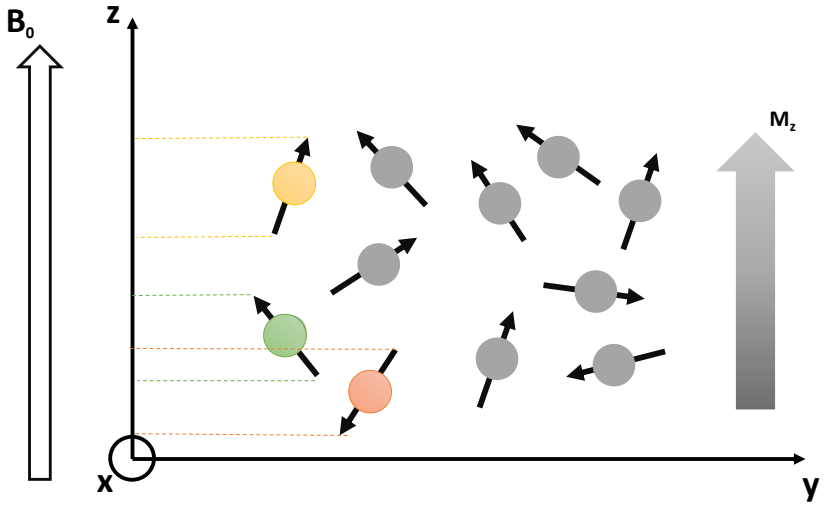


Figure 2. 4. Simplified representation of the single spin contribution, at a microscopic level, at the net macroscopic magnetization M_z: from the nuclear magnetic moments of each spin, making a projection on the z axis. The figure greatly exaggerates the anisotropy, for the sake of clarity.

Now it is possible to explain how the net longitudinal magnetization M_z come from the anisotropy of the polarization distribution at thermal equilibrium due to the fluctuating molecular fields. In fact at any given moment in the microscopic point of view, each spin precess about a field that is the sum of the external field, which is static, and a very small microscopic field, which varies in time, and which may have any possible direction in space. These second fields are small, come from the fact that each molecule contains many magnetic particles (electrons and nuclei) which are source of magnetic fields, and they fluctuate rapidly because of the thermal motion of the environment. The total magnetic field seen by each spin, therefore, has a slightly fluctuating magnitude, and also a slightly fluctuating direction. Hence, at any given time, the local magnetic field experienced by any one nuclear spin is slightly different, both in magnitude and direction, to that of its neighbors. In practice, the small fluctuating fields from the thermal environment cause a gradual breakdown of the constant-angle "cone precession" of the nuclear spins: for each

spin, the angle between the spin magnetic moment and the external field varies slightly. It is this tiny fluctuations that in the long term allow the isotropy of the nuclear spin polarization to be broken (creating an anisotropy) and, hence, a macroscopic nuclear magnetic moment to develop. This is the microscopic mechanism of nuclear paramagnetism (Levitt, 2008).

The longitudinal magnetization appears progressively (Figure 2. 5) with time according to the following law:

$$M_Z = M_0\left(1 - e^{\frac{-t}{T_1}}\right) \qquad (3)$$

where T_1 denotes the spin-lattice relaxation time or the longitudinal relaxation time.

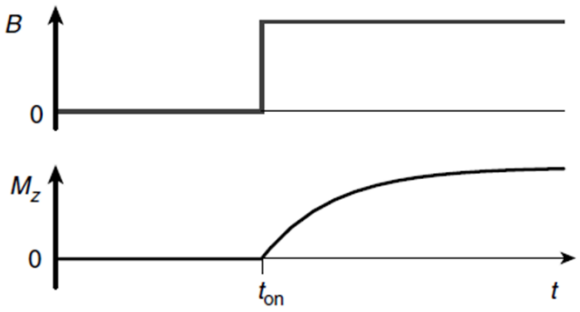


Figure 2. 5. The macroscopic nuclear magnetization is initially zero and gradually grow after the magnetic field is turned on, with an exponential curve.

Equation 3 implies that

$$\frac{\partial M_Z}{\partial t} = -\frac{M_Z - M_0}{T_1} \tag{4}$$

with M_0 the longitudinal magnetization at equilibrium at the temperature T given by Langevin's law

$$M_0 = N_0 \frac{\gamma^2 \hbar^2 B_0}{kT} \frac{I(I+1)}{3} = \chi_0 B_0 \tag{5}$$

where N_0 is the number of magnetic moments per unit volume, and $\chi_0 = \frac{M_0}{B_0}$ is the static magnetic susceptibility. At room temperature, population difference for the two orientations of the nuclear magnetic moments is very weak (e.g., it is of the order of 1 in 105 for ^{1}H spin in a magnetic field of 11.7 T) (Kalbitzer, 1997).

2.2.2. Nuclear Magnetic Resonance phenomenon

The Nuclear Magnetic Resonance phenomenon occurs by adding to the main static magnetic field $\vec{B}_0$, a secondary magnetic field $\vec{B}_1$, orthogonal to $\vec{B}_0$ and with $\left\|\vec{B}_1\right\| << \left\|\vec{B}_0\right\|$,

which oscillates at the nuclear Larmor frequency. This second radio frequency field flips down the longitudinal magnetization to the *xy* plane, and hence generates a transverse magnetization M_{xy}. Then, the radiofrequency field is switched off and the magnetization progressively returns to its initial equilibrium position according to relaxation processes. The motion of precession of the magnetization while it returns to equilibrium induces a voltage in a coil placed perpendicularly to the main static field (Figure 2. 6).

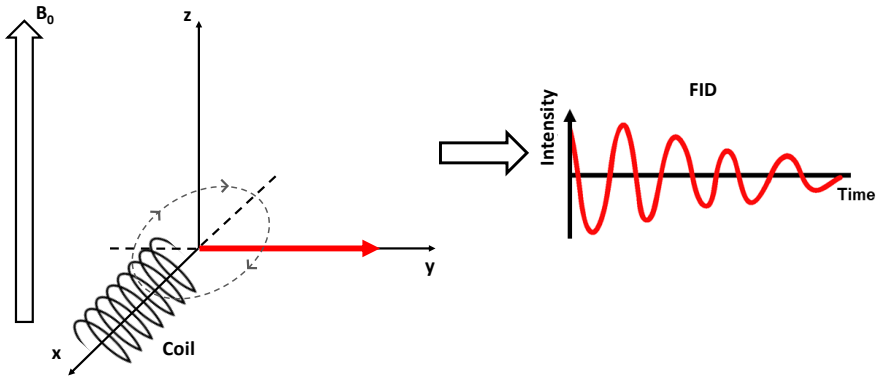


Figure 2. 6. Precession motion of the magnetization on the xy plane which induces in a coil, positioned perpendicular to B_0, an oscillating electric current which constitutes the NMR signal (FID).

This voltage constitutes the NMR signal and is called a Free Induction decay (FID): free of the influence of the radio frequency field, induced in the coil, and decaying back to equilibrium.

Many relaxation mechanisms dictate the evolution of the transverse magnetization. To describe this evolution, a transverse relaxation time T_2 must be introduced. Transverse relaxation does not necessarily involve energy exchange but increases the entropy of the nuclear spin system. T_2 is defined by

$$\frac{\partial M_X}{\partial t} = -\frac{M_X}{T_2} \quad \text{and} \quad \frac{\partial M_Y}{\partial t} = -\frac{M_Y}{T_2} \tag{6}$$

The system of nuclear magnetic moments can be associated with a macroscopic or bulk magnetization vector $\vec{M}$. In turn, the bulk magnetization vector $\vec{M}$ is related to a bulk angular momentum $\vec{J}$ through the nuclear gyromagnetic ratio γ according to

$$\vec{M} = \gamma \cdot \vec{J} \tag{7}$$

Under certain conditions, the macroscopic behavior of the system of magnetic moments can be described by the laws of classical mechanics. The fundamental equation of motion is

$$\frac{\partial \vec{J}}{\partial t} = \vec{T} \tag{8}$$

Where $\vec{T}$ is a torque. In the presence of a magnetic field $\vec{B}$, the torque exerted on the system of magnetic moments is given by

$$\vec{T} = \vec{M} \wedge \vec{B} \tag{9}$$

Thus, by combining eq (7), (8), and (9), we obtain

$$\frac{\partial \vec{M}}{\partial t} = \gamma \cdot \vec{M} \wedge \vec{B} \tag{10}$$

In the NMR experiment, as described before for the net magnetization moment development, the total magnetic field $\vec{B}$ is composed of two distinct components: an intense, static magnetic field oriented along the *z* axis, $\vec{B}_0$, and a weaker, oscillating field, $\vec{B}_1$.

Formally, the oscillating field $\vec{B}_1$ is linearly polarized along an axis that belongs to the *xy* plane. In this chapter, it is assumed

to be the x axis without loss of generality (Kalbitzer, 1997). As described elsewhere (S.L.S., 1988), a linearly polarized magnetic field of amplitude $2B_1$ is equivalent to two counters rotating magnetic fields of amplitude $2B_1$ rotating along the *z* axis. To 1st order, only one of these two counters rotating components can affect the bulk magnetization vector, and hence the other component will not be further considered here. In other words, the linearly polarized magnetic field $\vec{B}_1$ can be pictured as a magnetic field that rotates along the *z* axis with a frequency w, an amplitude B_1 and an initial phase *f*. By definition, *f* is the angle formed between the *x* axis and the polarization axis of the $\vec{B}_1$ field, that, in this case, implies that *f* is zero.

In these conditions, if $\gamma > 0$, the total effective field acting on the bulk magnetization $\vec{M}$ is given in the laboratory frame $(\vec{e}_x, \vec{e}_y, \vec{e}_z)$ by

$$(B_1 \cos \omega \cdot t)\vec{e}_x + (-B_1 \sin \omega \cdot t)\vec{e}_y + B_0 \vec{e}_z \qquad (11)$$

Thus, in the laboratory frame, the Bloch equations are given by

$$M'_X = \gamma \cdot \left[M_Y B_0 + M_Z B_1 \sin(\omega t) \right] - \frac{M_X}{T_2}$$

$$M'_Y = \gamma \cdot \left[-M_X B_0 + M_Z B_1 \cos(\omega t) \right] - \frac{M_Y}{T_2} \qquad (12)$$

$$M'_Z = \gamma \cdot \left[-M_Y B_1 \cos(\omega t) - M_X B_1 \sin(\omega t) \right] - \frac{M_Z - M_0}{T_1}$$

Additional simplification can be achieved by describing the NMR phenomenon in the so-called rotating frame, i.e. in an orthonormal frame that rotates along the *z* axis at the frequency of the radiofrequency field $\vec{B}_1$. In this case, if the frequency of the radiofrequency field is supposed to be equal the Larmor frequency of the nucleus (on-resonance case), both $\vec{M}$ and $\vec{B}_1$ appear fixed in the rotating frame. In other words, their time dependence has been mathematically, and artificially, removed.

At this moment of the NMR experiment, in the modern pulsed NMR spectrometer, an intense radiofrequency field $\vec{B}_1$ is applied for a very short period of time, typically a few μs.

Because the relaxation times T_1 and T_2 are much larger that the pulse duration t (note that, rigorously, T_1 and T_2 are not mere times but time constants), relaxation processes can be safely neglected during the pulse. Therefore, in the rotating frame, the effect of a radiofrequency pulse of duration t and phase x (i.e. applied along the *x* axis) can be pictured as the rotation of the bulk magnetization vector $\vec{M}$ around the *x* axis through an angle θ of $\gamma B_1 t$ (Figure 2. 7).

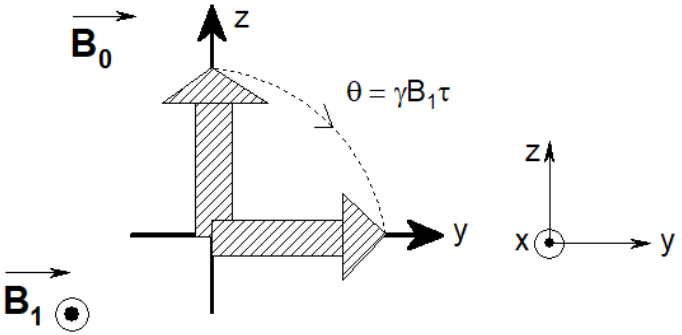


Figure 2. 7. Schematic representation of the effect on the longitudinal magnetization vector $\vec{M}$ (represented by the large dashed arrow) of a radiofrequency pulse of duration t applied with a x phase: $\vec{M}$ is rotated along the x axis of an angle θ that depends on the radiofrequency pulse amplitude B_1 and duration t. Here γ is supposed to be positive.

2.3. CW-NMR and FT-NMR

The original NMR experiment, the so called Continuous Wave NMR (CW-NMR) by Bloch, Purcell, and their respective colleagues, provided the sequentially measurement of each part of the spectrum.

To explain this original experiment and the modern pulsed experiment, called Fourier transform NMR (FT-NMR), it is possible to consider an NMR spectrum of a sample analogous to the frequency response of an amplifier, with the difference that in NMR we are dealing with the nuclei responding to radio frequencies in the MHz range.

If we want to find the frequency response of a high fidelity amplifier (an electronic device that can increase the power of a signal: is a two-port electronic circuit that uses electric power to increase the amplitude of a signal applied to its input terminals, producing a proportionally greater amplitude signal at its output.), i.e., what notes (frequencies) it amplifies and by how much, one way of doing this is to feed in a pure tone of constant volume (amplitude) and measure the output volume as the tone is changed. In that way, we might

learn that the amplifier does not pass very low tones (say, below 100 Hz or cycles per second) nor very high tones (say, above 20 kHz) but it passes everything else in between with quite constant amplification (gain). The plot of the response vs. frequency is called a spectrum and is entirely analogous to the NMR spectrum. This is a good method for accomplishing our goal and we would be perfectly happy with it as long as we did not have to measure the frequency response of a large number of amplifiers. If we were the impatient sort, however, we could think of several faster methods. One would be to get several tone generators (frequency sources) which put out different tones and use them with tuned detectors which can separately but simultaneously detect those tones. You could perform the required measurement all at once but it is simply not practical to assemble the required number of separate tone generators and detectors if any kind of frequency resolution were required. This example, with its impracticality, contains the seed for the best solution to the problem. We somehow want to put all the frequencies into the amplifier at once and detect all the frequencies which come out. The solution is the use of a short

square pulse. In fact a short pulse contains a continuous distribution of frequencies. Thus, for such a pulse, the amplifier sees many frequencies coming into it and will amplify them according to its characteristics. For example, if the amplifier does not respond to the high frequencies needed to shape the sharp corners , the corners will be rounded off in the pulse coming out of the amplifier. If some method were available to decompose the output pulse into its frequency components so they can be plotted out as a spectrum and this is compared with the spectrum of the input pulse, we will have accomplished our goal. The Fourier transform performs the desired decomposition.

To recapitulate, the frequency response of the amplifier can be obtained by measuring the gain at each frequency, how it happen in a CW experiment, or alternatively by measuring the response of the output of the amplifier to a rectangular input pulse, how it happen in a pulsed experiment, and a subsequent Fourier transform (clearly, there are other pulse shapes which contain many different frequency components, too, but the square pulse is easy to form and its frequency distribution is

well known). Hence, in a pulsed experiment, all the spectral information desired is already contained in the transient response to a pulse and the Fourier transform merely allows us to decompose the signal into its spectral components. The inefficient solution in the above example corresponds to a CW-NMR experiment, where each part of the spectrum is measured sequentially, whereas the final solution corresponds to FT-NMR.

Another way to figure out the CW and FT NMR experiments, is well described in (Fukushima & Roeder, 1981):"Consider an analogy: Suppose there were a series of bells, each with a different pitch or frequency, and suppose that one were asked to characterize the loudness and frequency of each of these bells. One might ring each bell and plot the amplitude against the frequency. For N bells this would require performing N different experiments. This would be comparable to the CW experiment in which each of the contributions for the magnetization at different frequency is sampled, one by one. On the other hand, all the bells can be struck simultaneously and the resulting ringing, which is a complex interferogram, can be

digitized and Fourier transformed to yield the spectrum of all the bells. It is clear that this experiment is far more efficient than the first" (Fukushima & Roeder, 1981).

However, when we speak about the FT-NMR, we refer to the pulsed NMR and the "Fourier transform" is not the reason since we are not taking the data at one frequency at a time, but the efficiency of this method is due to the multiplexing effect (is a way of sending multiple signals in the form of a single and from a source to a destination. Thein in the destination, a process called demultiplexing, recovers the separate signals and outputs them to individual lines), applied to high resolution NMR for the first time by Ernst and Anderson in 1966 (Ernst & Anderson, 1966). While, the Fourier transform is just the process that enables us to transform information in the time domain into equivalent information in the frequency domain (and vice versa) (Fukushima & Roeder, 1981).

One of the advantages of the pulsed method with respect to the continuous wave method, relies on the possibility to repeat each measurement in a faster way (typically every second). It then becomes possible to coherently add the results

of n measurements, hereby increasing the signal-to-noise ratio by a factor of $\sqrt{n}$. This come from the fact that the accumulation of the non-random signal is clearly proportional to the number of experiments. On the other hand, the noise accumulates at a rate proportional to the square root of the number of experiments. Therefore, S/N increases with the number of experiments n as $n/\sqrt{n} = \sqrt{n}$. Moreover, since the number of experiments n is proportional to the time t required to take data, S/N increases at $\sqrt{t}$. This means that the duration of the experiment must be quadrupled in order to double the S/N so that long time signal averaging becomes futile after a certain point (Ernst, R. R., Bodenhausen, G., Wokaun, A., & Redfield, 1989; Fukushima & Roeder, 1981).

The first pulse experiments followed shortly thereafter and Hahn published his famous spin echo paper in 1950 (Hahn, 1950). However, this first spin echo experiment by Hahn, with double $\pi/2$ pulses, is relatively weak and difficult to use. The "modern" type of spin echo, induced by a π pulse, was developed by Carr and Purcell (Carr & Purcell, 1954).

This sequence now is a component of a very large number of more complex experiments. In brief in the sequence we have a π pulse (indicated by an open rectangle as opposed to the closed one for a $\pi/2$ pulse) is in the center of a delay of duration 2τ, thus separating the sequence into two equal periods, τ. The signal is acquired after the second delay τ (Figure 2. 8a) (Jacobsen, 2007).

What happen at the magnetization vector in the spin echo experiment is described in the vector diagram in Figure 2. 8b. During the first delay τ the vector precesses from -*y* towards the *x* axis. The angle through which the vector rotates is simply (Ωt). The effect of the π pulse is to move the vector to a mirror image position, with the mirror in question being in the xz plane. So, the vector is now at an angle (Ωt) to the *y* axis rather than being at (Ωt) to the -y axis. During the second delay τ the vector continues to evolve; during this time it will rotate through a further angle of (Ωt) and therefore at the end of the second delay the vector will be aligned along the *y* axis. A few moments thought will reveal that as the angle through which the vector rotates during the first τ delay must be equal to that

through which it rotates during the second τ delay; the vector will therefore always end up along the *y* axis regardless of the offset, Ω). The π pulse is called a *refocusing pulse* because of the property that the evolution due to the offset during the first delay τ is refocused during the second delay.

This experiment resolve the problem of the different spin isochromats in the sample. Spin isochromat is a small segment of the sample that experience an homogeneous applied magnetic field, that contribute to the net magnetic moment. Hence, each spin isochromat precess with the same Larmor frequency ("isochromat" since spin with the same frequency means same colour). With only a $\pi/2$ pulse, rather than a spin echo, the different spin isochromats of a sample bring to a dephasing in the xy plane.

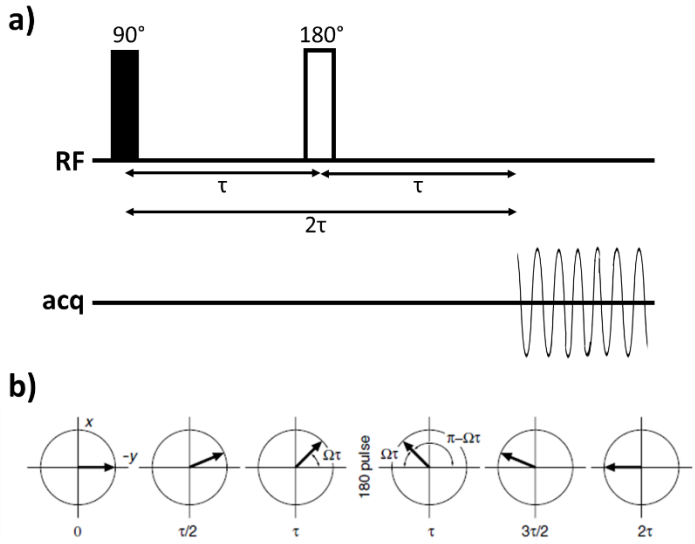


Figure 2. 8. a) Pulse sequence for the spin echo experiment; b) Vector diagrams showing how a spin echo refocuses the evolution of the offset (adapted from: (Jacobsen, 2007)*).*

2.4. The NMR spectrometer

After the general description of the theoretical principles on which NMR spectroscopy is based, in this section a brief explanation of the hardware and software that constitute the NMR spectrometer is provided, in order to have a more practical idea of all the steps that occur during an NMR experiment.

In Figure 2. 9 a schematic representation of a single-channel NMR spectrometer (Levitt, 2008), including a one pulsed field gradient channel, is presented:

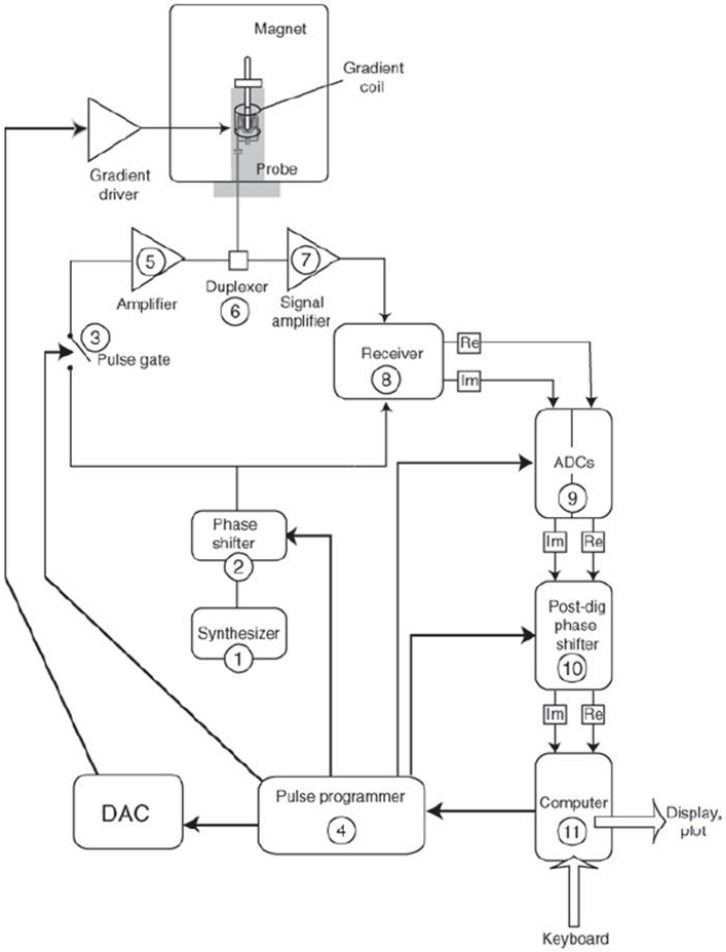


Figure 2. 9. Schematic overview of a single-channel spectrometer, incorporating one pulsed field gradient channel.

- The magnet: NMR experiments require a homogeneous magnetic field that must be maintained over the entire volume of the sample, and also be extremely stable with respect to time. A perfectly uniform magnetic field avoids inhomogeneous broadening of the NMR signal and allows the resolution of small differences in the nuclear Larmor frequency, due to chemical shifts, spin–spin couplings, or other molecular interactions. All NMR spectrometers employ superconducting magnets, capable of supporting large electric currents without any external source of power. Once charged with current, a superconducting magnet runs almost indefinitely, providing an extremely stable magnetic field with no outside interference. Superconducting materials (Nb-Sn) must be cooled at the boiling point of liquid He (4.18 K) to support large magnetic fields without electrical resistance. The liquid He bath is itself insulated by a large reservoir of liquid N_2 (77 K). In the center of the cylindrical can, and through the center of the superconducting coil, there is a large hole called the

bore. The sample is mounted in a cylindrical device called a probe, that is inserted into the bore to position the sample at the point of maximum field. Based on the magnetific field power we can have the wide-line or the high resolution NMR. The advantage of recording NMR spectra at high fields was soon recognized, in order to simplify the spectral analysis and increase the sensitivity (Freeman & Robert, 1990).

- The radio frequency (r.f.) synthesizer (1): this component of the spectrometer produces an oscillating electrical signal with a well-defined frequency. This electronic signal is usually subjected to several frequency conversion and electronic filtering steps. The result is a r.f. wave that oscillates at the spectrometer reference frequency ωref. The phase of an oscillating wave indicates the position (0, $\pi/2$, π, $3\pi/2$) of the oscillation at the time origin. In many NMR experiments, the r.f. phase is rapidly jumped between different values. In the NMR spectrometer, these phase

jump events (2) are controlled by a timing device called pulse programmer (4).

- The pulse gate (3): this is a fast switch that is opened at defined moments to allow the r.f. reference wave to pass through. The effect is to chop a 'time-slice' out of the r.f. waveform. The duration of an r.f. pulse is sometimes referred to as the pulse width. These events are controlled by the pulse programmer.
- The amplifier (5): the function of the r.f. amplifier is to scale up the gated waveform so as to produce a large-amplitude r.f. pulse for transmission to the probe. Typical r.f. amplifiers for NMR applications have ratings between several watts and about 1 kW of peak output power.
- The duplexer (6): the amplified r.f. pulse travels down a cable into the duplexer. From the duplexer, two more cables emerge. One cable leads to the probe, which is mounted inside the magnet, and which contains the sample. The second cable leads to the receiver section, which is used to detect the weak r.f. signals generated

by the nuclear spins. When a strong r.f. pulse arrives from the amplifier, the duplexer diverts it down the cable leading to the probe, not into the sensitive signal detection circuitry. On the other hand, the tiny NMR signal travels down the same cable from the probe to the duplexer and it is diverted into the signal detection path.

- The probe: The probe is the most specialized part of the NMR spectrometer and is often the only part that needs to be exchanged when switching between different NMR experiments. This piece of the apparatus has several functions such as locating the sample in the region of homogeneous magnetic field, includes r.f. electronic circuits for irradiating the sample with r.f. waves, rotating the sample. The probe electronic is formed by a r.f. circuit consisting of a coil and two capacitors. The function of the coil is twofold. First, during the r.f. pulse, electrical currents in the coil generate an oscillating magnetic field at the sample; second, when the r.f. pulse has terminated, the

precessing nuclear magnetization generates electrical currents in the coil that give rise to a detectable signal travelling back down the cable again towards the duplexer. In a very general way, the two capacitors have the function of making stable the incoming and the outcoming electronic signals.

- Signal preamplifier (7): The NMR signal first arrives at the duplexer, that diverts it down the cable towards the signal preamplifier. This is a low-noise r.f. amplifier that scales up the tiny signal to a more convenient voltage level.
- The quadrature receiver (8): The NMR signal must be fed into the computer for interpretation and presentation. Therefore, it is necessary to convert the NMR signal (an oscillating electrical current) into digital form (a sequence of 'ones' and 'zeros'). The process of converting a continuous current or voltage into digital form is called analogue-to-digital conversion. This task is accomplished by specialized electronic circuits called analogue-to-digital converters (ADCs). Anyway, the

'raw' NMR signal oscillates at many hundreds of megahertz, that is too fast for current ADCs. Therefore, it is necessary to 'down-convert' the frequency of the NMR signals, so that they may be handled by the digital electronics at the next stage. The quadrature receiver accomplishes the signal frequency conversion by comparing it with a reference wave of frequency, as supplied by the r.f. synthesizer. The quadrature receiver combines the NMR signal, that oscillates at the Larmor frequency, with the reference signal, to generate a new signal that oscillates at the relative Larmor frequency, usually of the order of 1MHz or less. In order to distinguish between spins that rotate faster or slower respect to the Larmor frequency, the receiver supplies two output signals that are interpreted as the real and imaginary components of a single complex signal.

- Analogue–digital converter (9): Each of the two outputs of the quadrature receiver are connected to their own ADC. This is an electronic circuit that rapidly measures the voltage level of an input signal and presents the

information as a digital signal, by repeating the measurement at a set of consecutive time points and storing the information in the computer as an ordered set of values. This is called digitization.

- Post-digitization phase shifter (10): this device which multiplies the signal by a complex phase factor before it is passed to the computer. This operation corrects the NMR signal phase variations that can occur during the experiment phases.
- Digital-to-analogue converter (DAC) and gradient driver: many NMR experiments require the application of pulsed static magnetic fields, as well as r.f. fields. In most spectrometers, each magnetic field gradient is controlled by a separate channel, that resembles the one used in the r.f. section. Each gradient channel consists of a digital-to-analogue converter (DAC) and a gradient driver. The DAC converts timed digital instructions from the pulse programmer into an analogue voltage level. It therefore performs the inverse function of the ADCs used in the receiver circuit. The gradient driver is

a powerful amplifier that converts the analogue input voltage into a strong, well-controlled current. This electric current is driven through the gradient coils, generating the desired magnetic field gradient pulse. These circuits allow each gradient pulse to be shaped accurately as a function of time.

2.5. NMR experiments

All the operations described in the previous paragraph are exploited to create different NMR pulse sequences, on the basis of which it is possible to generate different types of experiments and thus obtain different types of information about the analyzed sample (Jacobsen, 2007). In this section, a brief description of the main NMR mono (1D) and two-dimensional (2D) experiments that can be very useful for metabolomics studies is proposed:

- ^{1}D ^{1}H: the principle of all mono-dimensional experiments is based on the theory and the practical description previously described. Basing on the selected nucleus, the proper r.f. pulse and field adjustments are

carried out. ^{1}H NMR experiments are of sure the most used and the most indicative, since basing on the chemical shifts, signal shape, and J-coupling constants it is possible to obtain much information on the sample chemical features.

- ^{1}D ^{13}C: together with ^{1}H, ^{13}C nucleus is very informative for structural determination. Anyway, since the isotopic abundance of this nucleus is very low and the coupling interactions with ^{1}H generate high-lined multiplets in the spectra, the NMR experiments for this nucleus are slightly sensitive and the signal to noise ratio is very low. For these reasons, ^{13}C experiments are carried out by applying particular pulses that enhance the signal intensity namely decoupling and NOE (Nuclear Overhauser Effect).
- 2D CORRELATION SPECTROSCOPY (COSY): this is the first and the simplest 2D experiment. It correlates one proton to another via a single J coupling that may be 2-bond (geminal), 3-bond (vicinal) or in rare cases 4-bond or 5-bond (long range).

- 2D TOTAL CORRELATION SPECTROSCOPY (TOCSY): Provides $^{1}H–^{1}H$ spin–spin coupling connectivity for all hydrogen atoms within a spin system that forms an unbroken chain of couplings, and not just to the protons connected by a single J coupling, thereby unravelling the number and nature of the molecular fragments.
- 2D HETERONUCLEAR SINGLE QUANTUM COHERENCE (HSQC): this experiment shows correlations between hydrogen atoms and the carbon atom to which they are attached.
- 2D HETERONUCLEAR MULTIPLE BOND CORRELATION (HMBC): provides correlations between hydrogen and a carbon generally two or three bonds away.

2.6. NMR data processing

After finishing acquiring the NMR data, it is necessary to process the data into a spectrum and plot that spectrum on paper with a ppm axis, and possibly with integrals, peak lists,

and other features. Each NMR instrument has its own software for data processing, and it can be daunting to try to learn all of the different commands and operations. The actual data processing task, however, is the same in all cases. Starting with a FID (raw time-domain data), the following operations are generally applied:

- With zero filling the size of the data set can be artificially increased by adding zeroes to the end of the list of FID data. This process of zero filling has no effect on the peak positions, intensities, or linewidths of the spectrum, but it does increase the digital resolution (fewer hertz per data point) in the spectrum.
- Multiply the FID by a multiplier (line-broadening parameter) or window function. This operation allows to increase the signal to noise ratio but on the other hand, broader signals are obtained. So, this operation has to be regulated basing on the quality of the obtained spectrum.
- Fourier transform converts the time domain data to a frequency domain spectrum. In fact, the raw NMR data

obtained after an experiment is in the form of a series of intensity values collected as a function of time that die out gradually as the nucleus recover from the pulse and relax. In this form, the FID can not be interpretated because of the complexity of the FID. Fourier transform is a mathematical function that converts the time-domain data into a frequency-domain data, the NMR spectrum. The obtained spectrum allows to observe each type of detected frequency as a single signal well distinguished from the others thanks to the chemical shift phenomenon. Considering a mono-dimensional experiment, these signals.

- Phase adjusting of certain unavoidable instrumental errors involved in acquiring the FID.
- Find a reference standard peak and set its chemical shift to the reference value in parts per million. Generally, this operation is carried out by referring to the internal standard or residual solvent peak.
- Baseline adjustment. The "baseline" is the average of the noise part of your spectrum. Ideally, this would be a

straight, horizontal line representing zero intensity. In the practice, this line not always reflect these characteristics so, basing on the used software, several correction operations can be applied to adjust this line.

- Integration of peaks area for quantitative measurements.

For further information about the theorical and practical aspects of NMR, several texts have been realized during the time (Abragam, 1961; Callaghan, 1991; Canet, D., Boubel, J.C., Canet Soulas, 2002; Cavanagh et al., 2007; Ernst et al., 1987; Fukushima & Roeder, 1981; Keeler, 2010; Levitt, 2008). Reports about the history of NMR development and applications have been also created (Becker, 1993; Freeman & Robert, 1990).

2.7. References

Abragam, A. (1961). *The principles of nuclear magnetism*. Oxford University Press.

Becker, E. D. (1993). A Brief History of Nuclear Magnetic Resonance. *Analytical Chemistry*, *65*(6), 295A-302A. https://doi.org/10.1021/ac00054a716

Bloch, F, Hanse W.W, P. M. (1946). The Nuclear Experiment. *Physical Review*, *70*(5), 474–485.

Callaghan, P. T. (1991). *rinciples of Nuclear Magnetic Resonance Microscopy*. Oxford University Press.

Canet, D., Boubel, J.C., Canet Soulas, E. (2002). *La RMN : Concepts, méthodes et applications* (2nd ed.). Dunod.

Carr, H. Y., & Purcell, E. M. (1954). Effects of diffusion on free precession in nuclear magnetic resonance experiments. *Physical Review*, *94*(3), 630–638. https://doi.org/10.1103/PhysRev.94.630

Cavanagh, J., Wayne, J. F., Palmer, A. G., Rance, M., & Nicholas, J. S. (2007). *Protein NMR Spectroscopy* (2nd ed.). Academic Press. https://doi.org/https://doi.org/10.1016/B978-0-12-164491-8.50018-X

Ernst, R. R., Bodenhausen, G., Wokaun, A., & Redfield, A. G. (1989). Principles of Nuclear Magnetic Resonance in One and Two Dimensions. *Physics Today*, *42*(7), 75–76. https://doi.org/https://doi.org/10.1063/1.2811094

Ernst, R. R., & Anderson, W. A. (1966). Application of fourier transform spectroscopy to magnetic resonance. *Review of Scientific Instruments*, *37*(1), 93–102. https://doi.org/10.1063/1.1719961

Ernst, R. R., Bodenhausen, U., & Wokaun, A. (1987). *Principles of Nuclear Magnetic Resonance in One and Two Dimensions*. Clarendon Press. https://doi.org/https://doi.org/10.1002/bbpc.198800370

Freeman, R., & Robert, J. B. (1990). A Brief History of High Resolution NMR. In *NMR Basic Principles and Progress* (Vol. 25, pp. 1–16). Sp. https://doi.org/10.1007/978-3-642-48814-6_1

Fukushima, E., & Roeder, S. B. W. (1981). *Experimental pulse NMR: A Nuts and Bolts Approach*. Westview Press.

Hahn, E. L. (1950). Spin echoes. *Physical Review*, *80*(4), 580–594. https://doi.org/10.1103/PhysRev.80.580

Jacobsen, N. E. (2007). *NMR Spectroscopy Explained: Simplified Theory, Applications and Examples for Organic Chemistry and Structural Biology*. John Wiley & Sons, Inc. https://doi.org/https://doi.org/10.1002/9780470173350

Kalbitzer, H. R. (1997). Protein NMR Spectroscopy. Principles and Practice. *Zeitschrift Für Physikalische Chemie*, *176*(11), 30–32.

Keeler, J. (2010). *Understanding NMR Spectroscopy* (2nd ed.). Wiley.

Levitt, M. H. (2008). *Spin Dynamics: Basics of Nuclear Magnetic Resonance* (2nd Ed. (Ed.)). John Wiley & Sons, Ltd.

Purcell, E. M., Pound, R. V., & Bloembergen, N. (1946). Nuclear magnetic resonance absorption in hydrogen gas [17]. *Physical Review*, *70*(11–12), 986–987. https://doi.org/10.1103/PhysRev.70.986

S.L.S. (1988). Modern NMR Spectroscopy: A guide for Chemists. *Journal of Molecular Structure*, *189*(3–4), 397–400. https://doi.org/https://doi.org/10.1016/s0022-2860(98)80140-3

Chapter 3: Basics of High-Performance Liquid Chromatography

3.1. Introduction

The chromatography techniques are fundamentals for the separation and detection of a whole range of compound classes performing a proper matrix extraction and developing a separation method. The purpose of applying chromatography which is used as a method of quantitative analysis apart from its separation, is to achieve a satisfactory separation within a suitable timeinterval. Various chromatography methods have been developed to that end. Some of them include column chromatography, thin-layer chromatography (TLC), paper chromatography, gas chromatography (GC), ion-exchange chromatography, gel-filtration chromatography, high-pressure liquid chromatography (HPLC), supercritical fluid chromatography (SFC) and affinity chromatography (Figure 3. 1) (Coskun, 2016; Kumari et al., 2022).

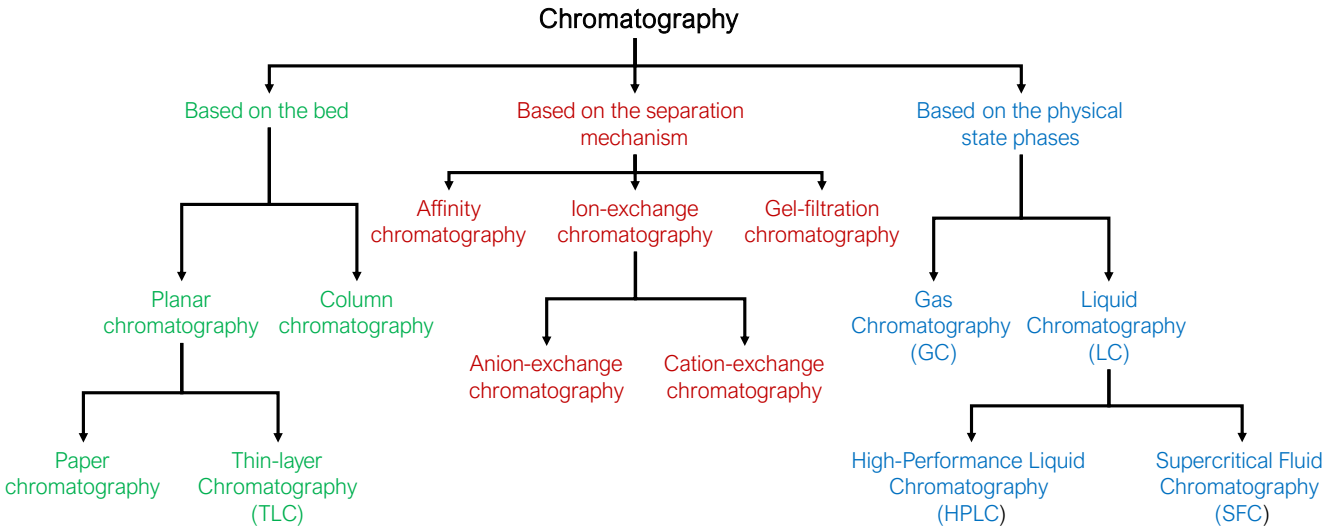


Figure 3. 1 Scheme of the different types of chromatography based on three different aspects: on the bed, on the separation mechanism and on the physical state phases.

3.2. Theory of the chromatographic techniques

This section describes the theoretical bases of chromatography describing the general principles of the chromatographic techniques with a focus for the liquid chromatography (LC). At the end, an explication of the High-Performance Liquid Chromatography (HPLC) is also provided.

3.2.1 Conventional parameters

The fundamental parameters for the understanding of the chromatographic process are briefly described below.

- **t_R**, retention time: is defined as the time that elapse among the injection of a sample into the chromatographic system and the detection of its peak at the detector (peak maximum).
- **$t'_R = t_R - t_0$**, corrected retention time: it is given by the sum of t_0, also called dead time, which is the elapsed time required for a compound not retained to cross the column, and the retention time t_R which is the time spent by a compound in the interaction with the stationary phase.

- **k**, retention factor (or capacity factor): is an experimental parameter used to describe the retention of the solute and therefore the retention rate of the solutes along the column. In LC the retention factors can be modified to obtain a better separation through changes in the composition of the mobile phase and the stationary phase. The retention factor represents the fraction of analyte that is divided between the stationary phase and the mobile phase in the column at any time.

$$\boldsymbol{k} = \frac{\mathrm{Ms}}{\mathrm{Mm}} = \frac{\mathrm{CsVs}}{\mathrm{CmVm}} = \frac{\mathrm{Vs}}{\mathrm{Vm}}\ \mathrm{Kd}$$

$$\boldsymbol{k} = \frac{\mathrm{Vr} - \mathrm{Vm}}{\mathrm{Vm}} = \frac{\mathrm{t_r} - \mathrm{t_0}}{\mathrm{t_0}}$$

- $\boldsymbol{\alpha}$, the selectivity factor: allows to evaluate the selectivity of the system through the complete separation of two species. It is equal to the ratio between the retention factors of the most retained solute and the least retained solute, under the same chromatographic conditions. To

obtain the complete separation of two different species it must be greater than 1.

$$\alpha = \frac{k'_2}{k'_1} = \frac{t_{r2} - t_0}{t_{r1} - t_0}$$

- **Rs**, resolution factor: this parameter allows to evaluate the separation of adjacent peaks, it can be calculated:

$$Rs = \frac{1.18\,\Delta t}{w_{h1} + w_{h2}}$$

Where Δt represents the difference between the retention times of the two analytes and wh_1 and wh_2 are the amplitude of the respective peaks at half height. The equation shown is the one that best suits the conditions in which the peaks are not separated up to the baseline. From the theoretical point of view, several equations have been formulated to correlate the resolution to some chromatographic variables such as selectivity and efficiency, and among these the most used is the following:

$$Rs = \left(\frac{\sqrt{N}}{4}\right)\left(\frac{\alpha - 1}{\alpha}\right)\left(\frac{k'}{1 + k'}\right)$$

where N is the number of theoretical plates, an index parameter of the column efficiency.

- **N**, theoretical plate: is a parameter of the separation efficiency and chromatographic performance of a column.

$$\mathbf{N} = \frac{\mathrm{L}}{\mathrm{H}}$$

where L and H are respectively the length and height of the theoretical plate. The term N is therefore directly proportional to the length of the column and is a purely mathematical value useful for establishing the chromatographic efficiency of the column for a given analytical method. However, the theory of the plate has limits and the plates are a completely ideal supposition, since in the experimental reality there are many factors that determine a dispersion. This justifies the typical Gaussian profile of the chromatographic peak. The width of the peak depends on some experimental parameters such as: longitudinal diffusion, multiple paths and mass transfer between mobile phase and

stationary phase. These parameters are correlated with each other through the Van Deemter equation.

3.2.2 Chromatographic efficiency: Van Deemter equation

The efficiency of a chromatographic column can be described by the Van Deemter equation where the height of the theoretical plate H (H = L / N) is correlated to the linear velocity of the mobile phase u through three terms:

$$H = A + B/u + Cu$$

$$H = 2\lambda d_p + \frac{2\gamma D_m}{u} + \frac{f(k) d_p^2 u}{D_m} + \frac{f(k) d_f^2 u}{D_s}$$

where d_p is the diameter of the particles, k the retention factor of the analyte, D_m and D_s are respectively the diffusion coefficients of the solute in the mobile phase and in the stationary phase, λ and γ are factors concerning the structure of the packing material of tortuosity or obstruction, d_f is the film thickness of the stationary phase. The three terms of the Van Deemter equation correspond to the different causes of

widening of the chromatographic peak. The first term A corresponds to the "vortical dispersion" or "eddy diffusion" due to the different path that the molecules can follow between the stationary phase particles; the second term B corresponds to the “longitudinal dispersion”, and is due to the longitudinal diffusion of the analyte band in the mobile phase. The third term C corresponds to the “dispersion of mass distribution”, and represents the resistance to mass transfer, which is often the factor that most influence the peak shape.

The Van Deemter curve shown in Figure 3. 2 allows to optimize the chromatographic performance as a function of the flow rate. Contribution B is significant only at very low linear speeds, while the influence of term C becomes important at high speeds. The optimum flow velocity is that which corresponds to the minimum of the curve.

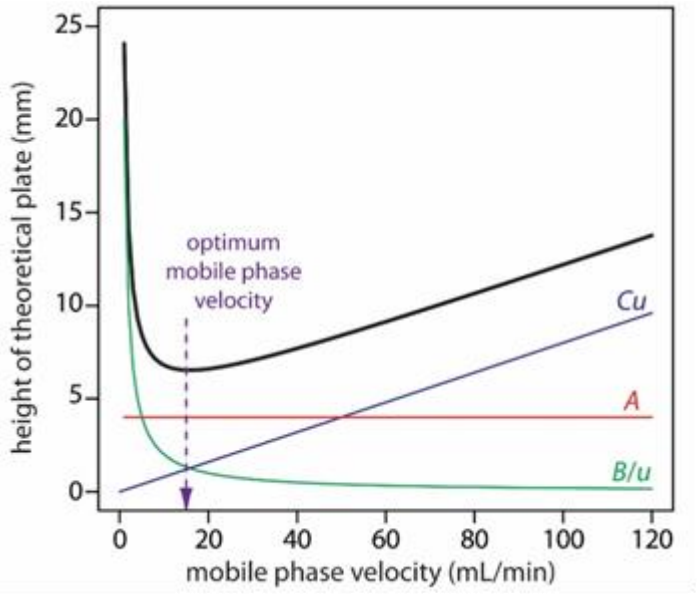


Figure 3. 2. Van Deemter curve with the three terms that contribute to the efficiency of the chromatographic column.

3.2.3 Broadening of the chromatographic band due to extra-column effects

The extra-column effects cause the chromatographic band to broaden.

To describe the chromatographic system, we start from a variance model expressed by the following equation:

$$\sigma^2 sys = \sigma^2 ext + \sigma^2 col$$

where σ^2ext and σ^2col represent the variance due to extra-column and in-column factors, respectively.

The maximum acceptable value relating to the "extra-column" variance is 10% of the value of σ^2col:

$$\sigma^2_{(acc)} \leq \sigma^2_{col} * 0.10 \leq \frac{\pi^2 L^2 \, r^4 \varepsilon^2 (1+k)^2}{N}$$

The phenomenon of the broadening of the peaks due to extra-column factors can be reduced by choosing the connection fittings of appropriate internal diameter and length, suitable injectors and detection cells in order to minimize the dead volumes, which can compromise the chromatographic efficiency. The last important factor to take into account is the maximum injection volume which is to be considered a function of the length of the column, the number of theoretical plates and the retention factor. On the other hand, it is not possible to inject larger volumes as there would be an overload of the column "overloading" with a consequent loss of chromatographic efficiency (Martin et al., 1975).

3.2.4 Stationary phases

The stationary phase for an HPLC analysis are chosen on the base of the chemical structure of the compounds to be analyzed. The proper stationary phase allow analytes separation, following the conventional chromatographic mechanisms of partition, adsorption, affinity, ion exchange, etc. Generally, silica-based particles functionalized with different groups, with a particle diameter of 3 μm or 5 μm, are used.

Recently, due to the continuous demand to obtain increasingly efficient, selectivity and rapid chromatographic methods, stationary phases characterized by small particles (1.1 μm and 1.8 μm) have been introduced. From the Van Deemter equation, it can be observed how the use of particles with small diameter leads to a decrease of the terms A and C. Hence, the choice of stationary phases based on porous sub-2 μm increase the efficiency at higher linear speeds and allow to considerably reduce the analysis times (Wang et al., 2012). However, the use of columns packed with sub-2 μm particles generates very high back pressures, making it necessary to introduce pumps capable of withstanding higher pressures than typical ones of

HPLC systems (400 bar). For this reason, Ultra High Performance Liquid Chromatography (UHPLC) are born, becoming the chromatographic technique of choice in many application sectors. In the event that a dedicated instrumentation is not available, a good compromise is represented by Core-Shell or Fused-Core technology. The core-shell particles consist of a solid inner core (silica, aluminum, gold, etc.) covered by a porous surface shell, available in different total diameters: 1.3 μm and 1.7 μm (for UHPLC columns); 2.6 μm (suitable for both UHPLC and HPLC columns); 5 μm (specific for HPLC columns) (Guillarme et al., 2010). These columns are characterized by small values of the Van Deemter coefficients. In fact compared with the completely porous particles, A is reduced by 40%, B decreases by 20% and consequently also C. These phases provide speed and chromatographic efficiency comparable to those of sub-2 μm particles, but at about half the back pressure for the same column length. This is the reason why columns packed with 5 μm and 2.6 μm particles can be handled by HPLC instruments. On the other hand, a limitation of the core-shell particles is

undoubtedly due to the reduced load capacity, a disadvantage partially overcome in the more recent stationary phases.

3.2.5 HPLC instrument

The main instrument of the liquid chromatography is the HPLC (Figure 3. 3). To perform the analysis on a column or a capillary, the typical set-up for analytical purposes entails a mobile phase supplier, one or more pumps delivering the eluent, the solvent programmer, the sample injection valve, the column (or the capillary) and one or more detectors (Degano, 2019).

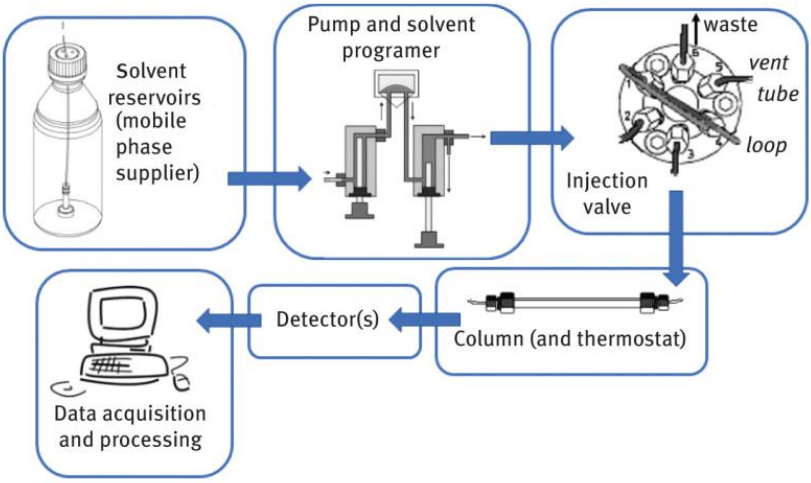


Figure 3. 3. General scheme of an HPLC instrument (adapted from: (Degano, 2019)*)*

The solvent reservoir(s) contains the eluents to be used for the analysis. The pump can operate up to 6000 psi for High-Performance Liquid Chromatography (HPLC) and up to 10000 psi for Ultra-High-Performance Liquid Chromatography (UPLC). Moreover, a precise and reproducible flow control is required and in the specific range needed for the target application. For HPLC the flow rates is of the order of mL/min, for nano-LC applications the flow rates is of the order of μL/min. The solvent programmer is necessary to perform the analysis in a gradient mode. The column is the core of the chromatographic separation and several columns are available on the market. In general, more than 80% of the commercial columns are packed in stainless steel to support high pressures and guarantee inertness towards the most common eluents. Tubing, fittings and frits holding the packing in the column are made of materials resistant to solvents and buffers, such as stainless steel or peek. The stationary phase is in most cases made of spherical packings, which might or might not be functionalized (in the case of normal or reverse phase chromatography, respectively), made of silica particles or

polymers. Both the pore size and the diameter of the particles influence the back-pressure needed to elute the sample components. Most important, they affect the superficial area of the stationary phase and the coefficient of diffusion of the analytes into the stationary phase, and ultimately have a strong effect on the retention mechanisms and the overall efficiency of the separation. The influence of different experimental parameters on the efficiency of a separation is considered by the van Deemter equation. Most columns are in the 10–30 cm length range, with 2-4.6 mm internal diameter and 2–10 μm particle size diameter. A common column for HPLC instruments is the one with an internal diameter of 4.6 mm and work with a flow rates enter 0.2 – 2.0 mL/min. UPLC allows the use of sub-2-μm particles for the stationary phase by exploiting more effective solvent pumps and shorter connections, which can resist to relatively higher back-pressures. UPLC allows obtaining a high chromatographic efficiency in shorter runtimes, thus providing faster analyses with lower solvent consumption. The sample is injected through an injection port, which includes a loop for sample loading and an internal valve. Rheodyne injector or

loop injector is the most popular injector and is widely used (Figure 3. 4). The Rheodyne model 7125 manual sample injector was firstly introduced by the Rheodyne Corporation (acquired by IDEX in 2002) and then became the industry-standard injector in the late 1970s (Paul et al., 2019). It is available with a fixed or variable amount of loop, to hold the sample until injected into the column (0.1 – 100 μL). It is placed just before the column's inlet. A manual Rheodyne sample injector has two positions, load and inject. In a load position, a sample is loaded into the loop with the help of a syringe. After loading, the sample is injected with the help of manual rotation by switching to the inject position. Then the sample is flow with the mobile phase in the columns and analyte is separate according to their affinity. If you use a fixed volume injector, only the set volume is passed to the stationary phase and excess is removed.

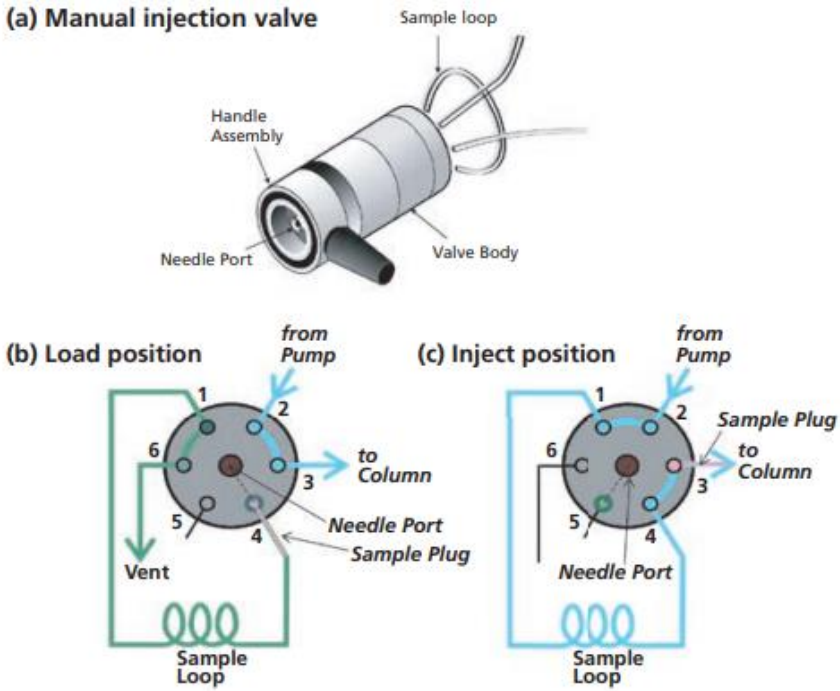


Figure 3. 4. Schematic diagram of (a) the manual injection valve (Rheodyne model 7125); (b) schematic of the 7125 injector in Load position; (c) and in Inject position. Figures adapted from reference (adapted from: (Paul et al., 2019)*)*

Most recent instruments are equipped with autosamplers, whose functioning is based on the same type of valves and loops as manual injection (Rheodyne is also used with the autosampler HPLC systems). Autosamplers allow multiple samples to be analysed in a sequence that can run overnight,

thus increasing the throughput of the analytical set up. Lastly, the instrument can be coupled with two main different types of detectors: detectors based on UV-Vis absorption and mass spectrometry (Paul et al., 2019). Regarding the spectrophotometric detectors, they can be coupled online to the chromatographic set up by employing conical flow cells to host the eluent as exited from the column. Single wavelength or multi-wavelength detectors can be used; Photodiode Array Detectors (PDA or also known as DAD) are also employed and provide information on the entire UV-Vis absorption spectrum of eluted species. The tridimensional information achieved by DAD allows obtaining chromatograms over a range of wavelengths during a single run, thus providing more information on the sample composition than a single wavelength detector. In particular, the combination of retention time and spectrum allows for the positive identification of the analytes, ruling out coelution of different compounds. Moreover, the acquisition of the UV-Vis spectrum of each separated peak allows for selecting an optimal wavelength for verifying peak purity and peak identity, and to quantify the

analytes with optimal detection limits. A scheme of a DAD detector is reported in Figure 3. 5.

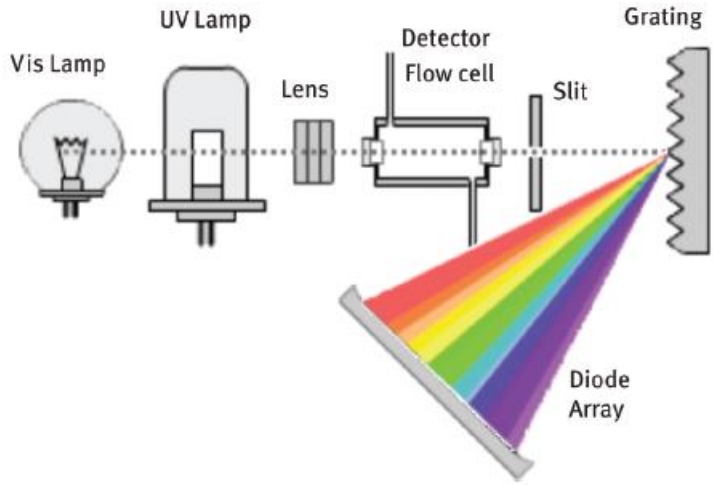


Figure 3. 5. Scheme of a Photodiode Array Detector (or Diode Array Detector) in the UV-Vis range (adapted from: (Degano, 2019))

Fluorescence detectors (FD) are also frequently used, providing higher selectivity and sensitivity towards fluorescent analytes. The sensitivity of FD is typically 2 or 3 orders of magnitude higher than that of absorption detectors; the outstanding selectivity is due to the possibility to change both excitation and emission wavelengths during the

chromatographic run. In order to improve the absorption or the fluorescence of the analytes, offline or online derivatization can be applied.

Regarding the mass spectrometry detectors, spray ionization techniques such as electrospray ionization (ESI) and atmospheric pressure chemical ionization (APCI) are the typical interfaces used for coupling mass spectrometry with HPLC. Differently from ESI, APCI produces singly charged ions with fragmentation to some extent. The most common analyser are the ones based on quadrupole, ion trap or Time of Flight (ToF). The mass spectra are acquired in sequence by scanning the selected mass interval repetitively in quadrupoles and ion traps, or by measuring the ToF of the ions through the flight tube in ToF detectors. The ions abundance in each spectrum is summed and reported in the Total Ion Current (TIC) chromatogram.

3.3. Extraction method to study food matrices by means of HPLC

The HPLC technique, when applying on a food matrices, is normally used to study a particular compound class. Hence, a fundamental part of the experiment is the sample preparation with the development of the extraction method (Slack & Snow, 2007). In general, the main objectives of sample preparation are the extraction of the targeted compounds form the matrix, their enrichment and the elimination of interfering species. Therefore, the primary criterion is always to find a method that provides acceptable recoveries for all the analytes under study based on the food matrix type. The extraction is defined as the transfer of one or more components from the food into, typically, a fluid phase.

For liquid foods (such as beverages), the conventional extraction method is a Liquid-Liquid extraction (LLE). While, for solid foods, the conventional extraction method is the Solid-Liquid Extraction (SLE).

3.3.1. Liquid-Liquid extraction (LLE)

The LLE is the conventional extraction method used for liquid food matrices. The extraction procedure is based on the transfer of the analyte from the aqueous phase of the liquid food (based in water) to a solvent immiscible with the water (based on the partition coefficient of the octanol / water mixture) (Daso & Okonkwo, 2015).

3.3.2. Solid-Liquid Extraction (SLE)

The SLE is the conventional extraction method used for solid food matrices. In fact, the SLE involves the removal of a desired component or a peculiar class of components from a solid material using a liquid (usually an organic solvent such as ethanol, methanol, acetone, hexane, or ethyl acetate, pure or mixed in water) able to dissolve the solute but not (or at a less extent) the other components of the solid matrix. The process consists of mixing the solid material and the solvent, and the mixture is maintained during the time needed to promote the transference of the solutes from the solid to the solvent. The SLE process is regulated by three essential mechanisms: the

extractant penetration in the solid matrix, the diffusivity of analytes to the outer space, and the solubility of the analytes in the extractant (Priego-Capote, 2021). In order to improve SLE, the application of high temperature with high pressure and the assistance with auxiliary energies, particularly, microwaves and ultrasound were performed.

3.3.3. Innovation in the extraction methods for solid foods

To date, a number of innovative extraction techniques applied to food matrices already exist. The aim is the reduction of the time required for extraction, avoid the use of organic solvents consumption (Mussatto, 2015) and enhance the extraction performance. Some of these techniques are:

- Microwave-Assisted Extraction (MAE): This process consists of mixing the solvent and sample in extraction vessels that are closed and submitted to controlled temperature and pressure conditions. The microwave energy penetrates into the closed vessels, producing a volumetrically distributed heat source due to molecular

friction resulting from dipolar rotation of polar solvents and from the conductive migration of dissolved ions. As a consequence, the temperature of the solvent rises above its boiling point, resulting in the extraction of the compounds from the material structure.

- Ultrasound-Assisted Extraction (UAE): consists of passing ultrasonic energy in the form of waves through a liquid solvent containing solid particles. As the waves hit the surface of the material, a force that is either perpendicular or parallel to the surface is generated. Sonic energy is converted into mechanical energy in the form of shock waves equivalent to several thousand atmospheres of pressure. It is believed that the rapid localized increases in pressure and temperature are responsible for the disruption of cellular membranes, thereby facilitating the solvent migration into the cell and the extraction of the desired component as a consequence (Cravotto & Binello, 2016).
- Supercritical Fluid Extraction (SFE): Supercritical fluid is the name given to a fluid that is forced to a

temperature and pressure above its critical point. Under these conditions, the fluid has several properties that are between those of a gas and a liquid. The SFE technique consists of using a supercritical fluid as a solvent to separate desired components from solid or liquid materials. Carbon dioxide is the fluid most commonly used in SFE processes since it is non-toxic and non-flammable, readily available, and has a low cost. Moreover, carbon dioxide can be easily removed from the solute after extraction, leaving no chemical residue.

- Subcritical Water Extraction (SWE): Subcritical water (also called hot liquid water, superheated water, or pressurized hot water) is defined as water maintained in the liquid state by pressurizing under temperature values varying between 100 and 374 °C. Under these conditions, the ionic product of the subcritical water is higher than that of water under normal temperature and pressure. Additionally, for temperatures above 200 °C, subcritical water has specific inductive capacity comparable to that of polar organic solvents such as

methanol, ethanol, acetonitrile, and acetone, being efficient for extract compounds from natural sources.

3.3.4. Innovation in the extraction methods for liquid foods

The inherent disadvantages associated with the conventional LLE techniques, including the use of a large volume of extraction solvent, labor-intensive operations, time-consuming phase separation processes, and the possible formation of emulsion during the extraction are well-known. As a result, other types of extraction methods suitable for aqueous matrices were developed, such as Solid-Phase Extraction (SPE) and vary miniaturized extraction techniques, namely Solid-Phase Micro-Extraction (SPME) and Liquid Phase Micro-Extraction (LPME).

- Solid-Phase Extraction (SPE): The functioning of the SPE is based on the retention of the analyte on a solid material and the subsequent elution with a suitable solvent. Due to its selectivity and affinity characteristics, the SPE allows not only the extraction and pre-

concentration of the analytes but also the purification of the extract which can be immediately analyzed. A large variety of adsorbent materials for SPEs exist on the market. The choice of the type of material strongly depends on the chemical-physical properties of the analytes and on the interactions of the latter with the material itself. Comparing this technique to the LLE, there is a reduced consumption of organic solvents and no formation of emulsions. Furthermore, it is a simple, fast, reproducible extraction technique and is easy to apply. Although this extraction procedure has several advantages, it is expensive because the cartridges, rather expensive, are one-use and cannot be remanufactured.

- Solid-Phase Micro-Extraction (SPME): it is one of the micro-extractive techniques. Generally in SPME, a silicon fiber is covered with the stationary phase through a "coating" and there is an interaction between the analyte contained in the matrix and the fiber (Arthur & Pawliszyn, 1990). The major advantage of this

technique is represented by the direct extraction of the analytes by immersing the fiber in the sample. SPME is a fast technique, easy to perform but present some disadvantages: the short life of the fibers and the poor sensitivity of analytes in complex matrices.

- Liquid Phase Micro-Extraction (LPME): In LPME, analytes are extracted from an aqueous phase of the sample (donor phase). with an immiscible solvent (acceptor phase) with water using a volume of a few microliters. Compared to the conventional LLE, the LPME allows the extraction of the analytes, their pre-concentration and the implementation of the process in a few steps with a considerable saving of time. This micro-extraction procedure can be performed in three different ways: Single Drop Micro-Extraction (SDME), Hollow Fiber Liquid Micro-Extraction (HF-LPME) and Dispersive Liquid-Liquid Micro-Extraction (DLLME) (Psillakis & Kalogerakis, 2003).

3.4. References

Arthur, C. L., & Pawliszyn, J. (1990). Solid Phase Microextraction with Thermal Desorption Using Fused Silica Optical Fibers. *Analytical Chemistry*, *62*(19), 2145–2148. https://doi.org/10.1021/ac00218a019

Coskun, O. (2016). Separation Tecniques: CHROMATOGRAPHY. *Northern Clinics of Istanbul*. https://doi.org/10.14744/nci.2016.32757

Cravotto, G., & Binello, A. (2016). Low-Frequency, High-Power Ultrasound-Assisted Food Component Extraction. In *Innovative Food Processing Technologies: Extraction, Separation, Component Modification and Process Intensification* (pp. 3–29). Elsevier. https://doi.org/10.1016/B978-0-08-100294-0.00001-8

Daso, A. P., & Okonkwo, O. J. (2015). Conventional Extraction Techniques: Soxhlet and Liquid-Liquid Extractions and Evaporation. In *Analytical Separation Science* (Issue Lc, pp. 1437–1468). DOI: 10.1002/9783527678129.assep053

Degano, I. (2019). Liquid chromatography: Current applications in Heritage Science and recent developments. *Physical*

Sciences Reviews, *4*(5), 1–14. DOI:10.1515/psr-2018-0009

Guillarme, D., Ruta, J., Rudaz, S., & Veuthey, J. L. (2010). New trends in fast and high-resolution liquid chromatography: A critical comparison of existing approaches. *Analytical and Bioanalytical Chemistry*, *397*(3), 1069–1082. https://doi.org/10.1007/s00216-009-3305-8

Kumari, V. B. C., Patil, S. M., Ramu, R., Shirahatti, P. S., Kumar, N., Sowmya, B. P., Egbuna, C., Patrick-Iwuanyanwu, K. C., & Uche, C. Z. (2022). Chromatographic techniques: Types, principles, and applications. In *Analytical Techniques in Biosciences: from Basics to Applications*. https://doi.org/10.1016/B978-0-12-822654-4.00013-0

Martin, M., Eon, C., & Guiochon, G. (1975). Study of the pertinency of pressure in liquid chromatography. II. Problems in equipment design. *Journal of Chromatography A*, *108*(2), 229–241. https://doi.org/10.1016/S0021-9673(00)84666-X

Mussatto, S. I. (2015). Generating Biomedical Polyphenolic Compounds from Spent Coffee or Silverskin. In *Coffee in Health and Disease Prevention* (pp. 93–106). Elsevier Inc.

https://doi.org/10.1016/B978-0-12-409517-5.00011-5

Paul, C., Frank, S., & Dong, M. W. (2019). HPLC Autosamplers: Perspectives, Principles, and Practices. *LCGC North Am.*, *37*(8), 514–529.

Priego-Capote, F. (2021). Solid–liquid extraction techniques. In *Analytical Sample Preparation With Nano- and Other High-Performance Materials*. https://doi.org/10.1016/b978-0-12-822139-6.00002-x

Psillakis, E., & Kalogerakis, N. (2003). Developments in liquid-phase microextraction. *TrAC - Trends in Analytical Chemistry*, *22*(10), 565–574. https://doi.org/10.1016/S0165-9936(03)01007-0

Slack, G. C., & Snow, N. H. (2007). HPLC sample preparation. In *HPLC Method Development for Pharmaceuticals* (Vol. 8, pp. 237–268). https://doi.org/10.1016/S0149-6395(07)80014-6

Wang, Y., Ai, F., Ng, S. C., & Tan, T. T. Y. (2012). Sub-2μm porous silica materials for enhanced separation performance in liquid chromatography. *Journal of Chromatography A*, *1228*, 99–109. https://doi.org/10.1016/j.chroma.2011.08.085

Chapter 4: Application of the NMR metabolomics approach in Food Science

4.1. NMR methodology approach for food analysis

The metabolite characterization of foodstuffs by means of NMR spectroscopy represent a very powerful tool since the application of this methodology can solve several food-related issues such as characterization of chemical composition, authentication (variety, geographical origin, harvest/production year,) as well as potential adulterations (Luisa Mannina et al., 2012). In fact, in a targeted technique such as chromatography, the chemical analysis of a foodstuff is generally focused on specific chemical classes that are chosen a priori before the analysis, thus limiting the possibility of identifying for new or unexpected metabolites. The described workflows and data analysis approaches that have to be applied in NMR food analysis, have shown to be very effective in solving several food-related issues such as chemical characterization, geographical origin, authenticity, fraud tracking. Basically, this can be accomplished by using three possible approaches, namely metabolite finger-printing, target analysis (1), metabolite profiling (2), and metabolomics (3), according to the specific application (Figure 4. 1).

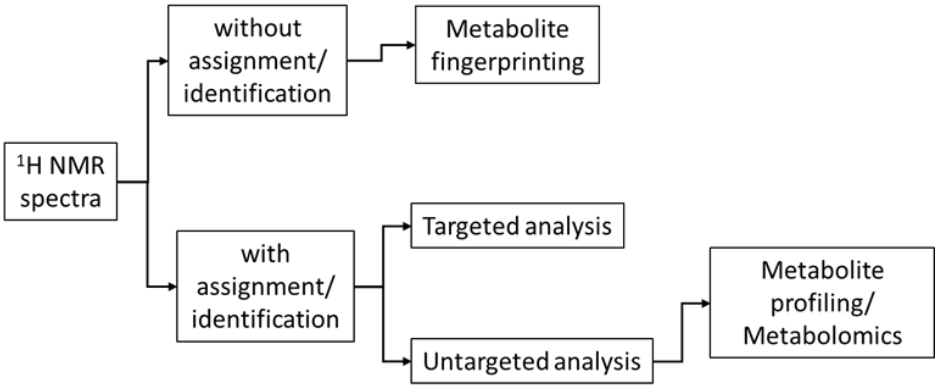


Figure 4. 1. Classification of high-resolution ¹H NMR spectroscopy's approaches to study foodstuffs.

1. **Targeted approach**: the NMR analysis is restricted to the identification and quantification of specific compounds, chosen according to previous knowledge about the food under investigation. So, for this reason, sample preparation and extraction are carried out in order to concentrate the targeted metabolites. This approach is mainly applied to identify compounds that are responsible for some peculiar characteristic of the analyzed foodstuff, thus characterizing its origin, variety or identifying adulterations. For instance, the NMR can be used for the identification and quantification of the 16-O-methylcafestol in coffee samples.

This compound is a characteristic terpen of the Robusta coffee and is absent in the Arabica one. Hence, the detection of 16-O-methylcafestol in ^{1}H NMR spectrum of the chloroform extract of the roasted coffee powder, thanks to the characteristic signal of the methoxide group at 3.17 ppm, can be used for the authenticity test of the most valuable Arabica coffee variety (Schievano et al., 2014).

2. **Metabolic profiling (untargeted analysis)**: consists in identification and quantification of a number of selected metabolites, belonging to various classes of compounds. It is usually applied when the problem doesn't present an hypothesis and therefore the solution may require the investigation of as many metabolites as possible. For instance, in this study about sea bass the high resolution NMR spectroscopy was used as an analytical tool to determine the complete metabolic profiling of sea bass extracts (L. Mannina et al., 2008). The ^{1}H spectra of sea bass extracts in aqueous and organic solvents were analyzed, all the NMR signals were assigned using 2D NMR spectra, and finally the intensity of the identified metabolites were

measured and submitted to chemometric analysis. Water-soluble metabolites belonging to different classes such as sugars, amino acids, dipeptides and organic acids as well as metabolites soluble in organic solvents such as lipids, sterols and fatty acids were identified. The identified metabolites together with a suitable statistical analysis were used to discriminate between wild and cultured sea bass samples. Preliminary results showed that discrimination between wild and cultured sea bass was obtained not only using fatty acid composition but also cholesterol and phosphatidylethanolamine and some water-soluble metabolites such as choline, trimethylamine oxide, glutamine, fumaric and malic acids.

3. **Metabolic fingerprinting**: is used when classification of samples without recognition of individual specific metabolites is sufficient: in this case, the NMR spectrum can be considered as a fingerprint of the foodstuff and all the NMR resonances are measured without any identification. The metabolomic approach is the most used approach often used to study different aspects of foods. An example is the

NMR study of the non-volatile organic honey components to determine its botanical origin (Schievano et al., 2010). Each ^{1}H spectrum was segmented into intervals ("buckets") and the signal intensity in each interval was integrated and the spectra were normalized to the total sum of integrals. The resulting normalized integrals composed the data matrix that was submitted to multivariate analysis. The realized PLS-DA allowed the classification of the samples. A classification index can be calculated and used to determine the floral origin of honey as an alternative to the melissopalinology test and possibly to determine the percentage of various botanical species in polyfloral samples.

All these approaches require a specific and well-studied methodology that comprise not only the NMR experiment but also the numerous phases that occur before and after the NMR analysis. Figure 4. 2 schematically explains all the phases that constitute a typical NMR metabolomics workflow for the study of a complex matrix such as food.

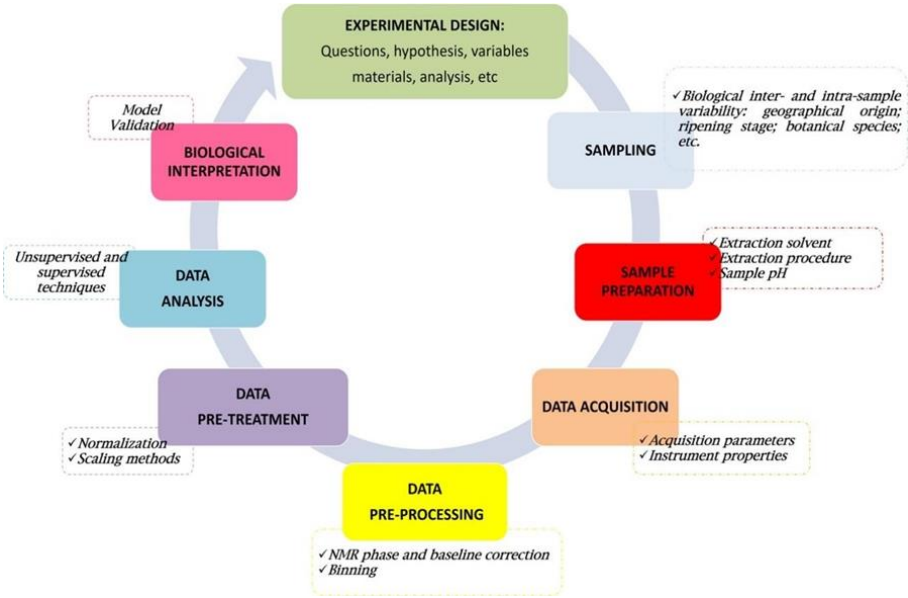


Figure 4. 2. Typical NMR metabolomics workflow and sources of variability for the study of foods.

4.2. NMR metabolomics workflow

4.2.1. Experimental design

The first step is represented by the experimental design, very important since all the experimental aspects, from the sampling size and collection to the data analysis, must be taken into consideration in order to maximize the possibilities of answering the research questions of interest as clearly and efficiently as possible. Well-designed experiments together

with appropriate analytical data and statistical analysis, enable researchers to increase the robustness and validity of their experimental results (Dunn & Ellis, 2005; Smlinska et al., 2012).

4.2.2. Sampling

Proper sampling is a crucial point of any analytical protocol from two different points of view. The first one is represented, mainly in the case of foodstuffs, by the choice of the proper characteristics of the sample (variety, harvesting period, agronomical practices, origin, etc) basing on the focus of the study. For this purpose, a deep knowledge of metadata including the growing conditions, the production practices, the botanical characteristics, the storage, and so on, is very important since the final results will be strictly correlated with the sample properties (Ben-Zvi et al., 2015).

Conservation occurring after sampling requires suitable care to preserve the quality and composition of foodstuffs. In fact, some operations such as harvesting for vegetables, and slaughter for animals can be followed by an enzymatic attack and other degradation processes. Freezing in liquid nitrogen

followed by storing in the dark at low temperature (-20° C or -80° C) are the most common procedures used to avoid chemical or enzymatic degradation.

The second aspect of sampling that is needed to be considered regards the treatment of the sample inside the laboratory, before the extraction or the direct analysis. In fact, as previously underlined, foodstuff is a complex matrix where the spatial distribution of metabolites can be not homogeneous. If it is necessary to analyze just a piece of sample, since it is impossible to put in the instrument the sample as a whole (this is the most common case), it is important to perform the sampling in a correct way. For instance, it can be chosen to take different parts of the foodstuff to have a "representative" sample to analyze, or the whole sample pool can be homogenized to uniformize the whole foodstuff. This concept has to be mainly applied for solid samples, since liquid ones are homogeneous matrices in each "point". Liquid samples such as olive oils, vinegars, wines, fruits juices are generally analyzed without any treatment, whereas dilution for a viscous liquid such as honey is recommended. Anyway, in some cases, liquid

samples can be dried with nitrogen flux or lyophilization in order to eliminate the solvent presence (water or alcohol), whose NMR signals could cover the signals of other components (Hu et al., 2020; Zhu et al., 2020). In the case of solid foodstuffs, after sample homogenization and/or disruption, an extraction with a suitable solvent has to be performed.

4.2.3. Sample extraction

The choice of the solvent is very important since it determines the metabolites that are extracted and thus analyzed. If a targeted analysis has to be carried out, the proper solvents and/or pH values represent a crucial point. On the contrary, when an untargeted NMR analysis has to be carried out, the extraction of the whole metabolite pattern is recommended. In this case, a biphasic extraction system, generally formed by a methanol/water/chloroform mixture in different proportions is often used to extract both hydrophobic and hydrophilic compounds. Below are reported some of the most used types of biphasic extraction systems: Folch extraction

(1), Bligh-Dyer extraction (2) and the Bligh-Dyer with alternative solvents (3).

1. **Folch extraction method**: The Folch extraction is a method for the preparation of lipid extracts from tissues developed by Folch et al. in 1951 (Folch et al., 1951). The method provide an extraction of the sample with a methanol/chloroform 1/2 % *v*/*v* solution. The obtained extract is then filtrated. The filtrate, which contained the tissue lipides accompanied by non-lipide substances, was freed from these substances by being placed in contact with at least 5-fold its volume of water.

   The method have been improved in 1957 (Folch et al., 1956). A chloroform methanol extract of the tissue, prepared as described in the original version of the method, is mixed with 0.2 its volume of water to which, for certain purposes, different mineral salts may be added. A biphasic system without any interfacial fluff is obtained. The upper phase contains all of the non-lipide substances, most of the strandin, and only negligible amounts of the other lipides. The lower phase contains

essentially all the tissue lipides, other than strandin, and only negligible amounts of the other lipides. In comparison with the original method, the present version has the advantage of being simpler, of being applicable to any scale desired, of substantially decreasing the losses of lipides incidental to the washing process, and, finally, of yielding a washed extract which can be taken to dryness without foaming and without splitting of the Proteolipids. Nevertheless there is a problem: in each phase contaminant from the other (in the organic phase there are trace of water and methanol and in the hydroalcoholic phase trace of chloroform.

2. **Bligh-Dyer extraction method**: The Bligh-Dyer extraction is another method for the extraction and purification of lipids from biological materials developed by E. G. Bligh and W. J. Dyer in 1959 that work with a ternary extraction system (Bligh, E.G. and Dyer, 1959). This method overcome the problem of the Folch extraction method: the lipid extract contain small

amounts of non-lipid materials. Briefly, the Bligh-Dyer method is described below (Figure 4. 3):

i. Make monophasic system for extraction: mix sample with chloroform/methanol 1:2 % *v*/*v* mixture, considering 0.8 % *v*/*v* ratio of water from tissue (resulting proportion: chloroform/methanol/water 1:2:0.8 % *v*/*v*/*v*);
ii. Homogenization in a blender for 2 min;
iii. Make biphasic system for separation of the lipid, in the lower phase (chlorophorm), and non-lipid component, in the upper phase (methanol/water): addition of 1 volume of chloroform and 1 volume of water (resulting proportion: chloroform/methanol/water 2:2:1.8 % *v*/*v*/*v*);
iv. After each addition, 30 sec of blending;
v. The homogenate is filtered;
vi. The volume of the chloroform layer is recorded and the alcoholic layer removed by aspiration.

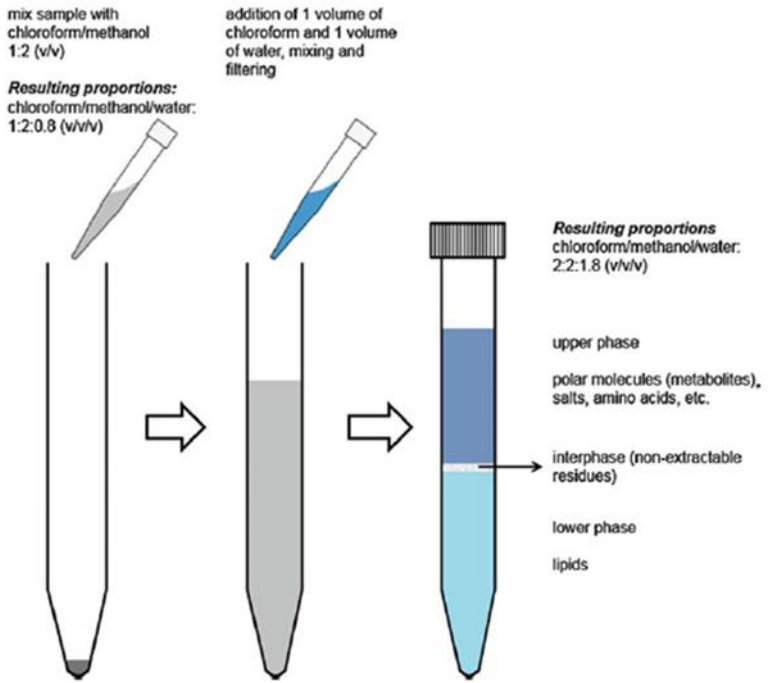


Figure 4. 3. Workflow to performing lipid extraction according to Bligh and Dyer (source: (Sundermann et al., 2016)*)*

This extraction is simply adapted to other matrices. In fact, for the extraction of materials that do not contain 80 % of water, either the size of the samples or the volume of chloroform and methanol can be adjusted to give the correct proportion of the ternary system, namely chloroform/methanol/water 1:2:0.8 % *v*/*v*/*v*. In cases

where the moisture content is much less than 80 % (e.g. fish meal), it is necessary to add distilled water.

This extraction protocol has been largely applied for the metabolomic study of several foodstuffs, such as vegetables and fruits and animal derived matrices (Capitani, Mannina, et al., 2013; Capitani, Sobolev, et al., 2013; Ingallina et al., 2020; Anatoli P. Sobolev et al., 2005; Anatoly P. Sobolev et al., 2018), due to its simplicity and quickness and the possibility to collect both the organic and the hydroalcoholic phases.

3. **Bligh-Dyer extraction with alternative solvents**: In order to replace the toxic petroleum solvents (one principle of the green chemistry), Breil et al. have developed an alternative Bligh-Dyer extraction with bio-sourced solvents in 2017 (Breil et al., 2017). Methanol and chloroform were replaced with ethanol and ethyl acetate (Figure 4. 4), demonstrating to be as effective as the classical system in terms of the yield of lipids extracted from microorganism tissues, independently of their apparent hydrophilicity.

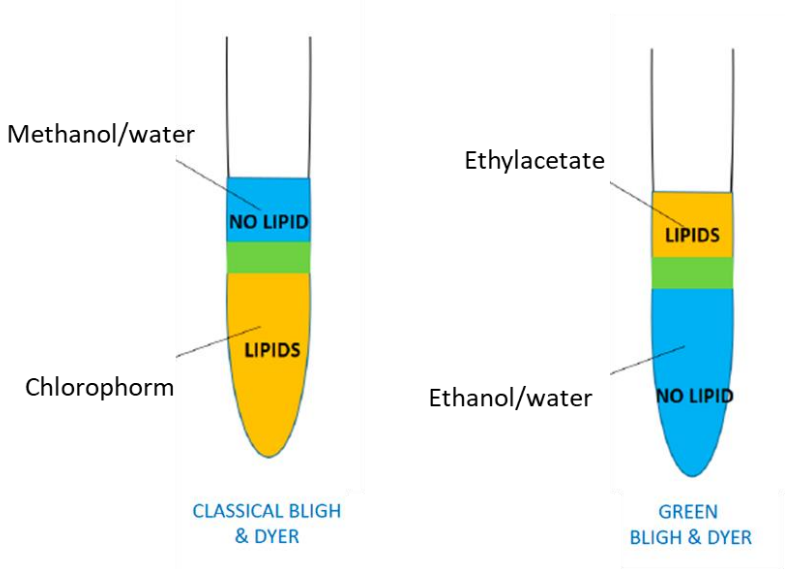


Figure 4. 4. Comparison of the classical Bligh-Dyer extraction vs. the modified green type developed by Breil et al. (source: (Breil et al., 2017)*).*

4.2.4. Sample preparation for NMR analysis

Although each research group follows its own optimal protocol, often developed after a case-by-case evaluation of the best compromise between quality of data and throughput of analysis, it is important, at the end of a research study, to give the possibility of comparing the obtained data among different laboratories. For this reason, it is recommended to provide detailed information of the experimental design and the relative

experimental protocol. In this context, it is important to reduce sources of variability and use a standardized procedure as much as possible. Sample preparation for NMR analysis represents one of the steps that have to be normalized and clearly indicated. In the case of both liquid and solid samples, there are some important aspects that have to be considered to obtain reproducible ^{1}H spectra without undesirable chemical shift variations between samples. Among these aspects, variation in pH between aqueous samples can cause a significant difference in the chemical shifts of signals belonging to organic acids, amino acids, and other metabolites with acidic or basic functional groups (Fan, 1996). Two different approaches to solve this problem can be applied: control of pH (buffered solution or pH adjustment) and specific data processing. Phosphate buffer is frequently used to stabilise pH in the range between 6 and 7, whereas oxalate buffer used for more acidic solutions (pH ~ 4). Both buffers do not give any additional proton signals in the spectrum. The other approach to control the pH is represented by the addition of small volumes of hydrochloric acid or sodium hydroxide solutions

basing on the starting pH value (Avenoza et al., 2006). The data processing approach to eliminate pH induced variations consists in using exponential multiplication of free-induction decays with high values (10–50 Hz) of line broadening factor (Duarte et al., 2004). Anyway, this last method causes a decrease in spectral resolution and only small chemical shifts differences can be levelled.

The liquid state NMR requires the presence of some deuterated solvent in the sample to provide an independent from proton channel field-frequency lock signal and a signal on which resolution adjustment can be carried out. Liquid food samples can be submitted to NMR analysis upon the addition of a small fraction of deuterated solvent to provide the lock signal for NMR. When samples are viscous or dry, they have to be dissolved in deuterated solvents. The deuterated solvents commonly used in NMR food analysis are D2O, methanol-d4, DMSO-d6, acetone-d6, acetonitrile-d3, and chloroform-d (Fulmer et al., 2010). The choice of solvent is determined by the nature of the sample, its preparation and solubility. For polar extracts usually D2O, methanol-d4 or a mixture of both of them

are used. Deuterated chloroform is usually used for non-polar extracts. It is important to consider that, when a different solvent is used, metabolites chemical shifts variations occur. It is noteworthy that the presence of paramagnetic cations (Fe3+, Mn2+) in plant derived aqueous extracts and foodstuffs can affect the signals of several organic acids (citric, malic) capable of chelating metal, causing a strong broadening of signals. This source of broadening of NMR signals can be avoided by adding ethylene diamine tetra-acetic acid (EDTA) to the supernatant to capture the paramagnetic ions.

Finally, the addition in the solvent of a soluble internal standard can be useful to have chemical shift reference and/or to make a quantification analysis if the standard concentration is well known.

4.2.5. Data acquisition, pre-processing and pre-treatment

Taking up the previous discussion regarding the factors that have to be considered to avoid chemical shift variations during the NMR experiments as more as possible, it is

important to make considerations about temperature control and instrumental drift. Within a set of samples, it is important to perform the NMR experiments using the same temperature, with most of the 1H NMR spectra of foodstuffs being acquired in the 25-27° C range of temperatures. When the temperature used in NMR experiment is not reported, the value of the results is drastically reduced. Instrumental drift (small gradual diminishing of the magnetic field strength of an NMR instrument), except in the most extreme circumstances, does not impact comparability of data. A modern instrument can expect to have a magnetic field drift of less than 1 Hz per hour (Evans et al., 2013).

Regarding the NMR experimental acquisition and process parameters that have to be properly adjusted before and after a NMR experiment, these aspects have been discussed in the previous chapter (Chapter 2). The identification of metabolites represents one of the most critical phases of the NMR metabolomics study. While the structural assignment of isolated organic compounds can usually be successfully performed by NMR, the NMR analysis of foodstuffs is

challenging because these samples, as all complex biological matrices, include a myriad of compounds (saccharides, polysaccharides, lipids, peptides, amino acids, organic acids, etc.), that are present in a large range of concentrations. These very complex mixtures inevitably give rise to 1H NMR spectra that are highly crowded due to the presence of numerous, often multiplet- resonances due to scalar couplings. In this context, the NMR analysis of complex mixtures represents an active field of research, not exclusively restricted to the study of foods samples. Various approaches for the structural assignment of compounds present in complex mixtures have been developed (McKenzie et al., 2011; Novoa-Carballal et al., 2011) and, regarding the NMR analysis and structural assignment of foodstuffs samples, two main approaches are generally applied: spectral comparison using databases of NMR spectra (database matching approach) or application of 1D and 2D/nD NMR experiments (NMR elucidation approach). In the database matching approach, similarly to what happen with other analytical methods, each compound in a mixture can be identified by its characteristic signals in the NMR spectrum

after comparison with the NMR spectrum of the pure compound. One of the main limitations of this approach is that an exhaustive database should be available, otherwise it would require an enormous number of compounds to be synthesized or isolated from natural sources. In order to solve this limitation, in the last years, several publicly available databases of NMR metabolite standard measurements (HMDB, MMCD, TOCCATA) (Bingol et al., 2012) have been developed (Tulpan et al., 2011). Anyway, further limitations are represented by the variation of NMR spectral parameters (chemical shifts, relaxation times, etc) that can occur when the compound is analyzed in a mixture, as opposed to alone in solution, due to interactions with other molecules or, more simply, due to changes in experimental conditions (ionic strength, pH, temperature, solvent, etc.). In this case, it is clear that some chemical shift values can be different from the values found in the library database, thereby precluding unambiguous identification.

In the NMR elucidation approach, together with 1D experiments, correlation 2D experiments between the proton

signals of the same molecule (^{1}H-^{1}H COSY, ^{1}H-^{1}H TOCSY, ^{1}H-^{1}H NOESY) or between ^{1}H and other nuclei, generally ^{13}C (^{1}H-^{13}C HSQC and ^{1}H-^{13}C HMBC), are carried out, in order to identify the chemical structure of the considered compound and so its identity. This type of approach is time consuming since these 2D experiments require more time to be acquired, as well as the compound structure elucidation. The correct identification of a compound can be very difficult, mainly when its presence in a given foodstuff has not been previously documented. For this reason, when possible, it is useful to confirm assignments by directly adding an appropriate amount of a pure chemical standard to the investigated sample, once its presence has been inferred or suspected. Moreover, it is recommended to compare the NMR assignment with data achieved by other techniques (mass spectrometry, chromatography, UV/Vis and IR spectroscopy) on the same analyzed foodstuff, as only the combination of several analytical techniques can reliably unravel the complexity of foodstuffs (Bernal et al., 2011).

Apart from qualitative and structural information, robust quantitative data can be obtained from NMR spectra. The main advantage of NMR for quantification purposes is the possibility to quantify, with a good accuracy and reproducibility, a large number of metabolites in a given sample using a single experiment, without the necessity of creating calibration curves (Dais et al., 2007). ^{1}H NMR is, in fact, a quantitative technique owing to the proportionality of signal integral to the molar concentration of the corresponding metabolite. Generally, two quantification strategies can be applied: absolute quantification provides the amount of metabolites in a given sample, whereas relative quantification provides the percentage of a given metabolite in the mixture.

When an absolute metabolite quantification is required, the duration of recycle time and number of scans to reach a suitable signal to noise ratio have to be optimised in each experiment to obtain reliable and accurate results. NMR relaxation properties of metabolite nuclei are the key factors influencing the accuracy of metabolite quantification. Generally, a recycle time of at least five times the longitudinal

relaxation time (T_1) of the slowest relaxing nuclei is required to allow a complete relaxation of all nuclei in metabolites and internal standard molecules. When extremely accurate quantitative measurements are required, T_1 measurements are usually performed on the sample of interest to set up the proper recycle time which essentially provides a complete nuclear relaxation. On the contrary, when a comparison between samples is needed without accurate quantifications, a recycle delay of 5-10 sec is generally applied, in order to have a good signal to noise ratio. The traditional widely used quantification method is the integration of a specific signal area vs. the signal area of a reference compound, whose exact quantity has to be known. Typically, in aqueous solutions, trimethylsilylpropanoic acid sodium salt (TSP), and sodium trimethylsilyl propanesulfonate (DSS) have been mainly used, whereas hexamethyl-disiloxane (HMDSO) has been proposed for organic solutions, since tetramethylsilane (TMS), generally used as a chemical shift reference is not stable because of its high volatility. Anyway, other "new" internal standards have been proposed (Harris et al., 2008; Rundlöf et al., 2010). An

alternative to the use of internal standard is represented by the Electronic REference To access In vivo Concentrations (ERETIC) method (Akoka et al., 1999) that provides a reference signal synthesized by an electronic device. A particular attention in the integration procedure has to be taken when the ^{1}H spectrum of a foodstuff sample is dominated by the water peak. In this case, it is difficult to perform a correct quantitative analysis of the signals close to the water signal tail. Moreover, water suppression procedures can also partially saturate the resonances near the water signal affecting their quantification. So, water suppression experimental parameters must be accurately calibrated. Other factors that can represent a source of error during integration are signals overlapping, solved with deconvolution or 2D J-resolved experiments, and chemical shifts variations. In this case, manual integration or bucketing approaches can be useful in solving these issues. Manual integration is a time-spending approach, mainly when many signals and many samples have to be considered.

Finally, another approach consisting in the measure of the signal height, reported as signal intensity, is used instead of the

integral for quantitative measurements, since, as in the case of the integral, signal intensity is proportional to the compound concentration. In order to use this approach, the signal linewidths of each specific resonance has to be the same in all the compared spectra. The measurement of the intensity can be performed manually or in the case of many signals using an automatic peak peaking procedure.

4.2.6. Data statistical analysis

The NMR metabolic analysis generates a large amount of data from which it is necessary to extract the desired information using chemometric methods that can identify possible patterns among samples. In fact, since the number of identified metabolites and the number of studied samples can be very consistent, the only possibility of generating some final consideration or hypothesis from the obtained data is represented by the application of several statistical approaches. The nature of quantitative data extracted from an NMR spectrum (all data points, buckets, integral or intensity of selected resonances) influences the choice of the statistical

approach for their elaboration. To be properly applied, any statistical approach has to take into account several important aspects of data, such as number of variables, the data redundancy, and possible noise. When a quantitative analysis is performed using all NMR spectral data points, the statistical elaboration has to face the problems of high data redundancy and noise introduction. The role of any single metabolite in statistical models is not easily deducible, but the data analysis is quick, and experimental data is not excluded a priori, thus avoiding the risk of losing any pertinent information. Bucketing reduces the number of variables and hence data redundancy, but again the variables (buckets) are not necessarily associated with single metabolites thus hindering the interpretation of statistical results in terms of individual metabolic contributions. In many cases, when data points or bucketing approaches are used after detecting the signals or spectral regions responsible for the most significant differences, the identification of corresponding metabolites can be carried out (Figure 4. 5).

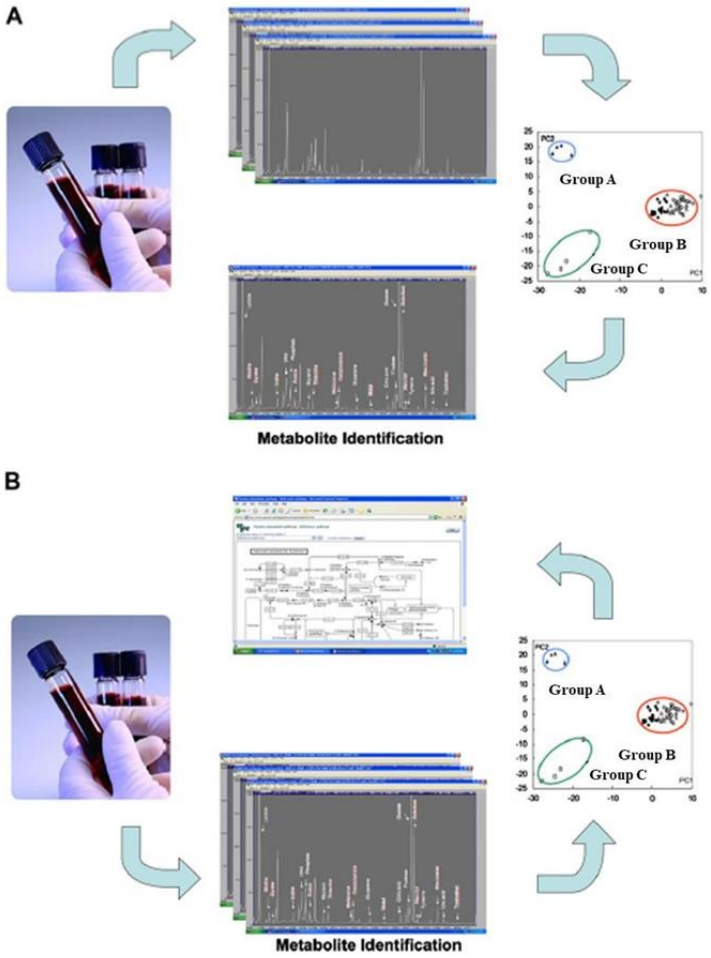


Figure 4. 5. Schematic illustration of the chemometric approaches to metabolomics. A) The multivariate statistical analysis is performed on the obtained spectra. After identifying significant differences, the most informative peaks in the spectra are assigned using a variety of methods. B) The multivariate statistical analysis is performed on the identified metabolites.

Finally, the statistical analysis of integrals or intensities of selected resonances requires time consuming assignment and quantification procedures. The selection of signals, avoiding the data-redundancy problem, is an advantage with respect to other quantitative approaches, but pertinent information deriving from non-selected resonances could be lost. Additionally, the interpretation of the statistical results in terms of individual metabolic contributions is straightforward.

Two types of statistical approaches can be used for data analysis, namely univariate and multivariate (Andre & Soukoulis, 2020). Among these, multivariate statistical analysis is generally applied for the processing of NMR data of complex matrices such as foodstuffs, by means of unsupervised and supervised approaches. Explorative unsupervised analysis is often the first step of statistical treatment. Structure of data, presence of outliers and natural grouping of samples can be revealed at this step and in many cases, the obtained results are sufficient to distinguish different groups of samples according to metabolic differences. However, in the case of classification

and prediction problems, the application of supervised multivariate techniques is necessary.

When multiple spectra are collected on a set of samples, after the necessary processing actions the obtained data are normally arranged into a rectangular matrix X, having as many rows as the number of samples and as many columns as the variables that have been chosen as descriptors for the system. This matrix represents the basis for the multivariate data analysis.

Explorative unsupervised analysis

The exploratory data analysis consists in trying to summarize the main characteristics of the data in an easy-to-understand way, mainly through the use of graphical tools and without the formulation of any statistical model or *a priori* hypothesis (Biancolillo et al., 2020). The main aims of unsupervised data analysis are to maximize insight into a data set, to uncover its underlying structure (e.g., spontaneous clustering, trends in data time series), to identify relevant variables, and to detect outliers and anomalies.

- *Principal Component Analysis (PCA):* The variables extracted from NMR spectra define a multidimensional space where every spectrum and corresponding sample can be represented by a single point. Considering that the number of variables typically used in metabolomic studies is always higher than 3, the data space cannot be simply visualized, but, using the PCA it is possible to transform the multidimensional space of experimental variables into a space with reduced mutually orthogonal dimensions that are a linear combination of variables, called principal components. PCA is the main chemometric tool for exploratory data analysis since it allows the compression of the relevant information of a data set into a reduced set of abstract variables (the principal components). PCA is commonly used as an explorative technique in multivariate analysis, having proven to be a powerful and widely applicable technique. However, PCA may not be suitable if the effect of interest is not the main source of data variability

and is masked in PCA by other factors with higher variability.

- *Tree clustering analysis (TCA),* also called hierarchical clustering analysis (HCA): It is another unsupervised exploration method used to discover the natural grouping (clustering) of samples. Tree clustering methods join together objects (samples) into successively larger clusters, using amalgamation rules for clusters and some measurements of the distance between single objects. The statistical results are reported as a dendrogram. All possible classifications in a prescribed number of groups can be obtained by cutting the tree at a suitable level.

Supervised classification/regression methods

In some situations, the spectral profiles recorded by NMR constitute the basis to build predictive models, i.e., models that allow not only the description of the main features of the samples under investigation, but also predict one or more characteristics of new samples. In particular,

depending on the nature of the properties to be predicted, two families of methods can be distinguished: calibration methods, used to predict quantitative properties, and classification methods, that provide qualitative answers. Since the final aim of these methods is to be able to accurately predict the desired properties on new (unknown) samples, it is mandatory that, at least, two requirements are met: a sufficient number of training samples, and a careful validation step, to test the reliability of the approach providing also a quantitative estimate of the error. Validation (Westad & Marini, 2015) is indeed an unavoidable step for any predictive model, as it guarantees the applicability of the methods to any future sample: in a very general way, it consists in applying the model to a new set of samples, that are treated as unknown by the model itself but for which the "true" values of the responses to be predicted are available to the experimenter.

Indeed, the aim of classification methods is to define a mathematical criterion to assign an individual (a sample) to one group (category or class) based on the measured

variables. The main applied supervised methods in foodstuffs NMR metabolomics are:

- *Partial Least Square (PLS) regression*: this approach can be chosen to create a prediction model, in which the features from PCA and multiple regression are generalised and combined. Unlike PCA, PLS studies the relationship between two data matrices, X and Y. Matrix X contains the data extracted from NMR spectra for each sample, whereas matrix Y contains extra information on samples obtained using reference methodologies. PLS transforms the multidimensional space of variables from matrix X into a new coordinate system with axes corresponding to the highest covariance between measured NMR data (matrix X) and the response variables (matrix Y). In this way, the relationship between the NMR spectra and other properties of food samples can be used to predict these properties directly based on NMR data.
- *Linear Discriminant Analysis (LDA):* this method is based on linear combinations of original variables, that

maximises the difference between a priori defined classes. In LDA the hyperspace of the variables is divided in as many regions as the number of available categories or classes. LDA is rather sensitive to data redundancy and a reliable model can be built only using a limited number of original non-correlated variables and a sufficient number of samples for each category.

- *PLS-DA*: taking advantages of both statistical approaches PLS and LDA, and avoiding their weaknesses, PLS-DA has found many applications in the analysis of NMR metabolomic data. In PLS-DA, the information about the variables responsible for the classification of samples is obtained by examining VIP scores (Variable Importance in Projection) and the regression coefficients.
- *Soft Independent Modelling of Class Analogies (SIMCA):* it is a class-modelling technique, that acts by defining the category space of one class at a time and is more focused on the similarities among samples of the same class than on the differences among the classes as in the case of

discriminant analysis. Consequently, each sample can be assigned to one or more classes or to none of them.

4.3. References

Akoka, S., Barantin, L., & Trierweiler, M. (1999). Concentration Measurement by Proton \textsc{nmr} Using the \textsc{eretic} Method. *Analytical Chemistry*, *71*(13), 2554\,–\,7.

Andre, C. M., & Soukoulis, C. (2020). Food quality assessed by chemometrics. *Foods*, *9*(7), 2–5. https://doi.org/10.3390/foods9070897

Avenoza, A., Busto, J. H., Canal, N., & Peregrina, J. M. (2006). Time course of the evolution of malic and lactic acids in the alcoholic and malolactic fermentation of grape must by quantitative 1H NMR (qHNMR) spectroscopy. *Journal of Agricultural and Food Chemistry*, *54*(13), 4715–4720. https://doi.org/10.1021/jf060778p

Ben-Zvi, D., Bakker, A., & Makar, K. (2015). Learning to reason from samples. *Educational Studies in Mathematics*, *88*(3), 291–303. https://doi.org/10.1007/s10649-015-9593-3

Bernal, J., Mendiola, J. A., Ibáñez, E., & Cifuentes, A. (2011). Advanced analysis of nutraceuticals. *Journal of Pharmaceutical and Biomedical Analysis*, *55*(4), 758–774.

https://doi.org/10.1016/j.jpba.2010.11.033

Biancolillo, A., Marini, F., & Ruckebusch, C. (2020). Chemometric Strategies for Spectroscopy-Based Food Authentication. *Applied Sciences (Switzerland)*, *10*, 6544. https://doi.org/doi:10.3390/app10186544

Bingol, K., Zhang, F., Bruschweiler-Li, L., & Brüschweiler, R. (2012). TOCCATA: A customized carbon total correlation spectroscopy NMR metabolomics database. *Analytical Chemistry*, *84*(21), 9395–9401. https://doi.org/10.1021/ac302197e

Bligh, E.G. and Dyer, W. J. (1959). A rapid method of total lipid extraction and purification. *Canadian Journal of Biochemistry and Physiology*, *37*(8).

Breil, C., Abert Vian, M., Zemb, T., Kunz, W., & Chemat, F. (2017). "Bligh and Dyer" and Folch methods for solid–liquid–liquid extraction of lipids from microorganisms. Comprehension of solvatation mechanisms and towards substitution with alternative solvents. *International Journal of Molecular Sciences*, *18*(4), 1–21. https://doi.org/10.3390/ijms18040708

Capitani, D., Mannina, L., Proietti, N., Sobolev, A. P., Tomassini, A., Miccheli, A., Di Cocco, M. E., Capuani, G., De Salvador, F. R., & Delfini, M. (2013). Metabolic profiling and outer pericarp water state in zespri, CI.GI, and hayward kiwifruits. *Journal of Agricultural and Food Chemistry*, *61*(8), 1727–1740. https://doi.org/10.1021/jf3028864

Capitani, D., Sobolev, A. P., Tomassini, A., Sciubba, F., De Salvador, F. R., Mannina, L., & Delfini, M. (2013). Peach fruit: Metabolic comparative analysis of two varieties with different resistances to insect attacks by NMR spectroscopy. *Journal of Agricultural and Food Chemistry*, *61*(8). https://doi.org/10.1021/jf303248z

Dais, P., Spyros, A., Christophoridou, S., Hatzakis, E., Fragaki, G., Agiomyrgianaki, A., Salivaras, E., Siragakis, G., Daskalaki, D., Tasioula-Margari, M., & Brenes, M. (2007). Comparison of analytical methodologies based on 1H and 31P NMR spectroscopy with conventional methods of analysis for the determination of some olive oil constituents. *Journal of Agricultural and Food Chemistry*,

55(3), 577–584. https://doi.org/10.1021/jf061601y

Duarte, I. F., Barros, A., Almeida, C., Spraul, M., & Gil, A. M. (2004). Multivariate Analysis of NMR and FTIR Data as a Potential Tool for the Quality Control of Beer. *J. Agric. Food Chem.*, *52*(5), 1031–1038. https://doi.org/https://doi.org/10.1021/jf030659z

Dunn, W. B., & Ellis, D. I. (2005). Metabolomics: Current analytical platforms and methodologies. *TrAC - Trends in Analytical Chemistry*, *24*(4), 285–294. https://doi.org/10.1016/j.trac.2004.11.021

Evans, C. J., Puts, N. A. J., Robson, S. E., Boy, F., McGonigle, D. J., Sumner, P., Singh, K. D., & Edden, R. A. E. (2013). Subtraction artifacts and frequency (Mis-)alignment in J-difference GABA editing. *Journal of Magnetic Resonance Imaging*, *38*(4), 970–975. https://doi.org/10.1002/jmri.23923

Fan, T. W. M. (1996). Metabolite profiling by one- and two-dimensional NMR analysis of complex mixtures. *Progress in Nuclear Magnetic Resonance Spectroscopy*, *28*(2), 161–219. https://doi.org/10.1016/0079-6565(95)01017-3

Folch, J., Ascoli, I., Lees, M., Meath, J. A., & Lebaron, F. N.

(1951). Preparation of lipid extracts from brain tisue. *J. Biol. Chem.*, *191*, 833–841.

Folch, J., Lees, M., & Sloane Stanley, G. . (1956). A simple method for the isolation and purification of total lipides from animal tissues. *J. Biol. Chem.*, *226*, 497–509.

Fulmer, G. R., Miller, A. J. M., Sherden, N. H., Gottlieb, H. E., Nudelman, A., Stoltz, B. M., Bercaw, J. E., & Goldberg, K. I. (2010). NMR chemical shifts of trace impurities: Common laboratory solvents, organics, and gases in deuterated solvents relevant to the organometallic chemist. *Organometallics*, *29*(9), 2176–2179. https://doi.org/10.1021/om100106e

Harris, R. K., Becker, E. D., Cabral De Menezes, S. M., Granger, P., Hoffman, R. E., & Zilm, K. W. (2008). Further conventions for NMR shielding and chemical shifts (IUPAC Recommendations 2008). *Pure and Applied Chemistry*, *80*(1), 59–84. https://doi.org/10.1351/pac200880010059

Hu, B., Gao, J., Xu, S., Zhu, J., Fan, X., & Zhou, X. (2020). Quality evaluation of different varieties of dry red wine based on

nuclear magnetic resonance metabolomics. *Applied Biological Chemistry*, *63*(1). https://doi.org/10.1186/s13765-020-00509-x

Ingallina, C., Spano, M., Sobolev, A. P., Esposito, C., Santarcangelo, C., Baldi, A., Daglia, M., & Mannina, L. (2020). Characterization of Local Products for Their Industrial Use : The Case of Italian Potato Cultivars Analyzed by Untargeted and Targeted Methodologies. *Foods*, *9*(9), 1–15.

Mannina, L., Sobolev, A. P., Capitani, D., Iaffaldano, N., Rosato, M. P., Ragni, P., Reale, A., Sorrentino, E., D'Amico, I., & Coppola, R. (2008). NMR metabolic profiling of organic and aqueous sea bass extracts: Implications in the discrimination of wild and cultured sea bass. *Talanta*, *77*(1), 433–444. https://doi.org/10.1016/j.talanta.2008.07.006

Mannina, Luisa, Sobolev, A. P., & Viel, S. (2012). Liquid state 1H high field NMR in food analysis. In *Progress in Nuclear Magnetic Resonance Spectroscopy* (Vol. 66). https://doi.org/10.1016/j.pnmrs.2012.02.001

McKenzie, J. S., Donarski, J. A., Wilson, J. C., & Charlton, A. J.

(2011). Analysis of complex mixtures using high-resolution nuclear magnetic resonance spectroscopy and chemometrics. *Progress in Nuclear Magnetic Resonance Spectroscopy*, *59*(4), 336–359. https://doi.org/10.1016/j.pnmrs.2011.04.003

Novoa-Carballal, R., Fernandez-Megia, E., Jimenez, C., & Riguera, R. (2011). NMR methods for unravelling the spectra of complex mixtures. *Natural Product Reports*, *28*(1), 78–98. https://doi.org/10.1039/c005320c

Rundlöf, T., Mathiasson, M., Bekiroglu, S., Hakkarainen, B., Bowden, T., & Arvidsson, T. (2010). Survey and qualification of internal standards for quantification by 1H NMR spectroscopy. *Journal of Pharmaceutical and Biomedical Analysis*, *52*(5), 645–651. https://doi.org/10.1016/j.jpba.2010.02.007

Schievano, E., Finotello, C., De Angelis, E., Mammi, S., & Navarini, L. (2014). Rapid authentication of coffee blends and quantification of 16-O-methylcafestol in roasted coffee beans by nuclear magnetic resonance. *Journal of Agricultural and Food Chemistry*, *62*(51), 12309–12314.

https://doi.org/10.1021/jf505013d

Schievano, E., Peggion, E., & Mammi, S. (2010). 1H nuclear magnetic resonance spectra of chloroform extracts of honey for chemometric determination of its botanical origin. *Journal of Agricultural and Food Chemistry*, *58*(1), 57–65. https://doi.org/10.1021/jf9022977

Smlinska, A., Blanchet, L., Buydens, L. M. C., & Wijmenga, S. S. (2012). NMR and pattern recognition methods in metabolomics: From data acquisition to biomarker discovery: A review. *Analytica Chimica Acta*, *750*, 82–97. https://doi.org/10.1016/j.aca.2012.05.049

Sobolev, Anatoli P., Brosio, E., Gianferri, R., & Segre, A. L. (2005). Metabolic profile of lettuce leaves by high-field NMR spectra. *Magnetic Resonance in Chemistry*, *43*(8), 625–638. https://doi.org/10.1002/mrc.1618

Sobolev, Anatoly P., Mannina, L., Capitani, D., Sanzò, G., Ingallina, C., Botta, B., Fornarini, S., Crestoni, M. E., Chiavarino, B., Carradori, S., Locatelli, M., Giusti, A. M., Simonetti, G., Vinci, G., Preti, R., Toniolo, C., Reverberi, M., Scarpari, M., Parroni, A., … Di Sotto, A. (2018). A

multi-methodological approach in the study of Italian PDO "Cornetto di Pontecorvo" red sweet pepper. *Food Chemistry*, *255*(February), 120–131. https://doi.org/10.1016/j.foodchem.2018.02.050

Sundermann, A., Eggers, L. F., & Schwudke, D. (2016). Liquid Extraction: Bligh and Dyer. In *Encyclopedia of Lipidomics*. Springer Science. https://doi.org/DOI 10.1007/978-94-007-7864-1_88-1

Tulpan, D., Léger, S., Belliveau, L., Culf, A., & Čuperlović-Culf, M. (2011). MetaboHunter: An automatic approach for identification of metabolites from 1H-NMR spectra of complex mixtures. *BMC Bioinformatics*, *12*, 1–22. https://doi.org/10.1186/1471-2105-12-400

Zhu, D., Kebede, B., Chen, G., McComb, K., & Frew, R. (2020). Impact of freeze-drying and subsequent storage on milk metabolites based on 1H NMR and UHPLC-QToF/MS. *Food Control*, *116*, 107017. https://doi.org/10.1016/j.foodcont.2019.107017

Chapter 5: NMR metabolomics for the valorization of Italian local products and for the quality preservation of vegetables

5.1. Introduction

A natural product is characterized by an extremely complex and variable composition depending on various factors. While, inside the natural products world, a given foodstuff is characterized by a "reproducible" well-defined chemical composition. However, qualitative and quantitative differences can be found due to several factors (origin, variety, pedoclimatic conditions, post-harvesting treatments). These differences can give rise to change in food nutritive and sensorial (colour, shape, aromas, etc.) characteristics.

Nowadays market is mainly focused on the extensive production of only few varieties of each foodstuff. In fact, in many Italian regions, local products are cultivated and used only for the local consumption. Therefore many varieties and biodiversity tend to be lost due to the agronomic and commercial selection of only a few varieties. Another factor that contribute to the loss of crop biodiversity is the replacement of local varieties with high-yielding species. Hence, a limited number of varieties are cultivated and products coming from extensive productions, sometimes deceptively labelled as

"Made in Italy", are imported to satisfy the high food request. In this context, high field NMR spectroscopy has been applied to characterize and therefore valorize local Italian products.

In this context, several local products typical of different Italian regions have been studied and characterized. The aim is to deepen the knowledge of the matrix in order to valorize the products and bring out the biodiversity of each food variety. In particular, the following case studies have been considered:

- Case study 1: Torpedino di Fondi and San Marzano tomato cultivars of Lazio region (Ingallina et al., 2020);
- Case study 2: Ten apple cultivars from the Piedmont Region (Di Matteo, Spano, et al., 2021);
- Case study 3: Goji berries cultivars cultivated in Lazio region (Spano et al., 2021).

Another aim of the chemical characterization of food matrices is the study of the shelf-life and the development of new solution for its extension. In fact the food packaging plays an essential role in preserving food throughout the distribution chain. Without packaging, the direct contact with physical, chemical, and biological contaminants can drastically

compromise food quality and nutritional health value. In this regard, food industries have increased attention towards products with improved nutritional quality and health promoting properties and towards the use of proper packaging materials. Packaging has to be capable of maintaining food sensorial and nutritional quality and guaranteeing food safety both in international and national markets even in complex conditions. In the twentieth century, the innovation of packaging underwent a rapid evolution thanks also to the discovery and marketing of new materials as plastics and derivatives. Nowadays, in many countries, including Italy, more than 70% of packaging is destined for the food industry. However, over time, the generation of a large amount of food packaging waste has become an extremely critical point, with Europe reaching 65% of the total packaging waste production. Traditional polymeric materials from mineral oils are characterized by long degradation times and are the main responsible for plastic pollution and environmental damage. In addition, this type of packaging can represent a possible carrier of food contaminants. The introduction of eco-sustainable bio

packaging in food packaging represents a current requirement to which the scientific community and national and international legislative bodies have been working together. In the following paper, the mechanical and chemical/physical properties (studied also by NMR methodology) as well as the functionality of three commercial biofilms on cut pumpkin were investigated.

- Case study 4: Metabolomic NMR profile of pumpkin packaged with commercial biofilms (Di Matteo, et al., 2021)

References

Di Matteo, G., Di Matteo, P., Sambucci, M., Tirill, J., Giusti, A. M., Vinci, G., Gobbi, L., Prencipe, S. A., Salvo, A., Ingallina, C., Spano, M., Sobolev, A. P., Proietti, N., Tullio, V. Di, Russo, P., Mannina, L., & Valente, M. (2021). Commercial Bio-Packaging to Preserve the Quality and Extend the Shelf-Life of Vegetables : The Case-Study of Pumpkin Samples Studied by a Multimethodological Approach. *Foods*, 1–24.

Di Matteo, G., Spano, M., Esposito, C., Santarcangelo, C., Baldi, A., Daglia, M., Mannina, L., Ingallina, C., & Sobolev, A. P. (2021). NMR Characterization of Ten Apple Cultivars from the Piedmont Region. *Foods*, *10*(289). https://doi.org/https://doi.org/10.3390/foods10020289

Ingallina, C., Maccelli, A., Spano, M., Di Matteo, G., Sotto, A. Di, Giusti, A. M., Vinci, G., Giacomo, S. Di, Rapa, M., Ciano, S., Fraschetti, C., Filippi, A., Simonetti, G., Cordeiro, C., Silva, M. S., Crestoni, M. E., Sobolev, A. P., Fornarini, S., & Mannina, L. (2020). Chemico-biological characterization of torpedino di fondi® tomato fruits: A comparison with san marzano cultivar at two ripeness stages. *Antioxidants*, *9*(10), 1–29. https://doi.org/10.3390/antiox9101027

Spano, M., Maccelli, A., Matteo, G. Di, Ingallina, C., Biava, M., Crestoni, M. E., Bardaud, J., Giusti, A. M., Mariano, A., Abusco, A. S. D., Sobolev, A. P., Lasalvia, A., Fornarini, S., & Mannina, L. (2021). Metabolomic Profiling of Fresh Goji (Lycium barbarum L .) A Multi-Methodological Approach. *Molecules*, 1–23.

5.2. Case study 1: Torpedino di Fondi and San Marzano tomato cultivars of Lazio Region

Torpedino di Fondi cultivar is a new hybrid variety known as "Mini-San Marzano" characterized by a peculiar sweetness and palatability. It is cultivated in the Lazio Region of Central Italy, in the Ciociaria area which is characterized by a sandy-loamy soil with a high degree of salinity and a Mediterranean climate with relatively dry and warm summers and humid winters.

In the present work, organic and hydroalcolic fractions obtained by Blight-Dyer extraction of San Marzano and Torpedino di Fondi varieties harvested in two developmental stages (ripe and unripe) were analyzed by untargeted methodologies namely high field NMR and ESI FT-ICR MS methodologies. Both NMR and ESI FT-ICR MS allowed to detect different classes of metabolites (sugars, amino acids, organic acid, fatty acids) and to monitor the metabolite concentration during the ripening

antioxidants

MDPI

Article

Chemico-Biological Characterization of Torpedino Di Fondi® Tomato Fruits: A Comparison with San Marzano Cultivar at Two Ripeness Stages

Cinzia Ingallina [1,†], Alessandro Maccelli [1,†], Mattia Spano [1], Giacomo Di Matteo [1], Antonella Di Sotto [2], Anna Maria Giusti [3], Giuliana Vinci [4], Silvia Di Giacomo [2], Mattia Rapa [4], Salvatore Ciano [4], Caterina Fraschetti [1], Antonello Filippi [1], Giovanna Simonetti [5], Carlos Cordeiro [6], Marta Sousa Silva [6], Maria Elisa Crestoni [1,*], Anatoly P. Sobolev [7,*], Simonetta Fornarini [1] and Luisa Mannina [1]

1 Dipartimento di Chimica e Tecnologie del Farmaco, Sapienza Università di Roma, P. le Aldo Moro 5, 00185 Rome, Italy; cinzia.ingallina@uniroma1.it (C.I.); alessandro.maccelli@uniroma1.it (A.M.); mattia.spano@uniroma1.it (M.S.); giacomo.dimatteo@uniroma1.it (G.D.M.); caterina.fraschetti@uniroma1.it (C.F.); antonello.filippi@uniroma1.it (A.F.); simonetta.fornarini@uniroma1.it (S.F.); luisa.mannina@uniroma1.it (L.M.)

2 Dipartimento di Fisiologia e Farmacologia "V. Ersparmer", Sapienza Università di Roma, P. le Aldo Moro 5, 00185 Rome, Italy; antonella.disotto@uniroma1.it (A.D.S.); silvia.digiacomo@uniroma1.it (S.D.G.)

3 Dipartimento di Medicina Sperimentale Sapienza, Università di Roma, P. le Aldo Moro 5, 00185 Rome, Italy; annamaria.giusti@uniroma1.it

4 Dipartimento di Management, Laboratorio di Merceologia, Sapienza Università di Roma, Via del Castro Laurenziano 9, 00161 Rome, Italy; giuliana.vinci@uniroma1.it (G.V.); mattia.rapa@uniroma1.it (M.R.); salvatore.ciano@uniroma1.it (S.C.)

5 Dipartimento di Biologia Ambientale, Sapienza Università di Roma, P. le Aldo Moro 5, 00185 Rome, Italy; giovanna.simonetti@uniroma1.it

6 Laboratório de FT-ICR e Espectrometria de Massa Estrutural, Faculdade de Ciências da Universidade de Lisboa, Campo-Grande, 1749-016 Lisboa, Portugal; cacordeiro@fc.ul.pt (C.C.); mfsilva@fc.ul.pt (M.S.S.)

7 Istituto per i Sistemi Biologici, Laboratorio di Risonanza Magnetica "Annalaura Segre", CNR, 00015 Rome, Italy

* Correspondence: mariaelisa.crestoni@uniroma1.it (M.E.C.); anatoly.sobolev@cnr.it (A.P.S.); Tel.: +39-06-4991-3596 (M.E.C.); +39-06-9067-2385 (A.P.S.)

† These authors gave an equal contribution to this work.

Received: 23 September 2020; Accepted: 15 October 2020; Published: 21 October 2020



Abstract: Torpedino di Fondi (TF) is a hybrid tomato landrace developed in Sicily and recently introduced in the south Lazio area along with the classical San Marzano (SM) cultivar. The present study aimed at characterizing TF tomatoes at both pink and red ripening stages, and at comparing them with traditional SM tomatoes. A multidisciplinary approach consisting of morphological, chemical (FT-ICR MS, NMR, HPLC, and spectrophotometric methods), and biological (antioxidant and antifungal in vitro activity) analyses was applied. Morphological analysis confirmed the mini-San Marzano nature and the peculiar crunchy and solid consistency of TF fruits. Pink TF tomatoes displayed the highest content of hydrophilic antioxidants, like total polyphenols (0.192 mg/g), tannins (0.013 mg/g), flavonoids (0.204 mg/g), and chlorophylls a (0.344 mg/g) and b (0.161 mg/g), whereas red TF fruits were characterized by the highest levels of fructose (3000 mg/100 g), glucose (2000 mg/100 g), tryptophan (2.7 mg/100 g), phenylalanine (13 mg/100 g), alanine (25 mg/100 g), and total tri-unsaturated fatty acids (13% mol). Red SM fruits revealed the greatest content of lipophilic antioxidants, with 1234 mg/g of total carotenoids. In agreement with phenolics content, TF cultivar showed the greatest antioxidant activity. Lastly, red TF inhibited *Candida* species (*albicans*, *glabrata* and *krusei*) growth.

Keywords: tomatoes; NMR spectroscopy; FT-ICR mass spectrometry; ripening stage; phenolics; antioxidant activity; metabolomics; phytochemicals

1. Introduction

San Marzano (SM) is a traditional tomato landrace grown in south Italy suitable for both fresh consumption and processing. The distinct SM organoleptic properties made this variety a worldwide model for tomato quality traits, although the scarcity of genetic resistance against pathogens represents a critical SM weakness [1]. Throughout the years, both natural and in vitro selections have led to new SM tomatoes with peculiar accessions; however, several ecotypes not suitable for local environments gradually disappeared. The term "San Marzano" refers to a population of tomatoes with a wide range of characteristics [2]. In this context, a new SM cultivar, namely, Torpedino di Fondi (TF) has been recently introduced in the south Lazio area. Developed in Sicily (Licata and Vittoria), TF is characterized by a peculiar sweetness and palatability and, due to its smaller size and weight compared to SM, it is defined as mini-San Marzano.

Different analytical methodologies, such as NMR, MS, GC-MS, and HPLC, have been applied to characterize different SM cultivars from chemical [2–7], sensorial [4,5], and genomic [1,4,8] points of view. However, to the best of our knowledge, TF tomatoes have not been characterized yet.

It is well established that plants and vegetable foodstuffs represent a unique reservoir of nutrients and phytochemicals with health implications [9]. Tomatoes and tomato-based food have proven to possess a wide variety of bioactive compounds that are beneficial for human well-being; among these, dietary antioxidants like carotenoids, polyphenols, and vitamins are the most abundant in tomato fruits. Indeed, carotenoids have shown to play an important role in reducing the incidence of some chronic diseases, like cancer and cardiovascular diseases [10], whereas polyphenols in tomatoes have proved to prevent the oxidative damage [11–14] in human cells. Recently, the influence of the cultivation system on the polyphenols content has been found to depend mostly on variety and year than the cultivation and drying methods [15,16].

Moreover, a recent study provided evidence on the activity of ethanolic extracts of *Solanum lycopersicum* at concentration of 6.25 mg/mL against *C. albicans*, *C. guilliermondii*, and *C. lusitaniae* isolated from HIV positive patients [17]. Conversely, extracts from tomato crop remains at the end of the cultivation cycle displayed a low antifungal activity against the microfungi *Aspergillus* and *Penicillium species* [18]. Interestingly, an antimicrobial snaking peptide (SN2) obtained from *Solanum lycopersicum* tested as a recombinant peptide in *E. coli* exhibited strong fungicidal bioactivity ascribed to biomembrane perforation [19]. *Candida* spp. is present in the gut, but an overproduction may lead to serious health problems. Some diseases, such as Crohn's disease and ulcerative colitis, are associated with an overgrowth of *Candida* in the gastrointestinal tract [20]. *Candida* overgrowth can be prevented by healthy foods.

The aim of the present study was to fully characterize for the first time TF tomatoes at pink and red ripeness stages, both considered ideal for fresh consumption, through the investigation of morphological characteristics, metabolite profile (carbohydrates, amino acids, organic acids, polyphenols, pigments, sterols, fatty acids), and the evaluation of antioxidant and antifungal (towards *Candida* spp.) properties of tomato extracts. In this study, a comparison with traditional SM tomatoes was also carried out at the same experimental conditions.

The present multidisciplinary analytical approach here employed was already successfully applied to other matrices such as sweet pepper [21], celery [22], extra-virgin olive oil [23], hemp inflorescences [24], but never to tomato fruits. In this study, the powerful combination of high-resolution NMR spectroscopy and FT-ICR MS, not yet widely exploited and largely complementing each other, allowed to obtain a broad untargeted chemical profile, whereas HPLC and spectrophotometric targeted methodologies enabled the content of biogenic amines, polyphenols, and pigments, respectively, to be quantified.

Herein, a biological evaluation of the extracts was finally carried out in terms of antioxidant properties, antifungal activity, and enzyme inhibition. The combined results of radical-scavenging activity, formation of advanced glycation final product (AGE), and the cytoprotective activity towards the oxidative damage induced by tert-butyl hydroperoxide solution (tBuOOH) has allowed to estimate the TF and SM tomatoes antioxidant properties. Moreover, in vitro antifungal activity of the tomatoes extracts towards four *C. albicans*, three *C. glabrata*, and two *C. krusei* strains was assayed.

2. Materials and Methods

2.1. Plant Material

Fresh fruits of *Solanum lycopersicum* L. TF variety were grown and collected by Mafalda SRL (41.342622, 13.420856), whereas SM fresh fruits were grown and collected by San Leone Agricultural Cooperative (41.293929, 13.397638) sited both in Fondi (Latina, Italy). Fondi is characterized by a Mediterranean climate with an average air temperature (T) = 19.5 °C and humidity = 54.1% during the growing season. Irrigation and plant protection, as well as the weed control were carried out following local practices. Samples were harvested at two different ripening stages according to market demand, namely pink (P) stage (from 30% to 60% of not green tomato skin) and red stage (R) (about 90% of not green tomato skin) showing a red colour (Figure S1). Peduncles were removed, some fresh fruits were subjected to morphological analysis and the extraction procedure, while other samples were instantly stored at −80 °C.

2.2. Chemicals

Rutin, quercetin, 2,2-diphenyl-1-picrylhydrazyl (DPPH), 2,2′-azino-bis(3-thylbenzothiazoline-6-sulfonic acid) diammonium salt (ABTS), 2,2′-azobis(2-methylpropionamidine) dihydrochloride (AAPH), trolox, polyvinylpyrrolidone (PVP), tert-butyl hydroperoxide solution (tBuOOH; 900 mg mL^{-1}), ferrozine, hydroxylamine hydrochloride, iron(III) chloride ($FeCl_3 \times 6H_2O$), iron(II) sulfate heptahydrate ($FeSO_4 \times 7H_2O$), potassium hexacyanoferrate(III), iron(II) chloride ($FeCl_2 \times 4H_2O$), magnesium oxide, doxorubicin, 3-(4,5-dimethylthiazol-2-yl)-2,5-diphenyltetrazolium bromide (MTT), 2,7-dichlorofluorescein diacetate (DCFH-DA), and the solvents (HPLC-MS purity grade) were purchased from Sigma-Aldrich (Milan, Italy). Methanol (HPLC-grade), formic acid (99%), perchloric acid (70%), acetone (analytical-grade), chloroform, acetonitrile (HPLC-grade) were obtained from Carlo Erba Reagenti (Milan, Italy). Double-distilled water was obtained using a Millipore Milli-Q Plus water treatment system (Millipore Bedford Corp., Bedford, MA). Sodium carbonate (Na_2CO_3; 99.999% purity), Folin–Ciocalteu's phenol reagent, tannic acid (Ph. Eur. purity) and aluminum chloride hexahydrate ($AlCl_3 \times 6H_2O$; Ph. Eur. purity) were purchased from Merck (Darmstadt, Germany). Deuterated water (D_2O) 99.97 atom% of deuterium, methanol-D4 99.80 atom% of deuterium, chloroform-D 99.80 atom% of deuterium + 0.03% tetramethylsilane (TMS), and 3-(trimethylsilyl)-propionic-2,2,3,3-d_4 acid sodium salt (TSP) were purchased from Euriso-Top (Saclay, France).

2.3. Morphological Analysis

Ten fresh fruits for both tomato varieties and redness stages were subjected to morphological analysis, in order to describe their size (length and diameter), weight, and shape. For each fruit, a careful separation of different components, including peel (i.e., exocarp of the fruit), pulp (i.e., mesocarp of the fruit), seeds (removed with the internal juice), and juice, was performed. The peel was gently separated from the pulp by using a scalpel. The detached components were examined and weighted, and their amount in the whole fruit was determined.

Pigments Characterization

The total carotenoids and chlorophylls analysis in peel and pulp of SM and TF tomatoes samples were performed according to Solovchenko and co-workers [25] with some modifications. The peel

was cut from the surface of the fruits, carefully freed from the pulp, and successively weighted. Both peel and pulp from each sample were twice washed with distilled water for 1 min and dried with filter paper. To remove the cuticular lipids, peel fraction was washed with 2 mL portion of chloroform for 1 min. Pigments were extracted according to the Folch method [26]. The samples were homogenized with mortar and pestle in 6 mL of chloroform-methanol (2:1, *v/v*) and, to prevent chlorophyll pheophytinization, 30 mg of MgO were added before the homogenization. The homogenate was passed through a paper filter and after an amount of distilled water equal to 1/5 of the extract volume was added. Finally, this mixture was centrifuged in a glass tube test for 20 min at 2469× *g* for 20 min at 10 °C to complete separation of chloroform fraction from hydroalcoholic one. Absorption spectra of the chloroform phase were recorded with a Beckman Coulter DU 800 instruments, in the range of 350–800 nm with a spectral resolution of 0.5 nm, at a temperature of 20 °C. The concentrations of chlorophyll a and b as well as total carotenoids (*mg/g* of sample) were determined according to Wellburn [27].

2.4. Extraction Procedures

Fifteen fresh whole fruits from pink TF (TF_P), red TF (TF_R), pink SM (SM_P), and red SM (SM_R) were frozen and ground in liquid nitrogen to obtain a homogeneous pool and subjected to the Bligh–Dyer extraction method, which allows to extract both water-soluble and liposoluble metabolites in a quantitative manner.

In details, about 1.0 g of samples (peel, pulp, and seeds) of each variety was added sequentially with 3 mL methanol/chloroform (2:1 *v/v*) mixture, 1 mL of chloroform, and 1.2 mL of distilled water. After each addition the sample was carefully shacked. The emulsion was maintained at 4 °C for 40 min. The sample was then centrifuged (4200× *g* for 15 min at 4 °C) and the upper (hydroalcoholic) and lower (organic) phases were carefully separated. The pellets were re-extracted using half of the solvent volumes (in the same conditions described above) and the separated fractions were pooled. Both hydroalcoholic and organic fractions were filtered with Whatman paper filters and dried under a gentle N_2 flow at room temperature until the solvent was completely evaporated [22]. The dried phases were stored at −20 °C until further analyses. The values of drug to extract ratio (DER) are reported in Table 1.

Table 1. Drug to extract ratio of Bligh–Dyer (hydroalcoholic and organic) extracts of both pink and red fruits from *Solanum lycopersicum* var. Torpedino di Fondi (TF) and San Marzano (SM) [a].

Sample	Drug/Extract Ratio (DER)	
	Hydroalcoholic	Organic
TF_P	20	274
TF_R	9	320
SM_P	20	447

[a] TF_P = pink TF; TF_R = red TF; SM_P = pink SM; SM_R = red SM.

2.5. Metabolite Profile

2.5.1. NMR Analysis

The dried organic fraction of each sample was dissolved in 0.7 mL of a $CDCl_3/CD_3OD$ mixture (2:1 *v/v*) and then placed into a 5 mm NMR tube. Finally, the NMR tube was flame sealed. Conversely, the dried hydroalcoholic phase of each sample was solubilized in 0.7 mL of 400 mM phosphate buffer/D_2O containing 1 mM solution of TSP as internal standard and then transferred into a 5 mm NMR tube. NMR spectra of all hydroalcoholic and organic extracts were recorded at 27 °C on a Bruker AVANCE 600 spectrometer operating at the proton frequency of 600.13 MHz and equipped with a Bruker multinuclear z-gradient 5 mm probe head. ^1H spectra were referenced to methyl group signals of TSP

(δ = 0.00 ppm) in D_2O and to the residual CHD_2 signal of methanol (set to 3.31 ppm) in $CD_3OD/CDCl_3$ mixture. ^1H spectra of hydroalcoholic extracts were acquired with 256 transients with a recycle delay of 5 s. The residual HDO signal was suppressed using a pre-saturation. The experiment was carried out by using 45° pulse of 6.5–7.5 μs, 32 K data points. ^1H spectra of extracts in $CD_3OD/CDCl_3$ were acquired with 256 transients, recycle delay of 5 s, and 90° pulse of 9–11 μs, 32 K data points. The two-dimensional (2D) NMR experiments, such as ^1H-^1H TOCSY, ^1H-^{13}C HSQC, and ^1H-^{13}C HMBC, were carried out under the same experimental conditions previously reported [28]. The integrals of 26 selected signals in hydroalcoholic extract (Table 2) were measured using the Bruker TOPSPIN software and normalized with respect to the resonance at 0.00 ppm, due to methyl group signal of TSP, set to 100. Results were expressed in mg/100 g fresh weight (FW). The quantification of components in organic extracts was described in a previous work [28].

Table 2. Compounds and relative signals ($\delta(^1H)$, ppm) selected for quantitative analysis in the hydroalcoholic and organic extracts.

Ppm	Compounds	Ppm	Compounds
		Hydroalcoholic	
0.96	Leucine	3.25	β-Glucose
0.99	Valine	4.04	Fructose
1.01	Isoleucine	4.31	Malic Acid
1.34	Threonine	4.59	β-Galactose
1.49	Alanine	5.25	α-Glucose
2.30	γ-amino butyric acid (GABA)	6.91	Tyrosine
2.35	Glutamic acid	7.34	Phenylalanine
2.46	Glutamine	7.74	Tryptophan
2.55	Citric Acid	8.14–8.17	Histidine
2.81	Aspartic acid	8.36	Adenosine
2.90	Asparagine	8.46	Formic Acid
3.04	Lysine	8.586	ADP
3.21	Choline	9.13	Trigonelline
		Organic	
0.66	β-Sitosterol	2.73	Di-unsaturated fatty acids (DUFAs)
0.68	Stigmasterol	2.77	Tri-unsaturated fatty acids (TUFAs)
2.30	Total fatty acids (FAs)	5.31	Total unsaturated fatty acids (UFAs)

2.5.2. FT-ICR MS Analysis

A portion (1 mg) of each dried Bligh–Dyer hydroalcoholic (H) and organic (O) fraction of TF and SM cultivars was dissolved in 1 mL (1:1) methanol/water and CH_2Cl_2, respectively. These stock solutions were then vortexed for 3 min, filtered through a 0.45 μm polypropylene Acrodisc (Sigma–Aldrich) syringe filter to remove debris and subsequently diluted in methanol so as to obtain a final concentration of 100 μg L^{-1}, a value chosen to limit ion suppression effects. For each extract, three distinct solutions prepared according to the above procedure were submitted to analysis. In positive mode MS, formic acid (1% *v*/*v*) was used to assist protonation, while leucine enkephalin (YGGFL, $C_{28}H_{37}N_5O_7$) was added to all samples at a final concentration of 0.5 μg L^{-1} as an internal reference (revealed as $[M+H]^+$ at *m*/*z* 556.27657 in positive mode and as $[M-H]^-$ at *m*/*z* 554.26202 in negative mode) to calibrate the spectra by means of the on-line calibration tool (Data Analysis 5.0, Bruker Daltonics). Further internal calibration was achieved by referring to a list of ubiquitous metabolites, including hexose/monosaccharides, citric and palmitic acids, reaching a routine mass accuracy lower than 0.2 ppm. Preliminary mass spectrometric surveys were carried out by using a Bruker BioApex Fourier transform ion cyclotron resonance (FT-ICR) [29] mass spectrometer (Bruker Daltonics GmbH, Bremen, Germany) equipped with an Apollo I electrospray ionization (ESI) source and a 4.7 T superconducting magnet (FT-ICR lab, Sapienza Università di Roma). Ultrahigh-resolution mass spectra were acquired on a Bruker SolariX

XR FT-ICR MS endowed with a 7 T superconducting magnet (Magnex Scientific Inc., Yarnton, UK), a ParaCell (Bruker Daltonics GmbH, Bremen, Germany), and an APOLLO II electrospray ionization (ESI) source operated in either the positive (ESI+) or negative ionization mode (ESI-), at Universidade de Lisboa. Samples were directly infused in the ESI source at a flow rate of 120 μL h^{-1}. The nebulizer gas pressure was set at 1.0 bar, the drying gas flow rate at 4.0 L min^{-1} at a temperature of 200 °C, and the capillary exit voltage at 200 V.

All MS spectra were acquired in absorption mode, over a mass range between *m/z* 100 and 3000 (resolution of 650,000 at *m/z* 400), with an acquisition size of 4 mega words, resulting in a free induction decay (FID) of 1.973 s. For each sample, two hundred scans were coadded, corresponding to a run time of 10 min.

Overall, 20 μL of dilute sample solution (corresponding to 2 ng of original dry sample) were used for acquiring one mass spectrum, which not only makes the FT-ICR MS analysis compatible for high sample throughput but also uses relatively small sample amounts.

The list of *m/z* values was exported with a cut-off signal-to-noise ratio (S/N) of 4 and submitted to the free tool MassTRIX [30], taking into account protonated, sodiated, and potassiated (ESI(+)), and deprotonated and chlorinated (ESI(−)) ions, with a maximum deviation range set to ± 1ppm. An accurate check of the isotopic pattern based on the natural abundances of 13C, 15N, 18O, 34S, and 37Cl isotopes, was also performed to minimize false positive results. Only singly charged species were revealed, in both polarity modes. In analyzing each cultivar, peaks with a reproducibility lower than 67% were removed. A large number of unambiguous molecular formulas, for which several isomers are possible, admitting the presence of the elements C, H, O, N, P, and S, could be assigned by both ESI(+) and ESI(−) analyses and were further filtered by application of several chemical constraints as indicated by Kind et al. [31]. Additional information was obtained by acquisition of collision induced dissociation (CID) spectra, though limited to components of adequate abundance, further verified against fragmentation patterns of reference compounds or data inserted into a specialized database. The formulas generated from each sample were then transposed to two-dimensional van Krevelen diagrams, known as elemental ratio analysis, constructed by plotting the molar hydrogen to carbon ratio (H/C) vs. the molar ratio of oxygen to carbon (O/C) for each data point. According to their own characteristic H/C and O/C ratios, main classes of compounds are specifically localized as areas in the plot, thus allowing a depiction of a sample's composition [32].

2.5.3. Phenolic Compounds (Polyphenols, Tannins, and Flavonoids)

Total polyphenols, tannins, and flavonoids per milligram of fresh fruit were determined by spectrophotometric methods according to previous published methods [24]. The total amount of both polyphenols and tannins was expressed as tannic acid equivalents (TAE), while flavonoids were expressed as quercetin equivalents (QE).

2.5.4. Biogenic Amines (BAs) Determination

The BAs determination was carried out as previously described [33]. Briefly, 8 g of tomato extract were added 15 mL 0.6 M $HClO_4$ aqueous solution and 0.5 mL of 1,7diaminoheptane 100 mg mL^{-1} (Internal Standard), then homogenized for 3 min with an Ultra-Turrax and centrifuged at 3000 RPM for 10 min. Supernatant was filtered through a 0.20 μm membrane Millipore filter and sediment was added with 8 mL of $HClO_4$ 0.6 M, mixed, and centrifuged again for 3 min. The second extract was then filtered and added to the first. The final volume was adjusted to 25 mL with $HClO_4$ 0.6M. An aliquot of 1 mL of the final extract was then derivatized by adding 200 μL of NaOH 2 M, 300 μL of saturated $NaHCO_3$ solution, and 2 mL of dansyl chloride solution (10 mg mL^{-1} in acetone). After shaking, samples were left in the dark at 45 °C for 60 min. The final volume was adjusted to 5 mL by adding acetonitrile. The dansylated extract was filtered using 0.22 μm (Polypro Acrodisc, PallGelman Laboratory, USA) filter, injected into the chromatograph, and analyzed with a previous

standard method [34]. The determination was carried out twice on 8 samples of each examined tomato cultivar.

2.6. Screening of Biological Activities

2.6.1. Antioxidant Activities

All tests were performed in 96-multiwell microplates away from direct light. To perform the assays, the extracts were assayed at the concentrations of 1, 10, 25, 50, 100, 250, 500, 1000, 1500, 2000, and 5000 μg mL^{-1} in order to achieve a concentration-response curve. The samples were dissolved in 50% or 100% *v/v* EtOH (organic and hydroalcoholic extracts, respectively). The experiments were repeated at least twice, and in every experiment, each concentration was tested in triplicate. Data obtained from at least two experiments were pooled for the statistical analysis.

In each experiment, the vehicle (negative control) and standard antioxidants (positive controls), i.e., trolox (assayed concentrations 0.1, 0.25, 1, 5, 10, 50, and 100 μg mL^{-1}) for the radical scavenger and reducing activity, and quercetin (assayed concentrations 1, 5, 10, 50, 100, and 200 μg mL^{-1}) for the chelating activity, were included too. The absorbance was measured by a microplate reader (Epoch Microplate Spectrophotometer, BioTeK® Instruments Inc., Winooski, VT, USA). Some wells containing only the test samples were also included to determine its possible absorbance.

Scavenging activity towards DPPH and ABTS radicals was determined according to the methods of Di Sotto et al. [35]. Furthermore, the ability of the extracts to indirectly interfere with the ROS-generation through blocking the Fenton reaction was evaluated by testing the iron chelating and reducing activities in the ferrozine assay [35]. Chelation ability was evaluated against both ferrous and ferric ions. The ability of the samples to inhibit the ROS-induced lipid peroxidation was assessed by the ferric thiocyanate method [36].

2.6.2. Advanced Glycation End-Product (AGE) Inhibition

The ability of the tested samples to inhibit the AGE formation was measured through the method of Di Sotto et al. [37]. The phenolics naringenin and rutin were included as standard inhibitors, while the vehicle (50% or 100% *v/v* EtOH for organic and hydroalcoholic extracts respectively) represented the lack of inhibition. The inhibitory activity was calculated as percentage of the control, as follow:

$$(A_{control} - A_{sample}/A_{control}) \times 100 \quad (1)$$

where $A_{control}$ is the fluorescence of the control, whereas A_{sample} is the fluorescence of the sample. Data from at least three replicated experiments (including six replicates for experiment) were pooled for the statistical analysis.

2.6.3. Cytoprotection towards the Oxidative Stress Induced by tBuOOH

Cytoprotective activity of the tested extracts was evaluated towards the oxidative damage induced by tert-butyl hydroperoxide solution (tBuOOH) in HepG2 liver cancer cells (American Type Culture Collection, Milan, Italy). The cells were grown at 37 °C in 5% CO_2 in Dulbecco's modified Eagle's medium, supplemented with fetal bovine serum (10% *v/v*), glutamine (2 mM), streptomycin (100 μg mL^{-1}), and penicillin (100 U mL^{-1}) [38]. All experiments were performed when cells reached the logarithmic growth phase.

Preliminarily, the extracts (1–1000 μg mL^{-1} concentration range) were tested for the mitochondrial cytotoxicity by the 3-(4,5-dimethylthiazol-2-yl)-2,5-diphenyl tetrazolium bromide (MTT) assay [39], in order to define the proper concentrations to be used in the subsequent experiments. Then, 50% or 100% *v/v* EtOH were used as vehicle for organic and hydroalcoholic extracts respectively; the vehicle was nontoxic at final concentration of 1% *v/v* in the medium.

The ability of the tested samples to counteract the oxidative stress induced by tBuOOH was evaluated by measuring the levels of intracellular ROS (reactive oxygen species) through the 2,7-dichlorofluorescein diacetate assay (DCFH-DA) [40]. To this end, 5×10^5 cells were grown into 6-well plates for 24 h, then treated with a nontoxic concentration of the extracts (100 μg mL^{-1}) for 24 h. At the end of incubation, the cells were treated with a low-toxic concentration (about 40% cytotoxicity as found in preliminary experiments) of the pro-oxidant agent tBuOOH (5 mM) for 2 h, then washed twice with Hank's Balanced Salt Solution (HBSS) (1×) and added with DCFH-DA (10 μM; 6 μL). Fluorescence of DCF, obtained by DCFH-DA oxidation, was measured though a BD Accuri™ C6 flow cytometer at an excitation wavelength of 485 nm and emission wavelength of 528 nm. In each experiment, proper treatment with the vehicle control (corresponding to the basal ROS level) and the pro-oxidant agent tBuOOH were included too; furthermore, the extracts alone were assayed to evaluate their effect on the basal ROS levels, released as a consequence of cell metabolism. The oxidation index was obtained by the ratio between the DCF fluorescence of the sample and vehicle control.

2.6.4. In Vitro Metabolic Enzyme Inhibition

The ability of the tested extracts to inhibit in vitro the α-amylase and α-glucosidase enzymes was measured by dinitrosalicilic acid (DNSA) and *p*-nitrophenyl-α-D-glucopiranoside (PNGP) methods described by Di Sotto et al. [37]. Acarbose was included in all the experiments as standard enzyme inhibitor (100% enzyme inhibition), while the vehicle (50% or 100% *v/v* EtOH for organic and hydroalcoholic extracts respectively) represented the maximum enzyme activity. Additional treatments, in which enzyme solution was replaced by buffer solution, were included to evaluate a possible interfering absorbance of the samples. The experiments were performed at least in triplicate and in each experiment about six replicates were prepared. Data obtained from at least two experiments were pooled in the statistical analysis. The inhibitory activity was calculated as percentage of inhibition with respect to the vehicle control.

2.6.5. Antifungal Susceptibility Test

To evaluate the minimal inhibitory concentration (MIC) of the extracts, the broth microdilution method was performed according to a standardized method for yeasts [41].

The assay was carried out with four *C. albicans* strains (ATCC10231, ATCC24433, 3153A, PMC1033), three *C. glabrata* strains (PMC0822, PMC0851, PMC0807), and two *C. krusei* strains (PMC0631, PMC0624). *Candida* spp. strains were grown on Sabouraud dextrose agar at 37 °C for 24 h. Then, cell suspensions of the strains were prepared in RPMI 1640 medium buffered to pH 7.0 with 0.165 mM MOPS. The final concentration of the inoculum was 1×10^3–5×10^3 cells mL^{-1}. The extracts were dissolved in DMSO and diluted 100 times in RPMI-1640 broth. Ten concentrations ranging from 1000 to 1.9 μg mL^{-1} were tested against *Candida* spp. strains in 96-well round-bottom microtitration plates. The antifungal activity is the result of four independent experiments. The MIC_{50}, MIC_{90}, and MIC_{100}, the lowest concentrations of extracts that caused growth inhibitions ≥50%, ≥90%, and 100% respectively, were evaluated. Data were reported as range and geometric mean (GM) of MIC.

2.7. Statistical Analysis

All values are expressed as mean ± standard error (SE). Statistical analysis was performed by GraphPad Prism™ (Version 4.00) software (GraphPad Software, Inc., San Diego, CA, USA). The one-way analysis of variance (one-way ANOVA), followed by a suitable multiple comparison post hoc test (i.e., Bonferroni post-test for comparison among means, while Dunnett's post-test for estimating a difference compared to the control), was used to analyze the difference between treatments. The concentration– response curves were constructed using the "Hill equation":

$$E = Emax/(1 + 10\hat{}(LogEC_{50}/A) \times HillSlope) \quad (2)$$

where E is the effect at a given concentration of agonist, Emax is the maximum activity, EC_{50} is the concentration that produces a 50% of the inhibitory response (namely IC_{50}), A is the agonist concentration in molarity, HillSlope is the slope of the agonist curve. p values < 0.05 were considered as significant. Correlation between two variables was evaluated by the Pearson correlation coefficient and the statistical significance was measured by the two-tailed t-test.

3. Results and Discussion

3.1. Morphological and Pigments Analyses

The sampled TF tomatoes showed a shape similar to SM fruits, but were smaller in length and circumference (about two-fold lower) and in weight (about five folds lower), thus supporting their nature of "Mini-San Marzano tomato" (Table 3). Despite a smaller size, peel amount in pink and red TF fruits was two- and ten-fold higher than those of SM at the same ripening stages, respectively (Table S1). Furthermore, at least a doubled peel amount was found in the red TF tomatoes compared to the pink ones, whereas an opposite trend was observed in SM fruits (Table S1).

Table 3. Color, weight, and size (length and diameter) of both pink and red fruits from Solanum lycopersicum TF and SM varieties. Data are displayed as mean ± SE (n = 10) [a].

Sample	Color	Weight (g)	Size (cm)	
			Length	Diameter
TF_P	dark-green	21.7 ± 0.1	6.3 ± 0.1	2.6 ± 0.1
TF_R	bright red	20.6 ± 0.1	5.6 ± 0.1	2.7 ± 0.1
SM_P	pale green	106.1 ± 0.9 **	10.1 ± 0.1 **	4.5 ± 0.1 *
SM_R	light red	110.7 ± 0.6 **,§	11.4 ± 0.1 **	4.4 ± 0.1 *

[a] * $p < 0.05$ and ** $p < 0.01$ denote a statistically significant difference compared to TF tomato at the same ripening stage (t-Student Test). § $p < 0.05$ denotes a statistically significant difference with respect to pink stage within the same cultivar (t-Student Test).

Ripeness also increased the pulp amount in both varieties. The TF pulp content per gram of fruit was at least four-fold higher with respect to SM tomatoes (Table S1). In spite of a lower pulp amount, both pink and red SM (SM_P, SM_R) tomatoes contained high amounts of juice (pH 4.0–4.2). Conversely, the juice content was at least two to six-fold lower in pink and red TF (TF_P, TF_R) tomatoes (Table S1). Altogether, these features support the claimed crunchy and solid consistency of TF tomatoes, likely ascribable to a high peel and pulp content, despite a significant low amount of juice.

A significant difference in the seed number and weight per gram of fruit was observed, which was about four-fold higher in TF compared to SM tomatoes at both ripening stages (Table S1). Conversely, the size and weight of each seed were similar in both varieties, with a slight increase in the SM_R fruits (Table S1). It is widely accepted that seed size and number are strictly linked to the plant reproductive potential. Small seeds were reported to possess lower reproductive capacity, due to a lower endosperm amount, which limits seedling survivorship and competitive ability [42]. On the other hand, a high seed number improves the competitive ability of the plant, due to the increased probability of seedling survivorship. In this context, TF tomatoes seem to possess a higher reproductive competition related to SM, along with similar plant reproductive capacity and survival.

The color of SM tomatoes varied from pale green in the pink fruits to light red in the red ones (Table 3 and Figure S1). The analysis of pigments i.e., chlorophyll a, chlorophyll b, and total carotenoids, carried out on the TF and SM organic extracts from peel and pulp justified these features. The dark-green colour of TF_P tomatoes can be ascribed to the higher content in chlorophylls a and b in peel (+70% and +52% higher amount, respectively) ($p < 0.01$) and in pulp (+10% and +82% higher amount, respectively) ($p < 0.01$) with respect to TF_R fruits (Table 4). On the contrary, carotenoids content (bright red color) was found about five-fold higher in TF_R peel and pulp than in pink ones ($p < 0.001$) (Figure S1).

Table 4. Amounts of chlorophyll a, chlorophyll b, and total carotenoids in the organic extracts of both pink and red fruits from Solanum lycopersicum var. Torpedino di Fondi (TF) compared San Marzano (SM) tomatoes [a].

Sample	Fruit Part	Chlorophyll a	Chlorophyll b	Total Carotenoids	Ratio (a + b)/ Total Carotenoids
		μg/g FW			
TF_P	peel	166 ± 32	67 ± 3	79 ± 7	3.16
	pulp	178 ± 30	94 ± 4	82 ± 9	
TF_R	peel	49 ± 5 §	32 ± 3 §	404 ± 22 §§	0.18
	pulp	18 ± 4 §§	17 ± 1 §§	455 ± 10 §§	
SM_P	peel	63 ± 3 **	33 ± 4 *	26 ± 5 **	3.9
	pulp	31 ± 3 ***	13 ± 3 **	13 ± 3 ***	
SM_R	peel	5 ± 2 *** §	9 ± 1 §	723 ± 4 ***,§§	0.02
	pulp	4 ± 2 §	8 ± 1	511 ± 13 ***,§§	

[a] * $p < 0.05$, ** $p < 0.01$ and *** $p < 0.001$ denote a statistically significant difference compared to TF tomato at the same ripening stage (ANOVA followed by Bonferroni multiple comparison post test). §§ $p < 0.01$ denotes a statistically significant difference with respect to pink stage within the same variety (ANOVA followed by Bonferroni multiple comparison post test).

The difference in chlorophyll a content between pink and red fruits was particularly marked in SM cultivar, where chlorophyll a amount was 90% higher in peel and pulp of SM_P compared to SM_R fruits ($p < 0.01$). SM_P tomatoes displayed both chlorophyll a and b content to be double in peel with respect to pulp, while in SM_R fruits, this difference was not evident (Table 4). The opposite trend was observed with regard to carotenoids content. SM_R peel showed a carotenoid amount 28 times higher with respect to SM_P peel ($p < 0.001$), while in SM_R pulp, a 40 times higher level of total carotenoids with respect to SM_P pulp ($p < 0.001$) was found.

TF fruits were characterized by higher levels of chlorophylls compared to SM ones at both ripening stages ($p < 0.01$). In particular, chlorophyll a and b content was found to be 60% and 80% higher in TF_P peel and pulp fruits than in SM_P peel and pulp, respectively ($p < 0.01$). A similar trend was observed in terms of total carotenoids content, which was 68% higher in TF_P fruits with respect to SM_P ($p < 0.01$). These findings agree with the different shade of green color observed in the TF_P (dark green) compared to SM_P fruits (pale green) (Figure S1). In addition, red fruits of both cultivars were characterized by different pigments proportion. In TF_R peel, chlorophyll levels were 90% higher compared to SM_R peel (+90%, $p < 0.001$), the latter showed 40% higher content of carotenoids than TF_R peel ($p < 0.001$; Table 4).

Carotenoids are mainly responsible for the red color of tomatoes and are involved in the fruit protection against excessive sun irradiation and harmful UV rays. Total carotenoids amount in fruits depends on the ripening stage and other factors, such as cultivar, climate, sun exposure, agronomic practices, irrigation. The ratio of chlorophyll a and b to total carotenoids (a + b/total carotenoids) can be considered as an indicator of tomato ripening stage. During chromoplast development in fruit maturation, the ratio a + b/total carotenoids tends to decrease continuously, thus reaching a value below 1.0 [43]. Our findings confirmed the differences in ripening stages selected for the study, revealing a ratio value of 3.16 in TF_P tomatoes and 0.18 in TF_R ones. In SM fruits, this trend was even wider, in fact, pink fruits showed a ratio value of 3.9, whereas in red fruits, this ratio was 0.02 (far below of 1).

3.2. Metabolite Profiling

FT-ICR MS and NMR untargeted analyses were carried out for a thorough metabolite profile characterization of TF and SM in relation to their pink and red states. The high mass accuracy typically achieved with FT-MS implies that elemental formulas can be determined, pertaining to a large number of metabolites, based on their accurate mass, whereas the NMR capacity of structural determination allows the unambiguous compound identification and quantification.

The ESI FT-ICR MS analysis of both Bligh–Dyer hydroalcoholic and organic fractions of TF_P, TF_R, SM_P, and SM_R fruits has allowed to detect both polar and non-polar metabolites. Each sample was analyzed in both positive and negative ionization mode (Figures S2–S5), detecting up to 1138 molecular formulas; however, a larger number of compounds were detected in positive ionization mode (Table 5). Overall, the TF cultivar was characterized by a smaller number of compounds with respect to SM and the ripeness process promotes a general increase in the number of putatively identified metabolites (Table 5). An overview of all the recorded plausible compounds is available in Tables S2 and S3.

Table 5. Number of chemical formulas detected in hydroalcoholic and organic extracts of pink and red SM and TF by ESI FT-ICR MS.

Sample		Ion Mode	Detected Molecular Formulas	
San Marzano				
Hydroalcoholic	Pink	ESI(+)	824	935
		ESI(−)	132	
	Red	ESI(+)	808	1031
		ESI(−)	240	
Organic	Pink	ESI(+)	401	508
		ESI(−)	113	
	Red	ESI(+)	865	1138
		ESI(−)	286	
Torpedino di Fondi				
Hydroalcoholic	Pink	ESI(+)	488	652
		ESI(−)	261	
	Red	ESI(+)	549	751
		ESI(−)	204	
Organic	Pink	ESI(+)	381	586
		ESI(−)	208	
	Red	ESI(+)	800	948
		ESI(−)	151	

Specific data analysis allows to organize the vast amount and complexity of detected formulas to uncover interesting information. Among the detected molecular formulas, the relative frequency distribution was investigated (Figure 1E,F) showing that all tomato extracts contain a majority of CHO species followed by CHON, CHOP and, in smaller amount, CHNOP and CHNOS. In particular, CHO components correspond mainly to polyphenols (more hits in SM_R extracts), steroids (more hits in TF), and fatty acids (more entries in TF), followed by di- and tri-glycerides (more entries in SM_P), terpenoids, organic acids, and arachidonic derivatives (Supplementary Figure S6A). When considering CHON components, they can be ascribed mainly to amino fatty acids, amino-sugars, amines (more hits in red extracts), N-acylamines (more hits in TF_P), followed by amino acids (more entries in pink extracts), solanidines, nucleosides (more hits in SM_P), and vitamins (more hits in TF_R) as shown in Figure S6B.

Van Krevelen diagrams were used to classify the detected molecular formulas in different classes of natural compounds such as lipids, terpenoids, carbohydrates, amino acids, aminosugars, nucleic acids, polyphenols, polyketides, unsaturated hydrocarbons and condensed hydrocarbons (Figure 1A–D). TF and SM tomato extracts showed marked similarities, covering several classes of metabolite families. A relatively higher compound density is present in the area of lipids, terpenoids, and polyketides, followed by components in the areas of amino acids, unsaturated hydrocarbons, polyphenols and (relatively less) in the regions of carbohydrates, aminosugars, nucleic acids, and condensed hydrocarbons (Figure 1A–D).

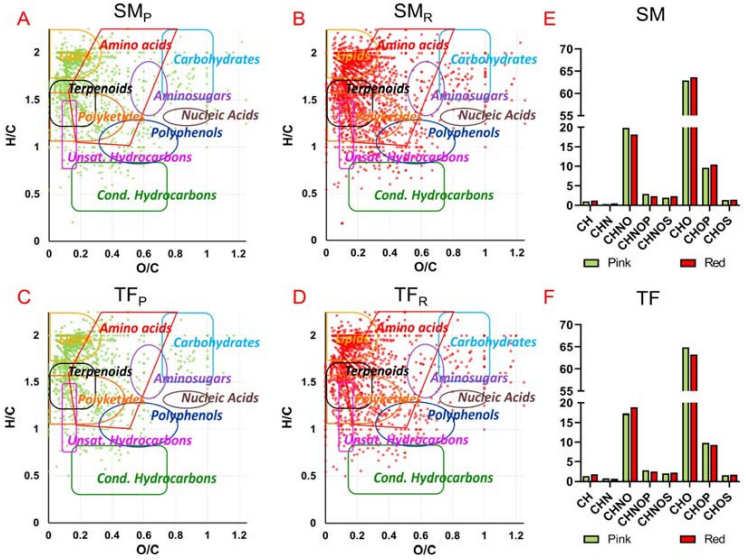


Figure 1. Van Krevelen plot (elemental plot) obtained from the molecular formulas obtained by ESI FT-ICR MS analysis of total hydroalcoholic and organic fractions of: (**A**) SM_P; (**B**) SM_R; (**C**) TF_P; (**D**) TF_R. Histograms of the relative frequency of CH, CHN, CHNO, CHNOP, CHNOS, CHO, CHOP, CHOS compounds: (**E**) in SM_P (green), SM_R (red); (**F**) TF_P (green) and TF_R (red).

Moreover, Venn diagrams (Figure S7) pointed out possible similarities and differences in the metabolic profile of the sampled TF and SM fruits. The combined pattern of hydroalcoholic and organic fractions of pink and red extracts of the two cultivars showed that overall only 19% of the molecular formulas were found to be common, thus suggesting a noticeable extent of chemical diversity, whereas more than 40% of molecular formulas were shared between pink and red samples of each variety.

This wide metabolomics survey supported the untargeted and targeted analyses driving the identification of selected classes of metabolites. In particular, 1D NMR spectra assignment of the TF and SM hydroalcoholic extracts solubilized in D_2O phosphate buffer and organic extracts solubilized in $CDCl_3/CD_3OH$ (Table 2) were obtained by means of literature data [28,44–46]. Furthermore, targeted analytical approaches provided the identification and quantification of total polyphenols, tannins, and flavonoids content and BAs.

Results will be presented and discussed according to compound classes.

3.2.1. Amino Acids and Derivatives

NMR spectra of both red and pink TF and SM hydroalcoholic extracts showed signals of sixteen amino acids, namely leucine, valine, isoleucine, threonine, alanine, GABA, glutamic acid, glutamine, aspartic acid, asparagine, lysine, arginine, tyrosine, phenylalanine, tryptophan, and histidine, as also confirmed by ESI FT-ICR MS. All of them were quantifiable, except arginine. In addition, ESI FT-ICR MS revealed the presence of proline, serine, the non-essential amino acid citrulline, and other amino-acids-related metabolites, like hydroxyproline and phosphoserine. Some peptides were also found. In particular, glutathione was detected in all hydroalcoholic extracts, S-nitrosoglutathione in red fruits, glutathione disulfide in pink fruits.

Alanyl-alanine (in hydroalcoholic SM_P), glycyl-proline (in organic SM_R), glycyl-leucine (in organic TF_R), glutamyl-valine and glutamyl-glutamine (in hydroalcoholic SM_R) were also revealed.

According to NMR scrutiny, TF and SM samples showed some/several similarities (Figure 2A): glutamine was found to be the most abundant amino acid in both cultivars at the pink stage, followed by GABA and glutamic acid, whereas, at the red stage, glutamic acid increased, becoming the most abundant amino acid. The pattern of SM developmental changes in free amino acid content was in agreement with literature data, being glutamic acid characterized by a remarkable increase in all ripe fruits [2–4,45,47–52]. Glutamic acid, aspartate, tryptophan, and alanine rose upon the fruit ripening; asparagine and phenylalanine turned out to be constant; tyrosine, isoleucine, valine, threonine, GABA, and glutamine content decreased from pink to red SM fruits. These findings reflect data reported in literature about the analyses of SM [2,4] and other cultivars [3,45,47–52].

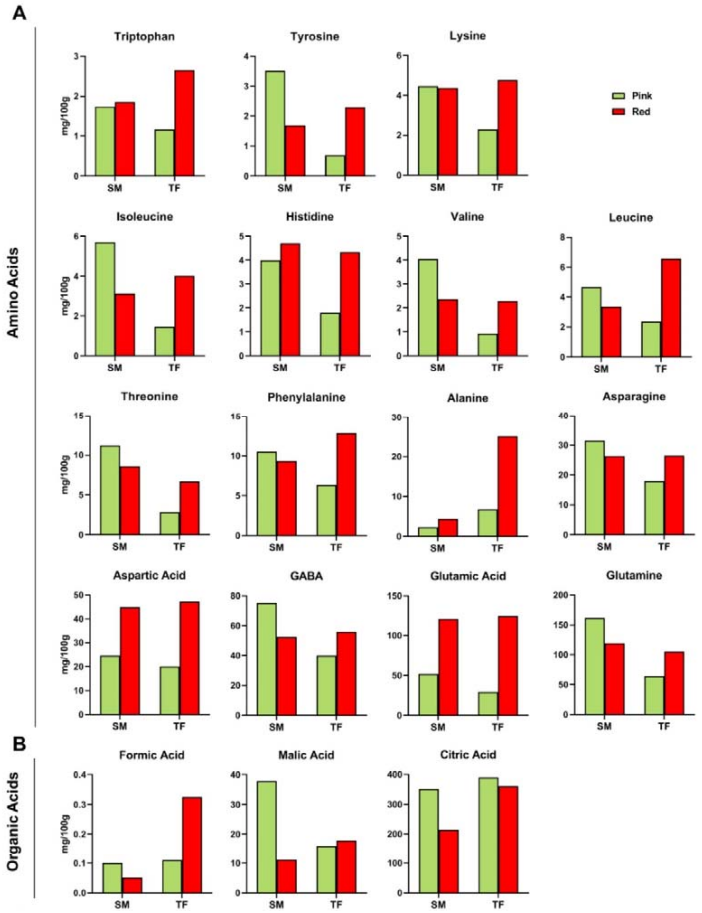


Figure 2. *Cont.*

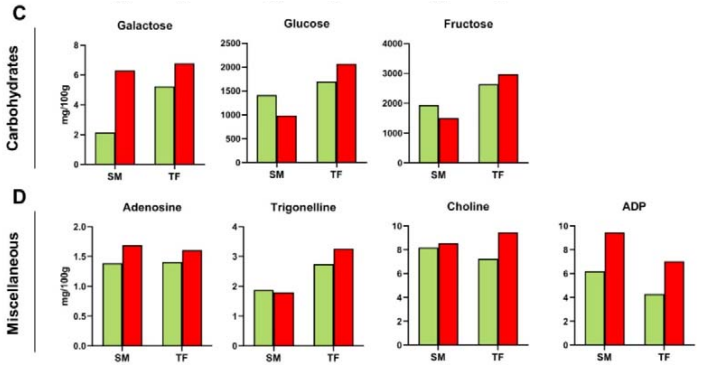


Figure 2. Histograms relative to metabolites identified by H^1-NMR spectroscopy in tomato hydroalcoholic extracts from pink (green) and red (red) SM and TF cultivars: (**A**) Amino acids; (**B**) Organic acids; (**C**) Carbohydrates; (**D**) Other compounds. Data are expressed as mg/100 g FW.

Interestingly, the TF fruit ripening showed a peculiar trend in the amino acid profile, being characterized by an increase in the content of all the amino acids from the pink to red stage. In particular, except for asparagine, GABA, and glutamine, the content of the remaining twelve amino acids rose more than two-fold.

3.2.2. Organic Acids

Ascorbic, citric, chlorogenic, malic and formic acids were detected by NMR analysis. Chlorogenic acid (5-caffeoylquinic acid) was identified only in hydroalcoholic TF_P extracts. The ESI FT-ICR mass spectra in negative mode provided additional peaks corresponding to deprotonated organic acids identified in one or a few samples, like succinic and glutaric (in organic SM_R and hydroalcoholic TF_P extracts), maleic (in hydroalcoholic TF_P extracts), quinic and shikimic (in hydroalcoholic TF_R and TF_P extracts), and lactic (absent only in red hydroalcoholic samples) acids, as the most prominent signals. In addition, sugar esters of caffeic and ferulic acids, caffeoyl- and feruloyl-hexose, were revealed, with both metabolites being present in hydroalcoholic extracts. Although the present method does not allow to recognize which constitutional isomer is formed, glycosylated forms of phenolic acids have been previously identified in methanol extracts of tomato fruit by a HPLC/DAD/MS approach [53].

Histograms reporting NMR data (Figure 2B) showed that formic acid was always present in a minor amount, whereas citric acid represented the main organic acid, contributing to sourness [5] and confirming literature data [2–4,45,47,48]. During the developmental process, both malic and citric acids contents stayed constant in TF fruits and decreased in SM tomatoes. Previous results concerning the organic acid trends are contradictory: Mounet et al. [48] and Jezequel et al. [54] described an increasing citric acid content from the pink to red stage, whereas Perez et al. [45] found out a decrease in citric and malic acids content. These differences might be ascribed to the combination of genetic, pedoclimatic, seasonal, and agronomic factors.

In terms of cultivar, the three organic acids were comparably abundant at the pink stage, except for malic acid which was significantly higher in SM than in TF fruits. At the red stage, formic, malic and citric acids contents were found nearly doubled in TF compared to SM fruits.

3.2.3. Sugars

Fructose, glucose and galactose were the monosaccharides identified in the ^{1}H NMR spectrum of hydroalcoholic extracts. Besides, confirming the widespread incidence of mono and disaccharides, ESI FT-ICR results reported an Amadori compound, fructosyl lysine, in all hydroalcoholic extracts, providing a sensitive marker of early modifications in food nutrients previously described also in unprocessed tomato extracts [55].

Fructose was the most abundant sugar in both cultivars at both ripeness stages, followed by glucose; however, higher levels of both carbohydrates were found in TF compared to SM fruits (Figure 2C). Fructose, glucose, and galactose levels increased in TF cultivar over the ripening period, whereas the opposite trend was observed in SM fruits. Loiudice et al. [2] reported glucose and fructose contents of eleven SM tomato cultivars at three harvesting years: fructose was always found the most abundant sugar in all samples characterized by a mean content of 1.4g/100 g, whereas glucose mean content was 1.2 g/100 g. These data are consistent with the values reported in Figure 2C: fructose was the main sugar in SM with a mean value of 1.7 g/100 g and glucose content was 1.2 g/100 g, with a total amount of 2.9 g/100 g. However, sugars content in hybrid cultivars tended to increase [2], confirming the higher amount of both fructose and glucose in TF, which reached 5 g/100 g as mean value.

3.2.4. Other Compounds

NMR signals of choline, trigonelline, uridine, adenosine, and ADP were identified and, except for uridine, quantified (Figure 2D). A rich variety of miscellaneous compounds were detected by ESI FT-ICR analysis, comprising small amines (serotonin), nucleosides (adenosine, methylthioadenosine, orotidine), and nucleotides (guanosine-, cytidine-, and uridine-monophosphate), sugar alcohols (sorbitol, mannitol), sugar acids (galactonic and glucuronic acids), aminosugars (glucosamine, lactosamine), terpenes (*p*-cymene, caryophyllene, limonene), terpenoid (apiole, oxo-campholide), vitamins and derivatives (ascorbic acid, retinol, α-tocopherol). As expected, both cultivars contained several key secondary metabolites characteristic of tomato fruits, including alkaloids (trigonelline, narciclasine, and catharanthine, only in hydroalcoholic extracts, nicotine and sauroxine, spread in all samples), polyketides such as lycoflexine, mostly in pink fruits, and glycoalkaloids as tomatine and tomatidine, only in pink hydroalcoholic extracts [56,57]. Several phytohormones, recognized as key signaling molecules, were observed in most samples, like derivatives of abscisic acid, only in hydroalcoholic extracts, jasmonic acid, only in red hydroalcoholic fractions, and salicylic acid, mostly in TF_P and SM_R, and several gibberellins, mainly detected in red organic samples [58].

The concentration of choline and adenosine were comparable in SM and TF fruits, slightly increasing at the red stage, whereas trigonelline content was found to be lower in SM with respect to TF at both developmental stages. ADP content severely increased in both cultivars at the red stage, almost doubling its level.

The presence of hydroxyl-substituted fatty acids, metabolites with strong anti-inflammatory and antioxidative effects, confirms the nutraceutical potential of tomato. Hydroxy-stearic acid was observed in all samples except for organic SM_R, hydroxy-linoleic acid, in all extract excluding hydroalcoholic SM_P, and hydroxylinolenic acid, in organic SM_R and all TF extracts [59].

3.2.5. Phenolic Compounds (Polyphenols, Tannins, and Flavonoids)

Spectrophotometric targeted analyses provided the total content of phenolic compounds expressed as polyphenols, tannins, and flavonoids. Highest levels of total polyphenols were found in hydroalcoholic extracts from pink fruits of both cultivars, being TF_P the most enriched sample (triple content compared SM_P); conversely, their levels were reduced of about 14- and 6-fold with ripeness (Table 6). Similarly, a 1.6-fold reduction in total polyphenols was found in TF_R organic extracts with respect to those from TF_P, whereas an opposite trend occurred in the SM variety (Table 6).

Table 6. Amounts of total polyphenols, tannins and flavonoids in Bligh–Dyer hydroalcoholic and organic extracts of both pink and red fruits from *Solanum lycopersicum* var. TF and SM [a].

Sample	ADD HEADING	Polyphenols	Tannins	Flavonoids
		[μg TAEs/g Fruit] [b]		[μg QEs/g Fruit] [c]
TF_P	Hydroalcoholic	155.0 ± 0.1	5.0 ± 0.4	149.7 ± 0.6
	Organic	36.9 ± 0.3	7.7 ± 0.3	54.4 ± 0.4
TF_R	Hydroalcoholic	11.1 ± 0.3 §§§	6.4 ± 0.1 §	101.3 ± 0.8 §§
	Organic	22.9 ± 0.5 §§	0.9 ± 0.1 §§§	12.8 ± 0.5 §§§
SM_P	Hydroalcoholic	55.0 ± 0.4 ***	5.0 ± 0.6	50.0 ± 0.7 ***
	Organic	13.7 ± 0.1 ***	4.7 ± 0.2 **	2.2 ± 0.1 ***
SM_R	Hydroalcoholic	9.1 ± 0.6 §§§	5.8 ± 0.2	91.0 ± 0.3 * §§
	Organic	27.8 ± 0.7 §§§	4.3 ± 0.3 ***	132.2 ± 1.2 *** §§§

[a] * $p < 0.05$, ** $p < 0.01$ and *** $p < 0.001$ denote a statistically significant difference compared to TF tomato at the same stage of ripening (ANOVA followed by Bonferroni multiple comparison post test). § $p < 0.05$, §§ $p < 0.01$ and §§§ $p < 0.001$ denotes a statistically significant difference with respect to pink stage within the same variety (t-Student Test). [b] TAEs, tannic acid equivalents. [c] QEs, quercetin equivalents.

TF_P and SM_P hydroalcoholic extracts contained similar levels of tannins, which slightly increased with ripening (Table 6). Comparing the ripening stages, both SM_P and SM_R organic extracts contained an analogue content of tannins, whereas a marked 8-fold reduction in their levels occurred in TF_R organic extracts compared to TF_P (Table 6).

Flavonoids were mainly concentrated in the hydroalcoholic extracts of both TF and SM tomatoes at both the ripening stages, although high levels were also found in the organic extracts of TF_P and SM_R fruits (Table 6). TF_P hydroalcoholic extract resulted in the most enriched sample in flavonoids, being three times more concentrated than SM_P; similarly, the same trend was observed in pink organic fractions, being TF the cultivar characterized by an almost 30-fold higher flavonoid content compared to SM (Table 6). At the red stage, TF fruits showed a flavonoid reduction of about 1.5- and 4-fold in organic and hydroalcoholic extracts respectively, whereas an opposite trend was registered for SM tomatoes. Indeed, a 2- and 66-fold flavonoid increase was found in the hydroalcoholic and organic SM_R with respect to SM_P (Table 6). This evidence revealed that the highest levels of total polyphenols, tannins, and flavonoids were concentrated in the TF_P tomatoes, although a high flavonoid content was retained in TF_R and SM_R fruits. Our data agree with previous evidence that highlighted a total flavonoid content of 200 μg/g (calculated as quercetin equivalents) in SM_R tomatoes [60]. Conversely, to the best of our knowledge, no comparison data are available in the literature regarding TF landrace.

In addition, ESI FT-ICR MS experiments have revealed flavanols (dihydroxy-methoxy-isoflavanol), flavan-3-ols (epigallocatechin sulfate), flavonoids (apigeniflavan, tetrahydroxyflavanone glucoside), and polyphenol derivatives like catechin-O-glucoside, catechin-O-rutinoside, dihydrokaempferol, trihydroxy-prenyldihydrochalcone glucosyl-coumarate, quercetin glucoside-glucuronide [61].

3.2.6. Sterols

β-Sitosterol and stigmasterol were detected and quantified by NMR analysis in the organic extracts of both cultivars at pink and red developmental stages.

β-Sitosterol content showed a decreasing trend in SM_R fruits, opposite to TF fruits. Conversely, stigmasterol content significantly increased (3-fold higher) over the ripening stage in both cultivars (Figure 3). According to ESI FT-ICR results, cholesterol- and hydroxycholesterol-sulfate were found in all samples, whereas methylstigmasterol was detected in the hydroalcoholic TF_R sample.

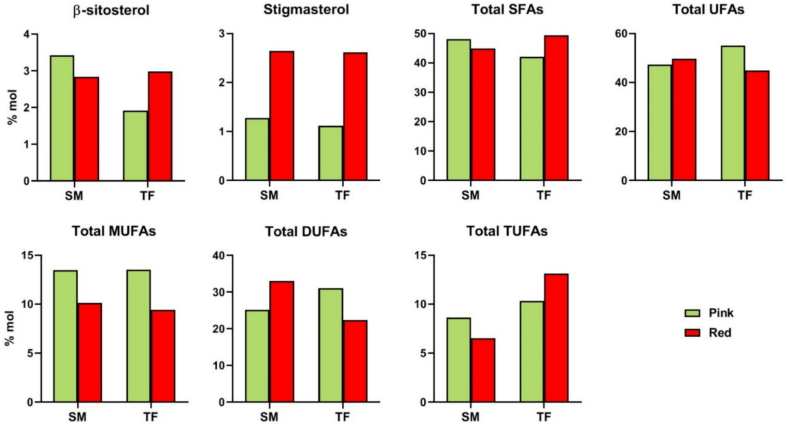


Figure 3. Histograms comparing the concentration (% molar) of metabolites present in tomato organic extracts from pink and red SM and TF. SFA: saturated fatty acids; UFA: unsaturated fatty acids; MUFA: mono-unsaturated fatty acids; DUFA: di-unsaturated.

3.2.7. Fatty Acid Chains

NMR analysis allowed the identification and quantification of the total saturated (SFA) and unsaturated (UFA) fatty acid chains, the latter ones including mono- (MUFA), di- (DUFA) and tri-unsaturated (TUFA) fatty acid chains. The amount of the selected metabolites was comparable in SM and TF cultivars at both ripening stages, except for the case of TUFA, more abundant in TF fruits (Figure 3). Regarding the ripening stages, total UFA content was found to slightly increase in SM fruits and decrease in TF cultivar, conversely total SFA showed the opposite trend.

A drop from pink to red fruits was noticed in MUFA (both SM and TF), DUFA (TF), and TUFA (SM) content, whereas an opposite trend/increase with the ripening stage emerged DUFA (SM) and TUFA (TF) amount.

Despite untargeted investigation, direct infusion ESI FT-ICR MS analysis delivers consistent solution composition and maximum metabolome coverage, ion-suppression effects and differences of signal response are a concern in view of an accurate quantitation. However, careful tuning of experimental conditions has recently allowed a successful quantification of numerous isomeric groups of intact wax esters, where relative ionization efficiency was found to be influenced only by lipid class and saturation degree, while independent on carbon chain length [62]. On this basis, the abundances of molecular formulas classified as free fatty acids (FA) and presenting the expected $(CH_2)_2$ increments were obtained from the lists of organic extracts in the negative ionization mode, relatively richer in lipids (Table S4). Then, these values were summed up within each specific class, namely saturated SFA, containing the series 12:0-20:0, MUFA, with the series 14:1–20:1, DUFA and TUFA, including compounds 18:2, 20:2, 18:3, 20:3, 18:4, 20:4, respectively, to evaluate their relative abundance. Notably, four FAs at *m/z* 227, 255, 277, and 279 have been assigned to myristic (14:0), palmitic (16:0), linolenic (18:3), and linoleic (18:2) acids, respectively, on the basis of their characteristic fragmentation in CID experiments. As shown in Figure 4, an overall similar composition is highlighted in both organic SM_R and TF_R extracts, with the highest percentages found for: (i) 16:0 (ca. 60%) and 18:0 (ca. 28%) among SFAs; (ii) 16:1 (ca. 58%) and 18:1 (ca. 39%) among MUFAs; (iii) 18:2 (ca. 77%) and 20:2 (ca. 17%) among DUFAs; (iv) 18:3 (ca. 37%) and 20:3 (ca. 64%), among TUFAs.

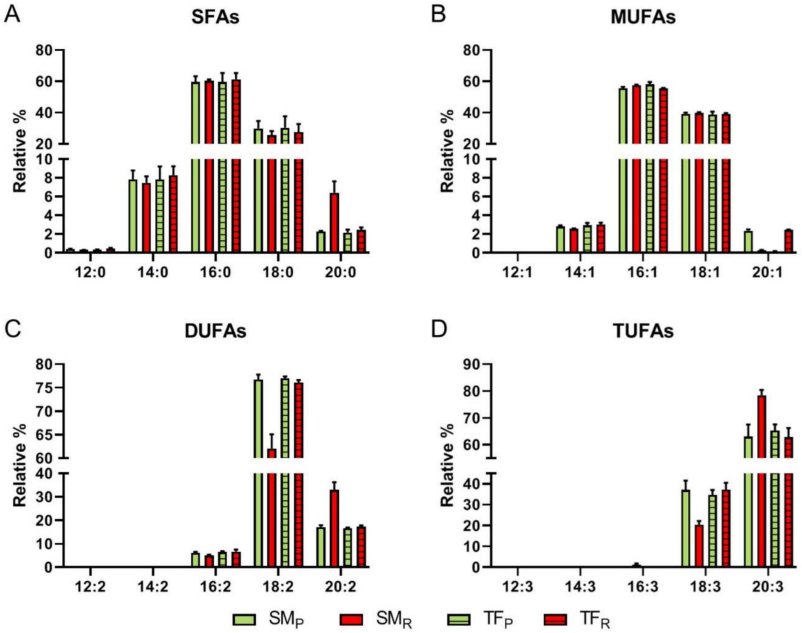


Figure 4. Histograms of the relative abundance distribution within specific classes of FA: saturated (**A**); mono-unsaturated (**B**); di-unsaturated (**C**); tri-unsaturated (**D**) obtained by ESI(−) FT-ICR MS analyses of organic SM_R (red), SM_P (green), TF_R (red), TF_P (green) extracts.

The presence and chemical diversity of long chain fatty acids pointed out in both cultivars is intriguing, since these compounds are known to have a wide range of biological properties, including the promotion of type 2 immune responses [63].

Noteworthy, SM_R organic fraction contains both the lowest percentage of relatively shorter chain di- and tri-unsaturated FA, including 18:2 (ca. 62% vs. the above reported value of 77%) and 18:3 (ca. 21% vs. 37% above reported), and the highest amount of longer chain FA, including 20:2 (ca. 33% vs. 17%) and 20:3 (ca. 78% vs. 64%).

The availability of appropriate unsaturated fatty acids is reported as a significant factor responsible for specific fruit flavor and aroma development, due to the action of lipase enzymes that may release a rich milieu of metabolites from acyl lipids during the ripeness processes.

3.2.8. Biogenic Amines

High performance liquid chromatography allowed to detect seven BAs (Table 7), namely putrescine (PUT), cadaverine (CAD), histidine (HIS), serotonin (SER), spermidine (SPD), and spermine (SPM). All BAs investigated are found in tomato samples, except for tyramine (TYM), an amine with negative health effect, which was not detected in any samples. By contrast, HIS, another BA with negative health effect, was detected in all samples. Histamine presence is regulated in some food, but none in tomatoes. The tolerance presence of histamine in wine and fish is up to 100 μg/g [64]. The maximum HIS level was found in TFR at 1.463 ± 0.015 μg/g, far less than the regulation limits (Commission Regulation (EU) No 1019/2013 of 23 October 2013 amending Annex I to Regulation (EC) No 2073/2005 as regards to histamine in fishery products.) For these reasons, these tomato cultivars appear to be safe

for human health. The rest of BAs are usually related to cultivar and storage condition of samples. Indeed, a great variability of BAs concentration was found between SM and TF. In all the tomatoes, SER, an important neurotransmitter, was also detected in high concentration. This BA has positive effects on human health; SER plays an important role in regulating mood, sleep, body temperature, sexuality, and appetite. SER is involved in many neuropsychiatric disorders such as migraine, bipolar disorder; serotonin deficiency causes obsessive-compulsive disorder, repetition, and mania. So, its assumption by diet is highly recommended [65]. About the different level of the BAs in pink with respect to red tomatoes, is possible to highlight that in almost all samples, the highest concentration was found in red fruits (Table 7). This is in accordance with previously studies which demonstrated the accumulation of BAs during ripening of meat [66] or dairy products [67]. Finally, based on the obtained data, BAs could be also used as ripening markers of tomatoes.

Table 7. Biogenic amines determined by HPLC in SM and TF samples, at red and pink ripening stages ± Std. Dev. (μg/g) [a].

ADD HEADING	BPEA	PUT	CAD	HIS	SER	TYM	SPD	SPM
SM_P	0.170 ± 0.001	2.777 ± 0.137	1.127 ± 0.055	0.448 ± 0.027	277.760 ± 5.226	n.d.	0.235 ± 0.010	0.253 ± 0.013
SM_R	0.168 ± 0.001	7.564 ± 0.289	1.888 ± 0.025	1.363 ± 0.037	394.054 ± 12.725	n.d.	0.122 ± 0.006	0.346 ± 0.019
TF_P	0.165 ± 0.001	3.289 ± 0.006	1.287 ± 0.006	0.589 ± 0.032	258.679 ± 7.360	n.d.	0.116 ± 0.001	0.191 ± 0.002
TF_R	0.272 ± 0.050	6.293 ± 0.113	1.533 ± 0.033	1.463 ± 0.015	326.848 ± 8.850	n.d.	0.249 ± 0.010	0.477 ± 0.031

[a] BPEA: β-phenylethylamine, PUT: putrescine; CAD: cadaverine; HIS: histidine; SER: serotonin; TYM: tyramine; SPD: spermidine; SPM: spermine; n.d.: not detected.

3.3. Screening of Biological Activities

3.3.1. Antioxidant Activities

The radical scavenging properties of the tested extracts were evaluated against the synthetic chromogenic DPPH and ABTS radicals. Under our experimental conditions, all extracts (1–5000 μg mL^{-1}) were able to counteract the ABTS radical, despite a weak radical scavenger activity against DPPH, which achieved a lower than 40% inhibition at the highest tested concentration, thus hindering the IC_{50} evaluation (Figure S8). As expected, the positive control trolox (concentration range of 1–100 μg mL^{-1}) was found to be a potent scavenger of both DPPH and ABTS (Figure S8). The measurable IC_{50} values for the extracts and Trolox were displayed in Table 8.

Table 8. Effects of hydroalcoholic and organic extracts from both pink (*p*) and red (R) fruits of *Solanum lycopersicum* var. TF and SM, and standard antioxidant agents in the antioxidant assays [a].

Sample	IC_{50} (CL) (μg mL^{-1}) [a]			
	ADD HEADING	ABTS Radical Scavenging Activity	Ferric Ion Chelating Activity	Ferric Ion Reducing Activity
TF_P	Hydroalcoholic	371.2 (296.6–494.8)	106.6 (69.3–163.6)	-
	Organic	174.9 (119.6–255.8)	-	184.6 (109.3–433.6)
TF_R	Hydroalcoholic	-	208.5 (143.1–303.1)	-
	Organic	573.1 (463.3–708.9)	-	250.0 (152.1–410.5)
SM_P	Hydroalcoholic	629.9 (475.9–720.5)	93.5 (63.9–116.6)	-
	Organic	479.6 (358.7–663.3)	-	397.8 (319.3–438.7)
SM_R	Hydroalcoholic	-	242.7 (233.9–276.6)	-
	Organic	-	-	368.5 (289.3–468.6)
Positive control		2.5 (1.3–5.6) [b]	45.2 (13.1–75.5) [c]	1.5 (1.1–2.0) [b]

[a] CL, confidence limits; - not evaluable since a lower than 40% effect was achieved. [b] trolox; [c] quercetin.

Comparing the tomato varieties at the pink developmental stage, TF_P organic extract displayed the most potent ABTS scavenging activity, being the IC_{50} value about 2-, 3-, and 4-fold less than that of TF_P hydroalcoholic, and both SM_P organic and hydroalcoholic fractions, respectively (Table 8). Similarly, TF_R organic extract was the most effective scavenging sample from red fruits, followed by TF_R hydroalcoholic extract, although with a 3-fold lower potency compared to the TF_P sample (Table 8). Conversely, SM_R organic and hydroalcoholic extracts produced a lower than 50% ABTS inhibition at the highest tested concentrations, thus hindering the evaluation the IC_{50} value (Table 8).

ABTS and DPPH radicals are scavenged by electron- or hydrogen-transfer mechanisms, although with a different specificity and kinetic profile [68]. ABTS usually reacts with both lipophilic and hydrophilic compounds and possesses a poor selectivity in the reaction with hydrogen-atom donors; conversely, DPPH is more selective for small molecules, likely due to the limited steric accessibility of the radical site to larger compounds [68]. ABTS assay has been also reported to better estimate the antioxidant power of fruits and vegetables rich in hydrophilic, lipophilic, and high-pigmented antioxidant compounds compared to DPPH assay [69]. Particularly, carotenoids seem to not react with DPPH, while being able to bleach ABTS [70].

On the base of this evidence, the scavenging abilities of TF and SM extracts towards ABTS radical can be ascribed to the presence of both hydrophilic and lipophilic antioxidant phytochemicals. Among them, the antioxidant contribution of polyphenols, carotenoids, tocopherols, and vitamins C and E to the ABTS scavenging properties of tomato fruits has been previously hypothesized [71]. Further studies are required to clarify their involvement in the radical scavenging activity of TF and SM extracts.

When assessed in ferrozine assay, all samples exhibited a weak chelating activity of ferrous ion; conversely, the hydroalcoholic extracts of TF and SM fruits were able to chelate ferric ions (Table 8), being hydroalcoholic TF_P and SM_P extracts the most potent (IC_{50} values about two-fold lower than that of the corresponding red extracts). The positive control quercetin resulted to be about two- and four-fold more potent than the tested extracts (Table 8).

Despite a marked ferric chelating activity, the hydroalcoholic samples were ineffective as reducing agents; conversely, the organic extracts significantly reduced ferric ions, being that from TF_P the most potent (Table 8). According to the Pearson analysis, a significant correlation occurs between the ABTS scavenger power of TF hydroalcoholic and organic extract and the respective chelating and reducing activities (correlation coefficient r of 0.81 and 0.95, respectively).

Regarding the ferric thiocyanate assay, all the extracts showed an inhibitory activity of linoleic acid peroxidation, being the organic samples from both pink and red tomatoes the most effective ones (Figure 5). Among the tested extracts, TF_P and TF_R organic fractions induced about a 60 and 50% inhibition of lipid peroxidation already after 24 h incubation (Figure 5B), followed by a 50% of SM_P organic fraction and a lower than 40% inhibition of the other samples (Figure 5B).

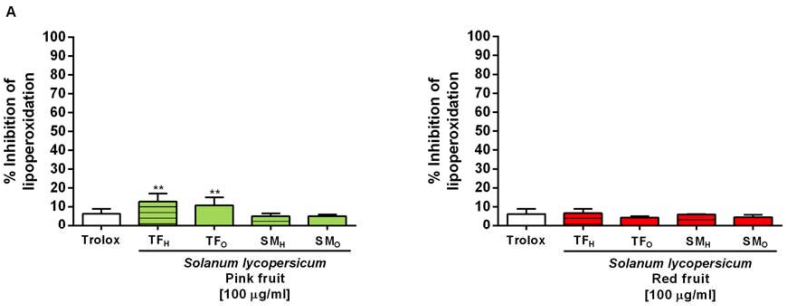


Figure 5. *Cont.*

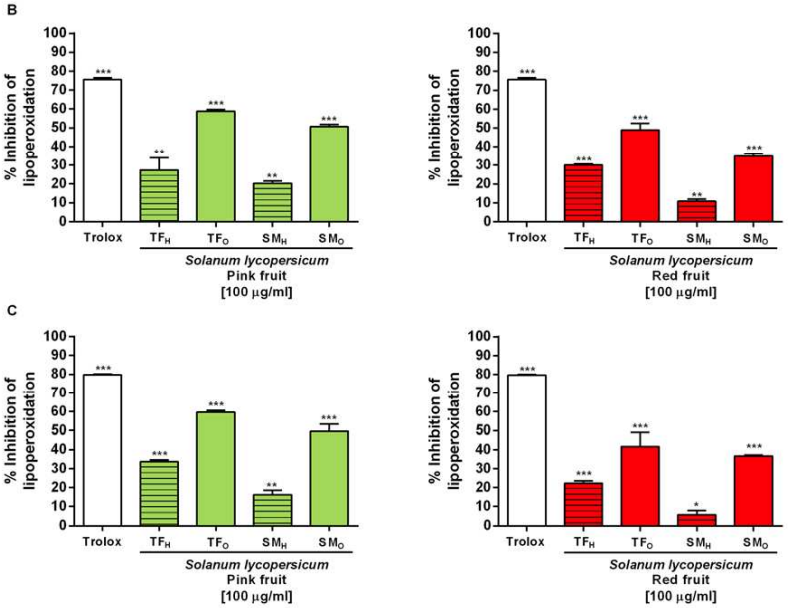


Figure 5. Inhibitory effects of the organic and hydroalcoholic extracts from *Solanum lycopersicum* var. TF and SM tomatoes, at pink (left) and red (right) stages, on linoleic acid peroxidation after different time exposure (**A**) t = 0, (**B**) t = 24 h, and(**C**) t = 48 h. TF organic (TF_O), TF hydroalcoholic (TF_H), SM organic (SM_O), SM hydroalcoholic (SM_H), extracts 100 µg mL^{-1}. * $p < 0.05$, ** $p < 0.01$, and *** $p < 0.01$, represent a statistically significant lipoperoxidation inhibition respect to the basal effect at t = 0 (Anova + Dunnett's multiple comparison post test).

3.3.2. Advanced Glycation End-Product (AGE) Inhibition

Growing evidence highlighted that phenolic compounds are able to prevent the production of advance glycation end products (AGEs), toxic metabolites accumulated under different pathologies, and responsible for the inflammatory and oxidative stress [37]. According to these data, the ability to interfere with AGE formation was assessed as a possible mechanism correlated to the antioxidant and cytoprotective power of TF and SM extracts. Therefore, treatment with AGEs inhibitors is believed to be a potential strategy for preventing diabetes complications.

Under the experimental conditions, despite a null activity of SM samples, both TF_P and TF_R hydroalcoholic fractions produced a concentration-dependent and statistically significant inhibition of the AGE production, although with a potency about 3-fold lower compared to rutin (positive control). The maximum 47% inhibition was achieved at the concentration of 1000 µg mL^{-1} of TF_R hydroalcoholic extract (Figure 6B). Furthermore, that from TF_P produced a maximum 44% inhibition at the highest tested concentration. According to literature [37], phenolic compounds could contribute to the observed effects.

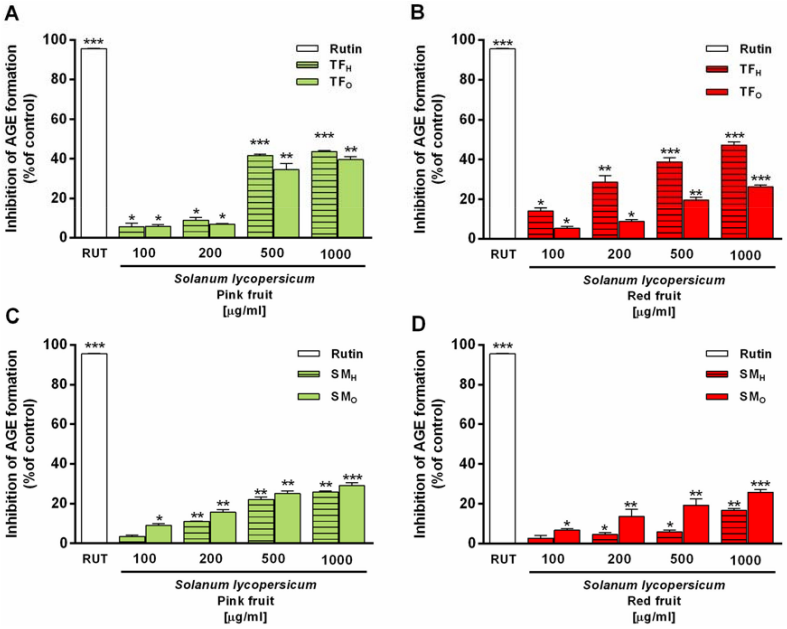


Figure 6. Inhibition of formation of advanced glycation end-products (AGE) induced by organic (O) and hydroalcoholic (H) extracts from *Solanum lycopersicum* var. (**A**) TF_P, (**B**) TF_R, (**C**) SM_P, (**D**) SM_R, and the positive control rutin [200 μg mL^{-1}]. RUT, rutin, TF_H, TF_O, SM_H, SM_O. Each value represents mean ± SEM ($n = 6$). * $p < 0.05$, ** $p < 0.01$, and *** $p < 0.01$, represent a statistically significant AGE inhibition compared to the basal level (Anova + Dunnett's multiple comparison post test).

3.3.3. In Vitro Metabolic Enzyme Inhibition

Taking into account that dietary phenolics are known to decrease the activity of α-amylase and α-glucosidase, thus lowering carbohydrate digestion and absorption [37], the ability of the tested samples was also evaluated to affect the function of both enzymes. Under our experimental conditions, the extracts resulted ineffective towards α-amylase enzyme, whereas a partial α-glucosidase inhibition (maximum 50% inhibition at the highest concentration of 1000 μg mL^{-1}) was found in the presence of the hydroalcoholic extracts of both pink and red TF tomatoes (data not shown), likely ascribable to the highest phenolic content.

3.3.4. Cytoprotection towards the Oxidative Stress Induced by tBuOOH

Preliminarily, the cytotoxicity of selected tomatoes samples on HepG2 cells was evaluated by MTT assay, thus highlighting that the extracts did not affect significantly the cell viability up to the concentration of 100 μg mL^{-1} after 24 h exposure, with early toxicity signs at higher concentrations (data not shown). On the basis of this evidence, the concentration of 100 μg mL^{-1} was used to study the ability of the extracts to inhibit the intracellular oxidative stress induced by tBuOOH after 2 h exposure.

Under our experimental conditions, tBuOOH produced a statistically significant increase of the intracellular ROS-level with respect to the vehicle control, reaching an oxidation index of 2.17 ± 0.04 (Figure 7), while the extracts alone did not affect the ROS levels (data not shown).

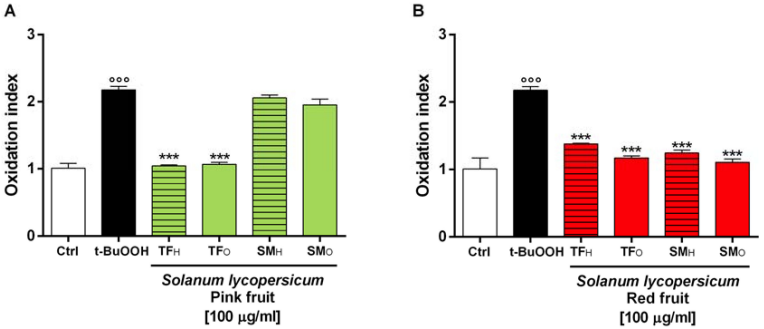


Figure 7. Effect of the organic and hydroalcoholic extracts from the fruits of *Solanum lycopersicum* var. Torpedino di Fondi (TF) and San Marzano (SM) at (**A**) pink and (**B**) red ripening stages on the *t*BuOOH-induced intracellular ROS levels by the DCFH-DA (2,7-dichlorofluorescein diacetate) assay. *t*BuOOH (5 mM) TF_H, TF_O, SM_H, SM_O. The oxidation index was obtained by the ration between the DCF fluorescence of the sample and that of the vehicle control (i.e., EtOH 1% *v*/*v*). *** $p < 0.001$, represent a statistically significant difference of the treatment with respect to *t*BuOOH (Anova + Dunnett's multiple comparison post test). °°° $p < 0.001$, represent a statistically significant difference of *t*BuOOH vs. Ctrl. $p < 0.001$, represent a statistically significant difference of *t*BuOOH vs. Ctrl.

When the cells were pre-treated overnight with the tested extracts, the pro-oxidant effect of tBuOOH resulted significantly reduced, although with different potency. Among pink tomato samples, both TF hydroalcoholic and organic extracts were able to halve the tBuOOH-induced oxidation (with 48% and 54% inhibition index respectively), thus exhibiting a strong antioxidant activity (Figure 7A). Conversely, the organic and hydroalcoholic extracts from SM_P fruits resulted ineffective, being the oxidation index similar to that of tBuOOH (Figure 7A). All the extracts from red tomatoes displayed marked antioxidant activity, with the oxidation index of tBuOOH reduced from 1.7- to 2-fold. For both varieties, the organic extracts were the most potent samples, achieving the inhibition levels of 46.0 and 49% for TF and SM, respectively (Figure 7B). Analogously, the hydroalcoholic extracts produced antioxidant effects against tBuOOH, although with lower potency, being the inhibition values of 36 and 43% for TF and SM, respectively (Figure 7B).

3.3.5. Antifungal Activity of SM and TF Hydroalcoholic and Organic Extracts

Irving and colleagues have shown antifungal activity of tomato plant extracts against *Candida albicans* ATCC 2091 [72]. In the present study, for the first time has been analyzed the anti-*Candida* activity of different extracts of tomato fruits from TF and SM cultivars against different *Candida* species such as *C. albicans*, *glabrata*, and *krusei*.

Candida is a human commensal in several anatomically distinct sites such as in the gastrointestinal tract. In specific environmental condition, *Candida* can switch to pathogen and can be responsible of some diseases. In the gut, patients with intestinal inflammation have high levels of *Candida* species when compared to healthy individuals [73]. The main *Candida* species isolated from the human gastrointestinal tract are *C. albicans*, *C. glabrata*, and *C. krusei* [74]. Antifungal activity of plants extracts was demonstrated on these species by the broth microdilution method. Between the two varieties tested, TF showed a better activity, against all *Candida* strains (Table S5). Moreover, organic fractions showed the best antifungal activity compared to the hydroalcoholic ones. In particular, organic TF_R and TF_P and hydroalcoholic TF_R and TF_P extracts showed a geometric (GM) MIC_{50} of 707 µg mL^{-1}, 841 µg mL^{-1}, 1361 µg mL^{-1}, 1101 µg mL^{-1}, respectively. Organic SM_R and SM_P, hydroalcoholic SM_R and SM_P fractions showed a GM MIC_{50} of 1236 µg mL^{-1}, 891 µg mL^{-1}, 1442 µg mL^{-1}, 1414 µg mL^{-1},

respectively (Table S5) In particular, TF_R organic extracts showed a GM MIC_{50} of 707 μg mL^{-1}, while the TF_R hydroalcoholic showed a GM MIC_{50} 1442 μg mL^{-1} against all *Candida* strains (Table S5).

Antibacterial and antifungal activity of several plant secondary metabolites and their derivatives such as alkaloids and polyphenols has been reported [75]. The alkaloid such as glycoalkaloid α-tomatine depicted antifungal effects against a variety of fungi [76]. In our results, tomatine was found only in TF_P and not in TF_R, indicating that probably, as hypothesized by some authors, the synergy of several compounds is responsible for the antifungal activity shown.

In conclusion, TF reduces *Candida* cells in the intestinal tract intake of TF, which have a growth inhibiting activity against different *Candida* species, and could be a strategy to restore the intestinal microbiota present in the healthy individual.

4. Conclusions

The combined application of both targeted and untargeted methodologies allowed to outline the chemical profile of both TF, a new hybrid cultivar recently introduced in south Lazio (Italy), and SM tomatoes at two ripening stages. We wish to itemize here in some detail both single important molecules and chemical classes to stimulate an active consideration of these highly complex natural mixtures, rich in compounds that may reveal novel important, hopefully beneficial roles in forthcoming studies. Some metabolites were shared by all extracts, though at different concentration, such as macronutrients like sugars and derivatives (hexose, sorbitol, mannosylglycerate), and amino acids (tryptophan and citrulline), the Amadori adduct fructoselysine, relevant biochemical intermediates (ornithine, chorismic acid, and GABA), terpenes (caryophyllene), nucleobase (adenosine), vitamin precursors and metabolites (diapophytoene, diapolycopene, α-tocopheronolactone), fatty alcohol (panaxytriol), organic acids (citric, chlorogenic, and azelaic acid) and conjugates (caffeic acid 3-glucoside, O-feruloylquinate), sterols (solagenin), free fatty acids (myristic, myristoleic, lauric, palmitic, oleic, linoleic, linolenic, eicosenoic acids). Differently, other metabolites might be considered marker compounds, being detected only in one or a few extracts, like glycyphyllin, maleic and tartaric acids (TF_P), cinnamoyl glucoside (TF_R), the vitamins dihydroretinol, dehydroretinal, retinoic and tocopheronic acids, and the antifungal terpenoid phytuberin (SM_R), the solanine derivative, tomatidinol (SM_P), the vitamin-E precursors, phytol (SM_R, TF_P), and γ-tocotrienol (SM_P, SM_R), the glycoalkaloids tomatine and tomatidine, suberic and ascorbic acids (SM_P, TF_P), quinic, phosphogluconic and shikimic acids (TF_R, TF_P), the polyketide lycoflexine (SM_R, SM_P, TF_P). These characteristic chemical features may concur to the excellent organoleptic properties as well as to antioxidant, antiglycative, and antifungal activities of Torpedino di Fondi, an emerging south Lazio tomato belonging to the mini-San Marzano type. This study may contribute to the unceasing buildup of reliable reference databases useful to guarantee food authenticity and freshness, and to support consumers and further nutraceutical evaluations.

Supplementary Materials: Supplementary materials can be found at http://www.mdpi.com/2076-3921/9/10/1027/s1, Figures S1–S5: TF and SM tomato fruits from Fondi area (Lazio region), Figure S6: Comparison between TFP and TFR and SMP and SMR their ripening stage for the number of possible CHO (A) and CHNO (B) metabolites, Figure S7: Common and uncommon features (in%) in the combined pattern of hydroalcoholic and organic extracts, Table S1: Amount of peel, pulp, seeds and juice in both pink and red Solanum lycopersicum var. TF and SM fruits; Table S2–3: Comprehensive list of metabolites detected in hydroalcoholic and organic fractions of pink and red San Marzano (SM) and Torpedino di Fondi (TF) extracts, Table S4: Overview of the relative abundancies of specific classes of saturated, mono-, di- and poly-unsaturated fatty acids (FA), Table S5: Antifungal activity of extracts against 4 *C.albicans* strains, 3 *C. glabrata* strains and 2 *C. krusei*.

Author Contributions: Conceptualization, C.I., A.M., M.E.C., and L.M.; methodology, A.F., and C.F.; validation, A.P.S., A.D.S., C.C., M.S.S., and A.F.; formal analysis, A.M.G., M.S., G.D.M., M.R., S.C., A.F., C.F., G.S., A.D.S. and S.D.G.; investigation, A.M.G., M.S., G.D.M., M.R., S.C., G.S., A.F., C.F., C.C., M.S.S., A.D.S. and S.D.G.; resources, C.I., A.M., M.S., and G.D.M.; data curation, A.P.S., A.D.S., S.F., C.C., M.S.S. and G.V.; writing—original draft preparation, C.I., A.M., A.D.S. and M.E.C.; writing—review and editing, C.I., A.M. and M.E.C.; visualization, C.I., A.M., and M.E.C.; supervision, S.F., M.E.C., G.V., A.P.S., and L.M.; project administration, L.M.; funding acquisition, S.F., M.E.C., and L.M. All authors have read and agreed to the published version of the manuscript.

Funding: This research was funded by REGIONE LAZIO, "e-ALIERB" Project LR13/2008–Dipartimento di Chimica e Tecnologie del Farmaco and Italian Ministry of Education, Universities and Research-Dipartimenti di Eccellenza-L. 232/2016 and by the EU Horizon 2020 Programme (EU_FT-ICR_MS, under grant number 731077). We also acknowledge the support from the Portuguese Mass Spectrometry Network (LISBOA-01-0145-FEDER-022125) and The Portuguese Foundation for Science and Technology FCT for contract CEECIND/02246/2017 to MSS.

Acknowledgments: Authors wish to thank the Società Cooperativa Agricola "San Leone" (Fondi-Sperlonga, Lazio region, Central Italy) and Mafalda s.r.l. for supplying the fresh raw material. Fellowship of Cinzia Ingallina and Silvia Di Giacomo was financed by "e-ALIERB" Project. Antonella Di Sotto was supported by Enrico and Enrica Sovena Foundation.

Conflicts of Interest: The authors declare no conflict of interest. The funders had no role in the design of the study; in the collection, analyses, or interpretation of data; in the writing of the manuscript, or in the decision to publish the results.

References

1. Rao, R.; Corrado, G.; Bianchi, M.; Di Mauro, A. (GATA)4 DNA fingerprinting identifies morphologically characterized "San Marzano" tomato plants. *Plant Breed.* **2006**, *125*, 173–176. [CrossRef]
2. Loiudice, R.; Impembo, M.; Laratta, B.; Villari, G.; Lo Voi, A.; Siviero, P.; Castaldo, D. Composition of San Marzano tomato varieties. *Food Chem.* **1995**, *53*, 81–89. [CrossRef]
3. Dono, G.; Rambla, J.L.; Frusciante, S.; Granell, A.; Diretto, G.; Mazzucato, A. Color mutations alter the biochemical composition in the san marzano tomato fruit. *Metabolites* **2020**, *10*, 110. [CrossRef]
4. D'Esposito, D.; Ferriello, F.; Molin, A.D.; Diretto, G.; Sacco, A.; Minio, A.; Barone, A.; Di Monaco, R.; Cavella, S.; Tardella, L.; et al. Unraveling the complexity of transcriptomic, metabolomic and quality environmental response of tomato fruit. *BMC Plant Biol.* **2017**, *17*, 1–18. [CrossRef] [PubMed]
5. Ercolano, M.R.; Carli, P.; Soria, A.; Cascone, A.; Fogliano, V.; Frusciante, L.; Barone, A. Biochemical, sensorial and genomic profiling of traditional Italian tomato varieties. *Euphytica* **2008**, *164*, 571–582. [CrossRef]
6. Sobolev, A.P.; Circi, S.; Capitani, D.; Ingallina, C.; Mannina, L. Molecular fingerprinting of food authenticity. *Curr. Opin. Food Sci.* **2017**, *16*. [CrossRef]
7. Sobolev, A.P.; Thomas, F.; Donarski, J.; Ingallina, C.; Circi, S.; Cesare Marincola, F.; Capitani, D.; Mannina, L. Use of NMR applications to tackle future food fraud issues. *Trends Food Sci. Technol.* **2019**, *91*, 347–353. [CrossRef]
8. Dono, G.; Picarella, M.E.; Pons, C.; Santangelo, E.; Monforte, A.; Granell, A.; Mazzucato, A. Characterization of a repertoire of tomato fruit genetic variants in the San marzano genetic background. *Sci. Hortic.* **2020**, *261*, 108927. [CrossRef]
9. Macone, A.; Fontana, M.; Barba, M.; Botta, B.; Nardini, M.; Ghirga, F.; Calcaterra, A.; Pecci, L.; Matarese, R.M. Antioxidant Properties of Aminoethylcysteine Ketimine Decarboxylated Dimer: A Review. *Int. J. Mol. Sci.* **2011**, *12*, 3072–3084. [CrossRef]
10. Burton-Freeman, B.; Reimers, K. Tomato Consumption and Health: Emerging Benefits. *Am. J. Lifestyle Med.* **2011**, *5*, 182–191. [CrossRef]
11. Del Giudice, R.; Raiola, A.; Tenore, G.C.; Frusciante, L.; Barone, A.; Monti, D.M.; Rigano, M.M. Antioxidant bioactive compounds in tomato fruits at different ripening stages and their effects on normal and cancer cells. *J. Funct. Foods* **2015**, *18*, 83–94. [CrossRef]
12. García-Valverde, V.; Navarro-González, I.; García-Alonso, J.; Periago, M.J. Antioxidant Bioactive Compounds in Selected Industrial Processing and Fresh Consumption Tomato Cultivars. *Food Bioprocess Technol.* **2013**, *6*, 391–402. [CrossRef]
13. Slimestad, R.; Verheul, M. Review of flavonoids and other phenolics from fruits of different tomato (*Lycopersicon esculentum Mill.*) cultivars. *J. Sci. Food Agric.* **2009**, *89*, 1255–1270. [CrossRef]
14. Fratianni, F.; Cozzolino, A.; D'Acierno, A.; Nazzaro, F.; Riccardi, R.; Spigno, P. Qualitative Aspects of Some Traditional Landraces of the Tomato "Piennolo" (*Solanum lycopersicum* L.) of the Campania Region, Southern Italy. *Antioxidants* **2020**, *9*, 565. [CrossRef] [PubMed]
15. Anton, D.; Matt, D.; Pedastsaar, P.; Bender, I.; Kazimierczak, R.; Roasto, M.; Kaart, T.; Luik, A.; Püssa, T. Three-Year Comparative Study of Polyphenol Contents and Antioxidant Capacities in Fruits of Tomato (*Lycopersicon esculentum Mill.*) Cultivars Grown under Organic and Conventional Conditions. *J. Agric. Food Chem.* **2014**, *62*, 5173–5180. [CrossRef] [PubMed]

16. Tan, S.; Ke, Z.; Chai, D.; Miao, Y.; Luo, K.; Li, W. Lycopene, polyphenols and antioxidant activities of three characteristic tomato cultivars subjected to two drying methods. *Food Chem.* **2021**, *338*, 128062. [CrossRef] [PubMed]
17. Devadas, S.M.; Giffen, S.R.; Kumar, N.; Lobo, R.; Ballal, M. Activity of Solanum lycopersicum against Candida species isolated from retro-positive patients—An invitro study. *J. Pharm. Sci. Res.* **2017**, *9*, 1233–1236.
18. Añibarro-Ortega, M.; Pinela, J.; Ćirić, A.; Martins, V.; Rocha, F.; Soković, M.D.; Barata, A.M.; Carvalho, A.M.; Barros, L.; Ferreira, I.C.F.R. Valorisation of table tomato crop by-products: Phenolic profiles and in vitro antioxidant and antimicrobial activities. *Food Bioprod. Process.* **2020**, *124*, 307–319. [CrossRef]
19. Herbel, V.; Schäfer, H.; Wink, M. Recombinant Production of Snakin-2 (an Antimicrobial Peptide from Tomato) in *E. coli* and Analysis of Its Bioactivity. *Molecules* **2015**, *20*, 14889–14901. [CrossRef]
20. Vasile Rusu, A.; Alvarez Penedo, B.; Schwarze, A.-K.; Trif, M. The Influence of Candida spp. in Intestinal Microbiota; Diet Therapy, the Emerging Conditions Related to Candida in Athletes and Elderly People. In *Candidiasis [Working Title]*; IntechOpen: London, UK, 2020.
21. Sobolev, A.P.; Mannina, L.; Capitani, D.; Sanzò, G.; Ingallina, C.; Botta, B.; Fornarini, S.; Crestoni, M.E.; Chiavarino, B.; Carradori, S.; et al. A multi-methodological approach in the study of Italian PDO "Cornetto di Pontecorvo" red sweet pepper. *Food Chem.* **2018**, *255*. [CrossRef]
22. Ingallina, C.; Capitani, D.; Mannina, L.; Carradori, S.; Locatelli, M.; Di Sotto, A.; Di Giacomo, S.; Toniolo, C.; Pasqua, G.; Valletta, A.; et al. Phytochemical and biological characterization of Italian "sedano bianco di Sperlonga" Protected Geographical Indication celery ecotype: A multimethodological approach. *Food Chem.* **2020**, *309*, 125649. [CrossRef] [PubMed]
23. Circi, S.; Capitani, D.; Randazzo, A.; Ingallina, C.; Mannina, L.; Sobolev, A.P. Panel test and chemical analyses of commercial olive oils: A comparative study. *Chem. Biol. Technol. Agric.* **2017**, *4*. [CrossRef]
24. Ingallina, C.; Sobolev, A.P.; Circi, S.; Spano, M.; Fraschetti, C.; Filippi, A.; Di Sotto, A.; Di Giacomo, S.; Mazzoccanti, G.; Gasparrini, F.; et al. *Cannabis sativa* L. Inflorescences from Monoecious Cultivars Grown in Central Italy: An Untargeted Chemical Characterization from Early Flowering to Ripening. *Molecules* **2020**, *25*, 1908. [CrossRef]
25. Solovchenko, A.E.; Chivkunova, O.B.; Merzlyak, M.N.; Reshetnikova, I.V. A Spectrophotometric Analysis of Pigments in Apples. *Russ. J. Plant Physiol.* **2001**, *48*, 693–700. [CrossRef]
26. Folch, J.; Lees, M.; Sloane Stanley, G.H. A simple method for the isolation and purification of total lipides from animal tissues. *J. Biol. Chem.* **1957**, *226*, 497–509.
27. Wellburn, A.R. The Spectral Determination of Chlorophylls a and b, as well as Total Carotenoids, Using Various Solvents with Spectrophotometers of Different Resolution. *J. Plant Physiol.* **1994**, *144*, 307–313. [CrossRef]
28. Ingallina, C.; Sobolev, A.P.; Circi, S.; Spano, M.; Giusti, A.M.; Mannina, L. New hybrid tomato cultivars: An NMR-based chemical characterization. *Appl. Sci.* **2020**, *10*, 1887. [CrossRef]
29. Marshall, A.G.; Hendrickson, C.L.; Jackson, G.S. Fourier transform ion cyclotron resonance mass spectrometry: A primer. *Mass Spectrom. Rev.* **1998**, *17*, 1–35. [CrossRef]
30. MassTRIX. Available online: http://masstrix3.helmholtz-muenchen.de/masstrix3/start) (accessed on 20 April 2020).
31. Kind, T.; Fiehn, O. Seven Golden Rules for heuristic filtering of molecular formulas obtained by accurate mass spectrometry. *BMC Bioinform.* **2007**, *8*, 105. [CrossRef] [PubMed]
32. Kim, S.; Kramer, R.W.; Hatcher, P.G. Graphical Method for Analysis of Ultrahigh-Resolution Broadband Mass Spectra of Natural Organic Matter, the Van Krevelen Diagram. *Anal. Chem.* **2003**, *75*, 5336–5344. [CrossRef] [PubMed]
33. Preti, R.; Rapa, M.; Vinci, G. Effect of Steaming and Boiling on the Antioxidant Properties and Biogenic Amines Content in Green Bean (*Phaseolus vulgaris*) Varieties of Different Colours. *J. Food Qual.* **2017**, *2017*, 1–8. [CrossRef]
34. Chiacchierini, E.; Restuccia, D.; Vinci, G. Evaluation of two different extraction methods for chromatographic determination of bioactive amines in tomato products. *Talanta* **2006**, *69*, 548–555. [CrossRef] [PubMed]
35. Di Sotto, A.; Vecchiato, M.; Abete, L.; Toniolo, C.; Giusti, A.M.; Mannina, L.; Locatelli, M.; Nicoletti, M.; Di Giacomo, S. *Capsicum annuum* L. var. Cornetto di Pontecorvo PDO: Polyphenolic profile and in vitro biological activities. *J. Funct. Foods* **2018**, *40*, 679–691. [CrossRef]
36. Di Sotto, A.; Di Giacomo, S.; Toniolo, C.; Nicoletti, M.; Mazzanti, G. *Sisymbrium Officinale* (L.) Scop. and its Polyphenolic Fractions Inhibit the Mutagenicity of Tert-Butylhydroperoxide in Escherichia Coli WP2 uvr AR Strain. *Phyther. Res.* **2016**, *30*, 829–834. [CrossRef]

37. Di Sotto, A.; Locatelli, M.; Macone, A.; Toniolo, C.; Cesa, S.; Carradori, S.; Eufemi, M.; Mazzanti, G.; Di Giacomo, S. Hypoglycemic, Antiglycation, and Cytoprotective Properties of a Phenol-Rich Extract from Waste Peel of *Punica granatum* L. var. Dente di Cavallo DC2. *Molecules* **2019**, *24*, 3103. [CrossRef] [PubMed]
38. Di Sotto, A.; Irannejad, H.; Eufemi, M.; Mancinelli, R.; Abete, L.; Mammola, C.L.; Altieri, F.; Mazzanti, G.; Di Giacomo, S. Potentiation of Low-Dose Doxorubicin Cytotoxicity by Affecting P-Glycoprotein through Caryophyllane Sesquiterpenes in HepG2 Cells: An in Vitro and in Silico Study. *Int. J. Mol. Sci.* **2020**, *21*, 633. [CrossRef]
39. Vitalone, A.; Di Giacomo, S.; Di Sotto, A.; Franchitto, A.; Mammola, C.L.; Mariani, P.; Mastrangelo, S.; Mazzanti, G. Cassia angustifolia Extract Is Not Hepatotoxic in an in vitro and in vivo Study. *Pharmacology* **2011**, *88*, 252–259. [CrossRef]
40. Di Giacomo, S.; Abete, L.; Cocchiola, R.; Mazzanti, G.; Eufemi, M.; Di Sotto, A. Caryophyllane sesquiterpenes inhibit DNA-damage by tobacco smoke in bacterial and mammalian cells. *Food Chem. Toxicol.* **2018**, *111*, 393–404. [CrossRef]
41. Clinical and Laboratory Standards Institute. *Reference Method for Broth Dilution Antifungal Susceptibility Testing of Yeasts CLSI Document M27*, 4th ed.; Clinical and Laboratory Standards Institute: Wayne, PA, USA, 2017; ISBN 1-56238-827-4.
42. Schaal, B.A. Reproductive Capacity and Seed Size in Lupinus Texensis. *Am. J. Bot.* **1980**, *67*, 703–709. [CrossRef]
43. Lichtenthaler, H.K.; Buschmann, C. Chlorophylls and Carotenoids: Measurement and Characterization by UV-VIS Spectroscopy. *Curr. Protoc. Food Anal. Chem.* **2001**, *1*, F4.3.1–F4.3.8. [CrossRef]
44. Sobolev, A.P.; Segre, A.; Lamanna, R. Proton high-field NMR study of tomato juice. *Magn. Reson. Chem.* **2003**, *41*, 237–245. [CrossRef]
45. Pérez, E.M.S.; Iglesias, M.J.; Ortiz, F.L.; Pérez, I.S.; Galera, M.M. Study of the suitability of HRMAS NMR for metabolic profiling of tomatoes: Application to tissue differentiation and fruit ripening. *Food Chem.* **2010**, *122*, 877–887. [CrossRef]
46. Hohmann, M.; Christoph, N.; Wachter, H.; Holzgrabe, U. 1 H NMR Profiling as an Approach To Differentiate Conventionally and Organically Grown Tomatoes. *J. Agric. Food Chem.* **2014**, *62*, 8530–8540. [CrossRef]
47. Carrari, F.; Baxter, C.; Usadel, B.; Urbanczyk-Wochniak, E.; Zanor, M.-I.; Nunes-Nesi, A.; Nikiforova, V.; Centero, D.; Ratzka, A.; Pauly, M.; et al. Integrated Analysis of Metabolite and Transcript Levels Reveals the Metabolic Shifts That Underlie Tomato Fruit Development and Highlight Regulatory Aspects of Metabolic Network Behavior. *Plant Physiol.* **2006**, *142*, 1380–1396. [CrossRef]
48. Mounet, F.; Lemaire-Chamley, M.; Maucourt, M.; Cabasson, C.; Giraudel, J.L.; Deborde, C.; Lessire, R.; Gallusci, P.; Bertrand, A.; Gaudillère, M.; et al. Quantitative metabolic profiles of tomato flesh and seeds during fruit development: Complementary analysis with ANN and PCA. *Metabolomics* **2007**, *3*, 273–288. [CrossRef]
49. Agius, C.; von Tucher, S.; Poppenberger, B.; Rozhon, W. Quantification of Glutamate and Aspartate by Ultra-High Performance Liquid Chromatography. *Molecules* **2018**, *23*, 1389. [CrossRef]
50. Sorrequieta, A.; Ferraro, G.; Boggio, S.B.; Valle, E.M. Free amino acid production during tomato fruit ripening: A focus on l-glutamate. *Amino Acids* **2010**, *38*, 1523–1532. [CrossRef]
51. Boggio, S.B.; Palatnik, J.F.; Heldt, H.W.; Valle, E.M. Changes in amino acid composition and nitrogen metabolizing enzymes in ripening fruits of Lycopersicon esculentum Mill. *Plant Sci.* **2000**, *159*, 125–133. [CrossRef]
52. Ghirga, F.; Quaglio, D.; Ghirga, P.; Berardozzi, S.; Zappia, G.; Botta, B.; Mori, M.; D'Acquarica, I. Occurrence of Enantioselectivity in Nature: The Case of (S)-Norcoclaurine. *Chirality* **2016**, *28*, 169–180. [CrossRef] [PubMed]
53. Gómez-Romero, M.; Segura-Carretero, A.; Fernández-Gutiérrez, A. Metabolite profiling and quantification of phenolic compounds in methanol extracts of tomato fruit. *Phytochemistry* **2010**, *71*, 1848–1864. [CrossRef] [PubMed]
54. Jézéquel, T.; Deborde, C.; Maucourt, M.; Zhendre, V.; Moing, A.; Giraudeau, P. Absolute quantification of metabolites in tomato fruit extracts by fast 2D NMR. *Metabolomics* **2015**, *11*, 1231–1242. [CrossRef]
55. Sanz, M.L.; del Castillo, M.D.; Corzo, N.; Olano, A. Presence of 2-Furoylmethyl Derivatives in Hydrolysates of Processed Tomato Products. *J. Agric. Food Chem.* **2000**, *48*, 468–471. [CrossRef] [PubMed]

56. Bueno, M.J.M.; Díaz-Galiano, F.J.; Rajski, Ł.; Cutillas, V.; Fernández-Alba, A.R. A non-targeted metabolomic approach to identify food markers to support discrimination between organic and conventional tomato crops. *J. Chromatogr. A* **2018**, *1546*, 66–76. [CrossRef]
57. Iijima, Y.; Watanabe, B.; Sasaki, R.; Takenaka, M.; Ono, H.; Sakurai, N.; Umemoto, N.; Suzuki, H.; Shibata, D.; Aoki, K. Steroidal glycoalkaloid profiling and structures of glycoalkaloids in wild tomato fruit. *Phytochemistry* **2013**, *95*, 145–157. [CrossRef]
58. Van Meulebroek, L.; Bussche, J.V.; Steppe, K.; Vanhaecke, L. Ultra-high performance liquid chromatography coupled to high resolution Orbitrap mass spectrometry for metabolomic profiling of the endogenous phytohormonal status of the tomato plant. *J. Chromatogr. A* **2012**, *1260*, 67–80. [CrossRef]
59. Liberati-Čizmek, A.-M.; Biluš, M.; Brkić, A.L.; Barić, I.C.; Bakula, M.; Hozić, A.; Cindrić, M. Analysis of Fatty Acid Esters of Hydroxyl Fatty Acid in Selected Plant Food. *Plant Foods Hum. Nutr.* **2019**, *74*, 235–240. [CrossRef]
60. Tommonaro, G.; de Prisco, R.; Abbamondi, G.R.; Marzocco, S.; Saturnino, C.; Poli, A.; Nicolaus, B. Evaluation of Antioxidant Properties, Total Phenolic Content, and Biological Activities of New Tomato Hybrids of Industrial Interest. *J. Med. Food* **2012**, *15*, 483–489. [CrossRef] [PubMed]
61. Iijima, Y.; Suda, K.; Suzuki, T.; Aoki, K.; Shibata, D. Metabolite Profiling of Chalcones and Flavanones in Tomato Fruit. *J. Jpn. Soc. Hortic. Sci.* **2008**, *77*, 94–102. [CrossRef]
62. Chen, J.; Green, K.B.; Nichols, K.K. Quantitative Profiling of Major Neutral Lipid Classes in Human Meibum by Direct Infusion Electrospray Ionization Mass Spectrometry. *Investig. Opthalmol. Vis. Sci.* **2013**, *54*, 5730. [CrossRef]
63. Berer, K.; Martínez, I.; Walker, A.; Kunkel, B.; Schmitt-Kopplin, P.; Walter, J.; Krishnamoorthy, G. Dietary non-fermentable fiber prevents autoimmune neurological disease by changing gut metabolic and immune status. *Sci. Rep.* **2018**, *8*, 10431. [CrossRef]
64. Guo, Y.-Y.; Yang, Y.-P.; Peng, Q.; Han, Y. Biogenic amines in wine: A review. *Int. J. Food Sci. Technol.* **2015**, *50*, 1523–1532. [CrossRef]
65. Briguglio, M.; Dell'Osso, B.; Panzica, G.; Malgaroli, A.; Banfi, G.; Zanaboni Dina, C.; Galentino, R.; Porta, M. Dietary Neurotransmitters: A Narrative Review on Current Knowledge. *Nutrients* **2018**, *10*, 591. [CrossRef] [PubMed]
66. Suzzi, G. Biogenic amines in dry fermented sausages: A review. *Int. J. Food Microbiol.* **2003**, *88*, 41–54. [CrossRef]
67. Linares, D.M.; del Río, B.; Ladero, V.; Martínez, N.; Fernández, M.; Martín, M.C.; Álvarez, M.A. Factors Influencing Biogenic Amines Accumulation in Dairy Products. *Front. Microbiol.* **2012**, *3*. [CrossRef]
68. Prior, R.L.; Wu, X.; Schaich, K. Standardized Methods for the Determination of Antioxidant Capacity and Phenolics in Foods and Dietary Supplements. *J. Agric. Food Chem.* **2005**, *53*, 4290–4302. [CrossRef]
69. Floegel, A.; Kim, D.-O.; Chung, S.-J.; Koo, S.I.; Chun, O.K. Comparison of ABTS/DPPH assays to measure antioxidant capacity in popular antioxidant-rich US foods. *J. Food Compos. Anal.* **2011**, *24*, 1043–1048. [CrossRef]
70. Müller, L.; Fröhlich, K.; Böhm, V. Comparative antioxidant activities of carotenoids measured by ferric reducing antioxidant power (FRAP), ABTS bleaching assay (αTEAC), DPPH assay and peroxyl radical scavenging assay. *Food Chem.* **2011**, *129*, 139–148. [CrossRef]
71. Kotíková, Z.; Lachman, J.; Hejtmánková, A.; Hejtmánková, K. Determination of antioxidant activity and antioxidant content in tomato varieties and evaluation of mutual interactions between antioxidants. *LWT Food Sci. Technol.* **2011**, *44*, 1703–1710. [CrossRef]
72. Irving, G.W.; Fontaine, T.D.; Doolittle, S.P. Partial Antibiotic Spectrum Of Tomatin, an Antibiotic Agent from the Tomato Plant 12. *J. Bacteriol.* **1946**, *52*, 601–607. [CrossRef]
73. Charlet, R.; Bortolus, C.; Sendid, B.; Jawhara, S. Bacteroides thetaiotaomicron and Lactobacillus johnsonii modulate intestinal inflammation and eliminate fungi via enzymatic hydrolysis of the fungal cell wall. *Sci. Rep.* **2020**, *10*, 11510. [CrossRef]
74. Biasoli, M.S.; Tosello, M.E.; Magaró, H.M. Adherence of Candida strains isolated from the human gastrointestinal tract. *Mycoses* **2002**, *45*, 465–469. [CrossRef]

75. Othman, L.; Sleiman, A.; Abdel-Massih, R.M. Antimicrobial Activity of Polyphenols and Alkaloids in Middle Eastern Plants. *Front. Microbiol.* **2019**, *10*. [CrossRef] [PubMed]
76. Khan, H.; Mubarak, M.S.; Amin, S. Antifungal Potential of Alkaloids As An Emerging Therapeutic Target. *Curr. Drug Targets* **2017**, *18*. [CrossRef] [PubMed]

Publisher's Note: MDPI stays neutral with regard to jurisdictional claims in published maps and institutional affiliations.



© 2020 by the authors. Licensee MDPI, Basel, Switzerland. This article is an open access article distributed under the terms and conditions of the Creative Commons Attribution (CC BY) license (http://creativecommons.org/licenses/by/4.0/).

5.3. Case study 2: Ten apple cultivars from the Piedmont Region

The story of Piedmont apple growing dates back to the Middle Ages, when the monastic orders cultivated and improved the varieties that had survived barbarian invasions. By the early 20th century, Piedmont was home to thousands of varieties, but with the advent of industrial agriculture, decisions with great impact were made regarding selection. The market preferred more productive and attractive apple cultivars, characterized by a bigger size, more attractive appearance, and less delicate flavor, leading to the loss of traditional Italian apple cultivars.

In the present work, ten variety of traditional apple cultivars of the Piedmont Region of Italy were extracted through the Bligh-Dyer protocol and characterize by the combined NMR and PCA analysis in order to discriminate their differences/similarities and to compare their composition with the commercial cultivars.

foods

MDPI

Article

NMR Characterization of Ten Apple Cultivars from the Piedmont Region

Giacomo Di Matteo [1], Mattia Spano [1], Cristina Esposito [2], Cristina Santarcangelo [2], Alessandra Baldi [3], Maria Daglia [2,4], Luisa Mannina [1], Cinzia Ingallina [1,*] and Anatoly P. Sobolev [5]

[1] Department of Chemistry and Technology of Drugs, Sapienza University of Rome, Piazzale Aldo Moro 5, 00185 Rome, Italy; giacomo.dimatteo@uniroma1.it (G.D.M.); mattia.spano@uniroma1.it (M.S.); luisa.mannina@uniroma1.it (L.M.)
[2] Department of Pharmacy, University of Naples Federico II, 80138 Naples, Italy; cristina.esposito@unina.it (C.E.); cristina.santarcangelo@unina.it (C.S.); maria.daglia@unina.it (M.D.)
[3] Tefarco Innova, Parco Area delle Scienze 27/A—Campus, 43124 Parma, Italy; alessandra.baldi.alimenti@gmail.com
[4] International Research Center for Food Nutrition and Safety, Jiangsu University, Zhenjiang 212013, China
[5] Institute for Biological Systems, Magnetic Resonance Laboratory "Segre-Capitani", CNR, Via Salaria Km 29.300, 00015 Monterotondo, Italy; anatoly.sobolev@cnr.it
* Correspondence: cinzia.ingallina@uniroma1.it

Abstract: The metabolite profile of ten traditional apple cultivars grown in the Piedmont region (Italy) was studied by means of nuclear magnetic resonance spectroscopy, identifying an overall number of 36 compounds. A more complete assignment of the proton nuclear magnetic resonance (^{1}H NMR) resonances from hydroalcoholic and organic apple extracts with respect to literature data was reported, identifying fructose tautomeric forms, galacturonic acid, γ-aminobutyric acid (GABA), *p*-coumaroyl moiety, phosphatidylcholine, and digalactosyldiacylglycerol. The chemical profile of each apple cultivar was defined by thorough quantitative NMR analysis of four sugars (fructose, glucose, sucrose, and xylose), nine organic acids (acetic, citric, formic, citramalic, lactic, malic, quinic, and galacturonic acids), six amino acids (alanine, asparagine, aspartate, GABA, isoleucine, and valine), rhamnitol, *p*-coumaroyl derivative, phloretin/phloridzin and choline, as well as β-sitosterol, fatty acid chains, phosphatidylcholine, and digalactosyldiacylglycerol. Finally, the application of PCA analysis allowed us to highlight possible differences/similarities. The Magnana cultivar showed the highest content of sugars, GABA, valine, isoleucine, and alanine. The Runsé cultivar was characterized by high amounts of organic acids, whereas the Gamba Fina cultivar showed a high content of chlorogenic acid. A significant amount of quinic acid was detected in the Carla cultivar. The knowledge of apple chemical profiles can be useful for industries interested in specific compounds for obtaining ingredients of food supplements and functional foods and for promoting apple valorization and preservation.

Keywords: *malus domestica*; local apple cultivars; NMR; metabolite profile; PCA; food ingredients

check for updates

Citation: Di Matteo, G.; Spano, M.; Esposito, C.; Santarcangelo, C.; Baldi, A.; Daglia, M.; Mannina, L.; Ingallina, C.; Sobolev, A.P. NMR Characterization of Ten Apple Cultivars from the Piedmont Region. *Foods* **2021**, *10*, 289. https://doi.org/10.3390/foods10020289

Academic Editor: Luca Laghi
Received: 30 December 2020
Accepted: 25 January 2021
Published: 1 February 2021

Publisher's Note: MDPI stays neutral with regard to jurisdictional claims in published maps and institutional affiliations.

Copyright: © 2021 by the authors. Licensee MDPI, Basel, Switzerland. This article is an open access article distributed under the terms and conditions of the Creative Commons Attribution (CC BY) license (https://creativecommons.org/licenses/by/4.0/).

1. Introduction

Apples are the third most produced fruits in the world [1] after bananas and watermelons, consumed in the human diet as raw or dried products, juice, paste, jam and syrups. From a nutritional point of view, apples are a low-fat (less than 1%) and low-protein food (less than 1%) [2], whereas sugars represent about 10% of total apple weight, with fructose being the most abundant sugar (6%). Micronutrients, such as minerals (mainly potassium, phosphorus, calcium, and magnesium), vitamins (mainly vitamin C), and secondary metabolites (such as phenolic compounds [3,4]) are also present. Moreover, apples represent an important source of pectin, a gelling agent obtained from apple pomaces, used for many food industrial productions [5,6].

In 2018, more than 86 million tons of apples were produced worldwide, with China being the main producer (39 million tons). Italy is the sixth largest producer in the world with 2.4 million tons in 2018 [1]. In many Italian regions, local apple cultivars, used and consumed by the local population, represent an important crop, especially in terms of the local economy. In particular, Alto Adige (912.757 tons in 2020) and Trentino (496.783 tons in 2020) are the most important growing areas of high-quality apples throughout Europe, despite the fact that the cultivation area is not particularly large. However, Piedmont represents today the third largest Italian producer, contributing 225.281 tons of apples to the national production and with an increase of +13% with respect to 2019. Indeed, although Piedmont apple cultivation is not well-known, the story of Piedmont apple growing dates back to the Middle Ages, when the monastic orders cultivated and improved the varieties that had survived barbarian invasions [7–9]. By the early 20th century, Piedmont was home to thousands of varieties, but with the advent of industrial agriculture, decisions with great impact were made regarding selection. The market preferred more productive and attractive apple cultivars, characterized by a bigger size, more attractive appearance, and less delicate flavor, leading to the loss of traditional Italian apple cultivars [10], which survived only in local and niche areas. Today, a turnaround can be observed—the rediscovery of traditional and ancient cultivars that often represent more environmentally sustainable cultivation than commercial ones [11], maintaining both biodiversity and the historical and cultural links [12]. In this scenario, deep characterization and valorization of this heritage is fundamental in order to preserve the special quality of these fruits and to avoid the loss of precious and useful germplasms [12].

Apples' flavor, consistency, taste and, health-related properties strictly depend on the fruit's chemical composition and on the balance between apple component levels. For instance, each organic acid gives rise to a particular acidity sense, and each sugar has its own sweetness level. Apple chemical composition has been largely investigated using targeted chromatographic techniques, such as high-performance liquid chromatography (HPLC) to determine phenolic content [13–16] and gas chromatography (GC) for the determination of sugars, polyols, sugar phosphates, organic acids, sterols, polyphenols [17], fatty acids [18], and other aromatic compounds [19,20]. Untargeted proton nuclear magnetic resonance (^{1}H NMR) methodologies [21] have focused mainly on apple juice matrixes [19,22,23] to study the chemical composition of new cultivars [24], cultivars with different resistances against fungi attacks [25], and commercial cultivars from Japan and New Zealand [26]. ^{1}H high field NMR spectroscopy has already shown to be a valuable tool to investigate local typical products, such as red sweet peppers [27], white celery [28], tomatoes [29], and olive oils [30]. To date, ancient apple cultivars from Piedmont have been investigated in term of sensory parameters, nutritional aspects [12,31], and genetic characterization [32] through the application of standard analytical techniques. Both Donno et al. and Contessa et al. highlighted superior nutritional traits of ancient Piedmont apple cultivars, with a generally high content of organic acids, sugars, and total phenolic compounds [31]. However, deep chemical characterization by means of advanced analytical methodologies has never been performed.

In this paper, the hydroalcoholic and organic extracts of ten traditional apple cultivars grown in the Piedmont region (northwest Italy) were investigated by means of the NMR methodology to determine their apple metabolite profiles. The application of principal component analysis (PCA) to NMR data allowed us to summarize and highlight the differences and similarities between the selected apple cultivars. Indeed, mathematical tools, better known as chemometrics, are widely used for metabolomic data analysis. In particular, unsupervised methods are utilized to summarize, explore, and discover clusters or trends in the data without a priori attribution of any class membership [33].

The knowledge of chemical apple profile can be extremely important for the introduction of local products in national and international markets and for industries interested in specific apple compounds.

2. Materials and Methods

2.1. Sampling

Ten apple cultivars (*Malus domestica*) typical of Piedmont region, Italy (Figure 1) were collected in the period of their complete maturity, specific for every cultivar, as reported in Table 1. The apples were provided by three farms: "Azienda Agricola Melamangio", "Scuola Malva Arnaldi", and "Azienda Agricola Turaglio". In particular the "Azienda Agricola Melamangio" farm, located in Odalengo Piccolo, provided the variety Canditina (A1); "Scuola Malva Arnaldi", located in Bibiana, provided five varieties: Grigia di Torriana (A2), Magnana (A3), Runsé (A4), Carla (A5) and Gamba Fina (A6); "Azienda Agricola Turaglio", located in Cavour, provided four varieties: Ross Giambon (A7), Dominici (A8), Calvilla (A9) and Grenoble (A10). Some features of the ten cultivars, such as maturity time, size, peel tactility and color, pulp consistency, and color, are reported in [7–9].

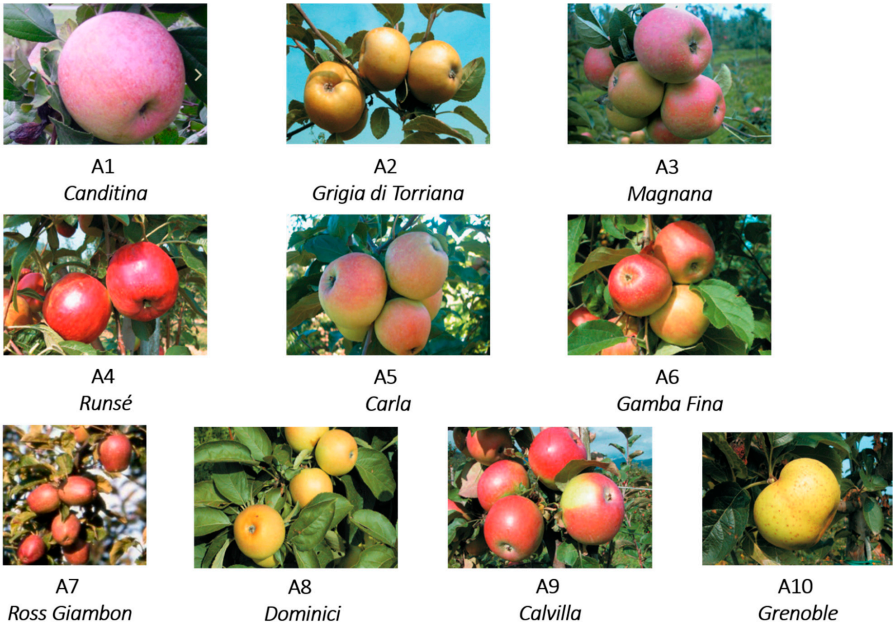


Figure 1. Apple cultivars from the Piedmont region.

2.2. Chemicals

Deuterated water (D_2O) 99.97% D, methanol-D4 99.80% D, chloroform-D 99.80% D + 0.03% tetramethylsilane (TMS), and 3-(trimethylsilyl)-propionic-2,2,3,3-d4 acid sodium salt (TSP) were purchased from Euriso–Top (Saclay, France). Anhydrous potassium phosphate dibasic (K_2HPO_4) and anhydrous potassium phosphate monobasic (KH_2PO_4) were purchased from Sigma–Aldrich (St. Louis, MO, USA). Methanol (HPLC-grade) and chloroform (HPLC-grade) were purchased from Carlo Erba Reagenti (Milan, Italy). Millipore grade water was purchased from Tito Menichelli S.r.l. (Rome, Italy).

Table 1. Characteristics (maturity time, peel, pulp and size) of the ten investigated apple cultivars [7–9,34].

N°	Cultivar	Maturity Time	Peel	Pulp	Size
A1	Canditina	Late October	Smooth, green with red overcolour	Juicy, white/green	Medium
A2	Grigia di Torriana	Mid/late October	Rough, green	Soft, white	Medium
A3	Magnana	Late October/early November	Smooth/rough, white/green with red overcolour	Soft, white/green	Medium
A4	Runsé	Late October/early November	Smooth, red	Juicy, white/pink	Medium
A5	Carla	Mid/late September	Smooth, yellow with red/orange overcolour	Soft, white	Medium/small
A6	Gamba Fina	Early/Mid October	Smooth, yellow/green with red overcolour	Soft, white	Medium/small
A7	Ross Giambon	Mid October	Smooth, yellow/green	Juicy, white	Large
A8	Dominici	Mid October	Rough, yellow/green with red overcolour	Crisp, white	Large
A9	Calvilla	Mid October	Smooth, green with red overcolour	Crisp and juicy, white/green	Medium
A10	Grenoble	Late October	Rough, green	Crisp, white/green	Small

2.3. Sample Preparation

In the sample preparation step, apple skin and pulp and seeds were removed. Seven apples were sampled for each cultivar. The apples were first washed with water and Na_2CO_3 to eliminate every dirt residue. A clove was taken from each apple and subsequently shredded with a ceramic knife. To control the oxidation during preparation, the samples were cut in an ice bath. All the samples were transferred to the falcon and lyophilized for 7 days. All apples were cut into eight parts, and seven pieces (one from each apple of the cultivar) were chopped together into smaller pieces. Each sample was then freeze-dried and pulverized with mortar and pestle. The freeze-drying process promotes water removal, thereby reducing the oxidation process.

2.4. Extraction Procedure for NMR Analysis

Extracts for NMR analysis were obtained following the protocol previously described [35] with some modifications. Powder (0.5 g) was sequentially added with a 3 mL methanol/chloroform (2:1 v/v) mixture, containing 1 mL of chloroform and 1.8 mL of Millipore-grade water, which was shaken slightly after each solvent addition. The obtained emulsion was stored at 4 °C for 40 min and then centrifuged at 4200× g for 15 min at 4 °C. The organic and hydroalcoholic phases were separated, and the residual pellet was extracted again using half of the solvent volumes to ensure complete extraction of the soluble metabolites. A slow N_2 flow was used for drying. The obtained extracts were stored at −20 °C until analysis.

2.5. Metabolic Profile by NMR Analysis

Hydroalcoholic and organic extracts were analyzed using a Bruker AVANCE 600 spectrometer (Bruker, Milan, Italy) at 28 °C operating at 600.13 MHz (proton frequency) and equipped with a Bruker multinuclear z-gradient 5 mm probe head. The temperature for NMR spectral analysis (28 °C) was chosen according to the internal laboratory protocol that assures temperature maintenance within (±0.1 °C) limits and is close to the experimental conditions reported in most databases. Each dried hydroalcoholic extract was solubilized in 1 mL of D_2O; 0.2 mL of the obtained solution was mixed with 0.5 mL of 400 mM phosphate buffer (pH 7.4)/D_2O containing 2 mM solution of TSP (internal standard) and transferred into a 5 mm NMR tube. The use of TPS as internal standard

does not interfere with the protein in apple extracts, as the balk of apple proteins is not easily soluble in water [36]. ^{1}H spectra (Bruker pulse sequence *zgpr*) of hydroalcoholic extracts were acquired with 200 transients, a recycle delay of 5 s, an acquisition time of 2.28 s, a 90° flip angle pulse of 14 µs, and 32K data points. The water signal was suppressed using solvent pre-saturation. Each dried organic extract was solubilized in 0.7 mL of the $CDCl_3/CD_3OD$ (2:1 *v*/*v*) mixture and transferred into a 5 mm NMR tube that was flame sealed. ^{1}H spectra (Bruker pulse sequence *zg*) of the organic extracts were acquired with 128 transients, a recycle delay of 5 s, an acquisition time of 1.82 s, a 90° flip angle pulse of 10.5 µs, and 32K data points.

Two-dimensional (2D) NMR experiments (^{1}H-^{1}H TOtal Correlated SpectroscopY (TOCSY), ^{1}H-^{13}C Heteronuclear Single Quantum Coherence (HSQC), and ^{1}H-^{13}C Heteronuclear Multiple Bond Correlation (HMBC) were performed on each hydroalcoholic and organic extract under the experimental conditions previously reported [29].

In order to evaluate the repeatability of the protocol and to ensure the complete extraction of the soluble metabolites, all dry matter after freeze-drying was recovered, and the entire procedure (from the extraction to NMR analysis) was carried out in triplicate.

In Table 2, the signals of the identified metabolites in the hydroalcoholic extracts ^{1}H NMR spectra are reported. Among them, the 26 selected signals marked with asterisks were integrated using the Bruker TOPSPIN 1.3 software and normalized with respect to the methyl group signal of TSP (0.00 ppm), set to 100. The quantified metabolites were expressed in mg/100 g of the dried sample ± SD (standard deviation) (Table S1).

Table 2. Metabolites identified in the 600.13 MHz proton nuclear magnetic resonance (^{1}H NMR), ^{1}H-^{1}H TOCSY, ^{1}H-^{13}C HSQC, and ^{1}H-^{13}C HMBC spectra of Bligh–Dyer hydroalcoholic extracts of apple in 0.7 mL of phosphate buffer/D_2O at 28 °C. Asterisks (*) indicate signals selected for integration.

Compound	Assignment	^{1}H (ppm)	Multiplicity (J(Hz))	^{13}C (ppm)
		Carbohydrates		
α-D-Fructofuranose	C-2			105.5
	CH-3	4.13 *		83.0
	CH-4	4.00		77.2
	CH-5	4.07		82.4
β-D-Fructofuranose	C-2			102.6
	CH-3	4.12 *		76.6
	CH-4	4.12 *		75.5
	CH-5	3.84		81.7
	CH2-6,6′	3.83; 3.68		
β-D-Fructopyranose	CH_2-1,1′	3.57; 3.72		64.9
	C-2			99.2
	CH-3	3.80		68.6
	CH-4	3.90		70.7
	CH-5	4.01		70.2
	CH_2-6,6′	3.72; 4.03		64.5
α-Xylose	CH-1	5.20 *	d [a] (3.8)	93.4
	CH-2	3.55		
	CH-3	3.65		
β- Xylose	CH-1	4.59 *	d (8.0)	97.7
	CH-2	3.54		
	CH-3	3.69		
α-Glucose	CH-1	5.24 *	d (3.8)	93.2
	CH-2	3.55		72.2
	CH-3	3.73		73.7
	CH-4	3.42		70.3
	CH-5	3.84		72.8
β-Glucose	CH-1	4.66 *	d (8.0)	97.0

Table 2. *Cont.*

Compound	Assignment	^{1}H (ppm)	Multiplicity (J(Hz))	^{13}C (ppm)
	CH-2	3.25	dd [b] (9.4; 7.9)	75.1
	CH-3	3.51		76.9
	CH-4	3.43		70.7
	CH-5	3.49		76.9
	CH_2-6,6′	3.90; 3.75		61.8
Sucrose	CH-1 (glucose)	5.42 *	d (3.8)	93.3
	CH-2	3.57		72.0
	CH-3	3.77		73.7
	CH-4	3.47		70.1
	CH-5	3.85		73.5
	C-2 (fructose)			104.8
	CH-3	4.22	d (8.8)	77.3
Rhamnitol	CH_3	1.28 *	d (6.4)	20.0
	CH-2	3.88		68.2
	CH-3	3.61		74.3
	Organic acids			
Acetic acid	α-CH_3	1.92 *	s [c]	
Citric acid	α,γ-CH	2.54 *	d (15.2)	46.7
	α′,γ′-CH	2.67		46.7
	β-C			76.5
	1,5-COOH			180.8
	6-COOH			183.0
Formic acid	HCOOH	8.46 *	s	
Citramalic acid	β-CH_3	1.33 *	s	26.5
	β-CH_2	2.44	d (15.8)	47.7
	β′-CH_2	2.74	d (15.8)	47.7
	α-C			75.5
	1,4-COOH			184.2
Lactic acid	β-CH_3	1.33 *	d (7.0)	21.4
	α-CH	4.12		69.8
	COOH			183.4
Malic acid	α-CH	4.30 *	dd (9.9; 3.2)	71.6
	β-CH	2.67	dd (15.4; 3.2)	43.9
	β′-CH	2.37	dd (15.4; 9.9)	43.9
Quinic acid	C-1			78.3
	CH_2-2, 2′	1.88 *; 2.06	dd (13.5; 10.8); m	41.9
	CH-3	4.03	m [d]	68.0
	CH-4	3.57	m	76.2
	CH-5	4.16	m	71.3
α-Galacturonic acid	CH-1	5.31	d (3.8)	93.1
	CH-2	3.80		
	CH-3	3.90		
	CH-4	4.29		
	CH-5	4.41*	d (1.2)	72.5
	COOH			177.1
	Amino acids			
Alanine	α-CH	3.80		51.5
	β-CH_3	1.49 *	d (7.3)	17.3
	COOH			176.8
Asparagine	α-CH	4.05		52.3
	β,β′-CH_2	2.88 *; 2.96	dd (7.4; 16.9); dd (4.3; 12.6)	35.6
	COOH			175.5
Aspartate	β,β′-CH_2	2.70; 2.81 *	dd(3.7; 17.4)	
γ-Aminobutyrate	α-CH_2	2.30 *	t [e] (7.4)	35.3

Table 2. *Cont.*

Compound	Assignment	^{1}H (ppm)	Multiplicity (J(Hz))	^{13}C (ppm)
	β-CH_2	1.90		24.7
	γ-CH_2	3.01		
Isoleucine	γ-CH_3	1.01 *	d (7.1)	
Valine	γ-CH_3	0.99 *	d (7.1)	
	γ′-CH_3	1.05	d (7.1)	
	Miscellaneous metabolites			
Chlorogenic acid	CH_2-2	2.20		
	CH-3	5.33	m	72.2
	CH_2-6	2.04		
	CH-1′	6.42 *	d (16.0)	115.8
	CH-2′	7.67	d (16.0)	147.3
	CH-3′	7.22	d (2.0)	116.3
	CH-6′	6.98		116.7
	CH-7′	7.15		123.8
	CH_2-6, 6′	1.97;2.05	m	38.5
Choline	$N(CH_3)_3$+	3.21 *	s	55.1
p-Coumaric acid derivative	CH-2,6	7.62 *	d (8.8)	131.9
	CH-3,5	6.97		
	CH=CH	7.79; 6.51	d (16.1)	
Phloretin/Phloridzin	CH-2,6	7.16	d (8.3)	130.7
	CH-3,5	6.85 *	d (8.3)	116.5
	CH-3′,5′	6.19; 6.24	s	96.6; 97.3
	β-CH_2	2.92		31.0

[a] d = doublet; [b] dd = double doublet; [c] s = singlet; [d] m = multiplet; [e] t = triplet.

The integral areas of the 7 selected signals in the ^{1}H NMR spectra of organic extracts (Table 3) were measured using the Bruker TOPSPIN 1.3 software and normalized with respect to the integral (I_{FA}) of the α-CH_2 group signal of all fatty acids (2.30 ppm), set to 100. The molar % values ± SD of fatty acids, β-sitosterol, phosphatidylcholine, and digalactosyldiacylglycerol were calculated with consideration of the number of equivalent protons using the following equations:

$$\%_{STE} = 100(0.66I_{STE}/I_{tot}) \quad (1)$$

$$\%_{TRI} = 100(0.5I_{TRI}/I_{tot}) \quad (2)$$

$$\%_{DI} = 100(I_{DI}/I_{tot}) \quad (3)$$

$$\%_{MONO} = 100(I_{UNS} - 2I_{DI} - 1.5I_{TRI})/I_{tot} \quad (4)$$

$$\%_{SAT} = 100(I_{FA} - I_{DI} - 0.5I_{TRI} - \%_{MONO})/I_{tot} \quad (5)$$

$$\%_{PC} = 100(4I_{PC}/9I_{tot}) \quad (6)$$

$$\%_{DGDG} = 100(4I_{DGDG}/I_{tot}) \quad (7)$$

where $\%_{STE}$, $\%_{TRI}$, $\%_{DI}$, $\%_{MONO}$, $\%_{SAT}$, $\%_{PC}$, and $\%_{DGDG}$ are the molar % of β-sitosterol, tri-unsaturated fatty acids, di-unsaturated fatty acids, mono-unsaturated fatty acids, saturated fatty acids, phosphatidylcholine, and digalactosyldiacylglycerol, respectively. I_{STE}, I_{TRI}, I_{DI}, I_{UNS}, I_{FA}, I_{PC}, and I_{DGDG} are integrals, whereas I_{tot} is calculated according to the following equation:

$$I_{tot} = I_{FA} + 0.66I_{STE} \quad (8)$$

Table 3. Metabolites identified in the 600.13 MHz ^{1}H NMR, ^{1}H-^{1}H TOCSY, ^{1}H-^{13}C HSQC, and ^{1}H-^{13}C HMBC spectra (28 °C) of Bligh–Dyer organic extracts of apple in $CDCl_3$/CD_3OD (2:1 *v*/*v*) mixture at 28 °C. Asterisks (*) indicate signals selected for integration. For the integration of total fatty acids (I_{FA}), the region of 2.22–2.35 was considered. For the integration of total unsaturated fatty acids (I_{UNS}), the region of 5.25–5.384 was considered.

Compound	Assignment	^{1}H (ppm)	Multiplicity (J(Hz))	^{13}C (ppm)
Oleic fatty chain	COO			174.4
(C18:1 Δ^{9})	CH_2-2	2.30		34.6
	CH_2-3	1.58	m [a]	25.3
	CH_2-4,7	1.30	m	29.5
	CH_2-8	2.01	m	27.6
	CH=CH 9,10	5.31	m	130.6
	CH_2-11	2.01	m	27.6
	CH_2-12,15	1.33–1.30	m	29.4–30.2
	CH_2-16	1.28	m	31.6
	CH_2-17	1.26	m	23.0
	CH_3-18	0.84	t [b]	14.4
Linoleic fatty chain	COO			174.4
(C18:2 $\Delta^{9,12}$)	CH_2-2	2.30		34.6
	CH_2-3	1.58	m	25.3
	CH_2-4,7	1.32–1.28	m	29.5
	CH_2-8	2.02	m	27.6
	CH= 9	5.34	m	130.6
	CH= 10	5.31	m	128.6
	CH_2-11	2.73 * (I_{DI})	t (6.8)	26.0
	CH= 12	5.31	m	128.6
	CH= 13	5.34	m	130.6
	CH_2-14	2.02	m	27.6
	CH_2-15	1.29	m	29.4
	CH_2-16	1.29	m	31.6
	CH_2-17	1.23	m	23.0
	CH_3-18	0.85	t	14.4
Linolenic fatty chain	COO			174.4
(C18:3 $\Delta^{9,12,15}$)	CH_2-2	2.30		34.9
	CH_2-3	1.58	m	25.3
	CH_2-4,7	1.30	m	29.5
	CH_2-8	2.03	m	27.6
	CH= 9	5.34	m	130.6
	CH= 10	5.30	m	128.6
	CH_2 11	2.77 * (I_{TRI})	t (6.2)	26.0
	CH=CH 12,13	5.30	m	128.6
	CH_2-14	2.77 * (I_{TRI})	t (6.2)	26.0
	CH= 15	5.28	m	127.4
	CH= 16	5.34	m	132.2
	CH_2-17	2.03	m	20.9
	CH_3-18	0.94	t (7.6)	14.4
Saturated fatty acids	COO			174.4
	CH_2-2	2.28		34.6
	CH_2-3	1.58	m	25.3
	CH_2	1.28–1.22	m	29.6-32.0
	CH_2 n-1	1.26		22.9
	CH_3 n	0.84	t	14.4
Diacylglycerol moiety	CH-*sn* 2	5.06		72.5
	CH-*sn* 1	4.15, 4.33		62.5
	CH-*sn* 3	3.65		61.0

Table 3. *Cont.*

Compound	Assignment	^{1}H (ppm)	Multiplicity (J(Hz))	^{13}C (ppm)
β-Sitosterol	CH_3-18	0.66 * (I_{STE})	s [c]	12.2
Squalene	CH_3-a	1.56		16.3
	CH_3-b	1.64		25.8
	CH-c	5.07	m	124.8
	CH_2-d	2.02		27.4
	CH_2-e	1.96		40.1
1,2-Diacyl-*sn*-glycero-3-phosphatidylcholine	$N(CH_3)_3$+	3.22 * (I_{PC})	s	54.5
	CH_2N+	3.75		66.4
	CH_2OP	4.45		60.6
	CH-*sn* 2	5.06		72.5
	CH-*sn* 1	4.15, 4.33		62.5
	CH-*sn* 3	3.65		61.0
Digalactosyldiacylglycerol	CH″-1	4.87 * (I_{DGDG})	d [d] (3.8)	99.8
	CH″-2	3.77		69.2
	CH″-3	3.69		70.6
	CH″-4	3.91		70.2
	CH′-1	4.19		104.5
	CH′-2,3	3.51–3.53		
	CH′-4	3.90		
	CH-*sn* 2	5.06		72.5
	CH-*sn* 1	4.15, 4.33		62.5
	CH-*sn* 3	3.65		61.0

[a] m = multiplet; [b] t = triplet; [c] s = singlet; [d] d = doublet.

The amount of each quantified metabolite in organic extracts is reported in Table S2.

2.6. Multivariate Statistical Analysis

Principal component analysis (PCA) was carried out on 30 selected variables corresponding to 23 metabolites from the hydroalcoholic extract and 7 from the organic extract. In the case of fructose, glucose, and xylose, the sum of their alpha and beta anomeric forms instead of the individual isomer content was used in statistics. Before statistical analysis, the data were preprocessed using autoscaling: all of the variables were mean centered, and each variable was divided by its standard deviation. Principal component analysis was carried out using SIMCA software (version 12).

3. Results

3.1. Assignments of Aqueous and Organic Extracts

The ^{1}H and ^{13}C NMR spectra assignments apple aqueous (Figure 2) and organic (Figure 3) extracts of apple were carried out using 2D NMR experiments, standard compound addition, and literature data [24–26,37]. A more complete spectral assignment (Table 2) of the aqueous extracts with respect to literature data was obtained, identifying fructose tautomeric forms, galacturonic acid, GABA, and *p*-coumaroyl moiety. Fructose tautomeric forms, namely α-D-fructofuranose and β-D-fructopyranose, were identified by means of their diagnostic ^{1}H NMR signals and 2D experiments. In particular, the presence of α-D-fructofuranose was suggested by its characteristic signal at 4.13 ppm due to the CH-3 proton. ^{1}H-^{1}H TOCSY experiment allowed us to identify the correlation with the CH-4 proton (4.00 ppm), whereas the ^{1}H-^{13}C HMBC experiment showed the correlation of the CH-3 proton with the C-2 carbon at 105.5 ppm, typical of ketoses. Analogously, β-D-fructopyranose was recognized by the signal of the CH-5 proton at 4.01 ppm, and the diagnostic spin system detected by the ^{1}H-^{1}H TOCSY experiment allowed us to identify the other protons of this sugar, namely CH-3 (3.80 ppm), CH-4 (3.90 ppm), and CH_2-6,6′ (3.72, 4.03 ppm). C-2 carbon at 99.2 ppm was also identified by means of the ^{1}H-^{13}C HMBC

map. The presence of α-galacturonic moiety was suggested by the diagnostic chemical shifts of the spin systems in the ^{1}H-^{1}H TOCSY experiment, the coupling constants, and the correlations in the ^{1}H-^{13}C HMBC experiment. In particular, the doublet at 4.41 ppm with a J coupling constant of 1.2 Hz due to CH-5 proton indicates single coupling between H-5 and the equatorial H-4. The ^{1}H-^{1}H TOCSY experiment allowed us to identify the other protons of this metabolite, namely CH-4 (4.29 ppm), CH-3 (3.90 ppm), CH-2 (3.80 ppm), and CH-1 (5.31 ppm, doublet with J = 3.80 Hz). The correlation of the CH-5 proton with carboxylic carbon at 177.1 ppm was confirmed by the ^{1}H-^{13}C HMBC map.

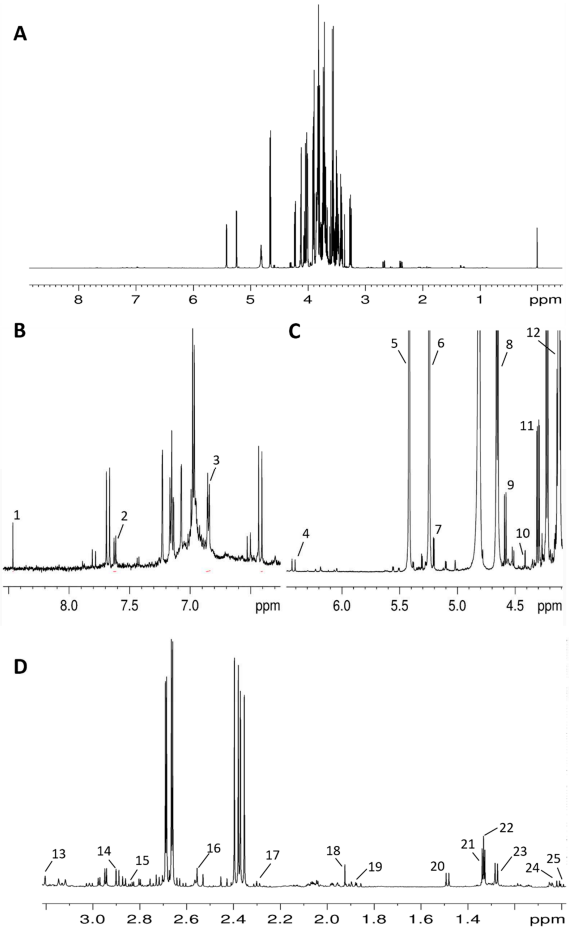


Figure 2. 600 MHz ^{1}H NMR spectrum of hydroalcoholic extract from apple fruit (var. Magnana) in a 400 mM phosphate buffer (pH 7.4)/D_2O mixture with 2mM of 3-(trimethylsilyl)-propionic-2,2,3,3-d4 acid sodium salt (TSP). (**A**) Entire spectrum. (**B**) Low field region: 1, formic acid; 2, *p*-coumaric acid derivative; 3, phloretin/phloridzin. (**C**) Middle field region: 4, chlorogenic acid; 5, sucrose; 6, α-glucose; 7, α-xylose; 8, β -glucose; 9, β-xylose; 10, α-galacturonic acid; 11, malic acid; 12, D-fructofuranose, (**D**) High field region**:** 13, choline; 14, aspartate; 15, asparagine; 16, citric acid; 17, γ-aminobutyrate; 18, acetic acid; 19, quinic acid; 20, alanine; 21, lactic acid; 22, citramalic acid; 23, rhamnitol; 24, isoleucine; 25, valine.

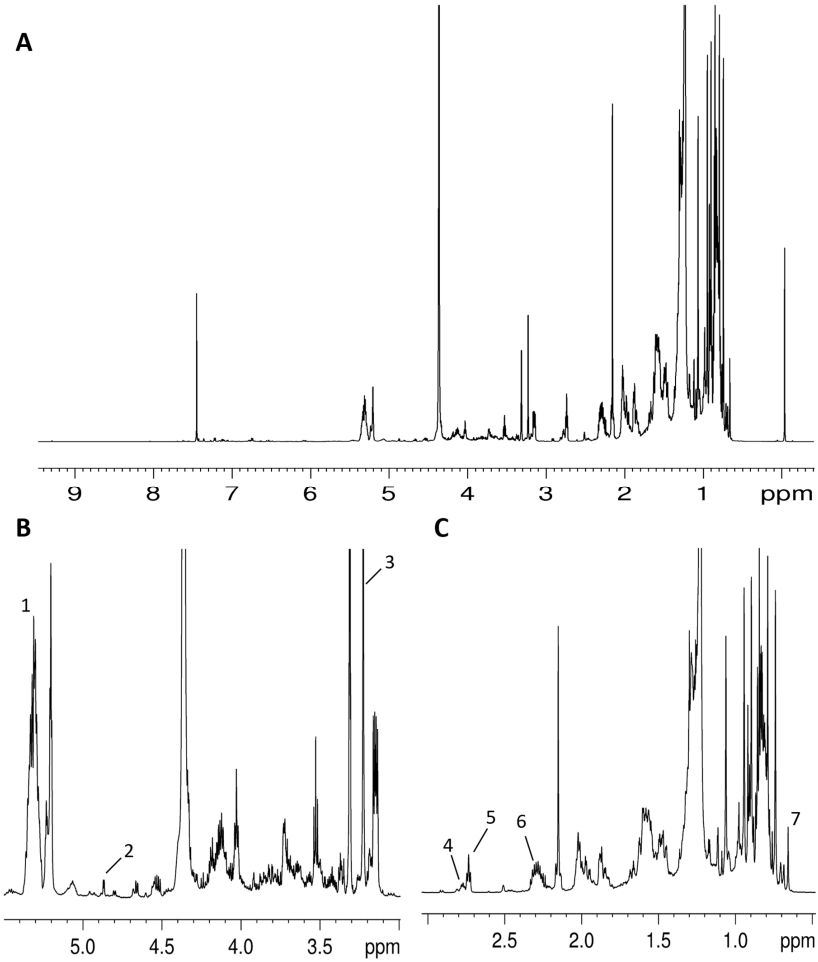


Figure 3. ^{1}H NMR spectrum at 600 MHz of organic extract from apple fruit (var. Magnana) in the $CDCl_3/CD_3OH$ 2:1 (*v*/*v*) mixture. (**A**) Entire spectrum. (**B**) Middle field region: 1, total unsaturated fatty acids; 2, digalactosyldiacylglycerol; 3, 1,2-diacyl-*sn*-glycero-3-phosphatidylcholine. (**C**) High field region**:** 4, linolenic fatty chain; 5, linoleic fatty chain; 6, total fatty acids; 7, β-sitosterol.

The presence of GABA was confirmed by its typical triplet at 2.30 ppm (J = 7.4 Hz) assigned to α-CH_2 protons. The diagnostic spin systems identified in the ^{1}H-^{1}H TOCSY experiment allowed us to observe the correlations with β-CH_2 and γ-CH_2 protons at 1.90 and 3.01 ppm, respectively.

The diagnostic spin systems identified in the ^{1}H-^{1}H TOCSY experiment suggested the presence of *p*-coumaroyl moiety due to the correlation between H-2/H-6 equivalent

aromatic signals at 7.62 ppm and H-3/H-5 equivalent signals at 6.97 ppm (J = 8.8 Hz corresponding to *ortho* position) and the correlation between the double bond protons at 7.79 and 6.51 ppm with J = 16.1 Hz corresponding to *trans* configuration of the double bond. The low intensity of these signals—and, therefore, the low concentration of the corresponding compound—does not allow further correlations to be observed in the 2D experiments to complete the structural assignment. *p*-Coumaroyl quinic acid is the principal *p*-coumaroyl ester previously identified in apples using the targeted HPLC methodology [13,38,39]. Therefore, the identified *p*-coumaroyl moiety can be bound to quinic acid; however, the esterified quinic acid moiety was not detected due to the signal overlapping.

It was not possible to distinguish phloretin from its glycosides (such as phloridzin) using the available signals from aromatic protons region. Unfortunately, the signals expected for β-glucose moiety were not observed due to the strong overlapping with markedly more intense signals of other carbohydrates. The *orto*- and *meta*- protons of the *para*-substituted aromatic ring, a common moiety for all phloretin derivatives, gave rise to the signals at 7.16 and 6.85 ppm, respectively.

In Table 2, the assignment of four sugars (fructose, glucose, sucrose, and xylose), nine organic acids (acetic, citric, formic, citramalic, lactic, malic, quinic, and galacturonic acids), six amino acids (alanine, asparagine, aspartate, GABA, isoleucine, and valine), rhamnitol, *p*-coumaroyl derivative, phloretin/phloridzin, and choline is reported.

A more complete assignment of organic extracts of apples (Table 3) with respect to the literature data was obtained, reporting the assignment of glycerogalactolipid and glycerophospholipid polar heads. The presence of digalactosyldiacylglycerol (DGDG), the most abundant galactolipid in apples [40], was suggested by the characteristic doublet (J = 3.8 Hz) at 4.87 ppm due to the equatorial CH″-1 proton of the external galactose ring [41]. The ^{1}H-^{1}H TOCSY experiment allowed us to identify other protons of the ring, namely CH-2″ (3.77 ppm), CH-3″ (3.69 ppm), and CH-4″ (3.91 ppm). Analogously, the CH-1′ proton of the internal DGDG galactose was also assigned at 4.19 ppm, together with the CH-2′/CH-3′ and CH-4′ protons (3.50–3.53 and 3.90 ppm, respectively).

Methyl groups of phosphatidylcholine N^{+}-$(CH_3)_3$ moiety were detected by the diagnostic ^{1}H and ^{13} C signals at 3.22 ppm at 54.5 ppm, respectively. Moreover, the ^{1}H-^{1}H TOCSY experiment allowed us to identify proton correlation between the CH_2OP group at 4.45 ppm (^{13}C 60.6 ppm) and the CH_2N^{+} protons at 3.75 ppm (^{13}C 66.4 ppm).

In Table 3, the assignment of β-Sitosterol, fatty acid chains, phosphatidylcholine, and digalactosyldiacylglycerol is also reported.

3.2. Metabolite Profiles of Apple Cultivars

In this section, each class of compounds is discussed separately, and a comparison of the ten cultivars is conducted.

3.2.1. Sugars and Polyols

The highest content of total sugars was measured in cultivars A9, A7, A3, and A2, whereas the lowest content was found in cultivars A1 and A6 (Figure 4). In particular, fructose, glucose and, sucrose were the most abundant sugars in all apple cultivars (Figure 5A). As expected [18], fructose turned out to be the main sugar in all samples, with the highest content detected in cultivars A5 and A7 and the lowest content in A1. The highest value of glucose content was measured in cultivar A2, whereas the lowest content (more than three times less) was identified in sample A6. According to literature data [18,42,43], the fructose-to-glucose ratio was higher than 1.7 in all of the analyzed samples. Moreover, the fructose/glucose, fructose/sucrose, and sugar/acid weight ratios were calculated (Table 4). Cultivar A3 showed the highest sucrose content, whereas the lowest content was observed in A5 (more than four times less). Xylose was present in low concentrations in all of the cultivars, with cultivar A5 showing the highest content, whereas A1 showed the lowest content (more than six times). The highest content of rhamnitol, a polyol, was measured in cultivar A10, whereas the lowest content was found in A7.

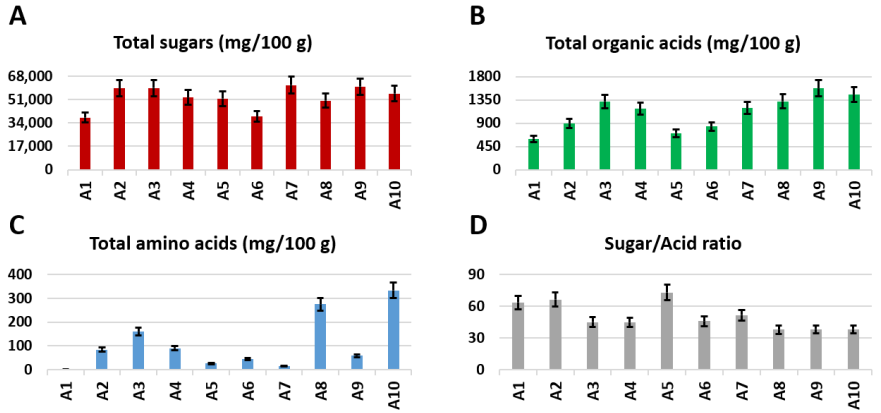


Figure 4. Bar charts of the total content of (**A**) sugars, (**B**) organic acids, (**C**) amino acids, (**D**) sugar/acid ratio, identified and quantified (mg/100 g of DW ± SD) in the ^{1}H NMR spectra of hydroalcoholic extracts of apples.

Table 4. Fructose/glucose, fructose/sucrose, and sugar/acid weight ratios in the ten studied Piedmont region apple cultivars and in three commercial cultivars (calculated using literature data).

Cultivar	Reference	Fru/Glc	Fru/Suc	Sugar/Acid
Golden Delicious	[18]	2.0	2.3	34
Golden Delicious	[44]	2.9	1.8	
Golden Delicious	[45]	3.6	1.9	60
Fuji	[18]	1.7	2.8	42
Fuji	[44]	15.0	2.0	
Fuji	[45]	1.9	3.0	90
Jonagold	[18]	1.7	2.6	31
Jonagold	[44]	7.3	1.1	
Jonagold	[45]	3.2	1.8	127
A1	Present work	2.3	2.4	57
A2	Present work	1.8	3.2	61
A3	Present work	3.6	1.3	44
A4	Present work	3.5	3.1	43
A5	Present work	2.9	6.5	69
A6	Present work	4.2	2.0	42
A7	Present work	3.6	2.1	49
A8	Present work	3.8	2.3	37
A9	Present work	4.3	1.5	37
A10	Present work	3.2	1.3	38

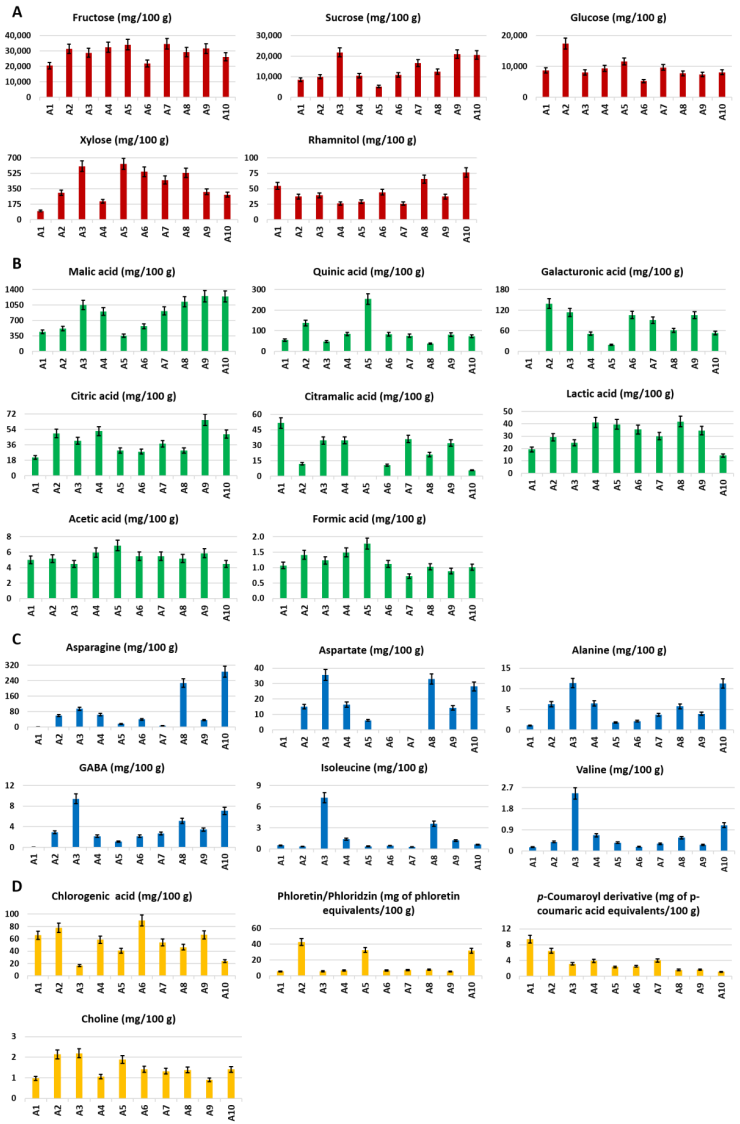


Figure 5. Bar charts of the metabolites identified and quantified (mg/100 g of DW ± SD) in the ^{1}H NMR spectra of hydroalcoholic extracts of apples. (**A**) Sugars and polyols, (**B**) organic acids, (**C**) amino acids, (**D**) miscellaneous metabolites. Phloretin/phloridzin and *p*-coumaroyl derivative contents are expressed as phloretin equivalents and p-coumaric acid equivalents, respectively.

3.2.2. Organic Acids

The highest total organic acids content (Figure 4) was found in cultivars A9 and A10, whereas the lowest amount was observed in cultivar A1 (more than two times less). In particular, malic acid was the most abundant acid in apples. The highest concentrations of malic acid were found in samples A9 and A10, whereas the lowest concentration was observed in A5 (Figure 5B). Cultivar A5 presented by far the highest content of quinic acid, whereas the lowest content (almost seven times less) was found in sample A8. The highest content of galacturonic acid was measured in cultivar A2, whereas it was not detected in sample A1. Cultivar A9 showed the highest amount of citric acid, whereas the lowest content was measured in A1 (more than three times less). Citramalic acid was not detected in sample A5; conversely, the highest amount was measured in sample A1. Cultivars A4 and A8 showed the highest content of lactic acid, whereas the lowest content was found in A10. Sample A10 was also characterized by the lowest amount of acetic acid, whereas cultivar A5 showed the highest amount. Finally, formic and acetic acids were found in very low concentrations, below 2 mg/100 g.

3.2.3. Amino Acids

The content of free amino acids (total and those of individual components) was extremely variable among the different cultivars (Figure 5C). The highest total amino acid content was found in cultivars A8 and A10, whereas the lowest amount was observed in cultivars A1, A7, and A5 (Figure 4). In particular, cultivar A3 showed the highest amount of GABA, valine, and isoleucine, and, together with cultivar A10, alanine. Asparagine content varied from 280 mg/100 g in A10 to less than 1 mg/100 g (below the limit of detection) in A1. Aspartate was not found in cultivars A1, A6, or A7, and GABA was not detected in cultivar A1.

3.2.4. Miscellaneous

Cultivar A6 showed the highest amount of chlorogenic acid, whereas cultivar A3 the lowest amount (5 times less). A2, A5, and A10 showed by far the highest amounts of phloretin/phloridzin, whereas the lowest amount was observed in cultivar A1. The highest amount of *p*-coumaroyl derivatives was detected in cultivar A1, whereas the lowest amount was found in A10. The highest amount of choline was measured in cultivars A2 and A3, whereas the lowest amount was found in samples A1 and A9 (Figure 5D).

3.2.5. β-Sitosterol

This molecule was found in appreciable concentrations in all of the analyzed cultivars. In particular, the highest value was measured in cultivar A2, whereas the lowest amount was identified in A1 (Figure 6).

3.2.6. Fatty Acids

The content of unsaturated fatty acids (TOT UFA) was higher than the content of saturated fatty acids (TOT SFA) in all of the ten cultivars. Di-unsaturated fatty acids (DUFA) were the most abundant unsaturated fatty acids in all of the samples, the highest level being measured in cultivar A2 and the lowest in A1. Sample A1 was also characterized by the lowest value of mono-unsaturated fatty acids (MUFA) and the highest value of tri-unsaturated fatty acids (TUFA). Cultivar A4 showed an opposite trend, having the highest amount of MUFA and the lowest amount of TUFA. Finally, the highest concentration of TOT SFA was found in cultivar A1, whereas the lowest concentration was measured in sampleA8 (Figure 6).

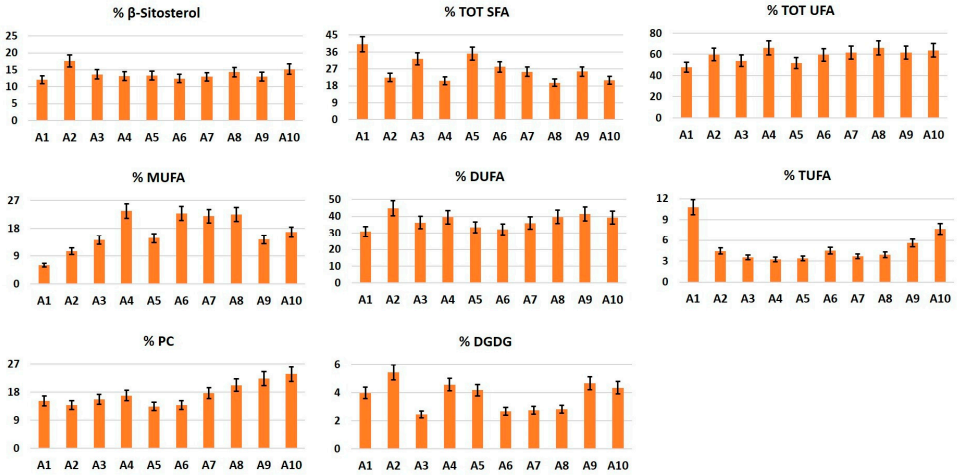


Figure 6. Bar charts of the metabolites (molar % ± SD) identified and quantified in the ^{1}H NMR spectra of organic extracts of apples.

3.2.7. Polar Lipids

The highest content of phosphatidylcholine (PC) was observed in cultivar A10, whereas the lowest content was measured in A5. Cultivar A2 showed the highest concentration of digalactosyldiacylglycerol (DGDG), whereas the lowest content was observed in sample A3 (Figure 6).

3.3. Multivariate Statistycal Analysis (PCA)

The overall analysis of the histograms made it possible to find characteristic features relative to each cultivar. Moreover, PCA applied to all of the NMR variables allowed us to highlight possible cultivar similarities and differences (Figure 7).

Cultivar A1 (Canditina) was observed to be well separated from all of the others for the high content of citramalic acid, *p*-coumaroyl moiety, TUFA, and TOT SFA, and low amounts of xylose, fructose, sucrose, malic acid, citric acid, alanine, and MUFA. Notably, galacturonic acid, asparagine, aspartate, and GABA were not detected.

Carla, cultivar A5, was characterized by high contents of fructose, xylose, and organic acids (such as quinic acid, lactic acid, acetic acid, and formic acid) and low amounts of sucrose, chlorogenic acid, malic acid, amino acids (namely, asparagine aspartate, and alanine), and malic and galacturonic acids. Citramalic acid was not detected.

Gamba Fina, cultivar A6, was characterized by high content of MUFA and chlorogenic acid and low amounts of fructose, glucose, and citramalic acid. Aspartate was not detected.

Ross Giambon, cultivar A7, was characterized by high fructose and MUFA contents and low amounts of rhamnitol and asparagine. The level of aspartate was beyond the limit of detection.

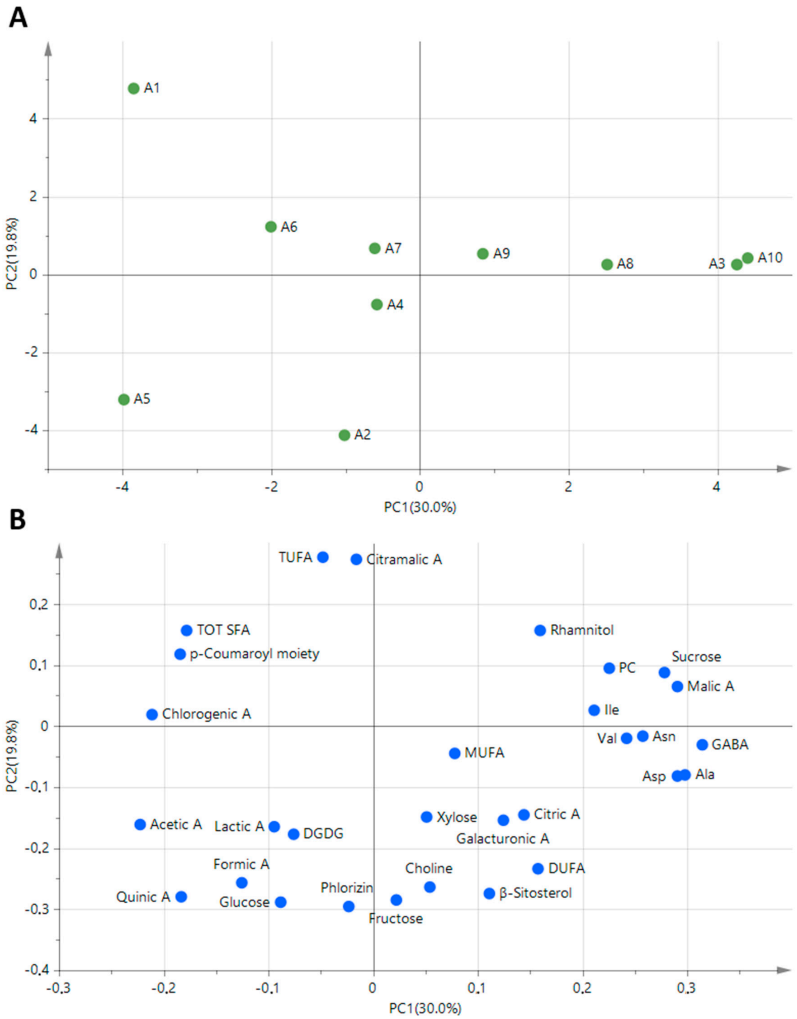


Figure 7. PCA applied to NMR data of the ten apple cultivars. (**A**) Sample scores and (**B**) loadings. PC1 and PC2 represent 30.0% and 19.8% of the total variance, respectively.

Runsé, cultivar A4, was characterized by high amounts of organic acids and MUFA.

Grigia di Torriana, cultivar A2, showed high amounts of glucose, galacturonic acid, choline, DUFA, and DGDG and a low level of citramalic acid.

Calvilla, cultivar A9, was characterized by high levels of sucrose, organic acids, DUFA and PC.

Dominici, cultivar A8, showed high contents of rhamnitol, lactic acid, asparagine, aspartate, isoleucine, and MUFA and a low concentration of quinic acid.

The Magnana (A3) and Grenoble (A10) cultivars, situated nearby on the PCA score plot (PC1 > 4, Figure 3a), were characterized by high levels of sucrose, rhamnitol, malic acid, asparagine, alanine, and PC and low content of *p*-coumaroyl moiety.

4. Discussion

The present data on the chemical composition of traditional apple cultivars of the Piedmont region can be compared with those of some of the most widely cultivated apple cultivars in the world [46,47], such as Golden Delicious, Fuji, Granny Smith, and Jonagold [18,44,45]. Taking into account the fact that the data reported in the literature are related to apple juice composition (usually expressed as g/L or g/kg FW), while our data are related to dried tissue (expressed as mg/100 g of DW), it is clear that only the ratios between the components and not the absolute values can be directly compared.

The sugar content in apple fruit is very important, especially for diabetic patients who adapt their insulin intake in relation to the carbohydrate content of each food. Table 4 shows the ratios of fructose/glucose and fructose/sucrose calculated using the literature data [18,44,45] for the most popular apple cultivars (Golden Delicious, Fuji, and Jonagold) in comparison with our data on Piedmont region cultivars. It is noteworthy that among three different studies of the same apple cultivars, there is a lack of agreement regarding sugar content. The studies only agree on the fact that fructose seemed to be the most abundant in all apple cultivars, whereas the relative content of glucose and sucrose was highly variable. The fructose/glucose ratio was always higher than 1.7 for all apple cultivars, whereas the upper limit can be as high as 15 (calculated for Fuji according to literature data [44]). In the case of Piedmont cultivars, the fructose/glucose ratio was in the range of 4.3 (A9)–1.8 (A2). The fructose/sucrose ratio was less variable, ranging from 1.1 (Jonagold, [44]) to 3.0 (Fuji, [45]). The corresponding values for Piedmont cultivars are inside this range, except for one (6.5), corresponding to cultivar A5 with the lowest sucrose content and a high fructose level.

The sugar-to-acid ratio is another important parameter indicating the taste and flavor of apples. In particular, a high level of the sugar/acid ratio is related to higher sweetness [48,49]. Again, the literature data on the sugar-to-acid ratio in Golden Delicious, Fuji, and Jonagold are not consistent—see Table 4. For example, for the Jonagold cultivar, values from 31 [18] to 127 [45] were reported. In our study, the cultivars with the highest sugar/acid ratio were Canditina (A1), Grigia di Torriana (A2), and Carla (A5) due to a low level of total organic acid, whereas a lower sugar/acid ratio was observed for the Dominici (A8), Calvilla (A9), and Grenoble (A10) cultivars.

The content of chlorogenic acid, one of the most abundant polyphenols in apple, has been reported to range from 34.9 (Golden Delicious) to 39.4 mg/100 g of DW (Jonagold) in the pulp of commercial cultivars [45]. Almost all Piedmont cultivars (except A3 and A10) were generally characterized by a higher content of chlorogenic acid with the maximum observed in Gamba Fina A6 (89 mg/100 g DW).

The fatty acid composition observed in the analyzed apple cultivars was similar to that of the literature data [18]. In particular, DUFA was by far the main class of fatty acids, followed by saturated fatty acids, MUFA, and TUFA. A high percentage of DUFA has been reported for Golden Delicious and Jonagold (more than 50 mol %) [11], whereas among the Piedmont cultivars, the highest DUFA content (45 mol%) was observed in Canditina A1.

The identification of some characteristic metabolites of apples, such as phloridzin/phloretin, rhamnitol, and citramalic acid, is particularly noteworthy. [26,33,50,51] Their content is largely variable both in the analyzed cultivars and in others described in the literature [18,25,26,52]. These molecules are also widely studied to assign their role in the human body and in apple biosynthetic pathways.

Phloridzin as a polyphenol compound with antioxidant activity [53] shows some health benefits; in particular, it can be useful in the prevention of the type 2 diabetes mellitus [54,55] by reducing intestinal sugar uptake. Rhamnitol has been considered as a dietary biomarker in relation to the consumption of apples [56] and also as an important

metabolite for the geographical discrimination of apple varieties with different geographical origins [26]. Finally, citramalic acid has been studied for its contribution to the development of anthocyanin in apple skin [57] and for its correlation with the storage of apples [58].

5. Conclusions

The presented results show that every local variety has its own chemical profile responsible for the sensorial, nutritional, and health-related properties, and they may be used as sources of specific substances that are utilized as ingredients of health products, such as food supplements, functional foods, and cosmetics. For instance, the Gamba Fina (A6) cultivar showed a significant content of chlorogenic acid with recognized properties against metabolic syndrome disorder [59,60], and the Grigia di Torriana (A2), Carla (A5), and Grenoble (A10) cultivars, with their high content of phloretin and phloridzin, could be considered very interesting for their possible properties against insulin resistance [54,55,61]. From a nutritional point of view, being rich in sugars, the Magnana cultivar (A3) can be used to prepare apple juice with no added sugars. Moreover, as the morphological characteristics (especially of the medium/small fruits) make these apple cultivars unattractive to the market for direct consumption, most of them could be successfully employed for the preparation of ingredients of nutraceutical products with high added value.

Although further studies should be performed to gain further understanding of the genetic and environmental basis that leads to these peculiar chemical compositions and the accumulation of polyphenols or nutrients, the reported data could be useful for national and international information systems to reinforce food and agriculture sectors, giving producers and industries accurate information regarding local food peculiarities [62].

Supplementary Materials: The following are available online at https://www.mdpi.com/2304-8158/10/2/289/s1, Table S1: Metabolite content in the hydroalcoholic extract of the analyzed apple cultivars from the Piedmont region (mg/100 g ± SD); Table S2: Metabolite content in the organic extract of the analyzed apple cultivars from the Piedmont region (molar % ± SD).

Author Contributions: Conceptualization, L.M. and A.P.S.; methodology, M.S., G.D.M.; software, G.D.M.; validation, A.P.S., C.I. and L.M.; formal analysis, C.E., C.S.; investigation, M.S., G.D.M.; resources, C.I.; data curation, A.P.S.; writing—original draft preparation, M.S., G.D.M. and A.P.S.; writing—review and editing, M.D., A.B.; visualization, C.I.; supervision, A.P.S. and L.M. All authors have read and agreed to the published version of the manuscript.

Funding: This research was funded by Dipartimento di Chimica e Tecnologie del Farmaco and Italian Ministry of Education, Universities and Research-Dipartimenti di Eccellenza-L. 232/2016.

Data Availability Statement: The data presented in this study are available on request from the corresponding author.

Acknowledgments: The authors wish to thank "Azienda Agricola Melamangio", "Scuola Malva Arnaldi", and "Azienda Agricola Turaglio" for supplying apple samples, as well as Clara Bonifacio and Cinzia Pizzo for their contribution to the identification and collection of ancient cultivars.

Conflicts of Interest: The authors declare no conflict of interest. The funders had no role in the design of the study; in the collection, analyses, or interpretation of data; in the writing of the manuscript, or in the decision to publish the results.

References

1. FAO FAOSTAT Data. Available online: http://www.fao.org/faostat/en/#data/QC (accessed on 18 May 2020).
2. U.S. Department of Agriculture Food Data Central. Available online: https://fdc.nal.usda.gov/ (accessed on 18 May 2020).
3. Lee, K.W.; Kim, Y.J.; Kim, D.O.; Lee, H.J.; Lee, C.Y. Major Phenolics in Apple and Their Contribution to the Total Antioxidant Capacity. *J. Agric. Food Chem.* **2003**, *51*, 6516–6520. [CrossRef] [PubMed]
4. Francini, A.; Sebastiani, L. Phenolic compounds in apple (Malus x domestica borkh.): Compounds characterization and stability during postharvest and after processing. *Antioxidants* **2013**, *2*, 181–193. [CrossRef]
5. Wikiera, A.; Mika, M.; Grabacka, M. Multicatalytic enzyme preparations as effective alternative to acid in pectin extraction. *Food Hydrocoll.* **2015**, *44*, 156–161. [CrossRef]

6. Güzel, M.; Akpınar, Ö. Valorisation of fruit by-products: Production characterization of pectins from fruit peels. *Food Bioprod. Process.* **2019**, *115*, 126–133. [CrossRef]
7. Caruso, T.; Ciarmiello, L.F.; Cutino, I.; Malvolti, M.E.; Murri, G.; Piccirillo, P. *Atlante dei Fruttiferi Autoctoni Italiani*; Crea—Centro di Frutticoltura: Roma, Italy, 2016; Volume III, pp. 1276–1285.
8. Arnaldi, S.M. Antiche Varietà Piemontesi, le Mele. Available online: https://www.antichevarietapiemontesi.it/mele/ (accessed on 6 August 2020).
9. Bounous, G. Antiche Cultivar di Melo in Piemonte. Piemonte, R., Ed.; 2006. Available online: http://hdl.handle.net/2318/15310 (accessed on 18 May 2020).
10. Bounous, G.; Melo, D.G.I. *Collana Coltura & Cultura*; Script, A.R.T., Servizi, E.S.P.A., Eds.; Bayer Crop Science: Bologna, Italy, 2008; pp. 82–111.
11. Cerutti, A.K.; Bruun, S.; Donno, D.; Beccaro, G.L.; Bounous, G. Environmental sustainability of traditional foods: The case of ancient apple cultivars in Northern Italy assessed by multifunctional LCA. *J. Clean. Prod.* **2013**, *52*, 245–252. [CrossRef]
12. Donno, D.; Beccaro, G.L.; Mellano, M.G.; Torello Marinoni, D.; Cerutti, A.K.; Canterino, S.; Bounous, G. Application of sensory, nutraceutical and genetic techniques to create a quality profile of ancient apple cultivars. *J. Food Qual.* **2012**, *35*, 169–181. [CrossRef]
13. Ramirez-Ambrosi, M.; Abad-Garcia, B.; Viloria-Bernal, M.; Garmon-Lobato, S.; Berrueta, L.A.; Gallo, B. A new ultrahigh performance liquid chromatography with diode array detection coupled to electrospray ionization and quadrupole time-of-flight mass spectrometry analytical strategy for fast analysis and improved characterization of phenolic compounds in ap. *J. Chromatogr. A* **2013**, *1316*, 78–91. [CrossRef]
14. Mari, A.; Tedesco, I.; Nappo, A.; Russo, G.L.; Malorni, A.; Carbone, V. Phenolic compound characterisation and antiproliferative activity of "Annurca" apple, a southern Italian cultivar. *Food Chem.* **2010**, *123*, 157–164. [CrossRef]
15. Guo, J.; Yue, T.; Yuan, Y.; Wang, Y. Chemometric Classification of Apple Juices According to Variety and Geographical Origin Based on Polyphenolic Profiles. *J. Agric. Food Chem.* **2013**, *61*, 6949–6963. [CrossRef]
16. Bai, L.; Guo, S.; Liu, Q.; Cui, X.; Zhang, X.; Zhang, L.; Yang, X.; Hou, M.; Ho, C.T.; Bai, N. Characterization of nine polyphenols in fruits of Malus pumila Mill by high-performance liquid chromatography. *J. Food Drug Anal.* **2016**, *24*, 293–298. [CrossRef]
17. Ferruzza, S.; Natella, F.; Ranaldi, G.; Murgia, C.; Rossi, C.; Trošt, K.; Mattivi, F.; Nardini, M.; Maldini, M.; Giusti, A.M.; et al. Nutraceutical improvement increases the protective activity of broccoli sprout juice in a human intestinal cell model of gut inflammation. *Pharmaceuticals* **2016**, *9*, 48. [CrossRef] [PubMed]
18. Wu, J.; Gao, H.; Zhao, L.; Liao, X.; Chen, F.; Wang, Z.; Hu, X. Chemical compositional characterization of some apple cultivars. *Food Chem.* **2007**, *103*, 88–93. [CrossRef]
19. Iaccarino, N.; Varming, C.; Petersen, M.A.; Viereck, N.; Schütz, B.; Toldam-Andersen, T.B.; Randazzo, A.; Engelsen, S.B. Ancient danish apple cultivars—A comprehensive metabolite and sensory profiling of apple juices. *Metabolites* **2019**, *9*, 139. [CrossRef] [PubMed]
20. Aprea, E.; Gika, H.; Carlin, S.; Theodoridis, G.; Vrhovsek, U.; Mattivi, F. Metabolite profiling on apple volatile content based on solid phase microextraction and gas-chromatography time of flight mass spectrometry. *J. Chromatogr. A* **2011**, *1218*, 4517–4524. [CrossRef] [PubMed]
21. Sobolev, A.P.; Thomas, F.; Donarski, J.; Ingallina, C.; Circi, S.; Cesare Marincola, F.; Capitani, D.; Mannina, L. Use of NMR applications to tackle future food fraud issues. *Trends Food Sci. Technol.* **2019**, *91*, 347–353. [CrossRef]
22. Belton, P.S.; Delgadillo, I.; Gil, A.M.; Roma, P.; Casuscelli, F.; Colquhoun, I.J.; Dennis, M.J.; Spraul, M. High-field proton NMR studies of apple juices. *Magn. Reson. Chem.* **1997**, *35*, 52–60. [CrossRef]
23. Berregi, I.; del Campo, G.; Caracena, R.; Miranda, J.I. Quantitative determination of formic acid in apple juices by 1H NMR spectrometry. *Talanta* **2007**, *72*, 1049–1053. [CrossRef] [PubMed]
24. Eisenmann, P.; Ehlers, M.; Weinert, C.H.; Tzvetkova, P.; Silber, M.; Rist, M.J.; Luy, B.; Muhle-Goll, C. Untargeted NMR spectroscopic analysis of the metabolic variety of new apple cultivars. *Metabolites* **2016**, *6*, 29. [CrossRef]
25. Sciubba, F.; Di Cocco, M.E.; Gianferri, R.; Capuani, G.; De Salvador, F.R.; Fontanari, M.; Gorietti, D.; Delfini, M. Nuclear Magnetic Resonance-Based Metabolic Comparative Analysis of Two Apple Varieties with Different Resistances to Apple Scab Attacks. *J. Agric. Food Chem.* **2015**, *63*, 8339–8347. [CrossRef]
26. Tomita, S.; Nemoto, T.; Matsuo, Y.; Shoji, T.; Tanaka, F.; Nakagawa, H.; Ono, H.; Kikuchi, J.; Ohnishi-Kameyama, M.; Sekiyama, Y. A NMR-based, non-targeted multistep metabolic profiling revealed l-rhamnitol as a metabolite that characterised apples from different geographic origins. *Food Chem.* **2015**, *174*, 163–172. [CrossRef]
27. Sobolev, A.P.; Mannina, L.; Capitani, D.; Sanzò, G.; Ingallina, C.; Botta, B.; Fornarini, S.; Crestoni, M.E.; Chiavarino, B.; Carradori, S.; et al. A multi-methodological approach in the study of Italian PDO "Cornetto di Pontecorvo" red sweet pepper. *Food Chem.* **2018**, *255*, 120–131. [CrossRef] [PubMed]
28. Ingallina, C.; Capitani, D.; Mannina, L.; Carradori, S.; Locatelli, M.; Di Sotto, A.; Di Giacomo, S.; Toniolo, C.; Pasqua, G.; Valletta, A.; et al. Phytochemical and biological characterization of Italian "sedano bianco di Sperlonga" Protected Geographical Indication celery ecotype: A multimethodological approach. *Food Chem.* **2020**, *309*, 125649. [CrossRef] [PubMed]
29. Ingallina, C.; Sobolev, A.P.; Circi, S.; Spano, M.; Giusti, A.M.; Mannina, L. New hybrid tomato cultivars: An NMR-based chemical characterization. *Appl. Sci.* **2020**, *10*, 1887. [CrossRef]
30. D'Imperio, M.; Dugo, G.; Alfa, M.; Mannina, L.; Segre, A.L. Statistical analysis on Sicilian olive oils. *Food Chem.* **2007**, *102*, 956–965. [CrossRef]

31. Contessa, C.; Botta, R. Comparison of physicochemical traits of red-fleshed, commercial and ancient apple cultivars. *Hortic. Sci.* **2016**, *43*, 159–166. [CrossRef]
32. Cavanna, M.; Marinoni, D.T.; Bounous, G.; Botta, R. Genetic diversity in ancient apple germplasm from northwest Italy. *J. Hortic. Sci. Biotechnol.* **2008**, *83*, 549–554. [CrossRef]
33. Mannina, L.; Sobolev, A.P.; Viel, S. Liquid state 1H high field NMR in food analysis. *Prog. Nucl. Magn. Reson. Spectrosc.* **2012**, *66*, 1–39. [CrossRef]
34. Arnaldi, S.M. Piante di melo di Antiche Varietà piemontesi. Available online: http://www.scuolamalva.it/wp-content/uploads/2016/06/Descrizione-piante-melo-TRIO.pdf (accessed on 6 August 2020).
35. Ingallina, C.; Sobolev, A.P.; Circi, S.; Spano, M.; Fraschetti, C.; Filippi, A.; Di Sotto, A.; Di Giacomo, S.; Mazzoccanti, G.; Gasparrini, F.; et al. Cannabis sativa L. Inflorescences from Monoecious Cultivars Grown in Central Italy: An Untargeted Chemical Characterization from Early Flowering to Ripening. *Molecules* **2020**, *25*, 1908. [CrossRef]
36. Zhu, D.; Shen, Y.; Wei, L.; Xu, L.; Cao, X.; Liu, H.; Li, J. Effect of particle size on the stability and flavor of cloudy apple juice. *Food Chem.* **2020**, *328*, 126967. [CrossRef]
37. Vermathen, M.; Marzorati, M.; Baumgartner, D.; Good, C.; Vermathen, P. Investigation of different apple cultivars by high resolution magic angle spinning NMR. A feasibility study. *J. Agric. Food Chem.* **2011**, *59*, 12784–12793. [CrossRef]
38. Vrhovsek, U.; Rigo, A.; Tonon, D.; Mattivi, F. Quantitation of polyphenols in different apple varieties. *J. Agric. Food Chem.* **2004**, *52*, 6532–6538. [CrossRef] [PubMed]
39. Panzella, L.; Petriccione, M.; Rega, P.; Scortichini, M.; Napolitano, A. A reappraisal of traditional apple cultivars from Southern Italy as a rich source of phenols with superior antioxidant activity. *Food Chem.* **2013**, *140*, 672–679. [CrossRef] [PubMed]
40. Sugawara, T.; Miyazawa, T. Separation and determination of glycolipids from edible plant sources by high-performance liquid chromatography and evaporative light-scattering detection. *Lipids* **1999**, *34*, 1231–1237. [CrossRef] [PubMed]
41. Ingallina, C.; Spano, M.; Sobolev, A.P.; Esposito, C.; Santarcangelo, C.; Baldi, A.; Daglia, M.; Mannina, L. Characterization of Local Products for Their Industrial Use : The Case of Italian Potato Cultivars Analyzed by Untargeted and Targeted Methodologies. *Foods* **2020**, *9*, 1216. [CrossRef] [PubMed]
42. Ticha, A.; Salejda, A.M.; Hyšpler, R.; Matejicek, A.; Paprstein, F.; Zadak, Z.; Cukrów, W.S. Jabłkach Różnych Odmian I Ich Wpływ Na Cechy Sensoryczne. *Zywn. Nauk. Technol. Jakosc/Food. Sci. Technol. Qual.* **2015**, *22*, 137–150. [CrossRef]
43. Hermann, K.; Bordewick-Dell, U. Fructose in different apple varieties. Implications for apple consumption in persons affected by fructose intolerance. *Ernährungs Umschau* **2018**, *65*, 48–52. [CrossRef]
44. Hecke, K.; Herbinger, K.; Veberič, R.; Trobec, M.; Toplak, H.; Štampar, F.; Keppel, H.; Grill, D. Sugar-, acid- and phenol contents in apple cultivars from organic and integrated fruit cultivation. *Eur. J. Clin. Nutr.* **2006**, *60*, 1136–1140. [CrossRef]
45. Kim, I.; Ku, K.H.; Jeong, M.C.; Kwon, S., II; Lee, J. Metabolite profiling and antioxidant activity of 10 new early- to mid-season apple cultivars and 14 traditional cultivars. *Antioxidants* **2020**, *9*, 443. [CrossRef]
46. Agricultural Marketing Resource Center Apples. Available online: https://www.agmrc.org/commodities-products/fruits/apples (accessed on 6 August 2020).
47. Produce Report Global Trends in Apple Innovation. Available online: https://www.producereport.com/article/global-trends-apple-innovation (accessed on 6 August 2020).
48. Petkovsek, M.M.; Stampar, F.; Veberic, R. Parameters of inner quality of the apple scab resistant and susceptible apple cultivars (Malus domestica Borkh.). *Sci. Hortic.* **2007**, *114*, 37–44. [CrossRef]
49. Colaric, M.; Veberic, R.; Stampar, F.; Hudina, M. Evaluation of peach and nectarine fruit quality and correlations between sensory and chemical attributes. *J. Sci. Food Agric.* **2005**, *85*, 2611–2616. [CrossRef]
50. Hulme, A.C. The isolation of L-citramalic acid from the peel of the apple fruit. Biochim. *Biophys. Acta* **1954**, *14*, 36–43. [CrossRef]
51. Ehrenkranz, J.R.L.; Lewis, N.G.; Kahn, C.R.; Roth, J. Phlorizin: A review. *Diabetes. Metab. Res. Rev.* **2005**, *21*, 31–38. [CrossRef] [PubMed]
52. Escarpa, A.; González, M.C. High-performance liquid chromatography with diode-array detection for the determination of phenolic compounds in peel and pulp from different apple varieties. *J. Chromatogr. A* **1998**, *823*, 331–337. [CrossRef]
53. Boyer, J.; Liu, R.H. Apple phytochemicals and their health benefits. *Nutr. J.* **2004**, *3*, 1–15. [CrossRef]
54. Niederberger, K.E.; Tennant, D.R.; Bellion, P. Dietary intake of phloridzin from natural occurrence in foods. *Br. J. Nutr.* **2020**, *123*, 942–950. [CrossRef]
55. Kumar, S.; Sinha, K.; Sharma, R.; Purohit, R.; Padwad, Y. Phloretin and phloridzin improve insulin sensitivity and enhance glucose uptake by subverting PPARγ/Cdk5 interaction in differentiated adipocytes. *Exp. Cell Res.* **2019**, *383*, 111480. [CrossRef]
56. Posma, J.M.; Garcia-Perez, I.; Heaton, J.C.; Burdisso, P.; Mathers, J.C.; Draper, J.; Lewis, M.; Lindon, J.C.; Frost, G.; Holmes, E.; et al. Integrated Analytical and Statistical Two-Dimensional Spectroscopy Strategy for Metabolite Identification: Application to Dietary Biomarkers. *Anal. Chem.* **2017**, *89*, 3300–3309. [CrossRef]
57. Noro, S.; Kudo, N.; Kitzuwa, T. Differences in Sugars and Organic Acids between Red and Yellow Apple Cultivars at Time of Coloring, and Effect of Citramalic Acid on Development of Anthocyanin. *J. Jpn. Soc. Hortic. Sci.* **1988**, *57*, 381–389. [CrossRef]
58. Rudell, D.R.; Mattheis, J.P.; Curry, E.A. Prestorage ultraviolet-white light irradiation alters apple peel metabolome. *J. Agric. Food Chem.* **2008**, *56*, 1138–1147. [CrossRef]
59. Santana-Gálvez, J.; Cisneros-Zevallos, L.; Jacobo-Velázquez, D.A. Chlorogenic Acid: Recent advances on its dual role as a food additive and a nutraceutical against metabolic syndrome. *Molecules* **2017**, *22*, 358. [CrossRef]

60. Finamore, A.; Roselli, M.; Donini, L.M.; Brasili, D.E.; Rami, R.; Carnevali, P.; Mistura, L.; Pinto, A.; Giusti, A.M.; Mengheri, E. Supplementation with Bifidobacterium longum Bar33 and Lactobacillus helveticus Bar13 mixture improves immunity in elderly humans (over 75 years) and aged mice. *Nutrition* **2019**, *63*, 184–192. [CrossRef] [PubMed]
61. Boutaoui, N.; Zaiter, L.; Benayache, F.; Benayache, S.; Cacciagrano, F.; Cesa, S.; Secci, D.; Carradori, S.; Giusti, A.M.; Campestre, C.; et al. Atriplex mollis Desf. aerial parts: Extraction procedures, secondary metabolites and color analysis. *Molecules* **2018**, *23*, 1962. [CrossRef] [PubMed]
62. Toledo, Á.; Burlingame, B. Biodiversity and nutrition: A common path toward global food security and sustainable development. *J. Food Compos. Anal.* **2006**, *19*, 477–483. [CrossRef]

5.4. Case study 3: Goji berries cultivars cultivated in Lazio Region

Italy is one of the main Goji berries producers in Europe. Among the many Goji berries cultivars, Big Lifeberry and Sweet Lifeberry are of particular interest and are widely grown in Europe and North America. The beneficial effects contributed are widespread from the consumption of Goji berries as a functional food in many dietary, cosmetic, and pharmaceutical preparations and supplements.

In the present work, Big Lifeberry and Sweet Lifeberry Goji berries grown in the South Lazio Region of Italy and harvested in August and October were investigated by a multimethodological analytical protocol after their harvesting, before the post-harvesting treatments to obtain a complete metabolite profile. In particular, NMR spectroscopy, electrospray ionization Fourier transform ion cyclotron resonance (ESI FT-ICR) mass spectrometry, and UV-Vis spectrophotometry was applied to obtain the metabolite profile of the hydroalcoholic and organic Bligh-Dyer extracts.

molecules

MDPI

Article

Metabolomic Profiling of Fresh Goji (*Lycium barbarum* L.) Berries from Two Cultivars Grown in Central Italy: A Multi-Methodological Approach

Mattia Spano [1,†], Alessandro Maccelli [1,†], Giacomo Di Matteo [1], Cinzia Ingallina [1], Mariangela Biava [1], Maria Elisa Crestoni [1,*], Jean-Xavier Bardaud [2], Anna Maria Giusti [3], Alessia Mariano [4], Anna Scotto D'Abusco [4], Anatoly P. Sobolev [5,*], Alba Lasalvia [1], Simonetta Fornarini [1] and Luisa Mannina [1]

[1] Department of Chemistry and Technology of Drugs, Sapienza University of Rome, Piazzale Aldo Moro 5, 00185 Rome, Italy; mattia.spano@uniroma1.it (M.S.); alessandro.maccelli@uniroma1.it (A.M.); giacomo.dimatteo@uniroma1.it (G.D.M.); cinzia.ingallina@uniroma1.it (C.I.); mariangela.biava@uniroma1.it (M.B.); alba.lasalvia@uniroma1.it (A.L.); simonetta.fornarini@uniroma1.it (S.F.); luisa.mannina@uniroma1.it (L.M.)

[2] Institut de Chimie Physique, CLIO, Université Paris Saclay, Bât 200, BP34, CEDEX, 91898 Orsay, France; j.xavier.bardaud@gmail.com

[3] Department of Experimental Medicine, Sapienza University of Rome, P.le Aldo Moro 5, 00185 Rome, Italy; annamaria.giusti@uniroma1.it

[4] Department of Biochemical Sciences, Sapienza University of Roma, P.le Aldo Moro 5, 00185 Rome, Italy; alessia.mariano@uniroma1.it (A.M.); anna.scottodabusco@uniroma1.it (A.S.D.)

[5] Institute for Biological Systems, Magnetic Resonance Laboratory "Segre-Capitani", CNR, Via Salaria Km 29.300, 00015 Monterotondo, Italy

* Correspondence: mariaelisa.crestoni@uniroma1.it (M.E.C.); anatoly.sobolev@cnr.it (A.P.S.)

† These authors contributed equally to this work.

Abstract: The metabolite profile of fresh Goji berries from two cultivars, namely Big Lifeberry (BL) and Sweet Lifeberry (SL), grown in the Lazio region (Central Italy) and harvested at two different periods, August and October, corresponding at the beginning and the end of the maturation, was characterized by means of nuclear magnetic resonance (NMR) and electrospray ionization Fourier transform ion cyclotron resonance (ESI FT-ICR MS) methodologies. Several classes of compounds such as sugars, amino acids, organic acids, fatty acids, polyphenols, and terpenes were identified and quantified in hydroalcoholic and organic Bligh-Dyer extracts. Sweet Lifeberry extracts were characterized by a higher content of sucrose with respect to the Big Lifeberry ones and high levels of amino acids (glycine, betaine, proline) were observed in SL berries harvested in October. Spectrophotometric analysis of chlorophylls and total carotenoids was also carried out, showing a decrease of carotenoids during the time. These results can be useful not only to valorize local products but also to suggest the best harvesting period to obtain a product with a chemical composition suitable for specific industrial use. Finally, preliminary studies regarding both the chemical characterization of Goji leaves generally considered a waste product, and the biological activity of Big Lifeberry berries extracts was also investigated. Goji leaves showed a chemical profile rich in healthy compounds (polyphenols, flavonoids, etc.) confirming their promising use in the supplements/nutraceutical/cosmetic field. MG63 cells treated with Big Lifeberry berries extracts showed a decrease of iNOS, COX-2, IL-6, and IL-8 expression indicating their significant biological activity.

Keywords: Goji berries; metabolite profile; NMR; FT-ICR MS; Goji leaves; biological assays

check for updates

Citation: Spano, M.; Maccelli, A.; Di Matteo, G.; Ingallina, C.; Biava, M.; Crestoni, M.E.; Bardaud, J.-X.; Giusti, A.M.; Mariano, A.; D'Abusco, A.S.; et al. Metabolomic Profiling of Fresh Goji (*Lycium barbarum* L.) Berries from Two Cultivars Grown in Central Italy: A Multi-Methodological Approach. *Molecules* **2021**, *26*, 5412. https://doi.org/10.3390/molecules26175412

Academic Editors: Alessandra Biancolillo and Angelo Antonio D'Archivio

Received: 5 August 2021
Accepted: 2 September 2021
Published: 6 September 2021

Publisher's Note: MDPI stays neutral with regard to jurisdictional claims in published maps and institutional affiliations.

Copyright: © 2021 by the authors. Licensee MDPI, Basel, Switzerland. This article is an open access article distributed under the terms and conditions of the Creative Commons Attribution (CC BY) license (https://creativecommons.org/licenses/by/4.0/).

1. Introduction

Goji berries or wolfberries (*Lycium* fruits) are healthy fruits of closely related shrubs from the genus *Lycium*, belonging to the Solanaceae family. *L. barbarum* and *L. chinense*

species have a long history in ancestral Chinese medicine as traditional medicinal herbs and food supplements [1]. Beneficial effects on aging, neuroprotection, and well-being such as antioxidant, immunomodulatory, and anticancer properties [2–4] have been ascribed to Goji berries' chemical composition including polysaccharides, terpenoids, glycerogalactolipids, carotenoids, organic acids, phenolic acids (chlorogenic, caffeic acid, *p*-coumaric acids, quercetin, kaempferol) [5], flavonoids, vitamins, minerals, and fibers [6–10]. The beneficial effects contributed are widespread from the consumption of Goji berries as a functional food in many dietary, cosmetic, and pharmaceutical preparations and supplements in the Western countries, including Italy. Italy is one of the main Goji berries producers in Europe [11]. Among the many Goji berries cultivars, Big Lifeberry and Sweet Lifeberry are of particular interest and are widely grown in Europe and North America [12]. Generally, analytical studies on Goji berries have been focused on the chemical characterization of dried berries commercially available in markets. In particular, targeted techniques such as chromatography and UV-Vis spectrophotometry have been applied to study specific classes of compounds such as polyphenols, carotenoids, sugars, organic acids, fatty acids, polysaccharides, and fibers [5,6,9–11,13,14].

In this study, Big Lifeberry (BL) and Sweet Lifeberry (SL) Goji berries grown in the South Lazio region (Central Italy) and harvested in August and October [11] were investigated by a multimethodological analytical protocol after their harvesting, before the post-harvesting treatments to obtain a complete metabolite profile. In particular, high-resolution nuclear magnetic resonance (NMR) spectroscopy, electrospray ionization Fourier transform ion cyclotron resonance (ESI FT-ICR) mass spectrometry, and UV-Vis spectrophotometry was applied to obtain the metabolite profile of the hydroalcoholic and organic Bligh-Dyer method extracts. This multimethodological approach has been already exploited to other complex matrices, including essential oils [15] and foodstuffs [16–18], ensuring a reliable and extensive phytochemical coverage and quality assessment of the Lycium fruits analyzed from Central Italy. Finally, preliminary studies regarding both the metabolite profile of Goji leaves extracts [19,20] and the biological activity of Big Lifeberry berries was also carried out.

2. Results and Discussion

2.1. Goji Berries Metabolite Profile

Goji berries Bligh-Dyer extracts from BL and SL Goji berries harvested in August (BL1 and SL1) and October (BL2 and SL2) were analyzed using high-resolution NMR and direct infusion ESI FT-ICR MS methodologies. The ESI FT-ICR MS allowed us to detect many molecular formulas, whereas the less sensitive NMR methodology provided structural and quantitative information. The NMR and ESI FT-ICR assignments will be first discussed separately. Then, the metabolite profile will be discussed for the class of compounds assimilating the results obtained by the two complementary untargeted methodologies.

2.1.1. ^{1}H NMR Assignment

NMR spectroscopy represents a very powerful tool for metabolomic studies since this methodology allows us to resolve complex mixtures such as natural matrices extracts. This is due to the combined interpretation of both one-dimensional and two-dimensional NMR experiments. The ^{1}H NMR spectral assignments of hydroalcoholic (Table 1) and organic (Table 2) Bligh-Dyer extracts were carried out by means of 2D experiments and literature data regarding other vegetable matrices analyzed in the same experimental conditions [21,22]. Three sugars, six organic acids, fifteen amino acids, choline, and trigonelline were detected in all the hydroalcoholic Bligh-Dyer extracts and their characteristic ^{1}H NMR signals were used for compound quantification. Acetic acid, fumaric acid, arginine, and glutamine were not quantified because of their signals overlapping.

Table 1. Metabolites identified in the 600.13 MHz ^{1}H-NMR spectra of the Bligh-Dyer hydroalcoholic extracts of Goji berries dissolved in 400 mM phosphate buffer/D_2O containing TSP 1 mM. Signals selected for quantitative analysis (integration) are labeled with an asterisk (*).

Metabolite	Group	^{1}H (ppm)	Multiplicity [*J*(Hz)]	^{13}C (ppm)
Sugars				
α-D-Fructofuranose [b,l]	C-2			105.4
	CH-3	4.12 *		83.0
	CH-4	4.01		
	CH-5	4.07		82.5
β-D-Fructofuranose [b,l]	C-2			102.9
	CH-3	4.12 *		76.5
	CH-4	4.12 *		75.4
	CH-5	3.83		
β-D-Fructopyranose [b,l]	C-2			99.3
	CH-3	3.80		68.6
	CH-4	4.00		77.0
	CH_2-6,6′	3.72; 4.03		64.4
α-Glucose [b,l]	CH-1	5.25 *	d [3.8]	93.2
	CH-2	3.55		72.0
	CH-3	3.72		73.3
	CH-4	3.42		70.7
	CH-5	3.84		72.5
	CH_2-6,6′	3.89; 3.78		61.8
β-Glucose [b,l]	CH-1	4.66 *	d [8.0]	96.9
	CH-2	3.26		75.1
	CH-3	3.51		76.9
	CH-4	3.42		70.7
	CH-5	3.49		76.8
	CH_2-6,6′	3.90; 3.75		61.8
Sucrose [b,l]	CH-1 (Glucose)	5.42 *	d [3.8]	93.1
	CH-2	3.57		71.8
	CH-3	3.77		73.6
	CH-4	3.48		70.2
	CH-5	3.85		73.5
	C-2 (Fructose)			104.8
	CH-3′	4.23	d [8.8]	77.4
	CH-4′	4.07		75.1
	CH-5′	3.90		82.4
	CH_2-6′	3.83		61.2
Organic acids				
Acetic acid [b,l]	α-CH_3	1.93	s	24.4
	COOH			182.6
Citric acid [b,l]	α,γ-CH	2.55 *	d [15.4]	46.6
	α′,γ′-CH	2.68	d [15.4]	46.6
	β-C			76.5
	1,5-COOH			180.1
	6-COOH			183.0
Formic acid [b,l]	HCOOH	8.47 *	s	
Fumaric Acid [b,l]	α,β-CH=CH	6.53	s	
Malic acid [b,l]	α-CH	4.30 *	dd [9.9; 3.2]	71.3
	β-CH	2.70	dd [15.4; 3.2]	43.5
	β′-CH	2.39	dd [15.4; 9.9]	43.5
Quinic acid [b,l]	CH_2-2,2′	1.88 *; 2.07	dd [13.5; 10.8]; m	41.7
	CH-3	4.16		

Table 1. *Cont.*

Metabolite	Group	^{1}H (ppm)	Multiplicity [*J*(Hz)]	^{13}C (ppm)
Amino acids				
Alanine [b,l]	α-CH	3.80		51.7
	β-CH_3	1.49 *	d [7.3]	17.1
	COOH			177.1
Arginine [b,l]	α-CH	3.79		55.3
	β-CH_2	1.91	m	28.6
	γ-CH	1.67	m	25.1
	γ′-CH	1.74	m	25.1
	δ-CH_3	3.24		41.6
Asparagine [b,l]	α-CH	4.02		52.4
	β,β′-CH_2	2.89 *; 2.96	dd [7.3; 16.9]	35.5
	γ-$CONH_2$			175.4
Aspartate [b,l]	α-CH	3.94		53.1
	β,β′-CH_2	2.70; 2.81 *	dd [3.9; 17.4]	37.5
	γ-COO^-			179.9
GABA [b,l]	α-CH_2	2.30 *	t [7.4]	35.4
	β-CH_2	1.91		25.0
	γ-CH_2	3.02		41.0
Glycinebetaine [b,l]	$N(CH_3)_3$+	3.27 *	s	54.4
	α-CH_2	3.90		67.5
Glutamine [b,l]	α-CH	3.79		55.4
	β,β′-CH_2	2.14	m	27.5
	γ-CH	2.46	m	31.9
Isoleucine [b,l]	β-CH	1.99		37.1
	γ-CH_3	1.27		25.8
	γ-CH_3	1.01 *	d [7.1]	15.7
	δ-CH_3	0.95		12.0
Leucine [b,l]	β-CH_2	1.74		40.8
	γ-CH	1.71		
	δ-CH_3	0.97 *	d [6.2]	23.0
	δ′-CH_3	0.96	d [6.2]	22.0
Phenylalanine [b,l]	CH-2,6	7.34	m	130.3
	CH-4	7.38	m	128.6
	CH-3,5	7.43 *	m	130.2
Proline [b]	α-CH	4.15		62.3
	β,β′- CH_2	2.07, 2.35		30.3
	γ-CH_2	2.01 *	m	24.8
	δ,δ′- CH_2	3.35, 3.42		47.2
Threonine [b,l]	α-CH	3.61		61.6
	β-CH	4.27		67.2
	γ-CH_3	1.34 *	d [6.6]	20.4
Tyrosine [b,l]	CH-3,5	7.20	d [8.5]	131.8
	CH-2,6	6.90 *	d [8.5]	116.7
Tryptophan [b]	CH-4	7.27	m	
	CH-5	7.19	m	
	CH-6	7.73	d [8.0]	119.5
	CH-7	7.54 *	d [8.0]	113.0
Valine [b,l]	α-CH	3.62		61.4
	β-CH	2.28		30.3
	γ-CH_3	1.00	d [7.1]	17.7
	γ′-CH_3	1.05 *	d [7.1]	18.9
Miscellaneous metabolites				
Choline [b,l]	$N(CH_3)_3^+$	3.21 *	s	54.8
	α-CH_2	3.81		68.5
Trigonelline [b,l]	CH-1	9.13 *	s	
	CH-3,5	8.84		
	CH-4	8.09		

[b] Metabolite identified in Bligh-Dyer hydroalcoholic extract of Goji berries; [l] Metabolite identified in Bligh-Dyer hydroalcoholic extract of Goji leaves.

Table 2. Metabolites identified in the 600.13 MHz ^{1}H-NMR (Nuclear Magnetic Resonance) spectra of the Bligh-Dyer organic extracts of Goji berries dissolved in $CDCl_3$/MeOD 2:1 *v/v* mixture. Signals selected for quantitative analysis (integration) are labeled with an asterisk (*).

Metabolite	Group	^{1}H (ppm)	Multiplicity [*J* (Hz)]	^{13}C (ppm)
Oleic fatty chain [b,l]	COO			174.5
(C18:1 Δ^{9})	CH_2-2	2.30 *		34.6
	CH_2-3	1.59	m	25.4
	CH_2-4-7	1.30	m	29.5
	CH_2-8	2.03	m	27.6
	CH=CH-9,10	5.30 *	m	128.4
	CH_2-11	2.03	m	27.6
	CH_2-12-15	1.33–1.30	m	29.5–29.9
	CH_2-16	1.29	m	29.7
	CH_2-17	1.24	m	32.2
	CH_3-18	0.84	t	14.1
Linoleic fatty chain [b,l]	COO			174.5
(C18:2 $\Delta^{9,12}$)	CH_2-2	2.30 *		34.6
	CH_2-3	1.59	m	25.4
	CH_2-4-7	1.32–1.28	m	29.5
	CH_2-8	2.03	m	27.6
	CH= 9	5.33 *	m	130.5
	CH= 10	5.30 *	m	128.4
	CH_2-11	2.75 *	t [6.8]	25.9
	CH= 12	5.30 *	m	128.4
	CH= 13	5.33 *	m	130.5
	CH_2-14	2.03	m	27.6
	CH_2-15	1.29	m	29.7
	CH_2-16	1.29	m	29.7
	CH_2-17	1.24	m	32.2
	CH_3-18	0.86	t	14.1
Linolenic fatty chain [b,l]	COO			174.5
(C18:3 $\Delta^{9,12,15}$)	CH_2-2	2.30 *		34.6
	CH_2-3	1.57	m	25.4
	CH_2-4-7	1.30	m	29.5
	CH_2-8	2.04	m	27.5
	CH=CH 9,10	5.33 *	m	128.4
	CH_2 11	2.79 *	t [6.2]	25.9
	CH=CH 12,13	5.33 *	m	128.4
	CH_2-14	2.79 *	t [6.2]	25.9
	CH= 15	5.28 *	m	128.6
	CH= 16	5.35 *	m	132.2
	CH_2-17	2.04	m	20.6
	CH_3-18	0.95	t [7.5]	14.3
Saturated fatty acids [b,l]	COO			174.5
	CH_2-2	2.28 *		34.8
	CH_2-3	1.57	m	25.4
	CH_2	1.28–1.22	m	29.9–32.0
	CH_2 n-1	1.25		23.0
	CH_3 n	0.84	t	14.1
β-Sitosterol [b,l]	C-13			42.4
	CH-17	1.16		56.4
	CH_3-18	0.66 *	s	12.0
Squalene [b,l]	CH_3-a	1.56		
	CH_3-b	1.65		
	CH-c	5.08	m	124.7
	CH_2-d	2.04		
	CH_2-e	1.96		

Table 2. *Cont.*

Metabolite	Group	^{1}H (ppm)	Multiplicity [*J* (Hz)]	^{13}C (ppm)
1,2-Diacyl-*sn*-glycero-3-Phosphatidylcholine [b,l]	CH_2-*sn1*	4.30, 4.14		62.5
	CH-*sn2*	5.22		70.7
	CH_2-*sn3*	3.94, 3.70		68.2
	$N(CH_3)_3$+	3.19 *	s	54.4
Digalactosyldiacylglycerol [b,l]	CH_2-*sn1*	4.30, 4.14		62.5
	CH-*sn2*	5.06		70.7
	CH_2-*sn3*	3.66		68.2
	CH″-1	4.87 *	d [3.8]	99.7
	CH″-2	3.78		68.5
	CH″-3,5	3.70		70.6
	CH″-4	3.92		70.1
	CH′-1	4.20		104.3
	CH′-2	3.50		71.3
	CH′-3	3.47		73.5
	CH′-4	3.87		66.6
Carotenoids [b]	CH-7	6.09		125.6
	CH-8	6.09		139.2
	CH-10	6.14		131.7
	CH-11	6.63		125.2
	CH-12	6.35 *		138.0
	CH-14	6.24		133.0
	CH-15	6.62		130.4

[b] Metabolite identified in Bligh-Dyer hydroalcoholic extract of Goji berries; [l] Metabolite identified in Bligh-Dyer hydroalcoholic extract of Goji leaves.

Regarding the organic Bligh-Dyer extracts, β-sitosterol, fatty acids, phosphatidylcholine, digalactosyldiacylglycerol, squalene, and carotenoids were identified in ^{1}H NMR spectra of all samples. Squalene was not quantified due to signal overlapping.

2.1.2. ESI FT-ICR Assignment

ESI(+) FT-ICR mass spectra of hydroalcoholic extracts from BL and SL berries (Figures S1 and S2) showed peaks due to protonated compounds or alkali metal adducts. The list of assigned elemental formulas together with the experimental and theoretical *m/z* ratios, the mass deviation, and the putative compound annotations are available in either ionization mode in Tables S1 and S2 (hydroalcoholic extracts), and Tables S3 and S4 (organic extracts).

The distribution of the identified molecular formulas is reported in Table 3. Numerous compounds assayed by CID-MS^{n} (n = 2,3) experiments provided additional structural information useful to validate peak assignments of likely isomers (Figure S3). Globally, a higher number of molecules were revealed in positive mode, and the hydroalcoholic extracts were relatively richer than the organic ones for each sample.

BL and SL samples collected in August showed a similar chemical profile in both hydroalcoholic and organic extracts. When harvested in October, more metabolites were observed in BL than in SL in hydroalcoholic extracts, whereas the opposite trend was observed in organic extracts.

A large amount of assigned molecular formulas was visualized by two-dimensional van Krevelen diagrams (vKd) where elemental formulas are sorted based on their H/C versus O/C atomic ratios (Figure 1A–D). These plots enable the identified molecular compositions to be organized, thus providing a qualitative overview of densities of molecular classes, including lipids, amino acids, carbohydrates, polyketides, nucleic acids, and polyalcohols [23]. Regardless of the harvest period, SL and BL cultivars were characterized by strong similarities, with a high density of phytochemicals in the regions of lipids, polyketides, amino acids, and polyphenols.

Table 3. Molecular formulas (MF) identified by electrospray ionization-mass spectrometry (ESI-MS) in Bligh-Dyer hydroalcoholic and organic extracts of Big Lifeberry (BL) and Sweet Lifeberry SL) berries harvested in periods 1 and 2.

Extract	Hydroalcoholic [a]			Organic [b]		
	Ion Mode	Identified MF		Ion Mode	Identified MF	
BL1	ESI(+)	96	191	ESI(+)	55	109
	ESI(−)	114		ESI(−)	65	
BL2	ESI(+)	118	219	ESI(+)	71	104
	ESI(−)	121		ESI(−)	38	
SL1	ESI(+)	165	273	ESI(+)	114	169
	ESI(−)	114		ESI(−)	63	
SL2	ESI(+)	93	138	ESI(+)	101	170
	ESI(−)	57		ESI(−)	84	

[a] Investigated by means of ESI FT-ICR MS. [b] Investigated by means of ESI Ion trap MS.

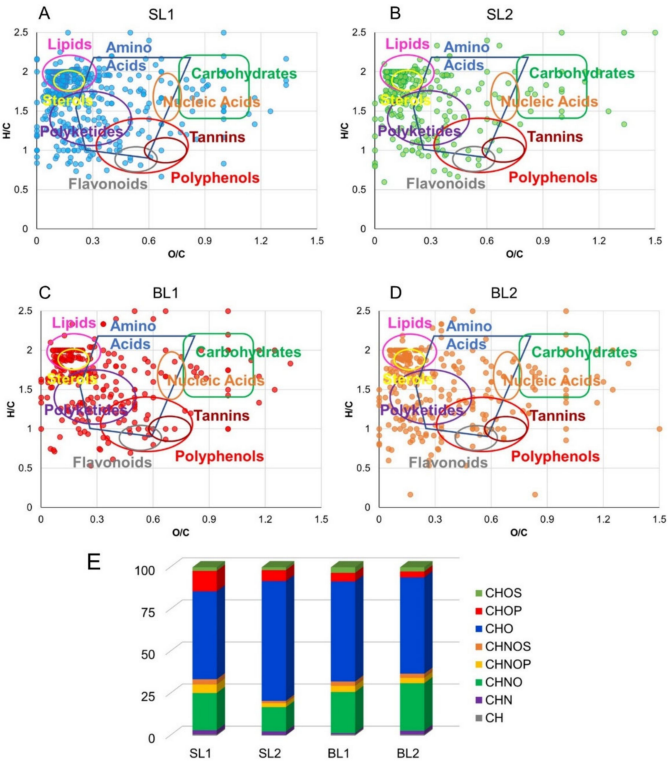


Figure 1. Van Krevelen diagram (elemental plot) obtained from the molecular formulas determined by ESI FT-ICR and Esquire 6000 MS analyses of hydroalcoholic and organic berries extracts of SL1 (panel **A**), SL2 (panel **B**), BL1 (panel **C**), BL2 (panel **D**). Each point represents a distinctive molecular formula. Relative frequency histograms of CH, CHN, CHO, CHNO, CHOP, CHOS, CHNOP, and CHNOS elemental compositions in SL and BL berries extracts (**E**).

In addition, homology series along trend lines with specific slopes can be identified as indicative of structural relationships among families of compounds brought about by chemical reactions such as (de)hydrogenation (A-lines), oxidation or reduction (B-lines), (de)hydration (C-lines) and (de)methylation routes (D-lines) [23]. In particular, hits along A-lines comprise, for example, lactic acid ($C_3H_6O_3$)/glycerol ($C_3H_8O_3$), fumaric ($C_4H_4O_4$)/succinic ($C_4H_6O_4$) acids, for O/C = 1.0; entries along B-lines include cinnamyl alcohol ($C_9H_{10}O$)/dihydrocinnamic acid ($C_9H_{10}O_2$), for H/C = 1.1, and rhamnose ($C_6H_{12}O_5$)/glucose ($C_6H_{12}O_6$)/gluconic acid ($C_6H_{12}O_7$), for H/C = 2.0; items along D-lines encompass palmitic ($C_{16}H_{32}O_2$)/ stearic ($C_{18}H_{36}O_2$)/ arachidic ($C_{20}H_{40}O_2$) acids (Figure S4).

The relative frequency distribution of the annotated molecular formulas in Figure 1E shows that the most abundant metabolites in all extracts are CHO species, alcohols, carbohydrates, lipids, and polyphenols, ranging from 59% (BL1) to 52% (SL1), and CHNO compounds, mainly amino acids, and alkaloids, from 14% (SL2) to 28% (BL2).

CHOS, CHOP, CHNOP, and CHNOS components were measured in low percentage, with SL1 comprising the majority of CHOP (12%) and CHNOP (5%) groups.

According to Figure 1E, SL1 presented the major biodiversity of CHOP (12%), CHNOP (5%), and CHNOS (3%) components, whereas BL2 contained the highest number of CHN (2%) and CHOS (2%) species. Some metabolites were identified in almost all extracts, such as phosphate, valine, arginine, aldohexose, sucrose, *O*-galloyl-glucose, lactic, aspartic, glutamic, malic, citric, myristic, palmitic, and stearic acids, found in the hydroalcoholic extracts; and limonene, arachidonic, eicosenoic, docosanedioic, linoleic, linolenic, palmitoleic and oleic acids, vitamin D3 derivatives, and mono- and diacylacylglycerols, detected in the organic one.

Conversely, other phytochemicals were detected only in few samples as hereafter reported in detail for a class of compounds.

2.1.3. Amino Acids and Derivatives

Glycinbetaine, a typical and characteristic metabolite of Goji berries [2,24] was the most abundant amino acid derivative detected in ^{1}H NMR spectra of berries, reaching the highest amount in the SL2 sample, that significantly increased ($p < 0.05$) in August, see Figure 2A. Asparagine was also present in high concentration, with the highest level in the SL cultivar, mainly in October. It was noteworthy that in the BL cultivar, the amounts of amino acids, mainly branched chains (no statistical difference), were generally the same in the two harvesting periods, whereas for the SL cultivar, peculiar trends were observed. Many amino acids such as proline, valine, isoleucine, and GABA significantly increased during the time, whereas tryptophan and aspartate showed a strong decrease from SL1 to SL2 ($p < 0.05$).

ESI FT-ICR MS also detected signals of glutamic acid, lysine, methionine, and histidine, covering almost all the proteinogenic amino acids. Other amino acid derivatives, including proline betaine, acetyltyrosine, nitroarginine, and small peptides, like aspartyl-lysine, glutamyl-carnitine, and prolylproline were also observed. FT-ICR allowed us to identify formally isobaric species, for example, protonated histidine, (*m/z* 156.07654) and potassiated valine, (*m/z* 156.04220) in BL1 (Figure S5). Conversely, histidine was barely present in SL2. *N*-Acetyl-phenylalanine was present only in BL2, whereas lysine discriminated the two cultivars in hydroalcoholic extracts, being present as an intense peak only in BL.

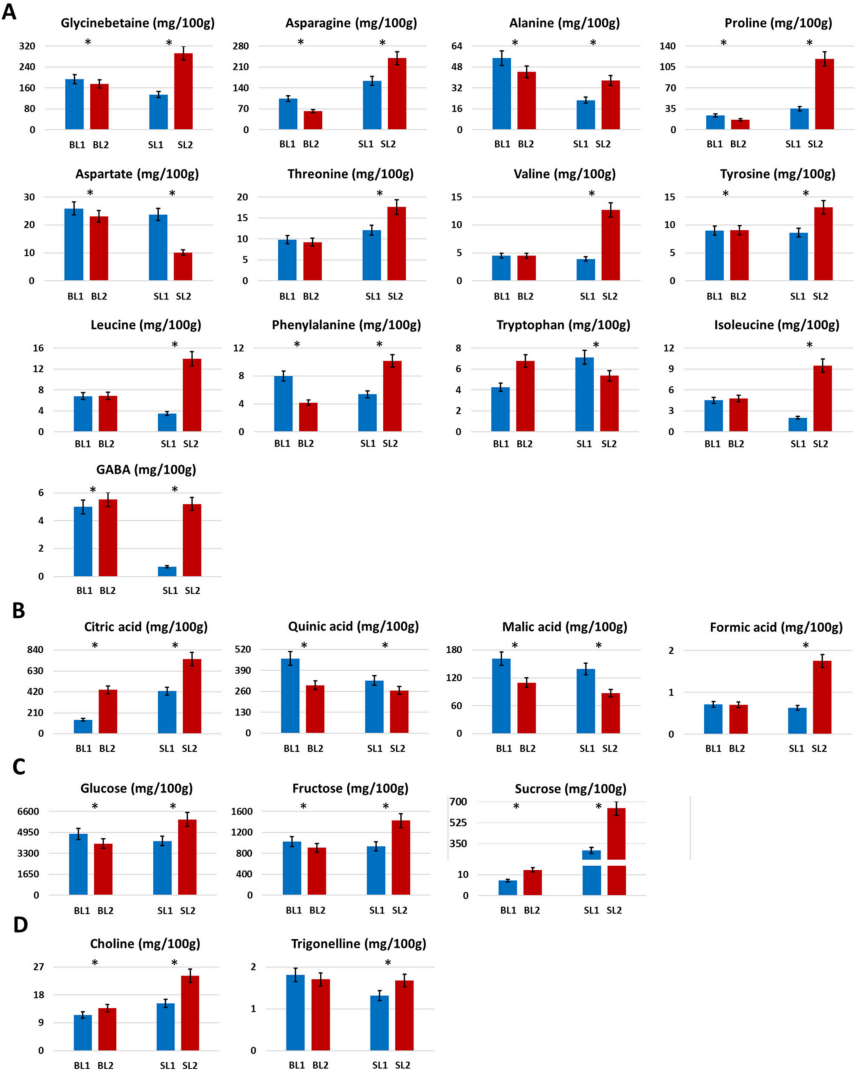


Figure 2. Histograms resulting from the quantitative NMR analysis of quantified compounds present in the Bligh-Dyer hydroalcoholic extracts of Goji berries cultivars Big Lifeberry (BL) and Sweet Lifeberry (SL) harvested in August (BL1, SL1) and October (BL2, SL2). (**A**) Sugars, (**B**) Organic acids, (**C**) Amino acids, (**D**) Other metabolites. Results were expressed as mg/100g ± SD of fresh sample. * $p < 0.05$ significantly difference between the two harvesting periods in the same cultivar, one-way ANOVA.

2.1.4. Organic Acids

The presence of citric, quinic, succinic, malic, lactic, and fumaric acids was confirmed by both NMR and ESI(−) FT-ICR MS analyses. For instance, regarding the NMR assignments of some of these metabolites, citric acid was firstly recognized in ^{1}H spectra by the typical "roofing" doublets (J = 15.4 Hz) at 2.55 and 2.68 ppm of its symmetric diastereotopic CH_2 groups. The long-range correlation with β-C, external and internal COOH groups at 76.5, 180.1, and 183.0 ppm, respectively, confirmed the identification of this metabolite. Similarly, malic acid was firstly recognized by its typical double doublets in the ^{1}H NMR spectra at 2.39, 2.70, and 4.30 ppm, corresponding to α-CH and diastereotopic β-CH protons (Table 1). The ^{1}H-^{1}H TOCSY experiment allowed us to identify the mutual correlations between these protons; moreover, the ^{1}H-^{13}C HSQC experiments confirmed the short-range correlation between each proton and their corresponding carbons [25]. According to literature data [26,27], citric and quinic acids were the most abundant organic acids in the Goji berries hydroalcoholic extracts, see Figure 2B, showing a different trend over the season. In particular, citric acid strongly increased ($p < 0.05$) from August to October whereas quinic acid decreased in both cultivars, mainly in BL. Moreover, citric acid was present in major concentrations in SL2, whereas quinic acid was in BL1. Malic acid content decreased over time, with both cultivars having the same concentrations at each harvesting period. Finally, formic acid was always present at low concentrations, increasing in SL2.

ESI(−) FT-ICR mass analysis allowed us to detect malonic acid and caffeic-quinone acid in SL2, 5-hydroxyferulic in BL2, and hydrocinnamic acid in all samples, except in SL2. Chlorogenic acid, already reported in a previous study on Italian Goji berries [10], was detected in BL1 and BL2 samples, as well as chorismic acid, involved in the biosynthetic pathways of aromatic amino acids and alkaloids [28].

2.1.5. Sugars

Sugars turned out to be the most abundant metabolites in hydroalcoholic Bligh-Dyer extracts of Goji berries. Three sugars namely glucose, fructose, and sucrose were assigned and quantified in the NMR spectra of hydroalcoholic extracts. As previously described and in this case, the assignment of sugars, such as all the NMR identified metabolites, was carried out by means of mono and two-dimensional experiment interpretations. For instance, for sucrose identification, its typical doublet at 5.42 ppm which was due to the anomeric CH group of glucose moiety, was recognized in the ^{1}H NMR spectra. Proton spin system correlations confirmed the presence of glucose moiety; moreover, the ^{1}H-^{13}C HMBC experiment allowed us to observe the glucose anomeric group correlation with 104.8 ppm carbon typical of the C-2 fructose group, thus confirming the presence of this disaccharide. Glucose was measured as the most abundant sugar, followed by fructose and sucrose, Figure 2C. Significative variations during the time were observed for the three measured sugars. In particular, in the BL cultivar, a decrease of glucose and fructose was observed during the period, whereas sucrose slightly increased. In the SL cultivar, an increase of the three sugars was observed over time. In particular, it was noteworthy that sucrose was more abundant (at least 40 times) in the SL cultivar with respect to BL. A chromatographic quantification of glucose, fructose, and sucrose in the BL and SL cultivars harvested in Switzerland in September 2004, expressed as dried sample weight, has been reported in previous work [29]. Since the results have been expressed in a different way, a comparison between the absolute quantitative values was not possible. However, in the case of the cultivar harvested in Switzerland, fructose was reported as the most abundant sugar, whereas in the extracts investigated here, glucose turned out to be the most abundant. Moreover, the same level of sucrose has been reported in the BL and SL cultivars conversely to what was observed in the present study.

ESI(−) FT-ICR mass analysis allowed us also to detect mannitol-1-phosphate, only in BL2.

2.1.6. Fatty Acids and Polar Lipids

In organic Bligh-Dyer extracts of Goji berries analyzed with NMR, a significant decrease ($p < 0.05$) during the time of total saturated fatty acids (SFA) was observed in both BL and SL cultivars, whereas total unsaturated fatty acids had an opposite trend, Figure 3A. Regarding the single classes of unsaturated fatty acids, di-unsaturated fatty acids (DUFA) were measured as the most abundant, showing the same content in the BL cultivar and a slight increase in SL. Mono-unsaturated fatty acids (MUFA) generally increased during the time for both cultivars, with the lowest content measured in SL1 that, on the contrary, was characterized by the highest amount of tri-unsaturated fatty acids (TUFA), generally present in low concentrations [30,31]. Regarding polar lipids, the BL cultivar showed an increase of digalactosyldiacylglycerol (DGDG) and a decrease in phosphatidylcholine (PC) during the time. In SL, DGDG and PC maintained the same value from August to October.

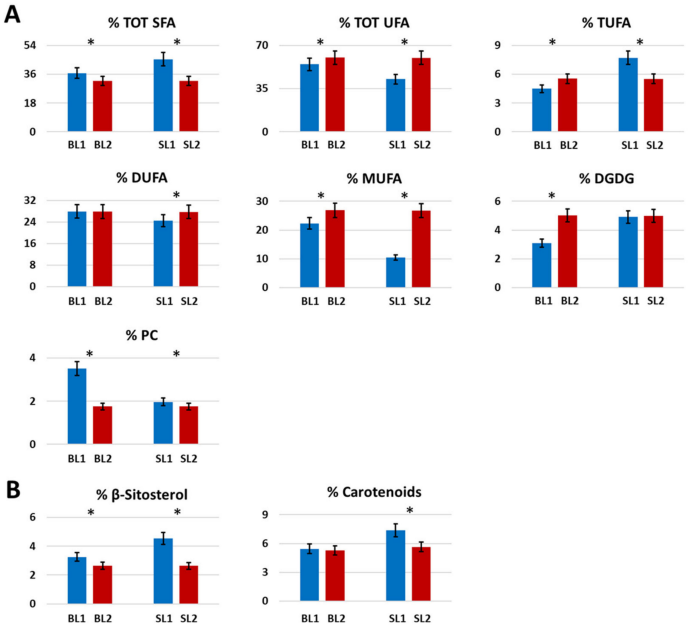


Figure 3. Histograms resulting from the quantitative NMR analysis of some metabolites present in the Bligh-Dyer organic extracts of Goji berries cultivars Big Lifeberry (BL) and Sweet Lifeberry (SL) harvested in August (1) and October (2). (**A**) fatty acids and polar lipids, (**B**) Other metabolites. Results were expressed as molar % ± SD. * $p < 0.05$ significantly difference between the two harvesting periods in the same cultivar, one-way ANOVA.

While NMR spectroscopy allowed to identify each general class of FAs (TOT SFA, TOT UFA, MUFA, DUFA, TUFA), ESI FT-ICR MS identified the specific FAs for each group. In particular, Goji berries were confirmed to be an important source of essential polyunsaturated FAs, comprising ω-3 (linolenic, stearidonic, and 12-hydroxyeicosatetraenoic) and ω-6 (linoleic, arachidonic, and docosadienoic) acids. Moreover, several species belonging to SFA (from 12:0 to 20:0) and MUFA (from 14:1 to 20:1) were detected in all samples.

2.1.7. Miscellaneous

Choline slightly increased during the time in both cultivars, whereas the content of trigonelline was quite the same in BL and slightly increased in SL, Figure 2D. β-sitosterol decreased over time in both cultivars whereas carotenoids were present at the same concentration in BL1 and BL2, whereas, in SL, its value significantly decreased ($p < 0.05$) during the time, Figure 3B.

Both cultivars presented numerous metabolites covering the classes of terpenes, such as limonene; terpenoids, such as apiole and phytuberin; hormones (cis-zeatin-*O*-glucoside); flavonoids (myricetin, cyanidin 3-4′′-acetylglucoside, quercetin 3-galactoside [32], flavonol 3-*O*-D-glycoside, apigenin-rhamnoside-rutinoside); vitamins (retinoic acid and pantothenic acid); nucleosides (dimethyladenosine, orotidine, methylguanosine); alkaloids (theophylline, nicotine, and caffeine). Furthermore, a precursor of lignins and lignols (caffeyl alcohol) were also identified in Goji berries, along with kinetin, a phytohormone able to modulate some aging-related disorders in animal models [33], revealed exclusively in the BL cultivar.

2.2. Pigments Analysis

In Table 4, the concentrations of chlorophyll a, chlorophyll b, and total carotenoids in Goji berries pulp and peel were reported. The three analyzed pigments were measured in higher concentrations in pulp with respect to peel in all samples. It was noteworthy that the chlorophylls trend was different in the two analyzed cultivars. In particular, chlorophylls a and b increased during the time in BL peel and pulp, whereas in SL, the opposite trend was observed. Moreover, chlorophyll a was measured in higher concentrations than chlorophyll b in the BL cultivar, observing the opposite trend in SL cultivars. On the contrary, the total carotenoids trend was the same in both peel and pulp of the BL and SL cultivars, showing a decrease during the time. According to the NMR results, the highest content of carotenoids was measured in the SL1 sample. Comparing the obtained results with those of a previous work where BL and SL have been cultivated in Switzerland and harvested in September 2014 [29], a different carotenoid content trend was observed. In particular, in the cited work, BL has shown to be richer in carotenoids, of more than 50% than in SL, suggesting how the variation of agronomical factors such as soil, harvesting, and climatic conditions can affect the chemical profile of a natural matrix.

Table 4. Chlorophyll a, chlorophyll b, and total carotenoid concentrations by spectrophotometric analysis (mg/g of fresh sample ± SD).

		Chlorophyll a	Chlorophyll b	Tot Carotenoids
BL1	Pulp	0.0112 ± 0.0011	0.0214 ± 0.0012	1.4210 ± 0.0452
	Peel	0.0043 ± 0.0008	0.0083 ± 0.0002	0.5300 ± 0.0340
BL2	Pulp	0.0195 ± 0.0015	0.0320 ± 0.0018	1.1980 ± 0.0420
	Peel	0.0139 ± 0.0018	0.0281 ± 0.0014	0.3274 ± 0.0285
SL1	Pulp	0.0300 ± 0.0080	0.0589 ± 0.0035	2.4130 ± 0.0490
	Peel	0.0157 ± 0.0023	0.0302 ± 0.0070	0.9822 ± 0.0130
SL2	Pulp	0.0184 ± 0.0026	0.0370 ± 0.0052	1.2810 ± 0.0772
	Peel	0.0046 ± 0.0003	0.0090 ± 0.0021	0.4652 ± 0.0084

2.3. Biological Assays on Berries Extracts and Metabolomic Characterization of Leaves

Preliminary studies of the berries' biological activities were carried out. In particular, for the preliminary biological assays regarding the anti-inflammatory activity of Goji berries extracts, MG63 osteoblasts were chosen since they are considered a good model to study bone diseases [34], largely widespread in the world population. In these pathologies, the inflammatory pathways are activated as stated by the production of cytokines and chemokines and in turn by secretion of inducible Nitric Oxide Synthase (iNOS) and inducible Cyclooxygenase (COX-2) [35,36]. iNOS and COX-2 generate nitric oxide (NO) and prostaglandins (PGS), respectively, that are involved in many cellular functions as well as in inflammatory settings [37].

Moreover, since Goji leaves are generally considered a waste product, a metabolomic characterization was carried out to define its metabolite profile and valorize a potential use of this matrix in the food field. In particular, both kinds of analyss were carried out considering the BL cultivar in period 1.

2.3.1. Effects of BL1 Goji Berries Extracts on MG63 Cell Viability

The effects of BL1 extracts on MG63 cell viability were determined by the MTS colorimetric method. The extracts did not show detrimental effects at any analyzed concentration, 100 μg/mL, 50 μg/mL, 25 μg/mL, 12.5 μg/mL and 6.5 μg/mL, or time point, 24, 48, and 72 h (Figure S6). For further experiments, 50 μg/mL and 12.5 μg/mL concentrations were used.

2.3.2. Effects of Goji Berries Extracts on Inflammatory Mediators in MG63 Cells

In order to test the effects of the hydroalcoholic and organic extracts of BL1 on inflammatory mediators in MG63 cells, they were added to the cell culture medium at a concentration of 50 and 12.5 μg/mL in presence of 10 ng/mL TNFα. The mRNA expression level of IL-6, IL-8, and IL-1β was analyzed by RT-PCR assay. Both hydroalcoholic and organic extract were able to decrease the examined cytokines mRNA expression level, and this effect is more pronounced in the presence of the organic extract (Figure S7, upper panel). Moreover, the mRNA expression level of iNOS and COX-2 following the pre-treatment with the LB (*L. Barbarum*) extracts, and the stimulus with TNFα was analyzed. A decrease to the basal level of iNOS and COX-2 expression after the treatment with hydroalcoholic and organic extracts with no statistically significant difference between the two extracts was observed (Figure S7, lower panel).

Considering the results obtained on mRNA expression, IL-6 and IL-8 protein production were verified by performing an ELISA assay. Similarly, to the effect on mRNA expression level, LBEHY (hydroalcoholic extract) and LBEORG (organic extract) at the analyzed concentration were able to decrease the production of IL-6 and IL-8 in MG63 cells, Figure S8.

Taking into account that the mRNA expression of COX-2 was decreased in MG63 cells by LBEHY and LBEORG, we verified whether the extracts were able to reduce the production of this enzyme, performing an immunofluorescence experiment. We found that both LBEHY and LBEORG after 5 h were able to reduce the COX-2 protein expression, Figure S9.

2.3.3. Metabolomic Characterization of Goji Leaves

In order to investigate the potential use of Goji leaves generally considered waste products, a preliminary study of the Goji leaves extracts was carried out. Up to now, the identification of Goji leaves metabolites has been mainly focused on the targeted chromatographic analysis of phenolic compounds [14,20]. In this work, the untargeted metabolomic analysis of Goji leaves was performed to identify as many compound classes as possible. In particular, Bligh-Dyer hydroalcoholic and organic extracts of a leaves pool collected from the Big Lifeberry cultivar in August were investigated by NMR and ESI(+) FT-ICR MS methodologies.

The same NMR experiments (^{1}H, ^{1}H-^{1}H TOCSY, ^{1}H-^{13}C HSQC, and ^{1}H-^{13}C HMBC) carried out for the analysis of Goji berries were used for Goji leaves metabolite identification. The ^{1}H NMR analysis of leaves extracts allowed us to identify and quantify (see Tables 5 and 6) the same metabolites present in Goji berries, except for proline, tryptophan, and carotenoids, absent in the leaves. Since the extraction and the NMR experiments were carried out at the same experimental conditions used for berries, the same NMR chemical shifts of Tables 1 and 2 were identified for metabolites in leaves. In the hydroalcoholic extract, significant quantitative differences were observed comparing leaves and berries, see Table 5: the content of alanine, asparagine, and citric acid was very low in leaves with respect to berries, as well the glucose and fructose levels were at least 10 times lower in leaves than in berries. On the contrary, the sucrose content was measured in high amounts,

over 50 times, with respect to berries. Similarly, GABA and malic acid were present in leaves in a higher amount with respect to berries. Betaine was present in a significant amount also in the Goji leaves. Among the other metabolites, comparative values were measured in both the leaves and berries. Regarding the organic extract, TUFAs represented the main class of unsaturated fatty acids in leaves, whereas in berries, they were present in very low concentrations. On the contrary, in leaves, DUFAs were present in very low concentrations and MUFAs were not measured since the error associated with Equation (4) (Section 3.4 of Materials and Methods) turned out to be higher than the MUFA value [18]. Since the quantification of organic extract metabolites is expressed relative to the sum of total metabolite intensities, a comparison between berries and leaves organic metabolites values can not be performed due to the absence of carotenoids in leaves.

Table 5. Compounds identified and quantified in the ^{1}H NMR spectrum of the Bligh-Dyer hydroalcoholic extracts of BL1 Goji leaves. In brackets, the value obtained in the correspondent berries sample for each metabolite was also reported for comparison. Results were expressed as mg/100 g of fresh sample ± SD.

Metabolite	mg/100 g	Metabolite	mg/100 g	Metabolite	mg/100 g
Valine	3.98 ± 0.40 (4.5)	Citric acid	52.67 ± 4.82 (139.9)	Glucose	356.66 ± 4.20 (4829.9)
Isoleucine	2.57 ± 0.31 (4.5)	Aspartate	27.38 ± 1.84 (39.4)	Sucrose	430.13 ± 4.32 (7.3)
Leucine	6.33 ± 0.56 (6.8)	Asparagine	5.57 ± 0.36 (103.9)	Tyrosine	4.49 ± 0.54 (9.0)
Threonine	5.30 ± 0.47 (9.8)	Choline	10.44 ± 1.40 (11.4)	Phenylalanine	3.81 ± 0.57 (8.0)
Alanine	3.84 ± 0.43 (54.7)	Glycinbetaine	110.09 ± 8.23 (194)	Formic acid	1.57 ± 0.09 (0.7)
Quinic acid	82.32 ± 2.31 (60.4)	Fructose	67.42 ± 5.42 (1025.5)	Trigonelline	7.60 ± 0.82 (1.8)
GABA	24.87 ± 3.78 (5.0)	Malic acid	306.02 ± 25.48 (161.7)		

Table 6. Quantitative NMR results for some metabolites present in the Bligh-Dyer organic extracts of BL1 Goji leaves. Results were expressed as molar % ± SD.

Metabolite	Molar %
TOT SFA	39.57 ± 3.21
TOT UFA	57.67 ± 4.83
TUFA	48.60 ± 4.65
DUFA	9.07 ± 1.03
MUFA	/
DGDG	17.70 ± 1.70
PC	5.02 ± 0.65
β-Sitosterol	6.80 ± 0.70

The same experimental conditions used for the ESI FT-ICR MS analysis of Goji berries were applied for leaves characterization. Surprisingly, the ESI FT-ICR MS analysis of Goji leaves extracts allowed to identify in both hydroalcoholic and organic extracts, a higher number of molecular formulas with respect to the corresponding BL1 sample. In particular, the analysis of the hydroalcoholic extract allowed the identification of 286 (vs. 96 in berries) and 100 (vs. 114 in berries) molecular formulas in positive and negative mode, respectively. For the organic extract, 202 (vs. 55 in berries) and 84 (vs. 65 in berries) molecular formulas were identified in positive and negative mode, respectively. The list of assigned elemental formulas together with the experimental and theoretical *m/z* ratios, the mass deviation, and the putative compound annotations are available in either ionization mode for Goji leaves in Tables S5 and S6 (hydroalcoholic extracts), and S7 and S8 (organic extracts). Interestingly,

the BL1 leaves presented a rich variety of phytochemicals, laying the basis for the helpful exploitation of such waste material.

As an example, the ESI(+) FT-ICR mass spectrum of BL1 leaves hydroalcoholic extract is reported in Figure S10.

In this study, almost 600 different molecular formulas/putative compounds were identified, distributed between hydroalcoholic (364) and organic (244) leaf extracts. More entries were collected for both portions in positive ionization mode. Similar to berries, Goji leaves' extracts cover several molecular classes in van Krevelen diagrams (Figure 4A), with a higher density of entries in the lipids, polyketides, amino acids, and polyphenols areas, and less represented carbohydrates, tannins, and nucleic acids. Accordingly, the relative frequency distribution donut chart of the elemental formulas shown in Figure 4B revealed CHO features (terpenoids, polyphenols, fatty acids, and carbohydrates) as the most populated class, similar to what was observed in the corresponding berries sample, followed by CHNO (amino acids and alkaloids) compounds. Interestingly, a high number of phosphorus-containing metabolites were found as CHOP (59 hits) and CHNOP (34 hits) components, measured in a relatively lower amount in berries. In these classes, phosphorylated-sugars, -amino acids, and -lipids were detected as key intermediates in the primary metabolic processes of the plant. Similar to what was observed above for goji berries, the homology series emerge (Figure S4) along trend A-lines, including entries for oleic ($C_{18}H_{34}O_2$)/linoleic ($C_{18}H_{32}O_2$)/linolenic ($C_{18}H_{30}O_2$) acids; B-lines, with hits for palmitic ($C_{16}H_{32}O_2$)/hydroxyhexadecanoic ($C_{16}H_{32}O_3$)/dihydroxyhexadecanoic ($C_{16}H_{32}O_4$) acids, and succinic ($C_4H_6O_4$)/malic ($C_4H_6O_5$)/tartaric ($C_4H_6O_6$) acids; D-lines, with items for asparagine ($C_4H_8N_2O_3$)/glutamine ($C_5H_{10}N_2O_3$), and lauric ($C_{12}H_{24}O_2$)/myristic ($C_{14}H_{28}O_2$)/palmitic ($C_{16}H_{32}O_2$)/stearic ($C_{18}H_{36}O_2$)/arachidic ($C_{20}H_{40}O_2$) acids.

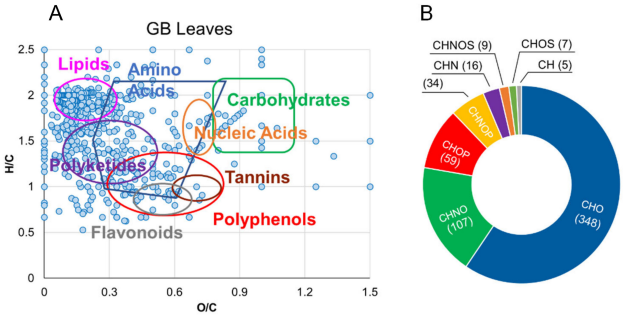


Figure 4. Van Krevelen diagram obtained from the molecular formulas determined by ESI FT-ICR analyses of hydroalcoholic and organic Big Lifeberry leaves extracts (panel **A**); donut chart describing the elemental composition concerning the same extracts (panel **B**).

As shown in Figure 4A, the lipids region comprised saturated (primarily 16:0), monounsaturated (mainly 18:1), ω-3 including hexadecatetraenoic, stearidonic and linolenic, and ω-6 like linoleic, arachidonic, and eicosadienoic acids identified as free fatty acids.

In the polyphenol region, the annotated metabolites could be grouped into two main subsets of tannins, with gallic acid and flavonoids, with anthocyanin, apigenin, myricetin-(galloylrhamnoside), naringenin-(*p*-coumaroylglucoside), isoquercetin, and rutin, already identified as a dominant component in Goji leaves [20]. According to previous evidence, flavonoids glycosidessuch as isoquercetin (quercetin-3-*O*-glucoside) were also found [14]. All these metabolites, mainly present in the hydroalcoholic extract, play significant health-promoting and anticancer activities. The organic fraction from Goji leaves exhibited peaks assigned to protonated and sodiated forms of pheophytin a and chlorophylls (Figure S10),

whose potential applications in the food industry and pharmacology have been amply described [38].

Other bioactive compounds responsible for radical scavenging, UV protective and anti-inflammatory effects, like carnosic acid, resveratrol [39], hydroxycinnamic (caffeic, ferulic, chlorogenic) acids [20,40] were also unveiled, concurring to describe the chemical space/metabolic profile of Goji leaves as a valuable source of bioactive/beneficial compounds.

3. Materials and Methods

3.1. Chemicals

Methanol (HPLC-grade), chloroform (HPLC-grade), and acetonitrile (HPLC-grade) were obtained from Carlo Erba Reagenti (Milan, Italy). Double-distilled water was obtained using a Millipore Milli-Q Plus water treatment system (Millipore Bedford Corp., Bedford, MA, USA). Deuterated water (D_2O) 99.97 atom% of deuterium, methanol-D4 99.80 atom% of deuterium, and chloroform-D 99.80 atom% of deuterium + 0.03% tetramethylsilane (TMS) was purchased from Euriso-Top (Saclay, France). 3-(trimethylsilyl)-propionic-2,2,3,3-d_4 acid sodium salt (TSP) was purchased from Merck (Milan, Italy).

3.2. Plant Material

Goji berries of two cultivars, namely Big Lifeberry and Sweet Lifeberry, of *Lycium barbarum* L. were grown in the South Lazio area of Subiaco (41°55′34.28″ N 13°05′20.62″ E). Fruits were collected in August (period 1, BL1, SL1) and October (period 2, BL2, SL 2), corresponding at the beginning and the end of the maturation period [2,26]. The berries of both cultivars were manually collected from the whole plant, they were homogenized and frozen using liquid nitrogen and, finally, they were stored at −80 °C until analysis.

3.3. Extraction Procedure

The Bligh-Dyer extraction protocol [41] was applied for both NMR and ESI FT-ICR analyses, in order to extract both hydrophilic and hydrophobic metabolites. In particular, 1.0 g of homogenized sample was added sequentially with 3 mL methanol/chloroform (2:1 *v*/*v*) mixture, 1 mL of chloroform, and 1.2 mL of bidistilled water, shaking the sample after each addition. The obtained emulsion was maintained at 4 °C for 40 min and then centrifuged at 4200× *g* for 15 min at 4 °C. Both phases, hydroalcoholic and organic, were carefully separated. The pellets were re-extracted using half of the solvent volumes in the same conditions described above. Finally, hydroalcoholic and organic fractions were dried using an N_2 flow at room temperature and the dried phases were stored at −20 °C until further analyses.

3.4. NMR Analysis

Dried Bligh-Dyer hydroalcoholic extracts were solubilized in 750 µL 400 mM phosphate buffer/D_2O, containing TSP 1 mM as internal standard, whereas dried Bligh-Dyer organic extracts were solubilized in 700 µL of a $CDCl_3/CD_3OD$ mixture (2:1 *v*/*v*). NMR analyses were carried out by using a Bruker AVANCE 600 spectrometer (Bruker, Milan, Italy) operating at the frequency ^1H frequency of 600.13 MHz and equipped with a multinuclear z-gradient 5 mm probe head (Bruker, Milan, Italy). Mono-dimensional (^1H) and two-dimensional (^1H-^1H TOCSY, ^1H-^{13}C HSQC, and ^1H-^{13}C HMBC) experiments were carried out using the same acquisition and processing parameters previously reported [21]. Two-dimensional experiments allowed us to identify long-range ^1H-^1H, and long- and short-range ^1H-^{13}C correlations within each considered molecule. This information, combined with data obtained from mono-dimensional spectra (chemical shift, multiplicity, coupling *J* constants), allowed us to define the chemical structure of the starting unknown compound and define its identity, also by comparing the obtained data with the literature data.

The complete procedures from the extraction to NMR measurement were repeated three times in order to evaluate the repeatability of the protocol. The integrals of 23 signals

in hydroalcoholic extracts ^{1}H spectra were selected, Table 1, and used for metabolite quantification, as mg/100 g fresh weight sample ± standard deviation (SD), referring to the internal standard TSP. The integrals of 8 signals in organic extracts ^{1}H spectra, referred to the area of total fatty acids signal set to 100, were selected, Table 2, and used for metabolite quantification as molar % ± SD by applying the following equations:

$$\%\beta\text{-SIT} = 100(0.66I_{\beta\text{-SIT}}/I_{tot}) \quad (1)$$

$$\%\text{TUFA} = 100(0.5I_{TUFA}/I_{tot}) \quad (2)$$

$$\%\text{DUFA} = 100(I_{DUFA}/I_{tot}) \quad (3)$$

$$\%\text{MUFA} = 100(I_{TOT\ UFA} - 2I_{DUFA} - 1.5I_{TUFA})/I_{tot} \quad (4)$$

$$\%\text{TOT FA} = 100(I_{TOT\ FA}/I_{tot}) \quad (5)$$

$$\%\text{TOT UFA} = \%\text{MUFA} + \%\text{DUFA} + \%\text{TUFA} \quad (6)$$

$$\%\text{TOT SFA} = \%\text{TOT FA} - \%\text{TOT UFA} \quad (7)$$

$$\%\text{PC} = 100(4I_{PC}/9I_{tot}) \quad (8)$$

$$\%\text{DGDG} = 100(4I_{DGDG}/I_{tot}) \quad (9)$$

$$\%\text{CAR} = 100(I_{CAR}/I_{tot}) \quad (10)$$

where %β-SIT, %TUFA, %DUFA, %MUFA, %TOT FA, %TOT UFA, %TOT SFA, %PC, %DGDG, and %CAR are molar % of β-sitosterol, tri-unsaturated fatty acids, di-unsaturated fatty acids, mono-unsaturated fatty acids, total fatty acids, total unsaturated fatty acids, total saturated fatty acids, phosphatidylcholine, digalactosyldiacylglycerol, and carotenoids respectively. $I_{\beta\text{-SIT}}$, I_{TUFA}, I_{DUFA}, $I_{TOT\ UFA}$, $I_{TOT\ FA}$, I_{PC}, I_{DGDG}, and I_{CAR} are integrals, whereas I_{tot} is calculated according to the following equation:

$$I_{tot} = I_{TOT\ FA} + 0.66I_{\beta\text{-SIT}} + I_{CAR} \quad (11)$$

One-way analysis of variance (ANOVA) was realized by Statistica software (Version 14.0.0.15) in order to determine significant differences ($p < 0.05$) among the quantified metabolites at different harvesting stages for each goji berry cultivar.

3.5. Mass-Spectrometry-Based Metabolomics

Stock solutions (1 mg/mL) of Bligh-Dyer hydroalcoholic and organic extracts of BL and SR fruits and BL leaves were filtered through a 0.45 µm hydrophobic polypropylene Acrodisc (VWR, Milan, Italy) to eliminate debris, and diluted in methanol and methanol/acetonitrile (50:50 *v/v*), respectively, to a final concentration of 0.2–0.5 mg L^{-1}. No ionization dopants were added. In order to avoid degradation, the stock solutions were kept at −20 °C and analyzed within 24 h after final dilution. Each diluted solution was directly infused with a flow rate of 120 µL/h in the electrospray ionization source of the mass spectrometer for untargeted analysis. All the analyses and Collision Induced Dissociation (CID) experiments were conducted on mass-selected ions with He gas using either a Paul ion trap (Esquire 6000, Bruker Daltonics, Bremen, Germany) or an LTQ XL (Thermo Scientific) in both positive (ESI(+)) and negative (ESI(−)) polarity modes. ESI settings were set as follows: solution flow rate of 120 µL/h, capillary spray voltage at –4.2 kV (in positive mode) or +3.8 kV (in negative mode), nebulizer pressure at 11 psi, drying gas flow at 6 L/min, and drying gas temperature at 300 °C. To gather proof of peak assignments, CID on mass-selected ions obtained from commercially available standards were carried out and further tested by reference spectra obtained from the literature or online libraries, like METLIN [42]. High-resolution mass analysis was carried out using a Fourier Transform-Ion Cyclotron Resonance (FT-ICR) mass spectrometer (Bruker Daltonics GmbH, Bremen, Germany) equipped with an Apollo I ESI source, a 4.7 T superconducting magnet, and an infinity cell (FT-ICR lab, Sapienza University of Rome, Rome, Italy) [43]. A

methanolic 10 µM solution of leucine enkephalin (YGGFL, $C_{28}H_{37}N_5O_7$, molecular weight: 556.26930) was added as an internal standard for precision and mass accuracy assessment. Additional internal frequency-to-*m/z* calibration was attained by relating to ubiquitous metabolites of known elemental composition, like arginine, monosaccharides, and organic acids. FT-ICR mass spectra were typically acquired in the *m/z* 90–1000 range (resolution of 70,000 at *m/z* 500) in at least three replicates. For each sample, the time domain signal was collected by co-adding 200 scans with an acquisition size of 1M.

3.6. Metabolomics Visualization Tools

The list of *m/z* values was subjected to preliminary filtering by retaining only peaks with a cut-off signal-to-noise ratio (S/N) of 3 and then submitted to the free tool MassTRIX [44] for metabolite assignment, by considering protonated, sodiated, and potassiated (ESI(+)), and deprotonated and chlorinated (ESI(−)) ions. The components of the extracts were assigned by comparing the high-resolution *m/z* values with the theoretical exact mass. All metabolite annotations were based on the "monoisotopic" ion. A qualitative description of the phytochemical composition of the samples has been gained by visualization tools, including van Krevelen diagrams (vKds) and relative elemental composition frequency histograms [17].

3.7. Spectrophotometric Pigments Analysis

Total carotenoids and chlorophylls were analyzed in the peel and pulp of the Goji berry varieties by using a previously described protocol [45]. In particular, the peel was cut from the surface of the fruits and carefully freed from the pulp. Samples were homogenized with mortar and pestle in 6 mL of chloroform/methanol mixture (2:1, *v/v*) and 30 mg of MgO to prevent chlorophyll pheophytinization. The obtained homogenate was filtered on a paper filter and then a volume of distilled water equal to 20% of the extract volume was added. Finally, the obtained biphasic system was centrifuged for 20 min at 2469× *g* at 10 °C to complete the separation of chloroform fraction from hydroalcoholic one. Absorption spectra of the chloroform phase were acquired with Beckman Coulter DU 800 instruments, in the range of 350–800 nm with a spectral resolution of 0.5 nm at 20 °C. The concentrations of chlorophyll a and b, as well as total carotenoids, were expressed as mg/g ± SD of fresh material were determined according to Wellburn equations [46].

3.8. Biological Assays

MG-63 osteosarcoma cell line, obtained from the American Type Culture Collection (ATCC, Rockville, MD, USA) was used as an osteoblast model. The cells were grown in Dulbecco's modified eagle medium Glutamax (Sigma, St. Louis, MI, USA), supplemented with 10% fetal bovine serum (GIBCO, Amarillo, TX, USA) with penicillin (100 µg/mL), streptomycin (100 U/mL), and 1% sodium pyruvate, at 37 °C with 5% CO_2, for 24 h, reaching a confluence of around 80%.

3.8.1. Cell Viability

To assess a potential cytotoxic effect of hydroalcoholic and organic extracts of BL1 on MG63 cells at different concentrations and time points, an MTS (3-[4,5-dimethylthiazol-2-yl]-5-[3-carboxymethoxyphenyl]-2-[4-sulfophenyl]-2*H*-tetrazolium)-based colorimetric assay was performed (Promega Corporation, Madison, WI, USA). Briefly, 5×10^3 cells per well were seeded in a 96-well plate. The day after seeding, cells were either left untreated (CTL) or treated with different concentrations of hydroalcoholic and organic extract of BL1 for 24, 48, and 72 h. After each time point, 100 µL MTS solution was added to the wells. Spectrophotometric absorbance was directly measured at 492 nm after 3 h incubation. MG63 cells were left untreated (CTL) or treated with 50 or 12.5 µg/mL of hydro-alcoholic and organic extract of *Lycium barbarum* and stimulated with TNFα (PeproTech House, London, UK) 10 ng/mL for the required time. Experiments were independently repeated at least three times.

3.8.2. Quantitative Real-Time PCR

Total RNA was extracted with a Total RNA extraction mini kit (Fisher Molecular Biology, Trevose, PA, USA), and reverse transcribed by Improm II enzyme, (Promega Corporation, Madison, WI, USA), according to the manufacturers' instructions. Quantitative real-time PCR analysis was performed using an ABI Prism 7300 (Applied Biosystems, Thermo Fisher Scientific, Waltham, MA, USA, accessed on 30 October 2019. Amplification was carried out using the SensimixPlus SYBR master mix (Bioline, London, UK). Primers were designed using Primer Express software (Applied Biosystems, accessed on 30 October 2019) and were synthesized by Biofab Research (Rome, Italy).

Data were analyzed by the $2^{-\Delta\Delta Ct}$ method, which determines the transcript abundance relative to the 18S housekeeping gene.

3.8.3. ELISA Assay

The amount of Interleukin -6(IL-6) and Interleukin-8 (IL-8) in the supernatant of cell cultures was determined using Enzyme-Linked Immunoadsorbent assay kits (Fine Test ELISA, Fine Biotech Co., Ltd., Wuhan, China) according to the manufacturer's instructions. Optical Density (O.D.) absorbance was measured at 450 nm by a microplate reader (Appliskan, Thermo Fisher, Waltham, MA, USA). The samples were analyzed after 5 h culture.

3.8.4. Immunofluorescence Measures

Cox-2 was visualized by immunofluorescence. Cells were fixed with 100% ethanol for 10 min at RT. After washing with PBS, cells were incubated with anti-Cox-2 mouse monoclonal antibody (Abcam) 1:250 for 1 h at RT. After washing with PBS, cells were incubated for 1 h at room temperature with Alexa Fluor 568 donkey anti-mouse antibody 1:400 (Invitrogen, Thermo Fisher Scientific), to stain Cox-2 in red. Cells were washed, incubated with DAPI (Invitrogen, Thermo Fisher Scientific) to visualize the nuclei, mounted, and analyzed with Leica DM microscope (Leica Microsystems, Milan, Italy).

4. Conclusions

In this work, for the first time, to our knowledge, the metabolite profile of Goji berries obtained using high-resolution NMR and ESI FT-ICR MS untargeted methodologies was reported. This approach contributed to enrich the knowledge of the chemical composition of this fruit by confirming the presence of carotenoids, polyphenols, fatty acids, and sugars; and by identifying other metabolite groups such as amino acids, terpenes, alkaloids, and chlorophylls. The rich phytochemical profile in both SL and BL cultivars confirmed Goji berries as a "superfruit" with remarkable potential bioactivity since the identified molecules are well known for their antioxidant, antimicrobial activities, together with a modulation activity of several metabolic biochemical processes of the organism. Moreover, the information obtained by the analysis of the considered Goji cultivars grown in Italy and harvested at two different ripening periods can be useful to produce Goji fruits with a peculiar chemical profile, since significative compositional differences were observed.

The preliminary biological studies represent a starting point to further characterize the biological effects of Goji berries, whose potential activities represent an important field of research for several applications of pharmaceutical/nutraceutical interest. Finally, the metabolite characterization of Goji leaves showed how this matrix, generally considered as a waste product, can be valorized as a raw material for several applications in the biological and food fields. Of course, further characterization of this matrix is still needed.

Supplementary Materials: The following are available online, Figure S1. Enlargement of ESI(+) FT-ICR MS Goji berries samples: BL1 (red profile), and BL2 (purple profile). Figure S2. Enlargement of ESI(+) FT-ICR MS Goji berries samples: SL1 (red profile), and SL2 (purple profile). Figure S3. Comparison between experimental ESI(–) CID assay performed by using LTQ XL ion trap and reference data obtained from Metlin database has allowed us to confirm the assignments of the following peaks at A) *m/z* 283 (stearic acid; B) *m/z* 309 (eicosenoic acid); C) *m/z* 311 (eicosanoic acid);

D) *m/z* 325 (eicosanoic acid, methyl ester); E) *m/z* 337 (docosenoic acid); F) *m/z* 339 (docosanoic acid). Figure S4. Van Krevelen diagram obtained by ESI MS analysis of hydroalcoholic and organic extracts from BL and SL fruits and BL leaves. The diagrams display broken lines with the following meaning: (A) lines related to (de)hydrogenation paths; (B) lines associated with oxidation or reduction reactions; (C) lines that describe hydration and condensation processes; (D) lines that correspond to (de)methylation paths. Figure S5. Differentiation between isobaric species by ESI FT-ICR MS: histidine (*m/z* 156.07654) and valine (*m/z* 156.04220) are discriminated in BL1 (purple profile). Otherwise, histidine appears lacking in SL2 (red profile). Figure S6. Cell viability was assessed by the MTS colorimetric method. MG63 cells were treated with different concentrations, 100 μg/mL, 50 μg/mL, 25 μg/mL, 12.5 μg/mL, and 6.5 μg/mL, of Lycium barbarum Hydro-alcoholic extract (LBEHY) dissolved in deionized water and Lycium barbarum organic extract (LBEORG) dissolved in DMSO, for 24, 48, and 72 h. Cell viability of treated samples was normalized to the untreated cells, which is reported as 100% and represented by a horizontal line. Figure S7. Effects of LBEHY and LBEORG extracts on IL-6, IL-8, IL-1β, iNOS, and COX-2 mRNA expression level in MG63 cells. After 2 h-treatment with 0.1 mg/mL of 50 and 12.5 μg/mL Lycium barbarum Hydro-alcoholic extract (LBEHY) dissolved in deionized water and Lycium barbarum organic extract (LBEORG) dissolved in DMSO, cells were stimulated for 30 min with 10 ng/mL of TNFα. Cells were harvested and mRNA was extracted and analyzed by RT-PCR. IL-6, IL-8, IL-1β, iNOS, and COX-2 mRNA levels were reported as relative mRNA expression levels with respect to 18S mRNA (2-ΔΔCt method). Results are expressed as mean ± S.E.M. of data obtained by three different experiments. * $p < 0.05$; # $p < 0.05$; * represents the comparison between TNFα and LBE-treated samples; # represents the comparison between untreated (CTL) and TNFα-stimulated samples. Figure S8. A measure of IL-6 and IL-8 secretion in cell culture medium. Cells were left untreated or treated with 10 ng/mL of TNFα in the absence or in presence of 50 and 12.5 μg/mL Lycium barbarum Hydro-alcoholic extract (LBEHY) dissolved in deionized water and Lycium barbarum organic extract (LBEORG) dissolved in DMSO, for 5 h and then analyzed for IL-6 and IL-8 by ELISA method. Results (in pg/mL) are expressed as mean ± standard error, obtained in three different experiments. * $p < 0.05$; *** $p < 0.005$; ## $p < 0.01$; ### $p < 0.005$. * represents the comparison between TNFα and LBE-treated samples; # represents the comparison between untreated (CTL) and TNFα-stimulated samples. Figure S9. Effects of LBEHY and LBEORG extracts on COX-2 protein production. Upper panel: Cells were left untreated or treated with 10 ng/mL of TNFα in the absence or in presence of 50 and 12.5 μg/mL Lycium barbarum Hydro-alcoholic extract (LBEHY) dissolved in deionized water and Lycium barbarum organic extract (LBEORG) dissolved in DMSO, for 5 h and then analyzed by immunofluorescence using anti-COX-2 primary antibody and Alexa Fluor 568 (red) secondary antibody. Nuclei were stained with DAPI (original magnification 40×), images are representative of two different experiments. Lower panel: The pixel intensities, in the region of interest, were obtained by ImageJ. * $p < 0.05$; # $p < 0.05$; * represents the comparison between TNFα and LBE-treated samples; # represents the comparison between untreated (CTL) and TNFα-stimulated samples. Figure S10. Enlargement of ESI(+) FT-ICR mass spectrum of hydroalcoholic extract of Big Lifeberry leaves. Figure S8. Enlargement of ESI(+) Esquire 6000 mass spectrum of organic extract of Big Life-berry Goji leaves showing protonated pheophytin, ([C55H74N4O5 + H]+, monoisotopic peak at *m/z* 871.4). The theoretical isotopic pattern is shown in the excerpt. Table S1: Untargeted metabolic profiling of Goji Berries hydroalcoholic extracts by ESI(+) FT-ICR MS. Table S2: Untargeted metabolic profiling of Goji Berries hydroalcoholic extracts by ESI(–) FT-ICR MS. Table S3: Untargeted metabolic profiling of Goji Berries organic extracts by ESI(+) Ion Trap MS. Table S4: Untargeted metabolic profiling of Goji Berries organic extracts by ESI(–) Ion Trap MS. Table S5: Untargeted metabolic profiling of Goji Berries leaves hydroalcoholic extracts by ESI(+) FT-ICR MS. Table S6: Untargeted metabolic profiling of Goji Berries leaves hydroalcoholic extracts by ESI(-) FT-ICR MS. Table S7: Untargeted metabolic profiling of Goji Berries leaves organic extracts by ESI(+) Ion Trap MS. Table S8: Untargeted metabolic profiling of Goji Berries leaves organic extracts by ESI(–) Ion Trap MS.

Author Contributions: Conceptualization, M.S., A.M. (Alessandro Maccelli), and G.D.M.; methodology, A.P.S., M.E.C. and A.M.G.; validation, A.P.S., M.E.C., A.M.G, and A.S.D.; formal analysis, M.S., A.M. (Alessandro Maccelli), G.D.M., J.-X.B., A.M.G., A.M. (Alessia Mariano), A.S.D. and A.L.; investigation, M.S., A.M. (Alessandro Maccelli), M.E.C. and A.P.S.; data curation, M.S., A.M. (Alessandro Maccelli), M.B., M.E.C. and C.I.; writing—original draft preparation, M.S., A.M.

(Alessandro Maccelli), and M.E.C.; writing—review and editing, L.M. and S.F.; visualization, A.P.S., C.I., M.B., L.M. and S.F. All authors have read and agreed to the published version of the manuscript.

Funding: This research was funded by Italian Ministry of Education, Universities and Research-Dipartimenti di Eccellenza-L. 232/2016.

Institutional Review Board Statement: Not applicable.

Informed Consent Statement: Not applicable.

Data Availability Statement: Not applicable.

Conflicts of Interest: The authors declare no conflict of interest.

Sample Availability: Samples of the compounds are available from the authors.

References

1. Yao, R.; Heinrich, M.; Weckerle, C.S. The genus Lycium as food and medicine: A botanical, ethnobotanical and historical review. *J. Ethnopharmacol.* **2018**, *212*, 50–66. [CrossRef] [PubMed]
2. Ma, Z.F.; Zhang, H.; Teh, S.S.; Wang, C.W.; Zhang, Y.; Hayford, F.; Wang, L.; Ma, T.; Dong, Z.; Zhang, Y.; et al. Goji berries as a potential natural antioxidant medicine: An insight into their molecular mechanisms of action. *Oxid. Med. Cell. Longev.* **2019**, *2019*, 1–9. [CrossRef] [PubMed]
3. Qian, D.; Zhao, Y.; Yang, G.; Huang, L. Systematic review of chemical constituents in the genus lycium (solanaceae). *Molecules* **2017**, *22*, 911. [CrossRef]
4. Kulczyński, B.; Gramza-Michałowska, A. Goji Berry (Lycium barbarum): Composition and Health Effects—A Review. *Polish J. Food Nutr. Sci.* **2016**, *66*, 67–75. [CrossRef]
5. Wang, C.C.; Chang, S.C.; Inbaraj, B.S.; Chen, B.H. Isolation of carotenoids, flavonoids and polysaccharides from Lycium barbarum L. and evaluation of antioxidant activity. *Food Chem.* **2010**, *120*, 184–192. [CrossRef]
6. Inbaraj, B.S.; Lu, H.; Kao, T.H.; Chen, B.H. Simultaneous determination of phenolic acids and flavonoids in Lycium barbarum Linnaeus by HPLC-DAD-ESI-MS. *J. Pharm. Biomed. Anal.* **2010**, *51*, 549–556. [CrossRef]
7. Masci, A.; Carradori, S.; Casadei, M.A.; Paolicelli, P.; Petralito, S.; Ragno, R.; Cesa, S. Lycium barbarum polysaccharides: Extraction, purification, structural characterisation and evidence about hypoglycaemic and hypolipidaemic effects. A review. *Food Chem.* **2018**, *254*, 377–389. [CrossRef]
8. Zou, S.; Zhang, X.; Yao, W.; Niu, Y.; Gao, X. Structure characterization and hypoglycemic activity of a polysaccharide isolated from the fruit of Lycium barbarum L. *Carbohydr. Polym.* **2010**, *80*, 1161–1167. [CrossRef]
9. Skenderidis, P.; Lampakis, D.; Giavasis, I.; Leontopoulos, S.; Petrotos, K.; Hadjichristodoulou, C.; Tsakalof, A. Chemical properties, fatty-acid composition, and antioxidant activity of Goji berry (Lycium barbarum l. and Lycium Chinense mill.) fruits. *Antioxidants* **2019**, *8*, 60. [CrossRef] [PubMed]
10. Mocan, A.; Cairone, F.; Locatelli, M.; Cacciagrano, F.; Carradori, S.; Vodnar, D.C.; Crișan, G.; Simonetti, G.; Cesa, S. Polyphenols from lycium barbarum (Goji) fruit european cultivars at different maturation steps: Extraction, hplc-dad analyses, and biological evaluation. *Antioxidants* **2019**, *8*, 562. [CrossRef] [PubMed]
11. Bertoldi, D.; Cossignani, L.; Blasi, F.; Perini, M.; Barbero, A.; Pianezze, S.; Montesano, D. Characterisation and geographical traceability of Italian goji berries. *Food Chem.* **2019**, *275*, 585–593. [CrossRef]
12. Dhekney, S.A.; Baldwin, M.R. Prospects for goji berry (*Lycium barbarum* L.) production in North America. In *Medicinal Plants: From Farm to Pharmacy*; SpringerLink: Berlin, Germany, 2019; pp. 129–140. ISBN 9783030312695.
13. Bondia-Pons, I.; Savolainen, O.; Törrönen, R.; Martinez, J.A.; Poutanen, K.; Hanhineva, K. Metabolic profiling of Goji berry extracts for discrimination of geographical origin by non-targeted liquid chromatography coupled to quadrupole time-of-flight mass spectrometry. *Food Res. Int.* **2014**, *63*, 132–138. [CrossRef]
14. Mocan, A.; Vlase, L.; Vodnar, D.C.; Bischin, C.; Hanganu, D.; Gheldiu, A.M.; Oprean, R.; Silaghi-Dumitrescu, R.; Crișan, G. Polyphenolic content, antioxidant and antimicrobial activities of Lycium barbarum L. And Lycium chinense Mill. Leaves. *Molecules* **2014**, *19*, 10056–10073. [CrossRef]
15. Vitanza, L.; Maccelli, A.; Marazzato, M.; Scazzocchio, F.; Comanducci, A.; Fornarini, S.; Crestoni, M.E.; Filippi, A.; Fraschetti, C.; Rinaldi, F.; et al. Satureja montana L. essential oil and its antimicrobial activity alone or in combination with gentamicin. *Microb. Pathog.* **2019**, *126*, 323–331. [CrossRef] [PubMed]
16. Sobolev, A.P.; Mannina, L.; Capitani, D.; Sanzò, G.; Ingallina, C.; Botta, B.; Fornarini, S.; Crestoni, M.E.; Chiavarino, B.; Carradori, S.; et al. A multi-methodological approach in the study of Italian PDO "Cornetto di Pontecorvo" red sweet pepper. *Food Chem.* **2018**, *255*, 120–131. [CrossRef]
17. Ingallina, C.; Maccelli, A.; Spano, M.; Matteo, G.D.; Sotto, A.D.; Giusti, A.M.; Vinci, G.; Giacomo, S.D.; Rapa, M.; Ciano, S.; et al. Chemico-biological characterization of torpedino di fondi® tomato fruits: A comparison with san marzano cultivar at two ripeness stages. *Antioxidants* **2020**, *9*, 1027. [CrossRef] [PubMed]

18. Ingallina, C.; Spano, M.; Sobolev, A.P.; Esposito, C.; Santarcangelo, C.; Baldi, A.; Daglia, M.; Mannina, L. Characterization of Local Products for Their Industrial Use: The Case of Italian Potato Cultivars Analyzed by Untargeted and Targeted Methodologies. *Foods* **2020**, *9*, 1216. [CrossRef]
19. Liu, H.; Fan, Y.; Wang, W.; Liu, N.; Zhang, H.; Zhu, Z.; Liu, A. Polysaccharides from Lycium barbarum leaves: Isolation, characterization and splenocyte proliferation activity. *Int. J. Biol. Macromol.* **2012**, *51*, 417–422. [CrossRef]
20. Mocan, A.; Zengin, G.; Simirgiotis, M.; Schafberg, M.; Mollica, A.; Vodnar, D.C.; Crişan, G.; Rohn, S. Functional constituents of wild and cultivated Goji (*L. barbarum* L.) leaves: Phytochemical characterization, biological profile, and computational studies. *J. Enzyme Inhib. Med. Chem.* **2017**, *32*, 153–168. [CrossRef] [PubMed]
21. Ingallina, C.; Sobolev, A.P.; Circi, S.; Spano, M.; Fraschetti, C.; Filippi, A.; Di Sotto, A.; Di Giacomo, S.; Mazzoccanti, G.; Gasparrini, F.; et al. Cannabis sativa L. inflorescences from monoecious cultivars grown in central Italy: An untargeted chemical characterization from early flowering to ripening. *Molecules* **2020**, *25*, 1908. [CrossRef] [PubMed]
22. Di Matteo, G.; Spano, M.; Esposito, C.; Santarcangelo, C.; Baldi, A.; Daglia, M.; Mannina, L.; Ingallina, C.; Sobolev, A.P. Nmr characterization of ten apple cultivars from the piedmont region. *Foods* **2021**, *10*, 289. [CrossRef] [PubMed]
23. Kim, S.; Kramer, R.W.; Hatcher, P.G. Graphical Method for Analysis of Ultrahigh-Resolution Broadband Mass Spectra of Natural Organic Matter, the Van Krevelen Diagram. *Anal. Chem.* **2003**, *75*, 5336–5344. [CrossRef]
24. Song, Y.; Xu, B. Diffusion profiles of health beneficial components from goji berry (Lyceum barbarum) marinated in alcohol and their antioxidant capacities as affected by alcohol concentration and steeping time. *Foods* **2013**, *2*, 32–42. [CrossRef] [PubMed]
25. Fan, T.W.M. Metabolite profiling by one- and two-dimensional NMR analysis of complex mixtures. *Prog. Nucl. Magn. Reson. Spectrosc.* **1996**, *28*, 161–219. [CrossRef]
26. Donno, D.; Beccaro, G.L.; Mellano, M.G.; Cerutti, A.K.; Bounous, G. Goji berry fruit (Lycium spp.): Antioxidant compound fingerprint and bioactivity evaluation. *J. Funct. Foods* **2015**, *18*, 1070–1085. [CrossRef]
27. Mikulic-Petkovsek, M.; Schmitzer, V.; Slatnar, A.; Stampar, F.; Veberic, R. Composition of Sugars, Organic Acids, and Total Phenolics in 25 Wild or Cultivated Berry Species. *J. Food Sci.* **2012**, *77*. [CrossRef] [PubMed]
28. Rekhter, D.; Lüdke, D.; Ding, Y.; Feussner, K.; Zienkiewicz, K.; Lipka, V.; Wiermer, M.; Zhang, Y.; Feussner, I. Isochorismate-derived biosynthesis of the plant stress hormone salicylic acid. *Science* **2019**, *365*, 498–502. [CrossRef]
29. Kosińska-Cagnazzo, A.; Weber, B.; Chablais, R.; Vouillamoz, J.F.; Molnár, B.; Crovadore, J.; Lefort, F.; Andlauer, W. Bioactive compound profile and antioxidant activity of fruits from six goji cultivars cultivated in Switzerland. *J. Berry Res.* **2017**, *7*, 43–59. [CrossRef]
30. Pedro, A.C.; Sánchez-Mata, M.C.; Pérez-Rodríguez, M.L.; Cámara, M.; López-Colón, J.L.; Bach, F.; Bellettini, M.; Haminiuk, C.W.I. Qualitative and nutritional comparison of goji berry fruits produced in organic and conventional systems. *Sci. Hortic.* **2019**, *257*. [CrossRef]
31. Ilić, T.; Dodevska, M.; Marčetić, M.; Božić, D.; Kodranov, I.; Vidović, B. Chemical Characterization, Antioxidant and Antimicrobial Properties of Goji Berries Cultivated in Serbia. *Foods* **2020**, *9*, 1614. [CrossRef] [PubMed]
32. Zheng, Y.Z.; Deng, G.; Liang, Q.; Chen, D.F.; Guo, R.; Lai, R.C. Antioxidant activity of quercetin and its glucosides from propolis: A theoretical study. *Sci. Rep.* **2017**, *7*. [CrossRef]
33. Maková, B.; Mik, V.; Lišková, B.; Gonzalez, G.; Vítek, D.; Medvedíková, M.; Monfort, B.; Ručilová, V.; Kadlecová, A.; Khirsariya, P.; et al. Cytoprotective activities of kinetin purine isosteres. *Bioorganic Med. Chem.* **2021**, *33*. [CrossRef] [PubMed]
34. Cao, D.; Pi, J.; Shan, Y.; Tang, Y.; Zhou, P. Anti-inflammatory effect of Resolvin D1 on LPS-treated MG-63 cells. *Exp. Ther. Med.* **2019**, *16*, 4283–4288. [CrossRef]
35. Leonidou, A.; Lepetsos, P.; Mintzas, M.; Kenanidis, E.; Macheras, G.; Tzetis, M.; Potoupnis, M.; Tsiridis, E. Inducible nitric oxide synthase as a target for osteoarthritis treatment. *Expert Opin. Ther. Targets* **2018**, *22*, 299–318. [CrossRef] [PubMed]
36. Tu, M.; Yang, M.; Yu, N.; Zhen, G.; Wan, M.; Liu, W.; Ji, B.; Ma, H.; Guo, Q.; Tong, P.; et al. Inhibition of cyclooxygenase-2 activity in subchondral bone modifies a subtype of osteoarthritis. *Bone Res.* **2019**, *7*. [CrossRef]
37. Salvemini, D.; Kim, S.F.; Mollace, V. Reciprocal regulation of the nitric oxide and cyclooxygenase pathway in pathophysiology: Relevance and clinical implications. *Am. J. Physiol. Regul. Integr. Comp. Physiol.* **2013**, *304*, 473–487. [CrossRef]
38. Solymosi, K.; Mysliwa-Kurdziel, B. Chlorophylls and their Derivatives Used in Food Industry and Medicine. *Mini-Rev. Med. Chem.* **2016**, *17*. [CrossRef]
39. Gülçin, I. Antioxidant properties of resveratrol: A structure-activity insight. *Innov. Food Sci. Emerg. Technol.* **2010**, *11*, 210–218. [CrossRef]
40. Taofiq, O.; González-Paramás, A.M.; Barreiro, M.F.; Ferreira, I.C.F.R.; McPhee, D.J. Hydroxycinnamic acids and their derivatives: Cosmeceutical significance, challenges and future perspectives, a review. *Molecules* **2017**, *22*, 281. [CrossRef] [PubMed]
41. BLIGH, E.G.; DYER, W.J. A rapid method of total lipid extraction and purification. *Can. J. Biochem. Physiol.* **1959**, *37*, 911–917. [CrossRef] [PubMed]
42. Guijas, C.; Montenegro-Burke, J.R.; Domingo-Almenara, X.; Palermo, A.; Warth, B.; Hermann, G.; Koellensperger, G.; Huan, T.; Uritboonthai, W.; Aisporna, A.E.; et al. METLIN: A Technology Platform for Identifying Knowns and Unknowns. *Anal. Chem.* **2018**, *90*, 3156–3164. [CrossRef]
43. Marshall, A.G.; Chen, T. 40 years of Fourier transform ion cyclotron resonance mass spectrometry. *Int. J. Mass Spectrom.* **2015**, *377*, 410–420. [CrossRef]

44. Wägele, B.; Witting, M.; Schmitt-Kopplin, P.; Suhre, K. Masstrix reloaded: Combined analysis and visualization of tran-scriptome and metabolome data. *PLoS ONE* **2012**, *7*. [CrossRef] [PubMed]
45. Spano, M.; Di Matteo, G.; Ingallina, C.; Botta, B.; Quaglio, D.; Ghirga, F.; Balducci, S.; Cammarone, S.; Campiglia, E.; Giusti, A.M.; et al. A multimethodological characterization of cannabis sativa l. Inflorescences from seven dioecious cultivars grown in Italy: The effect of different harvesting stages. *Molecules* **2021**, *26*, 2912. [CrossRef] [PubMed]
46. Wellburn, A.R. The Spectral Determination of Chlorophylls a and b, as well as Total Carotenoids, Using Various Solvents with Spectrophotometers of Different Resolution. *J. Plant. Physiol.* **1994**, *144*, 307–313. [CrossRef]

5.5. Case study 4: Metabolomic NMR profile of pumpkin packaged with commercial biofilms

Food packaging plays an essential role in preserving food throughout the distribution chain. To date the traditional polymeric materials from mineral oils are under prosecution due to the long degradation times responsible of plastic pollution and environmental damage and the contaminants that they can carry in foods. In this context, eco-sustainable bio-packaging represents a current exigency to which the scientific community and national and international legislative bodies have been working together. In this paper, the mechanical and chemical/physical properties as well as the functionality of three commercial biofilms were investigated. As food matrices, pumpkin has been chosen due to its large size, and thus the fact that have difficulties in marketing, storage and handling, which leads to many losses. To reduce these problems minimally processed pumpkin is proposed as an alternative.

The biofilm functionality was examined monitoring the chemical profile of fresh and packaged pumpkins by means of untargeted and targeted methodologies. The untargeted NMR

analysis was used to obtain a comprehensive metabolite profiling of pumpkin samples whereas target analyses were focused on a specific class of compounds: total carotenoids, chlorophylls and polyphenols in pumpkins were determined by spectrophotometric methods; volatile compounds were determined by SPME-GC-MS. To evaluate the quality of fresh and packaged pumpkins, the presence of biogenic amines was monitored by means of HPLC analysis and microbiological analyses carried out. The potential changes in water dynamics during sample preservation were also investigated by time-domain NMR portable relaxometry. Finally, the antioxidant capacity of pumpkin extracts was also evaluated by standard assays.

foods

MDPI

Article

Commercial Bio-Packaging to Preserve the Quality and Extend the Shelf-Life of Vegetables: The Case-Study of Pumpkin Samples Studied by a Multimethodological Approach

Giacomo Di Matteo [1,†], Paola Di Matteo [2,†], Matteo Sambucci [2], Jacopo Tirillò [2], Anna Maria Giusti [3], Giuliana Vinci [4], Laura Gobbi [4], Sabrina Antonia Prencipe [4], Andrea Salvo [1], Cinzia Ingallina [1], Mattia Spano [1], Anatoly P. Sobolev [5], Noemi Proietti [5], Valeria Di Tullio [5], Paola Russo [2,*], Luisa Mannina [1,*] and Marco Valente [2]

1 Dipartimento di Chimica e Tecnologie del Farmaco, Laboratorio di Chimica degli Alimenti, Sapienza Università di Roma, Piazzale Aldo Moro 5, 00182 Roma, Italy; giacomo.dimatteo@uniroma1.it (G.D.M.); andrea.salvo@uniroma1.it (A.S.); cinzia.ingallina@uniroma1.it (C.I.); mattia.spano@uniroma1.it (M.S.)

2 Dipartimento di Ingegneria Chimica Materiali Ambiente, Sapienza Università di Roma, Via Eudossiana 18, 00184 Roma, Italy; p.dimatteo@uniroma1.it (P.D.M.); matteo.sambucci@uniroma1.it (M.S.); jacopo.tirillo@uniroma1.it (J.T.); marco.valente@uniroma1.it (M.V.)

3 Dipartimento di Medicina Sperimentale, Sapienza Università di Roma, Viale Regina Elena 324, 00161 Roma, Italy; annamaria.giusti@uniroma1.it

4 Dipartimento di Management, Sapienza Università di Roma, Via del Castro Laurenziano 9, 00161 Roma, Italy; giuliana.vinci@uniroma1.it (G.V.); laura.gobbi@uniroma1.it (L.G.); sabrinaantonia.prencipe@uniroma1.it (S.A.P.)

5 Laboratorio di Risonanza Magnetica "Segre-Capitani", Istituto per i Sistemi Biologici, Area della Ricerca di Roma 1, CNR, Via Salaria Km 29.300, 00015 Monterotondo, Italy; anatoly.sobolev@cnr.it (A.P.S.); noemi.proietti@cnr.it (N.P.); valeria.ditullio@cnr.it (V.D.T.)

* Correspondence: paola.russo@uniroma1.it (P.R.); luisa.mannina@uniroma1.it (L.M.); Tel.: +39-06-44585565 (P.R.); +39-06-499137352 (L.M.)

† These authors contributed equally to this work.

check for updates

Citation: Di Matteo, G.; Di Matteo, P.; Sambucci, M.; Tirillò, J.; Giusti, A.M.; Vinci, G.; Gobbi, L.; Prencipe, S.A.; Salvo, A.; Ingallina, C.; et al. Commercial Bio-Packaging to Preserve the Quality and Extend the Shelf-Life of Vegetables: The Case-Study of Pumpkin Samples Studied by a Multimethodological Approach. *Foods* **2021**, *10*, 2440. https://doi.org/10.3390/foods10102440

Academic Editors: Patrizia Perego and Roberta Campardelli

Received: 14 September 2021
Accepted: 9 October 2021
Published: 14 October 2021

Publisher's Note: MDPI stays neutral with regard to jurisdictional claims in published maps and institutional affiliations.

Copyright: © 2021 by the authors. Licensee MDPI, Basel, Switzerland. This article is an open access article distributed under the terms and conditions of the Creative Commons Attribution (CC BY) license (https://creativecommons.org/licenses/by/4.0/).

Abstract: A multidisciplinary protocol is proposed to monitor the preservation of fresh pumpkin samples (FP) using three commercial polymeric films: A made of biodegradable cellophane from regenerated cellulose pulp; B from corn starch, cassava and eucalyptus, C made of polylactic acid from corn starch, and a polyethylene film used as reference (REF). Chemical, mechanical and microbiological analyses were applied on packaging and fresh and packaged samples at different times. After an 11-day period, NMR spectroscopy results showed a sucrose increase and a malic acid decrease in all the biofilms with respect to FP; fructose, glucose, galactose levels remained quite constant in biofilms B and C; the most abundant amino acids remained quite constant in biofilm A and decreased significantly in biofilm B. From microbiological analyses total microbial count was below the threshold value up to 7 days for samples in all the films, and 11 days for biofilm C. The lactic acid bacteria, and yeasts and molds counts were below the acceptability limit during the 11 days for all packages. In the case of biofilm C, the most promising packaging for microbiological point of view, aroma analysis was also carried out. In this paper, you can find all the analysis performed and all the values found.

Keywords: pumpkin; biofilm; shelf life; metabolomics; NMR spectroscopy; NMR relaxometry; SPME-GC-MS analysis; biogenic amines; mechanical characterization; microbiological analysis

1. Introduction

Food packaging plays an essential role in preserving food throughout the distribution chain. Without packaging, the direct contact with physical, chemical, and biological contaminants can drastically compromise food quality and nutritional health value. In

this regard, food industries have increased attention towards products with improved nutritional quality and health promoting properties and towards the use of proper packaging materials. Packaging has to be capable of maintaining food sensorial and nutritional quality and guaranteeing food safety both in international and national markets even in complex conditions. In the twentieth century, the innovation of packaging underwent a rapid evolution thanks also to the discovery and marketing of new materials as plastics and derivatives. Nowadays, in many countries, including Italy, more than 70% of packaging is destined for the food industry. However, over time, the generation of a large amount of food packaging waste has become an extremely critical point, with Europe reaching 65% of the total packaging waste production. Traditional polymeric materials from mineral oils are characterized by long degradation times and are the main responsible for plastic pollution and environmental damage. In addition, this type of packaging can represent a possible carrier of food contaminants. The introduction of eco-sustainable bio packaging in food packaging represents a current exigency to which the scientific community and national and international legislative bodies have been working together.

In this paper, the mechanical and chemical/physical properties as well as the functionality of three commercial biofilms were investigated. The application of these biofilm to food packaging is limited (i.e., biofilm A is used in dairy, chocolate and confectionery; biofilm B is used for meat, while C for sandwiches, cookies, or cold treats to go), and they were not previously applied for fresh fruits and vegetables.

The biofilm functionality on fresh-cut pumpkin sample preservation was examined. Pumpkins are generally large vegetables, and thus have difficulties in marketing, storage and handling, which leads to many losses. To reduce these problems minimally processed pumpkin is proposed as an alternative. However, this product is more perishable and needs conservation at refrigerated conditions and the use of a suitable packaging. Plastic packaging and modified atmosphere, but not biofilms, were investigated to this aim and their effect on physical and chemical properties of pumpkin were investigated [1–3]. Analyses of mass loss, microbiological growth, pH, aw, carotenoids content and sensory quality were carried out in order to obtain information on the shelf life of the minimally processed pumpkin [1–3].

The biofilm functionality was here examined monitoring the chemical profile of fresh and packaged products by means of untargeted and targeted methodologies. The untargeted NMR analysis was used to obtain a comprehensive metabolite profiling of pumpkin samples [4,5] whereas target analyses were focused on a specific class of compounds: total carotenoids, chlorophylls and polyphenols in pumpkins were determined by spectrophotometric methods; volatile compounds were determined by SPME-GC-MS. To evaluate the quality of fresh and packaged pumpkins, the presence of biogenic amines was monitored by means of HPLC analysis and microbiological analyses carried out. The potential changes in water dynamics during sample preservation were also investigated by time-domain NMR portable relaxometry. Finally, the antioxidant capacity of pumpkin extracts was also evaluated by standard assays.

2. Materials and Methods

2.1. Biodegradable Commercial Films

Commercial biodegradable films (biofilms) of vegetable origin, available on the market (here reported as A, B and C), and a commercial low-density polyethylene (LDPE) film used as a reference (REF), were used as food bags. The biofilm compositions as reported on the package label is reported in the Table 1. For polyethylene, which is a common packaging material (30 µm in thickness), oxygen transmission rate (OTR) and carbon dioxide transmission rate (CO_2TR) are data available from the supplier (i.e., OTR 5396 +/− 420 cm^3 m^{-2} day^{-1}; CO_2TR 26249 +/− 2918 cm^3 m^{-2} day^{-1}).

Table 1. Composition of commercial biofilms, as reported on the package label, and measured thickness, oxygen transmission rate (OTR) and carbon dioxide transmission rate (CO_2TR).

Biofilm Commercial	Biofilm Composition	Thickness (μm) (Measured Value)	OTR ($cm^3 \cdot pm^{-2} \cdot day^{-1}$) (Measured Value)	CO_2TR ($cm^3 \cdot m^{-2} \cdot day^{-1}$) (Measured Value)
A	Biodegradable cellophane from regenerated cellulose pulp	20	4.91 ± 0.27	10.78 ± 0.50
B	Corn starch, cassava and eucalyptus	40	4.30 ± 0.20	13.42 ± 0.71
C	Polylactic acid from corn starch	30	646.41 ± 32.33	2162.51 ± 110.13

2.2. Pumpkin and Packaged Food Preparation

Pumpkins (*Cucurbita moschata cultivar*) were provided by a local farm (Tenuta di Dragone Corsetti, Rome, Italy). A variety of French origin, with medium-sized fruits of 8–15 kg that can be kept whole for more than 6 months after harvest. This pumpkin has a reddish–ocher skin, with evident grooves. The pulp, orange in color, is very thick and tasty.

Pumpkins were harvested in October 2020, transported within 2 h directly from the field to the laboratory under refrigerated conditions and stored at 10°C before use. Pumpkins were washed with 2.5% sodium bicarbonate solution and then cut into cubes of about 2 cm side. The fresh pumpkin samples obtained at this stage (time zero) were reported as FP. FP cubes, about 100 g, were packaged using the three commercial biofilms (A, B, and C) and a polyethylene film (REF), see Table 1, each package having a volume of about 1000 cm^3 (Figure 1). All the packaged samples were stored at 5 °C for 11 days. For NMR, total chlorophyll, carotenoid and polyphenol analyses and the measurements of the antioxidant capacity, samples were freeze-dried by Lyovapor™ L-200 (Buchi, Milan, Italy) at 0.200 mbar for 12 h, blended and analyzed at 0 and 11 days.



Figure 1. Pumpkin cubes packaged in the commercial biofilms (A, B, C) and polyethylene film (REF).

For microbiological analyses, three samples for each package were randomly selected at 0, 4, 7 and 11 days.

2.3. Biofilms Analyses

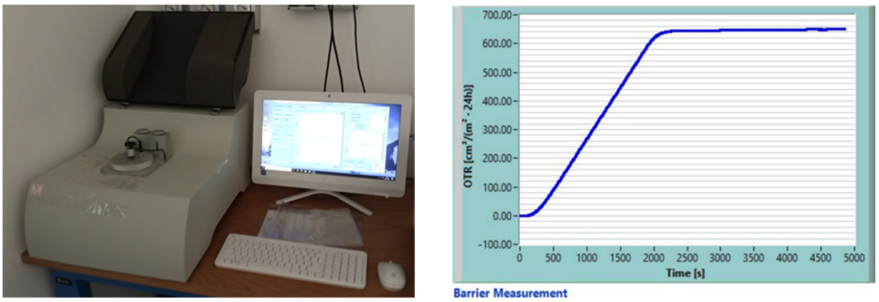
2.3.1. Mechanical Characterization: Tensile Test

Tensile properties of the commercial biofilms were evaluated using a Z10 mechanical testing machine (Zwick-Roell, Ulm, Germany), in accordance with ISO 527-3 standard method [6]. The specimens were extracted from the films by a MT1130 die-cutter (MinEuro, Turin, Italy), using a metallic dog-bone-shaped cutting edge to obtain samples with a width of 4 mm and a gauge length of 30 mm. Tests were performed with a 200 N load cell, a crosshead speed of 5 mm/min, and a pre-load of 5 MPa. The tensile strain of the specimens was obtained by recording the crosshead displacement of the test frame. TestXpert software (Zwick-Roell, Ulm, Germany) was used to record the data. For each type of biofilm, at least 3 representative samples were investigated and the mechanical properties, in terms of tensile strength (σ_t), elastic modulus (E), and elongation-at-break (ε_b) were reported.

Before the analysis, the thickness of each material was measured (three measuring points) with a centesimal micrometer (measuring range: 0–25 mm/graduation: 0.01 mm), see Table 1.

2.3.2. Gas Permeability Testing: Oxygen Transmission Rate (OTR) and Carbon Dioxide Transmission Rate (CO_2TR)

The oxygen transmission rate (OTR) and carbon dioxide transmission rate (CO_2TR) were considered as indicators to evaluate the gas permeability performance of the commercial biofilms. The measurements were performed using a Perme permeability tester (ExtraSolution, Pisa, Italy) conforming to ISO 15105-2 (2003) standard method [7]. The testing apparatus can operate in a temperature range of 10–50 °C, relative humidity (RH) up to 95%, and with high-purity permeating gases ($\geq$99.99% for CO_2 and $\geq$99.95% for O_2). The tests were performed at 23 °C, varying RH conditions in accordance with the type of measurement (50% RH for oxygen permeability test and 0% RH for carbon dioxide permeability test). The experimental set-up (Figure 2a) was based on gas/membrane/gas configuration. The film (sample surface of 50 cm^2) was placed inside the measurement chamber separating the side of the testing gas from the side of the carrier gas (nitrogen). Pressure of the two sides was equal but testing gas partial pressure is different. Testing gas was transmitted through the film and carried to the sensor by nitrogen with a flow rate of 12.05 mL/min. Sensor measured the testing gases permeance in the carrier one, providing the transmission rate values. OTR and CO_2TR, expressed in $cm^3\ m^{-2}\ day^{-1}$, were extrapolated from the slope of the linear steady-state part of the permeated gas volume–time curve (Figure 2b).



(**a**) (**b**)

Figure 2. Set-up for gas permeability testing (**a**) and experimental "permeated gas volume-time" curve extrapolated from oxygen permeability test (**b**).

2.3.3. NMR Analysis

For NMR analysis, Bligh–Dyer extracts were prepared according to the protocol previously described [8] with some modifications. Freeze dried sample (0.1 g) was sequentially added with a 3 mL methanol: chloroform (2:1 v/v) mixture and 0.8 mL of Millipore-grade water, shaking slightly after each addition. The obtained suspension was sonicated for 10 min in order to maximize the extraction yield. Then the extract was sequentially added with 1 mL of chloroform and 1 mL Millipore-grade water stirring with vortex for 30 s in order to achieve the phase separation. The emulsion was centrifugated at 7197× g for 15 min at 4 °C. The organic and hydroalcoholic phases were separated. To ensure the complete extraction of the soluble metabolites, the same procedure was repeated using pellet remained after the first extraction and half of the volumes of all the solvents. After phase separation a slow N_2 flow at room temperature was used for drying. The obtained extracts were stored at −20 °C until analysis. The hydroalcoholic and organic extracts were

analyzed using a Bruker AVANCE 600 spectrometer (Bruker, Milan, Italy) operating at the proton frequency 600.13 MHz and equipped with a Bruker multinuclear z-gradient 5 mm probe head. The NMR spectra were acquired at 28 °C according to the experimental conditions reported in most databases. Each dried hydroalcoholic extract was solubilized in 0.8 mL 400 mM phosphate buffer (pH 7.4)/D2O containing TSP 2 mM (internal standard) and EDTA-d16, filtered and transferred into a 5 mm NMR tube. ^{1}H spectra of hydroalcoholic extracts were acquired using the zgpr sequence to suppress water signal by solvent presaturation. The NMR acquisition parameters were 256 transients, a recycle delay of 5 s, an acquisition time of 2.28 s, a 90° flip angle pulse of 15.65 µs, and 32 K data points. Each dried organic extract was solubilized in 0.8 mL of the CDCl3/CD3OD (2:1 v/v) mixture with tetramethylsylane (TMS) as internal standard, filtered and transferred into a 5 mm NMR tube that was flame sealed. ^{1}H spectra (Bruker pulse sequence zg) of the organic extracts were acquired with 256 transients, a recycle delay of 5 s, an acquisition time of 1.82 s, a 90° flip angle pulse of 10.4 µs, and 32 K data points. Two-dimensional (2D) NMR experiments (^{1}H-^{1}H TOtal Correlated SpectroscopY (TOCSY), ^{1}H-^{13}C Heteronuclear single quantum coherence (HSQC), ^{1}H-^{13}C heteronuclear multiple bond correlation (HMBC), and ^{1}H homonuclear J-resolved experiment (JRES), were performed on each hydroalcoholic and organic extract under the experimental conditions previously reported [9]. In order to evaluate the repeatability of the protocol, the entire procedure (from the sample preparation to NMR analysis) was carried out in duplicate. The identified signals in the hydroalcoholic extracts were integrated by the TOPSPIN (Version 4.1.1) software (Bruker, Milan, Italy) and normalized with respect to the methyl group integral of TSP signal (at 0.00 ppm) set to 100 (Table S1) in order to obtain the metabolite absolute quantities [5]. The metabolite signals used for the quantification were showed in Table 2. The metabolites' amounts are expressed in mg/10 g of dried sample ± SD (standard deviation) (Figures S1 and S2).

Table 2. NMR signals selected for quantitative NMR analysis (qNMR).

ppm	Compound	ppm	Compound
0.94	Isoleucine	4.18	Pyro-glutamate
0.97	Leucine	4.30	Malic acid
1.05	Valine	4.60	β-Galactose
1.34	Threonine	4.66	β-Glucose
1.49	Alanine	5.25	α-Glucose
1.70	Arginine	5.28	α-Galactose
2.30	GABA	5.42	Sucrose
2.35	Glutamic acid	6.53	Fumaric acid
2.46	Glutamine	6.91	Tyrosine
2.54	Citric acid	7.44	Phenylalanine
2.81	Aspartic acid	7.55	Tryptophan
2.89	Asparagine	8.15	Istidine
3.21	Choline	8.47	Formic acid
3.30	Myo-inositol	8.84	Trigonelline
4.12	Fructose		

The integral areas of 4 selected signals in the ^{1}H NMR spectra of organic extracts (Figure S3) were measured using the TOPSPIN software and normalized with respect to the integral (I_{FA}) of the -CH_2 group signal of all fatty acids set to 100. The TMS signal was a chemical shift reference (0.00 ppm). The molar % values ± SD of fatty acids were calculated with consideration of the number of equivalent protons using the following equations:

$$\%_{TUFA} = 100(0.5I_{TUFA}/I_{FA}) \quad (1)$$

$$\%_{DUFA} = 100(I_{DUFA}/I_{FA}) \quad (2)$$

$$\%_{MUFA} = 100(I_{UFA} - 2I_{DUFA} - 1.5I_{TUFA})/I_{FA} \quad (3)$$

$$\%_{SFA} = 100 - \%_{MUFA} - \%_{DUFA} - \%_{TUFA} \quad (4)$$

where $\%_{TUFA}$, $\%_{DUFA}$, $\%_{MUFA}$ and $\%_{SFA}$ are the molar % of tri-unsaturated fatty acids, di-unsaturated fatty acids, mono-unsaturated fatty acids, saturated fatty acids, respectively. I_{TUFA}, I_{DUFA}, I_{UFA} and I_{FA} are integrals. The amount of each quantified fatty acid in the organic extracts is reported in Table S2.

One-way analysis of variance (ANOVA) was realized by the Statistica software (Version 14.0.0.15) in order to determine significant differences ($p < 0.05$) between the results (Tables S3 and S4).

2.3.4. Spectrophotometric Analysis of Chlorophylls, Total Carotenoids, Total Polyphenols and Antioxidant Activity

Pigments and total polyphenols were analyzed both in fresh and packaged samples at different times: time 0 (fresh, t_0) and after 11 days of storage (t_{11}) at T = 5 ± 1 °C. Chlorophylls a and b extraction was performed according to a protocol previously described [10] with some modifications. A Folch extraction was carried out on 10 mg of lyophilized sample adding 6 mL of a chloroform: methanol (2:1 *v*/*v*) mixture, together with 10 mg of MgO in order to neutralize plant acids and avoid pheophytin formation [11]. The obtained suspension was sonicated for 10 min to maximize the extraction yield. The pellet was removed by filtration through a filter paper under vacuum condition. Then 1.2 mL of Millipore-grade water was added to achieve the phase separation by centrifugation at 7197 g for 5 min at 20 °C. The lower organic phase was dried by N_2 flow and then solubilized in chloroform. The absorbance values at 648, 666 and 750 nm at 25 °C was detected by an UV/VIS spectrophotometer. The contents of chlorophyll a (Chl a), chlorophyll b (Chl b) were calculated according to Wellburn equations [12]. Data were reported as means of two replications and expressed as mg/g ± SD (standard deviation). Statistical significance was reached at $p < 0.05$.

Total carotenoid content was evaluated in the lipophilic fraction by UV-Vis methods at 449 nm, according to Rapa et al. [13] Briefly, 20 mL of ethanol:hexane mixture (4:3 *v*/*v*) was added to 0.015 g homogenized sample in a glass tube (protected from light). The carotenoids extraction was conducted by agitating the mixture for 1 h (darkness) at 200 rpm. Thereafter, 1 mL of distilled water was added to the mixture and stirred by inversion. The hexane fraction was then collected in an amber vial. The results were compared with a standard solution of β-carotene in n-hexane, and the quantification of total carotenoids was achieved by the linear regression (R^2 = 0.9967) and expressed as milligram of β-carotene (mg BCE).

Total phenolic content was determined by spectrophotometric analysis according to a previously published method [14]. Briefly, 0.08 g of lyophilized pumpkin was extracted with 20 mL of methanol in aqueous solution (60:40, *v*/*v*). Samples were homogenized in an Ultra-Turrax for 3 min and centrifuged at 3000× *g* for 5 min. The total content of polyphenols was expressed as milligrams of gallic acid equivalent (GAE) per kg. The final results were obtained through a calibration curve ranging from 10 to 100 mg/L (R^2 = 0.9997).

Antioxidant activities were determined by DPPH and ABTS assays, according to the methods of Preti et al. [15]. The DPPH and ABTS· free radical scavenging activity of the pumpkin extracts was evaluated by measuring the decrease in absorbance at 515 nm (DPPH), and 734 nm (ABTS). The absorbance was measured in 1-cm path length cuvettes against methanol in aqueous solution (60:40, *v*/*v*), using a UV-Vis spectrophotometer (Jenway, Stone, UK). Results were expressed as inhibition rate and were calculated based on Equation (5):

$$I\% = \frac{A_0 - A_f}{A_0} \times 100 \quad (5)$$

where A_0 is the radical cation's initial absorbance, and A_f is the absorbance after the addition of sample extract.

2.3.5. Biogenic Amines (BAs) Determination

The BAs determination was carried out according to a previously optimized method with some modifications [14]. About 0.4 g of lyophilized pumpkin sample was extracted with 10 mL of 0.6 M $HClO_4$, homogenized for 3 min, and centrifuged at 2700× *g* for 10 min. The supernatant was filtered through a 0.45 µm membrane millipore filter and collected in a flask. The residue was added with 10 mL of 0.6 M $HClO_4$, mixed, and again centrifuged for 10 min. Then, the second extract was then filtered and added to the first one. The final volume was adjusted to 25 mL with 0.6 M $HClO_4$. An aliquot of 1 mL of the final extract was then derivatized by adding 200 µL of 2 M NaOH, 300 µL of saturated $NaHCO_3$ solution, and 2 mL of dansyl chloride solution (10 mg mL^{-1} in acetone). After shaking, the samples were left in the dark for 60 min at 45 °C. About 100 µL of 25% NH_4OH was added to stop the derivatizing reaction. The final volume was adjusted to 5 mL by adding acetonitrile. The dansylated extract was filtered using 0.45-µm filter (Whatman® Puradisc filters, Sigma Aldrich, Milan, Italy), injected into the HPLC system, and analyzed with a previous standard method [15].

2.3.6. Microbiological Analysis

The microbiological analysis was performed on a sample (about 25 g) aseptically removed from the package, placed in a stomacher bag, diluted with 0.9% NaCl solution and homogenized with a Stomacher LAB Blender 400 (Pbi International). Further dilutions were carried out using the same diluent. The total aerobic count was determined on 3 M Petrifilm aerobic total count, with incubation at 30 °C for 24–48 h. Yeasts and molds were detected on 3M Petrifilm yeast and molds at 30 °C for 24–72 h and Lactic acid bacteria were enumerated on 3M Petrifilm lactic acid bacteria incubated at 30 °C for 24–72 h. Measurements were performed on 3 samples for each package randomly selected, at 0, 4, 7 and 11 days.

2.3.7. Mass Loss Measurement

The percentage mass loss was determined according to the following Equation (6):

$$\% M_{LOSS}(t) = \frac{M_0 - M_t}{M_0} \cdot 100 \quad (6)$$

where: $\% M_{LOSS}$ (t) is the percentage mass loss at time t, M_0 is the initial sample mass and M_t is the sample mass at time t. The sample mass was determined by a digital precision balance (±0.1 g) (Gibertini, Novate, Italy). The mass loss was measured in triplicate: three samples for each package were randomly selected, at 4, 7 and 11 days.

2.3.8. Water Activity Measurement

Water activity was measured by means of a Humimeter (Schaller Humimeter Rh2). Measurements were performed in triplicate at 0, 4, 7 and 11 days. The samples and the instrument were adjusted to the surrounding temperature for at least 30 min. The screw top jar of the device was filled with two pieces of pumpkin (50.00 ± 1.00 g) and the water activity measuring chamber was closed. The measure was carried out after 10 min.

2.3.9. pH Evaluation

The pH was evaluated on the homogenized pumpkin by a pH meter (Crison GLP 21 Crison Instruments). The pH measurement was carried in triplicate at 0, 4, 7 and 11 days.

2.3.10. Carbon Dioxide Measurement

CO_2 concentration in packaged pumpkin was measured using a Uniphos precision air sampling pump and gas detection tubes with different ranges of concentrations (0.03–0.5, 0.25–3.00 and 0.5–10% vol). For gas analysis, a volume of 100 cm^3 of package headspace was taken. To avoid modifications in the headspace gas composition due to gas sampling,

each package was used only for a single measurement of the headspace gas composition. Three bags were used for each measurement at 0, 4, 7 and 11 days.

2.3.11. Aroma Compounds by SPME-GC-MS Analysis

The aroma profile of pumpkin packaged in C film at initial time and at 11 days of storage at 5 °C was evaluated by SPME-GC-MS. 10 mL pumpkin pulps and 3.0 g of NaCl were added into 15 mL glass vial. The sample was equilibrated 40 min by oscillation at 45 °C [16]. A 100 µm polydimethylsiloxane fused silica coated fiber (Supelco Co., Bellefonte, PA, USA) was used for SPME. A micro-syringe was inserted into the headspace samples for 40 min at 45 °C. The desorption was carried out at 250 °C for 3.5 min in the injection port of an Agilent GC–MS (7890B–5977B). An Agilent Technologies, Inc., HP-5MS column was used (30 m, 0.25 mm I.D., 0.25 µm film thickness). The injection port was controlled in spitless type. The oven temperature program was from 45 to 140 °C at a rate of 5 °C/min, followed by an increase to 220 °C, at a rate of 10 °C/min; holding time was 5 min and finally the temperature was increased to 250 °C, and kept for 2 min in isothermal condition. The carrier gas was He at a constant flow rate of 1.0 mL/min. The MS fragmentation was carried through electronic effect EI at 70 eV, a source temperature of 230 °C and scan mode was between 50 and 550 mass units.

2.3.12. Portable Time Domain (TD)-NMR Relaxometry

Longitudinal and transverse relaxation times were measured at 13.62 MHz with a portable NMR instrument from Bruker Biospin interfaced with a purposely built single-sided sensor by RWTH Aachen University, Germany [17]. Longitudinal relaxation times T_1 were measured with the aperiodic saturation recovery sequence, using a logarithmic increment, 64 blocks were collected in each experiment [18]. Effective transverse relaxation times T_{2eff} were measured using the CPMG pulse sequence with TE of 80 µs, and 4096 echoes. Because the field generated by unilateral NMR is strongly inhomogeneous (G = 14.28 T/m), transverse relaxation times obtained are shorter than those measured in a homogeneous field. The shortening of the transverse relaxation time can be minimized by using an echo spacing as short as possible. It should be noted that, using the CPMG sequence for measuring T_2, only water components are observed, whereas T_2 of the rigid macromolecular matrix which is of the order of a few tens of µs is neglected.

T_1 and T_2 were collected on four pumpkin samples packaged in biofilm B and biofilm C. Measurements were carried out to a depth of 2 mm inside the pumpkin sample and collected for 1, 4, 7, and 11 days. T_1 data were obtained fitting the magnetization with the following equation:

$$M_z(t) = M_{ze}\left(1 - e^{-\frac{2t}{T_1}}\right) \quad (7)$$

where M_{ze} is the magnetization at the equilibrium.

The transverse relaxation times T_2 were obtained fitting the magnetization decay with the following equation:

$$M_{xy}(t) = \sum_{i\ i=1}^{N} M_{0i}\ \left(e^{-\frac{2t}{T_{2i}}}\right) \quad (8)$$

where T_{2i} is the ith time constant of magnetization decay, $M_{xy}(t)$ is the component of magnetization on the xy plane and M_0 is the initial magnetization for each ith T_2 component. The proton density was calculated applying Equation (2) and extrapolating at zero time the total M_{0t} value.

3. Results and Discussion

3.1. Mechanical and Chemical/Physical Characterization of the Commercial Biofilm

It is important to notice that the investigated commercial eco sustainable films had a different but very uniform thickness, see Table 1. The different mechanical performances of the three commercial samples are primarily attributable to the nature of the raw materials employed for their production.

3.1.1. Mechanical Characterization: Tensile Test

Tensile test results are shown in Figure 3 The maximum σ_t can be found in A sample, since the cellulose-based formulation confers a higher strength and more stiff behavior than the other biofilms (Figure 3). In this regard, due to their mechanical properties, cellulose fillers are often employed as strengthening agents in packaging film blends [19]. Moreover, as clear from the histograms refer to B samples, the tensile response of the eco-films is strongly correlated to the cutting direction (Figure 3). Figure 4 highlights the cuts performed on B film to mechanically test the sample in the two orientations with respect to the extrusion direction. The specimens extracted in the direction transversal to the film extrusion (labeled with "trasv") showed lower mechanical strength but significantly greater deformability than the specimens extracted in the longitudinal direction (labeled with "long"), resulting in an ε_b-increase of 165% (calculated as a percentage increment with respect ε_b-value found in B Long). Similar anisotropic behavior was demonstrated by Siracusa et al. [20] on C films for food packaging applications. Regardless of the specimen configurations, B film showed more ductile and deformable behavior than the other films, indicating better mechanical flexibility requirements for packaging applications, where it is crucial to avoid breaking during processing and use [21].

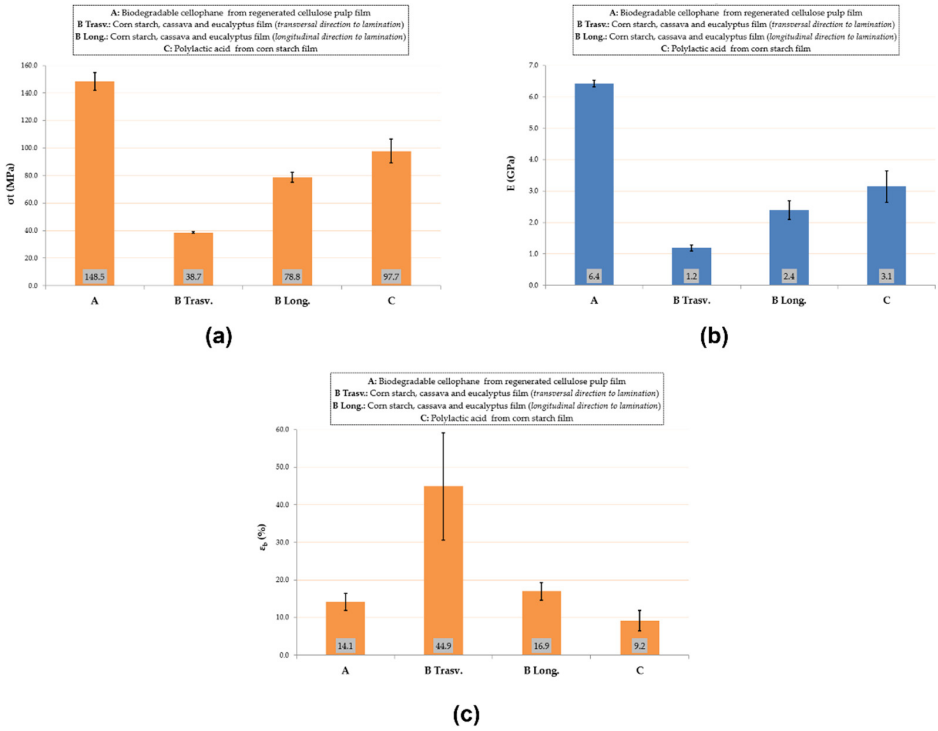


Figure 3. Tensile test results: tensile strength (**a**), elastic modulus (**b**), and elongation-at-break (**c**).



Figure 4. Cutting on B (Corn starch, cassava, and eucalyptus) biopolymer film to evaluate the mechanical properties with respect to the lamination direction.

3.1.2. Gas Permeability Testing: Oxygen Transmission Rate (OTR) and Carbon Dioxide Transmission Rate (CO_2TR)

The gas permeability of plastic films is of primary importance in food packaging. The ability to preserve the contents of the package from contact with the air is essential to avoid degradation phenomena, ensuring a correct and healthy shelf life of the products. Furthermore, the barrier property of a packaging film is crucial in the context of modified atmosphere packaging (MAP) technology: packaging systems that involve changing the gaseous atmosphere surrounding a food product inside a pack and employing packaging materials with an appropriate permeability to maintain the changed atmosphere at an acceptable level for preservation [22]. In this framework, the oxygen barrier performances of a film are fundamental because oxygen promotes a lot of degradation mechanisms of food, including corrosive phenomena, oxidation, and great modification of organoleptic properties. In addition, carbon dioxide plays a key role for MAP systems because it can potentially reduce the degradation phenomena associated with processed fresh vegetable products, leading to a significantly longer shelf-life [23]. Table 1 reports the experimental values of OTR and CO_2TR for the three films under examination.

Concerning the oxygen permeability performance, only A and B films provided proper requirements for food packaging applications as reported in [24], which defines recommended OTR value lower than 20 $cm^3\ m^{-2}\ day^{-1}$. The suitability of these films for the food packaging sector is also demonstrated in terms of carbon dioxide permeability, considering that the recommended CO_2TR index should range from 3 to 5 times the OTR value [25]. As verified by Piscopo et al. [26], the higher CO_2TRs values than OTR ones are to be attributed to the different behavior of carbon dioxide molecules in terms of solubility and diffusion through the polymeric chains, although the molecular size is larger.

The experimental results are in good agreement with the literature data. For A film, OTR values between 3.4 $cm^3\ m^{-2}\ day^{-1}$ and 11.1 $cm^3\ m^{-2}\ day^{-1}$ were detected [27]. Corn starch-based packaging materials (such as B sample investigated in this work) show an OTR value close to 1 $cm^3\ m^{-2}\ day^{-1}$ [28]. Discrepancies between the experimental and

literature/datasheet values are attributable to the different standard methods and test conditions (e.g., temperature and RH) involved in the analysis of the films. For PLA-based film under study, no reference values are available. However, analogous commercial films tested in other research works reported similar results: OTR of 487.67 cm^3 m^{-2} day^{-1} and CO_2TR of 1201 cm^3 m^{-2} day^{-1} reported in [20]; OTR of 617.6 cm^3 m^{-2} day^{-1} reported in [27]. Considering these values and the recommended level for packaging applications, C material would seem not suitable for medium or long shelf-life of some food products. This evidence finds agreement with previous gas permeability investigations on PLA bio packages [29,30], which stated inferior barrier properties with respect to conventional petroleum-based polymers.

3.2. Chemical Profile of Fresh and Packaged Samples

3.2.1. NMR Based Metabolite Profile

The metabolite profile of pumpkin samples, as obtained by the NMR methodology, is reported here for the first time. The assignment of ^{1}H NMR spectra of Bligh–Dyer hydroalcoholic extracts was carried out using two-dimensional NMR experiments (^{1}H-^{1}H TOCSY, ^{1}H-^{13}C HSQC, ^{1}H-^{13} HMBC and JRES experiments) and literature data regarding other vegetable matrices [31,32]. Sixteen free amino acids, five sugars, four organic acids and choline and trigonelline were identified and quantified (Table 3). In particular, pyroglutamate, generally identified only in vegetables, was identified by the typical doublet of doublets signal at 4.1 ppm (J = 5.9 Hz; 9.1 Hz) due to α-CH that showed cross peaks correlations with β-CH2, β′-CH2 and γ-CH2 at 2.04, 2.51 and 2.41 ppm, respectively, observed in the ^{1}H-^{1}H TOCSY map [33,34]. The most abundant sugars, namely sucrose, glucose, and fructose were identified taking into account their different isomeric form present in solution. Additionally, less abundant galactose and myo-inositol were also identified.

The assignment of ^{1}H NMR spectra of Bligh–Dyer organic extract was also carried out reporting the main classes of fatty acids (Table 4).

In order to establish the functionality of the three commercial biofilms, the metabolite profile of packed pumpkins after 11 days was compared to that of fresh samples FPs (time zero). Regarding sugars, the sucrose level increased for all the examined biofilms compared to FP, in particular for biofilm A it was 1.5 times higher. The fructose, glucose and galactose amounts were quite constant for all the tested biofilms, except for bio-film A package that showed a significant decrease of these metabolites. Myo-inositol content was quite steady for all the biofilms. Regarding organic acids, the malic acid amount decreased significantly for all the selected biofilms compared to FP, in particular, for biofilm REF it was more than 1.5-fold lower. On the contrary, an increment of citric acid was observed for both biofilms A and C (at least 1.5-fold), and those of fumaric acid for both biofilms B and REF (at least 1.4-fold). Formic acid remained quite constant for all the bio-film packages. Regarding amino acids, the most abundant amino acids in pumpkins (aspartate, glutamine, asparagine, arginine and pyro-glutamate) decrease in biofilm B packaged vegetable respect to FP, in particular pyro-glutamate was 1.5-fold lower. A decrease in asparagine was also observed for biofilm C and those of arginine for both bio-films C and REF. The tyrosine amount significantly decreased in the case of three commercial biofilms, in particular in biofilm B package it was 1.5-fold lower. Both alanine and histidine levels varied a lot for all the tested commercial packaging solutions. In particular, the alanine content decreased for bio-film A and increased more than 3 and 2 times for biofilms B and C, respectively, whereas the histidine amounts showed an opposite trend with an increment in biofilm A packed vegetable and a decrease in both biofilms B and C packed pumpkin respect to FP. Biofilm C package showed an increment of glutamate (1.5-fold) and a decrease of isoleucine, whereas biofilm B showed a decrease of both phenylalanine and tryptophan. All the other amino acids were quite steady for all the examined packaging's, except for the lowest one (leucine) that decreased significantly for both biofilms C and REF. The trigonelline level increased significantly for biofilm C and decreased for both biofilms B and REF, and the choline amount decreased for both bio-films A and B compared with FP.

Regarding the quantified fatty acids in the organic fraction, TOT SFA, TOT UFA and MUFA remained quite steady for all the tested biofilms. TUFA showed an increment for all the selected packaging, whereas DUFA increased for biofilm B and decreased for both biofilms C and REF.

Table 3. Carbohydrate, organic acid, amino acid and other metabolite amounts (mg/10 g ± SD) by NMR analysis of the pumpkins Bligh–Dyer hydroalcoholic fractions reported for fresh and packaged pumpkin samples. FP = fresh pumpkin sample (time 0); A, B and C = commercial biofilms; REF = polyethylene film. Analyses were carried out in duplicate.

	FP	A	B	C	REF
Carbohydrates					
Sucrose	759.42 ± 21.09	1425.34 ± 44.62	1026.61 ± 20.09	989.41 ± 26.60	1113.97 ± 87.08
Fructose	1095.69 ± 34.88	823.90 ± 26.82	1116.69 ± 36.09	1005.36 ± 9.47	1169.32 ± 135.70
Glucose	987.47 ± 36.58	641.06 ± 31.04	1053.60 ± 9.43	879.11 ± 15.30	1025.42 ± 125.89
Mio-inositol	170.66 ± 9.00	165.97 ± 2.98	147.79 ± 6.82	156.90 ± 5.16	162.15 ± 15.43
Galactose	80.97 ± 6.46	53.74 ± 2.68	67.18 ± 1.46	63.35 ± 0.58	70.46 ± 7.06
Organic acids					
Malic acid	340.84 ± 1.41	301.09 ± 5.97	255.01 ± 2.20	277.07 ± 1.38	178.78 ± 1.05
Citric acid	20.52 ± 0.77	34.76 ± 0.72	18.82 ± 0.24	36.14 ± 4.27	22.54 ± 0.11
Fumaric acid	0.94 ± 0.09	1.10 ± 0.04	1.81 ± 0.14	0.80 ± 0.05	1.35 ± 0.06
Formic acid	0.59 ± 0.19	0.69 ± 0.12	0.89 ± 0.06	0.73 ± 0.06	0.78 ± 0.10
Amino acids					
Aspartate	491.06 ± 16.94	456.09 ± 5.84	322.02 ± 2.76	457.88 ± 19.53	532.23 ± 47.67
Glutamine	272.77 ± 15.89	259.64 ± 4.08	196.37 ± 6.30	240.50 ± 5.44	286.30 ± 32.78
Asparagine	297.37 ± 8.98	284.24 ± 5.11	256.66 ± 2.86	238.47 ± 0.27	249.83 ± 20.12
Arginine	71.17 ± 0.20	70.62 ± 1.36	51.75 ± 0.78	63.40 ± 1.15	44.85 ± 4.30
Pyro-glutamate	57.24 ± 5.45	51.39 ± 2.01	37.13 ± 0.87	58.49 ± 8.72	40.31 ± 3.40
Tyrosine	55.17 ± 1.02	48.70 ± 0.70	35.85 ± 0.24	48.02 ± 0.45	46.05 ± 4.60
Alanine	12.47 ± 0.58	8.79 ± 0.07	43.42 ± 2.31	35.32 ± 1.35	9.47 ± 0.92
Glutamate	19.83 ± 1.58	15.46 ± 0.08	18.37 ± 1.80	36.07 ± 3.02	17.52 ± 1.33
GABA	29.99 ± 1.38	30.80 ± 1.94	28.03 ± 0.04	26.34 ± 0.05	24.13 ± 2.54
Phenylalanine	21.90 ± 0.63	20.26 ± 0.32	15.88 ± 0.17	20.90 ± 0.21	20.65 ± 1.82
Isoleucine	16.00 ± 1.04	18.07 ± 0.50	14.87 ± 0.59	12.71 ± 0.13	12.78 ± 1.71
Histidine	14.44 ± 0.13	15.99 ± 0.04	11.64 ± 0.76	13.07 ± 0.07	11.64 ± 1.40
Valine	16.22 ± 0.90	16.77 ± 0.46	13.82 ± 0.15	13.52 ± 0.24	13.54 ± 1.59
Threonine	15.87 ± 0.78	15.81 ± 0.22	14.83 ± 0.65	14.18 ± 0.01	15.18 ± 1.57
Tryptophan	12.31 ± 0.20	12.69 ± 0.75	8.50 ± 0.04	12.94 ± 0.10	10.33 ± 1.14
Leucine	2.04 ± 0.14	2.35 ± 0.11	2.02 ± 0.05	1.54 ± 0.05	1.12 ± 0.24
Miscellaneous metabolites					
Trigonelline	10.99 ± 0.30	9.49 ± 0.46	9.01 ± 0.43	14.65 ± 0.18	8.39 ± 0.68
Choline	9.99 ± 0.49	7.98 ± 0.14	6.23 ± 0.02	9.50 ± 0.24	7.66 ± 0.75

Table 4. Fatty acid percentages (molar % ± SD) by NMR analysis of the pumpkins Bligh–Dyer organic fractions reported for fresh and packaged pumpkin samples. FP = fresh pumpkin sample (time 0); A, B and C = commercial biofilms; REF = polyethylene film. Analyses were carried out in duplicate.

	FP	A	B	C	REF
Tot SFA	63.47 ± 0.92	58.90 ± 1.84	62.56 ± 0.78	62.69 ± 0.79	63.97 ± 3.51
Tot UFA	36.53 ± 0.92	41.10 ± 1.84	37.44 ± 0.78	37.31 ± 0.79	36.04 ± 3.51
TUFA	23.31 ± 0.17	25.52 ± 0.37	25.44 ± 0.25	25.23 ± 0.17	27.81 ± 1.26
MUFA	5.19 ± 1.13	7.19 ± 2.60	3.45 ± 1.10	4.88 ± 0.56	2.79 ± 2.20
DUFA	8.02 ± 0.04	8.40 ± 0.39	8.56 ± 0.07	7.20 ± 0.05	5.43 ± 0.05

It is noteworthy that after the contact of pumpkin with the packaging, in A and B samples at 11 days, new resonances appeared (doublet at 1.15 ppm) due to compounds not present in the fresh pumpkin. Selective TOCSY experiment indicated its correlations with 3.44, 3.55, and 3.89 ppm resonances, and all of them were assigned to propylene glycol. In a control experiment, packaging A was put in contact with deuterated water followed

by acquisition of ^{1}H NMR spectrum. The presence of all assigned signals of propylene glycol was confirmed; moreover, even more intense signals of glycerol were observed at 3.56, 3.66 and 3.79 ppm. Therefore, propylene glycol and glycerol from A and B packaging migrated in the pumpkin samples during storage. However, these compounds are allowed in foods and their presence in the food packaging depend on the industrial process applied for biofilm production.

3.2.2. Total Carotenoids, Chlorophylls a and b, Total Polyphenols and Antioxidant Activity

The pigments content (total carotenoids, chlorophylls a and b), total polyphenols and antioxidant activity was analysed in both fresh and packaged pumpkin samples at time = (t_0) and 11 days (t_{11}) and the results are displayed in Figure 5. In general, it is possible to note a decrease in all these bioactive compounds in the packaged products compared to the fresh one.

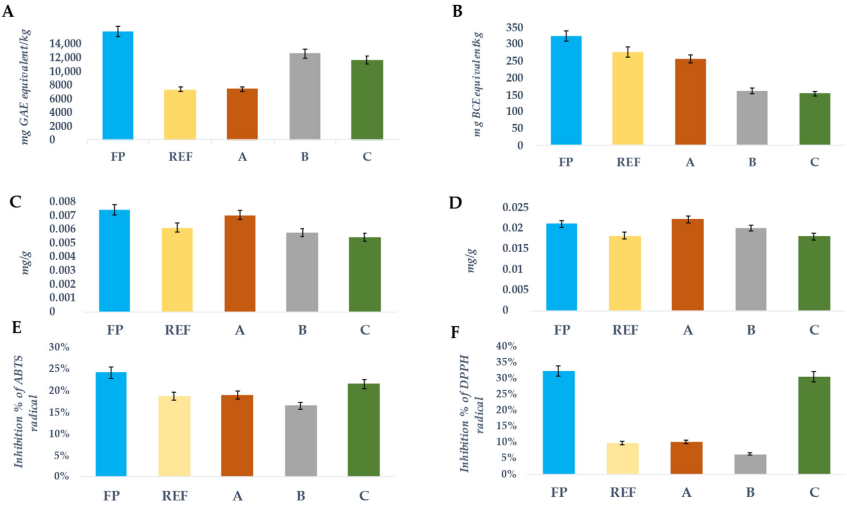


Figure 5. Histograms of total phenolic content (**A**) expressed in mg GAE/kg ± SD; total carotenoid content (**B**) expressed in mg BCE/kg± SD; chlorophyll a (**C**) and chlorophylls b (**D**) content expressed in mg/g± SD; ABTS (**E**) and DPPH (**F**) assays expressed as Inhibition %± SD, evaluated in fresh and packaged pumpkin samples, during shelf-life. FP: Fresh pumpkin (light blue trace); REF: polyethylene (yellow trace); A: biodegradable cellophane from regenerated cellulose (orange trace); B: biofilm obtained from maize starch, cassava, eucalyptus (grey trace); C: poly-lactate obtained from maize starch (green trace).

Regarding the chlorophyll content in pumpkin samples stored in different biofilms the results showed that the chlorophyll b concentration exceeded that of chlorophyll a by an average of 68% (the values ranged from 64% for the fresh samples (t_0) to 71% for packaging B (t_{11})) ($p < 0.01$). By comparing the different biofilms with respect to the REF, the highest level of chlorophyll a and chlorophyll b was detected in the packaging A sample, even if this difference did not reach statistical significance (Figure 5C,D).

A similar variability was also evaluated for the total polyphenols, TPC (Figure 5A) and for the total carotenoids, TCC (Figure 5B). During the 11-day storage period, REF and A—packaged pumpkin samples showed a reduction about 56% and 53%, respectively (REF: 6141.73 ± 0.06 mg GAE/kg, and A: 6210.57 ± 0.03 mg GAE/kg), compared with the fresh samples at t_0 (13,255.25 ± 0.02 mg GAE/kg). Regarding the total amount of carotenoids in pumpkin samples during shelf-life, the results showed that TCC decreased

more than 53%, especially in B and C packaged pumpkin samples (160.12 ± 1.36 mg BCE/kg, and 152.98 ± 1.1 mg BCE/kg); while, in REF packaged pumpkin, the content of carotenoids was almost unaltered towards fresh pumpkin (276.24 ± 2.27 mg BCE/kg). The antioxidant activity was measured by two widely used methods, DPPH and ABTS which are based on free radical scavenging and reducing power abilities of different type of antioxidant compounds found in plant food extracts. ABTS radical scavenging potential was comparatively higher than the DPPH radical scavenging activity, especially in polyethylene, A- and B-packaged pumpkin samples. ABTS is mainly oxidized by peroxyl radicals and it is soluble in both aqueous and organic solvents, so can be used to determine both hydrophilic and lipophilic antioxidant capacity (AOC) of extracts. While DPPH is a stable nitrogen radical that bears no resemblance to peroxyl radicals involved in lipid peroxidation. The decolourisation of the reagent occurs by both radical reaction and reduction, and steric accessibility is a determining factor in the reaction. Therefore, small molecules that have better access to the radical site have a higher AOC with this test [35]. Consequently, the combined use of these two assays provided an effective evaluation of antioxidant activity. The pumpkin samples stored in packaging C at t_{11} seemed to better preserve antioxidant activities both for ABTS and DPPH assays (21.47% and 30.34%, respectively) compared to fresh ones (24.02% and 32.10%) (Figure 5E,F). Different authors observed that the content of bioactive compounds in plant-origin foods, such as pumpkin, strictly de pended on storage period, plant varieties and post-harvest conditions [36,37].

3.2.3. Biogenic Amines Content

The content of eight BAs was evaluated in fresh and packaged pumpkin samples by high-performance liquid chromatography with fluorescence detection. The BAs investigated were spermine (SPM), spermidine (SPD), putrescine (PUT), and cadaverine (CAD) for polyamines, whereas β-phenylethylamine (β-PEA), histamine (HIS), serotonin (SER), and tyramine (TYR) were studied for monoamines. Figure 6 exhibited different trends of BA content for fresh and packaged pumpkin samples during the 11-day storage.

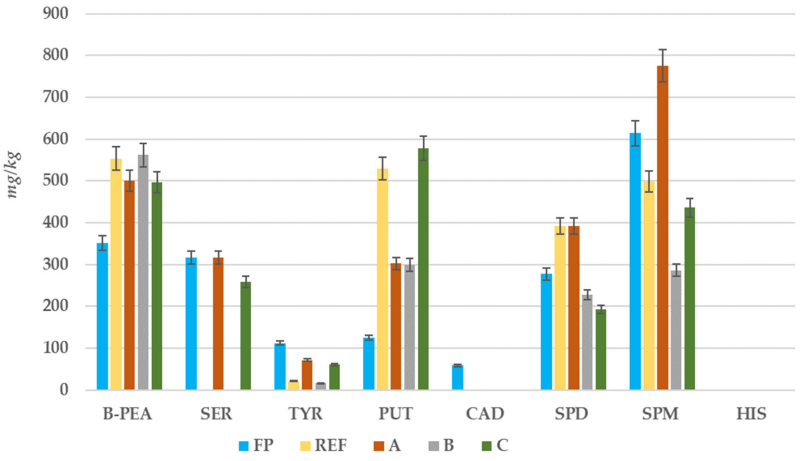


Figure 6. Biogenic amines content in fresh (t_0) and packaged pumpkin samples (t_{11}). FP: Fresh pumpkin (light blue trace); REF: polyethylene (yellow trace); A: biodegradable cellophane from regenerated cellulose (orange trace); B: biofilm obtained from maize starch, cassava, eucalyptus (grey trace); C: poly-lactate obtained from maize starch (green trace). β-PEA: β-phenylethylamine; PUT: putrescine; CAD: cadaverine; HIS: histamine; SER: serotonin; TYR: tyramine; SPD: spermidine; SPM: spermine.

All BAs investigated were found in pumpkin samples in a great variability, except for HIS, an amine with negative effects on health, which was not detected in any samples. Besides, TYR, another dangerous BA for human health was detected in all samples, and the fresh pumpkin presented the highest amount (112.24 ± 0.01 mg/kg). In plant-origin foods, tyramine content might be associated with microbial aminogenic activity [38]. While, during the storage period, TYR content was reduced in all type of packaged samples, especially in the packaging REF and B (20.68 ± 0.52 mg/kg, and 15.92 ± 0.90 mg/kg). Different authors observed that refrigeration temperatures (4–10 °C), delays or reduces the aminogenic potential of microorganisms, which could have been responsible for the formation of monoamines, such as TYR and HIS, during storage period [39,40].

3.3. Microbiological Analysis

Below are the results of the microbiological analysis together with mass loss, water activity, pH value, and carbon dioxide headspace concentration evaluation.

3.3.1. Mass Loss

Both moisture content and water activity are important in formulating products for safety and stability. Moisture content of fresh pumpkin was determined by weight loss upon drying equal to 95.58 ± 0.14% wet basis.

In Figure 7a, the pumpkin mass loss was plotted as a function of storage time for all the films investigated. The lower weight loss occurred for the biofilm C: its value remained constant at 4.58 ± 0.32% up to 11 days of storage at 5 °C. After 11 days, similar values were observed for biofilm B (7.24 ± 0.05%), and lower than those obtained for the polyethylene film. Only for biofilm A the weight loss was higher (15.36 ± 0.87%) than REF film.

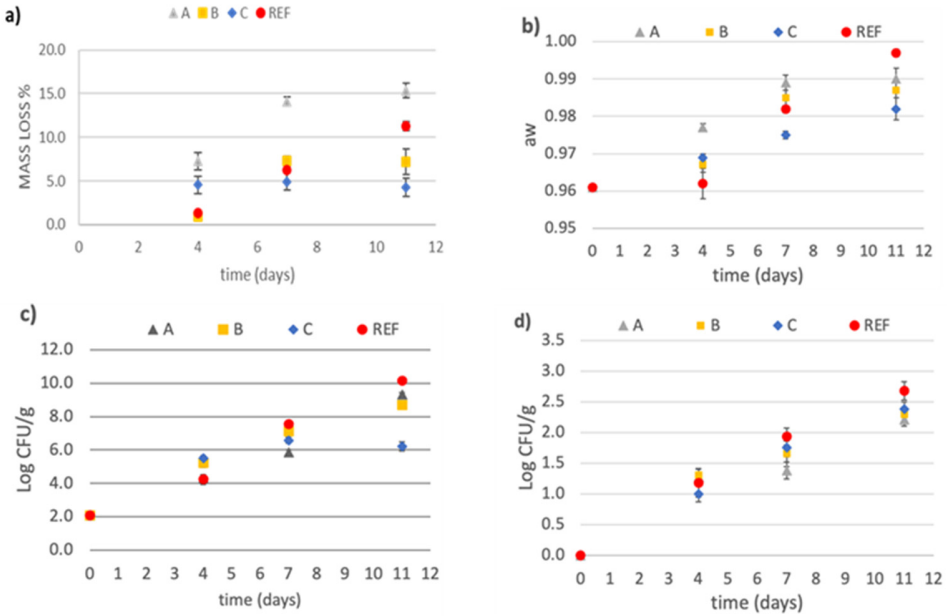


Figure 7. *Cont.*

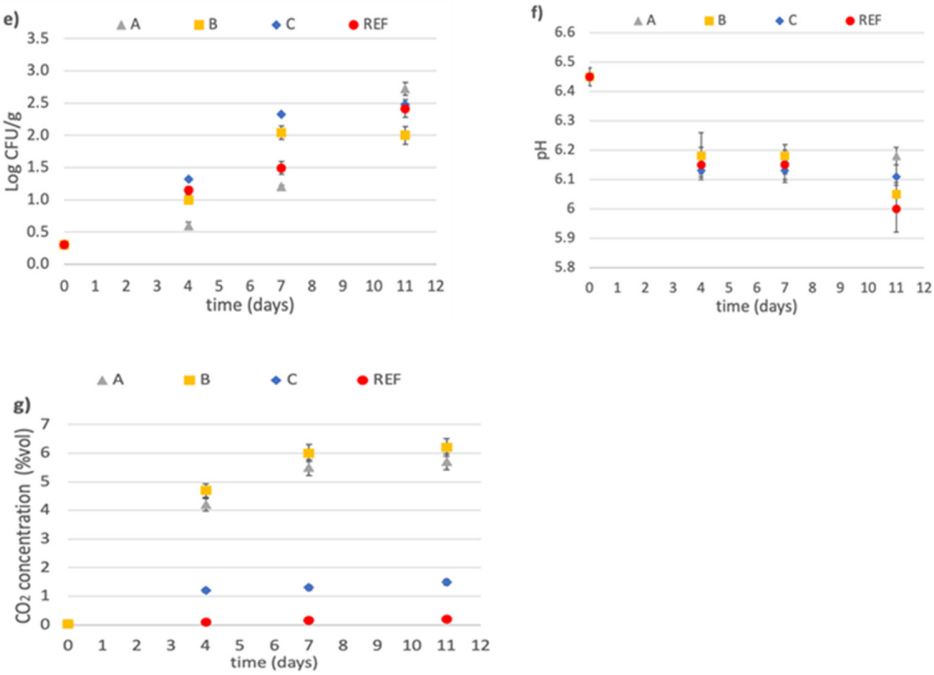


Figure 7. (**a**) Mass loss percentage, (**b**) water activity (a_w), (**c**) total microbial count, (**d**) lactic acid bacteria load, (**e**) yeasts and molds count, and (**f**) pH evaluated in fresh and packaged pumpkin samples, during shelf-life; (**g**) carbon dioxide concentration in headspace of pumpkin package in different films. REF: Polyethylene film; commercial biofilms: A, B and C.

3.3.2. Water Activity Evaluation

Water activity, a_W, is a measure of how much of that water is free, i.e., unbound, and thus available to microorganisms to use for growth. Therefore, it is important with regard to food safety. Microorganisms will not grow below a certain water activity level—$a_{W:}$ 0.90 for most pathogenic bacteria, 0.70 for spoilage molds, and 0.60 for all microorganisms. While temperature, pH, oxygen availability, and several other factors can influence whether an organism will grow in a product and at what rate, water activity is often the most important factor.

The water activity of fresh pumpkin was of 0.961 ± 0.001 and increased during the storage time for all the packages, especially for polyethylene film (Figure 8b), with values typical of high moisture foods in the range of 0.900 to 0.999 [41]. These conditions promoted the bacterial growth. At 11 days in the samples conserved in polyethylene film, the presence of water on the surface of the pumpkin cubes was observed (Figure 8). This caused deterioration and loss of product quality. On the contrary, the a_w measured in biofilm C reached a value of 0.982 ± 0.003, slightly lower than the other biofilms.

3.3.3. Microbiological Analysis

The total microbial count was plotted as a function of storage time in Figure 7c for all the tested packaging systems. The total count was below the threshold value (8.00 Log CFU/g) [42,43] up to 7 days of storage for all the films tested, and 11 days only for biofilm C, suggesting that microbial growth did not limit the shelf life of the pumpkin in

this time interval. The analysis of variance showed significant differences between samples at different times. In comparison, fresh cut pumpkins last for 2/3 days in refrigerators.



Figure 8. Pictures of pumpkins stored in biofilm C and in REF packaging at time 0 and after 11 days. (**a**) C at 0 days; (**b**) REF at 0 days; (**c**) C at 11 days; (**d**) REF at 11 days.

The lactic acid bacteria, and yeasts and molds counts were plotted as the function of storage time and reported in Figure 7d,e, respectively. In all samples, the values of microbial loads were always under the acceptability limit of 4.00 Log UFC/g [42] during the 11 days. The lactic acid bacteria load increased during the time up to 11 days; the values obtained with the different biofilms were similar, but lower than those obtained for polyethylene. It was probably the pH conditions at 4 days of storage (Figure 7f) that promoted the growth of lactic acid bacteria, which tolerate acidic conditions and are endogenous microbiota of the pumpkin [44].

For the yeasts and molds load (Figure 7e), an increasing value was observed in the first week which was maintained constant in the biofilm B up to 11 days (2.00 log CFU/g), but continuously increased in the other films. This behavior can be ascribed to the barrier effect of the biofilm B, higher than other films, and the consequent lower oxygen concentration in the package atmosphere, which avoids the growth of the aerobic organisms.

3.3.4. pH Value

pH values of pumpkin packaged in the four different films are shown in Figure 7f. The pH value of fresh pumpkin was 6.45 $\pm$ 0.03. In the first 4 days, a pH decreasing trend was observed for all the samples. The variations of pH among samples were not statistically significant up to 7 days. After 7 days, for biofilms C and A, the pH remained almost constant, 6.11 $\pm$ 0.02 and 6.18 $\pm$ 0.02, respectively.

The observed decreasing trend in the pH during the storage is a possible consequence of the accumulation of lactic acid produced in the lactic acid bacteria metabolism [45]. Moreover, the observed increase in CO_2 concentrations (Figure 7g) measured in the headspace of package can also contribute to a decrease in pH [46].

3.3.5. Carbon Dioxide Headspace Concentration

The headspace carbon dioxide concentration during shelf life of the packaged pumpkins is reported in Figure 7g. For both biofilms A and B, an increase was observed in carbon dioxide concentration from 0.04% to 5.70% vol in the first 4 days, and then it remained constant up to 11 days. This increase was higher than that measured for biofilm C and

polyethylene film, and in agreement with the measured CO_2 transmission rate obtained from the permeation tests.

3.3.6. Aroma Compounds

The aroma compounds of the pumpkin stored in biofilm C at the initial state (t = 0) and after 11 days were determined by headspace extraction followed by GC–MS analysis. The compounds were identified by comparison of mass spectra with NIST libraries. The elution order of the compounds agreed with the literature data [47].

Nineteen aroma compounds, including alcohols, esters, aldehydes and alkenes, were identified and reported in Table 5 with their retention times. The peak areas of the identified compounds were calculated by integration for both samples, and the difference in percentage between t = 0 and 11 days was valuated (ΔArea, %). After 11 days of storage in biofilm C, a general decreasing trend was observed in the aroma compounds with a maximum loss in hexanal.

Table 5. Volatile flavor compounds identified in pumpkin samples in C-PLA film and percentage variation of peak area recorded at 11 days at 5 °C.

Compound	Retention Time (min)	Δ Area, %
Ethanol	2.560	22.23 ± 0.12
Hexanal	3.951	−31.50 ± 1.23
Ethyl acetate	4.998	1.05 ± 0.24
1-Hexanol	5.347	−15.03 ± 2.87
1-Octen-3-ol	8.162	−14.00 ± 2.26
3-Hexen-1-ol	9.032	−11.71 ± 1.58
2 cyclohexen-1-ol-2.4.4-trimethyl	10.223	−5.10 ± 1.47
2-octenal	10.388	14.47 ± 1.51
iso-phorone	10.445	8.90 ± 1.04
Eucalyptol	10.765	−12.36 ± 1.78
6-nonenal	11.681	17.40 ± 1.24
2–6 nonadienal	13.123	−22.47 ± 0.60
6-nonen-1-ol	13.621	−27.11 ± 0.41
Decanal	14.616	13.49 ± 0.17
1-cyclohexene-1-carboxaldehyde-2,6,6-trimethyl	15.068	−6.32 ± 0.04
1-cyclohexene-1-acetaldehyde-2,6,6-trimethyl	16.081	−7.45 ± 0.02
Tetradecane	19.806	6.64 ± 0.05
Naftalene 1,4-dimethyl	20.281	−0.50 ± 0.06
3-buten-2-one,4-(2,6,6-trimethyl-1-cyclohexen-1-yl)	20.544	−26.14 ± 0.01
5,9-undecadien-2-one,6,10-dimethyl	21.071	−11.47 ± 0.09

3.4. T_1 and T_2 Relaxation Times of Fresh Pumpkin Packaged in Biofilm B and C by Portable TD-NMR

After 1 day in both packaging, the longitudinal magnetization decay of fresh packaged pumpkin showed a mono-exponential trend with a constant time of about 1.5–2 s. On the contrary, the transverse decay of the magnetization showed a bi-exponential trend due to the presence of water in two different proton domains. A long component of T_2 was found to be of about 35–40 ms affecting most of the spin protons (between 90–92% of the protons, depending on the sample), and a short component of T_2 of about 9–11 ms affecting the 8–10% of the protons. In food and plants cells, water molecules can experience particular physical and chemical environments due to various cell compartments and organelles, and by interacting with different macromolecules [48–51]. Consequently, the decay of magnetization is usually described by a multi-exponential function in which T_1 and T_2 show more than one component. However, water molecules or protons are in exchange between these compartments, and T_1 and T_2 relaxation times can be averaged by depending on both the exchange and the relaxation rates. In such a dynamic system, the direct assignment of relaxation times to particular compartments is a difficult task to be reached.

In fresh pumpkin, a single averaged T_1 value was found, indicating an exchange among water molecules from different compartments of pumpkin tissue. T_2 measurements yield a more detailed information on the partitioning of water in vegetable tissue than T_1. According to the literature, the two values of T_2 found in pumpkin may be categorized into "free water" mostly due to protons that shall be free-moving into vacuole, and "hindered water" possible due to water molecules that exchange across the other compartments such as cytoplasm, cell water/extracellular water.

During the storage period, both T_1 and T_2 were collected, see Figure 9. Because of the high variability of T_2 values collected during the storage time, and between each single pumpkin sample, the arithmetic mean of the relaxation times $<T_2>$ was calculated and compared to the T_1 values, and to the total proton density. The T_1 showed a slight increase during the storage period both in biofilm B and C. On the contrary, depending on the biofilm type, a different trend can be observed in the T_2. Biofilm B showed an initial elongation of the T_2, indicating a greater water mobility, followed by a decrease of T_2 value. In biofilm C, the T_2 values are rather stable expect to an initial shortening, indicating a slight decrease in the water mobility. Biofilm B and C showed a different behavior also in the proton density. For 7 days in both biofilms, the proton density was found to be quite constant. After the first week, the pumpkin in biofilm C showed a decrease in the proton density, whereas it showed a slow increase in biofilm B, possible indicating a higher water content at the sample surface.

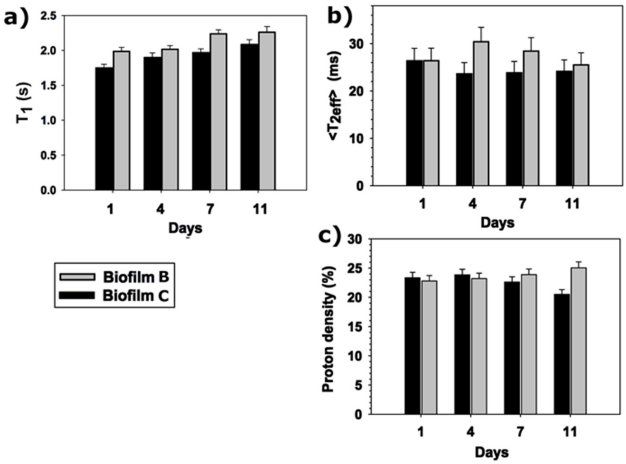


Figure 9. (**a**) Longitudinal relaxation times of packaged pumpkin; (**b**) mean transverse relaxation times and (**c**) proton density of packaged pumpkin in biofilm B and biofilm C as function of storage time.

These preliminary results indicate that biofilm B is less effective in preserving the mobility of water in fresh pumpkin compared to the biofilm C. However, many processes may affect the relaxation processes of water molecules in pumpkin during the storage, including the possible changes in cell membrane permeability, the diffusion of O_2 and CO_2 in the pumpkin tissue, and the variation in water activity and in food microstructure. Further investigations will be needed to correlate T_1, and T_2 values to other parameters used to assess the effectiveness of food packaging.

4. Conclusions

A comparison between different commercial biofilms for the preservation of pumpkin was reported. Among the films investigated, B film, based on Corn starch, cassava and eucalyptus, showed more ductile and deformable behavior, indicating better mechanical flexibility requirements for packaging applications, which is crucial to avoid breaking during processing and use. Moreover, biofilm B and A provided proper requirements in terms of oxygen and carbon dioxide transmission rate for food packaging applications.

Biofilm functionality was investigated through a multimethodological protocol consisting of chemical and microbiological analyses applied to fresh and packaged samples at different times.

Untargeted NMR spectroscopy allowed to obtain a comprehensive metabolite profiling of packaged and unpackaged pumpkin samples: organic acids, ammino acids, and sugars were identified and quantified showing a sucrose increase and a malic acid decrease in all the examined biofilms respect to FP; the other major sugars (fructose, glucose, galactose) levels remained quite steady in biofilms B and C; the most abundant amino acids (aspartate, glutamine, asparagine, arginine, pyro-glutamate) remained quite constant in biofilm A and decreased significantly in biofilm B.

Targeted methodologies allowed polyphenols, anthocyanins, carotenoids, volatile compounds, fatty acids and potential contaminants (i.e., biogenic amines as histamine, tyramine, etc.) to be tested and monitored.

In general, it is possible to note a trend of pigments decreasing in the packaged products compared to the fresh ones. After 11 days the content of total carotenoids tends to remain constant in the REF film compared to the fresh product, while it tends to decrease in biofilms A, B and especially in C.

After an 11-day period, A and C packaged samples showed the highest amount of total biogenic amines, especially for spermine, spermidine and putrescine, which could be considered as an index of food spoilage. Whereas the trends of TPC, antioxidant activities and TCC all decreased during the storage period, resulting in a significant loss of 56% for total phenolic content and 53% of total carotenoids content, especially in the REF and A packaged pumpkin samples. Regarding the chlorophylls content, the highest level of chlorophyll *a* and chlorophyll *b* was detected in the packaging A sample compared to the REF one.

Water activity was also measured to have indication of unbound water, which is thus available to microorganisms to use for growth. It is thus important with regard to food safety. The water activity of fresh pumpkin was of 0.961 ± 0.001 and increased during the storage time for all the packages, especially for polyethylene film, with water activity levels at which all microorganisms may grow.

Microbiological analyses were also carried out to assess the product quality. Microbiological analysis results suggest that microbial growth did not limit the shelf-life of the pumpkin up to 7 days for the biofilms A and B and up to 11 days for the biofilm C. The lactic acid bacteria and yeasts and molds counts increased but were for all packages below the acceptability limit during the 11 days. In particular, for biofilm B the yeasts and molds load increased in the first week and then was maintained constant up to 11 days. These are very promising results considering that fresh cut pumpkins last for 2/3 days in refrigerators.

The observed decreasing trend in the pH during the storage in all packages is a possible consequence of the accumulation of lactic acid produced in the lactic acid bacteria metabolism. Meanwhile, the lower increase of yeast and molds in biofilm B can be due to the observed increase in CO_2 concentrations measured in the headspace of package. In detail, for both biofilms A and B it was observed an increase in carbon dioxide concentration from 0.04% to 5.70% vol in the first 4 days, and then it remained constant up to 11 days. This increase is higher than that measured for biofilm C and polyethylene film. It is argued that the barrier effect of the biofilm B, higher than other films, and the consequent lower oxygen concentration in the package atmosphere, avoids the growth of the aerobic organisms.

In the case of samples packed with C film that turned to be the most promising packaging for microbiological point of view, the aroma analysis was also carried out by headspace extraction followed by GC–MS analysis. Nineteen compounds, including alcohols, esters, aldehydes and alkenes, were identified showing a general, but not too drastic, decreasing trend after 11 days.

The water dynamics were studied by time-domain NMR portable relaxometry. T_1 and T_2 relaxation times were measured in fresh and packaged samples pumpkin. A single averaged T_1 value was found in fresh and packaged pumpkin indicating an exchange among water molecules from different compartments of pumpkin tissue. During the whole period of preservation (11 days), T_1 showed a similar trend in both biofilm B and C with an increase of T_1 values during the storage period. In contrast, two values of T_2 were found in pumpkin possibly attributable to "free water" (water molecules free moving into vacuole), and "hindered water" (water molecules exchanging across the other compartments). The observed T_2 behavior in packaged sample during 11 days of conservation was depending on the biofilm type. Biofilm B showed an initial elongation of the T_2, indicating a greater water mobility, followed by a decrease of T_2 value. In biofilm C, the T_2 values show a stable trend after an initial shortening, indicating a slight decrease in the water mobility. In terms of water dynamics these preliminary results indicate that biofilm B is less effective in preserving the mobility of water in fresh pumpkin compared to the biofilm C.

Overall, results show that the biofilm C is the more suitable for applications of pumpkin in terms of the preservation of food quality properties (i.e., sugar content, organic acids, aminoacids, fatty acids in the organic fraction and aroma compounds). In contrast to A and B biofilms, pumpkin samples within C package resonances of propylene glycol (not present in the fresh pumpkin) were not observed.

Moreover, during the storage it was observed that in all the examined biofilms the total phenolic content and total carotenoids of pumpkin decreased compared to FP, but the biofilm C showed a better preservation of antioxidant activity.

Biofilm C also assured a low level of microorganisms' growth up to 11 days and a low amount of total biogenic amines which are an index of food spoilage.

In terms of water dynamics, the results of portable TD- NMR indicate that biofilm B is less effective in preserving the mobility of water in fresh pumpkin compared to the C biofilm.

Regarding mechanical properties, biofilm C has a good mechanical strength, but lower mechanical flexibility.

Supplementary Materials: The following are available online at https://www.mdpi.com/article/10.3390/foods10102440/s1, Figure S1: Bar charts of the amino acids identified and quantified (mg/10 g of DW ± SD) in the 1H NMR spectra of hydroalcoholic extracts of freeze-dried pumpkins samples. FP = Fresh pumpkin sample (time 0); A, B and C = commercial biofilms; REF = polyethylene film. Figure S2: Bar charts of the sugars (a), organic acids (b) and other metabolites (c) identified and quantified (mg/10 g of DW ± SD) in the 1H NMR spectra of hydroalcoholic extracts of pumpkins. FP = Fresh Pumpkin sample (time 0); A, B and C = commercial biofilms; REF= polyethylene film. Figure S3: Bar charts of the fatty acids identified and quantified (molar % ± SD) in the 1H NMR spectra of organic extracts of pumpkins. FP = Fresh Pumpkin sample (time 0); A, B and C = commercial biofilms; REF= polyethylene film. Table S1: Metabolites identified in the 600.13 MHz 1H NMR, 1H-1H TOCSY, 1H-13C HSQC, and 1H-13C HMBC spectra of Bligh–Dyer hydroalcoholic extracts of pumpkins in phosphate buffer/D2O acquired at 28 °C. Asterisks (*) indicate signals selected for integration. Table S2: Metabolites identified in the 600.13 MHz 1H NMR, 1H- 1H TOCSY, 1H-13C HSQC, and 1H-13C HMBC spectra of Bligh–Dyer organic extracts of pumpkins CDCl3/CD3OD (2:1 *v*/*v*) mixture acquired at 28 °C. Asterisks (*) indicate signals selected for integration. For the integration of total fatty acids (IFA) and total unsaturated fatty acids (IUFA), the region of 2.20–2.36 ppm and 5.25–5.40 ppm, respectively, were considered. Table S3: One-way analysis of variance (ANOVA) of the resulted NMR quantification of the polar metabolites. F and *p* values for the different examined packaging that reach a $p < 0.05$ respect to the FP were showed. Table S4: One-way analysis of variance (ANOVA) of the resulted NMR quantification of the fatty acids. F and *p* values for the different examined packaging that reach a $p < 0.05$ respect to the FP were showed.

Author Contributions: Conceptualization: L.M. and P.R.; Rheological methodology: M.V.; HR NMR methodology: G.D.M., A.P.S. and M.S. (Mattia Spano); TD-NMR methodology: V.D.T., A.S. and N.P.; Total carotenoids, chlorophylls a and b analyses: A.M.G.; Total polyphenols, antioxidant activity, bio-genic amines analyses: G.V., L.G., J.T., and S.A.P.; Microbiological analysis: P.D.M.; software: G.D.M.; validation: M.V., A.S. and M.S. (Matteo Sambucci); formal analysis: M.S. (Matteo Sambucci) and M.V.; investigation: G.D.M., M.V., J.T. and M.S. (Mattia Spano); writing and original draft preparation: G.D.M., P.D.M., M.S. (Matteo Sambucci), A.P.S., G.V., A.M.G., C.I., N.P. and V.D.T.; writing—review and editing: M.V., L.M. and P.R. All authors have read and agreed to the published version of the manuscript.

Funding: This work was realized with funds received from the following agencies: Ministero delle Politiche Agricole Alimentari e Forestali, progetto Ortopackhealth (n. 9049395, CUP: J56J200004200089; the Italian Ministry of Education, Universities, and Research—Dipartimenti di Eccellenza—L. 232/2016.

Data Availability Statement: The data presented in this study are available on request from the corresponding authors.

Acknowledgments: The authors wish to thank "Azienda Tenuta Agricola di Dragone Corsetti", for the samples.

Conflicts of Interest: The authors declare no conflict of interest. The funders had no role in the design of the study; in the collection, analyses, or interpretation of data; in the writing of the manuscript, or in the decision to publish the results.

References

1. Lima, K.S.; Sanches, A.G.; Cordeiro, C.A.M. Evalution of packaging in the conservation of minimally processed squash. *Appl. Res. Agrotechnol. Guarapuava-PR* **2019**, *12*, 75–84. [CrossRef]
2. Habibunnisa, R.; Baskaran, R.; Prasad, K.; Mysore, S. Storage behaviour of minimally processed pumpkin (Cucurbita maxima) under modified atmosphere packaging conditions. *Eur. Food Res. Technol.* **2001**, *212*, 165–169.
3. Lucera, A.; Simsek, F.; Conte, A.; Del Nobile, M.A. Minimally processed butternut squash shelf life. *J. Food Eng.* **2012**, *113*, 322–328. [CrossRef]
4. Ingallina, C.; Maccelli, A.; Spano, M.; Di Matteo, G.; Di Sotto, A.; Giusti, A.M.; Vinci, G.; Di Giacomo, S.; Rapa, M.; Ciano, S.; et al. Chemico-Biological Characterization of Torpedino Di Fondi® Tomato Fruits: A Comparison with San Marzano Cultivar at Two Ripeness Stages. *Antioxidants* **2020**, *9*, 1027. [CrossRef]
5. Mannina, L.; Sobolev, A.P.; Viel, S. Liquid state 1H high field NMR in food analysis. *Prog. Nucl. Magn. Reson. Spectrosc.* **2012**, *66*, 1–39. [CrossRef] [PubMed]
6. ISO 527-3:2008 Plastics—Determination of Tensile Properties Test Conditions for Films and Sheets. Available online: https://www.iso.org/standard/70307.html (accessed on 3 October 2021).
7. ISO 15105-2:2003 Plastics—Film and Sheeting—Determination of Gas-Transmission Rate—Part 2: Equal-Pressure Method. Available online: https://www.iso.org/standard/37514.html (accessed on 17 July 2021).
8. Ingallina, C.; Sobolev, A.P.; Circi, S.; Spano, M.; Fraschetti, C.; Filippi, A.; Di Sotto, A.; Di Giacomo, S.; Mazzoccanti, G.; Gasparrini, F.; et al. *Cannabis sativa* L. inflorescences from monoecious cultivars grown in central Italy: An untargeted chemical characterization from early flowering to ripening. *Molecules* **2020**, *25*, 1908. [CrossRef] [PubMed]
9. Sobolev, A.P.; Segre, A.; Lamanna, R. Proton high-field NMR study of tomato juice. *Magn. Reson. Chem.* **2003**, *41*, 237–245. [CrossRef]
10. Sobolev, A.P.; Mannina, L.; Capitani, D.; Sanzò, G.; Ingallina, C.; Botta, B.; Fornarini, S.; Crestoni, M.E.; Chiavarino, B.; Carradori, S.; et al. A multi-methodological approach in the study of Italian PDO "Cornetto di Pontecorvo" red sweet pepper. *Food Chem.* **2018**, *255*, 120–131. [CrossRef]
11. Lichtenthaler, H.K.; Buschmann, C. Chlorophylls and Carotenoids: Measurement and Characterization by UV-VIS Spectroscopy. *Curr. Protoc. Food Anal. Chem.* **2001**, *1*, F4.3.1–F4.3.8. [CrossRef]
12. Wellburn, A.R. The Spectral Determination of Chlorophylls a and b, as well as Total Carotenoids, Using Various Solvents with Spectrophotometers of Different Resolution. *J. Plant Physiol.* **1994**, *144*, 307–313. [CrossRef]
13. Rapa, M.; Ciano, S.; Gobbi, L.; Ruggieri, R.; Vinci, G. Quality and safety evaluation of new tomato cultivars. *Ital. J. Food Sci.* **2021**, *33*, 35–45. [CrossRef]
14. Rapa, M.; Ciano, S.; Ruggieri, R.; Vinci, G. Bioactive compounds in cherry tomatoes (*Solanum lycopersicum* var. Cerasiforme): Cultivation techniques classification by multivariate analysis. *Food Chem.* **2021**, *355*, 129630.
15. Preti, R.; Rapa, M.; Vinci, G. Effect of streaming and boiling on the antioxidant properties and biogenic amines content in green bean (*Phaselous vulgaris*) varieties of different colours. *J. Food Qual.* **2017**, 5329070. [CrossRef]
16. Liu, F.X.; Fu, S.F.; Bi, X.F.; Chen, F.; Liao, X.J.; Hu, X.S.; Wu, J.H. Physico-chemical and antioxidant properties of four mango (*Mangifera indica* L.) species in China. *Food Chem.* **2013**, *138*, 396–405. [CrossRef] [PubMed]
17. Blümich, B.; Perlo, J.; Casanova, F. Mobile single-sided NMR. *Progr. Nucl. Magn. Reson. Spectrosc.* **2008**, *52*, 197–269. [CrossRef]

18. Farrar, T.C.; Becker, E.D. *Pulse and Fourier Transform NMR*; Academic Press: New York, NY, USA, 1971.
19. Stark, N.M. Opportunities for cellulose nanomaterials in packaging films: A review and future trends. *J. Renew. Mater.* **2016**, *4*, 313–326. [CrossRef]
20. Siracusa, V.; Blanco, I.; Romani, S.; Tylewicz, U.; Rocculi, P.; Rosa, M.D. Poly (lactic acid)-modified films for food packaging application: Physical, mechanical, and barrier behavior. *J. Appl. Polym. Sci.* **2012**, *125* (Suppl. S2), E390–E401. [CrossRef]
21. Arrieta, M.P.; López, J.; Ferrándiz, S.; Peltzer, M.A. Characterization of PLA-limonene blends for food packaging applications. *Polym. Test.* **2013**, *32*, 760–768. [CrossRef]
22. Embleni, A. Modified atmosphere packaging and other active packaging systems for food, beverages and other fast-moving consumer goods. In *Trends in Packaging of Food, Beverages and Other Fast-Moving Consumer Goods (FMCG)*; Woodhead Publishing: Cambridge, UK, 2013; pp. 22–34. [CrossRef]
23. Siracusa, V. Food packaging permeability behaviour: A report. *Int. J. Polym. Sci.* **2012**, *2012*, 302029. [CrossRef]
24. Chinga-Carrasco, G.; Syverud, K. On the structure and oxygen transmission rate of biodegradable cellulose nanobarriers. *Nanoscale Res. Lett.* **2012**, *7*, 192. [CrossRef]
25. Available online: http://www.ecosign-project.eu/wp-content/uploads/2018/09/FOOD_UNIT11_IT_Lecture.pdf (accessed on 10 July 2021).
26. Piscopo, A.; Zappia, A.; De Bruno, A.; Pozzo, S.; Limbo, S.; Piergiovanni, L.; Poiana, M. Use of biodegradable materials as alternative packaging of typical Calabrian Provola cheese. *Food Packag. Shelf Life* **2019**, *21*, 100351. [CrossRef]
27. Peelman, N.; Ragaert, P.; Vandemoortele, A.; Verguldt, E.; Devlieghere, F.; De Meulenaer, B. Application of biobased materials for packing short, medium and long shelf life food products. In Proceedings of the 26th IAPRI symposium on Packaging 2013, Espoo, Finland, 10–13 June 2013; VTT Technical Research Centre of Finland; pp. 494–498.
28. Available online: https://thevacuumpouch.co.uk/wp-content/uploads/2021/03/VPC-Eco-Pouch-Spec-Sheet-50mu.pdf (accessed on 10 July 2021).
29. Panseri, S.; Martino, P.A.; Cagnardi, P.; Celano, G.; Tedesco, D.; Castrica, M.; Chiesa, L.M. Feasibility of biodegradable based packaging used for red meat storage during shelf-life: A pilot study. *Food Chem.* **2018**, *249*, 22–29. [CrossRef]
30. Tripathi, N.; Katiyar, V. PLA/functionalized-gum arabic based bionanocomposite films for high gas barrier applications. *J. Appl. Polym. Sci.* **2016**, 133–139. [CrossRef]
31. Ingallina, C.; Sobolev, A.P.; Circi, S.; Spano, M.; Giusti, A.M.; Mannina, L. New hybrid tomato cultivars: An NMR-based chemical characterization. *Appl. Sci.* **2020**, *10*, 1887. [CrossRef]
32. Sobolev, A.P.; Brosio, E.; Gianferri, R.; Segre, A.L. Metabolic profile of lettuce leaves by high-field NMR spectra. *Magn. Reson. Chem.* **2005**, *43*, 625–638. [CrossRef]
33. Schneider, T.; Butz, P.; Ludwig, H.; Tauscher, B. Pressure-induced formation of pyroglutamic acid from glutamine in neutral and alkaline solutions. *LWT—Food Sci. Technol.* **2003**, *36*, 365–367. [CrossRef]
34. Liang, T.; Wei, F.; Lu, Y.; Kodani, Y.; Nakada, M.; Miyakawa, T.; Tanokura, M. Comprehensive NMR analysis of compositional changes of black garlic during thermal processing. *J. Agric. Food Chem.* **2015**, *63*, 683–691. [CrossRef] [PubMed]
35. Prior, R.L.; Wu, X.; Schaich, K. Standardized Methods for the Determination of Antioxidant Capacity and Phenolics in Foods and Dietary Supplements. *J. Agric. Food Chem.* **2005**, *10*, 4290–4302. [CrossRef] [PubMed]
36. Kulczyński, B.; Gramza-Michałowska, A. The Profile of Secondary Metabolites and Other Bioactive Compounds in Cucurbita pepo L. and Cucurbita moschata Pumpkin Cultivars. *Molecules* **2019**, *24*, 2945. [CrossRef] [PubMed]
37. Can-Cauich, C.A.; Sauri-Duch, E.; Victor, M.M.; Betancur-Ancona, D.; Cuevas-Glory, L.F. Effect of extraction method and specie on the content of bioactive compounds and antioxidant activity of pumpkin oil from Yucatan, Mexico. *Food Chem.* **2019**, *285*, 186–193. [CrossRef] [PubMed]
38. Świder, O.; Roszko, M.L.; WòJcicki, M.; Szymczyk, K. Biogenic amines and free amino acids in traditional fermented vegetables –dietary risk evaluation. *J. Agric. Food Chem.* **2020**, *68*, 856–868. [CrossRef]
39. Sánchez-Pérez, S.; Comas-Basté, O.; Rabell-González, J.; Veciana-Nogués, M.; Latorre-Moratalla, M.; Vidal-Carou, M. Biogenic amines in plant-origin foods: Are they frequently underestimated in low-histamine diets? *Foods* **2018**, *7*, 205. [CrossRef] [PubMed]
40. Lavizzari, T.; Veciana-Nogués, M.T.; Weingart, O.; Bover-Cid, S.; Mariné-Font, A.; Vidal-Carou, M.C. Occurrence of biogenic amines and polyamines in spinach and changes during storage under refrigeration. *J. Agric. Food Chem.* **2007**, *55*, 9514–9519. [CrossRef] [PubMed]
41. Jay, J.M.; Golden, D.A.; Loessner, M.J. *Modern Food Microbiology*, 7th ed.; Springer: New York, NY, USA, 2005.
42. Ministere de l'Economie des Finances et du Budget. Marché consommation, Produits vegetaux prets a l'emploi dits de la 'IVemme Gamme': Guide de bonnes pratique hygieniques. *J. Off. De La Repub. Fr.* **1988**, *1621*, 1–29. Available online: https://catalogue.bnf.fr/ark:/12148/cb350090367 (accessed on 13 October 2021).
43. Corbo, M.R.; Altieri, C.; D'Amato, D.; Campaniello, D.; Del Nobile, M.A.; Sinigaglia, M. Effect of temperature on shelf life and microbial population of lightly processed cactus pear fruit. *Postharvest Biol. Technol.* **2004**, *31*, 93–104. [CrossRef]
44. Gutiérrez-López, G.; Barbosa-Canóvas, G.; WeltiChanes, J.; Parada-Arias, E. Use of Tapioca Starch Edible Film Containing Potassium Sorbate to Extend the Shelf Life of Minimally Processed Pumpkin. In *Food Engineering: Integrated Approaches*; Springer: New York, NY, USA, 2008; pp. 226–229.
45. Guzman Norleyn, M.N.; Orellana, L.E.; Obregon Quinones, L.G. Shelf Life of a Mixture of Pumpkin Puree (Cucurbita moschata) During Storage at 4 °C. *Adv. J. Food Sci. Technol.* **2018**, *15*, 152–157. [CrossRef]

46. Lucera, A.; Costa, C.; Mastromatteo, M.; Conte, A.; Del Nobile, M.A. Influence of different packaging systems on fresh-cut zucchini (*Cucurbita pepo*). *Innov. Food Sci. Emerg. Technol.* **2010**, *11*, 361–368. [CrossRef]
47. Zhou, C.L.; Mi, L.; Hu, X.Y.; Zhu, B.H. Evaluation of three pumpkin species: Correlation with physicochemical, antioxidant properties and classification using SPME-GC–MS and E-nose methods. *J. Food Sci. Technol.* **2017**, *54*, 3118–3131. [CrossRef]
48. Snaar, J.E.M.; Van As, H. Probing water compartments and membrane permeability in plantcells by ^{1}H NMR relaxation measurements. *Biophys. J.* **1992**, *63*, 1654–1658. [CrossRef]
49. Hills, B.P.; Remigereau, B. NMR studies of changes in subcellular water compartmentation in parenchyma apple tissue during drying and freezing. *Int. J. Food Sci. Tech.* **1997**, *32*, 51–61. [CrossRef]
50. Khan, M.I.H.; Wellard, R.M.; Nagy, S.A.; Joardder, M.U.H.; Karim, M.A. Investigation of bound and free water in plat-based food material using NMR T2 relaxometry. *Innov. Food Sci. Emerg.* **2016**, *38*, 252–261. [CrossRef]
51. Proietti, N.; Adiletta, G.; Russo, P.; Buonocore, R.; Mannina, L.; Crescitelli, V.; Capitani, D. Evolution of physicochemical properties of pear during drying by conventional techniques, portable-NMR, and modelling. *J. Food Eng.* **2018**, *230*, 82–98. [CrossRef]

Chapter 6: NMR characterization of foodstuff to find potential application for human health.

6.1. Introduction

Foods are complex systems containing macro- and micronutrients, as well as plant secondary metabolites, that can take part in biochemical processes and help to achieve or maintain a state of wellbeing.

To counteract a pathology the specific pharmacological interventions is clearly the only possibility. However, nutraceuticals, food supplements and functional foods are known to play an important role in the maintenance of human health and well-being. Today, there are a lot of efforts to deeply study foodstuff in order to find potential application for human health, since their safety based on their extensive use and knowledge. In fact, a substantial increase in the worldwide usage of vegetable extracts has been observed in recent decades, probably due to the increasing trend of consumer propensity towards preventive care through natural substances. Currently, more than 80% of world population is relying on the use of vegetable products for their primary health concerns.

In this scenario, it is important to start from the chemical characterization of these matrices to find their possible

application based on their composition and biological activities. When selected a foodstuff for a certain "health application", the NMR techniques with the metabolomic approach can be useful to quickly compare the profile of different food varieties and extraction methods, to identify bioactive molecules and to quantify a huge amounts of metabolites in a single analysis.

The related article to this chapter 6 is the following:

- Case study: Prunus domestica L. extracts as food supplement ingredients in the prevention of metabolic syndrome (Ullah et al., 2022)

References

Ullah, H., Sommella, E., Santarcangelo, C., Avino, D. D., Rossi, A., Dacrema, M., Di Minno, A., Di Matteo, G., Mannina, L., Campiglia, P., Magni, P., & Daglia, M. (2022). Hydroethanolic Extract of Prunus domestica L .: Metabolite Profiling and In Vitro Modulation of Molecular Mechanisms Associated to Cardiometabolic Diseases. *Nutrients*, *14*(2). https://doi.org/https://doi.org/10.3390/nu14020340

6.2. Case study: Prunus domestica L. extracts as food supplement ingredients in the prevention of metabolic syndrome

Prunus domestica L. (European plum) is known for its health benefits, which may be the result of its antioxidant potential and anti-inflammatory effects. Plums are fruits with low glycemic index, thus their consumption in adequate amount and on a regular basis could be a potential preventive strategy against metabolic syndrome.

In the present work, the hydroethanolic extracts of *P. domestica* L. subsp. Syriaca were characterize through NMR spectroscopy and UHPLC-HRMS analysis. Moreover, the in vitro modulatory effects of these extracts on the activity of a panel of enzymes differentially involved in the pathophysiology of metabolic syndrome and the modulation of proinflammatory mediator release were also carried out. The work could be the starting point to realize a new food supplements based on *P. domestica* extracts for the prevention of metabolic syndrome.

nutrients

MDPI

Article

Hydroethanolic Extract of *Prunus domestica* L.: Metabolite Profiling and In Vitro Modulation of Molecular Mechanisms Associated to Cardiometabolic Diseases

Hammad Ullah [1,†], Eduardo Sommella [2,†], Cristina Santarcangelo [1,†], Danilo D'Avino [1], Antonietta Rossi [1], Marco Dacrema [1], Alessandro Di Minno [1,3], Giacomo Di Matteo [4], Luisa Mannina [4], Pietro Campiglia [2,5], Paolo Magni [6,7,*] and Maria Daglia [1,8,*]

1 Department of Pharmacy, University of Napoli Federico II, Via D. Montesano 49, 80131 Naples, NA, Italy; hammad.ullah@unina.it (H.U.); cristina.santarcangelo@unina.it (C.S.); dani.davino@studenti.unina.it (D.D.); antrossi@unina.it (A.R.); marco.dacrema@unina.it (M.D.); alessandro.diminno@unina.it (A.D.M.)
2 Department of Pharmacy, University of Salerno, 84084 Fisciano, SA, Italy; esommella@unisa.it (E.S.); pcampiglia@unisa.it (P.C.)
3 CEINGE-Biotecnologie Avanzate, Via Gaetano Salvatore 486, 80145 Naples, NA, Italy
4 Department of Chemistry and Technology of Drugs, Sapienza University of Rome, Piazzale Aldo Moro 5, 00185 Rome, RM, Italy; giacomo.dimatteo@uniroma1.it (G.D.M.); luisa.mannina@uniroma1.it (L.M.)
5 European Biomedical Research Institute of Salerno, Via De Renzi 50, 84125 Salerno, SA, Italy
6 Department of Pharmacological and Biomolecular Sciences, Università degli Studi di Milano, 20133 Milan, MI, Italy
7 IRCCS MultiMedica, Sesto San Giovanni, 20099 Milan, MI, Italy
8 International Research Center for Food Nutrition and Safety, Jiangsu University, Zhenjiang 212013, China
* Correspondence: paolo.magni@unimi.it (P.M.); maria.daglia@unina.it (M.D.)
† These three authors share the first authorship.

check for updates

Citation: Ullah, H.; Sommella, E.; Santarcangelo, C.; D'Avino, D.; Rossi, A.; Dacrema, M.; Minno, A.D.; Di Matteo, G.; Mannina, L.; Campiglia, P.; et al. Hydroethanolic Extract of *Prunus domestica* L.: Metabolite Profiling and In Vitro Modulation of Molecular Mechanisms Associated to Cardiometabolic Diseases. *Nutrients* **2022**, *14*, 340. https://doi.org/10.3390/nu14020340

Academic Editors: Flávio Reis and Winston Craig

Received: 2 December 2021
Accepted: 10 January 2022
Published: 14 January 2022

Publisher's Note: MDPI stays neutral with regard to jurisdictional claims in published maps and institutional affiliations.

Copyright: © 2022 by the authors. Licensee MDPI, Basel, Switzerland. This article is an open access article distributed under the terms and conditions of the Creative Commons Attribution (CC BY) license (https://creativecommons.org/licenses/by/4.0/).

Abstract: High consumption of fruit and vegetables has an inverse association with cardiometabolic risk factors. This study aimed to chemically characterize the hydroethanolic extract of *P. domestica* subsp. syriaca fruit pulp and evaluate its inhibitory activity against metabolic enzymes and production of proinflammatory mediators. Ultra-high-performance liquid chromatography high-resolution mass spectrometry(UHPLC-HRMS) analysis showed the presence of hydroxycinnamic acids, flavanols, and glycoside flavonols, while nuclear magnetic resonance(NMR) analysis showed, among saccharides, an abundant presence of glucose. *P. domestica* fruit extract inhibited α-amylase, α-glucosidase, pancreatic lipase, and HMG CoA reductase enzyme activities, with IC50 values of 7.01 mg/mL, 6.4 mg/mL, 6.0 mg/mL, and 2.5 mg/mL, respectively. *P. domestica* fruit extract inhibited lipopolysaccharide-induced production of nitrite, interleukin-1 β and PGE_2 in activated J774 macrophages. The findings of the present study indicate that *P. domestica* fruit extracts positively modulate in vitro a series of molecular mechanisms involved in the pathophysiology of cardiometabolic diseases. Further research is necessary to better characterize these properties and their potential application for human health.

Keywords: *Prunus domestica* L.; chemical characterization; digestive enzyme inhibition; HMG-CoA reductase inhibition; anti-inflammatory activity

1. Introduction

The metabolic syndrome (MS), (also called as "Reaven's syndrome", "Syndrome X", "Insulin resistance syndrome", and "the deadly quartet") [1–3], is a cluster of pathological conditions including visceral obesity, hyperglycemia, or type 2 diabetes mellitus (T2DM), hypertension, and dyslipidemia, and is associated with higher cardiovascular disease (CVD) risk. A prolonged and persistent condition of MS may indeed silently progress towards serious complications such as T2DM, when not yet present, coronary heart disease (CHD), heart failure, stroke, cerebrovascular accidents (CVA) and stroke, as

well as liver complications (nonalcoholic fatty liver disease (NAFLD) and nonalcoholic steatohepatitis (NASH)) [4,5]. Adipose tissue dysfunction is commonly associated with MS, and dysregulated secretion of pro- or anti-inflammatory adipokines may contribute towards MS-induced complications [6,7]. Indeed, elevation of circulating tumor necrosis factor-alpha (TNF-α), interleukin-6 (IL-6), and C-reactive protein (CRP) are predominantly observed in patients with dysregulated metabolism [8,9].

Increasing age, sedentary lifestyle, female gender, lower socioeconomic class, positive family history, excessive alcohol intake, unhealthy dietary patterns, and intake of numerous medications are some of the risk factors associated with the prevalence of MS [10,11]. In this context, prevention is essential. Adopting a healthy lifestyle, aimed at weight normalization, increasing physical activity and adoption of a healthy diet, including increased intake of fruits, vegetables, and whole grains and a low consumption of salt, trans fatty acids, and cholesterol-rich foods [12]. However, as maintaining a healthy lifestyle on a daily basis is challenging, specific pharmacological interventions (i.e., statins, renin–angiotensin–aldosterone system (RAAS) inhibitors, and insulin-sensitizing agents, etc.) are often prescribed to target some selected pathogenetic mechanisms [12–14]. The main limitations of the pharmacological approach are the increase in the occurrence of adverse and side effects without beneficial effects on low-grade inflammation [15]. In this context, there is a growing attention to food supplements able to decrease the modifiable risk factors of MS [16]. One of the most widely used food supplement ingredients is red yeast rice (RYR), made by fermentation of rice with *Monascus purpureus*, producing monacolin K, which, in lactone form, is identical to lovastatin. RYR is used alone or in combination with plant extracts, coenzyme Q10, chromium, and vitamins. In 2018, the Panel on Food Additives and Nutrient Sources added to Food of the European Food Safety Authority (EFSA) has expressed doubts about the actual safety of RYR and concluded that EFSA is "unable to identify a dietary intake of monacolins from RYR that does not give rise to concerns about harmful effects to health" [17]. Besides RYR, other natural compounds could be effective strategies in the treatment of MS and prevention of MS progression towards serious complications through the inhibitory activity of the enzymes associated with carbohydrate/lipid digestion and cardiometabolic diseases (i.e., α-amylase, α-glucosidase, HMG-CoA reductase, and pancreatic lipase) [18–20].

Research analysis has shown an inverse association of increased consumption of fruits and vegetables with the incidence of MS risk factors [21,22], though there is a strong need to identify the specific effects of fruits and vegetables on the risk of MS development [23]. *Prunus domestica* L. (European plum) is known for its health benefits, which may be the result of its antioxidant potential and anti-inflammatory effects [24,25]. Plums are fruits with low glycemic index, thus their consumption in adequate amount and on a regular basis could be a potential preventive strategy against MS [25,26]. In addition, plums are commonly consumed when on a diet, they are commercially available at low cost, and as happens for many fruits, some of the plums produced are discarded as they do not reach the size requirements to be placed on the market.

As finding new food supplement ingredients which are safe and effective in the prevention of MS is an unmet need, especially after the concern of EFSA regarding RYR, the present study aimed to (1) characterize the metabolite profile of a hydroethanolic extract of *Prunus domestica*, using a multimethodological approach that was previously used for the study of different food matrices [27,28], and two analytical techniques, untargeted nuclear magnetic resonance (NMR) spectroscopy and targeted ultra-high-performance liquid chromatography high-resolution mass spectrometry (UHPLC-HRMS), and (2) study the in vitro modulatory effects of this extract on the activity of a panel of enzymes differentially involved in the pathophysiology of MS and the modulation of proinflammatory mediator release.

2. Materials and Methods

2.1. Preparation of Fruit Extracts

Two different varieties of *Prunus domestica* L. fruits (*P. domestica* L. subsp. domestica, also known as common plum, and *P. domestica* L. subsp. syriaca, also known as Mirabelle plum) (Figure 1) were collected from a local cultivator in the Campania Region (Italy) in October 2020. Eight fruits were sampled for each variety (Common Plum and Mirabelle Plum). All fruits were first washed with water to eliminate every dirt residue and were separated into skin and pulp. Both parts were cut into small pieces with a ceramic knife. To control oxidation during preparation, the samples were cut in an ice bath. The samples were freeze-dried and then ground into fine powder using a mortar and pestle. Aliquots of 1 and 2 g of the powdered skin and pulp were added to 20 mL and 40 mL of 50%, 70% and 99% ethanolic solution acidified with 0.1% HCL solution, respectively. The sample pH values were adjusted to 2.0, and the samples were subjected to magnetic stirring for 3 h at room temperature, followed by centrifugation at 6000 rpm for 10 min. The precipitate was separated from the supernatant. The same procedure was repeated three times and the supernatants of each sample were collected and filtered through Whatman cellulose filter paper. The filtrate was concentrated in a rotary evaporator at a temperature lower than 30 °C and submitted to freeze drying. The dry extracts were kept at −20 °C for subsequent determination of total polyphenol content, antioxidant activity, untargeted NMR spectroscopy, and targeted UHPLC-HRMS.



Figure 1. Plum varieties, collected from a local cultivator in the Campania Region (Italy). *P. domestica* L. subsp. domestica (Common plum) and *P. domestica* L. subsp. syriaca (Mirabelle plum).

Based on the assessment of total polyphenol content and antioxidant activity, the fruit pulp extract of *P. domestica* subsp. syriaca obtained with 50% hydroethanolic solution was selected, and in view of the high content of glucose and sucrose determined via NMR, it was subjected to the chemical precipitation of its sugars by treatment with absolute ethanol, followed by an ultra-freezing temperature. The organic solvent was removed under reduced pressure by a rotary evaporator and the dry extract obtained from the fruit pulp extract of *P. domestica* subsp. syriaca without sugars was kept at −20 °C for subsequent biological assays.

2.2. Total Phenolic Contents

Total phenolic content (TPC) was determined using a colorimetric assay (Folin-Ciocalteu method), following the same protocol as set by Singleton et al. with some modifications [29]. An aliquot (10 µL) of the samples (50 mg/mL) or gallic acid standard solutions (200–1000 µg/mL) was taken and added to 50 µL of Folin-Ciocalteu reagent. The solutions were cyclomixed for 4 min and added to 200 µL Na_2CO_3 (15%). The final volume was made to 1 mL with distilled water and allowed to incubate for 2 h at room temperature and under dark conditions. The solutions were read spectrophotometrically at 750 nm. Gallic acid was used as standard compound, with serial dilutions being prepared with

known concentrations ranging from 200 to 1000 µg/mL. The results were expressed as mg equivalent to gallic acid/g of extract on dry weight basis.

2.3. Antioxidant Assay

ABTS (2,2′-azino-bis3-ethylbenzthiazoline-6- sulfonic) assay was performed to evaluate the antioxidant potential of the fruit extracts following protocols set by Kok et al. with slight modifications [30]. The assay was conducted by placing 1 mL ABTS solution in a microtube, to which 10 µL of sample (50 mg/mL) or Trolox (0, 15, 20, 25, 30 and 35 µM) was added. The mixture was allowed to incubate for 2.5 min, and the absorbance was read at 734 nm. Thus, the antioxidant compounds present in the fruit extracts quench the color and produce a decoloration of the solution which is proportional to their antioxidant activity. The results were expressed as Trolox equivalent concentration (µM/g of extract on dry weight basis).

2.4. Metabolic Profiling of P. domestica Fruit Pulp Extract

The metabolic profiling of *P. domestica* fruit pulp extract was evaluated using UHPLC-HRMS and NMR analysis.

2.4.1. RP-UHPLC-HRMS Analysis

P. domestica fruit pulp extract was solubilized in methanol/water (50:50 *v/v*). The sample was then filtered through a cellulose acetate/cellulose nitrate mixed esters membrane (0.45 µm; Millipore Corporation, Billerica, MA, USA), and analyzed by RP-UHPLC-HRMS. UHPLC-HRMS analysis was performed on a Shimadzu Nexera UHPLC system, consisting of a CBM-20A controller, two LC-30AD dual-plunger parallel-flow pumps, a DGU-20 AR5 degasser, an SPD-M20A photo diode array detector (PDA), a CTO-20A column oven, and a SIL-30AC autosampler. The system was coupled online to a hybrid Ion trap Time of Flight Mass spectrometer (LCMS-IT-TOF, Shimadzu, Duisburg, F.R. Germany) equipped with an electrospray source (ESI). For RP-UHPLC analysis, a Kinetex Biphenyl 100 mm × 2.1 mm, 2.6 µm (L × I.D, particle size, Phenomenex®, Bologna, Italy) column was employed at a flow rate of 0.4 mL/min. The mobile phases consisted of (A) 0.1% CH_3COOH in H_2O and (B) ACN plus 0.1% CH_3COOH. Analysis was performed in gradient as follows: 0–20.0 min, 2–20% B; 20.01–22.0 min, 20.01–99% B; 99% B hold for 1 min; returning to initial conditions in 0.1 min. The column oven was set to 40 °C and 5 µL sample was injected. PDA detection parameters were sampling rate 12 Hz, time constant 0.160 s and chromatograms were extracted at 280 and 330 nm. LC data elaboration was performed by the LCMS solution® software (Version 3.50.346, Shimadzu, Duisburg, F.R. Germany). MS detection was performed in negative mode ionization as follows: curve desolvation line (CDL), 250 °C; Block Heater, 250 °C; Nebulizing and Drying gas, 1.5 and 10 L/min; ESI^- Capillary Voltage, −3.5 kV; MS range, m/z 150–1500; ion accumulation time, 30 ms; ion trap repeat, 3. MS/MS was performed in a data-dependent acquisition (DDA), precursor ions selection was based on the base peak chromatogram (BPC) intensity of 700,000. Collision-induced dissociation (CID), 50%, ion trap repeat. For analysis, the instrument was tuned using sodium trifluoroacetate (NaTFA). Metabolite annotation was based on accurate mass measurement, MS/MS fragmentation pattern and comparison within silico spectra with MS database searching [31,32]. "Formula Predictor" software (Shimadzu, Duisburg, F.R. Germany) was used for the prediction of the molecular formula using the following settings: maximum deviation from mass accuracy: 5 ppm, fragment ion information, and nitrogen rule.

2.4.2. NMR Analysis

P. domestica fruit pulp extract (500 mg) was solubilized in 10 mL of 400 mM phosphate buffer/D2O containing 3-(trimethylsilyl)-propionic-2,2,3,3-d4 acid sodium salt (TSPA), used as internal standard for quantitative measurements, and EDTA, used as a complexing agent for metal ions. Then, an aliquot of 0.7 mL was transferred in a 5 mm NMR tube. The NMR spectra were recorded at 25 °C on a JNM-ECZ 600R (JEOL Ltd., Tokyo, Japan) spectrometer

operating at the proton frequency of 600.17 MHz equipped with an autosampler and the SuperCOOL cryogenic probe (JEOL Ltd., Tokyo, Japan). The ^{1}H spectrum was acquired using a presaturation pulse sequence to suppress water signal, a 90° pulse of 12.8 µs and 65 K data points. All the NMR spectra were processed using the JEOL Delta v5.3.1. software (JEOL Ltd., Tokyo, Japan). The ^{1}H spectrum after Fourier transformation was manually phased, automatically base-corrected and referred to the β-glucose CH-1 signal set at 4.66 ppm. 2D NMR experiments, namely ^{1}H-^{1}H COSY, ^{1}H-^{1}H TOCSY,^{1}H-^{13}C HSQC and ^{1}H-13C HMBC, were performed using the following experimental conditions: ^{1}H-^{1}H COSY and ^{1}H-^{1}H TOCSY experiments were carried out with water presaturation during relaxation delay and 9 kHz of spectral width in both dimensions. ^{1}H-^{1}H COSY was acquired using 4 k × 256 points in F1 and F2, respectively, a relaxation delay of 2.5 s and 44 scans, whereas in the case of ^{1}H-^{1}H TOCSY experiment, 8 k × 256 points in F1 and F2 dimensions, respectively, a mixing time of 80 ms, a relaxation delay of 2 s and 52 scans were used. ^{1}H-^{13}C HSQC experiment was carried out using a 90° ^{1}H pulse of 12.8 µs and 90° ^{13}C pulse of 14.0 µs, a spectral width of 9 kHz and 33 kHz for the ^{1}H and ^{13}C dimensions, respectively, 8 k × 256 points, a relaxation delay of 2 s, 80 scans and a coupling constant 1JC–H of 150 Hz. ^{13}C spectra were referenced to the CH-1 resonance of β-glucose at 97.00 ppm. ^{1}H-13C HMBC experiment was carried out with 12.8 µs for ^{1}H and 14.0 µs for ^{13}C 90° pulse, a spectral width of 9 kHz and 38 kHz for the ^{1}H and ^{13}C dimensions, respectively, 8 k × 256 points in F1 and F2 dimensions, a relaxation delay of 2 s, a delay for the evolution of long-range couplings of 50 ms and 76 scans. In order to quantify the assigned compounds, the integral of the corresponding selected ^{1}H resonances were measured with respect to the integral of TSP methyl group signal normalized to 100. Quantitative results were expressed in µg/mg of dry weight.

2.5. Enzyme Inhibition Assays

Inhibition assays of different enzymes associated with the MS were performed as described below. The selected fruit extract (*P. domestica* subsp. syriaca fruit pulp), dissolved in 1% DMSO (SERVA Electrophoresis GmbH, Aurogene, Rome, Italy) and respective positive controls were tested using different concentrations to obtain half minimal inhibitory concentration (IC_{50}) for each enzyme, by nonlinear regression analysis. The absorbance of the sample blank (buffer in place of enzyme solution) and control (buffer in place of extract) was recorded as well. The inhibition of enzyme activity was calculated using following equation:

$$\% \text{ inhibition} = [(A_{\text{control}} - A_{\text{extract}})/A_{\text{control}}] \times 100$$

2.5.1. α-Amylase Inhibition Assay

The α-amylase from porcine pancreas inhibition assay was performed according to the protocol set up by Cicolari et al. with slight modifications [33]. The reaction mixture contained 20 µL fruit extract solution (concentration range: 0.0625–25 mg/mL) or acarbose (concentration range: 15.56–400 µg/mL), and 20 µL enzyme solution (0.5 mg/mL) in 0.02 M sodium phosphate buffer (pH 6.9 with 0.006 M NaCl), which was preincubated for 10 min at 25 °C. Then, 20 µL of 1% starch solution was added to each tube at timed intervals and allowed to incubate for 10 min at 25 °C. The reaction was stopped by the addition of 40 µL color reagent (DNSA). The test tubes were incubated in a boiling water bath for 10 min, and then cooled to room temperature. Finally, 600 µL of bidistilled water was added to dilute the reaction mixture and the absorbance was read at 540 nm using a microplate reader.

2.5.2. α-Glucosidase Inhibition Assay

The α-glucosidase from *Saccharomyces cerevisiae* inhibition assay was performed according to the protocols set by Cicolari et al. with slight modifications [33]. The reaction mixture containing 50 µL fruit extract solution (concentration range: 0.0313–25 mg/mL) or acarbose (concentration range: 15.56–900 µg/mL), and 100 µL enzyme solution (1 unit/mL) in 0.1 M phosphate buffer (pH 6.9), was incubated in a 96-well plate for 10 min at 25 °C.

After preincubation, 50 µL of 0.1 M phosphate buffer (pH 6.9) solution containing 5 mM p-nitrophenyl-α-D-glucopyranoside was added to each well at timed intervals, and was incubated for 5 min at 25 °C. The absorbance was read at 405 nm using a microplate reader.

2.5.3. HMG-CoA Reductase Inhibition Assay

The assay was conducted according to the manufacturer's protocol (Sigma-Aldrich). The assay was conducted by placing 910 µL phosphate buffer with 5 µL fruit extract (concentration range: 0.0625–30 mg/mL) or 5 µL pravastatin (concentration range: 18.75–300 µM) into microtubes; 20 µL of NADPH and 60 µL of HMG-CoA reductase substrate were then added. The analysis was initiated (time 0) by the addition of 5 µL of HMG-CoA reductase, and incubated at 37 °C. The rate of NADPH consumed was monitored every 15 s for up to 5 min by reading the decrease in absorbance at 340 nm, using the microplate reader.

2.5.4. Pancreatic Lipase Inhibition Assay

Porcine Pancreatic Lipase (PPL) inhibition assay was conducted according to the protocols reported by Nwakiban et al. (2019) [34]. The assay was conducted by mixing 30 µL PPL (2.5 mg/mL in 10 mM MOPS and 1 mM EDTA, pH 6.8) with 850 µL Tris buffer (100 mM Tris-HCl and 5 mM CaCl2, pH 7.0). Then, either 100 µL of fruit extract (concentration range: 1.30–12.5 mg/mL) or orlistat (concentration range: 1–500 µg/mL) was added to the mixture and incubated for at 37 °C for 15 min, followed by the addition of 10 µL substrate (10 mM p-NPB in dimethyl formamide). The mixtures were incubated again at 37 °C for 30 min. The absorbance was read at 405 nm using a microplate reader, to determine the lipase activity by quantifying the hydrolysis of p-NPB to p-nitrophenol.

2.6. Cell Culture

Murine monocyte/macrophage J774 cell line was obtained from the American Type Culture Collection (ATTC TIB 67). The cell line was grown in adhesion in Dulbecco's modified Eagles medium (DMEM) supplemented with glutamine (2 mM, Aurogene Rome, Italy) Hepes (25 mM, Aurogene Rome, Italy) penicillin (100 U/mL, Aurogene Rome, Italy), streptomycin (100 µg/mL, Aurogene Rome, Italy), fetal bovine serum (FBS, 10%, Aurogene Rome, Italy) and sodium pyruvate (1.2%, Aurogene Rome, Italy) (DMEM completed). The cells were plated at a density of ~1×10^6 cells in 75 cm^2 culture flasks and maintained at 37 °C under 5% CO_2 in a humidified incubator until 90% confluence. The culture medium was changed every 2 days. Before a confluent monolayer appeared, sub-culturing cell process was carried out. *P. domestica* subsp. syriaca fruit pulp extract was solubilized in DMSO at the concentration of 200 mg/mL (stock solution). Then, it was diluted in DMSO to obtain solutions at the concentrations of 150 mg/mL, 100 mg/mL, 20 mg/mL and 2 mg/mL. Cells were plated to a seeding density of 5.0×10^5 in 24 multiwell plates. After 2 h of adhesion, cells were pretreated (for 2 h) with increasing concentration of *P. domestica* subsp. syriaca fruit pulp extract (5 µL of 2, 20, 100, 150 and 200 mg/mL, which correspond to a final concentration in the well (1 mL) of 0.01, 0.1, 0.5, 0.75 and 1 mg/mL). After the preincubation, macrophages were stimulated with or without LPS from *Escherichia coli*, Serotype 0111:B4, (10 µg/mL; 100 µL of solution 100 µg/mL in DMEM completed with FBS, Sigma Aldrich, Milan, Italy) for 24 h [35].

2.6.1. Nitrite, IL-1β and PGE_2 Assay

After 24 h of incubation, the supernatants were collected for the nitrite, IL-1β and PGE_2 measurement. The nitrite concentration in the samples was measured by the Griess reaction, by adding 100 µL of Griess reagent (0.1% naphthylethylenediamide dihydrochloride in H_2O and 1% sulphanilamide in 5% concentrated H_2PO_4; vol. 1:1; Sigma Aldrich, Milan, Italy) to 100 µL samples. The optical density at 540 nm (OD_{540}) was measured immediately after Griess reagent addition, using ELISA microplate reader (Thermo Scientific, Multiskan GO, Milan Italy). Nitrite concentration was calculated by comparison with OD_{540} of standard solutions of sodium nitrite prepared in culture medium. IL-1β (R&D

Systems, Aurogene, Rome, Italy) and PGE_2 (Cayman Chemical, BertinPharma, Montigny Le Bretonneux, France) levels were measured with commercially available ELISA kits according to the manufacturer's instructions.

2.6.2. Cell Viability

Cell respiration, an indicator of cell viability, was assessed by the mitochondrial-dependent reduction of 3-(4,5-dimethylthiazol-2-yl)-2,5-diphenyltetrazolium bromide (MTT; Sigma Aldrich, Milan, Italy) to formazan. Cells were plated to a seeding density of 1.0×10^5 in 96 multiwell plates. After stimulation with LPS in the absence or presence of test compounds for 24 h, cells were incubated in 96-well plates with MTT (0.2 mg/mL), for 1 h. Culture medium was removed by aspiration and the cells were lysed in DMSO (0.1 mL). The extent of reduction of MTT to formazan within cells was quantified by the measurement of OD_{550}.

2.7. Statistical Analysis

Results from at least three independent experiments carried out in triplicate for TPC and antioxidant assay, and two independent experiments carried out in duplicate for enzyme inhibitory activities of the *P. domestica* fruit extract, were expressed as mean (±SD) values. Student's t-test was used to determine the level of significance and statistical differences among variables using GraphPad prism. For the in vitro anti-inflammatory studies, the results were expressed as mean ± standard error (SEM) of the mean of n observations, where n represents the number of experiments performed in different days. Triplicate wells were used for the various treatment conditions. The results were analyzed by one-way ANOVA followed by a Bonferroni post hoc test for multiple comparisons. A p-value less than 0.05 was considered significant. All graphs were generated using GraphPad prism, version 5 (GraphPad, San Diego, CA, USA).

3. Results

3.1. Description of P. domestica Extracts

Two different varieties of *Prunus domestica* L. fruits (*P. domestica* subsp. domestica and *P. domestica* subsp. syriaca), which were separated into pulp and skin, were submitted to three different hydroethanolic extractions to evaluate the effects of ethanol percentage in the extraction solvent on the total polyphenol content and antioxidant activity. The extraction yield calculated for the freeze-dried fruit skin ranged from 37 to 43% regardless of the *Prunus* variety. On the contrary, the extraction yield calculated for the freeze-dried fruit pulp ranged from 59.5 to 67% and from 45 to 49%, for subsp. domestica and subsp. syriaca, respectively (Table 1).

Table 1. Fruit samples and yield of extracts.

Prunus Variety	Common Name	Skin Color	Fruit Part Extracted	Ethanol (%)	Dry Extract (g/g) [1]	Extraction Yield (%)
P. domestica subsp. domestica	Common plum	Purple	Skin	99	0.42	42.0
				70	0.39	39.0
				50	0.38	38.0
			Pulp	99	0.60	59.5
				70	0.63	63.0
				50	0.67	67.0
P. domestica subsp. syriaca	Mirabelle plum	Yellow	Skin	99	0.37	37.0
				70	0.41	41.0
				50	0.43	43.0
			Pulp	99	0.45	45.0
				70	0.46	46.0
				50	0.49	49.0

[1] The weight of dry extract obtained in grams per gram of sample used for extraction.

3.2. Total Phenolic Contents and In Vitro Antioxidant Activity

A total of 12 hydroethanolic extracts were evaluated for their total phenolic content (TPC) and in vitro antioxidant activity (Table 2). The pulp of *P. domestica* subsp. syriaca extracted with 50% ethanol showed the highest TPC (12.9 mg GAE/g on dry weight basis), followed by fruit skin of *P. domestica* L. subsp. domestica extracted with 70% ethanol containing 12.8 mg GAE/g on dry weight basis. Overall, the fruit extracts extracted with 99% of ethanol exhibited relatively less phenolics, with fruit pulp of *P. domestica* subsp. syriaca showing the lowest content of total phenolics (6.5 mg GAE/g on dry weight basis). In general, fruit skin showed the highest antioxidant activity with fruit skin of *P. domestica* L. subsp. domestica (extracted with 50% ethanol) showing a Trolox equivalent concentration of 1944.1 µM/g, while fruit pulp of *P. domestica* subsp. syriaca (extracted with 99% ethanol) showed the lowest Trolox equivalent concentration of 585.5 µM/g. On the basis of the higher polyphenol content, to which the inhibitory activity of the enzymes involved in MS is generally ascribed [29], the good antioxidant activity, the higher yield (49%), and the lower percentage of ethanol used as extraction solvent (50%), the *P. domestica* subsp. syriaca fruit pulp extract obtained with 50% hydroethanolic solution was selected for the subsequent chemical characterization.

Table 2. Total phenolic content and Trolox equivalent concentration of the extracts obtained from the two varieties of *P. domestica*.

Prunus Variety	Fruit Part Extracted (Ethanol %)	TPC (GAE/g on Dry Weight Basis)	Trolox Equivalent Concentration (µM/g on Dry Weight Basis)
P. domestica subsp. domestica	skin (99%)	9.1 ± 1.0	1282.4 ± 84.1 [a]
	skin (70%)	12.8 ± 0.9 [a]	1826.2 ± 216.4
	skin (50%)	11.0 ± 0.6 [b]	1944.1 ± 138.1 [b]
	pulp (99%)	7.2 ± 1.0	630.5 ± 44.1 [a]
	pulp (70%)	11.3 ± 0.2 [a]	1611.9 ± 289.5
	pulp (50%)	9.7 ± 0.2 [b]	1290.7 ± 155.5 [b]
P. domestica subsp. syriaca	skin (99%)	7.0 ± 0.2	708.0 ± 25.1
	skin (70%)	11.2 ± 1.4	1597.4 ± 88.2 [c]
	skin (50%)	7.9 ± 0.8 [c]	1602.1 ± 368.1
	pulp (99%)	6.5 ± 0.4	578.5 ± 53.5
	pulp (70%)	10.0 ± 0.9	727.7 ± 43.9 [c]
	pulp (50%)	12.9 ± 1.7 [c]	1119.4 ± 93.1

Data are expressed as mean ± SD ($n = 3$). The assigned values of different letters in a column show significant difference among the mean values ($p < 0.05$); TPC, Total phenolic content.

Based on the assessment of total polyphenol content and antioxidant activity, on the higher yield (49%), and the lower percentage of ethanol used as extraction solvent (50%), the fruit pulp extract of *P. domestica* subsp. syriaca obtained with 50% hydroethanolic solution was selected, and in view of the high content of glucose and sucrose determined via NMR, it was subjected to the chemical precipitation of sugars by treatment with absolute ethanol, followed by ultra-freezing temperature. The organic solvent was removed under reduced pressure by a rotary evaporator, and the dry extract obtained from the fruit pulp extract of *P. domestica* subsp. syriaca without sugars was kept at −20 °C for subsequent biological assays.

3.3. UHPLC-HRMS Profile

The list of the metabolites occurring in the hydroethanolic (50%) extract obtained from *P. domestica* subsp. syriaca fruit pulp, with tentative identification based on accurate mass and fragmentation pattern compared against reference MS/MS spectra reported in silico and in previous literature, is reported in Table 3. In particular, 23 compounds belonging to different classes (organic and hydroxycinnamic acids and flavonoids, both aglycone and glycosylated) were identified in the extract (Figure 2). Hydroxycinnamic and quinic

acid derivatives were the most abundant compounds, retaining the 46.7% of total peak area, followed by procyanidins, in particular dimer (17%), monomers (13.10%) and trimers (6.9%). Lastly, flavonol glycosides represented the remaining 7.9%. (Table 4)

Table 3. Identified compounds in *P. domestica* subsp. syriaca fruit pulp extract according to the retention time (RT), compound, *m/z* and MS/MS, molecular formula, and mass accuracy, reported as part per million (ppm) error.

Peak	r_t	Compound	$[M-H]^-$	MS/MS	Molecular Formula	Error (ppm)
1	0.60	Citric acid	191.0227	111.0103; 173.0103	$C_6H_8O_7$	1.57
2	3.12	Chlorogenic acid	353.0874	173.0489; 191.0576	$C_{16}H_{18}O_9$	−1.13
3	4.68	Coumaroylquinic acid Isomer	337.0945	163.0417; 119.0558	$C_{16}H_{18}O_8$	4.75
4	5.45	Catechin	289.0729	245.0816	$C_{15}H_{14}O_6$	3.81
5	6.08	(+) Epicatechin dimer B type	577.1328	407.0787; 289.0728	$C_{30}H_{26}O_{12}$	−4.16
6	6.50	Feruloylquinic acid	367.1053	193.0531; 134.0390	$C_{17}H_{20}O_9$	4.90
7	6.70	Coumaroylquinic acid isomer	337.0928	163.0447; 191.0594	$C_{16}H_{18}O_8$	1.19
8	7.20	Coumaroylquinic acid isomer	337.0952	173.0458; 163.0418	$C_{16}H_{18}O_8$	2.30
9	8.12	(+) Epicatechin	289.0735	245.0816	$C_{15}H_{14}O_6$	5.88
10	8.48	(+) Epicatechin trimer B type	865.1979	407.0790; 287.0569; 577.1344	$C_{45}H_{38}O_{18}$	3.40
11	8.86	(+) Epicatechin dimer B type isomer	577.1344	407.0790; 289.0732	$C_{30}H_{26}O_{12}$	−1.39
12	9.70	Quinic acid derivative	393.1777	149.0465; 191.0561	$C_{17}H_{30}O_{10}$	2.80
13	10.50	Feruloyl-coumaroylquinic acid derivative	559.1665	337.0947; 193.0514	$C_{24}H_{32}O_{15}$	−0.54
14	11.29	Feruloyl-coumaroylquinic acid derivative	559.1670	337.0949; 193.0510	$C_{24}H_{32}O_{15}$	−0.50
15	12.19	Feruloyl-coumaroylquinic acid derivative	559.1677	337.0946; 193.0514	$C_{24}H_{32}O_{15}$	1.61
16	12.32	(+) Epicatechin dimer B type isomer	577.1358	407.0831; 289.0742	$C_{30}H_{26}O_{12}$	1.04
17	12.74	(+) Epicatechin B type trimer isomer	865.2015	407.0778; 287.0569; 577.1344; 543.0905	$C_{45}H_{38}O_{18}$	3.47
18	13.20	Quercetin-rutinoside	609.1477	301.0351; 271.0254; 255.0320	$C_{27}H_{30}O_{16}$	3.47
19	13.48	(+) Epicatechin A type trimer	863.1823	575.1180; 423.0711; 285.0393	$C_{45}H_{36}O_{18}$	−0.20
20	14.04	(+) Epicatechin A type trimer isomer	863.1828	575.1180; 423.0711; 285.0393	$C_{45}H_{36}O_{18}$	−0.12
21	14.82	(+) Epicatechin A type dimer	575.1197	423.0746; 285.0395	$C_{30}H_{24}O_{12}$	1.22
22	15.75	Quercetin-rhamnoside	447.0924	301.0371; 255.	$C_{21}H_{20}O_{11}$	−0.9
23	16.52	(+) Epicatechin A type dimer isomer	575.1187	423.0716; 285.0398	$C_{30}H_{24}O_{12}$	−1.39

Table 4. Retention time (min) and peak area, expressed as percentage of total area of the identified compounds in *P. domestica* subsp. syriaca fruit pulp extract.

Peak	Compound	Retention Time	Area %
1	Citric acid	0.6	7.92
2	Chlorogenic acid	3.12	15.43
3	Coumaroylquinic acid Isomer	4.68	0.74
4	Catechin	5.45	8.61
5	(+) Epicatechin dimer B type	6.08	5.74
6	Feruloylquinic acid	6.5	0.21
7	Coumaroylquinic acid isomer	6.7	0.39
8	Coumaroylquinic acid isomer	7.2	2.42
9	(+) Epicatechin	8.12	4.54

Table 4. *Cont.*

Peak	Compound	Retention Time	Area %
10	(+) Epicatechin trimer B type	8.48	0.24
11	(+) Epicatechin dimer B type isomer	8.86	5.47
12	Quinic acid derivative	9.7	1.98
13	Feruloyl-coumaroylquinic acid derivative	10.5	3.01
14	Feruloyl-coumaroylquinic acid derivative	11.29	19.55
15	Feruloyl-coumaroylquinic acid derivative	12.19	1.49
16	Feruloyl-coumaroylquinic acid derivative	12.32	1.47
17	(+) Epicatechin dimer B type isomer	12.74	6.27
18	(+) Epicatechin B type trimer isomer	13.2	0.79
19	Quercetin-rutinoside	13.48	3.20
20	(+) Epicatechin A type trimer	14.04	4.05
21	(+) Epicatechin A type trimer isomer	14.82	1.81
22	(+) Epicatechin A type dimer	15.75	0.16
23	Quercetin-rhamnoside	16.52	4.50

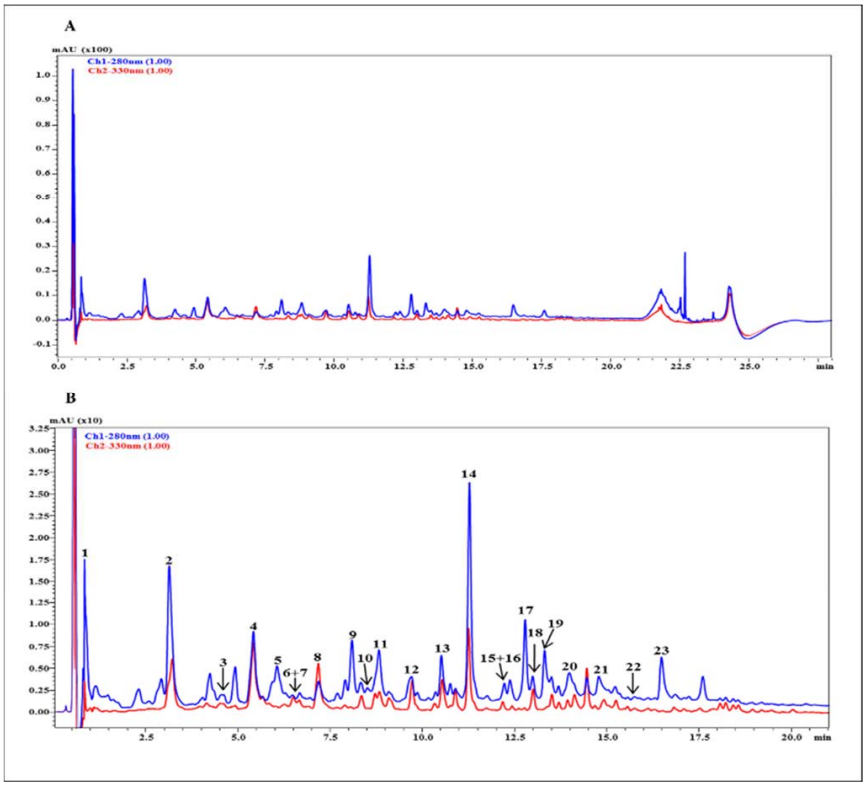


Figure 2. RP-UHPLC chromatograms of *P. domestica* subsp. syriaca fruit pulp extract with UV detection registered at λ 280 nm and 330 nm (**A**), and chromatogram expansion with corresponding peak HRMS assignment (**B**).

3.4. NMR Analysis and Quantification of Sugar and Organic Acid Contents

The ^{1}H spectrum of the *P. domestica* subsp. syriaca fruit pulp extract dissolved in phosphate buffer/D2O shows the presence of glucose, sucrose, xylose and citric, malic and quinic acids. The ^{1}H spectral assignment was obtained by literature data regarding other fruits [36,37] and 2D NMR experiments [38]. The integrals of selected signals due to sugars, namely xylose, glucose, and sucrose at 5.20 ppm, 5.25 ppm, and 5.42 ppm, respectively, and to organic acids, namely citric, malic and quinic acids at 1.88 ppm, 2.54 ppm, and 4.30 ppm, respectively, were used for compound quantification (Table 5). The ^{1}H NMR spectrum with the selected signals used for the quantification of metabolites (Figure 3) and the compound assignments table (Table S1) was also reported. In the case of some compounds, only a partial assignment was obtained due to low concentration of the compound. However, the partial assignment included diagnostic signals that allowed the identification of the reported compounds. Glucose and malic acid turned out to be the sugar and the organic acid, respectively, present in major amounts.

Table 5. Compounds identified in the ^{1}H NMR spectrum of *P. domestica* subsp. syriaca fruit pulp extract dissolved in phosphate buffer/D2O and the corresponding chemical shift signals (ppm) used in the integration process. The compound amounts in μg/mg of dry weight are also reported.

Compound	Chemical Shift (ppm) of Selected Resonances Used for Quantification	μg/mg Dry Weight
Quinic acid	1.88 (CH2-1)	7.50
Citric acid	2.54 (α,γ-CH)	0.84
Malic acid	4.30 (α-CH)	38.49
Xylose	5.20 (CH-1)	0.56
Glucose	5.25 (CH-1)	106.59
Sucrose	5.42 (CH-1)	31.59

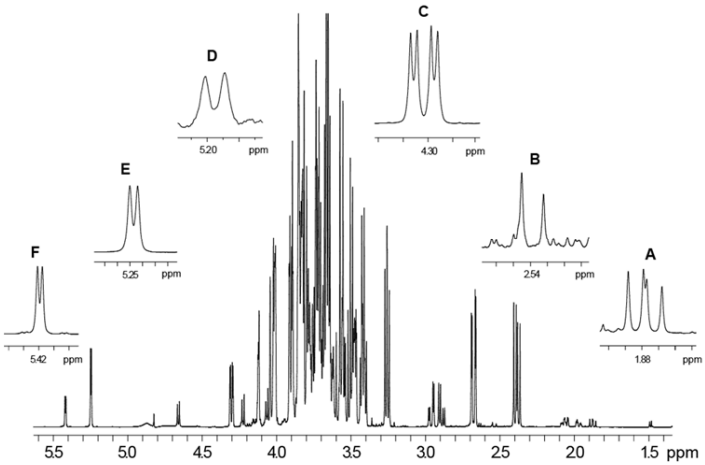


Figure 3. ^{1}H NMR spectrum of *P. domestica* subsp. syriaca fruit pulp extract. Quantified selected NMR signals are reported in expanded regions. (**A**) CH2-1 protons of quinic acid (1.88 ppm), (**B**) α,γ-CH protons of citric acid (2.54 ppm), (**C**) α-CH proton of malic acid (4.30 ppm), (**D**) CH-1 proton of in α-xylose (5.20 ppm), (**E**) CH-1 proton of α-glucose (5.25 ppm), (**F**) CH-1 proton of sucrose (5.42 ppm).

3.5. Preparation of *P. domestica* Fruit Extract without Sugar

In view of the high sugar content (about 14% of the whole extract) of *P. domestica* subsp. syriaca fruit pulp crude extract, it was subjected to chemical precipitation of sugar contents by treatment with absolute ethanol, supported by ultra-freezing temperature. The percent extraction yield following sugar precipitation was 41.8%.

3.6. Effect of *P. domestica* Subsp. Syriaca Fruit Pulp Extract on Enzyme Activities

P. domestica subsp. syriaca fruit pulp extract with reduced content of sugars was used for enzyme inhibition activities, with the aim of reducing the substances that may interfere with the enzyme inhibition activities of the vegetable extract. The inhibition of the enzyme activities performed by the extract at increasing concentration and the IC50 values for each enzyme, calculated with the nonlinear regression analysis, have been illustrated in Figure 4.

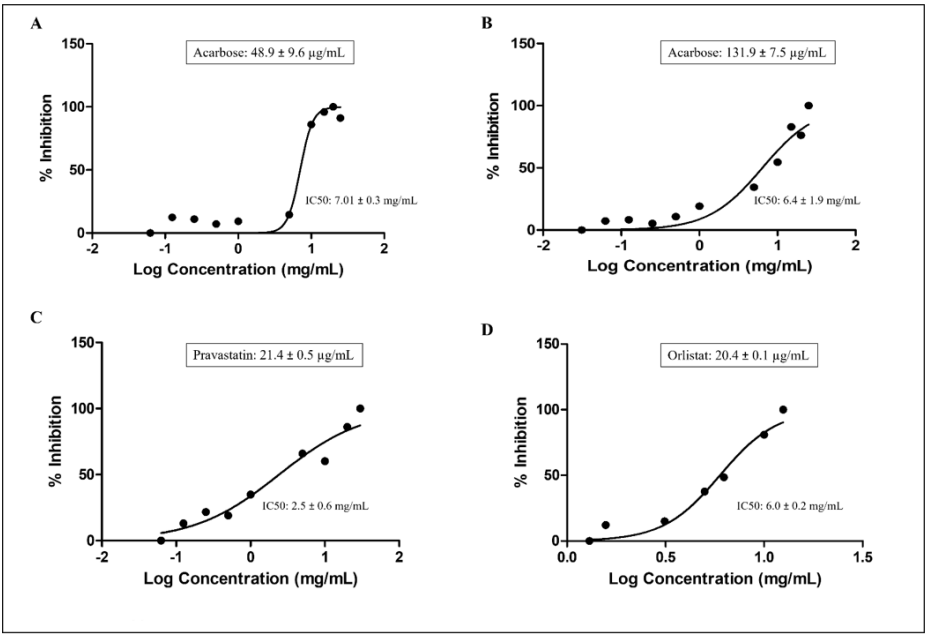


Figure 4. Enzyme inhibition activities and calculated IC50 values of *P. domestica* subsp. syriaca fruit pulp extract. α-amylases inhibition (**A**), α-glucosidase inhibition (**B**), HMG CoA reductase inhibition (**C**), Pancreatic lipase inhibition (**D**). Data expressed as mean ± SD. The IC50 values of the fruit extract against each enzyme were calculated using nonlinear regression analysis.

P. domestica subsp. syriaca fruit pulp extract inhibited α-amylase and α-glucosidase enzymes in a concentration-dependent manner, with an IC50 value of 7.01 mg/mL compared to acarbose, used as positive control (IC50: 48.9 µg/mL) (Figure 4A), and IC50 value of 6.4 mg/mL compared to acarbose (IC50: 131.9 µg/mL) (Figure 4B), respectively. As far as HMG-CoA reductase is concerned, *P. domestica* subsp. syriaca fruit extract inhibited HMG-CoA reductase enzyme in a concentration-dependent manner with an IC50 value of 2.5 mg/mL, while the reference inhibitor pravastatin inhibited HMG-CoA reductase with an IC50 value of 21.4 µg/mL (Figure 4C). Finally, regarding pancreatic lipase, the results suggest that *P. domestica* subsp. syriaca fruit pulp extract inhibited this enzyme in a

concentration-dependent manner with an IC50 value of 6.0 mg/mL compared to reference inhibitor orlistat (IC50 value: 20.4 µg/mL) (Figure 4D). Overall, the mean IC50 values of the fruit extract were found to be significantly different from the values obtained from the positive controls ($p < 0.05$).

3.7. In Vitro Anti-Inflammatory Effects of P. domestica Subsp. Syriaca Fruit Pulp Extract

In order to assess the anti-inflammatory proprieties of *P. domestica* subsp. syriaca fruit pulp extract, murine macrophage cell line J774 stimulated with LPS (10 µg/mL, 24 h), a well-known proinflammatory stimulus, was used. The anti-inflammatory activities were assessed by measuring the levels of proinflammatory mediators such as nitrites, PGE_2 and IL-1β. Preincubation of J774 macrophages with *P. domestica* subsp. syriaca fruit pulp extract (2 h before LPS treatment) inhibited significantly and in a concentration-dependent manner (0.01, 0.1, 0.5, 0.75 and 1 mg/mL) the production of nitrite (IC50 0.46 mg/mL, Figure 5A), PGE_2 (IC50 0.56 mg/mL, Figure 5B) and IL-1β (IC50 0.18 mg/mL, Figure 5C) induced by LPS, starting from the concentration of 0.1 mg/mL. No effects of P. domestica subsp. syriaca fruit pulp extract on proinflammatory mediator production were observed in unstimulated cells (without LPS) (Figure 5D–F). To rule out any alteration of cell viability, an MTT assay was performed and did not show any statistical reduction in cell viability after treatment with extract (Figure 5G).

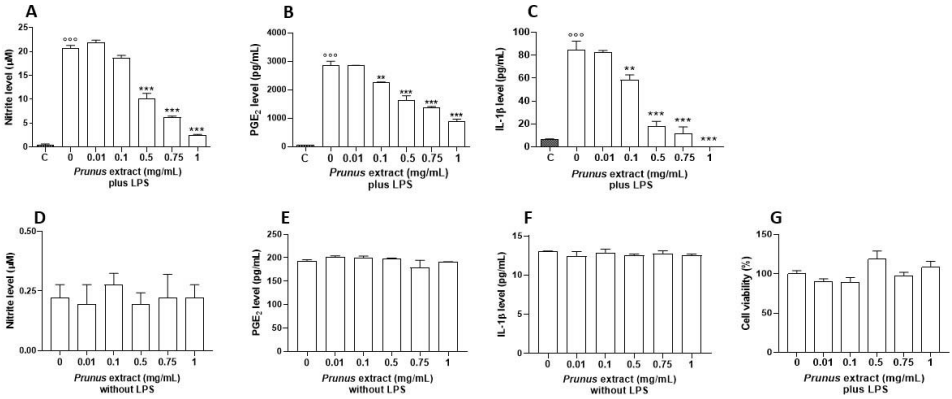


Figure 5. Effect of the *P. domestica* subsp. syriaca fruit pulp extract on LPS-induced nitrite, IL-1β and PGE_2 production. J774 cells were pretreated for 2 h with increasing concentrations of the extract ('0.01'. '0.1'. '0.5'. '0.75'. and '1' mg/mL) and then stimulated with LPS ('10' µg/mL) for 24 h (plus LPS). Effects of extract were also evaluated in absence of LPS (without LPS). Unstimulated J774 cells acted as a negative control (**C**). Nitrites (**A**,**D**), stable end products of NO, were measured in the supernatants by the Griess reaction, whereas IL-1β (**B**,**E**) and PGE_2 (**C**,**F**) were measured by ELISA. Cell viability was evaluated by the mitochondrial-dependent reduction of MTT to formazan (**G**). ○○○ $p < 0.001$ vs. unstimulated cells (**C**), $p < 0.001$ vs. unstimulated cells (**C**), *** $p < 0.001$ and ** $p < 0.01$ vs. LPS alone.

4. Discussion

The World Health Organization (WHO) reports that approximately 650 million people live today with obesity, 422 million with T2DM and 1.13 billion people with hypertension [39–41]. Thus, metabolic disorders remain a prevalent and urgent concern in the healthcare field, which today are remedied through pharmacological approaches prescribed to target some specific pathogenetic mechanisms. This, in turn, is often accompanied by adverse effects and poor compliance by patients. [42]. Therefore, the study of new food

supplement ingredients for the reduction of risk factors of MS is essential and finding new agents able to modulate the enzyme activities associated with carbohydrate/lipid digestion and cardiometabolic diseases is one of the essential targets in the prevention and treatment of cardiometabolic disorders. As evident by preclinical and clinical trials, *Prunus* species can improve energy homeostasis involving glucose and lipid metabolism, decrease inflammatory mediators, reduce lipid deposition, and modulate gut microbiota, and thus can reverse metabolic dysregulation states [43]. In this study, we explored the ability of a hydroethanolic extract of *P. domestica* subsp. syriaca (Mirabelle plum) fruit pulp to inhibit the activity of various enzymes associated with cardiometabolic disorders. Initially, fruit skin and pulp of two different *P. domestica* varieties (Common plum and Mirabelle plum), extracted with different concentrations of ethanolic solution, were evaluated for TPC, and the Mirabelle plum extract showing the highest TPC was selected for enzyme inhibition assays and evaluation of in vitro anti-inflammatory activity. Chemical profiling of *P. domestica* subsp. syriaca fruit pulp extract was evaluated using a multimethodological approach based on the application of new technologies, consisting of untargeted NMR spectroscopy and untargeted UHPLC-HRMS, which favors a holistic approach as opposed to the traditional reductionist methods, allowing us to overcome the concept of identifying one compound responsible for the obtained biological effect, and to ascribe the bioactivity to the whole phytocomplex [44]. The results suggested the presence of hydroxycinnamic acids (p-coumaroylquinic acid isomers and feruloylquinic acid derivatives), which resulted to be the most represented polyphenols followed by flavanols (catechin, epicatechin, procyanidins), flavonols (rutinoside and rhamnoside derivatives of quercetin), organic acids (quinic acid, citric acid, and malic acid), and carbohydrates (xylose, glucose, and sucrose). The carbohydrate quantitative analysis showed that glucose (106.6 mg/g dry weight of extract) is the main saccharide found in the fruit extract, in agreement with USDA Food Composition Databases, followed by sucrose (31.6 mg/g dry weight of extract) and xylose (0.6 mg/g dry weight of extract). Sugars of the fruit extract were at least in part chemically precipitated with ethanol before proceeding with the enzyme inhibition and the anti-inflammatory assays to remove the constituents that may interfere with the biological activities of the vegetable extract. The inhibition of α-amylase and α-glucosidase enzymes are important to reduce the digestion of complex carbohydrates and in turn the absorption of glucose, with the aim to normalize the blood glucose level both in subjects with mild hyperglycemia and in diabetic patients, to support glucose-lowering medication [19]. Acarbose is a pharmacologic drug currently employed in the treatment of subjects with diabetes due to its potential to inhibit α-amylase and α-glucosidase enzymes, thus reducing carbohydrate digestion, slowing down the absorption of carbohydrates, and decreasing postprandial insulin secretion, in addition to stimulating glucagon-like peptide (GLP-1) release [45]. The extract of *P. domestica* subsp. syriaca fruit pulp showed inhibitory activity against α-amylase and α-glucosidase enzymes with IC50 values of 7.01 mg/mL and 6.4 mg/mL, respectively. While evaluating antidiabetic activity of novel smoothies from selected *Prunus* fruits, Nowicka et al. demonstrated that anthocyanin and flavonol content have the highest impact on α-glucosidase enzyme, whereas flavanols may have the potential to inhibit α-amylase [46]. Some studies also reported that inhibition of α-glucosidase may be associated with the content of hydroxycinnamic acid derivatives such as ferulic acid or *p*-coumaric acids [47]. The researchers indicated that flavonols can interact with hydroxycinnamic acids or anthocyanins, which may increase the inhibition of α-glucosidase [48]. It has also been suggested that procyanidins-rich fruits are effective α-amylase inhibitors, possibly by the formation of enzyme-tannin complexes resulting in the prevention of the enzyme from interacting with starch [48]. The literature shows an inhibition of α-amylase and α-glucosidase enzymes with numerous botanical extracts, including *Elateriospermum tapos* Blume [49], *Xylopia parviflora* Spruce, *Monodora myristica* (Gaertn.) Dunal, *Tetrapleura tetraptera* (Schum. & Thonn.) Taub., *Dichrostachys glomerata* (Forssk.) Chiov., *Aframomum melegueta* K.Schum., *Aframomum citratum* (C.Pereira) K.Schum [34] and *Adansonia digitata* L. [33]. Different *Prunus* fruits (including Common European plum, 'vlaškača', damson

plum, white damson, purple-leaf cherry plum, white cherry plum, red cherry plum, sweet cherry, sweet cherry-wild type, sour cherry, steppe cherry, mahaleb cheery, blackthorn, and peach) extracted with 50% ethanol exhibited inhibition of α-amylase (IC50 value range: 1.11–136.23 mg/mL) and α-glucosidase (IC50 value range: 0.41–28.44 mg/mL) [50]. *Prunus* species in general showed a greater affinity towards α-glucosidase enzyme compared to α-amylase [50]. Altogether, these data suggest that inhibition of the enzymes involved in the digestion of carbohydrates by vegetable extracts may have promising potential in the management of glucose metabolism disorders. Statins are effective lipid-lowering agents, widely used as a first-line therapy in the atherosclerotic CVDs, which are known to competitively inhibit HMG-CoA reductase enzyme (rate-limiting enzyme of cholesterol synthesis) [51]. Considering the same approach of decreasing cholesterol synthesis, *P. domestica* subsp. syriaca fruit pulp extract was tested against the HMG-CoA reductase activity, showing an IC50 value of 2.5 mg/mL. The mean IC50 value calculated for the fruit extract was significantly higher from the reference statin (pravastatin). Susilowati et al. (2020) performed in silico analysis while evaluating antihyperlipidemic effects of apple peel extract, which showed the highest HMG CoA reductase inhibition by catechin, epicatechin, quercetin (aglycosidal form) and chlorogenic acid [52]. Several other vegetable extracts have already shown HMG-CoA reductase inhibitory activities, including, but not limited to *Basella alba* L. [53], *Syzygium polyanthum* (Wight) Walp. [54], *Ficus palmata* Forssk. [55], and *Amaranthus viridis* L. [56]. Inhibition of pancreatic lipase is a clinically validated approach in the treatment of obesity, as it reduces the hydrolysis of fats and decreases their absorption [57]. The Food and Drug Administration (FDA) approved orlistat in 1999 for the pharmacological management of obesity in conjunction with a reduced caloric diet, while in 2007 it was approved as an over-the-counter (OTC) agent for weight loss in overweight adults (18 years or older) [58]. Later, the FDA revised the label for orlistat by adding a new warning about severe liver injury, which has been reported rarely with this drug [59]. Following concerns about the possible cause of severe hepatic toxicities with orlistat, the European Medicines Agency completed a review for this medicine, where the Agency's Committee for Medicinal Products for Human Use (CHMP) concluded that the benefits of orlistat continue to outweighs the risks, but also recommended that marketing authorizations should ensure that the safety information on rarely occurring liver injuries be provided on the product information of all orlistat-containing medicines [60]. As reported in the present study, *P. domestica* subsp. syriaca fruit pulp extract inhibited the pancreatic lipase enzyme with an IC50 value of 6.0 mg/mL, although this value was significantly higher than that determined for orlistat. Hydroxycinnamic acids and proanthocyanidins have proven efficacy against lipase activity [61,62]. The presence of hydroxyl groups in the molecule (more potent), methoxy groups (less potent) and position of hydroxyl groups in the phenolic ring could influence the activity of polyphenols in inhibiting lipase enzyme [61]. Moreover, flavan-3-ol esters showed a stronger lipase inhibition compared to non-esterified flavanols such as catechin and epicatechin [61]. Plant species of different families (*Vitis vinifera* L., *Rhus coriaria* L., *Origanum dayi* Post, *Quercus infectoria* G.Olivier, *Eucalyptus galbie*, *Rosa damascene*, and *Levisticum officinale* W.D.J.Koch) showed considerable inhibition of pancreatic lipase enzyme [63,64]. Nowicka et al. observed an inhibition of pancreatic lipase enzyme with *Prunus persica* L. Batsch fruits (different cultivars), with an IC50 value ranging from 0.07 to 2.06 mg/mL [65]. On the whole, although the values of IC50 are much higher than those found for drugs, it must be considered that the extract, being derived from a food commonly consumed in diet and having been deprived of sugars, should not show adverse effects unlike medicines, and therefore it can be taken in larger quantities and for very long periods. In vivo studies are needed to confirm inhibitory activity against the enzymes considered. Lifestyle modifications (including diet and exercise) and pharmacological agents (such as peroxisome proliferator-activated receptor (PPAR)-α agonists, angiotensin-converting enzyme (ACE) inhibitors and angiotensin receptor blockers (ARBs)) all target inflammation in various ways, and thus can reduce MS-associated complications. Ongoing research studies are uncovering inflammatory pathways (related

to obesity, T2DM, and MS), which may be potential targets for novel preventive and treatment strategies with the aim of improving overall patient quality of life and reducing mortality, preferentially by preventing the adverse sequelae from MS [66]. *P. domestica* subsp. syriaca fruit pulp extract showed promising results against nitrite, IL-1β, and PGE_2 levels in LPS-stimulated macrophages in a concentration-dependent manner, with an IC50 of 0.46, 0.18 and 0.56 mg/mL, respectively. These results are in agreement with those previously published [67,68], although our extract was more active. In particular, dried plum polyphenols significantly suppressed the production of NO and COX-2 in LPS-stimulated RAW 264.7 macrophages at the concentration of 100 and 100 mg/mL, respectively [68]. The higher anti-inflammatory effects of *P. domestica* subsp. syriaca fruit pulp extract could be due to the presence of polyphenolic compounds in different concentrations, mainly flavonoids (catechin and (+) epicatechin) and hydroxy cinnamic acids (chlorogenic acid and feruloyl-coumaroylquinic acid derivative). Each compound inhibited the production of proinflammatory mediators at different concentrations, and whether the anti-inflammatory effects of this prunus extract are due to additively or synergistically polyphenolic action is not known. For example, inhibitory effects of catechin [69] and chlorogenic acid [70] on various inflammatory mediators using LPS-stimulated RAW 264.7 macrophages were reported. In particular, chlorogenic acid completely inhibited NO production in LPS-stimulated macrophage RAW 264.7 cells at the concentration of 40 ug/mL [70]. A medicinal plant *Inonotus (I.) sanghuang* (rich in rutin, chlorogenic acid, isorhamnetin, quercetin, and quercitrin) improved insulin resistance and MS by reducing inflammation via modulation of the crosstalk between macrophages and adipocytes [71]. Grape powder extract (rich in quercetin-3-glucoside, catechin, epicatechin, rutin, gallic acid and resveratrol) showed to decrease LPS-stimulated inflammation in macrophages by affecting the gene expression of IL-6, IL-8, IL-1β and TNF-α, and in turn decreased insulin resistance [72]. *Sambucus nigra* L. fruit extract alleviated insulin resistance by suppressing the enhanced production of NO, TNF-α, IL-6, and PGE_2, where the presence of cyanidin-based anthocyanins, flavan-3-ols, flavonols, and hydroxycinnamic acids were detected [73].

The main strength of this study is represented by the comprehensive characterization of the *P. domestica* extract by different and complementary technologies and the evaluation of some in vitro functional activities of this extract on mechanisms related to the pathophysiology of cardiometabolic diseases. A limitation of this study is that we did not evaluate additional specific aspects, such as modulation of triglyceride content or glucose uptake in appropriate cell models. The assessment of these and other related parameters will be the object of future research, in order to complete the functional characterization of *P. domestica* extracts and lay the scientific foundations for the placing on the market of new food supplements based on *P. domestica* extracts.

5. Conclusions

Nutraceuticals and functional foods are known to play an important role in the maintenance of human health and wellbeing through the prevention of chronic diseases. A substantial increase in the worldwide usage of vegetable extracts has been observed in recent decades, probably due to the increasing trend of consumer propensity towards preventive care through natural substances. Currently, more than 80% of world population is relying on the use of vegetable products for their primary health concerns [74]. The present investigation studied the potential nutraceutical benefits of *P. domestica* subsp. syriaca fruit pulp extract and found that it inhibited key enzymes involved in the metabolism of carbohydrates and lipids as well as in cholesterol synthesis, and attenuated LPS-stimulated release of proinflammatory mediators. The chemical characterization showed the presence of polyphenolic contents, which potentially justifies these biological properties. Taken together, these findings point towards a potential to modulate some molecular mechanisms involved in the pathophysiology of cardiometabolic diseases. Further studies using in vitro and in vivo models are required to better characterize these properties and their potential applications for human health.

Supplementary Materials: The following are available online at https://www.mdpi.com/article/10.3390/nu14020340/s1, Table S1: Sugars and organic acids identified in the 600.17 MHz ^{1}H spectra of P. domestica fruit pulp extracts. Asterisks indicate signals selected for integration.

Author Contributions: Conceptualization, M.D.(Maria Daglia), P.M. and A.D.M.; methodology, H.U., E.S., C.S., D.D. and G.D.M.; software, H.U., A.R., M.D.(Marco Dacrema); validation, H.U., E.S., C.S. and A.R.; formal analysis, H.U., A.R., L.M. and P.C.; investigation, H.U., E.S., A.R. and P.C.; resources, H.U., A.R., M.D.(Marco Dacrema) and P.C.; data cura1tion, H.U. and C.S.; writing—original draft preparation, H.U., E.S., C.S., and A.R.; writing—review and editing, H.U., E.S., C.S., A.R., P.M. and M.D.(Maria Daglia); visualization, H.U. and M.D.(Maria Daglia); supervision, M.D.(Maria Daglia). All authors have read and agreed to the published version of the manuscript.

Funding: This research received no external funding.

Informed Consent Statement: Not applicable.

Conflicts of Interest: The authors declare no conflict of interest.

References

1. Belwal, T.; Bisht, A.; Devkota, H.P.; Ullah, H.; Khan, H.; Pandey, A.; Bhatt, I.D.; Echeverría, J. Phytopharmacology and Clinical Updates of Berberis Species against Diabetes and Other Metabolic Diseases. *Front. Pharmacol.* **2020**, *11*, 41. [CrossRef] [PubMed]
2. Costa, L.A.; Canani, L.H.; Lisbôa, H.R.K.; Tres, G.S.; Gross, J.L. Aggregation of Features of the Metabolic Syndrome Is Associated with Increased Prevalence of Chronic Complications in Type 2 Diabetes. *Diabet Med.* **2004**, *21*, 252–255. [CrossRef]
3. McCracken, E.; Monaghan, M.; Sreenivasan, S. Pathophysiology of the Metabolic Syndrome. *Clin. Dermatol.* **2018**, *36*, 14–20. [CrossRef] [PubMed]
4. Åberg, F.; Helenius-Hietala, J.; Puukka, P.; Färkkilä, M.; Jula, A. Interaction between Alcohol Consumption and Metabolic Syndrome in Predicting Severe Liver Disease in the General Population. *Hepatology* **2018**, *67*, 2141–2149. [CrossRef]
5. Mongraw-Chaffin, M.; Foster, M.C.; Anderson, C.A.M.; Burke, G.L.; Haq, N.; Kalyani, R.R.; Ouyang, P.; Sibley, C.T.; Tracy, R.; Woodward, M.; et al. Metabolically Healthy Obesity, Transition to Metabolic Syndrome, and Cardiovascular Risk. *J. Am. Coll. Cardiol.* **2018**, *71*, 1857–1865. [CrossRef]
6. Scarpellini, E.; Tack, J. Obesity and Metabolic Syndrome: An Inflammatory Condition. *Dig. Dis.* **2012**, *30*, 148–153. [CrossRef]
7. Magni, P.; Liuzzi, A.; Ruscica, M.; Dozio, E.; Ferrario, S.; Bussi, I.; Minocci, A.; Castagna, A.; Motta, M.; Savia, G. Free and Bound Plasma Leptin in Normal Weight and Obese Men and Women: Relationship with Body Composition, Resting Energy Expenditure, Insulin-sensitivity, Lipid Profile and Macronutrient Preference. *Clin. Endocrinol.* **2005**, *62*, 189–196. [CrossRef]
8. Popko, K.; Gorska, E.; Stelmaszczyk-Emmel, A.; Plywaczewski, R.; Stoklosa, A.; Gorecka, D.; Pyrzak, B.; Demkow, U. Proinflammatory Cytokines Il-6 and TNF-α and the Development of Inflammation in Obese Subjects. *Eur. J. Med. Res.* **2010**, *15*, 120–122. [CrossRef]
9. Tangvarasittichai, S.; Pongthaisong, S.; Tangvarasittichai, O. Tumor Necrosis Factor-A, Interleukin-6, C-Reactive Protein Levels and Insulin Resistance Associated with Type 2 Diabetes in Abdominal Obesity Women. *Indian J. Clin. Biochem.* **2016**, *31*, 68–74. [CrossRef] [PubMed]
10. Chakraborty, S.; Roy, S.; Rahaman, M. Epidemiological Predictors of Metabolic Syndrome in Urban West Bengal, India. *J. Family Med. Prim. Care* **2015**, *4*, 535. [CrossRef]
11. de Filippis, A.; Ullah, H.; Baldi, A.; Dacrema, M.; Esposito, C.; Garzarella, E.U.; Santarcangelo, C.; Tantipongpiradet, A.; Daglia, M. Gastrointestinal Disorders and Metabolic Syndrome: Dysbiosis as a Key Link and Common Bioactive Dietary Components Useful for Their Treatment. *Int. J. Mol. Sci.* **2020**, *21*, 4929. [CrossRef] [PubMed]
12. Prasad, H.; Ryan, D.A.; Celzo, M.F.; Stapleton, D. Metabolic Syndrome: Definition and Therapeutic Implications. *Postgrad. Med.* **2012**, *124*, 21–30. [CrossRef] [PubMed]
13. Rask Larsen, J.; Dima, L.; Correll, C.U.; Manu, P. The Pharmacological Management of Metabolic Syndrome. *Expert Rev. Clin. Pharmacol.* **2018**, *11*, 397–410. [CrossRef] [PubMed]
14. Matfin, G. Developing Therapies for the Metabolic Syndrome: Challenges, Opportunities, and the Unknown. *Ther. Adv. Endocrinol. Metab.* **2010**, *1*, 89–94. [CrossRef] [PubMed]
15. Russo, R.; Gallelli, L.; Cannataro, R.; Perri, M.; Calignano, A.; Citraro, R.; Russo, E.; Gareri, P.; Corsonello, A.; de Sarro, G. When Nutraceuticals Reinforce Drugs Side Effects: A Case Report. *Curr. Drug Saf.* **2016**, *11*, 264–266. [CrossRef]
16. Li, X.T.; Liao, W.; Yu, H.J.; Liu, M.W.; Yuan, S.; Tang, B.W.; Yang, X.H.; Song, Y.; Huang, Y.; le Cheng, S.; et al. Combined Effects of Fruit and Vegetables Intake and Physical Activity on the Risk of Metabolic Syndrome among Chinese Adults. *PLoS ONE* **2017**, *12*, e0188533. [CrossRef]
17. EFSA Panel on Food Additives and Nutrient Sources added to Food (ANS); Younes, M.; Aggett, P.; Aguilar, F.; Crebelli, R.; Dusemund, B.; Filipič, M.; Frutos, M.J.; Galtier, P.; Gott, D.; et al. Scientific Opinion on the Safety of Monacolins in Red Yeast Rice. *EFSA J.* **2018**, *16*, e05368.
18. Birari, R.B.; Bhutani, K.K. Pancreatic Lipase Inhibitors from Natural Sources: Unexplored Potential. *Drug Discov.* **2007**, *12*, 879–889. [CrossRef] [PubMed]

19. Tundis, R.; Loizzo, M.R.; Menichini, F. Natural Products as α-Amylase and α Glucosidase Inhibitors and Their Hypoglycaemic Potential in the Treatment of Diabetes: An Update. *Mini Rev. Med. Chem.* **2010**, *10*, 315–331. [CrossRef]
20. Lin, S.-H.; Huang, K.-J.; Weng, C.-F.; Shiuan, D. Exploration of Natural Product Ingredients as Inhibitors of Human HMG-CoA Reductase through Structure-Based Virtual Screening. *Drug Des. Devel. Ther.* **2015**, *9*, 3313. [PubMed]
21. Young Shin, J.; Young Kim, J.; Tak Kang, H.; Hwa Han, K.; Yong Shim, J. Effect of Fruits and Vegetables on Metabolic Syndrome: A Systematic Review and Meta-Analysis of Randomized Controlled Trials. *Int. J. Food Sci. Nutr.* **2015**, *66*, 416–425. [CrossRef] [PubMed]
22. Lee, M.; Lim, M.; Kim, J. Fruit and Vegetable Consumption and the Metabolic Syndrome: A Systematic Review and Dose-Response Meta-Analysis. *Br. J. Nutr.* **2019**, *122*, 723–733. [CrossRef] [PubMed]
23. El-Beltagi, H.S.; El-Ansary, A.E.; Mostafa, M.A.; Kamel, T.A.; Safwat, G. Evaluation of the Phytochemical, Antioxidant, Antibacterial and Anticancer Activity of Prunus Domestica Fruit. *Not. Bot. Horti Agrobot. Cluj Napoca* **2019**, *47*, 395–404. [CrossRef]
24. Igwe, E.O.; Charlton, K.E. A Systematic Review on the Health Effects of Plums (*Prunus domestica* and *Prunus salicina*). *Phytother. Res.* **2016**, *30*, 701–731. [CrossRef]
25. Furchner-Evanson, A.; Petrisko, Y.; Howarth, L.; Nemoseck, T.; Kern, M. Type of Snack Influences Satiety Responses in Adult Women. *Appetite* **2010**, *54*, 564–569. [CrossRef]
26. Nilsson, A.; Ostman, E.; Holst, J.; Björck, I. Including Indigestible Carbohydrates in the Evening Meal of Healthy Subjects Improves Glucose Tolerance, Lowers Inflammatory Markers, and Increases Satiety after a Subsequent Standardized Breakfast. *J. Nutr.* **2008**, *138*, 732–739. [CrossRef]
27. di Matteo, G.; Spano, M.; Esposito, C.; Santarcangelo, C.; Baldi, A.; Daglia, M.; Mannina, L.; Ingallina, C.; Sobolev, A.P. NMR Characterization of Ten Apple Cultivars from the Piedmont Region. *Foods* **2021**, *10*, 289. [CrossRef]
28. Ingallina, C.; Spano, M.; Sobolev, A.P.; Esposito, C.; Santarcangelo, C.; Baldi, A.; Daglia, M.; Mannina, L. Characterization of Local Products for Their Industrial Use: The Case of Italian Potato Cultivars Analyzed by Untargeted and Targeted Methodologies. *Foods* **2020**, *9*, 1216. [CrossRef]
29. Singleton, V.L.; Rossi, J.A. Colorimetry of Total Phenolics with Phosphomolybdic-Phosphotungstic Acid Reagents. *Am. J. Enol. Vitic.* **1965**, *16*, 144–158.
30. Kok, J.M.L.; Jee, J.M.; Chew, L.Y.; Wong, C.L. The Potential of the Brown Seaweed Sargassum Polycystum against Acne Vulgaris. *J. Appl. Phycol.* **2016**, *28*, 3127–3133. [CrossRef]
31. Mass Bank of North America. Available online: https://mona.fiehnlab.ucdavis.edu/ (accessed on 18 July 2021).
32. Sirius. Available online: https://bio.informatik.uni-jena.de/software/sirius/ (accessed on 18 July 2021).
33. Cicolari, S.; Dacrema, M.; Tsetegho Sokeng, A.J.; Xiao, J.; Atchan Nwakiban, A.P.; di Giovanni, C.; Santarcangelo, C.; Magni, P.; Daglia, M. Hydromethanolic Extracts from *Adansonia digitata* L. Edible Parts Positively Modulate Pathophysiological Mechanisms Related to the Metabolic Syndrome. *Molecules* **2020**, *25*, 2858. [CrossRef] [PubMed]
34. Nwakiban, A.P.A.; Sokeng, A.J.; Dell'Agli, M.; Bossi, L.; Beretta, G.; Gelmini, F.; Tchamgoue, A.D.; Agbor, G.A.; Kuiaté, J.R.; Daglia, M.; et al. Hydroethanolic Plant Extracts from Cameroon Positively Modulate Enzymes Relevant to Carbohydrate/Lipid Digestion and Cardio-Metabolic Diseases. *Food Funct.* **2019**, *10*, 6533–6542. [CrossRef]
35. Galuppo, M.; Rossi, A.; Giacoppo, S.; Pace, S.; Bramanti, P.; Sautebin, L.; Mazzon, E. Use of Mometasone Furoate in Prolonged Treatment of Experimental Spinal Cord Injury in Mice: A Comparative Study of Three Different Glucocorticoids. *Pharmacol. Res.* **2015**, *99*, 316–328. [CrossRef] [PubMed]
36. Capitani, D.; Sobolev, A.P.; Delfini, M.; Vista, S.; Antiochia, R.; Proietti, N.; Bubici, S.; Ferrante, G.; Carradori, S.; Salvador, F.R.D.; et al. NMR Methodologies in the Analysis of Blueberries. *Electrophoresis* **2014**, *35*, 1615–1626. [CrossRef]
37. Mannina, L.; Sobolev, A.P.; Viel, S. Liquid State 1H High Field NMR in Food Analysis. *Prog. Nucl. Magn. Reson. Spectrosc.* **2012**, *66*, 1–39. [CrossRef] [PubMed]
38. Capitani, D.; Mannina, L.; Proietti, N.; Sobolev, A.P.; Tomassini, A.; Miccheli, A.; di Cocco, M.E.; Capuani, G.; de Salvador, R.; Delfini, M. Monitoring of Metabolic Profiling and Water Status of Hayward Kiwifruits by Nuclear Magnetic Resonance. *Talanta* **2010**, *82*, 1826–1838. [CrossRef]
39. WHO Hypertension. Available online: https://www.who.int/ne%0Aws-room/fact-sheets/detail/hypertension (accessed on 23 June 2021).
40. WHO Diabetes. Available online: https://www.who.int/news-roo%0Am/fact-sheets/detail/diabetes (accessed on 23 June 2021).
41. WHO Obesity and Overweight. Available online: https://www.who.int/news-room/fact-sheets/detail/obesity-and-overweight (accessed on 23 June 2021).
42. Mandlekar, S.; Hong, J.L.; Tony Kong, A.N. Modulation of Metabolic Enzymes by Dietary Phytochemicals: A Review of Mechanisms Underlying Beneficial versus Unfavorable Effects. *Curr. Drug Metab.* **2006**, *7*, 661–675. [CrossRef] [PubMed]
43. Ullah, H.; de Filippis, A.; Khan, H.; Xiao, J.; Daglia, M. An Overview of the Health Benefits of Prunus Species with Special Reference to Metabolic Syndrome Risk Factors. *Food Chem. Toxicol.* **2020**, *144*, 111574. [CrossRef] [PubMed]
44. Moracci, L.; Traldi, P.; Agostini, M. Mass Spectrometry for a Holistic View of Natural Extracts of Phytotherapeutic Interest. *Mass Spectrom. Rev.* **2020**, *39*, 553–573. [CrossRef]
45. Kumar Singla, R.; Singh, R.; Kumar Dubey, A. Important Aspects of Post-Prandial Antidiabetic Drug, Acarbose. *Curr. Top. Med. Chem.* **2016**, *16*, 2625–2633. [CrossRef]

46. Nowicka, P.; Wojdyło, A.; Samoticha, J. Evaluation of Phytochemicals, Antioxidant Capacity, and Antidiabetic Activity of Novel Smoothies from Selected Prunus Fruits. *J. Funct. Foods* **2016**, *25*, 397–407. [CrossRef]
47. Wang, T.; Li, X.; Zhou, B.; Li, H.; Zeng, J.; Gao, W. Anti-Diabetic Activity in Type 2 Diabetic Mice and α-Glucosidase Inhibitory, Antioxidant and Anti-Inflammatory Potential of Chemically Profiled Pear Peel and Pulp Extracts (*Pyrus* spp.). *J. Funct. Foods* **2015**, *13*, 276–288. [CrossRef]
48. Boath, A.S.; Stewart, D.; McDougall, G.J. Berry Components Inhibit α-Glucosidase in Vitro: Synergies between Acarbose and Polyphenols from Black Currant and Rowanberry. *Food Chem.* **2012**, *135*, 929–936. [CrossRef] [PubMed]
49. Nor-Liyana, J.; Siroshini, K.T.; Nurul-Syahirah, M.B.; Chang, W.L.; Nurul-Husna, S.; Daryl, J.A.; Khairul-Kamilah, A.K.; Hasnah, B. Phytochemical Analysis of Elateriospermum Tapos and Its Inhibitory Effects on Alpha-Amylase, Alpha-Glucosidase and Pancreatic Lipase. *J. Trop. For. Sci.* **2019**, *31*, 240–248.
50. Popović, B.M.; Blagojević, B.; Kucharska, A.Z.; Agić, D.; Magazin, N.; Milović, M.; Serra, A.T. Exploring Fruits from Genus Prunus as a Source of Potential Pharmaceutical Agents–In Vitro and in Silico Study. *Food Chem.* **2021**, *358*, 129812. [CrossRef]
51. Catapano, A.L.; Graham, I.; de Backer, G.; Wiklund, O.; Chapman, M.J.; Drexel, H.; Hoes, A.W.; Jennings, C.S.; Landmesser, U.; Pedersen, T.R.; et al. 2016 ESC/EAS Guidelines for the Management of Dyslipidaemias: The Task Force for the Management of Dyslipidaemias of the European Society of Cardiology (ESC) and European Atherosclerosis Society (EAS) Developed with the Special Contribution of the Europea. *Atherosclerosis* **2016**, *253*, 281–344. [CrossRef]
52. Susilowati, R.; Jannah, J.; Maghfuroh, Z.; Kusuma, M.T. Antihyperlipidemic Effects of Apple Peel Extract in High-Fat Diet-Induced Hyperlipidemic Rats. *J. Adv. Pharm. Technol. Res.* **2020**, *11*, 128. [CrossRef]
53. Baskaran, G.; Salvamani, S.; Ahmad, S.A.; Shaharuddin, N.A.; Pattiram, P.D.; Shukor, M.Y. HMG-CoA Reductase Inhibitory Activity and Phytocomponent Investigation of Basella Alba Leaf Extract as a Treatment for Hypercholesterolemia. *Drug Des. Devel. Ther.* **2015**, *9*, 509. [CrossRef]
54. Hartanti, L.; Yonas, S.M.K.; Mustamu, J.J.; Wijaya, S.; Setiawan, H.K.; Soegianto, L. Influence of Extraction Methods of Bay Leaves (Syzygium Polyanthum) on Antioxidant and HMG-CoA Reductase Inhibitory Activity. *Heliyon* **2019**, *5*, e01485. [CrossRef] [PubMed]
55. Iqbal, D.; Khan, M.S.; Khan, A.; Khan, M.; Ahmad, S.; Srivastava, A.K.; Bagga, P. In Vitro Screening for β-Hydroxy-β-Methylglutaryl-Coa Reductase Inhibitory and Antioxidant Activity of Sequentially Extracted Fractions of Ficus Palmata Forsk. *Biomed Res. Int.* **2014**, *2014*, 1–10. [CrossRef]
56. Salvamani, S.; Gunasekaran, B.; Shukor, M.Y.; Shaharuddin, N.A.; Sabullah, M.K.; Ahmad, S.A. Anti-HMG-CoA Reductase, Antioxidant, and Anti-Inflammatory Activities of Amaranthus Viridis Leaf Extract as a Potential Treatment for Hypercholesterolemia. *Evid. Based Complement. Alternat. Med.* **2016**, *2016*, 1–10. [CrossRef]
57. Pilitsi, E.; Farr, O.M.; Polyzos, S.A.; Perakakis, N.; Nolen-Doerr, E.; Papathanasiou, A.E.; Mantzoros, C.S. Pharmacotherapy of Obesity: Available Medications and Drugs under Investigation. *Metabolism* **2019**, *92*, 170–192. [CrossRef]
58. FDA Orlistat (Marketed as Alli and Xenical) Information. Available online: https://www.fda.gov/drugs/postmarket-drug-safety-information-patients-and-providers/orlistat-marketed-alli-and-xenical-information (accessed on 2 August 2021).
59. FDA FDA Drug Safety Communication: Completed Safety Review of Xenical/Alli (Orlistat) and Severe Liver Injury. Available online: https://www.fda.gov/drugs/postmarket-drug-safety-information-patients-and-providers/fda-drug-safety-communication-completed-safety-review-xenicalalli-orlistat-and-severe-liver-injury (accessed on 2 August 2021).
60. European Medicines Agency European Medicines Agency Starts Review of Orlistat-Containing Medicines. Available online: https://www.ema.europa.eu/en/news/european-medicines-agency-starts-review-orlistat-containing-medicines (accessed on 2 August 2021).
61. Buchholz, T.; Melzig, M.F. Polyphenolic Compounds as Pancreatic Lipase Inhibitors. *Planta Med.* **2015**, *81*, 771–783. [CrossRef] [PubMed]
62. McDougall, G.J.; Stewart, D. The Inhibitory Effects of Berry Polyphenols on Digestive Enzymes. *Biofactors* **2005**, *23*, 189–195. [CrossRef] [PubMed]
63. Gholamhoseinian, A.; Shahouzehi, B.; Sharifi-Far, F. Inhibitory Effect of Some Plant Extracts on Pancreatic Lipase. *Int. J. Pharmacol.* **2010**, *6*, 18–24. [CrossRef]
64. Jaradat, N.; Zaid, A.N.; Hussein, F.; Zaqzouq, M.; Aljammal, H.; Ayesh, O. Anti-Lipase Potential of the Organic and Aqueous Extracts of Ten Traditional Edible and Medicinal Plants in Palestine; a Comparison Study with Orlistat. *Medicines* **2017**, *4*, 89. [CrossRef]
65. Nowicka, P.; Wojdyło, A.; Laskowski, P. Inhibitory Potential against Digestive Enzymes Linked to Obesity and Type 2 Diabetes and Content of Bioactive Compounds in 20 Cultivars of the Peach Fruit Grown in Poland. *Plant Foods Hum. Nutr.* **2018**, *73*, 314–320. [CrossRef]
66. Welty, F.K.; Alfaddagh, A.; Elajami, T.K. Targeting Inflammation in Metabolic Syndrome. *Transl. Res.* **2016**, *167*, 257–280. [CrossRef] [PubMed]
67. Silvan, J.M.; Michalska-Ciechanowska, A.; Martinez-Rodriguez, A.J. Modulation of Antibacterial, Antioxidant, and Anti-Inflammatory Properties by Drying of *Prunus domestica* L. Plum Juice Extracts. *Microorganisms* **2020**, *8*, 119. [CrossRef]
68. Hooshmand, S.; Kumar, A.; Zhang, J.Y.; Johnson, S.A.; Chai, S.C.; Arjmandi, B.H. Evidence for Anti-Inflammatory and Antioxidative Properties of Dried Plum Polyphenols in Macrophage RAW 264.7 Cells. *Food Funct.* **2015**, *6*, 1719–1725. [CrossRef]

69. Sunil, M.A.; Sunitha, V.S.; Santhakumaran, P.; Mohan, M.C.; Jose, M.S.; Radhakrishnan, E.K.; Mathew, J. Protective Effect of (+)–Catechin against Lipopolysaccharide-Induced Inflammatory Response in RAW 264.7 Cells through Downregulation of NF-KB and P38 MAPK. *Inflammopharmacology* **2021**, *29*, 1139–1155. [CrossRef]
70. Lee, S.H.; Lee, S.Y.; Son, D.J.; Lee, H.; Yoo, H.S.; Song, S.; Oh, K.W.; Han, D.C.; Kwon, B.M.; Hong, J.T. Inhibitory Effect of 2′-Hydroxycinnamaldehyde on Nitric Oxide Production through Inhibition of NF-KB Activation in RAW 264.7 Cells. *Biochem. Pharmacol.* **2005**, *69*, 791–799. [CrossRef]
71. Zhang, M.; Xie, Y.; Su, X.; Liu, K.; Zhang, Y.; Pang, W.; Wang, J. Inonotus Sanghuang Polyphenols Attenuate Inflammatory Response via Modulating the Crosstalk between Macrophages and Adipocytes. *Front. Immunol.* **2019**, *10*, 286. [CrossRef] [PubMed]
72. Overman, A.; Bumrungpert, A.; Kennedy, A.; Martinez, K.; Chuang, C.C.; West, T.; Dawson, B.; Jia, W.; McIntosh, M. Polyphenol-Rich Grape Powder Extract (GPE) Attenuates Inflammation in Human Macrophages and in Human Adipocytes Exposed to Macrophage-Conditioned Media. *Int. J. Obes.* **2010**, *34*, 800–808. [CrossRef] [PubMed]
73. Zielińska-Wasielica, J.; Olejnik, A.; Kowalska, K.; Olkowicz, M.; Dembczyński, R. Elderberry (*Sambucus nigra* L.) Fruit Extract Alleviates Oxidative Stress, Insulin Resistance, and Inflammation in Hypertrophied 3T3-L1 Adipocytes and Activated RAW 264.7 Macrophages. *Foods* **2019**, *8*, 326. [CrossRef] [PubMed]
74. Ekor, M. The Growing Use of Herbal Medicines: Issues Relating to Adverse Reactions and Challenges in Monitoring Safety. *Front. Pharmacol.* **2014**, *4*, 177. [CrossRef]

Chapter 7: NMR metabolomics and HPLC analysis applied on plant matrices in the perspective of food applications

7.1. Introduction

Plants, as foods, are complex systems containing macro- and micronutrients, as well as secondary metabolites, that can take part in biochemical processes and help to achieve or maintain a state of well-being (Altemimi et al., 2017; Balandrin et al., 1993; Brusotti et al., 2014; Wijngaard et al., 2012). For instance, phenolic acids, known to serve as multipurpose bioactive compounds, are widely spread throughout the plant kingdom (Shahidi & Ambigaipalan, 2015).

Here are reported a series of articles related to two plant matrices that could be also applied in the food field: *Cannabis Sativa* L. and *Gentiana Lutea* L.

7.1.1. *Cannabis Sativa* L.

Cannabis sativa L. is one of the oldest plants cultivated by man, especially for its medicinal and textile uses. However, during 1950-2000 its name was associated with drugs of abuse (marijuana), due to the presence of high amount of the psychotropic compound Δ9-tetrahydrocannabinol (THC) in some hemp cultivars, leading to a slowly abandonment of this

crop for many States of the world. In 2000 the European Union published a regulation (Regulation EC No 1251/99) concerning the re-introduction of some industrial hemp cultivars, characterized by a low content of THC (under 0.2 % *w*/*w*) in the inflorescences, certified and included in the list of the "EU Plant variety database".

To date, although different classifications have been proposed, the generally accepted one is based on the content of psychotropic THC and non-psychotropic cannabidiol (CBD) cannabinoids: drug-type chemotype is characterized by higher levels of THC with respect to CBD, whereas fiber-type chemotype, also known as hemp, is characterized by low levels of THC (usually under 0.2%) and high levels of CBD (Piluzza et al., 2013). Drug-type chemotype is generally used for medical purpose, whereas fiber-type one is mainly used for industrial applications. Drug-type chemotype is generally used for medical purpose, whereas fiber-type one is mainly used for industrial applications. In particular, the different parts of fiber-type cannabis have been historically used for different applications (textile, paper, and rope production, food,

medicine). More modern applications such as biofuel and plastic production, cosmetic field, animal bedding, building materials have been developed in recent times.

Nevertheless, these years without hemp cultivation contributes to the loss of the traditional hemp cultivars, and so the available hemp cultivars come from foreign countries, chosen in different weather condition respect to the Mediterranean ones. For these reasons, their introduction in the agronomic Italian scenario need a careful investigation in order to avoid the diffusion of inadequate and not productive varieties. Therefore, a deep investigation of the exogenous factor (agronomical practices, seasoning and pedoclimatic conditions) that can influence the metabolomic profile is needed.

From a botanical point of view, *Cannabis* is naturally a dioecious cultivar; namely, the male and female flowers are presented on different plants: pollination occurs with the wind. Monoecious *Cannabis* cultivars are also obtained through breeding selection. The dioecious ones are mainly used for fiber production, whereas the monoecious ones for seed production.

The knowledge of the inflorescences chemical profile was a prerequisite to promote their use in several industrial fields, being a significant source of compounds with specific sensorial/nutraceutical/pharmaceutical properties.

In the last years have been undertaken to valorize and promote help cultivation and industrial use. In this context the project entitled “La Canapa industriale: sviluppo e valorizzazione di una nuova filiera agroalimentare ecosostenibile” funded by Lazio region in 2018 has been promoted for filling the "gap" of knowledge regarding the entire hemp chain. The project has proposed a research line to select varieties with a low THC content that can be reintroduced in Lazio region and also to suggest suitable cultivation techniques for the new requirements of environmental sustainability.

The related articles to this section 7.1.1. about the hemp products for food applications are reported in the following case studies:

- Case study 1: Multimethodological characterization of seven dioecious cultivars of industrial hemp over the season (Spano et al., 2021).
- Case study 2: Multimethodological characterization of Ferimon monoecious cultivar cultivated with different agronomical practices (Spano et al., 2022).
- Case study 3: Malted hempseeds characterization through HPLC analysis (Farinon et al., 2022).
- Case study 4: Hemp seed oils characterization by multimethodological approach (Spano et al., 2020).

7.1.2. *Gentiana Lutea* L.

Gentiana Lutea L. is a well-known plant for its use in bitters beverages preparation (Khan & Abourashed, 2010). *Gentiana Lutea* L. is a perennial herb, of the Gentianacee family, of 50-120 cm with an erect stem, broad lanceolate to elliptic leaves of 10–30 cm long and 4–12 cm broad and a characteristic yellow flower, diffused in the mountain of Central and Southern Europe (Aiello et al., 2013; Tutin et al., 1972; Venditti et al., 2013). The *Gentiana* plants were large used in the world for their activity. In particular, some Gentiana species are part of the Chinese Traditional Medicine (TCM) and are included in both the Chinese (Chinese Pharmacopeia Commission, 2015) and Japanese Pharmacopeia (Japanese Pharmacopeia Commission, 2001). Gentiana roots have also an herbal monography of EMA (European Medicines Agency, n.d., 2018) and are present in the European Pharmacopeia (PhEUR, 2020) for the loss of appetite and dyspeptic/gastrointestinal disorders based on long-standing traditional use. Single constituents have been identified as bioactive compounds with interesting pharmacological effects (Fadzil et al., 2021; Mei et al., 2021;

Yang et al., 2010). Also the whole Gentiana extract was studied for many pharmacological properties, like antioxidant and antibacterial activities (Joshi et al., 2017), anti-inflammatory and wound healing activities (Mathew et al., 2004) and antifungal activity (Mathew et al., 2004; "Studies on the antimicrobial activity and chemical composition of the essential oils and alcoholic extracts of Gentiana asclepiadea L.," 2011).

In Italy the use of the *Gentiana* plants is restricted to the preparation of a bitter liquor with their roots which possesses digestive and tonic properties due to the presence of the secoiridoid glycosides (Carnat et al., 2005; Mustafa et al., 2014) with amarogentin and gentiopicroside as the bitter ones (Khan & Abourashed, 2010). The wild *Gentiana Lutea* L. massive collection along century have brought to a depletion of the natural population. Now some species are in the European Red List regarding species threatened with extinction (Allen, D., Bilz, M., Leaman, D.J., Miller, R.M., Timoshyna, A. and Window, 2014; International Union for Conservation of Nature (IUCN), 2022) and so its collection is forbidden in many country of Europe, including Italy, thanks to European (European

Environment Agency, 2022), National and Regional level protective actions, leading at the start of the plant cultivation in many country, like France and Germany.

In this context, it is significance the study of plant species of uncontaminated or protected areas due to the genuine compounds profile.

The related article to this section 7.1.2. about the *Gentiana Lutea* L. for food applications is reported in the following case study:

- Case study 5: Metabolomic characterization of Gentian Lutea L.: analysis of the distribution of metabolites from root to leaves and flowers (in writing)

7.1.3. References

Aiello, N., Bontempo, R., & Vender, C. (2013). L'utilisation de caractères morphologiques et de la teneur en amarogentine pour la caractèrisation de populations spontanées de gentiane jaune (Gentiana lutea L.) du Nord Est de l'Italie. *Acta Botanica Gallica*, *160*(1), 33–41. https://doi.org/10.1080/12538078.2013.772497

Allen, D., Bilz, M., Leaman, D.J., Miller, R.M., Timoshyna, A. and Window, J. (2014). *European Red List of Medicinal Plants*. Publications Office of the European Union.

Altemimi, A., Lakhssassi, N., Baharlouei, A., Watson, D. G., & Lightfoot, D. A. (2017). Phytochemicals: Extraction, isolation, and identification of bioactive compounds from plant extracts. *Plants*, *6*(4). https://doi.org/10.3390/plants6040042

Balandrin, M., Douglas Kinghorn, A., & Farnsworth, N. R. (1993). Plant-Derived natural products in drug discovery and development. In *Human Medical Agents form Plants*. American Chemical Society. https://doi.org/10.1142/9789812790781_0002

Brusotti, G., Cesari, I., Dentamaro, A., Caccialanza, G., & Massolini, G. (2014). Isolation and characterization of bioactive compounds from plant resources: The role of analysis in the ethnopharmacological approach. *Journal of Pharmaceutical and Biomedical Analysis*, *87*, 218–228. https://doi.org/10.1016/j.jpba.2013.03.007

Carnat, A., Fraisse, D., Carnat, A. P., Felgines, C., Chaud, D., & Lamaison, J. L. (2005). Influence of drying mode on iridoid bitter constituent levels in gentian root. *Journal of the Science of Food and Agriculture*, *85*(4), 598–602. https://doi.org/10.1002/jsfa.2011

Chinese Pharmacopeia Commission. (2015). *Pharmacopoeia of the People's Republic of China, Volume I*. People's Medical publishing House.

European Environment Agency. (n.d.). *Gentiana Lutea L.* Retrieved October 15, 2022, from https://eunis.eea.europa.eu/species/172882#legal_status

European Medicines Agency. (n.d.). *Gentianae radix*. Retrieved October 15, 2022, from https://www.ema.europa.eu/en/medicines/herbal/gentian

ae-radix

European Medicines Agency. (2018). *European Union herbal monograph on Gentiana lutea L., radix*. https://www.ema.europa.eu/en/documents/herbal-monograph/european-herbal-monograph-gentiana-lutea-l-radix-revision-1_en.pdf

Fadzil, N. S. M., Sekar, M., Gan, S. H., Bonam, S. R., Wu, Y. S., Vaijanathappa, J., Ravi, S., Lum, P. T., & Dhadde, S. B. (2021). Chemistry, pharmacology and therapeutic potential of swertiamarin – a promising natural lead for new drug discovery and development. *Drug Design, Development and Therapy*, *15*(June), 2721–2746. https://doi.org/10.2147/DDDT.S299753

Farinon, B., Costantini, L., Molinari, R., Di Matteo, G., Garzoli, S., Ferri, S., Ceccantoni, B., Mannina, L., & Merendino, N. (2022). Effect of malting on nutritional and antioxidant properties of the seeds of two industrial hemp (Cannabis sativa L.) cultivars. *Food Chemistry*, *370*(April 2021). https://doi.org/10.1016/j.foodchem.2021.131348

International Union for Conservation of Nature (IUCN). (2022).

Gentian. The IUCN Red List of Threatened Species. https://www.iucnredlist.org/search?query=gentian&searchType=species

Japanese Pharmacopeia Commission. (2001). *The Japanese Pharmacopoeia*. Ministry of Health, Labour and Welfare.

Joshi, K., Pant, N. C., Kumar, V. A., & Kumar, A. (2017). Antioxidant and antibacterial activities of methanol, ethanol and aqueous extracts of leaf and root of Gentiana kurroo Royle. *Annals of Phytomedicine: An International Journal*, *6*(2), 138–148. https://doi.org/10.21276/ap.2017.6.2.14

Khan, I. A., & Abourashed, E. A. (2010). Gentian. In *Leung's Encyclopedia of Common Natural Ingredients Used in Food, Drugs, and Cosmetics* (Third edit). Wiley.

Mathew, A., Taranalli, A. D., & Torgal, S. S. (2004). Evaluation of anti-inflammatory and wound healing activity of Gentiana lutea rhizome extracts in animals. *Pharmaceutical Biology*, *42*(1), 8–12. https://doi.org/10.1080/13880200390502883

Mei, S., Ma, H., & Chen, X. (2021). Anticancer and anti-

inflammatory properties of mangiferin: A review of its molecular mechanisms. *Food and Chemical Toxicology*, *149*(October 2020), 111997. https://doi.org/10.1016/j.fct.2021.111997

Mustafa, A. M., Ricciutelli, M., Maggi, F., Sagratini, G., Vittori, S., & Caprioli, G. (2014). Simultaneous Determination of 18 Bioactive Compounds in Italian Bitter Liqueurs by Reversed-Phase High-Performance Liquid Chromatography-Diode Array Detection. *Food Analytical Methods*, *7*(3), 697–705. https://doi.org/10.1007/s12161-013-9727-0

PhEUR. (2020). Gentian root. Gentianae radix. Monograph 07/2015:0392. In *European Pharmacopoeia* (10th Editi).

Piluzza, G., Delogu, G., Cabras, A., Marceddu, S., & Bullitta, S. (2013). Differentiation between fiber and drug types of hemp (Cannabis sativa L.) from a collection of wild and domesticated accessions. *Genetic Resources and Crop Evolution*, *60*(8), 2331–2342. https://doi.org/10.1007/s10722-013-0001-5

Shahidi, F., & Ambigaipalan, P. (2015). Phenolics and

polyphenolics in foods, beverages and spices: Antioxidant activity and health effects - A review. In *Journal of Functional Foods* (Vol. 18). https://doi.org/10.1016/j.jff.2015.06.018

Spano, M., Di Matteo, G., Rapa, M., Ciano, S., Ingallina, C., Cesa, S., Menghini, L., Carradori, S., Giusti, A. M., Di Sotto, A., Di Giacomo, S., Sobolev, A. P., Vinci, G., & Mannina, L. (2020). Commercial hemp seed oils: A multimethodological characterization. *Applied Sciences (Switzerland)*, *10*(19), 1–15. https://doi.org/10.3390/app10196933

Spano, M., Matteo, G. Di, Ingallina, C., Botta, B., Quaglio, D., Ghirga, F., Balducci, S., Cammarone, S., Campiglia, E., Giusti, A. M., Vinci, G., Rapa, M., Ciano, S., Mannina, L., & Sobolev, A. P. (2021). A Multimethodological Characterization of Cannabis sativa L . Inflorescences from Seven Dioecious Cultivars Grown in Italy : The Effect of Different Harvesting Stages. *Molecules*, *26*(10), 2912. https://doi.org/https://doi.org/10.3390/molecules26102912

Spano, M., Matteo, G. Di, Ingallina, C., Sobolev, A. P., Giusti, A.

M., Vinci, G., Cammarone, S., Tortora, C., Lamelza, L., Prencipe, S. A., Gobbi, L., Botta, B., Marini, F., Campiglia, E., & Mannina, L. (2022). Industrial Hemp (Cannabis sativa L .) Inflorescences as Novel Food : The Effect of Different Agronomical Practices on Chemical Profile. *Foods*, *11*, 3658. https://doi.org/https://doi.org/10.3390/foods11223658

Studies on the antimicrobial activity and chemical composition of the essential oils and alcoholic extracts of Gentiana asclepiadea L. (2011). In *Journal of Medicinal Plants Research Vol. 5* (pp. 1164–1174).

Tutin, T. G., Heywood, S. M., Burges, N. A., Moore, D. M., Valentine, D. H., Walters, S. M., & Webb, D. A. (1972). Gentiana L. In *Flora Europea, vol. 3*. Cambridge University Press.

Venditti, A., Guarcini, L., Altieri, A., & Bianco, A. (2013). Phytochemical pattern of Gentiana species of Appennino in Central Italy. *Natural Product Research*, *27*(21), 2063–2065. https://doi.org/10.1080/14786419.2013.819863

Wijngaard, H., Hossain, M. B., Rai, D. K., & Brunton, N. (2012).

Techniques to extract bioactive compounds from food by-products of plant origin. *Food Research International*, *46*(2), 505–513. https://doi.org/10.1016/j.foodres.2011.09.027

Yang, J. L., Liu, L. L., & Shi, Y. P. (2010). Phytochemicals and biological activities of Gentiana species. *Natural Product Communications*, *5*(4), 649–664. https://doi.org/10.1177/1934578x1000500432

7.2. Case study 1: Multimethodological characterization of seven dioecious cultivars of industrial hemp

Cannabis inflorescences have been traditionally considered as a waste product in the industrial field but, in the last years, the interest for this part of the plant increased exponentially, mainly for the extraction of cannabinoids and essential oils. The chemical composition of hemp inflorescences can be affected by several factors such as genotype, pedoclimatic conditions, agronomical practices, and harvesting time.

In the present work, the chemical profile of the female inflorescence extracts from seven *Cannabis sativa* L. dioecious cultivars (Carmagnola, Fibranova, Eletta Campana, Antal, Tiborszallasi, Kompolti, and Tisza) was monitored at three harvesting stages, reaching from the beginning of flowering to end of flowering/beginning of seed formation, using untargeted NMR and targeted UHPLC and spectrophotometry analyses

molecules

MDPI

Article

A Multimethodological Characterization of *Cannabis sativa* L. Inflorescences from Seven Dioecious Cultivars Grown in Italy: The Effect of Different Harvesting Stages

Mattia Spano [1,†], Giacomo Di Matteo [1,†], Cinzia Ingallina [1], Bruno Botta [1], Deborah Quaglio [1], Francesca Ghirga [1], Silvia Balducci [1], Silvia Cammarone [1], Enio Campiglia [2], Anna Maria Giusti [3], Giuliana Vinci [4], Mattia Rapa [4], Salvatore Ciano [4], Luisa Mannina [1,*] and Anatoly P. Sobolev [5]

[1] Department of Chemistry and Technology of Drugs, Sapienza University of Rome, Piazzale Aldo Moro 5, 00185 Rome, Italy; mattia.spano@uniroma1.it (M.S.); giacomo.dimatteo@uniroma1.it (G.D.M.); cinzia.ingallina@uniroma1.it (C.I.); bruno.botta@uniroma1.it (B.B.); deborah.quaglio@uniroma1.it (D.Q.); francesca.ghirga@uniroma1.it (F.G.); silvia.balducci@uniroma1.it (S.B.); silvia.cammarone@uniroma1.it (S.C.)

[2] Department of Agricultural and Forest Sciences, University of Tuscia, Via San Camillo de Lellis snc, 01100 Viterbo, Italy; campigli@unitus.it

[3] Department of Experimental Medicine, Sapienza University of Rome, P.le Aldo Moro 5, 00185 Rome, Italy; annamaria.giusti@uniroma1.it

[4] Department of Management, Sapienza University of Rome, Via del Castro Laurenziano 9, 00161 Rome, Italy; giuliana.vinci@uniroma1.it (G.V.); mattia.rapa@uniroma1.it (M.R.); salvatore.ciano@uniroma1.it (S.C.)

[5] Institute for Biological Systems, Magnetic Resonance Laboratory "Segre-Capitani", CNR, Via Salaria Km 29.300, 00015 Monterotondo, Italy; anatoly.sobolev@cnr.it

* Correspondence: luisa.mannina@uniroma1.it; Tel.: +39-06-49913735

† These authors contributed equally to this work.

check for updates

Citation: Spano, M.; Di Matteo, G.; Ingallina, C.; Botta, B.; Quaglio, D.; Ghirga, F.; Balducci, S.; Cammarone, S.; Campiglia, E.; Giusti, A.M.; et al. A Multimethodological Characterization of *Cannabis sativa* L. Inflorescences from Seven Dioecious Cultivars Grown in Italy: The Effect of Different Harvesting Stages. *Molecules* **2021**, *26*, 2912. https://doi.org/10.3390/molecules26102912

Academic Editor: Severina Pacifico

Received: 15 April 2021
Accepted: 12 May 2021
Published: 14 May 2021

Publisher's Note: MDPI stays neutral with regard to jurisdictional claims in published maps and institutional affiliations.

Copyright: © 2021 by the authors. Licensee MDPI, Basel, Switzerland. This article is an open access article distributed under the terms and conditions of the Creative Commons Attribution (CC BY) license (https://creativecommons.org/licenses/by/4.0/).

Abstract: The chemical profile of the female inflorescence extracts from seven *Cannabis sativa* L. dioecious cultivars (Carmagnola, Fibranova, Eletta Campana, Antal, Tiborszallasi, Kompolti, and Tisza) was monitored at three harvesting stages (4, 14, and 30 September), reaching from the beginning of flowering to end of flowering/beginning of seed formation, using untargeted nuclear magnetic resonance (NMR) and targeted (ultra-high-performance liquid chromatography (UHPLC) and spectrophotometry) analyses. The tetrahydrocannabinol content was always below the legal limits (<0.6%) in all the analyzed samples. The NMR metabolite profile (sugars, organic acids, amino acids, and minor compounds) subjected to principal components analysis (PCA) showed a strong variability according to the harvesting stages: samples harvested in stage I were characterized by a high content of sucrose and myo-inositol, whereas the ones harvested in stage II showed high levels of succinic acid, alanine, valine, isoleucine, phenylalanine, and threonine. Samples harvested in stage III were characterized by high levels of glucose, fructose, choline, trigonelline, malic acid, formic acid, and some amino acids. The ratio between chlorophylls and carotenoids content indicated that all plants grew up exposed to the sun, the Eletta Campana cultivar having the highest pigment amount. Tiborszallasi cultivar showed the highest polyphenol content. The highest antioxidant activity was generally observed in stage II. All these results suggested that the *Cannabis sativa* L. inflorescences of each analyzed dioecious hemp cultivar presented a peculiar chemical profile affected by the harvesting stage. This information could be useful for producers and industries to harvest inflorescences in the appropriate stage to obtain samples with a peculiar chemical profile suitable for proper applications.

Keywords: industrial hemp; dioecious cultivars; inflorescences; phenological growth stages; cannabinoids; metabolite profile; antioxidant activity; multimethodological analysis

1. Introduction

Cannabis sativa L. is a plant of the *Cannabaceae* family widely used all over the world thanks to its multipurpose applications and climatic and territorial adaptability. From

a taxonomic point of view, different classifications of *Cannabis sativa* L. varieties exist causing sometimes some confusion. However, the generally accepted botanical classification is based on the content of psychotropic (Δ9-tetrahydrocannabinol, THC) and non-psychotropic (cannabidiol, CBD) cannabinoids: drug-type chemotype is characterized by higher levels of THC with respect to CBD, whereas fiber-type chemotype is characterized by low levels of THC (usually under 0.2%) and high levels of CBD [1]. Industrial hemp is a fiber-type *Cannabis sativa* L. traditionally cultivated and used worldwide for fiber (production of paper, ropes, and clothes) and seed (food uses) production [2]. During the 70′s, the illicit use of drug-type *Cannabis* for narcotic purposes led the European authorities to strongly restrict the cultivation and the industrial applications of *Cannabis sativa* L., including industrial hemp. In Italy, the second greatest hemp producer in the world after Russia [3], hemp cultivation almost disappeared due to legislative restrictions and the economic crisis. In the 90′s, the European Union published new regulations to promote and reintroduce the cultivation of *Cannabis sativa* L. cultivar with a low THC content ($\leq$0.2%, with a tolerance value of 0.6%) [4]. These cultivars are listed in an official European database [5], and their THC content is constantly monitored.

Following the European guidelines, Italy has started a process for the valorization of hemp cultivation and applications, and in 2017, the Lazio Region (Central Italy) approved a new regulation to enhance the reintroduction and the growth of *C. sativa* cultivations in the regional areas. In this scenario, the necessity of a better characterization and development of local *Cannabis sativa* L. products prompted the Lazio Region to support a project titled "Industrial Hemp: development and enhancement of a new eco-sustainable agro-food chain". *Cannabis* inflorescences have been traditionally considered as a waste product in the industrial field but, in the last years, the interest for this part of the plant increased exponentially, mainly for the extraction of cannabinoids and essential oils [6–8].

The chemical composition of hemp inflorescences can be affected by several factors such as genotype, pedoclimatic conditions, agronomical practices, and harvesting time [9–12].

Cannabis is naturally a dioecious cultivar; namely, the male and female flowers are presented on different plants: pollination occurs with the wind. Monoecious *Cannabis* cultivars are also obtained through breeding selection. The dioecious ones are mainly used for fiber production, whereas the monoecious ones for seed production [13,14].

In a previous paper [12], the chemical composition of the inflorescences from four *Cannabis sativa* L. monoecious cultivars, namely Ferimon, Uso-31, Felina 32, and Fedora 17, recently introduced in the Lazio Region, was monitored over the season using a multimethodological approach [15,16].

In this paper, the proposed protocol was extended to dioecious female inflorescences of seven *Cannabis sativa* L. cultivars (Carmagnola, Fibranova, Eletta Campana, Antal, Tiborszallasi, Kompolti, and Tisza) to determine their chemical composition and monitor possible variations according to three harvesting stages. Targeted methodologies, namely ultra-high-performance liquid chromatography (UHPLC) and spectrophotometry, were applied to analyze and to monitor cannabinoids, natural pigments, and total phenolics, as well as to evaluate the antioxidant activity of the inflorescences extracts. The seasonal time trend of sugars, amino acids, organic acids, and minor compounds was monitored using untargeted NMR spectroscopy, a very powerful tool to investigate the metabolite profile of vegetable matrices [17,18].

2. Results

Targeted and untargeted methodologies were used to determine the chemical profile of the inflorescences extracts at three harvesting stages (4 September, 14 September, and 30 September).

2.1. Targeted Analyses: Cannabinoids, Chlorophylls, Total Carotenoids, and Phenolics Content, Antioxidant Activity

The cannabinoid profile of the inflorescences methanol extracts was obtained using UHPLC. The concentrations of eight cannabinoids, namely CBDV, CBD, CBC, CBDA, CBG, CBN, Δ9-THC, and Δ9-THCA, are reported in Table 1. Δ8-THC, previously reported in medical cannabis samples [19], was not detected in the investigated samples. The total Δ9-THC/total CBD ratio was lower than 1.0 for all the analyzed samples, according to the fiber-type chemotype of all the selected hemp cultivars in the present study [20,21].

The chloroform extracts of *Cannabis sativa* L. inflorescences were analyzed with spectrophotometric technique in order to quantify the amount of chlorophyll a, chlorophyll b, and total carotenoids (Table 2). Chl a/chl b and chl (a+b)/carotenoid ratios are also reported in Table 2. Chl a/chl b ratio could be used as an indicator of the light exposition of the plants: a value of 1.1–1.3 was characteristic of shade exposition, whereas higher values were typical for sun-exposed plants. Chl (a+b)/car ratio was used as an indicator of both sun exposition and stress or senescence conditions of plants: a value of 4.2–5 was generally typical of sun-exposed plants, whereas a value below 3.5 was an indicator of senescence progress [22].

Total phenolics content and antioxidant activity (DPPH and ABTS assays) of hemp inflorescences (Table 3) were determined by spectrophotometric analysis. These untargeted assays were easy to perform, rapid, low-cost, and useful for achieving an overview of the antioxidant activity of the samples [23]. The ABTS•+ molecule showed low selectivity with aromatic OH- groups that gave a significant antioxidant contribution. In contrast, DPPH• (which was more selective with these compounds) had the disadvantage of steric accessibility. Small molecules had better access to the radical site showing higher apparent antioxidant activity [24]. For these reasons, the integrated use of these assays could complete the TPC assay's information. Hemp inflorescences exhibited high variability in antioxidant activity and total phenolic content.

2.2. Untargeted Analysis of Metabolite Profile by NMR and PCA

The NMR profile of hydroalcoholic Bligh–Dyer inflorescences extracts was obtained by using literature data [12]. Six sugars, six organic acids, thirteen amino acids, choline, and trigonelline were quantified at the three harvesting stages, and used for multivariate PCA, see Figure 1. In Table 4, the quantified metabolites in hydroalcoholic Bligh–Dyer extracts are listed, together with the chemical shift (ppm) of the signals used for quantification. Figure 1A,B show 2D PCA plots of sample scores and loading (PC1 versus PC2), whereas Figure 1C shows a 3D PCA plot of PC1, PC2, and PC3 sample scores. The first two PCs accounted for 63.2% of the variability within the data, whereas the first three PCs provided for 72.5% of the variability. PCs score plots showed a sample groping according to the harvesting stages. In particular, as it was clearly shown in the 3D score plot, the first two harvesting stages were separated along PC1 and PC3 (stage I having mainly negative PC1 values and positive PC3 values, stage II having positive PC1 values and negative PC3 values). Stage III (30 September) was well separated from the others and characterized by positive values of PC2. The contribution of the variables to this grouping given by the variable loadings reported in Figure 1B was discussed in detail in the Discussion paragraph.

Table 1. Cannabinoid concentrations by ultra-high-performance liquid chromatography (UHPLC analysis (% (*w*/*w*) ± SD) reported for each cultivar at three harvesting stages (stage I = 4 September, stage II = 14 September, stage III = 30 September). Analyses were carried out in triplicate.

Cultivar	Harvesting Stage	(–)-Δ9-THC	CBD	(–)-Δ9-THCA	CBDA	CBG	CBDV	CBC	CBN
Carmagnola	stage I	0.24 ± 0.02	3.10 ± 0.40	-	2.02 ± 0.30	0.13 ± 0.01	-	0.19 ± 0.02	-
	stage II	0.23 ± 0.01	3.12 ± 0.21	-	1.52 ± 0.02	0.17 ± 0.01	-	0.18 ± 0.01	-
	stage III	0.16 ± 0.01	3.82 ± 0.82	-	-	0.16 ± 0.01	-	0.13 ± 0.01	-
Fibranova	stage I	0.19 ± 0.01	2.05 ± 0.03	-	0.88 ± 0.04	0.18 ± 0.01	-	0.21 ± 0.01	-
	stage II	0.26 ± 0.01	2.97 ± 0.13	-	1.57 ± 0.07	0.18 ± 0.01	0.41 ± 0.01	0.33 ± 0.01	-
	stage III	0.11 ± 0.01	2.31 ± 0.30	-	-	-	-	-	0.11 ± 0.03
Kompolti	stage I	0.28 ± 0.01	2.90 ± 0.20	-	1.40 ± 0.10	0.15 ± 0.01	-	0.18 ± 0.01	-
	stage II	0.30 ± 0.01	5.09 ± 0.06	-	1.55 ± 0.02	0.18 ± 0.02	-	0.31 ± 0.01	-
	stage III	0.14 ± 0.01	4.64 ± 0.65	-	-	0.23 ± 0.01	-	0.15 ± 0.04	-
Tisza	stage I	0.193 ± 0.005	2.400 ± 0.100	-	1.280 ± 0.040	0.210 ± 0.010	-	0.17 ± 0.01	-
	stage II	0.250 ± 0.010	4.160 ± 0.220	-	1.910 ± 0.010	0.160 ± 0.010	-	0.21 ± 0.01	-
	stage III	0.061 ± 0.001	4.600 ± 0.090	-	-	0.091 ± 0.002	-	-	-
Antal	stage I	0.25 ± 0.01	4.30 ± 0.40	-	1.60 ± 0.30	0.22 ± 0.01	-	-	-
	stage II	0.14 ± 0.01	1.55 ± 0.15	-	1.11 ± 0.10	0.12 ± 0.01	-	-	-
	stage III	0.12 ± 0.01	1.96 ± 0.15	-	-	0.10 ± 0.01	0.09 ± 0.01	0.03 ± 0.01	-
Tiborszallasi	stage I	0.21 ± 0.01	2.76 ± 0.04	-	1.24 ± 0.03	0.24 ± 0.01	-	0.18 ± 0.01	-
	stage II	0.51 ± 0.07	4.54 ± 0.22	0.09 ± 0.01	1.87 ± 0.06	0.21 ± 0.01	-	0.22 ± 0.02	-
	stage III	0.13 ± 0.01	3.79 ± 0.41	-	-	0.12 ± 0.02	-	0.15 ± 0.02	-
Eletta Campana	stage I	0.17 ± 0.01	1.50 ± 0.10	-	1.00 ± 0.10	0.13 ± 0.01	-	-	-
	stage II	0.190 ± 0.01	2.04 ± 0.01	-	1.12 ± 0.02	0.12 ± 0.01	-	0.11 ± 0.01	-
	stage III	0.06 ± 0.01	1.37 ± 0.12	-	-	0.04 ± 0.01	-	0.05 ± 0.01	0.04 ± 0.01

Table 2. Chlorophyll a, chlorophyll b, and total carotenoid concentrations by spectrophotometric analysis (mg/g of fresh inflorescences ± SD) reported for each cultivar at three harvesting stages (stage I = 4 September, stage II = 14 September, stage III = 30 September). Chl a/b and Chl (a+b)/car ratios are also reported. Analyses were carried out in triplicate.

Cultivar	Harvesting Stage	Chlorophyll a	Chlorophyll b	Chl. a/b	Total Caroteoids	Chl. (a+b)/Car
Carmagnola	stage I	0.527 ± 0.050 §,e,c	0.337 ± 0.071 §,b,d,f	1.83 §,f	0.210 ± 0.023	4.03
	stage II	0.519 ± 0.004	0.272 ± 0.002	1.93	0.176 ± 0.002 §,f	4.49 §,c,d,f,g
	stage III	0.425 ± 0.008 *	0.235 ± 0.002	1.81	0.158 ± 0.002	4.16 §,c,d,e,f,g
Fibranova	stage I	0.540 ± 0.011 §,c,e	0.275 ± 0.004	2.27 §,f,g	0.201 ± 0.004	3.79
	stage II	0.683 ± 0.011 §,a,c,d,e,f,g	0.362 ± 0.004 §,a,c,d,e,f	1.89	0.223 ± 0.003 §,a,c,e,f	4.68 *,§,a,c,d,f,g
	stage III	0.271 ± 0.006	0.154 ± 0.001	1.76	0.106 ± 0.002	4.03 #,§,f
Kompolti	stage I	0.618 ± 0.002 §,a,b,d,e,f	0.330 ± 0.009 §,a,b,d,e,f	1.87	0.220 ± 0.001	4.32
	stage II	0.525 ± 0.004 §,f	0.290 ± 0.001	1.79	0.196 ± 0.002 §,a,f	4.15
	stage III	0.394 ± 0.002	0.219 ± 0.007	1.80	0.161 ± 0.001	3.81 *,#,§,f
Tisza	stage I	0.484 ± 0.003	0.241 ± 0.005	2.01 §,c,f,g	0.176 ± 0.001	4.13
	stage II	0.631 ± 0.006 *,§,a,c,e,f	0.324 ± 0.004 *,§,a,e,f	1.97 *	0.223 ± 0.003 *,§,a,c,e,f	4.29
	stage III	0.261 ± 0.004 *,#	0.161 ± 0.001 *,#	1.62 *	0.111 ± 0.002 *,#	3.79 *,#,§,f
Antal	stage I	0.565 ± 0.008 §,c,e	0.303 ± 0.008 §,d,f	1.86 §,f,g	0.218 ± 0.001 §,e,c	3.98
	stage II	0.580 ± 0.001 §,a,c,f	0.304 ± 0.003 §,a,f	1.93	0.188 ± 0.001	4.70 §,a,c,d,f,g
	stage III	0.354 ± 0.002 *,#	0.192 ± 0.003 *,#	1.84	0.142 ± 0.001	3.85 §,f
Tiborszallasi	stage I	0.335 ± 0.002	0.175 ± 0.003	1.91	0.129 ± 0.001	3.97
	stage II	0.449 ± 0.010 *	0.256 ± 0.002 *	1.73	0.162 ± 0.003 *	4.34 *,§,c
	stage III	0.218 ± 0.001 *,#	0.122 ± 0.001 *,#	1.79	0.106 ± 0.000 *,#	3.20 *,#
Eletta Campana	stage I	0.861 ± 0.010 §,a,b,c,d,e,f	0.432 ± 0.004 §,a,b,c,d,e,f	1.99	0.317 ± 0.003 §,d,e,f	4.08
	stage II	0.637 ± 0.001 *,§,a,c,e,f	0.366 ± 0.002 *,§,a,c,d,e,f	1.73	0.232 ± 0.001 *,§,a,c,e,f	4.32 *
	stage III	0.516 ± 0.004 *,#,§,d,f	0.275 ± 0.004*,#,§,d,f	1.88	0.205 ± 0.001 *,#,§,f	3.86 *

* $p < 0.001$, significantly different from the level in the same cultivar in stage I; # $p < 0.001$, significantly different from the level in the same cultivar in stage II; § $p < 0.001$, significantly different than the other cultivars in the same stage; [a] vs. Carmagnola; [b] vs. Fibranova; [c] vs. Kompolti; [d] vs. Tisza; [e] vs. Antal; [f] vs. Tiborszallasi; [g] vs. Eletta Campana (one-way ANOVA, followed by Bonferroni's Multiple Comparison Post Test).

Table 3. Total phenolic content (TPC) and antioxidant activity by spectrophotometric analysis (mg/g of fresh inflorescences or inhibition rate (I%) ± SD) reported for each cultivar in different harvesting stages (stage I = 4 September, stage II = 14 September, stage III = 30 September). Analyses were carried out in triplicate.

Cultivar	Harvesting Time	TPC (mg GAE/Kg FW)	DPPH (I%)	ABTS (I%)
Carmagnola	stage I	1.95 ± 0.06	72.87 ± 0.17	88.03 ± 0.39
	stage II	2.00 ± 0.06	78.74 ± 0.07	90.63 ± 0.74 ^{§,c,f}
	stage III	1.88 ± 0.08	75.38 ± 0.37	86.54 ± 0.89
Fibranova	stage I	1.65 ± 0.06	72.27 ± 0.17	85.56 ± 0.75 ^{§,e}
	stage II	2.38 ± 0.12	78.68 ± 0.15	92.68 ± 0.82 ^{§,c,f}
	stage III	2.01 ± 0.10	71.67 ± 0.43	86.66 ± 0.21
Kompolti	stage I	2.55 ± 0.08	75.42 ± 3.52	86.91 ± 0.39
	stage II	2.57 ± 0.10 ^{§,e}	75.57 ± 0.62	87.89 ± 0.69 *
	stage III	2.11 ± 0.06	72.63 ± 0.76	81.88 ± 0.33 $^{\#}$
Tisza	stage I	2.16 ± 0.09	73.17 ± 1.16	85.98 ± 0.29 ^{§,e,c}
	stage II	2.30 ± 0.10	75.29 ± 0.15	95.24 ± 0.16 ^{*,§,c,d}
	stage III	2.02 ± 0.06	71.97 ± 0.57	84.36 ± 0.42 *
Antal	stage I	1.84 ± 0.04	76.03 ± 1.34	95.35 ± 0.42
	stage II	1.67 ± 0.07	75.08 ± 0.81	84.84 ± 0.90 ^{§,c,d,f}
	stage III	1.54 ± 0.08	74.56 ± 0.52	84.56 ± 0.17 ^{§,a,b,c,d,f}
Tiborszallasi	stage I	2.41 ± 0.08	75.39 ± 0.86	87.32 ± 0.31
	stage II	2.68 ± 0.13 ^{§,e}	80.68 ± 1.07 ^{§,d}	88.03 ± 1.05 *
	stage III	2.42 ± 0.09 ^{§,a,e}	79.86 ± 0.79	84.18 ± 0.74 $^{\#}$
Eletta Campana	stage I	1.80 ± 0.0985.63	74.40 ± 0.51	91.67 ± 1.19 ^{§,e}
	stage II	2.10 ± 0.07	77.32 ± 0.44	93.05 ± 1.12 ^{§,c,f}
	stage III	2.05 ± 0.10	70.44 ± 3.66	92.40 ± 0.46 ^{§,a,b,c,d,f}

* $p < 0.001$, significantly different from the level in the same cultivar in stage I; $^{\#}$ $p < 0.001$, significantly different from the level in the same cultivar in stage II; § $p < 0.001$, significantly different than the other cultivars in the same stage; ^{a} vs. Carmagnola; ^{b} vs. Fibranova; ^{c} vs. Kompolti; ^{d} vs. Tisza; ^{e} vs. Antal; ^{f} vs. Tiborszallasi (one-way ANOVA, followed by Bonferroni's Multiple Comparison Post Test).

Table 4. Compounds, with relative ^{1}H NMR signals (ppm), quantified in *Cannabis sativa* L. inflorescences Bligh–Dyer hydroalcoholic extracts. Analyses were carried out in triplicate.

Compound	ppm	Compound	ppm
Isoleucine	1.02	Choline	3.21
Valine	1.05	Myo-inositol	3.30
Threonine	1.34	Fructose	4.04
Alanine	1.49	Malic acid	4.30
Proline	2.00	β-Glucose	4.66
Glutamic acid	2.07	α-Glucose	5.25
GABA	2.30	Sucrose	5.42
Succinic acid	2.41	Phenylalanine	7.43
Glutamine	2.46	Tryptophan	7.53
Aspartic acid	2.83	Formic acid	8.47
Asparagine	2.89	Trigonelline	9.12

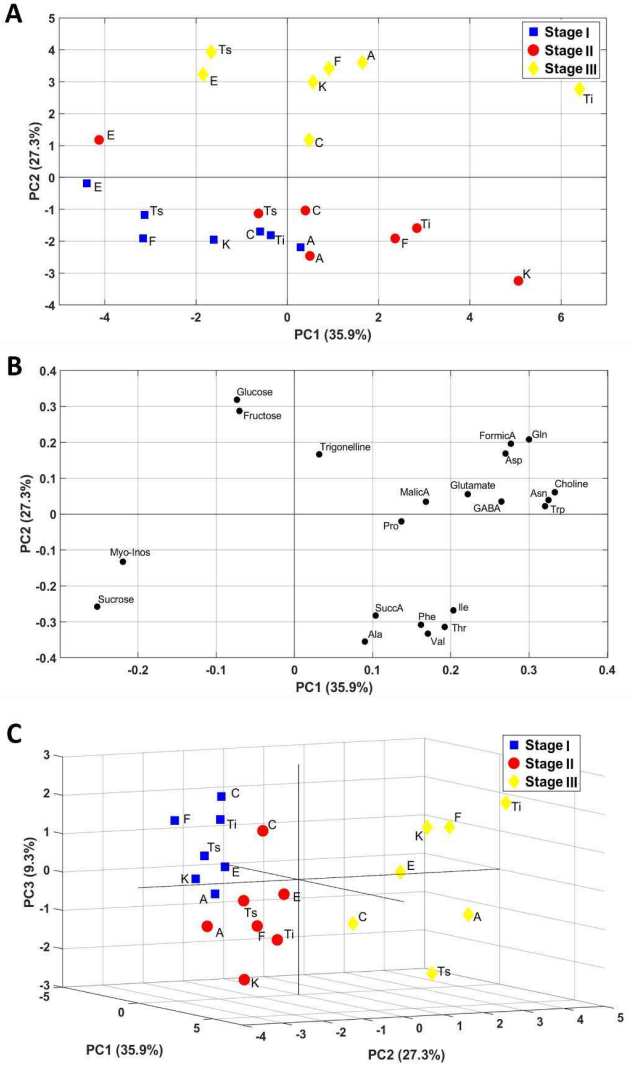


Figure 1. Principal components analysis (PCA) maps obtained using NMR data of inflorescences samples: (**A**) scores plot and (**B**) loadings plot relative to PC1 and PC2 (PCs); (**C**) score plot relative to PC1, PC2, and PC3. PC1, PC2, and PC3 represent 35.9%, 27.3%, and 9.3% of the total variance, respectively.

2.3. Metabolite Profile of the Inflorescences at Three Harvesting Stage

Trends of metabolite profiles during the three harvesting stages were discussed separately for each cultivar. Finally, a comparison among cultivars was also reported.

2.3.1. Carmagnola

Cannabinoids. CBD, the main cannabinoid, showed a gradual increase over the three different harvesting stages, reaching its maximum in stage III. The psychotropic cannabinoid THC remained constant over time, with a small decrease in stage III. The highest value of CBG was measured in stage II, whereas for CBC, the highest value was detected in stage I. CBDA was detected only in the first two stages, whereas THCA, CBDV, and CBN were not detected in all the harvesting stages (Table 1).

Free amino acids. Asparagine was found to be the main amino acid in hemp inflorescences. Asparagine amount, together with GABA and aspartic acid, increased during the time (Figure 2). Valine, glutamic acid, and proline showed an opposite trend. Glutamine content was quite constant in the first two harvesting stages and then slightly increased, whereas phenylalanine and isoleucine slightly decreased in stage III. Alanine and tryptophan concentrations were always constant.

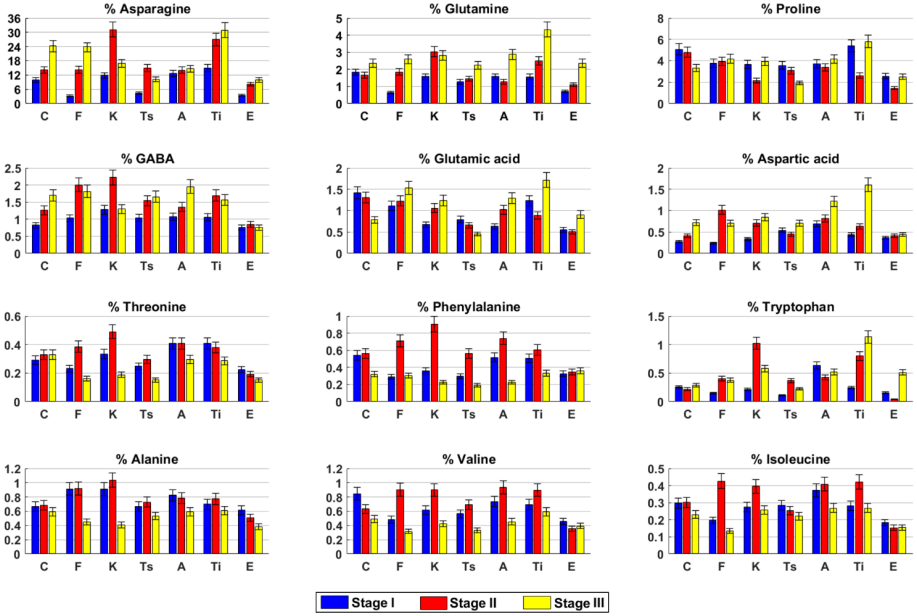


Figure 2. Free amino acids content in hydroalcoholic extracts of *Cannabis sativa* L. fresh inflorescences at three harvesting stages. C (Carmagnola), F (Fibranova), K (Kompolti), Ts (Tisza), A (Antal), Ti (Tiborszallasi), E (Eletta Campana).

Sugars. Sucrose, glucose, and fructose were the main sugars in hemp inflorescences. Sucrose drastically decreased from stage I to stage III (Figure 3A). Glucose and fructose remained quite constant. Myo-inositol content was constant in the first two stages and then doubled.

Organic acids. Malic acid increased over time, whereas succinic acid increased until stage II and then drastically decreased (Figure 3B). Formic acid was constant in the first two stages and then slightly increased.

Miscellaneous compounds. Trigonelline and choline increased over time (Figure 3C).

Pigments. Chlorophyll a, chlorophyll b, and total carotenoid contents decreased over time (Table 2). Chl a/chl b and chl (a+b)/car ratio values at the three stages were typical of sun-exposed plants, with the highest values in stage II.

Total phenolics and antioxidant activity. The highest content of total phenolic compounds (TPC) was measured in stage II, whereas the lowest one was found in stage III (Table 3). The same trend was also observed for both the inhibition rates in DPPH and ABTS assays.

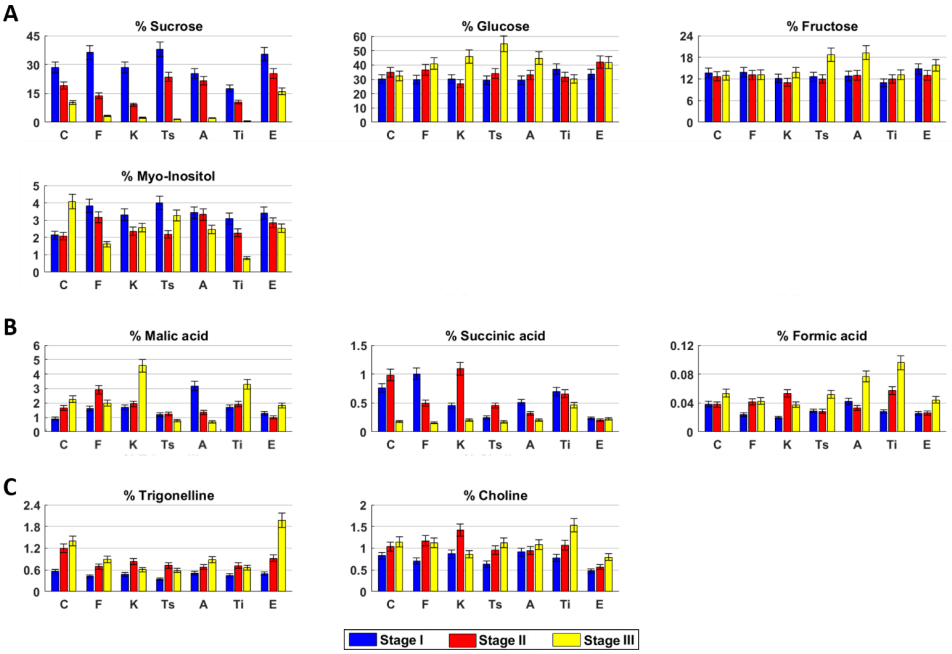


Figure 3. Sugars (**A**), organic acids (**B**), and miscellaneous compounds (**C**) content in hydroalcoholic extracts of *Cannabis sativa* L. fresh inflorescences at different harvesting stages. C (Carmagnola), F (Fibranova), K (Kompolti), Ts (Tisza), A (Antal), Ti (Tiborszallasi), E (Eletta Campana).

2.3.2. Fibranova

Cannabinoids. The highest contents of CBD and THC were measured in stage II (Table 1). Among the other cannabinoids, CBDA, CBG, and CBC were present only in the first two stages. Moreover, CBDV and CBN were detected only in stage II and stage III, respectively. THCA was never detected in all stages considered.

Free amino acids. Asparagine, glutamine, proline, and glutamic acid contents increased over time (Figure 2). Tryptophan and GABA increased from stage I to stage II and remained constant, whereas alanine was constant until stage II and then decreased. All the other amino acids analyzed reached their highest content in stage II.

Sugars. Sucrose and myo-inositol decreased during the time, whereas glucose showed an opposite trend. Fructose content was constant over time (Figure 3A).

Organic acids. The highest content of malic acid was measured in stage II, whereas succinic acid decreased over time. Formic acid slightly increased in stage II and then remained constant (Figure 3B).

Miscellaneous compounds. Choline and trigonelline concentrations increased from stage I to stage II and then remained constant (Figure 3C).

Pigments. Chlorophyll a, chlorophyll b, and total carotenoids content reached their highest value in stage II. Chl a/chl b and chl (a+b)/car ratio values at the three stages were typical of sun-exposed plants, with the highest value of chl a/chl b in stage I and the highest value of chl (a+b)/car in stage II (Table 2).

Total phenolics and antioxidant activity. The highest content of TPC was measured in stage II, whereas the lowest one was found in stage I. The same trend was also observed for the inhibition rate (I%) of ABTS assay, whereas in the DPPH assay, the highest and the lowest I% values were measured in stage I and stage III, respectively (Table 3).

2.3.3. Kompolti

Cannabinoids. The highest contents of THC, CBD, and CBC were measured in stage II, whereas for CBG, the highest value was measured in stage III. As a common trend, CBDA was not measured in stage III. THCA, CBDV, and CBN were never detected (Table 1).

Free amino acids. Asparagine, GABA, valine, isoleucine, threonine, phenylalanine, and tryptophan reached their highest concentrations in stage II. Conversely, in this stage, the lowest value of proline was measured. Glutamine, glutamic acid, and aspartic acid increased in stage II and remained constant (Figure 2).

Sugars. Sucrose drastically decreased over time (Figure 3A). Glucose and fructose slightly decreased in stage II and then increased. Myo-inositol decreased in stage II and then remained quite constant.

Organic acids. Malic acid slightly increased from stage I to stage II and then drastically decreased. Succinic and formic acids reached their highest content in stage II. (Figure 3B).

Miscellaneous compounds. Both choline and trigonelline reached their highest amount in stage II. (Figure 3C).

Pigments. Chlorophyll a, chlorophyll b, and total carotenoids, together with chl a/chl b and chl (a+b)/car ratios, decreased over time (Table 2).

Total phenolics and antioxidant activity. The highest content of TPC was measured in stage II, whereas the lowest one was found in stage III (Table 3). The same trend was also observed for both I % in DPPH and ABTS assays, although I % in the DPPH assay was quite the same in the first two harvesting stages.

2.3.4. Tisza

Cannabinoids. CBD drastically increased from stage I to stage III. The highest THC content was measured in stage II and drastically decreased (four times less) in stage III, whereas CBG content decreased during the time (Table 1). CBC and CBDA were measured only in stage II, whereas THCA, CBDV, and CBN were not detected.

Free amino acids. Asparagine, valine, threonine, phenylalanine, and tryptophan reached their highest contents in stage II, whereas proline, glutamic acid, and isoleucine slightly decreased over time (Figure 2). Glutamine and aspartic acid amounts were quite constant until stage II and then slightly increased. GABA increased in stage II and then remained constant, whereas the alanine amount was constant until stage II and then slightly decreased.

Sugars. Sucrose content drastically decreased over time, whereas glucose had an opposite trend (Figure 3A). Fructose content was constant until stage II and then increased, whereas myo-inositol content decreased in stage II and then increased.

Organic acids. Malic acid and formic acid contents were constant until stage II, then decreased and increased, respectively. Succinic acid amount was the highest in stage II (Figure 3B).

Miscellaneous compounds. Trigonelline content increased in stage II and then remained constant, whereas choline increased over time. (Figure 3C).

Pigments. Chlorophyll a, chlorophyll b, and total carotenoids, together with chl (a+b)/car, reached their highest value in stage II, whereas chl a/chl b ratio value was the highest in stage I (Table 2). However, both ratios were typical of sun-exposed plants.

Total phenolics and antioxidant activity. The highest content of TPC was measured in stage II, whereas the lowest one was found in stage III (Table 3). The same trend was also observed for both I% in DPPH and ABTS assays.

2.3.5. Antal

Cannabinoids. THC, CBD, and CBG reached their highest values in stage I and then decreased. Similarly, also the highest CBDA content was measured in stage I, although it was not detected in stage III. CBDV and CBC were detected only in stage III, whereas THCA and CBN were not detected in the stages considered (Table 1).

Free amino acids. Asparagine, GABA, glutamic acid, and aspartic acid slightly increased over time, whereas alanine had an opposite trend. Glutamine, proline, and tryptophan slightly decreased in stage II and then increased, whereas valine, isoleucine, and phenylalanine reached their highest content in stage II (Figure 2). Threonine remained constant until stage II and then decreased.

Sugars. Sucrose content drastically decreased over time, whereas glucose slightly increased (Figure 3A). Fructose and myo-inositol remained constant until stage II and then increased and decreased, respectively.

Organic acids. Malic and succinic acids decreased over time, whereas formic acid slightly decreased in stage II and then increased (Figure 3B).

Miscellaneous compounds. Trigonelline content was quite constant over time, whereas choline slightly increased. (Figure 3C).

Pigments. Chlorophyll a and total carotenoids content decreased over time, whereas chlorophyll b remained constant in the first two stages and then decreased. The highest values of chl a/chl b and chl (a+b)/car ratios were measured in stage II (Table 2).

Total phenolics and antioxidant activity. The highest values of TPC and I% in both DPPH and ABTS assays were measured in stage I then decreased over time (Table 3).

2.3.6. Tiborszallasi

Cannabinoids. THC, CBD, CBDA, and CBC reached their highest content in stage II, whereas the CBG amount decreased over time. THCA was detected only in stage II, whereas CBDV and CBN were never detected (Table 1).

Free amino acids. Asparagine, glutamine, aspartic acid, and tryptophan increased over time, whereas threonine had an opposite trend (Figure 2). Proline and glutamic acid reached their lowest content in stage II. Conversely, in this stage, the highest concentrations of GABA, alanine, valine, isoleucine, and phenylalanine were found.

Sugars. Sucrose, glucose, and myo-inositol concentrations decreased over time, whereas fructose had an opposite trend (Figure 3A).

Organic acids. Malic and formic acids increased over time, whereas succinic acid had an opposite trend (Figure 3B).

Miscellaneous compounds. Trigonelline increased in stage II and then remained constant. Choline slightly increased over time (Figure 3C).

Pigments. Chlorophyll a, chlorophyll b, and total carotenoids, together with chl (a+b)/car ratio, increased in stage II and then decreased (Table 3). Chl a/chl b ratio reached its highest content in stage I. Chl (a+b)/car ratio value in stage III indicated that the hemp plants were in the early stage of the senescence process.

Total phenolics and antioxidant activity. The highest content of TPC was measured in stage II, whereas the lowest one was found in stage I. The same trend was also observed for I% of the DPPH assay, whereas in the ABTS assay, the highest and the lowest I% values were measured in stage II and stage III, respectively (Table 4).

2.3.7. Eletta Campana

Cannabinoids. The highest contents of THC, CBD, CBDA, and CBC were measured in stage II, although CBDA and CBC were not detected in stage III and stage I, respec-

tively (Table 1). CBN was measured only in stage III, whereas THCA and CBDV were never detected.

Free amino acids. Asparagine and glutamine increased over the stages, whereas alanine and threonine showed an opposite trend (Figure 2). Proline, glutamic acid, valine, isoleucine, and tryptophan contents decreased in stage II and then increased. GABA, aspartic acid, and phenylalanine amounts remained quite constant over time.

Sugars. Sucrose and myo-inositol decreased over time, whereas glucose increased until stage II and then remained constant (Figure 3A). Fructose content had its highest concentration in stage II.

Organic acids. Malic acid content slightly decreased in stage II and then increased, whereas succinic acid remained quite constant during the three stages (Figure 3B). Formic acid concentration remained constant until stage II and then increased.

Miscellaneous compounds. Trigonelline and choline increased over time. (Figure 3C).

Pigments. Chlorophyll a, chlorophyll b, and total carotenoids decreased over time (Table 3). The highest values of chl a/chl b and chl (a+b)/car ratios were found in stage I and stage II, respectively. However, the ratio values in all the stages were indicators of the light exposition of the plant.

Total phenolics and antioxidant activity. The highest TPC content was measured in stage II, whereas the lowest one was found in stage I. The same trend was also observed for I% of ABTS assay, whereas in the DPPH assay, the highest and the lowest I% values were measured in stage II and stage III, respectively (Table 4).

3. Discussion

The cannabinoids content of the seven investigated cultivars (Carmagnola, Fibranova, Kompolti, Tisza, Antal, Tiborszallasi, and Eletta Campana) revealed common features but also important differences. In all the analyzed cultivars, the THC content was always under the legal limit, including Carmagnola, Fibranova, and Antal cultivars that, in 2019, were excluded from the European Plant Database because of the variable THC content. In particular, the lowest THC concentrations were measured in stage III in Tisza and Eletta Campana cultivars, whereas the highest one was measured in Tiborszallasi in stage II (0.51%). As expected for the fiber-type chemotype, CBD was found to be the most abundant cannabinoid, with the highest concentration measured in Kompolti cultivar in stage II (5.09%). The presence of high levels of CBD in female inflorescences of dioecious *Cannabis sativa* L. can be important from a pharmacological/nutraceutical point of view, considering that CBD is a non-psychotropic cannabinoid with several biological activities [25]. CBDA, the acid form of CBD, was present only in stage I and stage II, whereas THCA, the acid form of THC, was measured only in Tiborszallasi cultivar in stage II. Similarly, CBN was measured only in stage III in Fibranova and Eletta Campana cultivars, whereas CBDV was measured only in Fibranova and Antal cultivars in stage II and stage III, respectively. CBG and CBC were detected in most of the samples, as previously reported. Although these two cannabinoids were generally of less interest with respect to THC and CBD, they represented a new potential resource for the pharmaceutical/nutraceutical field [26,27].

In a previous HPLC study [21], the cannabinoids content of ethanolic extracts from Tisza, Tiborszallasi, Antal, and Carmagnola cultivars grown in Slovenia in September was reported: lower levels of THC and CBD with respect to those of THCA and CBDA had been detected. On the contrary, in our study, the neutral forms CBD and THC were more abundant than their acid forms: THCA was observed only in one sample, whereas CBDA was present only in stage I and stage II of all cultivars, confirming a decrement in this cannabinoid over the harvesting time. Therefore, the different contents of THCA and CBDA detected in the inflorescences grown in Slovenia were potentially due to different agronomic growing conditions.

In another study, the THC and CBD contents in hexane extracts of Kompolti air-dried inflorescences grown in Austria [28] were reported being at least two times lower than

those observed in the same cultivar in the present study. However, no indication regarding the harvesting stage was reported, making it difficult for comparison.

The spectrophotometric analysis of chlorophylls and total carotenoids showed that chlorophyll a was always more abundant with respect to chlorophyll b, underlining the major involvement of chlorophyll a in the photosynthetic process. The maximum content of chlorophyll a, chlorophyll b, and total carotenoids was observed in stage I or stage II, depending on the cultivar. Conversely, regardless the cultivar, the lowest concentrations of the analyzed pigments were always found in stage III. Among the cultivars, Eletta Campana cultivar was characterized by the highest values of all the analyzed pigments in all the harvesting stages, whereas Tiborszallasi cultivar showed the opposite trend. Considering the chl a/chl b ratio, all samples showed values above 1.3, revealing that hemp plants were grown in light exposition conditions at all the considered stages. Additionally, the chl (a+b)/car ratio indicated the light exposition conditions of the plants; moreover, the obtained values showed that, until the end of September, plants did not reach their senescence phase, except for Tiborszallasi cultivar (ratio value of 3.20). It was noteworthy that the quantitative trend of chlorophylls and carotenoids during the considered stages was strictly correlated. In particular, an increase in chlorophylls generally coincided with an increment of carotenoids, too, although with different rates. This correlation could be explained since chlorophylls and carotenoids synthesis were characterized by common pathways [29,30].

Regarding the total phenolic content, the lowest TPC value was measured in Fibranova in stage I, whereas the highest one was detected in Tiborszallasi in stage II. The TPC results suggested a different behavior of the investigated cultivars. Fibranova, Tisza, Tiborszallasi, and Eletta Campana presented a similar trend with an increment of TPC values in stage II, followed by a decrease (with different slopes) in stage III. Carmagnola and Kompolti, indeed, had a decrement in the last harvesting stage. Antal cultivar showed a unique trend, with a decrease in TPC values during the three harvesting stages. DPPH and ABTS showed different profiling of the cultivars during the harvesting stages. Carmagnola, Fibranova, Tisza, and Eletta Campana showed a similar trend for DPPH and ABTS assays with the highest values in stage II. Antal, here too, showed a unique trend with the decrease in the %I for both tests. Kompolti presented a different trend for the antioxidant activity tests; in the DPPH assay, its trend was the same as the Antal cultivars, whereas, in the ABTS assay, the trend was that of the other cultivars. In a previous work [31], the TPC and the antioxidant activity (DPPH assay) of Carmagnola, Antal, Kompolti, and Tiborszallasi cultivars were determined. However, since the sample treatment, the extraction procedure, and the expression of the results were different from those of the present work, and it was not possible to make a comparison. Among the analyzed classes of compounds, polyphenols were, of course, involved in the antioxidant activity of hydroalcoholic hemp extracts since this activity was well recognized for these compounds [32,33]. In particular, hemp inflorescences showed to be characterized by phenolic acids and flavonoids as the main polyphenolic compounds [31,34]. Moreover, also cannabinoids, mainly THC and CBD, proved to be characterized by antioxidant activity [35,36]. Since the chemical profile of hemp inflorescences was very complex, it could be not easy to correlate the antioxidant activity trend of hemp extracts with that of specific chemical compounds, which was also shown by literature data [37]. In fact, the Pearson correlation coefficient (Table S1) not always showed a strong correlation between TPC and antioxidant activity assays. However, it could be supposed that polyphenols and cannabinoids were strongly involved in the antioxidant activity of hemp inflorescences, which was supported by the obtained results. In particular, for the analyzed cultivars, the highest antioxidant activity was generally observed in stage II, as well as the content of cannabinoids and total polyphenols. Moreover, Antal cultivar, whose antioxidant activity was higher in stage I, was also characterized by the highest contents of polyphenols and cannabinoids, particularly CBD, in this period.

As for the metabolite profile of hemp inflorescences, it was possible to observe analogies and differences among cultivars and harvesting stages. Among amino acids, as-

paragine was found to be the most abundant in all cultivars, mainly in the last two harvesting stages, with the highest content measured in Kompolti cultivar in stage II (31%). Sucrose content was very high in all cultivars in stage I, with the highest concentration found in Tisza cultivar (38%), whereas in stage III its content was very low, reaching the lowest value in Tiborszallasi cultivar (0.6%). Malic acid was the main organic acid, with the highest concentration measured in Kompolti cultivar in stage III. These metabolites can affect the sensorial properties of hemp infusions and beverages that can be used for food or pharmacological purposes [38]. The PCA analysis of NMR data showed that in general, regardless of the cultivar, metabolite profiles could be differentiated owing to the harvesting stage. In particular, samples harvested in stage I were characterized by high contents of sucrose and myo-inositol, whereas the ones harvested in stage II showed higher levels of succinic acid, alanine, and essential amino acids. Samples harvested in stage III were distinguished by high levels of monosaccharides, choline, trigonelline, malic acid, formic acid, and some amino acids. In a previous work [12], the NMR metabolite profile of four monoecious hemp cultivars was determined by using the same analytical protocol of the present work. Comparing the quantitative results obtained for both monoecious and dioecious cultivars in September (considering the 14 September data for the present work), it was possible to observe that the two groups presented peculiar metabolites (Figure S1). In particular, higher levels of fructose, formic acid, malic acid, choline, and trigonelline were observed in monoecious cultivars, whereas dioecious cultivars were characterized by higher amounts of glucose and some amino acids: valine, threonine, alanine, and asparagine. The obtained results allowed us to observe how, basing on the cultivar and/or the harvesting stage, hemp inflorescences were characterized by a peculiar chemical profile suitable for several industrial applications. For instance, mid-September harvesting (stage II) was the most effective to obtain high concentrations of CBD and polyphenols; suggesting this harvesting stage as the main effective to obtain inflorescences with high pharmaceutical and nutraceutical properties. However, for Antal cultivar, the proper period to obtain inflorescences rich in bioactive compounds was early September (stage I). Moreover, secondary metabolites, such as sugars and organic acids, could affect the sensorial properties of hemp-based products, such as infuses. In this context, the Tisza cultivar was characterized by high levels of sugars in stage I and stage III harvesting periods, whereas Kompolti was particularly rich in malic acid in stage III.

4. Materials and Methods

4.1. Reagents and Chemicals

Gradient grade water, acetonitrile, chloroform, methanol, and formic acid were purchased from Merck Life Science (Milano, Italy). Cannabinoid reference standards dissolved in methanol, namely, cannabidivarin (CBDV, 1 mg/mL), cannabigerol (CBG, 1 mg/mL), cannabidiol (CBD, 1 mg/mL), cannabidiolic acid (CBDA, 1 mg/mL), cannabinol (CBN, 1 mg/mL), (–)-Δ9-tetrahydrocannabinol ((–)-Δ9-THC, 1 mg/mL), Δ9-tetrahydrocannabinolic acid ((–)-Δ9-THCA, 1 mg/mL), (–)-Δ8- tetrahydrocannabinol ((–)-Δ8-THC, 1 mg/mL), and cannabichromene (CBC, 1 mg/mL) with purity $\geq$ 99%, were purchased from Merck Life Science (Milano, Italy). Deuterated water (D_2O) 99.97 atom% of deuterium and 3-(trimethylsilyl)-propionic-2,2,3,3-d_4 acid sodium salt (TSP) were purchased from Euriso-Top (Saclay, France). Magnesium oxide (MgO), potassium phosphate monobasic (KH_2PO_4), and potassium phosphate dibasic (K_2HPO_4) 2,2-azino-bis (3-ethyl-benzothiazoline-6-sulfonic acid) diammonium salt (ABTS), 2,2-diphenyl-1-picrylhydrazyl (DPPH), Folin-Ciocalteu reagent, gallic acid (GA), and sodium carbonate (Na_2CO_3) were purchased from Merck Life Science (Milano, Italy).

4.2. Hemp Plant Material

Fresh inflorescences of seven dioecious female *Cannabis sativa* L. cultivars (Carmagnola, Fibranova, Eletta Campana, Antal, Tiborszallasi, Kompolti, and Tisza) were provided by the Canapa Live cultural association. They were grown in experimental fields located

in the North Lazio area (Italy, Rome) during the 2018 cultivation year. Carmagnola, Fibranova, and Eletta Campana are Italian cultivars, Antal is a cultivar from the Czech Republic, whereas Tisza, Tiborszallasi, and Kompolti are cultivars from Hungary. The same agronomical practices, previously described in [12], were used for plant cultivation. The inflorescences sampling was carried out by applying the following systematic pattern: for each cultivar, 25 plants were collected in the central part of the cultivation area by cutting the upper part (30 cm) of the stem. Considering the late (Antal, Tisza, Tiborszallasi, Kompolti) and very late (Carmagnola, Fibranova, Eletta Campana) vegetative cycles of the selected cultivars, female inflorescences were harvested in the following three stages: 4 September (stage I), 14 September (stage II), and 30 September (stage III) reaching from beginning of flowering to the end of flowering/beginning of seed formation. After harvesting, fresh inflorescences were ground under N_2 and stored at −80 °C until analysis. Analyzes were carried out within ten days of storage. Note that, since 2019, Carmagnola, Fibranova, and Antal cultivars were banned from the EU Plant Variety Database [5] because of their unstable THC content.

4.3. Cannabinoids Content by UHPLC Analyses

For each sample, 4 g of ground fresh inflorescences were dried at 70 °C for 48 h before extraction. After drying, 100 mg of inflorescences were extracted with 4 mL of methanol [39,40] in an ultrasonic bath for 30 min. The residual pellet was re-extracted again two times. Each extract was then filtered under vacuum conditions, diluted to 5 mL with methanol, filtered with a 0.45 μm PTFE membrane, and finally analyzed.

Analyses were carried out by using an Ultimate 3000 ultra-high-performance liquid chromatography (UHPLC; Thermo Fisher Scientific) (Rodano, Italy), with a binary gradient system, an automatic injector, a thermostatic column compartment, and a diode array detector. The system was controlled by Chromeleon Chromatography Data System software (Thermo Fisher Scientific, 1.0.5. v, Waltham, MA, USA, 2018. All separations were performed by using a Titan C 18 column (10 cm × 3 cm, 1.9 μm, Sigma Aldrich (Milan, Italy) with a mobile phase composed of 0.1% formic acid in both (A) water and (B) acetonitrile. The total run time was 22 min, and the chromatographic conditions were set as follows: 0–14 min from 65 to 100% B, 15–16 min isocratic elution with 100% B, 17–22 min from 100 to 65% B. The flow rate was 0.5 mL/min. The column temperature was set at 35 °C. A volume of 10 μL was injected. The PDA detector was set to 214 nm wavelength.

To prepare the calibration curve, standard cannabinoid solutions of CBDV, CBD, CBC, CBDA, CBG, CBN, Δ8-THC, Δ9-THC, and Δ9-THCA were prepared in the concentration range from 0.001 to 0.05 mg/mL.

Regression lines were calculated using the least squares method, and linearity was expressed by the determination coefficient (R^2). For each calibration curve, the R^2 value was always greater than 0.998, underlining good linearity.

Cannabinoid concentrations were expressed as percentage (*w/w*) ± SD (standard deviation; Table 2). Three replications were made for each sample.

4.4. Untargeted NMR Analysis and Multivariate Statistical Analysis

For the untargeted analysis, the fresh plant material was extracted by using the Bligh–Dyer protocol [41] already described in detail [12]. The dried hydroalcoholic extracts were solubilized in 0.75 mL of 400 mM phosphate buffer/D_2O, containing a 1 mM TSP as internal standard, and then transferred into a 5 mm NMR tube. NMR analyses were carried out on a Bruker AVANCE 600 spectrometer operating at the proton frequency of 600.13 MHz and equipped with a Bruker multinuclear z-gradient 5 mm probe head (Milan, Italy). ^{1}H spectra were registered using the following parameters: 28 °C sample temperature, 256 transients, suppression of residual water signal (HDO) using a presaturation, 5 s recycle delay, 45° pulse of 7.5 μs, and 32 K data points. Two-dimensional (2D) experiments (^{1}H-^{1}H TOCSY, ^{1}H-^{13}C HSQC, and ^{1}H-^{13}C HMBC) were carried out using the same experimental conditions previously reported [42]. Spectra were processed

using TopSpin software (version 4.0.6, Billerica, MA, USA, 2017). For quantitative analysis, the integrals of the corresponding selected resonances in ^{1}H NMR spectra (Table 2) were measured with respect to the internal standard TSP, allowing the molar concentration and the corresponding weight to be calculated. The amount of each metabolite was expressed as weight percentage with respect to the total weight of all quantified metabolites. Each sample was extracted and analyzed three times. The 21 quantified metabolites (Figures 2 and 3) in the hydroalcoholic phase were used as variables for the principal component analysis (PCA) by using MATLAB software (version R2020b). Before the analysis, the selected variables were processed using autoscaling and then mean centered.

4.5. Spectrophotometric Analysis of Chlorophylls and Total Carotenoids

Pigments extraction was carried out according to Mizliack–Solovchenko, with some modifications [43]: 30 mg of the sample was homogenized with mortar and pestle in 6 mL of a chloroform–methanol (2:1, *v/v*) mixture, together with 20 mg of MgO, in order to neutralize plant acids and prevent pheophytin formation [22]. After filtration, a volume of distilled water equal to the 20% of the organic extract volume was added, and the emulsion was centrifuged for 20 min (20 °C, 2500× *g*). The organic phase, which contained chlorophylls and carotenoids, was separated from the hydroalcoholic one and then analyzed. The absorption spectrum was acquired by an ONDA spectrophotometer UV-30 SCAN (spectral resolution 0.1 nm) in the wavelength range of 350–800 nm at 25 °C (sipper system A-100 series) (Milan, Italy). The absorbance values measured at 480, 648, and 666 were considered. The concentrations (µg/mL) of chlorophyll a (Chl a), chlorophyll b (Chl b), and total carotenoids (Car) were calculated according to Wellburn equations [44], where A is the measured absorbance at the selected wavelength:

$$C_{Chl\ a} = 11.47 \times A666 - 2 \times A648 \quad (1)$$

$$C_{Chl\ b} = 21.85 \times A648 - 4.53 \times A666 \quad (2)$$

$$C_{car} = (1000 \times A480 - 1.33 \times C_{Chl\ a} - 23.93 \times C_{Chl\ b})/202 \quad (3)$$

The obtained concentrations were then converted in mg/g ± SD (standard deviation) and reported as the means of three replications. Chl a/chl b and chl (a+b)/car ratios were also determined. Significant differences in the levels of the analyzed compounds among the cultivars at the same stage and among the same cultivar in different stages were evaluated by a one-way analysis of variance (one-way ANOVA), followed by Bonferroni's Multiple Comparison Post Test.

4.6. Spectrophotometric Analysis of Total Phenolics Content and Antioxidant Activity

The extraction of phenolic compounds was carried out following a protocol previously described [45], with some modifications. In particular, 0.5 g of fresh hemp inflorescences were added to 2.5 mL of MeOH/H_2O 7:3 *v/v* solution. Samples were then shacked for 1 min, sonicated in an ultrasonic bath for 5 min, and finally centrifuged for 10 min at 2500× *g*. After centrifugation, the supernatant was separated from the residual pellet that was extracted again using the same conditions described above. Supernatants obtained in both extractions were united, obtaining a final volume of 5 mL.

Total phenolics content (TPC) was determined using the Folin–Ciocalteu method [45], optimizing the protocol for hemp inflorescences: 1 mL of hydroalcoholic extract was added to 0.25 mL of Folin–Ciocalteu reagent and 0.5 mL of Na_2CO_3 (7.5% *w/v*) in a 10 mL volumetric flask, reaching the final volume with water. Each sample was stored in the dark for 45 min at room temperature, and the spectrophotometric analysis (Lenway 6705 UV-Vis spectrophotometer) (Milan, Italy) was performed at 750 nm. TPC was expressed as milligrams of gallic acid equivalents (GAE)/kg: a calibration curve was created, with a concentration range from 15 to 500 mg/L (R^2 = 0.9925). The measurements were carried out in triplicate for each sample and reported as mean value ± SD.

The antioxidant activity of hemp hydroalcoholic extracts was determined through DPPH and ABTS assays. For the DPPH assay, 1.5 mL of reagent were added to 1 mL of hydroalcoholic extract and left in the dark at room temperature. After 30 min, the absorbance of the solution was recorded. For the ABTS assay, 3.6 mL of reagent were added to 0.4 mL of hydroalcoholic extract and left in the dark at room temperature. After 15 min the absorbance of the solution was recorded. The reduction of radical concentration was evaluated by measuring the absorbance at 515 nm (for DPPH assay) and 734 nm (for ABTS assay), as previously reported [45]. Results were expressed as inhibition rate (I%) and were calculated according to the following equation:

$$I\% = (A_0 - A_f)/A_0 \times 100$$

where A_0 is the initial absorbance of the radical cation and A_f is the absorbance of the radical cation after the extract addition. The assays were carried out in triplicate for each sample and reported as mean value ± SD. Significant differences in the levels of the analyzed compounds among the cultivars at the same stage and among the same cultivar in different stages were evaluated by one-way analysis of variance (one-way ANOVA), followed by Bonferroni's Multiple Comparison Post Test. Pearson correlation coefficients were also evaluated and reported in Table S1.

5. Conclusions

The present study showed that the *Cannabis sativa* L. inflorescences of each analyzed hemp cultivar presented a peculiar chemical profile that could be affected by the harvesting stage. The knowledge of the inflorescences chemical profile was a prerequisite to promote their use in several industrial fields, being a significant source of compounds with specific sensorial/nutraceutical/pharmaceutical properties.

Supplementary Materials: The following are available online. Figure S1. PCA maps obtained comparing September inflorescences samples of monoecious and dioecious Cannabis sativa L. cultivars: (A) scores plot and (B) loadings plot relative to PC1 and PC2 (PCs); PC1 and PC2 represent 49.0% and 25.5% of the total variance, respectively. Table S1. Pearson correlation coefficient (r) between total polyphenolic compounds and antioxidant activity. * Significant at $p \leq 0.05$.

Author Contributions: Conceptualization, M.S., G.D.M., and L.M.; methodology, A.P.S., A.M.G., E.C., and G.V.; validation, A.P.S., M.S., G.D.M., E.C., G.V., M.R., F.G., and D.Q.; formal analysis, C.I., A.P.S., M.S., S.C. (Silvia Cammarone), S.B., S.C. (Salvatore Ciano), G.D.M., and M.R.; investigation, A.P.S., E.C., L.M., and G.V.; data curation, A.P.S., M.S., G.D.M., C.I., M.R., and A.M.G.; writing—original draft preparation, M.S. and G.D.M.; writing—review and editing, A.P.S. and L.M.; visualization, A.P.S., C.I., L.M., B.B., D.Q., F.G., E.C., S.B., S.C. (Silvia Cammarone), S.C. (Salvatore Ciano), A.M.G., and G.V.; supervision, L.M. and A.P.S.; project administration, L.M.; funding acquisition, L.M. All authors have read and agreed to the published version of the manuscript.

Funding: This work was realized with funds received from the following agencies: the Italian Ministry of Education, Universities, and Research—Dipartimenti di Eccellenza—L. 232/2016; Regione Lazio, LACanapa Project (Progetto di Ricerca, finanziato ai sensi della L.R. 13/08—Protocol 85-2017-15069 CUP: B86C18000730002).

Institutional Review Board Statement: Not applicable.

Informed Consent Statement: Not applicable.

Data Availability Statement: Not applicable.

Acknowledgments: This work is a part of a project supported by the Lazio Region entitled "La Canapa industriale: sviluppo e valorizzazione di una nuova filiera agroalimentare ecosostenibile".

Conflicts of Interest: The authors declare no conflict of interest.

Sample Availability: Samples are available from the authors.

References

1. Piluzza, G.; Delogu, G.; Cabras, A.; Marceddu, S.; Bullitta, S. Differentiation between fiber and drug types of hemp (*Cannabis sativa* L.) from a collection of wild and domesticated accessions. *Genet. Resour. Crop. Evol.* **2013**, *60*, 2331–2342. [CrossRef]
2. Andre, C.M.; Hausman, J.-F.; Guerriero, G. *Cannabis sativa*: The Plant of the Thousand and One Molecules. *Front. Plant Sci.* **2016**, *7*, 19. [CrossRef] [PubMed]
3. Ash, A.L. Hemp-production and utilization. *Econ. Bot.* **1948**, *2*, 158–169. [CrossRef]
4. EUR-Lex. Access to European Union Law. Available online: https://eur-lex.europa.eu/legal-content/EN/TXT/?uri=CELEX:01999R1251-20040701 (accessed on 3 March 2020).
5. EU. Plant Variety Database. Available online: https://ec.europa.eu/food/plant/plant_propagation_material/plant_variety_catalogues_databases/search/public/index.cfm?event=SearchVariety&ctl_type=A&species_id=240&variety_name=antal&listed_in=0&show_current=on&show_deleted=on (accessed on 20 March 2020).
6. Fiorini, D.; Molle, A.; Nabissi, M.; Santini, G.; Benelli, G.; Maggi, F. Valorizing industrial hemp (*Cannabis sativa* L.) by-products: Cannabidiol enrichment in the inflorescence essential oil optimizing sample pre-treatment prior to distillation. *Ind. Crop. Prod.* **2019**, *128*, 581–589. [CrossRef]
7. Verma, R.S.; Padalia, R.C.; Verma, S.K.; Chauhan, A.; Darokar, M.P. The essential oil of "bhang" (*Cannabis sativa* L.) for non-narcotic applications. *Curr. Sci.* **2014**, *107*, 645–650.
8. Bertoli, A.; Tozzi, S.; Pistelli, L.; Angelini, L.G. Fibre hemp inflorescences: From crop-residues to essential oil production. *Ind. Crop. Prod.* **2010**, *32*, 329–337. [CrossRef]
9. Ascrizzi, R.; Ceccarini, L.; Tavarini, S.; Flamini, G.; Angelini, L.G. Valorisation of hemp inflorescence after seed harvest: Cultivation site and harvest time influence agronomic characteristics and essential oil yield and composition. *Ind. Crop. Prod.* **2019**, *139*, 139. [CrossRef]
10. Amaducci, S.; Zatta, A.; Pelatti, F.; Venturi, G. Influence of agronomic factors on yield and quality of hemp (*Cannabis sativa* L.) fibre and implication for an innovative production system. *Field Crop. Res.* **2008**, *107*, 161–169. [CrossRef]
11. Mediavilla, V.; Meier, C. Factors influencing the yield and the quality of hemp (*Cannabis sativa* L.) essential oil. *J. Int. Hemp. Assoc.* **1998**, *5*, 16–20.
12. Ingallina, C.; Sobolev, A.P.; Circi, S.; Spano, M.; Fraschetti, C.; Filippi, A.; Di Sotto, A.; Di Giacomo, S.; Mazzoccanti, G.; Gasparrini, F.; et al. *Cannabis sativa* L. Inflorescences from Monoecious Cultivars Grown in Central Italy: An Untargeted Chemical Characterization from Early Flowering to Ripening. *Molecules* **2020**, *25*, 1908. [CrossRef]
13. Ranalli, P. Current status and future scenarios of hemp breeding. *Euphytica* **2004**, *140*, 121–131. [CrossRef]
14. ElSohly, M.A.; Radwan, M.M.; Gul, W.; Chandra, S.; Galal, A. *Phytochemistry of Cannabis sativa L.*; Springer: New York, NY, USA, 2017; Volume 103, ISBN 9783319455419.
15. Ingallina, C.; Capitani, D.; Mannina, L.; Carradori, S.; Locatelli, M.; Di Sotto, A.; Di Giacomo, S.; Toniolo, C.; Pasqua, G.; Valletta, A.; et al. Phytochemical and biological characterization of Italian "sedano bianco di Sperlonga" Protected Geographical Indication celery ecotype: A multimethodological approach. *Food Chem.* **2020**, *309*, 125649. [CrossRef]
16. Sobolev, A.P.; Mannina, L.; Capitani, D.; Sanzò, G.; Ingallina, C.; Botta, B.; Fornarini, S.; Crestoni, M.E.; Chiavarino, B.; Carradori, S.; et al. A multi-methodological approach in the study of Italian PDO "Cornetto di Pontecorvo" red sweet pepper. *Food Chem.* **2018**, *255*, 120–131. [CrossRef] [PubMed]
17. Sobolev, A.P.; Thomas, F.; Donarski, J.; Ingallina, C.; Circi, S.; Marincola, F.C.; Capitani, D.; Mannina, L. Use of NMR applications to tackle future food fraud issues. *Trends Food Sci. Technol.* **2019**, *91*, 347–353. [CrossRef]
18. Sobolev, A.P.; Circi, S.; Capitani, D.; Ingallina, C.; Mannina, L. Molecular fingerprinting of food authenticity. *Curr. Opin. Food Sci.* **2017**, *16*, 59–66. [CrossRef]
19. Mazzoccanti, G.; Ismail, O.H.; D'Acquarica, I.; Villani, C.; Manzo, C.; Wilcox, M.; Cavazzini, A.; Gasparrini, F. Cannabis through the looking glass: Chemo- and enantio-selective separation of phytocannabinoids by enantioselective ultra high performance supercritical fluid chromatography. *Chem. Commun.* **2017**, *53*, 12262–12265. [CrossRef]
20. Hillig, K.W.; Mahlberg, P.G. A chemotaxonomic analysis of cannabinoid variation inCannabis (Cannabaceae). *Am. J. Bot.* **2004**, *91*, 966–975. [CrossRef]
21. Glivar, T.; Eržen, J.; Kreft, S.; Zagožen, M.; Čerenak, A.; Čeh, B.; Benković, E.T. Cannabinoid content in industrial hemp (Cannabis sativa L.) varieties grown in Slovenia. *Ind. Crop. Prod.* **2020**, *145*, 112082. [CrossRef]
22. Lichtenthaler, H.K.; Buschmann, C. Chlorophylls and Carotenoids: Measurement and Characterization by UV-VIS Spectroscopy. *Curr. Protoc. Food Anal. Chem.* **2001**, *1*, F4-3. [CrossRef]
23. Rapa, M.; Ciano, S.; Ruggieri, R.; Vinci, G. Bioactive compounds in cherry tomatoes (Solanum Lycopersicum var. Cerasiforme): Cultivation techniques classification by multivariate analysis. *Food Chem.* **2021**, *355*, 129630. [CrossRef]
24. Cerretani, L.; Bendini, A. Rapid Assays to Evaluate the Antioxidant Capacity of Phenols in Virgin Olive Oil. In *Olives and Olive Oil in Health and Disease Prevention*; Academic Press: Cambridge, MA, USA, 2010; pp. 625–635.
25. Di Pierro, F. A nutraceutical role for cannabidiol. Why not? *Nutrafoods* **2015**, *14*, 111–117. [CrossRef]
26. Cascio, M.G.; Gauson, L.A.; Stevenson, L.A.; Ross, R.A.; Pertwee, R.G. Evidence that the plant cannabinoid cannabigerol is a highly potent α2-adrenoceptor agonist and moderately potent 5HT1A receptor antagonist. *Br. J. Pharmacol.* **2009**, *159*, 129–141. [CrossRef]

27. Delong, G.T.; Wolf, C.E.; Poklis, A.; Lichtman, A.H. Pharmacological evaluation of the natural constituent of Cannabis sativa, cannabichromene and its modulation by Δ9-tetrahydrocannabinol. *Drug Alcohol Depend.* **2010**, *112*, 126–133. [CrossRef] [PubMed]
28. Mechtler, K.; Bailer, J.; De Hueber, K. Variations of Δ9-THC content in single plants of hemp varieties. *Ind. Crop. Prod.* **2004**, *19*, 19–24. [CrossRef]
29. Stanley, L.; Yuan, Y. Transcriptional Regulation of Carotenoid Biosynthesis in Plants: So Many Regulators, So Little Consensus. *Front. Plant Sci.* **2019**, *10*, 1017. [CrossRef] [PubMed]
30. Wolken, J.J.; Mellon, A.D. The Relationship between Chlorophyll and the Carotenoids in the Algal Flagellate, Euglena. *J. Gen. Physiol.* **1956**, *39*, 675–685. [CrossRef] [PubMed]
31. Izzo, L.; Castaldo, L.; Narváez, A.; Graziani, G.; Gaspari, A.; Rodríguez-Carrasco, Y.; Ritieni, A. Analysis of Phenolic Compounds in Commercial Cannabis sativa L. Inflorescences Using UHPLC-Q-Orbitrap HRMS. *Molecules* **2020**, *25*, 631. [CrossRef]
32. Scalbert, A.; Johnson, I.T.; Saltmarsh, M. Polyphenols: Antioxidants and beyond. *Am. J. Clin. Nutr.* **2005**, *81*, 215S–217S. [CrossRef]
33. Khan, M.K.; Paniwnyk, L.; Hassan, S. Polyphenols as Natural Antioxidants: Sources, Extraction and Applications in Food, Cosmetics and Drugs. *Green Chem. Sustain. Technol.* **2019**, 197–235. [CrossRef]
34. Mkpenie, V.N.; Essien, E.E.; Udoh, I.I. Effect of extraction conditions on total polyphenol contents, antioxidant and antimicrobial activities of Cannabis sativa L. Electron. *J. Environ. Agric. Food Chem.* **2012**, *11*, 300–307.
35. Hacke, A.C.M.; Lima, D.; De Costa, F.; Deshmukh, K.; Li, N.; Chow, A.M.; Marques, J.A.; Pereira, R.P.; Kerman, K. Probing the antioxidant activity of Δ9-tetrahydrocannabinol and cannabidiol in Cannabis sativa extracts. *Analyst* **2019**, *144*, 4952–4961. [CrossRef]
36. Ramirez, C.L.; Fanovich, M.A.; Churio, M.S. Cannabinoids: Extraction Methods, Analysis, and Physicochemical Characterization. In *Studies in Natural Products Chemistry*; Elsevier BV: Amsterdam, The Netherlands, 2019; Volume 61, pp. 143–173.
37. Sulaiman, S.F.; Sajak, A.A.B.; Ooi, K.L.; Supriatno; Seow, E.M. Effect of solvents in extracting polyphenols and antioxidants of selected raw vegetables. *J. Food Compos. Anal.* **2011**, *24*, 506–515. [CrossRef]
38. Ferrante, C.; Recinella, L.; Ronci, M.; Menghini, L.; Brunetti, L.; Chiavaroli, A.; Leone, S.; Di Iorio, L.; Carradori, S.; Tirillini, B.; et al. Multiple pharmacognostic characterization on hemp commercial cultivars: Focus on inflorescence water extract activity. *Food Chem. Toxicol.* **2019**, *125*, 452–461. [CrossRef]
39. Nahar, L.; Uddin, S.J.; Alam, A.; Sarker, S.D. Extraction of naturally occurring cannabinoids: An update. *Phytochem. Anal.* **2021**, *32*, 228–241. [CrossRef] [PubMed]
40. Nahar, L.; Guo, M.; Sarker, S.D. Gas chromatographic analysis of naturally occurring cannabinoids: A review of literature published during the past decade. *Phytochem. Anal.* **2020**, *31*, 135–146. [CrossRef]
41. Bligh, E.G.; Dyer, W.J. A rapid method of total lipid extraction and purification. *Can. J. Biochem. Physiol.* **1959**, *37*, 911–917. [CrossRef]
42. Ingallina, C.; Sobolev, A.P.; Circi, S.; Spano, M.; Giusti, A.M.; Mannina, L. New Hybrid Tomato Cultivars: An NMR-Based Chemical Characterization. *Appl. Sci.* **2020**, *10*, 1887. [CrossRef]
43. Solovchenko, A.E.; Chivkunova, O.B.; Merzlyak, M.N.; Reshetnikova, I.V. A Spectrophotometric Analysis of Pigments in Apples. *Russ. J. Plant Physiol.* **2001**, *48*, 693–700. [CrossRef]
44. Wellburn, A.R. The Spectral Determination of Chlorophylls a and b, as well as Total Carotenoids, Using Various Solvents with Spectrophotometers of Different Resolution. *J. Plant Physiol.* **1994**, *144*, 307–313. [CrossRef]
45. Preti, R.; Rapa, M.; Vinci, G. Effect of Steaming and Boiling on the Antioxidant Properties and Biogenic Amines Content in Green Bean (*Phaseolus vulgaris*) Varieties of Different Colours. *J. Food Qual.* **2017**, *2017*, 1–8. [CrossRef]

7.3. Case study 2: Multimethodological characterization of Ferimon monoecious cultivar cultivated with different agronomical practices

Recently, hemp inflorescences have been proposed as Novel Food but for the final authorization due to the presence of cannabinoids, further studies have been required. With the aim of promote the authorization of industrial hemp as Novel Food, in the present work, the chemical composition of the inflorescences from seven *Cannabis sativa* L. dioecious cultivars, namely Carmagnola, Fibranova, Eletta Campana, Antal, Tiborszallasi, Kompolti, and Tisza, recently introduced in the Lazio Region, was monitored over the season using a multimethodological approach, including the NMR metabolomic analysis.

foods

MDPI

Article

Industrial Hemp (*Cannabis sativa* L.) Inflorescences as Novel Food: The Effect of Different Agronomical Practices on Chemical Profile

Mattia Spano [1], Giacomo Di Matteo [1], Cinzia Ingallina [1], Anatoly Petrovich Sobolev [2,*], Anna Maria Giusti [3], Giuliana Vinci [4], Silvia Cammarone [1], Carola Tortora [1], Lara Lamelza [1], Sabrina Antonia Prencipe [4], Laura Gobbi [4], Bruno Botta [1], Federico Marini [5], Enio Campiglia [6] and Luisa Mannina [1]

[1] Department of Chemistry and Technology of Drugs, Sapienza University of Rome, Piazzale Aldo Moro 5, 00185 Rome, Italy
[2] Magnetic Resonance Laboratory "Segre-Capitani", Institute for Biological Systems, CNR, Via Salaria Km 29.300, 00015 Monterotondo, Italy
[3] Department of Experimental Medicine, Sapienza University of Rome, Piazzale Aldo Moro 5, 00185 Rome, Italy
[4] Department of Management, Sapienza University of Rome, Via del Castro Laurenziano 9, 00161 Rome, Italy
[5] Department of Chemistry, Sapienza University of Rome, Piazzale Aldo Moro 5, 00185 Rome, Italy
[6] Department of Agricultural and Forest Sciences, University of Tuscia, Via San Camillo de Lellis Snc, 01100 Viterbo, Italy
* Correspondence: anatoly.sobolev@cnr.it

check for updates

Citation: Spano, M.; Di Matteo, G.; Ingallina, C.; Sobolev, A.P.; Giusti, A.M.; Vinci, G.; Cammarone, S.; Tortora, C.; Lamelza, L.; Prencipe, S.A.; et al. Industrial Hemp (*Cannabis sativa* L.) Inflorescences as Novel Food: The Effect of Different Agronomical Practices on Chemical Profile. *Foods* **2022**, *11*, 3658. https://doi.org/10.3390/foods11223658

Academic Editor: Ara Kirakosyan

Received: 10 October 2022
Accepted: 14 November 2022
Published: 16 November 2022

Publisher's Note: MDPI stays neutral with regard to jurisdictional claims in published maps and institutional affiliations.

Copyright: © 2022 by the authors. Licensee MDPI, Basel, Switzerland. This article is an open access article distributed under the terms and conditions of the Creative Commons Attribution (CC BY) license (https://creativecommons.org/licenses/by/4.0/).

Abstract: In this study, the effect of several agronomical practices on the chemical composition of hemp inflorescences, a potential novel food that needs to be further studied, was observed. Here, the case study of inflorescences from Ferimon cultivars is discussed and submitted to different agronomical practices (irrigation and fertilizers) in different years, and the inflorescences harvested in different periods were analyzed by a multimethodological approach. Targeted and untargeted methodologies allowed cannabinoids, total phenolic content, metabolite profile and antioxidant activity to be determined. The biomass and inflorescence yields were also reported. The whole data set was submitted to ANOVA-simultaneous component analysis. The statistic results allowed us to observe that irrigation was responsible for the (–)-Δ9-tetrahydrocannabinol (THC) and cannabidiol (CBD) increment. THC, cannabichromene (CBC), cannabigerol (CBG), succinate, and fructose resulted as higher in full female flowering than in the period of seed maturity. On the other hand, nitrogen supplementation led to an increase of iso-leucine, valine, and threonine. The obtained results underlined both the potential food application of hemp inflorescences, due to the rich chemical profile, and the strong effect of agronomical practices, mainly irrigation and harvesting, on the qualitative and quantitative characteristics of its metabolite profile.

Keywords: industrial hemp; agronomical practices; fertilization; harvesting; chemical profile

1. Introduction

Hemp (*Cannabis sativa* L.) is an herbaceous, annual plant of eastern Asian origin, whose cultivation was forbidden in many countries for a long time due to the presence of tetrahydrocannabinol (THC), a psychoactive secondary metabolite contained in different parts of the plant. Recently, the European Union reintroduced the cultivation of some genotypes of *Cannabis sativa* L., also called industrial hemp, with a THC content lower than 0.2% *w*/*w* for fiber, seed, and inflorescence production [1]. In 2016, the Italian government approved a new regulation (Law n°242/2016), following the European one, regarding industrial hemp production, commercialization, and utilization. Therefore, in the next few years, the cultivation of industrial hemp is expected to increase thanks to the positive regulatory framework and the new products obtainable from this crop. In fact, besides

the traditional utilization, industrial hemp products could be employed in several fields such as in functional food and nutraceuticals sectors [2,3]. In this regard, a rising interest in hemp metabolites such as fatty acids, flavonoids, amino acids, terpenes, terpenophenolics, sugars, and hydrocarbons, biosynthesized in the epidermal glands or glandular hairs of aerial parts of the plant [4], has been observed. These metabolites are contained in large amounts in inflorescences [5,6] and leaves [7,8].

To date, the European Union does not allow to use hemp inflorescences as food or food ingredient due to the presence of cannabinoids. Cannabinoids are now included in the novel food catalogue, but for the final authorization [9], further assessment studies are required.

Therefore, the prospect of using hemp inflorescences as a novel food has prompted scientific research to deepen the knowledge of the chemical composition of the hemp inflorescences with a particular focus on classes of molecules important in the food-nutraceutical sector. In this context, several studies on hemp inflorescences have reported the presence of amino acids, sugars, organic acids, polyphenols, etc. [10–13].

Several factors such as different genotypes [14,15], climatic conditions, and agronomic practices [11] can influence the hemp inflorescences development and, consequently, the chemical profile. Therefore, it is extremely important to know the effects of different management practices on the physiological accumulation of secondary metabolites and on the inflorescence yield for the economic sustainability and for choosing the proper agronomic practices to obtain inflorescences suitable for food uses.

Several studies have been carried out on the effect of specific agronomical practices such as fertilization [16–18], irrigation [19,20], and harvesting period variation [11,13,21] on hemp cultivation.

Regarding the fertilization, nitrogen (N) and phosphorus (P) fertilizers play an important role in crop growth and development [22]. The knowledge of the proper mineral nutrient requirement of industrial hemp is important not only for inflorescence yield and quality, but also to reduce the risks of environmental pollution from runoff or leaching of excess nutrients [23]. In a recent study on the growth of marijuana genotypes conducted in a controlled environment, inflorescence yield responded quadratically to N and P, with the optimal concentrations in nutrient solution predicted to be 194 and 59 mg L^{-1}, respectively [24]. Moreover, a negative correlation between cannabinoid content (THC and CBG) and increasing fertilizer rates [25,26] has been reported. However, information regarding N and P fertilization rates for inflorescence production in the open field is limited, and more research is needed to determine the proper use of fertilizers to obtain inflorescences with high yield and quality.

In the Mediterranean environment, another important agronomic factor for industrial hemp production is water availability, since during the cropping period, the climate is generally characterized by drought and high temperatures. Therefore, for the crop in a semi-arid Mediterranean environment, watering is often needed. Cosentino et al. [27] have suggested that irrigation water supply for industrial fiber hemp production ranges between 250 and 450 mm for early and late genotypes, respectively. However, it is feasible that the optimal water supply for irrigation is different for inflorescence production compared to fiber production. Low humidity conditions in open field have turned out to enhance the terpene content of essential oils [28]. The effect of irrigation on the cannabinoid content is still debated. Caplan et al. [29] have observed that drought-stressed hemp plants increased the concentrations and yield of major cannabinoids compared with a well-irrigated control, whereas other authors did not note clear responses of cannabinoid content in relation to the irrigation doses [30].

The harvesting period also plays a pivotal role in the chemical profile of inflorescences. Ingallina et al. [11] have found that, in monoecious industrial hemp cultivars, the content of proline drastically decreased after early flowering, whereas glucose, citrate and malate reached the highest content in the late flowering period. Similarly, in dioecious hemp cultivars, the chemical composition of inflorescences varies during the flowering period.

Spano et al. [13] have observed that at the beginning of flowering, female inflorescence extracts have been characterized by a high content of sucrose and myo-inositol, whereas at the end of flowering, the highest levels of glucose, fructose, choline, trigonelline, malic acid, formic acid, and some amino acids were observed.

Therefore, up to now, the research has been focused on the study of individual agronomical practices and their effect on cannabinoid content. A more complete chemical profile of hemp inflorescences has been reported in a few studies where only the harvesting period effect has been investigated [11,13].

In this paper, the combined effect of nitrogen and phosphorus fertilizer, irrigation, harvesting time and cultivation year on inflorescence chemical profile was investigated considering as a case study the monoecious Ferimon cultivar. A multimethodological approach based on both targeted (UHPLC-DAD, UV-Vis spectrophotometry) and untargeted (NMR) methodologies and chemometric analysis was applied.

2. Materials and Methods

2.1. Chemicals

Gradient grade water, acetonitrile, chloroform, methanol, and formic acid were purchased from Merck Life Science (Milano, Italy). Cannabinoid reference standards dissolved in methanol, namely, cannabidivarin (CBDV, 1 mg/mL), cannabigerol (CBG, 1 mg/mL), cannabidiol (CBD, 1 mg/mL), cannabidiolic acid (CBDA, 1 mg/mL), cannabinol (CBN, 1 mg/mL), (–)-Δ9-tetrahydrocannabinol ((–)-Δ9-THC, 1 mg/mL), Δ9-tetrahydrocannabinolic acid ((–)-Δ9-THCA, 1 mg/mL), (–)-Δ8-tetrahydrocannabinol ((–)-Δ8-THC, 1 mg/mL), and cannabichromene (CBC, 1 mg/mL) with purity $\geq$ 99%, were purchased from Merck Life Science (Milano, Italy). Deuterated water (D_2O) 99.97 atom% of deuterium and 3-(trimethylsilyl)-propionic-2,2,3,3-d_4 acid sodium salt (TSP) were purchased from Euriso-Top (Saclay, France). Magnesium oxide (MgO), potassium phosphate monobasic (KH_2PO_4), and potassium phosphate dibasic (K_2HPO_4) 2,2-azino-bis (3-ethyl-benzothiazoline-6-sulfonic acid) diammonium salt (ABTS), 2,2-diphenyl-1-picrylhydrazyl (DPPH), Folin–Ciocalteu reagent, gallic acid (GA), and sodium carbonate (Na_2CO_3) were purchased from Merck Life Science (Milano, Italy).

2.2. Experimental Site and Weather Conditions

Field experiments were conducted during the 2017 and 2018 growing seasons in Central Italy at the Experimental Farm of the University of Tuscia in Viterbo (latitude 42°25′ N, longitude 12°04′ E and altitude 295 m above sea level). The soil is volcanic with the following main characteristics at 0–30 cm depth: 11.2% clay, 14.7% silt, 74.1% sand, pH 6.7 (water, 1:2.5), organic matter 1.2% (Lotti method), total N 0.93 g kg^{-1} of dry soil (Kjeldahl method), available P_2O_5 41 mg kg^{-1}, and exchangeable K_2O 534 mg kg^{-1}. The climate of the experimental area is typically Mediterranean, characterized by a dry and hot summer and humid and mild winter. Weather data (rainfall, maximum and minimum air temperatures, and potential vapor-transpiration) were recorded daily from an automatic meteorological station located 100 m from the experimental fields. Meteorological data are reported at 10-day intervals for the period in which the experiment was conducted (Supplementary Table S1). As expected, in both experimental years, the average air temperatures gradually increased from sowing (April) to the hemp reproductive period and reached the maximum values in the first decade of August. However, there were remarkable differences between the experimental years. The range of temperature between minimum and maximum values was generally larger in 2017 compared to 2018. In fact, the temperature throughout the experimental period ranged from 8 °C in May to 38 °C in August 2017, whereas the temperature in the same period ranged from 11 °C in May 2018 to 34 °C in August 2018 (Supplementary Table S1). As a consequence, the average temperature in 2017 was significantly higher compared to 2018, especially during the flowering period. Furthermore, the total rainfall from hemp emergence until full flowering was 109 mm in 2017 and 306 mm in 2018; with a particular concentration in the last ten days of July 2017 (48 mm),

and May 2018 (150 mm). Similar values were observed for potential evapotranspiration in both cropping seasons (618 and 595 mm in 2017 and 2018, respectively). From the weather data it is evident that the 2017 was characterized by a longer period of drought compared to 2018 during the hemp growing period.

2.3. Field Experiment Description, Experimental Design, and Treatments

One week before hemp sowing, where foreseen, the plots were fertilized with phosphorus (P) at a dose of 45 or 90 kg P_2O_5 ha^{-1} as triple superphosphate. After applying the fertilizer, the soil was disked twice for seedbed preparation. The hemp variety used in this study was Ferimon, a French monoecious cultivar listed in the EU database of registered hemp varieties and commonly used for seed production, that also showed good performance for inflorescence yield in the Mediterranean environment of Central Italy [31]. Industrial hemp was sown with an experimental sowing machine (Wintersteiger, Ried im Innkreis, Austria) on 26 April 2017 and 3 May 2018 planting the seeds in rows at 0.25 m interrow spacing. The hemp seed rate was 15 kg ha^{-1}. In both years, in order to avoid emergence failure, the field was irrigated just after sowing by sprinkler irrigation. Ten days after emergence, the hemp seedlings were thinned manually in order to reach the density of 80 plants m^{-2}, in accordance with the density used in a similar environment in recent research on hemp cultivation [31]. Where foreseen, nitrogen (N) fertilization was applied at a ratio of 75 or 150 kg N ha^{-1} as ammonium nitrate, split into three doses applied at 15, 30 and 45 days after crop emergence (33% of the total amount for each application). Following each N fertilization, a manual hoe was applied to incorporate the N fertilizer and to control inter-row weeds. Potassium fertilizer was not applied due to the high levels present in the soil. Irrigation water was supplied in the irrigated plots by means of drip irrigation placing on the soil surface one pipeline per row immediately after hemp seedling thinning. The amount of water input was determined by evapotranspiration estimated by class A pan evaporimeter and converted by crop coefficients, returning 90% of the evapotranspirated water from the crop. The hemp inflorescences were harvested twice: at full female flowering stage (A), and at seed maturity stage (B). In 2017, the following experimental treatments were applied in factorial combination: (i) one irrigation regime (irrigated crop); (ii) two doses of phosphorus (0 and 90 kg P_2O_5 ha^{-1}); (iii) two doses of N fertilization (0 and 150 kg of N ha^{-1}). In 2018, further variables were considered, by applying the following treatments: (i) two irrigation regimes (irrigated and not-irrigated crop); (ii) three doses of phosphorus (0, 45 and 90 kg P_2O_5 ha^{-1}); and (iii) three doses of N fertilization (0, 75 and 150 kg of N ha^{-1}), Supplementary Figure S1.

In 2017, the experimental design of the field was a split-plot, where the main plots were represented by the phosphorus fertilization, and the sub-plots were the N fertilization. In 2018, the experimental design of the field was a split-split-plot, where the main plots were represented by the irrigation regimes, the sub-plots were the phosphorus fertilization, and the sub-sub-plots were the N fertilization. The main plot size was 135 m^2 (9 m × 15 m), the subplot size was 67.5 m^2 (4.5 m × 15 m), and the sub-sub-plot size was 22.5 m^2 (4.5 m × 5 m). In both years, the main plots in the field trial were separated by 8 m wide alleys for equipment operation.

2.4. Field Measurements and Data Collection

Immediately after hemp seedling thinning, a 2.0 m central row was randomly selected to carry out phenological observations, that were performed daily when the flowering stage was approaching. Two inflorescence harvests were carried out during the hemp reproductive period: the first one was carried out at full female flowering (50% of the bracts formed), encoded as phase 2302, whereas the second harvest occurred at seed maturity (50% of seeds hard), encoded as phase 2306 [32]. At each harvesting time, the plants in the 4 middle rows of each sub-sub-plot, corresponding at 1 m^2 area, were manually cut just above the soil surface. The aboveground biomass was split into two fractions: stems and inflorescence by cutting the upper part of the plant stem, and the stem ramifications when

present, at the insertion level of the first basal flower of the inflorescence. Both flowers and floral leaves were included in the inflorescence for determining the chemical profile, whereas the seeds present at the second inflorescence harvest were manually separated. The fresh material was immediately weighed, and a sub-sample was oven dried at 70 °C until constant weight to determine the dry matter content of stems, inflorescences, and seeds when present. The remaining part of the inflorescences were pulverized with liquid nitrogen by using mortar and pestle and then was preserved at a temperature of −80 °C until subsequent laboratory analyses.

In order to have information relevant for the economic sustainability, the biomass and inflorescences yield, inflorescences/biomass ratio (inf/bio) have been measured and reported.

2.5. UHPLC Analysis for Cannabinoid Profile

Fresh inflorescences were dried at 70 °C for 48 h before extraction. After drying, 100 mg of inflorescences were extracted with 4 mL of methanol in an ultrasonic bath for 30 min. The residual pellet was then extracted other two times. For each extract, an aliquot of 1 mL was filtered with a 0.45 µm PTFE membrane and finally analyzed.

Analyses were carried out by using an Ultimate 3000 ultra-high-performance liquid chromatography (UHPLC) (Thermo Fisher Scientific, Rodano, Italy), with a binary gradient system, an automatic injector, a thermostatic column compartment, and a diode array detector. The system was controlled by Chromeleon Chromatography Data System software (Thermo Fisher Scientific, 1.0.5. v, Waltham, MA, USA, 2018). All separations were performed by using a Titan C 18 column (10 cm × 3 cm, 1.9 µm, Sigma Aldrich (Milan, Italy)) with a mobile phase composed of 0.1% formic acid in water (A) and 0.1% formic acid in acetonitrile (B). The used elution conditions were the same previously described [13].

Cannabinoid concentrations were expressed as % w/w (g for 100 g of dried inflorescence) ± SD (standard deviation). Three replications were made for each sample.

2.6. Untargeted NMR Analysis

For the untargeted NMR analysis, Bligh–Dyer extraction procedure was applied, following the previously described conditions [33]. The hydroalcoholic extract was dried and then solubilized with 0.75 mL of 400 mM phosphate buffer/D_2O, containing a 1 mM 3-(trimethylsilyl)-propionic-2,2,3,3-d_4 acid sodium salt (TSP) as an internal standard, and then transferred into a 5 mm NMR tube. NMR analyses were carried out on a Bruker AVANCE 600 spectrometer operating at the proton frequency of 600.13 MHz and equipped with a Bruker multinuclear z-gradient 5 mm probe head (Milan, Italy). ^{1}H spectra were acquired at 28 °C using the following parameters: 256 transients, suppression of residual water signal (HDO) using a pre-saturation, 5 s recycle delay, 45° pulse of 7.5 µs, and 32 K data points. Metabolites identification, see Supplementary Table S2, was carried out based on the NMR results previously reported using the same experimental condition [11].

2.7. Spectrophotometric Analysis of Total Phenolics Content and Antioxidant Activity

The extraction of phenolic compounds was carried out as follows: 0.5 g of fresh hemp inflorescences were added to 2.5 mL of MeOH/H_2O 7:3 v/v solution. Samples were then shaken for 1 min, sonicated in an ultrasonic bath for 5 min, and finally centrifuged for 10 min at 2500× g. After supernatant removal, the residual pellet was extracted again using the same conditions. Both obtained supernatants were united to a final volume of 5 mL.

Total phenolics content (TPC) was determined using the Folin–Ciocâlteu method, optimized in a previous work for hemp inflorescences [13]. TPC was expressed as milligrams of gallic acid equivalents (GAE) kg^{-1}: a calibration curve was created, with a concentration range from 15 to 500 mg/L (R^2 = 0.9925). The measurements were carried out in triplicate for each sample and reported as mean value ± SD.

The antioxidant activity of hemp hydroalcoholic extracts was determined by applying DPPH and TEAC assays. The free radical scavenging activity of fresh hemp inflorescence

extracts was evaluated by means of DPPH assay, according to a previously reported method [34]. The scavenging activity was measured at 517 nm. Values were reported as EC_{50} value ± SD; EC_{50}, corresponded to the extracts' concentration providing 50% of radicals scavenging activity. Gallic acid dissolved in methanol, ranged between 1 and 100 mg/L, was used as reference compound.

The Trolox equivalent antioxidant capacity (TEAC) of hemp inflorescence extracts was estimated by the ABTS radical scavenging assay, according to Omono et al. [35], with some modifications. All measurements were performed by adding 3.6 mL of the ABTS radical solution to 0.4 mL of hemp extracts, leaving it in darkness for 15 min. The decolorization of ABTS•* was evaluated by measuring the absorbance at 734 nm, and then expressed as milligrams Trolox Equivalent (TE) per g of hemp inflorescence (mg TE/g), obtained by a calibration curve ranging from 0.5 µM TE to 200 µM TE (R^2 = 0.9963).

The assays were carried out in triplicate for each sample and reported as mean value ± SD.

2.8. Statistical Analysis

To evaluate the effect of the different cultivation conditions on the total defined chemical profile of hemp inflorescences, ANOVA-simultaneous component analysis (ASCA) was used. ASCA [36] is a multivariate method specifically proposed to analyze multivariate data coming from designed experiments and couples a multivariate ANOVA decomposition, to disentangle the contribution of each design term on the multivariate profile, with Simultaneous Component Analysis (SCA), that under the ANOVA constraints boils down to Principal Component Analysis (PCA), for the chemical interpretation of the observed effects.

If a term is found to be statistically significant, interpretation of the observed effect in terms of the multivariate profile recorded is made by SCA of the corresponding effect matrix. As explained above, under the constraints of ANOVA, the use of SCA is equivalent to a standard PCA on the matrix.

Since the effect matrices are only made of the mean profiles of the different factor/interaction levels, for the sake of a better interpretation, it is common practice, after the SCA model is calculated, to also project onto the resulting component the residuals, so as to have an idea of the expected within-level variability [37].

The obtained results, combined with the application of chemometric analysis, allowed us to observe the effect of the considered agronomical variables (nitrogen and phosphorus fertilization, irrigation, harvesting period) on the quali-quantitative features of the Ferimon metabolite profile.

3. Results and Discussion

3.1. Chemical Characterization

The chemical profile of Ferimon inflorescences was investigated by applying both targeted (UHPLC-DAD, UV-Vis spectrophotometry) analyses focused on cannabinoids and total phenols determination and NMR untargeted methodology to obtain the metabolite profile. The results will be discussed separately.

Cannabinoids. The UHPLC-DAD analysis of *Cannabis sativa* L. methanolic extracts allowed us to quantify Δ9-THC, CBD, Δ9-THCA, CBDA, CBG, and CBC. The concentrations, expressed as % *w*/*w* of dry matter ± SD, are reported in Table 1.

All the analyzed samples were characterized by a THC content below the legal limit, whereas CBD turned out to be the most abundant cannabinoid. In a previous study [11], the inflorescences of Ferimon hemp cultivar grown in 2016 in Central Lazio with different agronomical practices (irrigation and 100 kg ha^{-1} of N) have shown a different cannabinoids profile with the presence of CBDV and CBN not detected here. The cannabinoid profile of the Ferimon hemp cultivar grown in Slovenia in 2017 (agronomical practices not reported) [38] has shown a very high CBDA content, whereas CBD, THC, and CB contents were lower with respect to those here reported.

Table 1. Cannabinoid concentrations of the 2017 and 2018 samples reported for each phosphorus (P) and nitrogen (N) fertilization combination at two harvesting stages. Analyses were carried out in triplicate and expressed as % (*w*/*w*, g for 100 g of dried inflorescence) ± SD.

Harvesting Period	Fertilization	Δ9-THC % *w*/*w*	CBD % *w*/*w*	Δ9-THCA % *w*/*w*	CBDA % *w*/*w*	CBG % *w*/*w*	CBC % *w*/*w*
2017 year							
Stage A	P0 N0 I	0.08 ± 0.01 ^{a}	1.74 ± 0.14 ^{a}	/	0.77 ± 0.10 ^{a}	/	0.08 ± 0.01 ^{a}
	P0 N150 I	0.06 ± 0.01	1.58 ± 0.09	/	0.60 ± 0.14	/	0.07 ± 0.01
	P90 N0 I	0.06 ± 0.01	1.54 ± 0.07 ^{a}	/	0.84 ± 0.03 ^{a}	/	0.06 ± 0.01
	P90 N150 I	0.07 ± 0.01	1.71 ± 0.17 ^{a}	/	0.64 ± 0.04	/	0.08 ± 0.01 ^{a}
Stage B	P0 N0 I	0.05 ± 0.01	0.83 ± 0.01	/	0.52 ± 0.01	/	0.05 ± 0.01
	P0 N150 I	0.06 ± 0.01	1.28 ± 0.20	/	0.67 ± 0.05	/	0.06 ± 0.01
	P90 N0 I	0.05 ± 0.01	1.03 ± 0.08	/	0.71 ± 0.03	/	0.05 ± 0.01
	P90 N150 I	0.05 ± 0.01	0.97 ± 0.03	/	0.66 ± 0.03	/	0.05 ± 0.01
2018 year							
Stage A	P0 N0 D	0.08 ± 0.01	0.94 ± 0.04 ^{a}	0.07 ± 0.01 ^{a,b}	0.47 ± 0.02 ^{a,b}	0.07 ± 0.01 ^{b}	0.15 ± 0.04 ^{a}
	P0 N0 I	0.09 ± 0.01 ^{a}	0.60 ± 0.10 ^{a,b}	/	0.27 ± 0.03	/^{a}	0.19 ± 0.01 ^{a}
	P0 N75 D	0.06 ± 0.01	0.70 ± 0.10 ^{a}	/	0.39 ± 0.02 ^{a,b}	0.04 ± 0.01 ^{b}	0.12 ± 0.01 ^{a,b}
	P0 N75 I	0.08 ± 0.01 ^{a}	0.76 ± 0.02	/	0.29 ± 0.03 ^{a}	0.07 ± 0.01 ^{a}	0.19 ± 0.01 ^{a}
	P0 N150 D	0.06 ± 0.01	1.30 ± 0.02 ^{b}	/	0.39 ± 0.03 ^{a,b}	0.05 ± 0.01 ^{a}	0.12 ± 0.01 ^{a,b}
	P0 N150 I	0.07 ± 0.02	0.87 ± 0.02 ^{a}	/	0.16 ± 0.01 ^{a}	0.07 ± 0.01 ^{a}	0.19 ± 0.01 ^{a}
	P45 N0 D	0.08 ± 0.01	1.30 ± 0.20 ^{b}	0.08 ± 0.01 ^{a,b}	0.43 ± 0.01 ^{a}	0.05 ± 0.01 ^{a}	0.12 ± 0.01 ^{a,b}
	P45 N0 I	0.09 ± 0.01	0.45 ± 0.01 ^{a}	/	0.45 ± 0.01 ^{a}	0.07 ± 0.01 ^{a}	0.20 ± 0.01 ^{a}
	P45 N75 D	0.06 ± 0.01	0.60 ± 0.10 ^{a}	0.07 ± 0.01 ^{a,b}	0.34 ± 0.05 ^{b}	0.04 ± 0.01 ^{a}	0.11 ± 0.01 ^{a,b}
	P45 N75 I	0.08 ± 0.01	0.60 ± 0.10 ^{a}	/	0.10 ± 0.01 ^{a}	0.06 ± 0.02	0.19 ± 0.01 ^{a}
	P45 N150 D	0.06 ± 0.01 ^{b}	1.00 ± 0.10 ^{a,b}	0.08 ± 0.01 ^{a,b}	0.17 ± 0.01 ^{a,b}	0.05 ± 0.01 ^{a}	0.12 ± 0.01 ^{a,b}
	P45 N 150 I	0.09 ± 0.01	0.80 ± 0.04 ^{a}	/	0.48 ± 0.04	0.07 ± 0.01 ^{a}	0.20 ± 0.01 ^{a}
	P90 N0 D	0.07 ± 0.01	0.98 ± 0.01 ^{a}	/^{b}	0.46 ± 0.03 ^{a,b}	/^{b}	0.12 ± 0.01 ^{a,b}
	P90 N0 I	0.11 ± 0.03 ^{a}	1.30 ± 0.50	0.13 ± 0.01 ^{a}	0.35 ± 0.03	0.08 ± 0.01 ^{a}	0.22 ± 0.03 ^{a}
	P90 N75 D	0.06 ± 0.01 ^{b}	0.55 ± 0.05 ^{a,b}	0.07 ± 0.01 ^{b}	0.55 ± 0.04 ^{a,b}	/^{b}	0.11 ± 0.01 ^{b}
	P90 N75 I	0.09 ± 0.01	0.93 ± 0.01 ^{a}	/	0.31 ± 0.01 ^{a}	0.07 ± 0.01 ^{a}	0.20 ± 0.01 ^{a}
	P90 N150 D	0.07 ± 0.01	0.93 ± 0.08	/	0.18 ± 0.02 ^{a,b}	0.05 ± 0.01 ^{a,b}	0.12 ± 0.01 ^{a,b}
	P90 N150 I	0.09 ± 0.01	0.92 ± 0.07	/	0.46 ± 0.03 ^{a}	0.08 ± 0.01 ^{a}	0.20 ± 0.01 ^{a}

Table 1. *Cont.*

Harvesting Period	Fertilization	Δ9-THC % *w*/*w*	CBD % *w*/*w*	Δ9-THCA % *w*/*w*	CBDA % *w*/*w*	CBG % *w*/*w*	CBC % *w*/*w*
Stage B	P0 N0 D	0.07 ± 0.01	1.72 ± 0.09	/	0.30 ± 0.01	0.05 ± 0.01	0.07 ± 0.01
	P0 N0 I	0.06 ± 0.01	1.60 ± 0.27	/	0.30 ± 0.01	0.04 ± 0.01	0.09 ± 0.03
	P0 N75 D	0.07 ± 0.01	1.40 ± 0.01 [b]	/	0.72 ± 0.01 [b]	0.05 ± 0.01 [b]	0.07 ± 0.01 [b]
	P0 N75 I	0.05 ± 0.01	0.80 ± 0.10	/	0.36 ± 0.02	/	/
	P0 N150 D	0.08 ± 0.01	1.38 ± 0.06	/	0.74 ± 0.01 [b]	/ [b]	0.07 ± 0.01 [b]
	P0 N150 I	0.07 ± 0.01	1.30 ± 0.10	/	0.33 ± 0.03	0.04 ± 0.01	0.13 ± 0.01
	P45 N0 D	0.08 ± 0.01	1.43 ± 0.01	/	0.67 ± 0.02	/	0.07 ± 0.01 [b]
	P45 N0 I	0.08 ± 0.01	1.60 ± 0.27	/	0.66 ± 0.03	/	0.12 ± 0.01
	P45 N75 D	0.06 ± 0.01	1.33 ± 0.05 [b]	/	0.32 ± 0.01 [b]	/ [b]	0.07 ± 0.01 [b]
	P45 N75 I	0.08 ± 0.01	1.10 ± 0.10	/	0.55 ± 0.01	0.04 ± 0.01	0.12 ± 0.01
	P45 N150 D	0.06 ± 0.01	1.36 ± 0.01 [b]	/	0.30 ± 0.01 [b]	/ [b]	0.07 ± 0.01 [b]
	P45 N 150 I	0.08 ± 0.01	1.25 ± 0.01	/	0.56 ± 0.03	0.04 ± 0.01	0.13 ± 0.01
	P90 N0 D	0.08 ± 0.01	1.67 ± 0.01 [b]	/	0.29 ± 0.01 [b]	/	0.08 ± 0.01 [b]
	P90 N0 I	0.08 ± 0.01	1.13 ± 0.05	/	0.39 ± 0.01	/	0.11 ± 0.01
	P90 N75 D	0.07 ± 0.01	0.99 ± 0.13 [b]	0.05 ± 0.01 [b]	0.77 ± 0.02	/	0.09 ± 0.04
	P90 N75 I	0.08 ± 0.01	1.35 ± 0.13	/	0.80 ± 0.10	/	0.12 ± 0.01
	P90 N150 D	0.07 ± 0.01	1.01 ± 0.06	0.05 ± 0.01 [b]	0.53 ± 0.07 [b]	/	0.06 ± 0.01 [b]
	P90 N150 I	0.07 ± 0.01	1.01 ± 0.05	/	0.72 ± 0.03	/	0.12 ± 0.01

[a] $p < 0.05$, significantly different than the corresponding sample harvested in stage B, [b] $p < 0.05$, significantly different than the corresponding irrigated sample (one-way ANOVA, followed by Turkey HSD Test). Stage A = female flowering stage, stage B = seed maturity stage, I = irrigation, D = no irrigation.

NMR metabolite profile. The NMR metabolomic profile of hydroalcoholic Bligh–Dyer inflorescence extracts was obtained using literature data [11] relative to Ferimon cultivar. Four sugars, four organic acids, eleven amino acids, choline, and trigonelline were detected and quantified in all the investigated samples. The value relative to each compound was reported on Supplementary Tables S3–S6.

Total phenolic content (TPC) and antioxidant activity. The TPC and the antioxidant activity of Ferimon inflorescence were determined by means of DPPH and ABTS assays, see Table 2 for samples relative to 2017 and 2018. In the previously study [11], the TPC of Ferimon cultivar showed a value lower than the one here reported. Moreover, another study has analyzed the antioxidant activity of Ferimon cultivar cultivated in Central Italy [39] (irrigation and fertilization practices not reported) and harvested during the flowering stage; anyway, since the results have been expressed using another unit of measurement, a comparison with the reported results was not possible.

To take into account the whole set of data, ASCA analysis was carried out at first on data matrices relative to 2017 and 2018 separately, and successively on the joint data. The comparison between continuous irrigation and absence of irrigation was carried out only in 2018.

Table 2. Total phenolic content (TPC, mg kg^{-1} of fresh inflorescences ± SD) and antioxidant activity (inhibition rate I% ± SD) by spectrophotometric analysis of the 2017 and 2018 samples reported for each phosphorus (P) and nitrogen (N) fertilization combination at two harvesting stages. Analyses were carried out in triplicate.

Harvesting Period	Fertilization	TPC (mg kg^{-1} Fresh Hemp)	DPPH (EC_{50} in mg Fresh Hemp mL^{-1})	ABTS (mg TE g^{-1} Fresh Hemp)
2017 year				
Stage A	P0 N0 I	3788.15 ± 198.83 [a]	0.84 ± 0.32 [a]	0.75 ± 0.34
	P0 N150 I	3911.21 ± 158.83 [a]	0.82 ± 0.46 [a]	0.75 ± 0.42
	P90 N0 I	3859.71 ± 311.84 [a]	0.82 ± 0.14	0.75 ± 0.45
	P90 N150 I	3607.90 ± 278.35	0.88 ± 0.52	0.75 ± 0.46
Stage B	P0 N0 I	3201.61 ± 175.29	0.93 ± 0.01	0.75 ± 0.14
	P0 N150 I	3515.79 ± 88.44	0.97 ± 0.29	0.75 ± 0.19
	P90 N0 I	3031.07 ± 198.78	0.95 ± 0.37	0.75 ± 0.27
	P90 N150 I	3351.50 ± 33.45	0.96 ± 0.62	0.75 ± 0.24
2018 year				
Stage A	P0 N0 D	1686.54 ± 88.95 [a]	0.72 ± 0.26 [a]	0.76 ± 0.38
	P0 N0 I	1811.72 ± 190.37 [a]	0.74 ± 0.57	0.75 ± 0.43
	P0 N75 D	2958.75 ± 455.53 [a,b]	0.90 ± 0.52	0.76 ± 0.17
	P0 N75 I	1712.82 ± 4.04 [a]	0.68 ± 0.30	0.74 ± 0.29
	P0 N150 D	1610.49 ± 10.75 [a]	0.70 ± 0.23	0.75 ± 0.01
	P0 N 150 I	1605.26 ± 7.18 [a]	0.72 ± 0.19	0.76 ± 0.66
	P45 N0 D	1650.77 ± 206.59 [a]	0.75 ± 0.36	0.76 ± 0.15
	P45 N0 I	1766.50 ± 36.08	0.74 ± 0.43	0.74 ± 0.49
	P45 N75 D	1884.70 ± 103.77 [a]	0.70 ± 0.20	0.75 ± 0.11
	P45 N75 I	1752.48 ± 62.43 [a]	0.75 ± 0.18	0.76 ± 0.44
	P45 N150 D	1806.23 ± 3.89 [a,b]	0.69 ± 0.34	0.76 ± 0.51
	P45 N 150 I	1496.75 ± 5.26 [a]	0.79 ± 0.14	0.76 ± 0.58
	P90 N0 D	2806.45 ± 198.60 [a,b]	0.78 ± 0.11	0.76 ± 0.50
	P90 N0 I	1603.93 ± 8.84 [a]	0.71 ± 0.30	0.75 ± 0.16
	P90 N75 D	1598.98 ± 1.20 [a]	0.70 ± 0.17	0.76 ± 0.38
	P90 N75 I	1758.90 ± 118.94 [a]	0.86 ± 0.16	0.76 ± 0.18
	P90 N150 D	1478.74 ± 52.86 [a,b]	0.77 ± 0.15	0.75 ± 0.31
	P90 N150 I	2074.89 ± 144.55	0.87 ± 0.01	0.76 ± 0.65

Table 2. *Cont.*

Harvesting Period	Fertilization	TPC (mg kg^{-1} Fresh Hemp)	DPPH (EC_{50} in mg Fresh Hemp mL^{-1})	ABTS (mg TE g^{-1} Fresh Hemp)
Stage B	P0 N0 D	2114.52 ± 206.76	0.83 ± 0.06	0.74 ± 0.35
	P0 N0 I	2517.61 ± 158.69	0.79 ± 0.51	0.76 ± 0.66
	P0 N75 D	1827.67 ± 183.84 [b]	0.64 ± 0.60	0.76 ± 0.01
	P0 N75 I	2441.43 ± 69.45	0.83 ± 0.04	0.74 ± 0.25
	P0 N150 D	1235.93 ± 37.86 [b]	0.69 ± 0.42	0.76 ± 0.33
	P0 N150 I	1408.64 ± 37.68	0.91 ± 0.45	0.75 ± 0.19
	P45 N0 D	2176.90 ± 192.05	0.77 ± 0.03	0.76 ± 0.09
	P45 N0 I	2339.09 ± 490.98	0.86 ± 0.24	0.75 ± 0.17
	P45 N75 D	2514.91 ± 7.71 [b]	0.77 ± 0.46	0.76 ± 0.22
	P45 N75 I	2480.07 ± 0.35	0.83 ± 0.14	0.75 ± 0.07
	P45 N150 D	2089.19 ± 25.88 [b]	0.71 ± 0.38	0.75 ± 0.18
	P45 N 150 I	2535.18 ± 42.93	0.79 ± 0.29	0.76 ± 0.01
	P90 N0 D	2183.52 ± 104.90 [b]	0.68 ± 0.17	0.75 ± 0.17
	P90 N0 I	2618.61 ± 10.21	0.86 ± 0.43	0.75 ± 0.22
	P90 N75 D	2283.75 ± 67.69	0.66 ± 0.24	0.75 ± 0.22
	P90 N75 I	2462.76 ± 234.60	0.91 ± 0.67	0.76 ± 0.21
	P90 N150 D	2335.18 ± 60.61	0.67 ± 0.05	0.75 ± 0.02
	P90 N150 I	2177.69 ± 191.41	0.91 ± 0.23	0.76 ± 0.48

[a] $p < 0.05$, significantly different than the corresponding sample harvested in stage B, [b] $p < 0.05$, significantly different than the corresponding irrigated sample (one-way ANOVA, followed by Turkey HSD Test). Stage A = female flowering stage, stage B = seed maturity stage, I = irrigation, D = no irrigation.

3.2. The 2017 Year-Data

The 2017 year-data, relative only to irrigated fields, were acquired as a result of three controlled factors, each factor at two levels: harvesting period ((female flowering stage (A) and seed maturity stage (B)), P dose (0 and 90 kg P_2O_5 ha^{-1}), and N dose (0 and 150 kg of N ha^{-1}). ASCA applied to the matrix of experimental data, underlined that the largest part of the variance was due to the effect of harvesting (40.37%), followed by N dose (10.08%) and P dose (6.61%) factors. Permutation testing used to evaluate the significance of each of the design terms (main effects and interactions) showed that only the effect of harvesting period and N were statistically significant ($p < 0.05$). However, the effect of P fertilization was only slightly above the significance threshold ($p = 0.0558$). Accordingly, only the effect matrices for harvesting time and N fertilization were subjected to the successive SCA analysis.

Harvesting. The harvesting period was the agronomical factor that mainly affected the chemical variability of the analyzed samples with stage A being characterized by higher levels of Val (Valine), Pro (Proline), Myo-inositol, Malate, TPC, THC, and CBC, whereas stage B samples were richer in Gln (Glutamine), Asp (Aspartate), Asn (Asparagine), Formate, Trigonelline, Succinate, and DPPH, see scores and loadings of ASCA displayed on Figure 1.

The scores plot on the SC component shows that stages A and B correspond to negative and positive scores, respectively. This information is fundamental to interpret the corresponding loadings plot, where the variables that significantly contribute to the component are highlighted as red bars. Indeed, all the variables with positive loadings are higher in stage B samples, whereas the ones with negative loadings are higher in stage A.

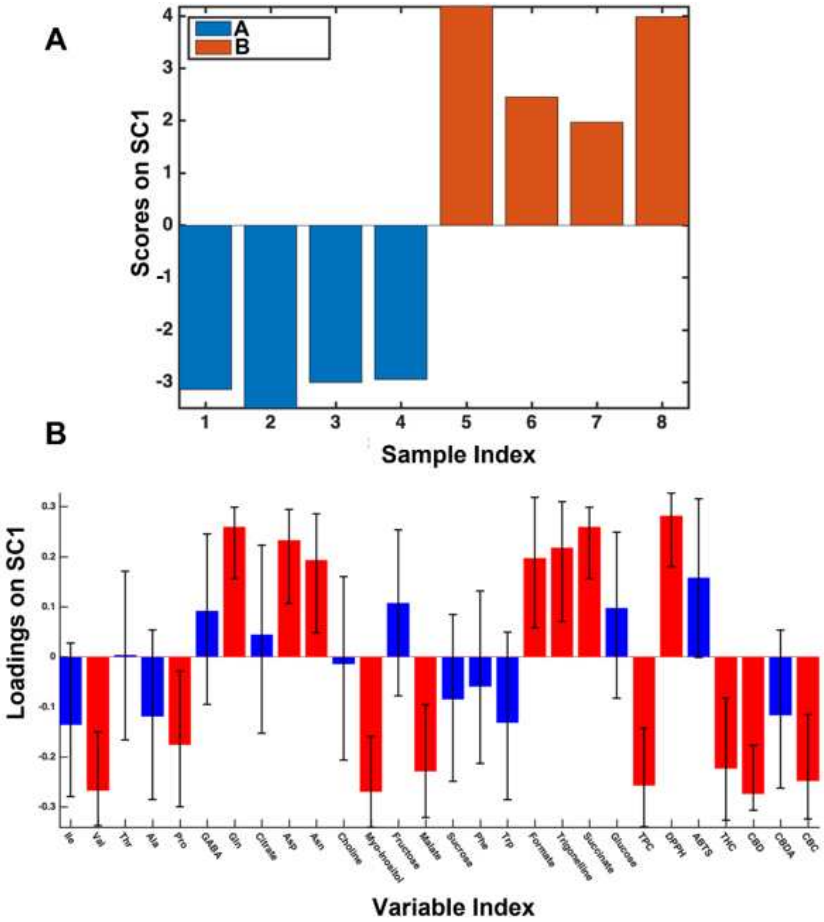


Figure 1. Scores (**A**) and loadings (**B**) plots of SC1 component extracted from SCA analysis regarding the harvesting effect on 2017 samples.

Moreover, an increase of biomass and inflorescences yield was observed from stage A to stage B, Table 3.

Fertilization. The 150 kg ha^{-1} dose of N caused an increase of several amino acids, namely Ile (Isoleucine), Phe (Phenylalanine), Thr (Threonine), Pro, and Trp (Tryptophan). Among these, Ile and Phe were the most statistically significant increased, as shown by scores and loadings plot of the SC component extracted from the SCA analysis regarding the effect of N fertilization, Figure 2. In particular, the scores plot highlights that levels of 0 kg ha^{-1} and 150 kg ha^{-1} correspond to positive and negative scores, respectively. On the other hand, in the loadings plot, the red error bars indicate the 95% confidence interval of the coefficients, estimated by bootstrapping. On the contrary, no statistically significant

effect of 0 kg ha^{-1} N were observed, although an increase of GABA (γ-aminobutyrate), Sucrose, and CBDA was observed.

Table 3. Biomass yield, inflorescences yield, and inflorescences/biomass ratio (inf/bio) of the 2017 and 2018 samples reported for each phosphorus (P) and nitrogen (N) fertilization combination at two harvesting stages. Measurements were carried out in triplicate.

Harvesting Period	Fertilization	Biomass (kg ha^{-1})	Inflorescences (kg ha^{-1})	Inf/Bio
2017 year				
Stage A	P0 N0 I	4540.11 ± 346.75 ^{a}	616.61 ± 34.16 ^{a}	0.14 ± 0.01 ^{a}
	P0 N150 I	6476.78 ± 293.35 ^{a}	840.66 ± 38.91 ^{a}	0.13 ± 0.01 ^{a}
	P90 N0 I	4932.39 ± 380.13 ^{a}	616.09 ± 60.50 ^{a}	0.12 ± 0.01 ^{a}
	P90 N150 I	6717.79 ± 173.38 ^{a}	862.28 ± 45.66 ^{a}	0.13 ± 0.01 ^{a}
Stage B	P0 N0 I	5618.85 ± 258.66	967.38 ± 112.69	0.17 ± 0.01
	P0 N150 I	8115.37 ± 133.85	1281.79 ± 89.10	0.16 ± 0.01
	P90 N0 I	5967.57 ± 288.33	1032.14 ± 79.09	0.17 ± 0.01
	P90 N150 I	8429.39 ± 478.14	1446.22 ± 99.63	0.17 ± 0.01
2018 year				
Stage A	P0 N0 D	1567.65 ± 161.07 ^{b}	217.15 ± 27.87 ^{a,b}	0.14 ± 0.01 ^{a}
	P0 N0 I	4839.72 ± 346.76 ^{a}	679.69 ± 24.19 ^{a}	0.14 ± 0.01 ^{a}
	P0 N75 D	1245.49 ± 80.32 ^{a,b}	170.37 ± 4.56 ^{a,b}	0.14 ± 0.01 ^{a}
	P0 N75 I	5636.54 ± 682.71 ^{a}	776.25 ± 72.03 ^{a}	0.14 ± 0.01 ^{a}
	P0 N150 D	1061.00 ± 106.68 ^{a,b}	143.97 ± 19.53 ^{a,b}	0.14 ± 0.01 ^{a}
	P0 N 150 I	6877.93 ± 221.06 ^{a}	976.34 ± 56.00 ^{a}	0.14 ± 0.01 ^{a}
	P45 N0 D	1533.95 ± 49.27 ^{a,b}	210.27 ± 18.05 ^{a,b}	0.14 ± 0.01 ^{a}
	P45 N0 I	5215.94 ± 579.36 ^{a}	718.69 ± 100.28 ^{a}	0.14 ± 0.01 ^{a}
	P45 N75 D	1373.71 ± 131.17 ^{b}	174.38 ± 29.37 ^{a,b}	0.13 ± 0.01 ^{a}
	P45 N75 I	5990.38 ± 199.68 ^{a}	824.92 ± 25.75 ^{a}	0.14 ± 0.01 ^{a}
	P45 N150 D	1085.79 ± 12.56 ^{b}	143.32 ± 17.78 ^{a,b}	0.13 ± 0.01 ^{a}
	P45 N 150 I	7181.05 ± 380.83 ^{a}	993.08 ± 47.33 ^{a}	0.14 ± 0.01 ^{a}
	P90 N0 D	1534.55 ± 93.93 ^{a,b}	209.62 ± 20.90 ^{a,b}	0.14 ± 0.01 ^{a}
	P90 N0 I	5356.79 ± 475.80 ^{a}	700.44 ± 50.03 ^{a}	0.13 ± 0.01 ^{a}
	P90 N75 D	1292.04 ± 187.33 ^{b}	177.43 ± 14.05 ^{a,b}	0.14 ± 0.01 ^{a}
	P90 N75 I	6046.85 ± 366.29 ^{a}	807.35 ± 68.69 ^{a}	0.13 ± 0.01 ^{a}
	P90 N150 D	1154.10 ± 231.08 ^{b}	170.97 ± 18.02 ^{a,b}	0.15 ± 0.01 ^{a}
	P90 N150 I	7125.98 ± 313.94 ^{a}	984.88 ± 51.93 ^{a}	0.14 ± 0.01 ^{a}
Stage B	P0 N0 D	1883.45 ± 154.60 ^{b}	341.47 ± 37.53 ^{b}	0.18 ± 0.01
	P0 N0 I	6265.84 ± 422.05	1100.76 ± 41.47	0.18 ± 0.01
	P0 N75 D	1548.50 ± 88.45 ^{b}	261.39 ± 31.92 ^{b}	0.17 ± 0.01
	P0 N75 I	7213.44 ± 565.81	1284.05 ± 96.02	0.18 ± 0.0
	P0 N150 D	1363.78 ± 78.17 ^{b}	226.66 ± 29.39 ^{b}	0.17 ± 0.01
	P0 N150 I	8377.37 ± 223.66	1510.85 ± 85.60	0.18 ± 0.01
	P45 N0 D	1945.90 ± 142.73 ^{b}	329.57 ± 50.37 ^{b}	0.17 ± 0.01
	P45 N0 I	6489.49 ± 468.28	1180.99 ± 177.02	0.18 ± 0.01
	P45 N75 D	1558.84 ± 92.52 ^{b}	285.11 ± 17.12 ^{b}	0.18 ± 0.01
	P45 N75 I	7451.66 ± 364.56	1308.29 ± 90.31	0.18 ± 0.01
	P45 N150 D	1204.93 ± 144.89 ^{b}	233.02 ± 24.49 ^{b}	0.19 ± 0.01
	P45 N 150 I	8655.74 ± 514.37	1629.76 ± 102.02	0.19 ± 0.01
	P90 N0 D	1945.84 ± 168.74 ^{b}	334.18 ± 54.75 ^{b}	0.17 ± 0.01
	P90 N0 I	6528.28 ± 410.66	1215.83 ± 135.20	0.19 ± 0.01
	P90 N75 D	1536.66 ± 129.23 ^{b}	274.72 ± 28.83 ^{b}	0.18 ± 0.01
	P90 N75 I	7408.61 ± 105.87	1363.41 ± 60.00	0.18 ± 0.01
	P90 N150 D	1177.53 ± 109.00 ^{b}	250.68 ± 31.20 ^{b}	0.21 ± 0.01 ^{b}
	P90 N150 I	8635.76 ± 396.31	1590.19 ± 97.10	0.18 ± 0.01

^{a} $p < 0.05$, significantly different than the corresponding sample harvested in stage B, ^{b} $p < 0.05$, significantly different than the corresponding irrigated sample (one-way ANOVA, followed by Turkey HSD Test). Stage A = female flowering stage, stage B = seed maturity stage, I = irrigation, D = no irrigation.

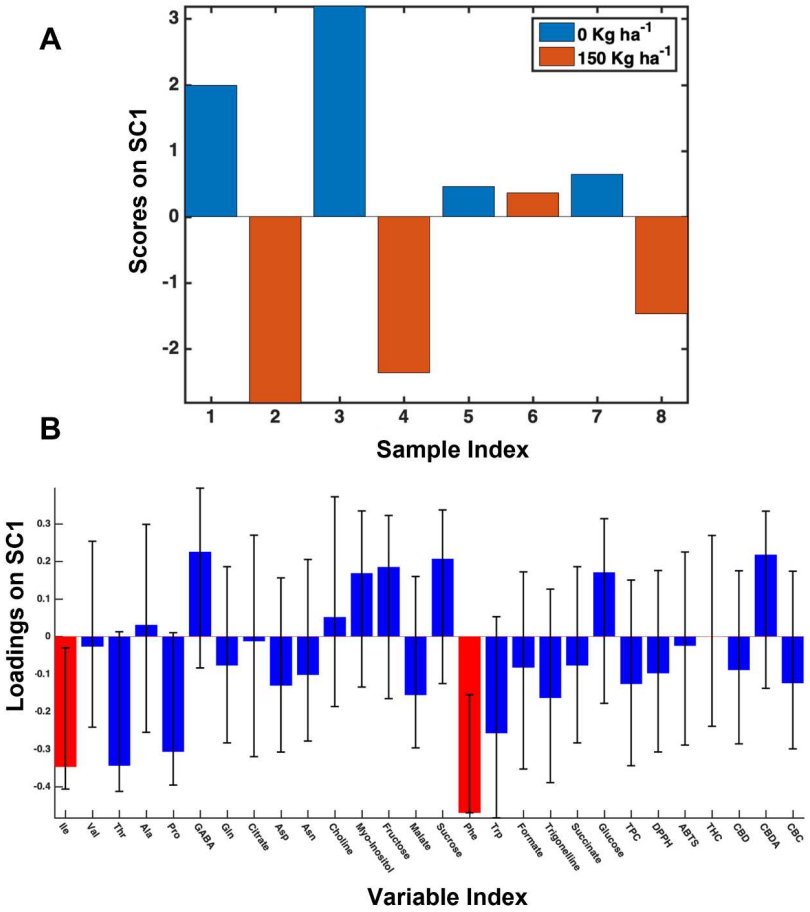


Figure 2. Scores (**A**) and loadings (**B**) plots of SC1 component extracted from SCA analysis regarding the N fertilization effect on 2017 samples.

Note that high N dosed caused an increase of both biomass and inflorescences yield, see Table 3.

3.3. The 2018 Year-Data

The 2018 year-data were acquired as a result of four controlled factors: P dose (0, 45 and 90 kg P_2O_5 ha^{-1}), N dose (0, 75 and 150 kg of N ha^{-1}), irrigation (irrigated or not), and harvesting period (female flowering stage (A) and seed maturity stage (B)). ASCA applied to the matrix of experimental data allowed us to observe that the largest part of the variance was due to the effect of irrigation (23.95%), followed by harvesting (21.76%), N fertilization (4.27%) and P dose (3.14%). On the other hand, permutation testing evidenced that all the design terms (main effects and interactions) are statistically significant ($p < 0.05$).

Harvesting effect. An increase of Choline, Myo-inositol, Fructose, Sucrose, Succinate, THCA, CBC, and CBG was observed in stage A, whereas stage B was characterized by an increase of Gln, Asp, Asn, Malate, Trp, Formate, TPC, CBD, and CBDA, as obtained by SCA.

Irrigation. Irrigation turned out to have the highest influence on hemp inflorescences chemical variability. When continuous irrigation was applied, an increase of DPPH, THC, and CBC was observed as underlined by SCA. It is noteworthy that DPPH increment was more appreciable in stage B. On the contrary, from SCA analysis, it emerged that the absence of irrigation caused an increase of several metabolites such as Val, Ala (Alanine), GABA, citrate, Asn, choline, fructose, malate, sucrose, formate, trigonelline, succinate, and glucose.

Additionally, the irrigation practice strongly affected the biomass and inflorescences yield. The absence of irrigation caused a strong stress condition in plants, thus reducing biomass and inflorescences at least of three times, see Table 3. It is noteworthy that in both irrigation and absence of irrigation conditions, the inf/bio ratio remained the same. This behavior has also been previously observed in Ermes and Carma cultivars grown in Spain, where a reduction of irrigation caused a decrease of biomass yield [19].

Fertilization. The inspection of the scores plot (Figure 3A) indicates a clear effect of nitrogen supplementation, whereas at the same time little difference in increasing the N level from 75 to 150 kg ha^{-1} is observed. When this fertilizer was applied, a significant increment of Ile and Thr was observed. Additionally, Val, Pro, GABA, Asp, Myo-inositol, Formate, and GABA also increased, as shown by scores and loadings plot of the SC component extracted from the SCA. On the contrary, high supplementation of N caused a decrease of some cannabinoids, namely THC, THCA, and CBD, and also Phe, Trp, succinate, and TPC. Among these metabolites, THC was subjected to the most statistically significant decrease, see Figure 3. The obtained results allowed us to observe how N fertilization mainly affects the amino acids content, with most of them increasing when it was supplied. Moreover, the use of 75 kg ha^{-1} had the same effect of the higher 150 kg ha^{-1} dose, thus giving helpful information that can be used for reducing fertilizer waste [40].

Although P fertilization did not appear to have a significant influence on the inflorescences chemical profile, an increase of Phe was observed when this fertilizer was used.

N fertilization strongly affected hemp yield, with the behavior being connected with the presence or the absence of irrigation. In particular, in irrigated plants, the use of high N doses caused an increase of both biomass and inflorescences yield. These data were confirmed by literature data where high dosages of N have caused an increase of hemp biomass yield [16–18]. Moreover, a synergistic effect of combination of N fertilization and irrigation on hemp biomass yield was observed, with the highest yield when the highest dosage of N (150 kg ha^{-1}) was used. On the contrary, when no irrigation was supplied, the use of high N doses caused a reduction of biomass and inflorescences yield, since high N dosages enhance the plant stress condition in not-irrigated plants. Similarly to what was observed for the chemical profile variations, P fertilization did not appear to influence the biomass and inflorescences yield.

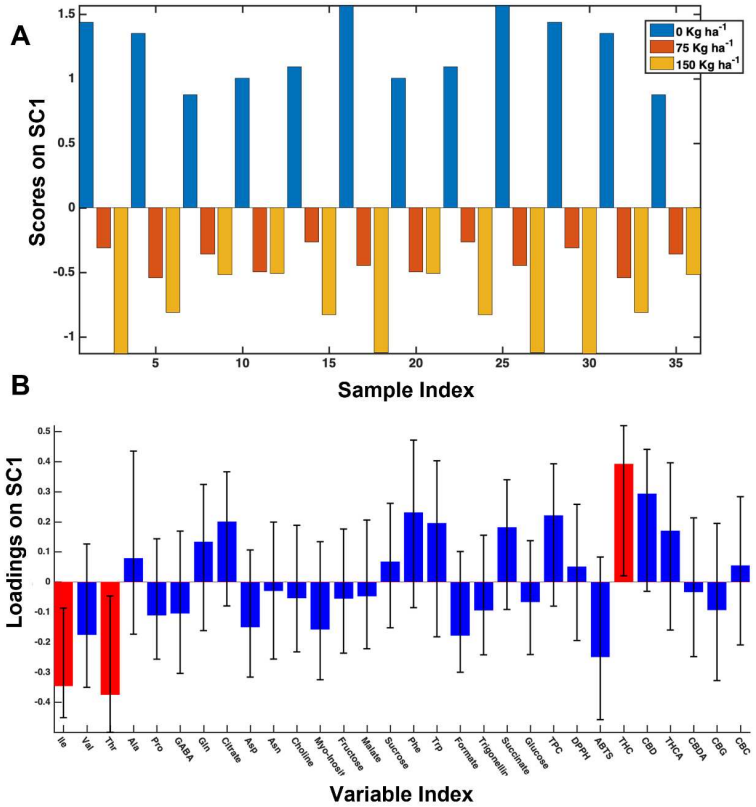


Figure 3. Scores (**A**) and loadings (**B**) plots of SC1 component extracted from SCA analysis regarding the N fertilization effect on 2018 samples.

3.4. 2017- and 2018-Years Data Set

The cultivation year represents an important factor that can strongly affect the chemical profile of food and vegetable matrices. Additionally, in this case, comparing the data obtained in 2017 and 2018, it was possible to observe a clear change of the chemical profile of hemp inflorescences. Interestingly some differences were observed in the cannabinoids profile, with THCA and CBG not being detected in inflorescences grown in 2017. The relevant effect of cultivation year was demonstrated by ASCA carried out on the joint data, by considering four factors: P dose (0 and 90 kg P_2O_5 ha^{-1}), N dose (0 and 150 kg of N ha^{-1}), harvesting (A and B) and year (2017 and 2018). All data were referred to irrigated crops. ASCA applied to the matrix of experimental data underlined that the largest part of the variance was due to the effect of year (48.59%), followed by that of harvesting (14.16%), N dose (3.79%), and P dose (2.08%). On the other hand, permutation testing evidenced that all the design terms (main effects and interactions) are statistically significant ($p < 0.05$).

The SCA regarding the effect matrix for the two years shows that almost all the metabolites were found to be present at significantly higher levels in 2018. The only

exceptions were TPC, CBDA, and DPPH values, which higher in 2017, whereas Pro, Gln, Asp, Asn, Malate, CBD, THCA, and ABTS values did not show any significant difference.

Comparing the results obtained in 2017 and 2018, it was possible to observe that some metabolites such as Gln, Asp, Asn, and formate increased their content during the harvesting period in both years in agreement with data previously reported for the Ferimon cultivar [11].

Regarding yield data, only a slight increase of biomass and inflorescence was observed in 2018 with respect to 2017. In both 2017 and 2018, harvesting stage B was characterized by higher values of biomass and inflorescences yield, with a major value of inflorescences/biomass (inf/bio) ratio with respect to those calculated in stage A. This data suggested that the biomass increase observed in stage B was mainly due to a major inflorescences production, as also demonstrated by the inf/bio increase.

The reported results underlined that the agronomical practices as well as the cultivation year can strongly influence the chemical profile and the yield of hemp inflorescences. In particular, cultivation year and harvesting period and N fertilization significantly affected the inflorescences chemical profile. It is also important to note that irrigation and harvesting during the full female flowering period cause an increase of THC and CBD (THC content always below the legal limit). On the other hand, the absence of irrigation caused an increase of several amino acids, sugars, and organic acids, as well as a reduction of biomass and inflorescences yield, by triggering a stress condition in the plant. Regarding the harvesting period, some metabolites such as glutamate, asparagine, aspartate, and formate increased during the time in both 2017 and 2018, as observed previously [13]. Among fertilization, nitrogen supplementation had a major influence on inflorescence chemical variation with respect to phosphorus by affecting the content of amino acids and cannabinoids. Moreover, nitrogen fertilization strongly affected the biomass and inflorescences yield with the behavior being strictly related to the presence or absence of irrigation. In particular, when irrigation is applied, the use of high nitrogen dosages causes important yields to increase.

Up to now, the studies on the inflorescences reported in the literature are often not comparable since they were carried out in different conditions or more simply since the agronomical conditions are not reported. For this reason, it is important to improve the research in this field since, as demonstrated in this study, the agronomic practices can influence the chemical composition of hemp inflorescences. This issue can be firstly a notable factor if, for instance, THC concentration is considered. Indeed, its amount has to be below the legal limits to avoid the cultivation and the industrial uses of *C. sativa* plants; so it is auspicious to apply proper practices that do not cause an increase of this cannabinoid. Moreover, in the perspective of using hemp inflorescences as a novel food, the possibility of using proper agronomic practices to obtain a specific chemical profile can strongly contribute to enhance the potential nutritional value of this matrix.

4. Conclusions

Considering that the food application of hemp inflorescences is a debated topic, this study can contribute to further underline the potential use of this matrix as a food or food ingredient, since several metabolites important from a nutritional and biological point of view were measured. Of course, these kinds of studies, based on chemical characterization, also have to be supported by safety, toxicity, and biological studies to further improve the total eligibility of hemp inflorescences as a novel food. The here reported results suggest the importance to choose the proper cultivation conditions to obtain products with a determined chemical composition, thus offering the possibility to have potential foods or food ingredients with a variable profile based on specific applications. The here reported investigation that involves chemical and agronomic aspects aims to propose a methodological approach that could be useful for future applications in this sector and also for the design of the experimental phase.

Supplementary Materials: The following supporting information can be downloaded at: https://www.mdpi.com/article/10.3390/foods11223658/s1, Figure S1. Schematic diagram explaining the practices of nitrogen (N) and phosphorus (P) fertilizations and irrigation applied for the cultivation of Ferimon cultivar. Subscript numbers refer to the kg of fertilizer applied for ha. Table S1. Means of minimum (T. min) and maximum (T. max.) air temperatures, total rainfall and potential evapotranspiration (ET0) throughout the periods of study at 10-days intervals from March to September in 2017 and 2018 cropping season. Table S2. Quantified metabolites in Bligh-Dyer hydroalcoholic extracts of Ferimon inflorescences, with relative ^{1}H NMR signals (ppm) used for quantification. Table S3. NMR quantitative results of amino acids measured in Bligh-Dyer hydroalcoholic extracts of Ferimon inflorescences in 2017. Table S4. NMR quantitative results of organic acids, sugars and other molecules measured in Bligh-Dyer hydroalcoholic extracts of Ferimon inflorescences in 2017. Table S5. NMR quantitative results of amino acids measured in Bligh-Dyer hydroalcoholic extracts of Ferimon inflorescences in 2018. Table S6. NMR quantitative results of organic acids, sugars and other molecules measured in Bligh-Dyer hydroalcoholic extracts of Ferimon inflorescences in 2018.

Author Contributions: Conceptualization, M.S., G.D.M. and L.M.; methodology, A.P.S., A.M.G., E.C. and G.V.; validation, A.P.S., M.S., G.D.M., E.C. and G.V.; formal analysis, C.I., A.P.S., F.M., M.S., S.C., G.D.M., L.L., C.T. and S.A.P.; investigation, A.P.S., E.C., L.G., L.M. and G.V.; data curation, A.P.S., M.S., G.D.M., C.I. and A.M.G.; writing—original draft preparation, M.S. and G.D.M.; writing—review and editing, A.P.S. and L.M.; visualization, A.P.S., C.I., L.M., L.G., B.B., E.C., F.M., S.C., L.L., C.T., S.A.P., A.M.G. and G.V.; supervision, L.M. and A.P.S.; project administration, L.M.; funding acquisition, L.M. All authors have read and agreed to the published version of the manuscript.

Funding: This work has been realized with funds received from the following agencies: Italian Ministry of Education, Universities and Research—Dipartimenti di Eccellenza—L. 232/2016; Regione Lazio, "LACanapa" Project (Progetto di Ricerca, finanziato ai sensi della L.R. 13/08—Protocol 85-2017-15069 CUP: B86C18000730002).

Data Availability Statement: Not applicable.

Acknowledgments: This work is part of a project supported by Lazio Region entitled "La Canapa industriale: sviluppo e valorizzazione di una nuova filiera agroalimentare ecosostenibile". The manuscript involved the contribution of researchers from the Italian Society of Food Sciences (SISA).

Conflicts of Interest: The authors declare no conflict of interest.

References

1. EUR-Lex. Access to European Union Law. Available online: https://eur-lex.europa.eu/legal-content/EN/TXT/?uri=CELEX:01999R1251-20040701 (accessed on 3 June 2022).
2. Montserrat-De La Paz, S.; Marín-Aguilar, F.; García-Giménez, M.D.; Fernández-Arche, M.A. Hemp (*Cannabis sativa* L.) seed oil: Analytical and phytochemical characterization of the unsaponifiable fraction. *J. Agric. Food Chem.* **2014**, *62*, 1105–1110. [CrossRef] [PubMed]
3. Lewis-Bakker, M.M.; Yang, Y.; Vyawahare, R.; Kotra, L.P. Extractions of Medical Cannabis Cultivars and the Role of Decarboxylation in Optimal Receptor Responses. *Cannabis Cannabinoid Res.* **2019**, *4*, 183–194. [CrossRef] [PubMed]
4. Kim, E.-S.; Mahlberg, P.G. Secretory Cavity Development in Glandular Trichomes of *Cannabis sativa* L. (Cannabaceae). *Am. J. Bot.* **1991**, *78*, 220. [CrossRef]
5. Jin, D.; Dai, K.; Xie, Z.; Chen, J. Secondary Metabolites Profiled in Cannabis Inflorescences, Leaves, Stem Barks, and Roots for Medicinal Purposes. *Sci. Rep.* **2020**, *10*, 3309. [CrossRef] [PubMed]
6. Drinić, Z.; Vladić, J.; Koren, A.; Zeremski, T.; Stojanov, N.; Kiprovski, B.; Vidović, S. Microwave-assisted extraction of cannabinoids and antioxidants from *Cannabis sativa* aerial parts and process modeling. *J. Chem. Technol. Biotechnol.* **2020**, *95*, 831–839. [CrossRef]
7. Lanyon, V.S.; Turner, J.C.; Mahlberg, P.G. Quantitative Analysis of Cannabinoids in the Secretory Product from Capitate-Stalked Glands of *Cannabis sativa* L. (Cannabaceae). *Bot. Gaz.* **1981**, *142*, 316–319. [CrossRef]
8. Hemphill, J.K.; Turner, J.C.; Mahlberg, P.G. Cannabinoid content of individual plant organs from different geographical strains of *Cannabis sativa* L. *J. Nat. Prod.* **1980**, *43*, 112–122. [CrossRef]
9. European Commission EU Novel Food Catalogue. Available online: https://webgate.ec.europa.eu/fip/novel_food_catalogue/# (accessed on 27 July 2022).
10. Cerino, P.; Buonerba, C.; Cannazza, G.; D'Auria, J.; Ottoni, E.; Fulgione, A.; Di Stasio, A.; Pierri, B.; Gallo, A. A review of hemp as food and nutritional supplement. *Cannabis Cannabinoid Res.* **2021**, *6*, 19–27. [CrossRef]

11. Ingallina, C.; Sobolev, A.P.; Circi, S.; Spano, M.; Fraschetti, C.; Filippi, A.; Di Sotto, A.; Di Giacomo, S.; Mazzoccanti, G.; Gasparrini, F.; et al. *Cannabis sativa* L. inflorescences from monoecious cultivars grown in central Italy: An untargeted chemical characterization from early flowering to ripening. *Molecules* **2020**, *25*, 1908. [CrossRef]
12. Izzo, L.; Castaldo, L.; Narváez, A.; Graziani, G.; Gaspari, A.; Rodríguez-Carrasco, Y.; Ritieni, A. Analysis of Phenolic Compounds in Commercial *Cannabis sativa* L. Inflorescences using UHPLC-Q-Orbitrap HRMs. *Molecules* **2020**, *25*, 631. [CrossRef]
13. Spano, M.; Di Matteo, G.; Ingallina, C.; Botta, B.; Quaglio, D.; Ghirga, F.; Balducci, S.; Cammarone, S.; Campiglia, E.; Giusti, A.M.; et al. A multimethodological characterization of *Cannabis sativa* L. Inflorescences from seven dioecious cultivars grown in Italy: The effect of different harvesting stages. *Molecules* **2021**, *26*, 2912. [CrossRef]
14. Jankauskiene, Z.; Gruzdeviene, E.; Ivanovs, S.; Maumevicius, E. Screening hemp (*Cannabis sativa* L.) biomass and chemical composition as influenced by seed rate and genotype. *Proc. Eng. R. Dev.* **2017**, *16*, 317–322.
15. Pieracci, Y.; Ascrizzi, R.; Terreni, V.; Pistelli, L.; Flamini, G.; Bassolino, L.; Fulvio, F.; Montanari, M.; Paris, R. Essential oil of *Cannabis sativa* l: Comparison of yield and chemical composition of 11 hemp genotypes. *Molecules* **2021**, *26*, 4080. [CrossRef]
16. Tang, K.; Struik, P.C.; Yin, X.; Calzolari, D.; Musio, S.; Thouminot, C.; Bjelková, M.; Stramkale, V.; Magagnini, G.; Amaducci, S. A comprehensive study of planting density and nitrogen fertilization effect on dual-purpose hemp (*Cannabis sativa* L.) cultivation. *Ind. Crops Prod.* **2017**, *107*, 427–438. [CrossRef]
17. Vera, C.L.; Malhi, S.S.; Raney, J.P.; Wang, Z.H. The effect of N and P fertilization on growth, seed yield and quality of industrial hemp in the Parkland region of Saskatchewan. *Can. J. Plant Sci.* **2004**, *84*, 939–947. [CrossRef]
18. Vera, C.L.; Malhi, S.S.; Phelps, S.M.; May, W.E.; Johnson, E.N. N, P, and S fertilization effects on industrial hemp in Saskatchewan. *Can. J. Plant Sci.* **2010**, *90*, 179–184. [CrossRef]
19. García-Tejero, I.F.; Durán-Zuazo, V.H.; Pérez-Álvarez, R.; Hernández, A.; Casano, S.; Morón, M.; Muriel-Fernández, J.L. Impact of plant density and irrigation on yield of hemp (*Cannabis sativa* L.) in a mediterranean semi-arid environment. *J. Agric. Sci. Technol.* **2014**, *16*, 887–895.
20. Pejić, B.; Sikora, V.; Milić, S.; Mačkić, K.; Koren, A.; Bajić, I. Effect of drip irrigation on yield and evapotranspiration of fibre hemp (*Cannabis sativa* L.). *Ratar. i Povrt.* **2018**, *55*, 130–134. [CrossRef]
21. Liu, M.; Fernando, D.; Daniel, G.; Madsen, B.; Meyer, A.S.; Ale, M.T.; Thygesen, A. Effect of harvest time and field retting duration on the chemical composition, morphology and mechanical properties of hemp fibers. *Ind. Crops Prod.* **2015**, *69*, 29–39. [CrossRef]
22. Maathuis, F.J. Physiological functions of mineral macronutrients. *Curr. Opin. Plant Biol.* **2009**, *12*, 250–258. [CrossRef]
23. Zheng, Y. Current nutrient management practices and technologies used in North American greenhouse and nursery industries. *Acta Hortic.* **2018**, *1227*, 435–442. [CrossRef]
24. Bevan, L.; Jones, M.; Zheng, Y. Optimisation of Nitrogen, Phosphorus, and Potassium for Soilless Production of *Cannabis sativa* in the Flowering Stage Using Response Surface Analysis. *Front. Plant Sci.* **2021**, *12*, 764103. [CrossRef] [PubMed]
25. Coffman, C.B.; Gentner, W.A. Responses of Greenhouse-grown *Cannabis sativa* L. to Nitrogen, Phosphorus, and Potassium 1. *Agron. J.* **1977**, *69*, 832–836. [CrossRef]
26. Caplan, D.; Dixon, M.; Zheng, Y. Optimal rate of organic fertilizer during the flowering stage for cannabis grown in two coir-based substrates. *HortScience* **2017**, *52*, 1796–1803. [CrossRef]
27. Cosentino, S.L.; Riggi, E.; Testa, G.; Scordia, D.; Copani, V. Evaluation of European developed fibre hemp genotypes (*Cannabis sativa* L.) in semi-arid Mediterranean environment. *Ind. Crops Prod.* **2013**, *50*, 312–324. [CrossRef]
28. Mediavilla, V.; Meier, C. Factors influencing the yield and the quality of hemp (*Cannabis sativa* L.) essential oil. *J. Int. Hemp. Assoc.* **1998**, *5*, 16–20.
29. Caplan, D.; Dixon, M.; Zheng, Y. Increasing inflorescence dry weight and cannabinoid content in medical cannabis using controlled drought stress. *HortScience* **2019**, *54*, 964–969. [CrossRef]
30. Campbell, B.J.; Berrada, A.F.; Hudalla, C.; Amaducci, S.; McKay, J.K. Genotype × Environment Interactions of Industrial Hemp Cultivars Highlight Diverse Responses to Environmental Factors. *Agrosyst. Geosci. Environ.* **2019**, *2*, 1–11. [CrossRef]
31. Campiglia, E.; Radicetti, E.; Mancinelli, R. Plant density and nitrogen fertilization affect agronomic performance of industrial hemp (*Cannabis sativa* L.) in Mediterranean environment. *Ind. Crops Prod.* **2017**, *100*, 246–254. [CrossRef]
32. Allen, R.G.; Pereira, L.S.; Raes, D.; Smith, M. *Crop evapotranspiration—Guidelines for computing crop water requirements—FAO Irrigation and drainage paper 56*; FAO: Rome, Italy, 1998; Volume 300, p. D05109.
33. Spano, M.; Maccelli, A.; Matteo, G.D.; Ingallina, C.; Biava, M.; Crestoni, M.E.; Bardaud, J.X.; Giusti, A.M.; Mariano, A.; D'abusco, A.S.; et al. Metabolomic profiling of fresh goji (*Lycium barbarum* L.) berries from two cultivars grown in central italy: A multi-methodological approach. *Molecules* **2021**, *26*, 5412. [CrossRef]
34. Gómez, J.; Simirgiotis, M.J.; Manrique, S.; Piñeiro, M.; Lima, B.; Bórquez, J.; Feresin, G.E.; Tapia, A. Uhplc-esi-ot-ms phenolics profiling, free radical scavenging, antibacterial and nematicidal activities of "yellow-brown resins" from *Larrea* spp. *Antioxidants* **2021**, *10*, 185. [CrossRef]
35. Pierre, E.O.; Nicolas, N.; Pierre, F.o.D.; Martine, L.O.; Denis, O.N. Heritability of polyphenols, anthocyanins and antioxidant capacity of Cameroonian cocoa (*Theobroma cacao* L.) beans. *Afr. J. Biotechnol.* **2015**, *14*, 2672–2682. [CrossRef]
36. Smilde, A.K.; Jansen, J.J.; Hoefsloot, H.C.J.; Lamers, R.J.A.N.; van der Greef, J.; Timmerman, M.E. ANOVA-simultaneous component analysis (ASCA): A new tool for analyzing designed metabolomics data. *Bioinformatics* **2005**, *21*, 3043–3048. [CrossRef]
37. Zwanenburg, G.; Hoefsloot, H.C.J.; Westerhuis, J.A.; Jansen, J.J.; Smilde, A.K. ANOVA–principal component analysis and ANOVA–simultaneous component analysis: A comparison. *J. Chemom.* **2011**, *25*, 561–567. [CrossRef]

38. Glivar, T.; Eržen, J.; Kreft, S.; Zagožen, M.; Čerenak, A.; Čeh, B.; Tavčar Benković, E. Cannabinoid content in industrial hemp (*Cannabis sativa* L.) varieties grown in Slovenia. *Ind. Crops Prod.* **2020**, *145*, 112082. [CrossRef]
39. Palmieri, S.; Fanti, F.; Oliva, E.; Viteritti, E.; Sergi, M.; Pepe, A.; Compagnone, D. Chemical characterization and evaluation of antioxidant activity from different cultivars of *Cannabis sativa* L. of Abruzzo's region. *Nat. Prod. Res.* **2022**, *2022*, 1–15. [CrossRef]
40. Anas, M.; Liao, F.; Verma, K.K.; Sarwar, M.A.; Mahmood, A.; Chen, Z.L.; Li, Q.; Zeng, X.P.; Liu, Y.; Li, Y.R. Fate of nitrogen in agriculture and environment: Agronomic, eco-physiological and molecular approaches to improve nitrogen use efficiency. *Biol. Res.* **2020**, *53*, 47. [CrossRef]

7.4. Case study 3: Malted hempseeds characterization through HPLC analysis

In Italy, among the hemp parts, hempseeds are the only one authorized for food applications (Decreto 4 novembre 2019). It can be consumed as such (whole, hulled seed) or dehulled (hempseed kernel), as well as its processing products, including oil, flour, and protein powder. Despite the fact that some studies highlighted high variability in the hempseed composition according to the genotypes and environmental factors it typically contains 25–35% lipids with a unique and perfectly balanced fatty acids composition; 20–25% proteins easy to digest and rich in essential amino acids; 20–30% carbohydrates, a great part of which are constituted in dietary fibre, mainly insoluble; as well as vitamins, and minerals. In addition to its nutritional value, hempseed is also rich in natural antioxidants and other bioactive components such as bioactive peptides, phenolic compounds, tocopherols, carotenoids, and phytosterols, the content of which appears to be mostly a ected by the environmental and agronomic factors and, to a lesser extent, by genetic variability. Moreover, hempseed

contains also some antinutritional compounds that could negatively influence its nutritional value.

For their nutritional and functional properties, hempseed and its derivatives could represent potential ingredients for the development of new functional and/or healthy food, and some biotechnological transformations could be useful to improve their nutritional and functional values. Among these, it is possible to mention the malting process, an ancient biotechnological process traditionally performed on cereal grains, consisting in the following three main steps: (1) steeping to hydrate and reactivate the resting seed's metabolism, (2) germination during which the seed undergoes modifications including the activation of several enzymes involving in catabolic and anabolic reactions needed for the embryo's growth, and (3) kilning to stop metabolic processes and ensure stability and storability of the dried product. Through using malting, drastically changes of the seed's content and physic and biochemical compositions occur, which are often associated with health benefits and can be useful to improve the nutritional and functional quality of malted seeds.

Therefore, in the present paper, two experimental malting procedures were performed on two certified industrial hemp varieties and the effect of malting on the antioxidant features were investigated, also through the HPLC analysis of polyphenol compounds.

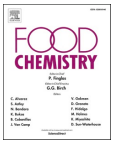
Food Chemistry 370 (2022) 131348



Contents lists available at ScienceDirect

Food Chemistry

journal homepage: www.elsevier.com/locate/foodchem





Effect of malting on nutritional and antioxidant properties of the seeds of two industrial hemp (*Cannabis sativa* L.) *cultivars*

Barbara Farinon [a,*], Lara Costantini [a], Romina Molinari [a], Giacomo Di Matteo [b], Stefania Garzoli [b], Serena Ferri [c], Brunella Ceccantoni [c], Luisa Mannina [b], Nicolò Merendino [a,*]

[a] Department of Ecological and Biological Sciences (DEB), Tuscia University, Largo dell'Università snc, 01100 Viterbo, Italy
[b] Department of Chemistry and Technology of Drugs, Sapienza University of Rome, Piazzale Aldo Moro 5, Rome 00185, Italy
[c] Department for Innovation in Biological, Agro-food and Forest Systems (DIBAF), Tuscia University, Via San Camillo de Lellis Snc, 01100 Viterbo, Italy

ARTICLE INFO

Keywords:
Cannabis sativa L. seeds
Industrial hemp
Malting
Antioxidant capacity
Phenolic compound
Tocopherols

ABSTRACT

The impact of malting on antioxidant, nutritional, and antinutritional features of two industrial hemp *cultivars* was investigated. The seeds were steeped (5 h; RT), germinated (3-days; 24 °C), and kilned at different temperatures (6 h; 50 °C or 70 °C). The following determinations were performed on malted and unmalted samples: total phenolic content, polyphenol profile, total antioxidant capacity, tocopherol composition, proximate analysis, fatty acids profile, trypsin inhibitors and phytate content. The results showed that malting increased the protein content up to 9%, without affecting the fat amount, and the fatty acids profile. Total phenolic content, tocopherol profile and total antioxidant capacity were also improved. 70 °C kilning temperature resulted effective to reduce the trypsin inhibitors (up to −27%), increase the reducing power and the level of *N-trans*-caffeoyltyramine and cannabisin A. Based on this, malting using 3 germination days and 70 °C as kilning temperature could be considered suitable transformation process for improving hempseeds quality.

1. Introduction

Cannabis sativa L., commonly hemp, is an herbaceous, anemophilous plant belonging to the *Cannabaceae* family. It is a multipurpose and low environmental impact crop, traditionally cultivated for fiber production, especially in the Western World. However, the progressive diffusion of synthetic fibers and the use of some narcotic strains to produce intoxicant drugs led to forbid its cultivation. Only since the last two decades, the cultivation of varieties popularly called "industrial hemp", containing a level of Δ9-tetrahydrocannabinol (THC) (*i.e.,* the only one psychoactive compound of the plant) less than 0.2% (Europe) or 0.3% (Canada and USA), has been authorized.

In the last decades, there has been a growing interest in the seeds of this plant, which were once considered a waste product of fiber production, or, at most, used as animal feed. Despite the high variability in hempseed's composition due to the genotypes and environmental factors, hempseed typically contains 25–35% lipids with a unique and perfectly balanced fatty acids (FAs) composition; 20–25% proteins easy to digest and containing all essential amino acids; 20–30% carbohydrates, whose main part is represented by insoluble dietary fiber; as well as vitamins, and minerals. In addition to its nutritional value, hempseed is also rich of natural antioxidants and other bioactive components like bioactive peptides, polyphenols, tocopherols, carotenoids, and phytosterols, but it does not completely lack in some antinutrients that could negatively influence its nutritional value (Farinon, Molinari, Costantini, & Merendino, 2020).

For their nutritional and functional properties, hempseed and its derivatives could represent potential ingredients for the development of new functional and/or healthy food, and some biotechnological transformations could be useful to improve their nutritional and functional values. Among these, it is possible to mention the malting process, an ancient biotechnological process traditionally performed on cereal grains, consisting in the following three main steps: (1) steeping to hydrate and reactivate the resting seed's metabolism, (2) germination during which the seed undergoes modifications including the activation of several enzymes involving in catabolic and anabolic reactions needed

* Corresponding authors.
E-mail addresses: b.farinon@unitus.it (B. Farinon), lara.cost@libero.it (L. Costantini), rominamolinari@libero.it (R. Molinari), giacomo.dimatteo@uniroma1.it (G. Di Matteo), stefania.garzoli@uniromal.it (S. Garzoli), serenaferri@unitus.it (S. Ferri), b.ceccantoni@unitus.it (B. Ceccantoni), luisa.mannina@uniroma1.it (L. Mannina), merendin@unitus.it (N. Merendino).

https://doi.org/10.1016/j.foodchem.2021.131348
Received 23 April 2021; Received in revised form 1 October 2021; Accepted 4 October 2021
Available online 7 October 2021
0308-8146/© 2021 Elsevier Ltd. All rights reserved.

for the embryo's growth, and (3) kilning to stop metabolic processes and ensure stability and storability of the dried product (MacLeod & Evans, 2016). Through using malting, drastically changes of the seed's content and physic and biochemical compositions occur, which are often associated with health benefits and can be useful to improve the nutritional and functional quality of malted seeds. Different studies highlighted the benefits resulting from germination and malting of cereal and pseudocereal grains and oilseeds such as linseed (Aguilar, Miano, Obregón, Soriano-Colchado, & Barraza-Jáuregui, 2019; Carciochi, Dimitrov, & Galván D'Alessandro, 2016; Carvalho, Gonçalves, & Guido, 2016; Lemmens et al., 2018; Li et al., 2019; Obadina et al., 2017; Terpinc, Cigić, Polak, Hribar, & Požrl, 2016; Udeh, Duodu, & Jideani, 2018). Recently, Frassinetti and et al. reported that germination of hempseeds of *Futura 75* (*F75*) *cultivar* increased the total phenolic content (TPC) and the antioxidant capacity of the hemp sprouts compared to the ungerminated seeds (Frassinetti et al., 2018). However, to the best of our knowledge, there is no study investigating the malting process on hempseeds and its effect on hempseeds' nutritional, antinutritional and antioxidant properties. Therefore, in the present paper, two experimental malting procedures differing in the temperature used for the kilning (*i.e.,* 50 °C or 70 °C) were performed on two certified industrial hemp varieties (*i.e.*, varieties registered in the EU plant variety database) and the effect of malting on the antioxidant features (*i.e.*, TPC, polyphenol profile, tocopherol composition, and total antioxidant capacity) were investigated. In addition, whether and how the malting process affects the nutritional (*i.e.*, proximate composition and FAs profile) and antinutritional (*i.e.,* trypsin inhibitors (TIs), and phytate content) properties of hempseeds was also evaluated.

2. Materials and methods

2.1. Plant materials and chemicals

The seeds of two certified industrial hemp *cultivars F75* (French monoecious) and *Secuieni jubileu* (*Sj*) (Romanian monoecious) were used. *F75* seeds were kindly provided by Molino Crisafulli (Caltagirone, CT, Italy); *Sj* seeds were purchased by Agricola Matteucci (Civita Castellana, VT, Italy). *F75* is a *cultivar* already described in the scientific literature, whose seeds are largely used in food preparation, while *Secueini jubileu* is a locally farmed hemp *cultivar* not still described in the literature. For each *cultivar*, seeds with a diameter ≥ 3 mm were selected and stored at −20 °C until the analyses. All chemicals were purchased from Sigma-Aldrich (St. Louis, MO, USA), unless otherwise specified.

2.2. Malting procedure

Selected seeds (100 g) were steeped in deionized sterile water (1:15, *w/v*) at room temperature (RT), in the dark for 5 h on an air-rest period of 5 min every 30 min. After each hour of steeping, an aliquot (3 g) of seeds was collected to assess the steeping behavior of hempseeds by evaluating the moisture content. Remaining seeds were germinated for 3 days in the dark, at 24 °C and 85% relative humidity in an incubator. Briefly, the steeped seeds were placed between two layers of wet filter paper (Whatman No. 1) on perforated germination trays. The seeds were daily moistened with sterile distilled water. Germinated seeds were dried (kilned) in a static oven (TCN 30, ARGO LAB, Modena, Italy) at 50 °C or 70 °C, for 6 h. Kilned seeds were immediately collected and stored at −20 °C.

2.3. Sample preparation

For all experiments, seeds' samples were freeze-dried (FreeZone 2.5, Labconco, Kansas City, MO, USA) and ground by IKA® A11 basic Analytical mill (IKA®-Werke GmbH & CO. KG, Staufen im Breisgau, Deutschland). Ground seeds were immediately used or stored at −80 °C until analyses.

2.4. Extracts' preparation for polyphenol compounds and antioxidant activity determination

For the analyses of the TPC and antioxidant activity, samples were extracted according to Frassinetti et al. (Frassinetti et al., 2018), the detailed description is reported in Supplementary Appendix B.1. For the RP-HPLC analysis of polyphenol profile, samples were extracted according to Siano et al. (Siano et al., 2018) with some modifications, reported in Supplementary Appendix B.2.

2.5. Total phenolic compounds content

The TPC was determined using the Folin–Ciocalteu standard method as modified by Costantini et al. (Costantini et al., 2014) and adapted for 96-wells plates and an automatic reader (Infinite 2000, Tecan, Salzburg, Austria), as described in Supplementary Appendix B.3. A gallic acid standard curve was prepared and the results were expressed as mg of gallic acid equivalents (GAE)/g of dry weight (DW) of the sample.

2.6. Polyphenol profile determination by RP-HPLC analysis

Determination of polyphenol compounds was performed according to Smeriglio et al. (Smeriglio et al., 2016) with some modifications. A Shimadzu Prominence-i LC-2030C 3D (Milan, Italy) system equipped with autosampler, binary pump, column oven and a photodiode array (PDA) (Milan, Italy) detector was used. 10 μL of extracts or external standards were separately injected into a Kinetex Evo C_{18} column (150 × 4.6 mm, 5 μm; Phenomenex, BO, Italy) pre-heated at 30 °C. The separation was performed employing a binary mobile phase consisted of methanol (A) and water/acetic acid (97:3 *v/v*) (B), at 1.2 mL/min, combined in a gradient as follows: 0 min, 90% B; 0–6 min, 90–85% B; 6–10 min, 85% B; 10–12 min, 85–77% B; 12–13 min, 77–67% B; 13–18 min, 67–60% B; 18–45 min, 60–0% B. Separations were monitored at 310 nm (for *N-trans*-caffeoyltyrammine, cannabisin B) and 260 nm (for cannabisin A, *p*-hydroxybenzoic acid), and the peaks were integrated using the LabSolutions software (version 5.71 SP2). *N-trans*-caffeoyltyrammine and *p*-hydroxybenzoic acid were identified comparing their retention times and UV spectrums with the external standards. Quantification was based on external standard method and the results were expressed as μg/g of DW. Cannabisin A (UV λ_{max} in ethanol 257 nm) (Sakakibara, Katsuhara, Ikeya, Hayashi, & Mitsuhashi, 1991) and cannabisin B (UV λ_{max} in methanol 250, 277, 337 nm) (Sakakibara, Ikeya, Hayashi, & Mitsuhashi, 1992) were tentatively identified based on their UV spectrum (Chen et al., 2012; Irakli et al., 2019; Leonard, Zhang, Ying, & Fang, 2021; Nigro et al., 2020; Sakakibara et al., 1991) due to the lack of the corresponding commercial standards and the results were expressed as μg of *trans*-cinnamic acid equivalents (CAE)/g of DW. A detailed description of the identification of cannabisin A and cannabisin B is reported in Supplementary Appendix B.4.

2.7. Tocopherols' composition

Tocopherols' compositions was assessed as described by Urvaka et al. (Urvaka, Mišina, Soliven, & Górnaś, 2019). Briefly, tocopherols were extracted through micro-saponification then, the tocopherol isomers were separated by RP-HPLC analysis performed on a HPLC Dionex Ultimate 3000 (Thermo Fisher Scientific, Waltham, MA, USA) equipped with a PDA detector. 20 μL of the extract were injected into a Dionex Acclaim 120 C_{18} column (150 mm × 4.6 mm, 5 μm; Thermo Fisher Scientific, Waltham, MA, USA) and eluted in isocratic mode with 0.8 mL/min methanol. The run time of each sample was 30 min. Tocopherols were detected at 295 nm. Quantification of individual tocopherols was performed based on gamma-, delta-, and alpha-tocopherol standards calibration curves. Individual tocopherols' concentrations were summed up to obtain the total tocopherol amount.

2.8. Total antioxidant capacity

The total antioxidant capacity was assessed by Cupric Reducing Antioxidant Capacity (CUPRAC) and 2,2′-azino-bis(3-ethylbenzothiazoline-6-sulfonic acid) ($ABTS^{\bullet+}$) radical scavenging activity assays as described in supplementary Appendix B.5. For both assays, a standard curve for Trolox was prepared and the antioxidant capacity was expressed as μmol of Trolox equivalents (TE)/g of DW.

2.9. Proximate composition

Proximate composition of the seeds was determined according to the standard procedures of AOAC International (2006), as described in Supplementary Appendix B.6.

2.10. Fatty acid profile

FAs composition was determined by gas chromatography/mass spectrometry (GC/MS) technique after lipid extraction and FAs methyl esters synthesis performed according to Costantini et al. (Costantini et al., 2014). GC/MS analyses were carried out on a gas chromatograph with a flame ionization detector (FID) directly coupled to a mass spectrometer (MS) Perkin Elmer Clarus 500 model (Waltham, MA, USA). GC was equipped with a 60 m × 0.25 mm, film thickness of 0.5 μm, Restek Stabilwax polar capillary column. Helium was used as the carrier gas at 1.0 mL/min constant flow rate. The injector was set to a 280 °C and the oven temperature was programmed from 170 °C, at rate of 3° C/min to 260 °C for 10 min. 2 μL of each sample were injected into the column in splitless mode; the mass spectra were recorded at 70 eV (EI) and were scanned in the range of 40–500 *m/z*. The ion source and the connection parts temperature were 220 °C. The GC-TIC mass spectra were obtained by the TurboMass data analysis software. Electronic integration measurements of peak areas by the FID detector were used to generate quantitative data of all the compounds without the use of an internal standard or correction factors and expressed in percentages; the identification was performed by matching their mass spectra with those stored in the Wiley and NIST 02 mass spectra libraries database.

2.10.1. Antinutritional compounds analysis

Analyses of antinutritional compounds were performed on the defatted materials, obtained as described in Supplementary Appendix B.7. Results were expressed on defatted materials to make them comparable with other literature data.

2.10.2. Trypsin inhibitors

TIs were extracted overnight from 0.1 g of defatted sample with 25.0 mL 2 mM glycine buffer, pH 11.0, containing 2 mM NaCl, 10 mM urea and 25 mM EDTA. The extract was centrifuged for 15 min at 4 °C and 24,500 × g. TIs activity (TIA) was measured by reading the absorbance at 410 nm with Uvikon spectrophotometer (942, Kontron Instruments, Zurich, Switzerland) as described by Galasso et al. (Galasso et al., 2016). Hempseed TIs content was expressed as unit of TI (TIU)/mg of DW of the defatted material. One TIU was defined as 0.01 decrease in absorbance at 410 nm compared with the control (without inhibitor) under the assay condition.

2.10.3. Phytate

Phytic acid was extracted overnight from the defatted samples with 0.66 M HCl and analyzed with the Phytic acid assay kit (Megazyme®) according to the manufacturer's instructions. Hempseed phytate content was expressed as g/100 g DW of defatted material after recording the absorbance at 655 nm on Uvikon spectrophotometer (942, Kontron Instruments, Zurich, Switzerland).

2.11. Statistical analysis

Malting treatments were repeated three times and each sample was analyzed in triplicate or duplicate. Results are presented as means ± standard deviation. One-way analysis of variance (ANOVA) followed by Tukey's post hoc test was applied using R software (Version 1.0.153). To assess differences between the analyzed varieties and due to the treatment (*i.e.,* malting) within each *cultivar*, a one-way analysis of variance for each variable parameter (*i.e.,* variety or treatment) was performed. Differences were considered significant at the $p \leq 0.05$ level.

3. Results and discussion

3.1. Steeping characteristics of hempseeds

The moisture content of *F75* and *Sj* seeds during the steeping is shown in Fig. 1. Steeping is the first stage of the malting process which aims to achieve a rapid uptake of water and oxygen by the seed, to promote the activation of embryo's enzymes involved in the germination step and needed for the embryo's growth and development (MacLeod & Evans, 2016). For the seeds of both analyzed varieties, the water uptake was very rapid in the first hour of steeping, increasing over than 3-fold compared to raw seeds. This rapid imbibition is related to the low water potential of dry seeds, due to their low moisture content (Weitbrecht, Müller, & Leubner-Metzger, 2011). After 3 h of steeping, the seed's moisture content of both *cultivars* increased significantly, reaching a 4-fold higher value compared to raw seeds. Furthermore, after 3 h of steeping, the moisture reached a plateau (Fig. 1). Interestingly, moisture content of *Sj* seeds increased faster than *F75* seeds. Shaban (Shaban, 2013) reported that seeds have a critical moisture content for germination, specific for each species. Once this critical value is attained in the seed, sufficient water amount is present to start germination, therefore the seed is committed to that event and cannot turn back. In the literature there is no information concerning the critical moisture content for hempseeds, however, we found that after 5 h of steeping some seeds of both *cultivars* were "chitted" showing the testa rupture and radicle protrusion, proving that the germination phase was started. Hence, according to our results, the hempseeds' critical moisture content amounted around 34% and 36%.

3.2. Total phenolic compounds content of raw and malted hempseeds

Several studies performed on different plant species, highlighted that processes like germination and malting have a positive impact on the antioxidant value of a seed, as a consequence to the rise in the content of antioxidant compounds such as polyphenols and tocopherols (Dabina-Bicka, Karklina, & Kruma, 2011; Li et al., 2019; Pająk, Socha, Broniek, Królikowska, & Fortuna, 2019; Terpinc et al., 2016). Therefore, we evaluated the effects of each step of the malting process on the TPC, polyphenols' and tocopherol's profile and antioxidant capacity of the analyzed seeds. Results concerning the TPC are reported in Fig. 2A. Statistically, there were no significant differences for the TPC values of the raw seeds of both analyzed *cultivars* (3.76 ± 0.55 and 3.56 ± 0.76 mg GAE/g DW for *F75* and *Sj*, respectively). The obtained values were similar to those found by Frassinetti et al. (Frassinetti et al., 2018) for the *F75* seeds, whilst Irakli et al. (2019) reported an almost 2-fold higher value for the same *cultivar*. However, in this latter paper, the analysis was performed on defatted seeds instead of whole seeds. This may result in higher concentration of phenolics in the defatted matter explaining the higher TPC value obtained compared to our results. When compared to other oilseeds such as flaxseed and chia seed, the TPC value we found for both *cultivars* resulted to be over 3-fold higher (Pająk et al., 2019).

5 h of steeping did not affect the TPC level of the seeds of both *cultivars*. Khandelwal et al. (Khandelwal, Udipi, & Ghugre, 2010) reported a negative impact of steeping on the TPC of some pulses as a consequence of their leaching into the soaking water and/or the formation of

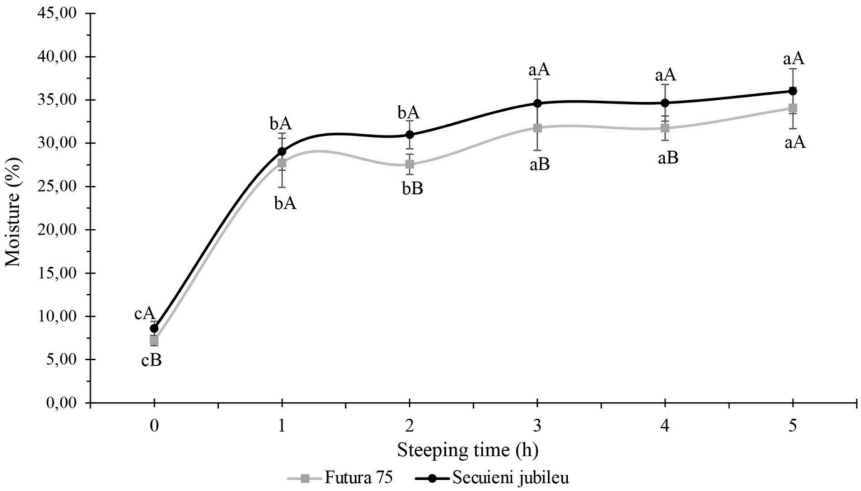


Fig. 1. Steeping characteristics of *Futura 75* and *Secuieni jubileu* seeds. Data are means ± standard deviation of at least three replicates (n = 3). Different letters indicate significant differences ($p \leq 0.05$) according to one-way analysis of variance. Lowercase letters represent Tukey's test comparison among different steeping time and uppercase letters represent comparison between *cultivars* at the same steeping time.

insoluble complexes with proteins or polymerization of lower molecular weight polyphenols. By contrast, Cevallos-Casals et al. (Cevallos-Casals & Cisneros-Zevallos, 2010) showed that for some edible seeds the imbibition represents an active period of phenolic synthesis. Similarly to our results, 8 h of steeping of the two buckwheat varieties' seeds did not significantly influence the TPC level (Terpinc et al., 2016).

After 3-days of germination, the TPC value increased 2-fold (+121%) in *F75* seeds and 3-fold (+188%) in *Sj* seeds in comparison to untreated seeds, and it was not significantly affected by the heat treatment at 50 °C or 70 °C (Fig. 2A). Frassinetti et al. (Frassinetti et al., 2018) demonstrated that 3-days of germination at 24 °C led to an increase of 116% in the TPC of *F75* seeds, similarly to our results. It was suggested that the increase in phenolic compounds during malting could be attributed both to the *de novo* synthesis of polyphenols during germination induced by enzymatic system activation (*e.g.,* enzymes involved in the phenylpropanoids pathway), and to structural changes in plant cell-wall caused by heat treatment, able to improve the release of glycosylated/esterified polyphenols (Aguilar et al., 2019; Carciochi et al., 2016). Indeed, some investigations reported that the heat treatment of germinated seeds can further increase the TPC values in the final malt, but the processing temperature is an important factor to take into account, since high temperatures can negatively affect the TPC value (Carciochi et al., 2016; Terpinc et al., 2016). Based on our results, the two adopted kilning temperatures did not have negative impact on the TPC value of germinated seeds.

3.3. RP-HPLC analysis of polyphenol compounds of raw and malted hempseeds

Ethanol extracts of unmalted and malted seeds were subjected to RP-HPLC analysis and the content of 4 main phenolic compounds detected by chromatographic separation and successfully identified and quantified are presented in Table 1. Major polyphenols found in hempseeds are lignans belonging to the two groups of phenolic amides and lignanamides (Farinon et al., 2020). Accordingly with other literatures data (Alasalvar, Chang, Bolling, Oh, & Shahidi, 2021), we found that the most abundant phenolic amide in both *F75* and *Sj* raw seeds was *N-trans*-caffeoyltyramine. Whereas the most abundant lignanamide in both varieties was the cannabisin A, followed by cannabisin B. We also detected the phenolic acid *p*-hydroxybenzoic acid. Although this profile was qualitatively comparable to that obtained in other studies (Alasalvar et al., 2021), we found value quantitatively slightly lower. Differences could be explained by different varieties and quantification methods, as well as the environment that represent an important factor which largely influences the plants' polyphenols profile (Irakli et al., 2019).

Malting significantly rose the content of *N-trans*-caffeoyltyramine and cannabisin A in both *cultivars*, especially the *F75* one, and particularly, when the kilning temperature was 70 °C. These polyphenols were defined as the major contributors to the antioxidant activity in hempseeds (Irakli et al., 2019), hence, their increase may play an important role in the total antioxidant activity of malted seeds. As said, in cereals, changes in the polyphenols profile after malting were attributed both to polyphenols' *de novo* biosynthesis and release of bound polyphenols, resulting in the increase in polyphenols' extractability and bioavailability (Carvalho et al., 2016; Lemmens et al., 2018). Actually, *N-trans*-caffeoyltyramine is found to be mainly located in the hempseeds hull, so their increase after malting at the higher kilning temperature (*i.e.*, 70 °C) may be effectively related to thermal-induced changes in the structure of the molecules connected to bound phenolics and consequently increase in their release. Interestingly, in both *cultivars* the amount of *p*-hydroxybenzoic acid significantly ($p \leq 0.05$) decreased after malting. It is a phenolic acid and considering that phenolic acids are constituents of lignanammides (Leonard, Zhang, Ying, Xiong, & Fang, 2021), it could be speculated that *p*-hydroxybenzoic acid may be addressed and used in the lignanammide's biosynthesis pathway. Chromatograms of the unmalted and malted samples (Supplementary Appendix A, Figure A.1) show the presence of additional peaks that it was not possible to identify and that overall, probably contributing to the TPC and antioxidant activity values. Hence, further and more resolutive analysis could be appropriated.

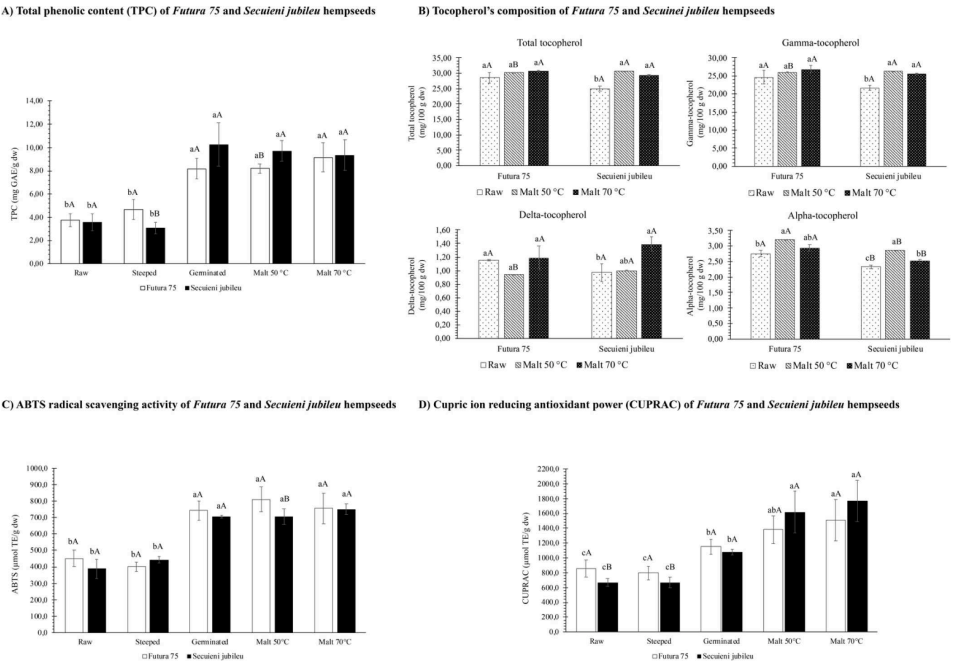


Fig. 2. Antioxidant profile of *Futura 75* and *Secuieni jubileu* hempseeds. A) Total phenolic content (TPC) (mg GAE/g DW) of untreated (Raw), Steeped, Germinated, and malted at 50 °C (Malt 50 °C) and 70 °C (Malt 70 °C) samples. Data are means ± standard deviation of three replicates (n = 3); B) Total tocopherol, gamma-tocopherol, delta-tocopherol and alpha-tocopherol amount (mg/100 g DW) of untreated (Raw) and malted at 50 °C (Malt 50 °C) and 70 °C (Malt 70 °C) samples. Data are mean ± standard deviation of two replicates (n = 2); C) ABTS$^{\bullet+}$ radical scavenging activity (μM TE/g DW) of untreated (Raw), Steeped, Germinated, and malted at 50 °C (Malt 50 °C) and 70 °C (Malt 70 °C) samples. Data are means ± standard deviation of three replicates (n = 3); D) Cupric ion reducing antioxidant power (CUPRAC) (μM TE/g DW) of untreated (Raw), Steeped, Germinated, and malted at 50 °C (Malt 50 °C) and 70 °C (Malt 70 °C) samples. Data are means ± standard deviation of three replicates (n = 3). Different letters within the same *cultivar* indicate significant differences (p less than 0.05), according to one-way analysis of variance. Lowercase letters represent Tukey's test comparison among malted and raw seeds. Uppercase letters represent comparison between *cultivars*. GAE: Gallic Acid Equivalent; TE: Trolox Equivalent; DW: dry weight.

3.4. Tocopherol profile of raw and malted hempseeds

Together with polyphenols, tocopherols represent another class of important antioxidants. Since they are thermolabile compounds, we focused on analyzing the effect of the two different kilning temperatures on the tocopherols profile of the analyzed seeds, to investigate any possible negative impact of the heat treatment. The obtained results are depicted in Fig. 2B. The total tocopherol amount was 28.57 ± 1.76 and 25.00 ± 0.82 mg/100 g DW for *F75* and *Sj* raw seeds, respectively, and there were no significant differences between the *cultivars*. According to previous studies, among the tocopherol isoforms, hempseed includes the alpha-, delta-, and gamma-tocopherols, the latter of which is the most abundant, representing almost 90% of the total tocopherol, followed by alpha- and delta-isoforms, present in lower concentration (Galasso et al., 2016). We found slight but significant differences only for the alpha-tocopherol which resulted higher in the *F75* than *Sj* raw seeds (2.76 ± 0.10 *vs.* 2.33 ± 0.06 mg/100 g DW, respectively). The found values were comparable to that reported for the hempseeds oil fraction (Farinon et al., 2020), and it pointed out that hempseeds of both analyzed varieties are a source of tocopherol as good as other edible seeds such as flaxseed, traditionally considered an excellent source of these compounds. According to the contribution of each isomer to the vitamin E biological activity as defined by the European Food Safety Authority (alpha-tocopherol, 1.0 mg; beta-tocopherol, 0.5 mg; gamma-tocopherol, 0.1 mg; delta-tocopherol, 0.03 mg) (EFSA Nda Panel, 2015), the medium vitamin E content in *F75* and *Sj* raw seeds was 4.88 and 4.13 mg/100 g of fresh weight (FW), respectively. Hence, a serving portion (*i.e.,* 30 g) of hempseeds would contribute to satisfying the vitamin E average intake (AI) up to 11.3% for males and 13.3% for females, in the case of *F75 cultivar* and up to 9.5% for males and 11.3% for females, in the case of *Sj* variety.

Malting at 50 °C and 70 °C did not significantly affect the total tocopherol content of the *F75* seeds; conversely, a significant increase in the *Sj* seeds' total tocopherol was observed after malting (+22% at 50 °C and + 18% at 70 °C). Similar results were found for the gamma-tocopherols amount. Delta-tocopherol was found unchanged in the *F75* malted seeds, instead a growing, but not significant trend was obtained for *Sj* seeds malted at 50 °C. The delta-tocopherol amount was found to be significantly higher (+43%) in the *Sj* seeds malted at 70 °C in comparison to raw seeds. Alpha-tocopherol significantly increased after malting at 50 °C and 70 °C compared to unmalted seeds for both *cultivars*, and the increase was more remarkable for *Sj* variety than *F75*. However, for both *cultivars*, the value for sample "Malt 70 °C" was lower than those for "Malt 50 °C", indicating that alpha-tocopherol is probably

Table 1
Phenolic compounds (μg/g DW) identified in ethanol extract of *Futura 75* and *Secuieni jubileu* hempseeds *cultivars*, untreated (Raw seed) and malted at either 50 °C (Malt 50 °C) or 70 °C (Malt 70 °C), by RP-HPLC analysis. Data are means ± standard deviation of two (n = 2) replicates. Different letters indicate significant differences ($p \leq 0.05$), according to one-way analysis of variance. Lowercase letters represent Tukey's test comparison among treatments and uppercase letters represent comparison between cultivars. DW: dry weight.

Hempseed *cultivar*	*N-trans*-caffeoyltyramine	Cannabisin A*	Cannabisin B*	*p*-hydroxybenzoic acid
Futura 75				
Raw Seed	69.28 ± 0.60^{bA}	88.34 ± 0.43^{bA}	18.95 ± 1.79^{bA}	7.46 ± 0.17^{aA}
Malt 50 °C	60.04 ± 2.44^{cA}	121.14 ± 9.91^{abA}	16.00 ± 0.64^{abA}	6.14 ± 0.20^{bA}
Malt 70 °C	91.13 ± 1.22^{aA}	140.93 ± 15.98^{aA}	25.24 ± 1.96^{aA}	5.50 ± 0.15^{bA}
Secuieni jubileu				
Raw Seed	32.45 ± 2.42^{bB}	57.58 ± 3.70^{bB}	9.64 ± 2.17^{aB}	6.81 ± 0.86^{aA}
Malt 50 °C	31.06 ± 0.67^{bB}	68.66 ± 0.43^{bB}	7.42 ± 0.06^{aB}	3.27 ± 0.01^{bB}
Malt 70 °C	42.47 ± 2.59^{aB}	90.59 ± 5.55^{aA}	11.17 ± 0.50^{aB}	2.95 ± 0.12^{bB}

*Expressed as μg *trans*-cinnamic acid equivalents (CAE)/g of dry weight (DW).

more susceptible to heating. The significant increase of the alpha-tocopherol amount in the malted samples is accompanied with an increment of the vitamin E biological activity, which ranged from 5.26 to 5.82 and 5.63 mg/100 g DW in *F75* "Malt 50 °C" and "Malt 70 °C", respectively and from 4.52 to 5.57 and 5.11 mg/100 g DW in *Sj* "Malt 50 °C" and "Malt 70 °C", respectively. This indicated that malting of hempseed using 50 °C as the kilning temperature could help to improve the vitamin E bioactivity in hempseed, especially for *Sj cultivar*. To the best of our knowledge, this is the first study exploring the changes in tocopherols' profile of hempseeds after malting, therefore, comparison with other literature data is rather difficult. Moreover, limited investigation and conflicting results about this topic are present also regarding other seeds commonly malted, such as barley. For example, Dabina-Bicka et al. (Dabina-Bicka et al., 2011) reported a 38% increase in the vitamin E content during malting of barley, attributed to the beginning of biochemical reactions in the grains during the germination stage. By contrast, Do et al. (Do, Cozzolino, Muhlhausler, Box, & Able, 2015) reported that the vitamin E content of most barley genotypes was reduced after malting due to the leaching of tocopherols by steeping. Studies on lupin and flaxseed, highlighted that germination induced an increase in the total tocopherol and alpha-tocopherol contents attributed to the synthesis of tocopherol as a material needed for young plants' growth (Frias, Miranda, Doblado, & Vidalvalverde, 2005; Li et al., 2019). Overall, malting conditions, genotype, and species probably have an important role in affecting the total tocopherol content and tocopherols profile of a seed and further investigations concerning the changes in the tocopherol isomers and total tocopherol content across each malting step would be interesting to explore in future studies.

3.5. Antioxidant activity of raw and malted hempseeds

We evaluated the antioxidant capacity of ethanolic extracts through two assays commonly used for food matrix: the TEAC and the CUPRAC assays, able to determine both lipophilic and hydrophilic antioxidants simultaneously (Rafi et al., 2018), and therefore, seem to be methods particularly suitable for samples containing both lipophilic and hydrophilic antioxidants, including tocopherols and phenolic compounds, such as hempseeds.

Results of TEAC and CUPRAC assays of raw, steeped, 3-days germinated, and malted seeds of *F75* and *Sj cultivars* are presented in Fig. 2C and 2D, respectively. Differences in the extraction methods and in the analytical procedure used for the analysis, as well as the scarcity of investigation concerning the antioxidant capacity of whole hempseeds, make the comparison with the literature rather difficult. Irakli et al. (Irakli et al., 2019) reported a mean value of 29.33 μmol TE/g in defatted flour of *F75* seeds, measured by $ABTS^{\bullet+}$ assay, whereas Galasso et al. (Galasso et al., 2016) obtained a value of 168 μmol TE/g in defatted flour of *F75* seeds, using a different analytical method. Compared to these results, we found higher values for both *F75* and *Sj* raw seeds. This could be related to the fact that we analyzed whole rather than defatted seeds, thus avoiding removing all or a large amount, of lipophilic antioxidants potentially present in hempseeds, including tocopherols. Frassinetti et al. (Frassinetti et al., 2018) assessed the antioxidant power of *F75* whole seeds' ethanolic extract (without defatting) obtaining a value lower than ours. The difference could be due to the use of different techniques for evaluating the antioxidant capacity. Overall, our results showed that the $ABTS^{\bullet+}$ scavenging activities of the raw seeds of both analyzed *cultivars* were similar (Fig. 2C), whereas a slight but significant difference ($p \leq 0.05$) was found for the reducing power measured by CUPRAC assay, which resulted higher in *F75* than *Sj* raw seeds (Fig. 2D).

Since polyphenols and tocopherols are the two major classes of antioxidants in hempseeds, it is reasonable to hypothesize that an increase in their amount during malting may be related to a concomitant increase in the total antioxidant activity. Results obtained by the TEAC assay (Fig. 2C) revealed that the $ABTS^{\bullet+}$ scavenging ability of the analyzed samples had a trend similar to that found for TPC (Fig. 2A): it was not affected by 5 h of steeping, and after germination it significantly increased by 64% and 82% in *F75* and *Sj cultivars*, respectively. Kilning at 50 °C or 70 °C did not negatively affect the antioxidant scavenging activity of germinated seeds for both *cultivars*. Similarly, the reducing power did not significantly change in both varieties after steeping, but it increased by 44% and 56% after germination of *F75* and *Sj* seeds, respectively (Fig. 2D). Interestingly, the heat treatment at 50 °C and especially at 70 °C led to a further increase in the CUPRAC value of both *cultivars*, resulting 2-folds for *F75*, and 2.5-folds for *Sj*, higher than the untreated seeds after malting at 70 °C. In general, an increase in the antioxidant activity of seeds was reported as a consequence of the metabolic changing occurring during germination (Lemmens et al., 2018). Frassinetti et al. (Frassinetti et al., 2018) reported an increase of the ORAC assay value by 78% in the seeds of *F75* after 3-days of germination, and this result was in good agreement with our findings. Some studies reported that according to the temperature, thermal treatment could negatively affect the antioxidant activity of seeds (Carciochi et al., 2016; Terpinc et al., 2016), but neither 50 °C nor 70 °C showed to be deleterious for the antioxidant activity of *F75* and *Sj* seeds. Contrarily, an increased reducing power after kilning was revealed by CUPRAC assay, and it could reflect a higher presence of donor electron compounds in the malted hempseeds, generated following the heat treatment. *N-trans*-caffeoyltyramine was shown to possess high reducing power (Trabelsi et al., 2014) and its higher amount found in the "Malt 70 °C" samples can explain at least in part, the increased CUPRAC value observed for these samples. In addition, in cereals, thermal treatment performed on germinated grains led to the production of Maillard reaction products (MRPs), resulting from complex reactions between reducing sugars and amino acids or peptides generated by the hydrolysis of reserve substances like starch and proteins occurring during germination. MRPs have shown to possess antioxidant activity, acting as reducing compounds (Carciochi et al., 2016). Temperature and time represent important factors to regulate the rate of Maillard reaction and the MRPs properties. Higher temperatures lead to an increase in the Maillard reaction's rate and hence, in the amount of MRPs with a concomitant raise in the reducing power of the sample (Carciochi et al., 2016). This evidence is in accordance with the increase in the reducing power found in hempseeds after the thermal treatment, however the kilning temperature used in this study was lower than 100 °C and to date, there is no evidence about the production of MRPs in hempseeds.

Therefore, further investigation about the metabolomic profile's changing induced by malting could be appropriate to better understand these results.

3.6. Proximate composition of raw and malted hempseeds

To evaluate whether malting may affect the nutritional properties of hempseeds, the proximate composition of raw and malted seeds of the two analyzed varieties were assessed and the obtained results are presented in Table 2. The moisture content of the raw seeds of both *cultivars* significantly ($p \leq 0.05$) decreased after malting because of the kilning. In malting, the kilning step aims to remove water to inactivate the enzymes and stop the germination, thus preventing further growth of the embryo and modification of the seeds' content. Moreover, it reduces the moisture content of the germinated seeds until 5% or below, a condition important to ensure stability during storage (Carvalho et al., 2016).

Fat is the most representative nutritional component of the *C. sativa* L. seed as it is an oilseed. In this study, the crude fat of *F75* and *Sj* seeds accounted for over 30% of the dry matter, without differences between the two varieties. The obtained values are in good agreement with previously published data (Farinon et al., 2020) and highlight that both varieties can be considered an excellent source of oil. Several papers reported a decrease in the fat amount after germination or malting of different types of seeds (Aguilar et al., 2019; Chaturvedi, 2015; Li et al., 2019; Obadina et al., 2017), as a consequence of the increased lipolytic activities and the utilization of fat to obtain the energy required for the biochemical and physiological modifications occurring during germination. However, we obtained a slight, but not significant, increase in the fat amount for both *cultivars* after malting. Similar result was reported for oat and barley after germination (Khang, Vasiljevic, & Xuan, 2016; Özcan, Aljuhaimi, & Uslu, 2018). These differences could be due to the malting condition which may differently influence the level of lipid degradation.

Concerning the protein content, a slight but significant difference between the two varieties was found, being the seeds of *F75 cultivar* those with the highest amount. Nevertheless, the values obtained for both *cultivars* ranged between 20 and 25% DW according to other literature data (Farinon et al., 2020). Differences in the hempseed protein content can be related to genetic and environmental factors (Irakli et al., 2019). When compared to the unmalted seeds, the protein content significantly ($p \leq 0.05$) increased by 7.5% and 9.2% for *F75* seeds and by 5.2% and 5.3% for *Sj* seeds after malting at 50 °C and 70 °C, respectively. Works concerning the protein content of seeds after malting are conflicting. Some studies reported a significant decreased in the protein amount of malted seeds compared to unmalted ones, due to the fact that during germination, proteins are catabolized into soluble amino acids which can be lost by lixiviation (Aguilar et al., 2019). Other studies showed an increase in the crude protein content of malted seeds (Chaturvedi, 2015; Obadina et al., 2017) attributed to the synthesis of enzymes and proteins needed for embryo growth, or by loss of carbohydrates through respiration (Aguilar et al., 2019; Lemmens et al., 2018). Interestingly, Mäkinen and Arendt (2015) reported that during germination of cereals, pseudocereals, and legumes an increase in albumins content occurred as a consequence of *de novo* synthesis. Considering that albumin is one of the most abundant proteins in hempseed (Farinon et al., 2020), it could be speculated that the increase in the protein content after malting may be due at least in part, to albumin synthesis during the germination step (Table 2).

Analogously to proteins, the energy value of malted seeds showed little but significant increased for both *cultivars*, which could be actually related to the enrichment in the protein content after malting. Nevertheless, no differences in energy values between the *cultivars* neither in the kilning temperature used for malting were observed. Similar result was obtained by Adebiyi et al. (Adebiyi, Obadina, Adebo, & Kayitesi, 2017) after malting pearl millet grains.

The carbohydrate content was similar in the raw seeds of *F75* and *Sj cultivars* and it represented up to 39% DW (Table 2). This result is consistent with other literature data which demonstrated that a great part of carbohydrates was constituted by dietary fiber, mostly the insoluble fraction (Farinon et al., 2020). After malting, the carbohydrates showed a decreasing trend, but the change was significant only for the *Sj* seeds malted at 70 °C. Similarly, Obadina et al. (Obadina et al., 2017) found a decreasing trend in the carbohydrates content of the malted pearl millet, which was attributed to the enzymatic hydrolysis of starch granules into free simple sugars used as an energy source for the growing embryo. Nevertheless, since the great part of total carbohydrates in hempseed is constituted by dietary fiber instead of starch, the decrease in the carbohydrates amount of *Sj* seeds malted at 70 °C is unlikely due to starch hydrolysis. By contrast, other studies reported an increase in the carbohydrates content of different seeds' types after malting, explained by the increase in the crude fiber for building dry matter during the growth and development of the new plant (Adebiyi et al., 2017; Chaturvedi, 2015). Interestingly, Koehler et al. (Koehler, Hartmann, Wieser, & Rychlik, 2007) observed that the total dietary fiber of wheat grains increased after 7 days of germination, but after 2 days of germination the values were trending downwards. During the germination step, the activation of wall-cell degrading enzymes occurs and leads to the breakdown of the cell walls and to the degradation of cell wall polysaccharides including cellulose, hemicellulose, and lignin (Lemmens et al., 2018) which are constituents of dietary fiber. Hence, it is possible to speculate that early germination tends to induce a decrease in the total fiber content as a result of the hydrolytic enzymes activity on the seed's wall-cell; when germination is further prolonged, the catabolic to anabolic shift occurs to promote the growth of the new seedling.

Regarding the ash amount, Table 2 shows a significant ($p \leq 0.05$) difference between *Sj* and *F75* seeds and *Sj* was the *cultivar* with the highest content. Ash can widely vary based on environmental conditions, mineral soil composition, the use or not of fertilizers, the type of fertilizer if used, as well as the hemp variety (Farinon et al., 2020). Literature data reported a decrease in the ash content after malting due

Table 2
Proximate composition (g/100 g DW) and energy value (Kcal/100 g FW), of *Futura 75* and *Secuieni jubileu* hempseeds *cultivars*, untreated (Raw seed) and malted at either 50 °C (Malt 50 °C) or 70 °C (Malt 70 °C). Data are means ± standard deviation of two (n = 2) replicates. Different letters indicate significant differences ($p \leq 0.05$), according to one-way analysis of variance. Lowercase letters represent Tukey's test comparison among treatments and uppercase letters represent comparison between cultivars. DW: dry weight. FW: fresh weight.

Hempseed *cultivar*	Moisture	Protein[1]	Fat	Carbohydrate[2]	Ash	Energy value
Futura 75						
Raw Seed	7.20 ± 0.58^{aB}	23.88 ± 0.05^{bA}	32.73 ± 1.27^{aA}	39.02 ± 1.29^{aA}	4.38 ± 0.04^{aB}	506.50 ± 5.49^{bA}
Malt 50 °C	3.15 ± 0.07^{bA}	25.65 ± 0.72^{abA}	35.34 ± 1.16^{aA}	34.87 ± 1.85^{aA}	4.15 ± 0.04^{bB}	542.57 ± 6.02^{aA}
Malt 70 °C	1.15 ± 0.09^{cA}	26.06 ± 0.50^{aA}	34.75 ± 0.06^{aA}	34.92 ± 0.60^{aA}	4.29 ± 0.04^{abB}	550.11 ± 0.66^{aA}
Secuieni jubileu						
Raw Seed	8.61 ± 0.81^{aA}	21.50 ± 0.32^{bB}	33.20 ± 1.17^{aA}	39.20 ± 0.83^{aA}	6.11 ± 0.02^{aA}	490.47 ± 3.32^{bA}
Malt 50 °C	2.85 ± 0.47^{bA}	22.62 ± 0.13^{aB}	34.44 ± 0.45^{aA}	36.91 ± 0.28^{abA}	6.04 ± 0.03^{aA}	530.60 ± 0.15^{aA}
Malt 70 °C	1.24 ± 0.11^{cA}	22.64 ± 0.04^{aB}	35.24 ± 0.88^{aA}	35.75 ± 1.07^{bA}	6.38 ± 0.15^{aA}	544.28 ± 5.96^{aA}

[1] Conversion factor: 6.25. [2]As difference (*i.e.,* 100 – (g [protein + fat + ash] in 100 g of DW sample)).

to lixiviation during steeping and/or germination (Aguilar et al., 2019), assimilation of available minerals into cell constituents, or their utilization as coenzymes during germination (Obadina et al., 2017). Nevertheless, the malting condition applied in this study did not induce significant changes in the ash content of *Sj* malted seeds. By contrast, we obtained a significant decrease for *F75* seeds after malting.

3.7. FAs composition of raw and malted hempseeds

FAs composition and the percentages of saturated FAs (SFAs), monounsaturated FAs (MUFAs), and polyunsaturated FAs (PUFAs) of *F75* and *Sj* raw and malted at 50 °C or 70 °C are given in Table 3. For both analyzed *cultivars*, the oil fraction was characterized by high unsaturated FAs content, with the PUFAs fraction amounting to 70.5% and 74.8% of total FAs, and MUFAs content represented 17.9% and 14.6% of the total FAs found in *F75* and *Sj* raw seed's oil, respectively. SFAs was found to be the lowest FAs of the oil of raw hempseeds for both *cultivars*. The principal SFA found in the raw seeds of both varieties was palmitic acid (PA; 16:0), followed by stearic acid (SA; 18:0), while the major MUFA was oleic acid (OA; 18:1, n-9). Regarding the essential FAs, the raw seeds of *F75* and *Sj cultivars* contained on average 57.92% and 61.15% of linoleic acid (LA; 18:2, n-6), and 11.38% and 12.40% of alpha-linolenic acid (ALA, 18:3, n-3), respectively. Among the minor unsaturated FAs, gamma-linolenic acid (GLA; 18:3, n-6) was found in the raw seeds in an average percentage of 1.23% and 1.28% of *F75* and *Sj* total FAs, respectively. These results agree with previous reports (Irakli et al., 2019; Galasso et al., 2016) and demonstrated that the oil fraction of the analyzed hempseed's *cultivars*, including the underexplored *Sj* variety, has good nutritional value, related to the high content of PUFAs, the presence of anti-inflammatory GLA, and low amount of SFAs, resulting in relatively high PUFAs/SFAs ratio. Additionally, the n-6/n-3 ratio was found to be equal to 5:1 for the raw seeds of both varieties. This is in accordance with what was reported by Irakli et al. (Irakli et al., 2015) and confers to both *F75* and *Sj* raw seeds a good, nutritionally balanced, and healthy amounts of n-6 and n-3 PUFAs. Interestingly, we found that the SA and OA amounts were significantly lower, while the LA content was significantly higher in *Sj* raw seeds than *F75* ones. It was reported that the FAs composition of hempseeds was highly affected by genotype (Galasso et al., 2016; Irakli et al., 2019), and between the two most abundant FAs in hempseeds, ALA was found to be more affected by genotype than LA (Irakli et al., 2019). Contrarily, for the raw seeds, we obtained that LA, but not ALA, was significantly different between the two *cultivars*.

Table 3
Fatty acid composition (% of oil) of *Futura 75* and *Secuieni jubileu*, untreated (Raw seed) and malted at either 50 °C (Malt 50 °C) or 70 °C (Malt 70 °C). Data are means ± standard deviation of two (n = 2) replicates. Different letters indicate significant differences ($p \leq 0.05$), according to one-way analysis of variance. Lowercase letters represent Tukey's test comparison among treatments and uppercase letters represent comparison between *cultivars*.

	Futura 75			*Secuieni jubileu*		
	Raw Seed	Malt 50 °C	Malt 70 °C	Raw Seed	Malt 50 °C	Malt 70 °C
PA (16:0)	8.33 ± 0.16^{aA}	7.91 ± 0.08^{bB}	8.55 ± 0.01^{aA}	8.08 ± 0.06^{bA}	8.51 ± 0.00^{aA}	8.10 ± 0.01^{bB}
PAL (16:1, n-7)	0.13 ± 0.04^{bA}	0.11 ± 0.01^{bB}	0.23 ± 0.01^{aA}	0.22 ± 0.04^{aA}	0.33 ± 0.01^{aA}	0.27 ± 0.01^{aA}
SA (18:0)	2.86 ± 0.05^{aA}	2.76 ± 0.08^{aA}	2.84 ± 0.02^{aA}	2.19 ± 0.08^{aB}	2.28 ± 0.00^{aB}	2.14 ± 0.01^{aB}
OA (18:1, n-9)	17.72 ± 0.04^{aA}	15.28 ± 0.04^{bA}	14.76 ± 0.05^{cB}	14.33 ± 0.04^{cB}	15.00 ± 0.08^{bA}	15.25 ± 0.01^{aA}
LA (18:2, n-6)	57.92 ± 0.24^{bB}	61.41 ± 0.12^{bA}	61.17 ± 0.02^{aA}	61.15 ± 0.81^{aA}	60.62 ± 0.02^{aA}	61.06 ± 0.01^{aA}
GLA (18:3, n-6)	1.23 ± 0.01^{aA}	1.04 ± 0.02^{bA}	1.12 ± 0.03^{bA}	1.28 ± 0.38^{aA}	1.03 ± 0.01^{aA}	1.03 ± 0.01^{aA}
ALA (18:3, n-3)	11.38 ± 0.04^{aA}	11.11 ± 0.03^{bB}	11.10 ± 0.01^{bB}	12.40 ± 0.37^{aA}	11.82 ± 0.04^{aA}	11.76 ± 0.01^{aA}
ARA (20:0)	0.44 ± 0.00^{bA}	0.52 ± 0.01^{aA}	0.25 ± 0.01^{cB}	0.37 ± 0.04^{aA}	0.42 ± 0.01^{aB}	0.41 ± 0.02^{aA}
∑ SFAs	11.6	11.2	11.6	10.6	11.2	10.6
∑ MUFAs	17.9	15.4	15.0	14.6	15.3	15.5
∑ PUFAs	70.5	73.6	73.4	74.8	73.5	73.9
PUFAs/ SFAs	6.1	6.6	6.3	7.0	6.6	6.9
n-6/n-3	5.2	5.6	5.6	5.0	5.2	5.3

PA: Palmitic Acid; PAL: Palmitoleic Acid; SA: Stearic Acid; OA: Oleic Acid; LA: Linoleic Acid; GLA: gamma-Linolenic Acid; ALA: alpha-Linolenic Acid; ARA: Arachidic Acid; SFAs: Saturated Fatty Acids; MUFAs: Monounsaturated Fatty Acids; PUFAs: Polyunsaturated Fatty Acids.

FAs profile of hempseed represents one of the most important nutritional features of this oilseed. Therefore, although the total fat content of both *F75* and *Sj* hempseed was not significantly affected by malting, we assessed the FAs composition of the seeds of both *cultivars*. after malting, to evaluate whether and if any, how malting could potentially affect it. No remarkable changes were observed for both *cultivars*. Specifically, some slight, but significant ($p \leq 0.05$) differences were noticed in the *F75* seeds, where a decreased in OA, GLA, and ALA content was observed after malting, independently from the kilning temperature, while a slight increase was found for ALA, but only with a kilning temperature of 70 °C. Whereas, in *Sj* seeds, the most relevant modification was shown for OA, which slightly increased after malting, differently to *F75* seeds. Variation in the FAs changes after malting among different varieties was reported in barley too and it was attributed to different biosynthesis of lipids during the germination step (Bravi, Marconi, Perretti, & Fantozzi, 2012).

3.8. Antinutritional compounds of raw and malted hempseeds

We assessed the content of the antinutrients TIs and phytate in the raw seeds of *Sj* and *F75 cultivars* and evaluated the effect of the malting process on these parameters. The obtained results are graphically reported in Fig. 3. The TIs amount was almost the same for the raw seeds of both *cultivars* and amounted to 29.42 ± 0.51 and 27.38 ± 1.72 TIU/mg DW of the defatted sample, respectively (Fig. 3A). These results are in good agreement with those obtained for *F75* seeds by Galasso et al. (Galasso et al., 2016), and placed hempseeds in the group including edible seeds with medium content of TIs (Farinon et al., 2020). Methods as thermal treatment, soaking, and germination have shown to be efficient to inactivate the TIs in soybean (Vagadia, Vanga, & Raghavan, 2017). Therefore, we evaluated the TIs activity in hempseeds before and after malting. As depicted in Fig. 3A, malting induced significant ($p \leq 0.05$) decrease in the TIs content for both varieties. Particularly, 70 °C of kilning appeared to be more efficient than 50 °C in the reduction of TIs, especially for *F75* seeds, leading a decrease by 25.0% and 26.7% for *F75* and *Sj cultivars*, respectively. Bueno-Borges et al. (Bueno-Borges et al., 2018) demonstrated that 80 °C of thermal treatment on the sacha inchi (*Plukenetia volubilis*) oilseeds reduced the TIs activity by 26.3% compared to control (*i.e.*, untreated seeds), obtaining comparable result.

The phytate content was significantly ($p \leq 0.05$) higher in *Sj* raw seeds than *F75* one, amounting to 4.14 ± 0.37 g/100 g DW and 2.45 ± 0.16 g/100 g DW of defatted sample, respectively (Fig. 3B). These results are in agreement with previous reports (Galasso et al., 2016). Steeping, germination, and kilning are all processes may be useful to reduce the phytate content in some seeds increasing the activity of endogenous phytases (Lemmens et al., 2018). However, we did not obtain significant differences in the phytate content after malting for both *cultivars*. (Fig. 3B). This could be due to the fact that the effect of germination/malting on the seed's phytate content depends on the species and the parameters used for each step of malting (Mäkinen & Arendt, 2015). Analogously, Udeh et al. did not observe any decrease in the phytate

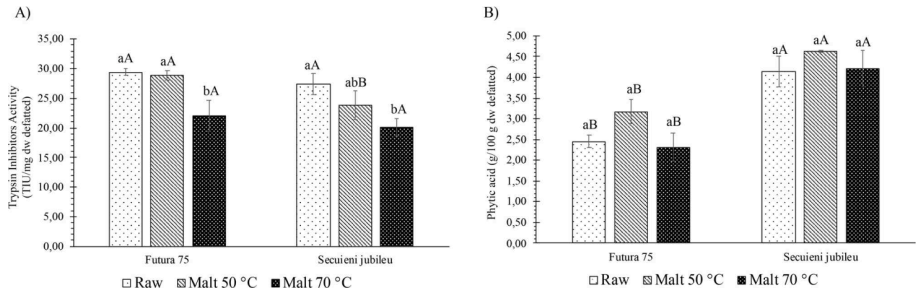


Fig. 3. Antinutritional Compounds of *Futura 75* and *Secuieni jubileu* defatted hempseeds untreated (Raw) and malted at 50 °C (Malt 50 °C) and 70 °C (Malt 70 °C). A) Trypsin Inhibitors Activity (TIU/mg DW); B) Phytic acid (g/100 g DW). Data are means ± standard deviation of three replicates (n = 3). Different letters indicate significant differences ($p \leq 0.05$), according to one-way analysis of variance. Lowercase letters represent Tukey's test comparison between raw and malted seeds and uppercase letters represent comparison between cultivars. TIU: Trypsin inhibitor unit; DW: dry weight.

content of the finger millet grains after malting (Udeh et al., 2018). Our results could be ascribed to low phytases amount in hempseed or to the fact that the adopted malting conditions may not be suitable enough to induce an adequately high phytase activity. It was reported that in cereals, phytases have a temperature *optimum* between 37 °C and 55 °C (Lemmens et al., 2018). Thus, it is possible that the modification of steeping and/or germination temperature to those optimal for hempseed's phytases could enhance the phytate breakdown. Nevertheless, more investigation concerning the hempseed's phytases activity would be required before making any changes to the process, also considering that increasing steeping temperatures could boost the loss of minerals by leaching, and it could negatively affect the seed's germinability (Lemmens et al., 2018). Despite its antinutritional activity, phytate has also health beneficial effects related to its ability to chelate iron ions (Nissar, Tehmeena, Naik, & Hussain, 2017). Unfortunately, to date, accurate and clear information on the phytate dosage required to elicit beneficial effects in human is still missing.

4. Conclusions

To conclude, the data obtained in this study showed that malting similarly influences the antioxidant profile of *F75* and *Sj* hempseeds, increasing their radical scavenging activity and reducing power, improving their tocopherol profile and TPC value. Concerning the polyphenols, malting with the higher tested kilning temperature (*i.e.*, 70 °C) significantly increased the amount of *N-trans*-caffeoyltyramine and cannabisin A, two typical hempseeds' polyphenols considered as the major contributors to the hempseeds' antioxidant activity. Nutritionally, malting increased the seeds' protein content without affecting the fat content, ash amount, and FAs profile. The kilning temperature of 70 °C resulted suitable also to reduce the amount of the antinutrients TIs, although the phytate content was not affected. In this work we analyzed TIs and phytate as antinutrients because they are found to be the main antinutrients in hempseeds (*i.e.*, nutritionally more harmful for their amounts), although other antinutritional compounds such as condensed tannins and saponins, are present, but at level lower than the attention threshold (Farinon et al., 2020). Therefore, analysis concerning the effect of malting on these other antinutrients could be advisable to be done in future works.

To the best of our knowledge, this is the first study concerning the nutritional and functional characterization of *Sj* seeds as well as the effect of malting on hempseeds, which could be attractive for food industry as hempseed's transformation process. In the last decades, the interest in hempseeds as a healthy, and nutritionally valuable ingredient has grown by the food industries, although hempseeds' processing/transformation methods are still poor. Therefore, this study may be industrially relevant to provide practical information about the possible strategies suitable to hempseed's industrial processing, useful to increase and valorize not only the hempseeds' healthy benefits, but also their potential commercial value. Additional investigation about this transformation process, including metabolomic analysis and microbiological monitoring, could be suitable to better understand the benefits of malting on hempseeds' nutritional and functional features, as well as to analyze the microbial growth eventually occurred throughout malting. This additional research would allow to find out how this process may be further optimized to obtain a healthy and safety food ingredient.

Funding

This research did not receive any specific grant from funding agencies in the public, commercial, or not-for-profit sectors.

CRediT authorship contribution statement

Barbara Farinon: Conceptualization, Methodology, Formal analysis, Investigation, Data curation, Writing - Original Draft. **Lara Costantini:** Validation. **Romina Molinari:** Validation. **Giacomo Di Matteo:** Methodology. **Serena Ferri:** Methodology. **Brunella Ceccantoni:** Methodology. **Stefania Garzoli:** Methodology. **Luisa Mannina:** Resources, Supervision. **Nicolò Merendino:** Validation, Resources, Funding acquisition, Supervision. **All authors:** Writing - Review & Editing.

Declaration of Competing Interest

The authors declare that they have no known competing financial interests or personal relationships that could have appeared to influence the work reported in this paper.

Acknowledgements

The authors would like to thank prof. Andrea Bellincontro for their technical HPLC instrument support, and Molino Crisafulli for kindly donating *Futura 75* seeds.

Appendices A and B. Supplementary figure and Supplementary data

Supplementary data to this article can be found online at https://doi.org/10.1016/j.foodchem.2021.131348.

References

Adebiyi, J. A., Obadina, A. O., Adebo, O. A., & Kayitesi, E. (2017). Comparison of nutritional quality and sensory acceptability of biscuits obtained from native, fermented, and malted pearl millet (Pennisetum glaucum) flour. *Food Chemistry, 232*, 210–217. https://doi.org/10.1016/j.foodchem.2017.04.020

Aguilar, J., Miano, A. C., Obregón, J., Soriano-Colchado, J., & Barraza-Jáuregui, G. (2019). Malting process as an alternative to obtain high nutritional quality quinoa flour. *Journal of Cereal Science, 90*, Article 102858. https://doi.org/10.1016/j.jcs.2019.102858

Alasalvar, C., Chang, S. K., Bolling, B., Oh, W. Y., & Shahidi, F. (2021). Specialty seeds: Nutrients, bioactives, bioavailability, and health benefits: A comprehensive review. *Comprehensive Reviews in Food Science and Food Safety, 1541–4337*, 12730. https://doi.org/10.1111/1541-4337.12730

AOAC International (Ed.), 2006. Official methods of analysis of AOAC International, 18. ed., current through rev. 1, 2006. ed. AOAC International, Gaithersburg, Md.

Bravi, E., Marconi, O., Perretti, G., & Fantozzi, P. (2012). Influence of barley variety and malting process on lipid content of malt. *Food Chemistry, 135*, 1112–1117. https://doi.org/10.1016/j.foodchem.2012.06.041

Bueno-Borges, L. B., Sartim, M. A., Gil, C. C., Sampaio, S. V., Rodrigues, P. H. V., & Regitano-d'Arce, M. A. B. (2018). Sacha inchi seeds from sub-tropical cultivation: Effects of roasting on antinutrients, antioxidant capacity and oxidative stability. *Journal of Food Science and Technology, 55*, 4159–4166. https://doi.org/10.1007/s13197-018-3345-1

Carciochi, R. A., Dimitrov, K., & Galván D'Alessandro, L. (2016). Effect of malting conditions on phenolic content, Maillard reaction products formation, and antioxidant activity of quinoa seeds. *Journal of Food Science and Technology, 53*, 3978–3985. https://doi.org/10.1007/s13197-016-2393-7

Carvalho, D. O., Gonçalves, L. M., & Guido, L. F. (2016). Overall Antioxidant Properties of Malt and How They Are Influenced by the Individual Constituents of Barley and the Malting Process. *Comprehensive Reviews in Food Science and Food Safety, 15*, 927–943. https://doi.org/10.1111/1541-4337.12218

Cevallos-Casals, B. A., & Cisneros-Zevallos, L. (2010). Impact of germination on phenolic content and antioxidant activity of 13 edible seed species. *Food Chemistry, 119*, 1485–1490. https://doi.org/10.1016/j.foodchem.2009.09.030

Chaturvedi, N. L. G. (2015). The Impact of Malting on Nutritional Composition of Foxtail Millet, Wheat and Chickpea. *J Nutr Food Sci, 05*. https://doi.org/10.4172/2155-9600.1000407

Chen, T., He, J., Zhang, J., Li, X., Zhang, H., Hao, J., & Li, L. (2012). The isolation and identification of two compounds with predominant radical scavenging activity in hempseed (seed of Cannabis sativa L.). *Food Chemistry, 134*, 1030–1037. https://doi.org/10.1016/j.foodchem.2012.03.009

Costantini, L., Lukšič, L., Molinari, R., Kreft, I., Bonafaccia, G., Manzi, L., & Merendino, N. (2014). Development of gluten-free bread using tartary buckwheat and chia flour rich in flavonoids and omega-3 fatty acids as ingredients. *Food Chemistry, 165*, 232–240. https://doi.org/10.1016/j.foodchem.2014.05.095

Dabina-Bicka, I., Karklina, D., & Kruma, Z. (2011). *Polyphenols and vitamin e as potential antioxidants in barley and malt.* Innovations for Food Science and Production.

Do, T. T. D., Cozzolino, D., Muhlhausler, B., Box, A., & Able, A. J. (2015). Effect of malting on antioxidant capacity and vitamin E content in different barley genotypes: Antioxidant capacity and vitamin E during malting. *Journal of the Institute of Brewing, 121*, 531–540. https://doi.org/10.1002/jib.271

EFSA Nda Panel. (2015). Scientific Opinion on Dietary Reference Values for vitamin E as α-tocopherol. *EFSA Journal, 13*, 4149.

Farinon, B., Molinari, R., Costantini, L., & Merendino, N. (2020). The Seed of Industrial Hemp (Cannabis sativa L.): Nutritional Quality and Potential Functionality for Human Health and Nutrition. *Nutrients, 12*, 1935. https://doi.org/10.3390/nu12071935

Frassinetti, S., Moccia, E., Caltavuturo, L., Gabriele, M., Longo, V., Bellani, L., … Giorgetti, L. (2018). Nutraceutical potential of hemp (Cannabis sativa L.) seeds and sprouts. *Food Chemistry, 262*, 56–66. https://doi.org/10.1016/j.foodchem.2018.04.078

Frias, J., Miranda, M., Doblado, R., & Vidalvalverde, C. (2005). Effect of germination and fermentation on the antioxidant vitamin content and antioxidant capacity of L. var. *Multolupa. Food Chemistry, 92*, 211–220. https://doi.org/10.1016/j.foodchem.2004.06.049

Galasso, I., Russo, R., Mapelli, S., Ponzoni, E., Brambilla, I. M., Battelli, G., & Reggiani, R. (2016). Variability in Seed Traits in a Collection of Cannabis sativa L. *Genotypes. Front. Plant Sci., 7*. https://doi.org/10.3389/fpls.2016.00688

Irakli, M., Tsaliki, E., Kalivas, A., Kleisiaris, F., Sarrou, E., & Cook, C. M. (2019). Effect of Genotype and Growing Year on the Nutritional, Phytochemical, and Antioxidant Properties of Industrial Hemp (Cannabis sativa L.) Seeds. *Antioxidants, 8*, 491. https://doi.org/10.3390/antiox8100491

Khandelwal, S., Udipi, S. A., & Ghugre, P. (2010). Polyphenols and tannins in Indian pulses: Effect of soaking, germination and pressure cooking. *Food Research International, 43*, 526–530. https://doi.org/10.1016/j.foodres.2009.09.036

Khang, D. T., Vasiljevic, T., & Xuan, T. D. (2016). Bioactive compounds, antioxidant and enzyme activities in germination of oats (Avena sativa L.). *International Food Research Journal, 23*, 1980–1987.

Koehler, P., Hartmann, G., Wieser, H., & Rychlik, M. (2007). Changes of Folates, Dietary Fiber, and Proteins in Wheat As Affected by Germination. *Journal of Agriculture and Food Chemistry, 55*, 4678–4683. https://doi.org/10.1021/jf0633037

Lemmens, E., Moroni, A. V., Pagand, J., Heirbaut, P., Ritala, A., Karlen, Y., … Delcour, J. A. (2018). Impact of Cereal Seed Sprouting on Its Nutritional and Technological Properties: A Critical Review. *Comprehensive Reviews in Food Science and Food Safety, 1541–4337*, 12414. https://doi.org/10.1111/1541-4337.12414

Leonard, W., Zhang, P., Ying, D., & Fang, Z. (2021). Lignanamides: Sources, biosynthesis and potential health benefits – a minireview. *Critical Reviews in Food Science and Nutrition, 61*, 1404–1414. https://doi.org/10.1080/10408398.2020.1759025

Leonard, W., Zhang, P., Ying, D., Xiong, Y., & Fang, Z. (2021). Extrusion improves the phenolic profile and biological activities of hempseed (Cannabis sativa L.) hull. *Food Chemistry, 346*, Article 128606. https://doi.org/10.1016/j.foodchem.2020.128606

Li, X., Li, J., Dong, S., Li, Y., Wei, L., Zhao, C., … Wang, Y. (2019). Effects of germination on tocopherol, secoisolariciresinol diglucoside, cyanogenic glycosides and antioxidant activities in flaxseed (*Linum usitatissimum* L.). *International Journal of Food Science & Technology, 54*, 2346–2354. https://doi.org/10.1111/ijfs.14098

MacLeod, L., & Evans, E. (2016). Malting. p. B9780081005965000000. In *Reference Module in Food Science*. Elsevier. https://doi.org/10.1016/B978-0-08-100596-5.00153-0.

Mäkinen, O. E., & Arendt, E. K. (2015). Nonbrewing Applications of Malted Cereals, Pseudocereals, and Legumes: A Review. *Journal of the American Society of Brewing Chemists, 73*, 223–227. https://doi.org/10.1094/ASBCJ-2015-0515-01

Nigro, E., Crescente, G., Formato, M., Pecoraro, M. T., Mallardo, M., Piccolella, S., … Pacifico, S. (2020). Hempseed Lignanamides Rich-Fraction: Chemical Investigation and Cytotoxicity towards U-87 Glioblastoma Cells. *Molecules, 25*, 1049. https://doi.org/10.3390/molecules25051049

Nissar, J., Tehmeena, A., Naik, H., & Hussain, S. (2017). A review phytic acid: As antinutrient or nutraceutical. *Journal of Pharmacognosy and Phytochemistry, 6*, 1554–1560.

Obadina, A. O., Arogbokun, C. A., Soares, A. O., de Carvalho, C. W. P., Barboza, H. T., & Adekoya, I. O. (2017). Changes in nutritional and physico-chemical properties of pearl millet (Pennisetum glaucum) Ex-Borno variety flour as a result of malting. *Journal of Food Science and Technology, 54*, 4442–4451. https://doi.org/10.1007/s13197-017-2922-z

Özcan, M. M., Aljuhaimi, F., & Uslu, N. (2018). Effect of malt process steps on bioactive properties and fatty acid composition of barley, green malt and malt grains. *Journal of Food Science and Technology, 55*, 226–232. https://doi.org/10.1007/s13197-017-2920-1

Pająk, P., Socha, R., Broniek, J., Królikowska, K., & Fortuna, T. (2019). Antioxidant properties, phenolic and mineral composition of germinated chia, golden flax, evening primrose, phacelia and fenugreek. *Food Chemistry, 275*, 69–76. https://doi.org/10.1016/j.foodchem.2018.09.081

Rafi, M., Febriany, S., Wulandari, P., Suparto, I. H., Ridwan, T., Rahayu, S., & Siswoyo, D. M. (2018). Total Phenolics, Flavonoids, and Anthocyanin Contents of Six Vireya Rhododendron from Indonesia and Evaluation of their Antioxidant Activities. *J App Pharm Sci, 8*, 49–54. https://doi.org/10.7324/JAPS.2018.8908

Sakakibara, I., Katsuhara, T., Ikeya, Y., Hayashi, K., & Mitsuhashi, H. (1991). Cannabisin A, an arylnaphthalene lignanamide from fruits of Cannabis sativa. *Phytochemistry, 30*, 3013–3016. https://doi.org/10.1016/S0031-9422(00)98242-6

Sakakibara, I., Ikeya, Y., Hayashi, K., & Mitsuhashi, H. (1992). Three phenyldihydronaphthalene lignanamides from fruits of Cannabis sativa. *Phytochemistry, 31*, 3219–3223. https://doi.org/10.1016/0031-9422(92)83479-I

Shaban, M. (2013). Effect of water and temperature on seed germination and emergence as a seed hydrothermal time model. *International journal of Advanced Biological and Biomedical Research, 1*, 1686–1691.

Siano, F., Moccia, S., Picariello, G., Russo, G., Sorrentino, G., Di Stasio, M., … Volpe, M. (2018). Comparative Study of Chemical, Biochemical Characteristic and ATR-FTIR Analysis of Seeds, Oil and Flour of the Edible Fedora Cultivar Hemp (Cannabis sativa L.). *Molecules, 24*, 83. https://doi.org/10.3390/molecules24010083

Smeriglio, A., Galati, E. M., Monforte, M. T., Lanuzza, F., D'Angelo, V., & Circosta, C. (2016). Polyphenolic Compounds and Antioxidant Activity of Cold-Pressed Seed Oil from Finola Cultivar of *Cannabis sativa* L.: Polyphenolic Compounds and Antioxidant Activity of FHSO. *Phytotherapy Research, 30*, 1298–1307. https://doi.org/10.1002/ptr.5623

Terpinc, P., Cigić, B., Polak, T., Hribar, J., & Požrl, T. (2016). LC–MS analysis of phenolic compounds and antioxidant activity of buckwheat at different stages of malting. *Food Chemistry, 210*, 9–17. https://doi.org/10.1016/j.foodchem.2016.04.030

Trabelsi, N., Oueslati, S., Ksouri, R., Nassra, M., Marchal, A., Krisa, S., … Waffo-Téguo, P. (2014). The antioxidant properties of new dimer and two monomers of phenolic acid amides isolated from Limoniastrum guyonianum. *Food Chemistry, 146*, 466–471. https://doi.org/10.1016/j.foodchem.2013.09.077

Udeh, H. O., Duodu, K. G., & Jideani, A. I. O. (2018). Effect of malting period on physicochemical properties, minerals, and phytic acid of finger millet (*Eleusine coracana*) flour varieties. *Food Sci Nutr, 6*, 1858–1869. https://doi.org/10.1002/fsn3.696

Urvaka, E., Mišina, I., Soliven, A., & Górnaś, P. (2019). Rapid Separation of All Four Tocopherol Homologues in Selected Fruit Seeds via Supercritical Fluid Chromatography Using a Solid-Core C18 Column. *Journal of Chemistry, 2019*, 1–10. https://doi.org/10.1155/2019/5307340

Vagadia, B. H., Vanga, S. K., & Raghavan, V. (2017). Inactivation methods of soybean trypsin inhibitor – A review. *Trends in Food Science & Technology, 64*, 115–125. https://doi.org/10.1016/j.tifs.2017.02.003

Weitbrecht, K., Müller, K., & Leubner-Metzger, G. (2011). First off the mark: Early seed germination. *Journal of Experimental Botany, 62*, 3289–3309. https://doi.org/10.1093/jxb/err030

7.5. Case study 4: Hemp seed oils characterization by multimethodological approach

Hempseed oil are a derived product of hempseed by cold pression. The high nutritional value lies in the presence of secondary metabolites and the characteristic fatty acids profile, which stands out for the higher levels of polyunsaturated fatty acids (PUFAs) with respect to saturated ones. The two essential fatty acids, linoleic acid and α-linolenic acid, account for more than 50% and 15–25% respectively, resulting in a perfect balanced 3:1 ratio ω-6:ω-3, optimal for healthy human nutrition. Moreover, the presence of secondary metabolites such as phenolic compounds and tocopherols, with antioxidant properties, improves the health benefits and helps to prevent the PUFA oxidation process, improving hemp seed oil shelf-life.

It is important to underline that a specific regulation concerning the analytical parameters for the quality assessment of hemp seed oils is still lacking, although the increasing interest towards hemp food products for human consumption. In the present work, nine commercial hemp seed oils were

analyzed, by a multimethodological approach, including the untargeted NMR methodology, to provide information regarding the quality of the products present on the markets

applied sciences

MDPI

Article

Commercial Hemp Seed Oils: A Multimethodological Characterization

Mattia Spano [1,†], Giacomo Di Matteo [1,†], Mattia Rapa [2], Salvatore Ciano [2], Cinzia Ingallina [1,*], Stefania Cesa [1], Luigi Menghini [3], Simone Carradori [3], Anna Maria Giusti [4], Antonella Di Sotto [5], Silvia Di Giacomo [5], Anatoly P. Sobolev [6], Giuliana Vinci [2] and Luisa Mannina [1]

1 Department of Chemistry and Technology of Drugs, Sapienza University of Rome, P.le Aldo Moro 5, 00185 Rome, Italy; mattia.spano@uniroma1.it (M.S.); giacomo.dimatteo@uniroma1.it (G.D.M.); stefania.cesa@uniroma1.it (S.C.); luisa.mannina@uniroma1.it (L.M.)
2 Department of Management, Sapienza University of Rome, via del Castro Laurenziano 9, 00161 Rome, Italy; mattia.rapa@uniroma1.it (M.R.); salvatore.ciano@uniroma1.it (S.C.); giuliana.vinci@uniroma1.it (G.V.)
3 Department of Pharmacy, University "G. d'Annunzio" of Chieti-Pescara, Via dei Vestini 31, 66100 Chieti, Italy; luigi.menghini@unich.it (L.M.); simone.carradori@unich.it (S.C.)
4 Department of Experimental Medicine, Sapienza University of Rome, P.le Aldo Moro 5, 00185 Rome, Italy; annamaria.giusti@uniroma1.it
5 Department of Physiology and Pharmacology "V. Ersparmer", Sapienza University of Rome, P.le Aldo Moro 5, 00185 Rome, Italy; antonella.disotto@uniroma1.it (A.D.S.); silvia.digiacomo@uniroma1.it (S.D.G.)
6 Institute for Biological Systems, Magnetic Resonance Laboratory "Segre-Capitani", CNR, Via Salaria Km 29.300, 00015 Monterotondo, Italy; anatoly.sobolev@cnr.it
* Correspondence: cinzia.ingallina@uniroma1.it
† These authors contributed equally to this work.

Received: 10 September 2020; Accepted: 1 October 2020; Published: 3 October 2020



Abstract: Nine commercial hemp seed oils from different countries were studied using a multimethodological approach to obtain information about their quality and chemical composition. Due to the lack of a specific regulation for hemp seed oils, quality parameters used in the case of olive oils (free acidity, peroxides number, spectrophotometer parameters) and anisidine number were measured and compared with those reported for extra virgin olive oil (EVOO). Free acidity and peroxides number showed a great variability, ranging from 0.4 to 17.24% and from 4.32 to 22.14 meqO_2/kg, respectively, whereas the anisidine number ranged from 0.11 to 3.58. K_{232} value turned out to be generally below the limit reported for EVOO, whereas K_{270} and ΔK values were higher, with respect to EVOO limits, due to the high amount of tri-unsaturated fatty chains. Colorimetric analysis showed a peculiar curve trend that could represent the fingerprint of this product. Untargeted nuclear magnetic resonance methodology allowed to measure the amount of fatty chains, ω-6:ω-3 ratio, β-sitosterol, and aldehydes. The ω-6:ω-3 ratio turned out to be, in some cases, different from that reported on the bottle labels. Finally, lipoperoxidation assays were also carried out under different storage (light and temperature) and time exposure conditions, confirming that the exposure to direct light is the condition that interferes more with the product quality.

Keywords: hemp seed oil; quality parameters; NMR; colorimetric analysis; lipoperoxidation

1. Introduction

Cannabis sativa L. is an annual plant belonging to the family of Cannabinaceae, widely spread in all five continents. Although its name is frequently associated with drugs of abuse (marijuana), due to the presence of psychotropic Δ^9-tetrahydrocannabinol (THC) [1], the recent evidence of *Cannabis sativa*

L. cultivars characterized by low amounts of Δ^9-THC (known as industrial hemp) raised a growing interest toward this plant in different fields, including pharmaceutical, food, and cosmetic sectors. In Europe, hemp cultivars with an amount of Δ^9-THC lower than 0.2% (in dry matter basis) are allowed for cultivation, and are reported in the EU approved list [2].

Among the different parts of the plant, hemp seeds are the only one to be authorized for food applications [3], as cannabinoids are present mainly due to cross-contamination during harvesting and processing [4]. Since ancient times, hemp seeds were consumed in the human diet; however, they were replaced by other seeds and used as feed materials for all animal species. Only in recent times the discovery of hemp seeds' high nutritional value led to a revaluation of this source for human consumption. Literature regarding the investigation of hemp seeds' composition has increased, making them an emerging source for value-added functional food ingredients and nutraceuticals [5,6]. Hemp seeds are consumed shelled in salad dressings, and in the production of snack bars, or they can be cold pressed to obtain edible hemp seed oil, and the residual cake is grinded to have a fiber-rich flour used in processed food (such as bread, biscuits, and pasta). The high nutritional value lies in the presence of secondary metabolites and the characteristic fatty acids profile, which stands out for the higher levels of polyunsaturated fatty acids (PUFAs) with respect to saturated ones. The two essential fatty acids, linoleic acid (C18:2 ω-6) and α-linolenic acid (C18:3 ω-3), account for more than 50% and 15–25% respectively, resulting in a perfect balanced 3:1 ratio ω-6:ω-3, optimal for healthy human nutrition [5]. Moreover, the presence of secondary metabolites such as phenolic compounds and tocopherols [7–11], with antioxidant properties, improves the health benefits and helps to prevent the PUFA oxidation process, improving hemp seed oil shelf-life. Some studies recommend a dietary intake of hemp seed oils [12–14], nowadays largely present in the markets of different countries (Canada, the European Union, Australia, and China) [15].

It is important to underline that a specific regulation concerning the analytical parameters for the quality assessment of hemp seed oils is still lacking, although the increasing interest towards hemp food products for human consumption has prompted few countries to issue guidelines about the acceptable level of Δ^9-THC in hemp seeds, hempseed oil, or processed food [4,16–18]. Indeed, some studies discuss the development of a proper analytical procedure for the detection of cannabinoids levels and ratio in hemp seeds and hempseed oils [4,19–22].

However, a plethora of different factors could influence the oil quality, such as the area of cultivation [23,24], the type of cultivars [25], the origin of seeds [26], agronomic practices, and extraction processing [27,28] that usually indicate the cold pressing as the preferred method to preserve the ω-3:ω-6 ratio [11]. Moreover, the price of commercial hempseed oil ranges from 20 to 100 €/L, making it an expensive food product sold on the market without any quality assurance. Taking into account the variability in composition and the price, quality parameters need to be established in order to both valorize products and preserve consumer safety and awareness.

Hemp seed oils are sold as food, and labeled accordingly [29]. In this context, the final product has to guarantee the safety standard for consumers, but relevant information, such as plant identity, variety, chemical characterization in terms of unsaturated fatty acid, secondary metabolites, and similar, are not mandatory, and therefore not reported in the bottle labels.

In the present study, nine commercial hemp seed oils were analyzed, by a multimethodological approach, to provide information regarding the quality of the products present on the markets. Due to the lack of a specific regulation for hemp seed oils, quality criteria reported in the olive oil Regulation (EU) 2015/1830 (European commission), namely free acidity, peroxides number, and spectrophotometric parameters such as K_{270}, ΔK, and K_{232}, were measured and compared with those reported for extra virgin olive oil (EVOO). Moreover, anisidine number, colorimetric analysis, and lipoperoxidation assays were also evaluated. Untargeted nuclear magnetic resonance (NMR) methodology was applied to identify and quantify simultaneously different classes of compounds [30,31].

2. Materials and Methods

2.1. Reagents and Materials

All chemical reagents (potassium hydroxide (KOH), phenolphthalein, potassium iodide (KI), acetic acid (CH_3COOH), sodium thiosulfate ($Na_2S_2O_3$), *p*-anisidine, glacial acetic acid, linoleic acid, iron (II) chloride ($FeCl_2$), potassium thiocyanate (KSCN), and solvents (ethanol (EtOH), methanol (MeOH), chloroform ($CHCl_3$), diethyl ether (Et_2O), iso-octane, and cyclohexane) were purchased from Sigma-Aldrich Co (St. Louis, MO, USA) (all purity ≥98%). Deionized water, purified with a Milli-Q system (Millipore, Bedford, USA), was used. Dimethyl sulfoxide D6 99.80% and chloroform D 99.80% were purchased from Euriso-Top (Saclay, France).

2.2. Sampling

Nine commercial hemp seed oils were purchased in organic foods stores and in the e-marketplace, chosen as the best representatives of the consumer's choices (the most common hempseed oils from greatly organized distribution, and the ones with top customer reviews from the e-marketplace). Hemp seed oils are usually sold in 250 mL bottles. Provenience and prices (€/L) are reported in Table 1. The labels of samples 2, 4, 5, 7, 8, and 9 stated that the preparation was performed using cold extraction. In all labels, the ω-6:ω-3 ratio was indicated. Before carrying out analysis, samples were stored in a cool and dry place, away from sources of light and heat, in order to prevent oxidation reactions. All analyses were carried out 6 months before the expiry date. The original bottle was opened just before analysis and divided in 10 mL tubes, completely fulfilled, hermetically closed, and stored in a cold place in the dark, in order to prevent oil–air and oil–light interactions.

Table 1. Geographical provenience and price of the commercial hemp seed oils.

Sample	1	2	3	4	5	6	7	8	9
Origin	Italy	EU	EU	NON-EU	NON-EU	Italy	NON-EU	NON-EU	Italy
Price (€/L)	44	20	24	25	26	30	52	64	80

2.3. Quality Parameters

Hemp seed oil quality was evaluated measuring free acidity, peroxides number, anisidine number, and spectrophotometer parameters (K_{232}, K_{270}, and ΔK). Since the methodologies usually applied to determine all these parameters require great quantities of samples and reagents, specific miniaturized methods were applied to analyze the hemp seed oil, according to Rapa et al. [32]. All the experiments were performed three times, and the results were expressed as the mean value ± SD (standard deviation).

2.3.1. Free Acidity

An aliquot of 3.33 g of hemp seed oil was dissolved in 10 mL of diethyl ether/ethanol (60/40 *v*/*v*) mixture. Then, free fatty acids were titrated with KOH 0.01 N until the tuning of the phenolphthalein indicator. Free acidity (A%) was determined, following Equation (1):

$$A\% = (V \times C \times M)/(10 \times m) \quad (1)$$

where: V is the titrant volume (expressed in mL); C is the exact concentration of KOH (expressed in mol/L); M is the molar weight of the oleic acid (282 g/mol) used for the expression of the result; and m is the weight of the analyzed substance (expressed in g) [33] (Table 2).

2.3.2. Peroxides Number (P.N.)

An aliquot of 0.5 g hemp seed oil was introduced in a flask with 2 mL of chloroform. After shaking (30 s), 3 mL of glacial acetic acid and 0.1 mL of potassium iodide saturated aqueous solution were

added. The flask was shaken for 1 min and then left, protected from light, at a temperature between 15 and 25 °C. After 5 min, 75 mL of distilled water was added. The released iodine was titrated with a sodium thiosulfate solution (0.0005 N) by vigorously shaking, using a starch solution as indicator. The peroxides number (P.N.), expressed as meqO_2/kg, and was calculated as follows (Equation (2)):

$$P.N. = (V \times T)/m \times 1000 \quad (2)$$

where: V is the volume of titrant (expressed in mL); T is the normality of the sodium thiosulfate solution (expressed in n.eq./L); and m is the weight in g of the analyzed sample [33].

Table 2. Free acidity (A%), peroxides number (P.N.), anisidine number (A.N.), and spectrophotometric parameters (K_{232}, K_{270}, and ΔK) of the analyzed hemp seed oil samples.

Sample	A%	P.N. (meqO_2/kg)	A.N.	K_{232}	K_{270}	ΔK
1	17.24 ± 0.63	4.31 ± 0.37	3.58 ± 0.17	2.65 ± 0.09	0.69 ± 0.01	0.03
2	1.86 ± 0.07	16.68 ± 1.28	1.14 ± 0.04	2.04 ± 0.02	0.41 ± 0.01	0.01
3	0.40 ± 0.01	16.42± 1.39	2.84 ± 0.11	2.35 ± 0.04	0.57 ± 0.01	0.02
4	4.15 ± 0.12	8.36 ± 0.75	1.60 ± 0.07	2.12 ±0.03	0.47 ± 0.01	0.01
5	1.47 ± 0.08	10.69 ± 0.96	1.17 ± 0.03	2.01 ± 0.17	0.39 ± 0.01	0.01
6	2.22 ± 0.02	22.14± 1.88	3.30 ± 0.28	2.26 ± 0.05	0.49 ± 0.01	0.01
7	0.76 ± 0.03	10.50 ± 1.26	0.11 ± 0.02	1.85 ± 0.02	0.26 ± 0.01	0.01
8	0.43 ± 0.02	17.13 ± 0.89	0.12 ± 0.01	1.72 ± 0.01	0.19 ± 0.01	0.01
9	1.50 ± 0.06	17.03 ± 1.17	2.80 ± 0.02	2.21 ± 0.02	0.46 ± 0.01	0.02

2.3.3. Anisidine Number (A.N.)

An amount of 0.2 g of hemp seed oil was dissolved in 10 mL of iso-octane (2,2,4-trimethylpentane) (solution A). Then, the extinction at 350 nm was determined in a 10 mm quartz cuvette. A 2.5% (*w/v*) solution of *p*-anisidine was prepared in glacial acetic acid. An aliquot of 2.5 mL of solution A was added to 0.5 mL of *p*-anisidine (2.5% in glacial acetic acid). The mixture (solution B) was shaken and set to rest for 10 min. Then, the extinction at 350 nm was measured. To obtain the *p*-anisidine number (A.N.), the following expression (Equation (3)) was applied:

$$A.N. = [25 \times (1.2\ Ea - Eb)]/m \quad (3)$$

where: Ea is the extinction of solution A; Eb is the extinction of the solution B; and m is the weight of the sample (expressed in g) [34].

2.3.4. Spectrophotometric Investigation in the Ultraviolet

An amount of 0.25 g of hemp seed oil was dissolved in 25 mL of cyclohexane solvent and homogenized to obtain a 1% solution (*w/v*). The extinction coefficients were measured at 232 nm, 266 nm, 270 nm, and 274 nm, with respect to the pure solvent as reference in a 10 mm quartz cuvette. The extinction absolute value (ΔK) was calculated as follows (Equation (4)):

$$\Delta K = K_{270} \times (K_{266} + K_{274})/2 \quad (4)$$

where K_{270}, K_{266}, and K_{274} are the wavelength-specific extinction [33].

2.4. Colorimetry

The hemp seed oils were submitted to colorimetric analyses. CIEL*a*b* parameters (L*, a*, b*, C^*_{ab}, and h_{ab}) were obtained using a colorimeter X-Rite SP-62 (X-Rite Europe GmbH, Regensdorf, Switzerland), equipped as previously described [35]. The color description is based on three parameters: L* (lightness), a* (greenness for negative, or redness for positive, values) and b* (blueness for negative,

or yellowness for positive, values). Cylindrical coordinates C^*_{ab} and h_{ab} were calculated from the parameters a* and b*, as described in our previous works [36]. All the experiments were performed four times, and the results were expressed as the mean value ± SD (Table 3).

Table 3. Colorimetric parameters obtained by CIELAB analyses performed on hemp seed oils 1–9.

Sample	L*	a*	b*	C^*_{ab}	h_{ab}
1	29.33 ± 0.15	3.54 ± 0.04	7.30 ± 0.22	8.11 ± 0.21	64.12 ± 0.56
2	25.40 ± 0.02	0.82 ± 0.00	1.19 ± 0.01	1.44 ± 0.01	55.68 ± 0.19
3	33.52 ± 0.04	3.96 ± 0.02	15.11 ± 0.09	15.62 ± 0.08	75.32 ± 0.09
4	46.32 ± 0.05	0.40 ± 0.02	24.60 ± 0.02	24.61 ± 0.02	89.08 ± 0.06
5	42.71 ± 0.88	1.50 ± 0.08	23.66 ± 0.17	23.71 ± 0.16	86.38 ± 0.20
6	39.20 ± 0.53	0.96 ± 0.05	6.28 ± 0.14	6.36 ± 0.13	81.27 ± 0.58
7	44.52 ± 0.09	0.72 ± 0.02	9.89 ± 0.15	9.92 ± 0.15	85.85 ± 0.09
8	52.33 ± 0.08	-0.62 ± 0.02	2.91 ± 0.09	2.98 ± 0.09	102.03 ± 0.47
9	40.13 ± 0.27	5.17 ± 0.10	25.80 ± 0.57	26.32 ± 0.57	78.68 ± 0.15

[1] L* = lightness; [2] a* = greenness for negative, or redness for positive, values; [3] b* = blueness for negative, or yellowness for positive, values; [4] C^*_{ab} and [5] h_{ab} = cylindrical coordinates.

2.5. NMR Analysis

Each hemp seed oil sample (20 µL) was dissolved in DMSO-d6 (20 µL) and $CDCl_3$ (700 µL) in a 5 mm NMR tube, which was flame-sealed. The NMR spectra were recorded at 27 °C on a Bruker AVANCE 600 spectrometer (Milan, Italy) operating at the proton frequency of 600.13 MHz and equipped with a Bruker multinuclear z-gradient 5 mm probe head. ^{1}H spectra were acquired using the following conditions: number of scans 1024, 90° pulse 9.5 µs, time domain 64 K data points, relaxation delay plus acquisition time 3.5 s, and spectral width 10,802 Hz. ^{1}H NMR spectra were obtained by the FT (Fourier transform) of the free induction decay, applying an exponential multiplication with a line-broadening factor of 0.3 Hz and a zero filling (size 64 K) procedure. ^{1}H NMR spectra were manually phased. Chemical shifts were reported with respect to the residual $CHCl_3$ signal set at 7.26 ppm. The baseline was corrected using the Cubic Spline Baseline Correction routine in the Bruker Topspin software. The integrals of seven selected signals were measured. In particular, the selected proton resonances were due to hexanal (CH) at 9.699 ppm, *trans*-2-hexenal (CH) at 9.448 ppm, diallylic protons of tri-unsaturated fatty acids (CH_2) at 2.778 ppm, diallylic protons of di-unsaturated fatty acids (CH_2) at 2.729 ppm, α-methylene protons of all fatty acids (CH_2) at 2.251 ppm, allylic protons of all unsaturated fatty acids (CH_2) at 1.999 ppm, and β-sitosterol (CH_3) at 0.622 ppm. The integrals of the selected resonances were normalized with respect to the resonance at 2.251 ppm set to 100. β-Sitosterol, fatty acids, and aldehydes were expressed as molar %, following the Equations previously described [37], with some modifications:

$$\%_{\beta\text{-SIT}} = 100 \times 0.66 I_{\beta\text{-SIT}}/I_{tot} \quad (5)$$

$$\%_{TRI} = 100 \times 0.5 I_{TRI}/I_{tot} \quad (6)$$

$$\%_{DI} = 100 \times I_{DI}/I_{tot} \quad (7)$$

$$\%_{MONO} = 100 \times 0.5(I_{UNS} - 2I_{DI} - I_{TRI})/I_{tot} \quad (8)$$

$$\%_{SAT} = 100 \times (I_{FA} - I_{DI} - 0.5 I_{TRI} - \%_{MONO})/I_{tot} \quad (9)$$

$$\%_{INS} = \%_{MONO} + \%_{DI} + \%_{TRI} \quad (10)$$

$$\%_{t\text{-}2\text{-}HEX} = 100 \times 2I_{t\text{-}2\text{-}HEX}/I_{tot} \quad (11)$$

$$\%_{HEX} = 100 \times 2I_{HEX}/I_{tot} \quad (12)$$

where $\%_{\beta\text{-SIT}}$, $\%_{TRI}$, $\%_{DI}$, $\%_{MONO}$, $\%_{SAT}$, $\%_{INS}$, $\%_{t\text{-2-HEX}}$, and $\%_{HEX}$ are molar % of β-sitosterol, tri-unsaturated fatty acids, di-unsaturated fatty acids, mono-unsaturated fatty acids, saturated fatty acids, unsaturated fatty acids, *trans*-2-hexenal, and hexanal, respectively. $I_{\beta\text{-SIT}}$, I_{TRI}, I_{DI}, I_{UNS}, I_{FA}, $I_{t\text{-2-HEX}}$, and I_{HEX} are integrals of β-sitosterol, tri-unsaturated fatty acids, di-unsaturated fatty acids, allylic protons of all unsaturated fatty acids, α-methylene protons of all fatty acids, *trans*-2-hexenal, and hexanal, respectively. I_{tot} was calculated according to Equation (13).

$$I_{tot} = I_{FA} + 0.66I_{\beta\text{-SIT}} + 2I_{t\text{-2-HEX}} + 2I_{HEX} \quad (13)$$

2.6. Lipoperoxidation

The assay was carried out by the ferric thiocyanate method according to Di Sotto et al. [38], with minor changes. Preliminarily, both linoleic acid and the oil samples were subjected to storage for 24 h under different temperature conditions, including room temperature (RT), room temperature plus light exposure (RT plus white light; distance of lamp, 30 cm), refrigerated temperatures of +4 °C and −20 °C, and warm temperature of +60 °C. After storage sodium phosphate buffer (625 µL; 0.2 M, pH 7.0) was added to linoleic acid or the hemp seed oil samples (625 µL; 2.5% *v/v* in pure EtOH) and incubated at 37 °C for 72 h. Various aliquots (10 µL) were taken at different incubation times (0, 24, 48, 72 h) and mixed with ethanol (970 µL; 75% *v/v*), $FeCl_2$ (10 µL; 200 mM in 3.5% *w/v* HCl) and KSCN (10 µL; 30% *w/v* in deionized water). Peroxides, generated during fatty acid peroxidation, oxidize Fe^{+2} to Fe^{+3}; the latter ion forms a complex with thiocyanate that can be measured spectrophotometrically at 500 nm.

The percentage of the Lipid Peroxidation (LP) was calculated, as follows (Equation (14)):

$$LP = A_{sample}/A_{standard} \times 100 \quad (14)$$

where $A_{standard}$ is the highest absorbance of linoleic acid used as reference, whereas A_{sample} is the absorbance of the tested sample. The experiments were repeated two times, and, in each experiment, three technical replicates were assayed for each storage condition.

3. Results and Discussion

3.1. Quality Parameters

Due to the lack of a specific regulation on hemp seed oils, quality parameters established for olive oils [33], namely free acidity, peroxides number, anisidine number, and spectrophotometric parameters (K_{232}, K_{270}, and ΔK) (ISO 6885:2016), were evaluated.

3.1.1. Free Acidity

Free Acidity (A%), expressed as oleic acid, points out the degree of fat hydrolytic alteration. Triglycerides hydrolysis occurs in the presence of water and enzymes (lipases), naturally present in raw vegetable matrix. In the Regulation (EU) 2015/1830 for virgin oils, a maximum limit of 2.0% is provided [33]. However, the Pharmacopoeia provides a maximum value of 6% in A% for seeds oils [39]. Among the commercial hemp seed oils here investigated (Table 2), samples 3, 7, and 8 showed an A% less than 1% (0.40%, 0.76% and 0.43%, respectively), whereas samples 1, 4, and 6 showed a value above the 2.0% threshold (17.24%, 4.15% and 2.22%, respectively). Considering the limit established by the Pharmacopoeia for seed oils, only sample 1 exceeds the 6% limit. It possible that this commercial product was not stored using adequate temperature and light conditions.

In literature, few studies have investigated the free acidity of hemp seed oils, and a great variability of values was found. A% of 0.074–0.890% has been reported for noncommercial hemp seed oils [32,40], whereas for Italian commercial hemp seed oils, the maximum value of 9.9% has been reported [7].

3.1.2. Oxidation Parameters: Peroxides Number and Anisidine Number

Fatty acids oxidation can occur in two steps. First, unsaturated fatty acids react with oxygen, producing odorless peroxides that, in the second step, decompose in aldehydes, responsible for rancid taste. The degree of the first oxidation step is evaluated by peroxides number (P.N.) (EU Regulation (EU) 2015/1830); a limit of 20 meqO_2/kg P.N. is reported for virgin and extra virgin olive oils. The peroxides value is useful for assessing the spoilage progression, especially in fresh oils or oil produced with low temperature technologies [41]. On the other hand, the anisidine number (A.N.) provides the assessment of the second oxidation step: an acceptable number for fat matrices is 10.

The nine hemp seed oils here investigated showed a relevant variability for P.N. values, ranging from 4.32 to 22.14 meqO_2/kg. Only sample 6 showed a P.N. value above 20 meqO_2/kg. Again, as in the case of A%, these values are higher than the values from 1.94 to 7.20 meqO_2/kg reported in the case of noncommercial samples [40,42,43] and Italian commercial hemp seed oils [7].

All the investigated samples showed A.N. values ranging from 0.11 to 3.58 (below the limit), in agreement with literature data [44].

3.1.3. K_{232}, K_{270}, and ΔK Spectroscopic Values

Regarding the spectroscopic measurements, the K_{232} value evaluates the presence of conjugated dienes, whereas K_{270} and ΔK indicate the presence of conjugated trienes. Almost all the samples showed a K_{232} value below the EVOO limit (2.6 L/g·cm), with sample 8 showing the lowest value (1.72 L/g·cm). The only exception was sample 1, with a value of 2.65 L/g·cm. Generally, the values here reported were lower than those reported by Anwar et al. for Pakistan samples [23].

The K_{270} and ΔK values turned out to be higher than the limits reported in the Regulation (0.25 L/g·cm, 0.01), in agreement with the previously reported data [45]. The higher conjugated trienes content, with respect to olive oils, is due to the high amount of PUFAs in hemp seed oils.

3.2. Colorimetry

The color of a product plays a preeminent role in the consumer acceptance and, consequently, in the choice of a food. In the case of oils, color could represent an index of good manufacturing practice, a warranty of quality and genuineness, and, not least important, of the right storage conditions. To evaluate the color properties of hemp seed oils, the tristimulus colorimetry was employed. To our knowledge, only one work is available in literature regarding colorimetric studies on hemp seed oil samples, reporting an L* value of 18.13, an a* of 2.40 and a b* of 30.87 [46], so that a significant yellow parameter (+b*) can be shown, compared to a very weak red value (+a*) and a quite dark sample.

In a previous work [46], a comparison among medium reflectance profiles of hemp seed, olive, and neem oils has been carried out: a similarity among olive oils and hemp oils has been observed, although hemp seed oils turned out to be darker.

The analyses, performed on the selected nine samples, only in part confirm these data (Table 3). Two samples (6 and 7) were turbid, and were analyzed before and after filtration. All samples covered a very wide range between 25 to 46 of lightness, −0.6–5.4 of a* and 1.2–33 of b*, substantially confirming a yellow color completely dominant on the slight reddish nuance, but also showing significant differences in the lightness and the tonality, $h_{ab} = \tan^{-1}(a^*/b^*)$, most likely due to the different cultivars, the work-up, and the purification steps applied by the producers. All the obtained reflectance curves, shown in Figure 1, account for the relevant differences found among the samples.

The profile of sample 2 corresponded to a very dark oil, whereas the profile of sample 8 corresponded to a very faded oil. In samples 6 and 7, turbidity and sediments were present. Therefore, when samples 2, 8, 6, and 7 were discarded, a clear reflectance profile was observed (Figure 1), accounting for a different lightness, corresponding to a higher b*/a* ratio, that indicates a dominant yellow color with respect to a reddish nuance. Samples 4 and 5, characterized by a quite different profile in the region between 450 and 500 nm, showed the lowest a* values and, consequently, the highest b*/a* ratios.

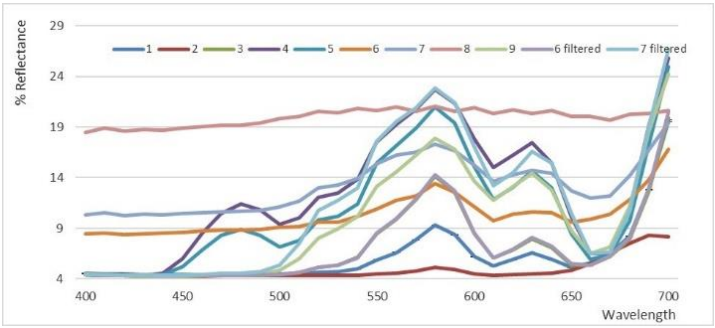


Figure 1. Spectral reflectance curves obtained by CIEL*a*b* analyses applied to 1–9 hemp seed oils. Samples 6 and 7 were measured after filtration.

Therefore, with respect to the reflectance profiles of other commercially available oils, such as corn, rice, and EVOO, hemp seed oils showed a peculiar curve trend that could represent a fingerprint for this product [40].

3.3. NMR Analysis

In Figure 2, the ^{1}H spectrum of a hemp seed oil is reported. Hemp seed oils spectra, similarly to other vegetable oils, were characterized by strong signals, due to the fatty chains on the glycerol moiety and minor compounds. The amount of β-sitosterol, hexanal, *trans*-2-hexenal, saturated fatty chains, and unsaturated fatty chains (including mono-unsaturated, di-unsaturated, and tri-unsaturated fatty chains) are reported as molar percentages in Figure 3.

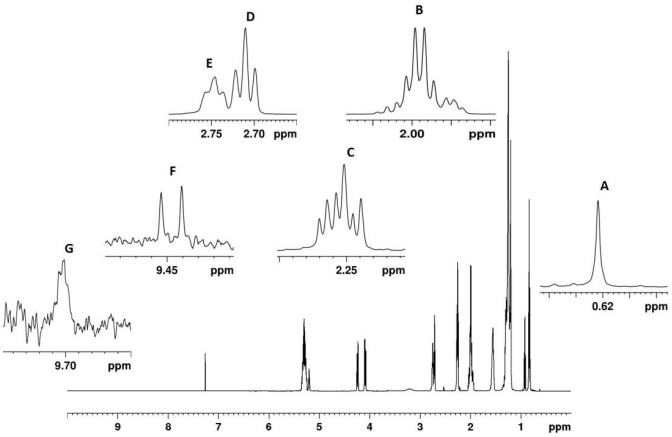


Figure 2. 600.13 MHz ^{1}H NMR spectrum of a hemp seed oil. Quantified selected NMR signals are reported in expanded regions. (**A**) β-sitosterol (0.622 ppm); (**B**): allylic protons of all fatty chains (1.999 ppm); (**C**): α-methylene protons of all acyl chains (2.251 ppm); (**D**): diallylic protons of linoleic fatty chains (2.729 ppm); (**E**): diallylic protons of linolenic fatty chains (2.778 ppm); (**F**): *trans*-2-hexenal (9.448 ppm); (**G**): hexanal (9.699 ppm).

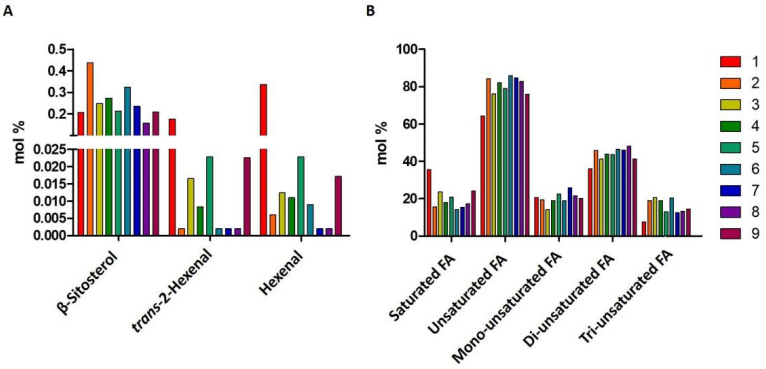


Figure 3. Histograms resulting from the quantitative NMR analysis of (**A**) β-sitosterol and aldehydes, and (**B**) fatty acids. The relative molecular abundances (molar percentage) are reported.

As expected, fatty acid chain profiles of all nine hemp seed oils were characterized by a higher content of unsaturated fatty acid chains with respect to saturated ones, and, among them, di-unsaturated fatty chains resulted in more abundance (35–48%), compared to mono- (15–28%) and tri-unsaturated ones (8–20%). In particular, sample 1 was characterized by the lowest tri-unsaturated fatty chain content.

Hemp seed oils are renowned for their optimal 3:1 ratio in ω-6:ω-3. However, on the bottle labels of samples 2, 6, and 9 (see Table 4), a ratio lower than 3:1 was reported, and, in some cases, the ω-6:ω-3 ratio measured by NMR was different from the ratio reported on the labels. For instance, 2, 3, and 4 hemp seed oil samples showed an ω-6:ω-3 ratio lower than that declared in the labels. Only 7, 8, 5, and 1 hemp seed oil samples, with values of 3.6, 3.6, 3.3, and 4.7, respectively, turned out to have an optimal ω-6:ω-3 ratio. In particular, sample 1 presented a particularly high ratio compared to other ones. According to NMR data, samples 4, 2, 9, and 6 did not reach the 3:1 ω-6:ω-3 ratio value, with sample 3 having a particularly low value.

Table 4. Comparison between ω-6:ω-3 ratios reported on the bottle labels and the ones measured by NMR analysis. Integrals of signals D (diallylic protons of linoleic fatty chains at 2.729 ppm) and E (diallylic protons of linolenic fatty chains at 2.778 ppm) of the nine commercial hemp seed oils analyzed were measured.

	ω-6:ω-3 Ratio	
Samples	**Bottle Label**	**NMR Results**
1	4.20	4.71
2	2.80	2.40
3	3.37	1.99
4	3.17	2.30
5	3.21	3.36
6	2.39	2.27
7	3.11	3.64
8	3.37	3.61
9	2.57	2.86

It is interesting to note that sample 9, with an ω-6:ω-3 ratio of 2.86, was sold at 80 €/L, whereas sample 5, with a 3.36 ratio value, was sold at 26 €/L, a much more affordable price.

Regarding the content of minor compounds, the β-sitosterol amount ranged from 0.15% (sample 8) to 0.33% and 0.45% (samples 6 and 5, respectively).

The content of *trans* 2-hexanal and hexanal was generally low in all the samples (between 0 and 0.5%). However, sample 1 showed the highest content of hexanal (0.34%) and *trans*-2-hexenal (0.17%).

3.4. Evaluation of Oxidation Susceptibility

In order to evaluate the susceptibility of hemp seed oils to lipid peroxidation, the samples were subjected to different temperatures of storage and to a specific light exposure condition under laboratory testing [7,47]. The results showed peculiar stability profiles of the oils with respect to linoleic acid, used as reference. Lipoperoxidation of hemp seed oils was not significantly increased over 24 h of incubation time, since the susceptibility to lipid peroxidation after 48 and 72 h was the same as of 24 h (Figure 4). Differences among the percentage of lipoperoxidation were estimated at time zero and after 24 h of exposure of the samples to different storage conditions (Table 5).

Table 5. Lipoperoxidation (%) of linoleic acid, used as standard, and the hemp seed oils 1–9 under different storage conditions.

	Lipoperoxidation (%)				
	RT *	**RT/light**	**+4 °C**	**−20 °C**	**+60 °C**
Linoleic acid					
t_0	40.1 ± 0.3	61.3 ± 1.1 ***	41.8 ± 0.8	37.3 ± 0.4	54.2 ± 0.3 **
t_{24}	76.6 ± 1.0 §§§	96.6 ± 0.8 ***§§	76.6 ± 1.0 §§§	69.1 ± 1.3 *§§	77.0 ± 0.3 §§
1					
t_0	27.4 ± 0.4	88.0 ± 2.4 ***	25.9 ± 1.2	21.5 ± 0.1 *	41.8 ± 1.9 ***
t_{24}	21.7 ± 0.5	98.2 ± 0.5 ***§	21.2 ± 1.1	19.5 ± 0.3 *	23.7 ± 1.4
2					
t_0	16.6 ± 0.3	26.1 ± 1.1 **	16.5 ± 0.3	17.1 ± 0.3	17.4 ± 0.5
t_{24}	48.9 ± 0.7 §§§	56.0 ± 3.1 *§§§	49.3 ± 0.4 §§§	48.4 ± 2.2 §§§	50.8 ± 4.6 §§§
3					
t_0	34.5 ± 1.1	37.8 ± 1.0	34.6 ± 0.7	26.4 ± 1.4	32.4 ± 0.8
t_{24}	25.6 ± 1.3	29.6 ± 1.3	24.5 ± 0.2	24.0 ± 2.3	24.7 ± 0.2
4					
t_0	37.6 ± 0.9	49.2 ± 1.1 *	31.8 ± 0.5	33.4 ± 2.4 *	28.5 ± 0.2
t_{24}	24.2 ± 0.3	32.8 ± 1.6 *	23.9 ± 0.4	21.9 ± 3.4	24.9 ± 0.3
5					
t_0	25.6 ± 0.1	40.4 ± 1.0 ***	25.8 ± 0.8	26.4 ± 3.4	26.5 ± 0.3
t_{24}	21.9 ± 1.2	23.2 ± 0.6	21.1 ± 1.1	20.8 ± 2.4	21.0 ± 0.4
6					
t_0	18.7 ± 0.3	29.6 ± 0.5 **	21.9 ± 0.3 *	16.5 ± 0.2 *	18.7 ± 0.2
t_{24}	54.2 ± 1.6 §§§	53.8 ± 0.7 §§§	55.7 ± 0.1 §§§	53.8 ± 0.5 §§§	49.7 ± 4.4 §§§
7					
t_0	15.9 ± 0.4	22.7 ± 0.2 **	16.8 ± 0.1	15.6 ± 0.2	16.4 ± 0.3
t_{24}	51.0 ± 0.6 §§§	48.9 ± 1.4 §§§	49.3 ± 0.4 §§§	45.8 ± 0.1 §§§	47.6 ± 3.1 §§§
8					
t_0	14.4 ± 0.4	20.4 ± 0.1 **	13.2 ± 0.5	13.6 ± 0.3	14.5 ± 0.5
t_{24}	48.6 ± 0.8 §§§	46.4 ± 1.3 §§§	45.8 ± 1.1 §§§	47.1 ± 0.6 §§§	46.7 ± 0.6 §§§
9					
t_0	28.3 ± 0.5	34.7 ± 0.4 *	26.4 ± 0.4	22.7 ± 0.4	22.5 ± 0.3
t_{24}	21.6 ± 0.7	24.2 ± 1.6 *	21.0 ± 0.3	21.2 ± 0.2	21.5 ± 0.7

* RT: room temperature; RT/light: room temperature with direct exposure to light; +4 °C: cold temperature; −20 °C: ultra-frost temperature; + 60 °C: warm temperature. * $p < 0.05$, ** $p < 0.01$ and *** $p < 0.001$ denote a statistically significant difference with respect to RT (ANOVA followed by Dunnet's Multiple Comparison Post Test). § $p < 0.05$, §§ $p < 0.01$, §§§ $p < 0.001$ denote a statistically significant increase with respect to time zero under the same storage conditions (ANOVA followed by Dunnet's Multiple Comparison Post Test).

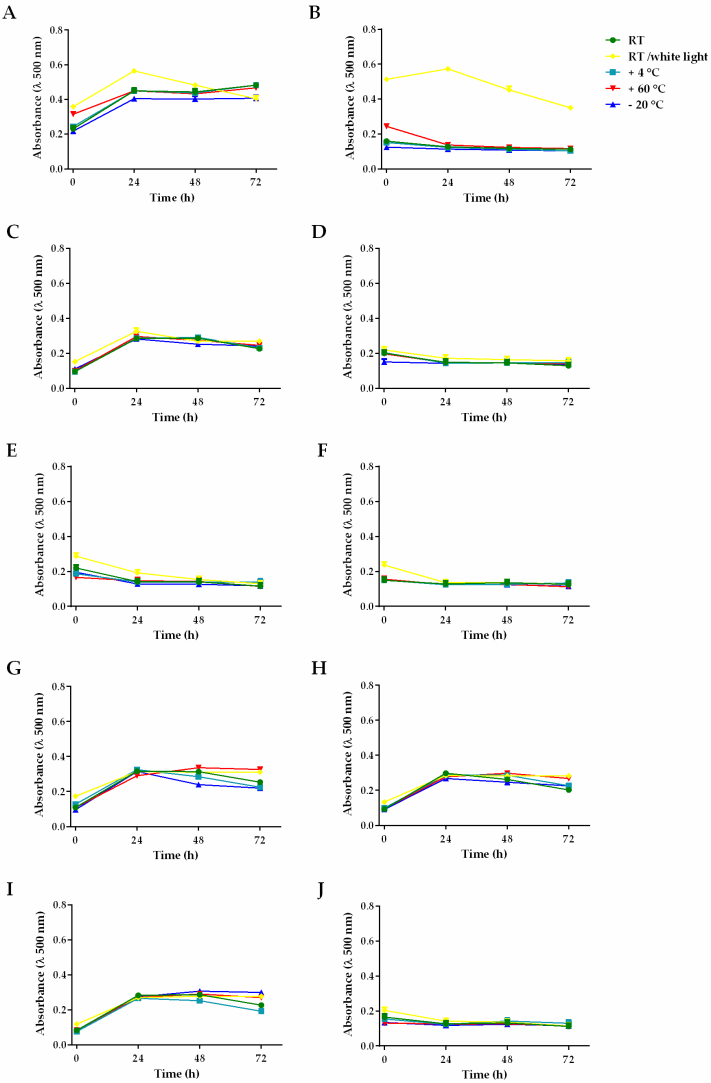


Figure 4. Absorbance (λ 500 nm) of lipoperoxides produced in different hemp seed oils, with respect to linoleic acid (**A**) under multiple storage conditions and incubation times (t = 0, 24, 48, and 72 h). Hemp seed oils: (**B**) 1, (**C**) 2, (**D**) 3, (**E**) 4, (**F**) 5, (**G**) 6, (**H**) 7, (**I**) 8, (**J**) 9.

Linoleic acid displayed a very low stability, being significantly oxidized under all storage conditions (Figure 4A): the maximum percentage of peroxidation was achieved after 24 h incubation at RT/light (about 2.4-fold higher than RT at time zero), followed by storage at 60 °C warm temperature

(1.5-fold higher than the RT oxidation at time zero). Conversely, an oxidation reduction (almost twofold, compared to RT oxidation at time zero) occurred under ultra-frost temperature (−20 °C).

Sample 1 exhibited a high stability under almost all the experimental conditions, except for RT/light, wherein it resulted in being strongly oxidized already at time zero (Figure 4B), with about a 3.3- and 4.5-fold peroxidation increase, compared to the RT oxidation at time zero and after 24 h, respectively. Moreover, after warm storage (60 °C), it showed about a twofold increase in oxidation with respect to RT at time zero, although the basal level was recovered during incubation (Figure 4B). Conversely, the ultra-frost temperature (−20 °C) weakly (about 1.2-fold) affected the basal oxidation of sample 1.

The other commercial hemp seed oils displayed a different behavior compared to sample 1. Samples 3, 4, 5, and 9 were only slightly affected by storage at warm and cold temperatures, or by light, at all incubation times (Figure 4D–F,L).

Regarding the hemp seed oils 4, 5, and 9, the storage at RT/light induced a weak but significant lipoperoxidation increase (1.3–1.6-fold), compared RT at time zero, which progressively disappeared during incubation time. Conversely, sample 3 turned out to be stable, also, to light exposure.

On the basis of this evidence, hemp seed oils appear to be stable under the tested storage conditions, although the direct exposure to light should be considered with caution, because of the higher susceptibility of some samples to oxidation, likely due to a high content of polyunsaturated fatty acids or to the presence of antioxidant constituents. Further studies could clarify this issue.

4. Conclusions

In this paper, nine commercial hemp seed oils were analyzed, by both targeted and untargeted analyses, to determine their chemical composition and, therefore, to obtain information regarding the quality of the products present in the markets. The results show a great variability between the samples. Applying the parameters used for EVOO, the quality was poor in above 50% of the samples, as showed by A%, P.N., and ω-6:ω-3 ratio, although price was very high. Lipoperoxidation assay confirmed that storage conditions can affect the shelf life of the product, however, the quality, in terms of healthy properties, should be assured at least until the expiration date. It is well established that several parameters (cultivars, pedoclimatic conditions, and agronomical practices) do affect the chemical composition and sensorial features of foodstuffs, however, the great variability of data obtained on the commercial hemp seed oil matrix highlights the urgent need to find reference parameters that define the quality of this product. Moreover, although in some European countries hemp seed oil has been a product on the market for years, in other countries, such as Italy, hemp seed oil can be considered a young product, with no history of production.

These results, together with other data recently reported on hemp oils [7], can constitute the starting point for development, and drawing up, of harmonized guidelines with suitable quality and safety parameters specific for hemp seed oils. Furthermore, these studies might drive producers to standardize procedures of hemp seed oil production, guaranteeing the achievement of a good food objective, consumer safety, and the further expansion of the hemp food industry.

Author Contributions: L.M. (Luisa Mannina) and G.V.; methodology: A.P.S., A.D.S., S.D.G., A.M.G., S.C. (Salvatore Ciano), S.C. (Simone Carradori), M.R., S.C. (Stefania Cesa), and C.I.; validation: M.S. and G.D.M.; formal analysis: M.R. and S.C. (Salvatore Ciano); investigation: A.P.S., C.I., A.D.S., S.C. (Salvatore Ciano), L.M. (Luigi Menghini), and G.V.; data curation: A.P.S., C.I., A.D.S., S.C. (Stefania Cesa), A.M.G., and G.V.; writing—original draft preparation: G.V.; writing—review and editing: G.V. and L.M. (Luisa Mannina); visualization: M.S., G.D.M., A.D.S., S.C. (Salvatore Ciano), S.C. (Simone Carradori), and G.V.; supervision: L.M. (Luisa Mannina) and G.V., project administration and funding acquisition: L.M. (Luisa Mannina). All authors have read and agreed to the published version of the manuscript.

Funding: This work has been realized with funds received from the following agencies: Italian Ministry of Education, Universities and Research—Dipartimenti di Eccellenza—L. 232/2016; Regione Lazio, "LACanapa" Project (Progetto di Ricerca, finanziato ai sensi della L.R. 13/08 -Protocol 85-2017-15069 CUP: B86C18000730002).

Acknowledgments: This work is part of a project supported by Lazio Region entitled "La Canapa industriale: sviluppo e valorizzazione di una nuova filiera agroalimentare ecosostenibile".

Conflicts of Interest: The authors declare no conflict of interest.

References

1. TNI. The UN Drug Control Conventions. Available online: https://www.tni.org/en/publication/the-un-drug-control-conventions#box3 (accessed on 6 September 2020).
2. European Commission. EU Plant Variety Database. Available online: https://ec.europa.eu/food/plant/plant_propagation_material/plant_variety_catalogues_databases/search/public/index.cfm?event=SearchVariety&ctl_type=A&species_id=240&variety_name=&listed_in=0&show_current=on&show_deleted= (accessed on 6 September 2020).
3. Ministero della Salute. *Produzione e Commercializzazione di Prodotti a Base di Semi di Canapa Per L'utilizzo nci Settori Dell'alimentazione Umana*; Ministero della Salute: Roma, Italy, 2009; pp. 1–4.
4. Jang, E.; Kim, H.; Jang, S.; Lee, J.; Baeck, S.; In, S.; Kim, E.; Kim, Y.; Han, E. Concentrations of THC, CBD, and CBN in commercial hemp seeds and hempseed oil sold in Korea. *Forensic Sci. Int.* **2020**, *306*, 110064. [CrossRef] [PubMed]
5. Farinon, B.; Molinari, R.; Costantini, L.; Merendino, N. The seed of industrial hemp (*Cannabis sativa* L.): Nutritional Quality and Potential Functionality for Human Health and Nutrition. *Nutrients* **2020**, *12*, 1935. [CrossRef] [PubMed]
6. Xu, Y.; Li, J.; Zhao, J.; Wang, W.; Griffin, J.; Li, Y.; Bean, S.; Tilley, M.; Wang, D. Hempseed as A Nutritious and Healthy Human Food or Animal Feed Source: A Review. *Int. J. Food Sci. Technol.* **2020**, 14755. [CrossRef]
7. Izzo, L.; Pacifico, S.; Piccolella, S.; Castaldo, L.; Narváez, A.; Grosso, M.; Ritieni, A. Chemical Analysis of Minor Bioactive Components and Cannabidiolic Acid in Commercial Hemp Seed Oil. *Molecules* **2020**, *25*, 3710. [CrossRef] [PubMed]
8. Smeriglio, A.; Galati, E.M.; Monforte, M.T.; Lanuzza, F.; D'Angelo, V.; Circosta, C. Polyphenolic Compounds and Antioxidant Activity of Cold-Pressed Seed Oil from Finola Cultivar of *Cannabis sativa* L. *Phytother. Res.* **2016**, *30*, 1298–1307. [CrossRef]
9. Crescente, G.; Piccolella, S.; Esposito, A.; Scognamiglio, M.; Fiorentino, A.; Pacifico, S. Chemical composition and nutraceutical properties of hempseed: An ancient food with actual functional value. *Phytochem. Rev.* **2018**, *17*, 733–749. [CrossRef]
10. Pojić, M.; Mišan, A.; Sakač, M.; Hadnađev, T.D.; Šarić, B.; Milovanović, I.; Hadnađev, M. Characterization of Byproducts Originating from Hemp Oil Processing. *J. Agric. Food Chem.* **2014**, *62*, 12436–12442. [CrossRef]
11. Ustun-Argon, Z. Phenolic Compounds, Antioxidant Activity and Fatty Acid Compositions of Commercial Cold-Pressed Hemp Seed (*Cannabis Sativa* L.) Oils from Turkey. *Int. J. Sci. Eng. Res.* **2019**, *10*, 166–173.
12. Callaway, J.; Schwab, U.; Harvima, I.; Halonen, P.; Mykkänen, O.; Hyvönen, P.; Järvinen, T. Efficacy of dietary hempseed oil in patients with atopic dermatitis. *J. Dermatol. Treat.* **2005**, *16*, 87–94. [CrossRef]
13. Rodriguez-Leyva, D.; Pierce, G.N. The cardiac and haemostatic effects of dietary hempseed. *Nutr. Metab.* **2010**, *7*, 32. [CrossRef]
14. Ghirga, F.; Quaglio, D.; Ghirga, P.; Berardozzi, S.; Zappia, G.; Botta, B.; Mori, M.; D'Acquarica, I. Occurrence of Enantioselectivity in Nature: The Case of (S)-Norcoclaurine. *Chirality* **2016**, *28*, 169–180. [CrossRef] [PubMed]
15. Carus, M.; Karst, S.; Kauffmann, A. *The European Hemp Industry: Cultivation, Processing and Applications for Fibres, Shivs and Seeds*; European Industrial Hemp Assocaition: Hürth, Germany, 2016.
16. Skoczinski, P.; Carus, M.; Grotenhermen, F.; Beitzke, B.; Kruse, D. *Limit and Guideline Values for THC (Tetrahydrocannabinol) in Hemp Foods*; European Industrial Hemp Assocaition: Hürth, Germany, 2019.
17. Ministero della Salute. *DECRETO 4 Novembre 2019 Definizione di Livelli Massimi di Tetraidrocannabinolo (THC) Negli Alimenti*; Ministero della Salute: Roma, Italy, 2019; pp. 1–5.
18. Berardozzi, S.; Bernardi, F.; Infante, P.; Ingallina, C.; Toscano, S.; De Paolis, E.; Alfonsi, R.; Caimano, M.; Botta, B.; Mori, M.; et al. Synergistic inhibition of the Hedgehog pathway by newly designed Smo and Gli antagonists bearing the isoflavone scaffold. *Eur. J. Med. Chem.* **2018**, *156*, 554–562. [CrossRef] [PubMed]
19. Di Marco Pisciottano, I.; Guadagnuolo, G.; Soprano, V.; De Crescenzo, M.; Gallo, P. A rapid method to determine nine natural cannabinoids in beverages and food derived from Cannabis sativa by liquid chromatography coupled to tandem mass spectrometry on a QTRAP 4000. *Rapid Commun. Mass Spectrom.* **2018**, *32*, 1728–1736. [CrossRef] [PubMed]

20. Meng, Q.; Buchanan, B.; Zuccolo, J.; Poulin, M.-M.; Gabriele, J.; Baranowski, D.C. A reliable and validated LC-MS/MS method for the simultaneous quantification of 4 cannabinoids in 40 consumer products. *PLoS ONE* **2018**, *13*, e0196396. [CrossRef]
21. Christinat, N.; Savoy, M.-C.; Mottier, P. Development, validation and application of a LC-MS/MS method for quantification of 15 cannabinoids in food. *Food Chem.* **2020**, *318*, 126469. [CrossRef]
22. Citti, C.; Linciano, P.; Panseri, S.; Vezzalini, F.; Forni, F.; Vandelli, M.A.; Cannazza, G. Cannabinoid Profiling of Hemp Seed Oil by Liquid Chromatography Coupled to High-Resolution Mass Spectrometry. *Front. Plant Sci.* **2019**, *10*, 120. [CrossRef]
23. Anwar, F.; Latif, S.; Ashraf, M. Analytical characterization of hemp (*Cannabis sativa*) seed oil from different agro-ecological zones of Pakistan. *J. Am. Oil Chem. Soc.* **2006**, *83*, 323–329. [CrossRef]
24. Chen, T.; He, J.; Zhang, J.; Zhang, H.; Qian, P.; Hao, J.; Li, L. Analytical Characterization of Hempseed (Seed of *Cannabis sativa* L.) Oil from Eight Regions in China. *J. Diet. Suppl.* **2010**, *7*, 117–129. [CrossRef]
25. Dimić, E.; Romanić, R.; Vujasinović, V. Essential fatty acids, nutritive value and oxidative stability of cold pressed hempseed (*Cannabis sativa* L.) oil from different varieties. *Acta Aliment.* **2009**, *38*, 229–236. [CrossRef]
26. Abdollahi, M.; Sefidkon, F.; Calagari, M.; Mousavi, A.; Mahomoodally, M.F. A comparative study of seed yield and oil composition of four cultivars of Hemp (Cannabis sativa L.) grown from three regions in northern Iran. *Ind. Crop. Prod.* **2020**, *152*, 112397. [CrossRef]
27. Devi, V.; Khanam, S. Optimization of the Ratio of ω-6 Linoleic and ω-3 α-Linolenic Fatty Acids of Hemp Seed Oil with Jackknife and Bootstrap Resampling. *Chem. Prod. Process. Model.* **2019**, *15*. [CrossRef]
28. Da Porto, C.; Decorti, D.; Tubaro, F. Fatty acid composition and oxidation stability of hemp (*Cannabis sativa* L.) seed oil extracted by supercritical carbon dioxide. *Ind. Crop. Prod.* **2012**, *36*, 401–404. [CrossRef]
29. European Parliament and Council. Regulation (EC) No 178/2002 Reguarding the General Principles and Requirements of Food Law, Establishing the European Food Safety Authority and Laying down Procedures in Matters of Food Safety. *Off. J.* **2002**, *31*.
30. Mannina, L.; Sobolev, A.P.; Viel, S. Liquid state 1H high field NMR in food analysis. *Prog. Nucl. Magn. Reson. Spectrosc.* **2012**, *66*, 1–39. [CrossRef]
31. Mannina, L.; D'Imperio, M.; Gobbino, M.; D'Amico, I.; Casini, A.; Emanuele, M.C.; Sobolev, A.P. Nuclear magnetic resonance study of flavoured olive oils. *Flavour Fragr. J.* **2012**, *27*, 250–259. [CrossRef]
32. Rapa, M.; Ciano, S.; Rocchi, A.; D'Ascenzo, F.; Ruggieri, R.; Vinci, G. Hempseed Oil Quality Parameters: Optimization of Sustainable Methods by Miniaturization. *Sustainability* **2019**, *11*, 3104. [CrossRef]
33. European Commission. COMMISSION DELEGATED REGULATION (EU) 2015/1830 of 8 July 2015 amending Regulation (EEC) No 2568/91 on the characteristics of olive oil and olive-residue oil and on the relevant methods of analysis. *Off. J.* **2015**, *L266*, 9–13.
34. British Standards Institution Animal and Vegetable Fats and Oils. Determination of Anisidine Value. Available online: https://www.iso.org/standard/40052.html (accessed on 6 September 2020).
35. Patsilinakos, A.; Ragno, R.; Carradori, S.; Petralito, S.; Cesa, S. Carotenoid content of Goji berries: CIELAB, HPLC-DAD analyses and quantitative correlation. *Food Chem.* **2018**, *268*, 49–56. [CrossRef]
36. Cairone, F.; Carradori, S.; Locatelli, M.; Casadei, M.A.; Cesa, S. Reflectance colorimetry: A mirror for food quality—A mini review. *Eur. Food Res. Technol.* **2020**, *246*, 259–272. [CrossRef]
37. Ingallina, C.; Sobolev, A.P.; Circi, S.; Spano, M.; Giusti, A.M.; Mannina, L. New Hybrid Tomato Cultivars: An NMR-Based Chemical Characterization. *Appl. Sci.* **2020**, *10*, 1887. [CrossRef]
38. Di Sotto, A.; Di Giacomo, S.; Toniolo, C.; Nicoletti, M.; Mazzanti, G. *Sisymbrium Officinale* (L.) Scop. and its Polyphenolic Fractions Inhibit the Mutagenicity of Tert-Butylhydroperoxide in *Escherichia Coli* WP2 uvr AR Strain. *Phytother. Res.* **2016**, *30*, 829–834. [CrossRef] [PubMed]
39. European Directorate for the Quality of Medicines & HealthCare. *Council of Europe European Pharmacopoeia*, 9th ed.; European Directorate for the Quality of Medicines & HealthCare: Strasbourg, France, 2016.
40. Teh, S.-S.; Birch, J. Physicochemical and quality characteristics of cold-pressed hemp, flax and canola seed oils. *J. Food Compos. Anal.* **2013**, *30*, 26–31. [CrossRef]
41. Lutterodt, H.; Luther, M.; Slavin, M.; Yin, J.-J.; Parry, J.; Gao, J.-M.; Yu, L. Fatty acid profile, thymoquinone content, oxidative stability, and antioxidant properties of cold-pressed black cumin seed oils. *LWT Food Sci. Technol.* **2010**, *43*, 1409–1413. [CrossRef]
42. Borhade, S.S. Chemical Composition and Characterization of Hemp (*Cannabis sativa*) Seed oil and essential fatty acids by HPLC Method. *Arch. Appl. Sci. Res.* **2013**, *5*, 5–8.

43. Rezvankhah, A.; Emam-Djomeh, Z.; Safari, M.; Askari, G.; Salami, M. Microwave-assisted extraction of hempseed oil: Studying and comparing of fatty acid composition, antioxidant activity, physiochemical and thermal properties with Soxhlet extraction. *J. Food Sci. Technol.* **2019**, *56*, 4198–4210. [CrossRef]
44. Oomah, B.D.; Busson, M.; Godfrey, D.V.; Drover, J.C. Characteristics of hemp (*Cannabis sativa* L.) seed oil. *Food Chem.* **2002**, *76*, 33–43. [CrossRef]
45. Da Porto, C.; Decorti, D.; Natolino, A. Potential Oil Yield, Fatty Acid Composition, and Oxidation Stability of the Hempseed Oil from FourCannabis sativaL. Cultivars. *J. Diet. Suppl.* **2015**, *12*, 1–10. [CrossRef]
46. Cesa, S.; Sisto, F.; Zengin, G.; Scaccabarozzi, D.; Kokolakis, A.K.; Scaltrito, M.M.; Grande, R.; Locatelli, M.; Cacciagrano, F.; Angiolella, L.; et al. Phytochemical analyses and pharmacological screening of Neem oil. *S. Afr. J. Bot.* **2019**, *120*, 331–337. [CrossRef]
47. Singh, A.P.; Fathordoobady, F.; Guo, Y.; Singh, A.; Kitts, D.D. Antioxidants help favorably regulate the kinetics of lipid peroxidation, polyunsaturated fatty acids degradation and acidic cannabinoids decarboxylation in hempseed oil. *Sci. Rep.* **2020**, *10*, 1–12. [CrossRef]



© 2020 by the authors. Licensee MDPI, Basel, Switzerland. This article is an open access article distributed under the terms and conditions of the Creative Commons Attribution (CC BY) license (http://creativecommons.org/licenses/by/4.0/).

7.6. Case study 5: Metabolomic characterization of *Gentian Lutea* L.: analysis of the distribution of metabolites from root to leaves and flowers

An NMR based metabolomic characterization of roots, leaves and flowers of *Gentiana Lutea L.* harvested in the "Majella National Park" (Central Italy) was carried out. *Gentiana Lutea* L. is a perennial herb of 50-120 cm with an erect stem, broad lanceolate to elliptic leaves of 10–30 cm long and 4–12 cm broad and a characteristic yellow flower, diffused in the mountain of Central and Southern Europe. Unfortunately, due to the Gentiana roots massive collection along century there is a depletion of the natural population. The Gentiana roots are largely used in the world as source of many bioactive compounds with interesting pharmacological effects, reported also in the Chinese, Japanese and European Pharmacopeias and also to prepare some bitter beverages.

In this scenario, it is of interest the study of the chemical profile of the Italian wild *Gentiana Lutea* L., in order to valorize the different plant parts (roots, leaves and

flowers) and to find an utilization for the aerial plant parts. For this purpose, the high field NMR spectroscopy has been applied for the first time to study the Blight-Dyer hydroalcoholic and organic extracts obtaining the whole chemical profile (sugars, amino acids, organic acids, fatty chains and sterols). The amount of these iridoids, secoiridoids and xanthones, the most studied Gentiana bioactive compounds, were also determined by the HPLC-DAD technique. Moreover a comparison among the *Gentiana Lutea* and *Gentiana Dinarica* (another species of the *Gentiana* genus of 8-10 cm with broadly elliptical leaves and only one large deep blue trumpet-shaped flower diffused in Southern-West Jugoslavia, Albania and in Central Italy) leaves and their possible applications are also reported.

Introduction

Gentiana Lutea L. is a well-known plant for its use in bitters beverages preparation (Khan & Abourashed, 2010). Gentiana Lutea L. is a perennial herb, of the Gentianacee family, of 50-120 cm with an erect stem, broad lanceolate to elliptic leaves of 10–30 cm long and 4–12 cm broad and a characteristic yellow flower, diffused in the mountain of Central and Southern Europe(Aiello et al., 2013; Tutin et al., 1972; Venditti et al., 2013). *Gentiana Dinarica* G. Beck is another species of the Gentiana genus of 8-10 cm with broadly elliptical leaves and only one large deep blue trumpet-shaped flower, diffused in Southern-West Jugoslavia, Albania and in Central Italy (Abruzzo Region) (Tutin et al., 1972; Venditti et al., 2013). The wild *Gentiana Lutea* L. from Italian National parks were already studied in previous works. The iridoid profile of Gentiana Lutea L. seeds from "Majella National Park" was determine by ethanol extraction, chromatographic separation and NMR analysis of the isolated compounds obtaining the identification of four iridoid compounds: sweroside, gentiopicroside, loganic acid and trifloroside (Bianco et al., 2003). The iridoids, secoiridoids and xanthones profile of *Gentiana Lutea* L. wild roots of "Monti Sibillini National Park" was determine by HPLC method finding gentiopicroside as most abundant compounds, followed by loganic acid, isogentisine, sweroside, swertiamarin and amarogentin (Mustafa et al., 2015).

On other hand, it is of interest the study of the chemical constituents distribution in the other part of the Italian wild Gentiana Lutea L. in order to find possible utilization of the aerial parts. The same issue was treated by Zeng et al. (Zeng et al., 2017) to characterize all the Salvia miltiorrhiz parts (roots, leaves, stems, and flowers) using Ultra-High Performance Liquid Chromatography-Triple Quadrupole Mass Spectrometer (UPLC-TQ-MS/MS) and High-Performance Liquid Chromatography coupled with Evaporative Light Scattering Detector (HPLC-ELSD) founding that not only the roots, used in the TCM, but also the plant aerial parts are rich in interesting bioactive compounds like phenolic acids and flavonoids. The same issue was also explored by Li et al. (Y. Li et al., 2019) for the chemical characterization of the Astragalus Membranaceus, used in the TCM, in order to find a rational utilization of the plant, carrying out an Ultra-Pressure Liquid Chromatography coupled with tandem Mass Spectrometry (UPLC-MS/MS) analysis of the various plant parts (root, rhizome, stem, leaf and flower). Regarding the target chemical characterization of the Gentiana species, the most studied bioactive compounds are the iridoids, secoiridoids and xanthones (Mustafa et al., 2015; Xu et al., 2017; Yang et al., 2010) through High-Performance Liquid Chromatography (HPLC) coupled with Diode Array Detector (DAD) (Aberham et al., 2011; Szucs et al., 2002) or Capillary Electrophoresis (CE) (Zhao et al., 2004). Other studies reports the Gentiana

species untargeted analysis realized by Mass Spectrometry (MS) coupled with Liquid Chromatography (LC) (Lv et al., 2018) or CE (Takahashi et al., 2012) for a comprehensive chemical characterization. The volatile profile by Gas Chromatography (GC) analysis was also determined (Lee et al., 2010; Mustafa et al., 2016). About the NMR methodologies there aren't available studies regarding the complete metabolomic characterization of this kind of matrices and its aerial parts. By now the NMR technique was huge utilized in the Gentiana investigation with three main aims: to elucidate the chemical structure of isolated compounds from the plants (Hou et al., 2020; W. Li et al., 2015; Wu et al., 2010), to make purity test of natural compounds like iridoids and secoiridoids (W. Li et al., 2015; Tanaka et al., 2014) and to quantify a targeted compound in a complex matrix like a crude drug extract (Tanaka et al., 2014). The NMR technique applied to the metabolomic filed is a powerful tool for a complete chemical characterization of a plant matrices with a quickly extraction and a single analysis (Ingallina et al., 2020; Spano et al., 2021)

In the present study, the complete metabolomic profile by NMR methodologies and the iridoids, secoiridoids and xanthones quantification by HPLC-DAD technique of the roots, leaves and flowers of wild *Gentiana Lutea* L. from Majella National Park of Central Italy were performed. Moreover a comparison among the *Gentiana Lutea* and *Gentiana Dinarica* leaves and their possible applications are also reported.

Material and methods

Gentiana plant material

The *Gentiana* plant parts were provided and harvested by "Parco Nazionale della Majella", an Italian National Park in the Apennine area, in Abruzzo Region, around the Majella massive, characterized by calcareous rocks with an altitude range from 130 m to 2793 m (of the highest mountain named Amaro Mountain) with more than 2300 different plant species including many autochthonous and endemic ones. The *Gentiana Lutea* L. roots and flowers and leaves were collected in July 2021. The *Gentiana Lutea* L. leaves were collected in July, August and September 2021. The *Gentiana Dinarica* L. leaves were collected in July, August and September 2021. In Figure 1 are reported the collected *Gentiana Lutea* parts. All the collected samples were stored at -20°C until the sample preparation.

Sample preparation

All the fresh Gentiana samples were freeze-dried by LyovaporTM L-200 (Buchi, Milan, Italy) at 0.200 mbar for 48 h and then grounded by IKA® A11 basic Analytical mill (IKA®-Werke GmbH & CO. KG, Staufen im Breisgau, Deutschland). The dry samples were stored at -20°C until extraction and analysis.



Figure 1. Photography of the collected Gentiana Lutea parts from "Parco Nazionale della Majella": A) root; B) shredded root; C) flowers; D) leaves.

Extraction procedure for HPLC-DAD analysis

For the HPLC-DAD analysis, the methanol extraction of iridoids, secoiridoids and xanthones from the Gentiana parts was performed following a previous reported method (doi:10.1016/j.jpba.2007.07.001) with some modifications in order to obtained a complete extractions of the compound of interest. Briefly, 0.1000 g of Gentiana dry roots, leaves or flowers was extracted with 3 mL of methanol (rate of 1:30 w/v) by 20 min of ultrasonic bath (DU-100 Digital Ultrasonic cleaner, ArgoLab, Carpi, MO, Italy) at room temperature. Then pellet and extract were separated by centrifugation at 7,000 rpm for 5 min and the supernatant was collected. All the extraction procedure was repeated two more times on the same pellet and the supernatants were collected together. Finally, the extracts were filtered through 0.45 μm PTFE syringe filter (Whatman, Kent, United Kingdom) and 10 μL injected in the HPLC-PDA system.

Extraction procedure for NMR analysis

The Bligh-Dyer protocol (Bligh, E.G. and Dyer, 1959), already applied at the NMR metabolomic field for food matrices extraction (Di Matteo et al., 2021), was optimize for the quantitative extraction of the hydroalcoholic and organic metabolites from the various parts of Gentiana plant. In detail, 0.5000 g of dry grounded root, leaf or flower were sequentially added with 0.8 mL of Millipore grade water and 3 mL of methanol/chloroform (2:1 % *v*/*v*) mixture to obtained the monophasic system methanol/chloroform/water (2:1:0.8 % *v*/*v*/*v*) for the extraction phase. The emulsion was sonicated at room temperature for 10 min to promote the extraction yield. Then the extract was sequentially added with 1 mL of chloroform and 1 mL of Millipore grade water to obtained the biphasic system methanol/chloroform/water (2:2:1.8 % *v*/*v*/*v*) for the separation phase. Finally, the hydroalcoholic phase, the upper one, was collected and the residue pellet was extracted again two more times in the same conditions described above. A slow N_2 flow was used for drying the obtained hydroalcoholic phases that were lastly stored at -20°C until analysis.

HPLC-DAD analysis of iridoids, secoiridoids and xanthones

The HPLC-DAD determination of iridoids, secoiridoids and xanthones in the methanol extract of Gentiana roots, leaves and flowers was performed according to a previous work with some modifications (Qi et al., 2017). A Shimadzu LC-40D (Shimadzu Italia srl, Milan, Italy) system equipped with autosampler, binary pump, column oven and a photodiode array (PDA) (Milan,

Italy) detector was used. 10 μL of samples (mix of commercial standards, methanol extract of Gentiana roots, leaves or flowers) were directly injected into a Shim-pack GIST C18 column (150 mm × 4.6 mm, 5 μm; Shimadzu, Milan, Italy) pre-heated at 30°C. The separation was performed employing a binary mobile phase consisting of 0.1 % formic acid (A) and acetonitrile (B), at 1.0 mL/min. The gradient program was set as follow: 0 min, 5% B; 0–5 min, 5-5% B; 5–30 min, 5-30 % B; 30–35 min, 30–80% B; 35–37 min, 80–80% B; 37–39 min, 80–100% B; 39–45 min, 100–100% B. Separations were monitored at 258 nm and the peaks were integrated using the LabSolutions software (version 6.106 SP1, Shimadzu, Milan, Italy). The signals of loganic acid, mangiferin, isogentisin, sweroside, swertiamarin, amarogentin and gentiopicroside (Figure 2) were identified comparing the retention time and UV spectrum with the corresponding commercial standards. Quantification was based on external standard method realizing a calibration curve with the commercial standards from 1 to 50 μg/mL with 7 points and from 0.1 to 1 μg/mL with 6 points. The resulted compound quantities were expressed as μg/g of DW ± SD. All the protocol from the extraction to the HPLC analysis was carried out in duplicate.

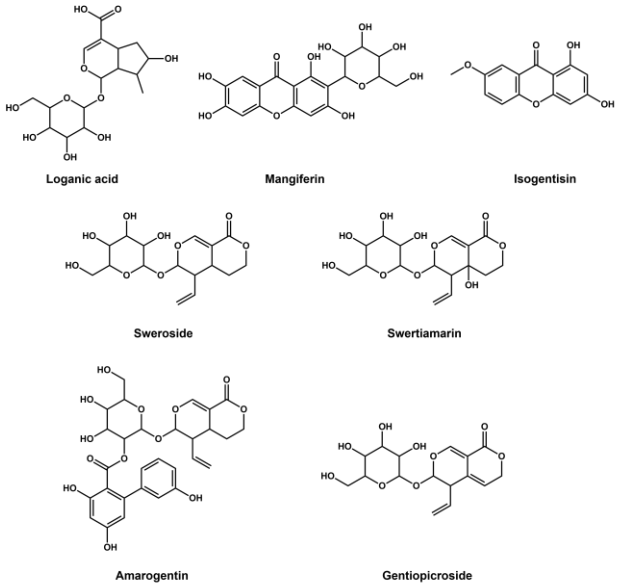


Figure 2. Chemical structures of the identified compounds in the chromatograms: one iridoid (loganic acid), four secoiridoids (sweroside, swertiamarin, amarogentin and gentiopicroside) and two xanthones (mangiferin, isogentisin).

Metabolic profile by NMR analysis

All the Gentiana parts Bligh-Dyer hydroalcoholic extracts were analyzed by the NMR methodologies. In particular, the Gentiana dried Bligh-Dyer hydroalcoholic phase was solubilized in 1 mL of 400 mM phosphate buffer/D_2O containing 2 mM 3-(trimethylsilyl)-propionic-2,2,3,3-d4 acid (TSP), as internal standard for quantitative measurements, and EDTA-d16, as complexing agent for metal ions. Then the solutions was centrifugated and 0.7 mL transferred in a 5 mm NMR tube. The NMR spectra were recorded at 25 °C on a JNM-ECZ 600R (JEOL Ltd, Tokyo, Japan) spectrometer operating at the proton frequency of 600.17 MHz equipped with an autosampler. The ^1H spectrum of the hydroalcoholic fraction was acquired using a presaturation pulse sequence to suppress water signal, a 90° pulse of 12.8 μs, 256 transients and 65 K data points. All the NMR spectra were processed using the JEOL Delta v5.3.1. software (JEOL Ltd, Tokyo, Japan). The ^1H NMR spectra were Fourier transformed, manually phased, automatically base corrected and referred to the internal standards: β-glucose CH-1 signal set at 4.66 ppm for the hydroalcoholic phase. 2D NMR experiments namely ^1H-^1H COSY, ^1H-^1H TOCSY,^1H-^{13}C HSQC and ^1H-^{13}C HMBC were performed for the hydroalcoholic Bligh-Dyer extracts using previous optimized parameters (Ullah et al., 2022). In order to absolute quantify the assigned metabolites in the hydroalcoholic phase, the integral of the corresponding selected ^1H resonances were measured with respect to the integral of TSP methyl group signal normalized to 100 and the quantitative results were expressed as mg/100g of dry weight (DW) ± SD (standard deviation). All the protocol from the extraction to the NMR analysis for both hydroalcoholic and organic phase was carried out in duplicate.

Results and discussion

HPLC-PDA analysis of iridoids, secoiridoids and xanthones distribution in Gentiana Lutea L. parts

First of all, the extraction and HPLC parameters were optimized starting from the article of (Aberham et al., 2007). Different solvents (methanol, ethanol), extraction methods (sonication at room temperature or at high temperature) and extraction time were evaluated. Finally the extraction was realized at room temperature to not degrade the secoiridoids compounds and three cycles of extraction were performed to achieve a complete extraction yield of the detected compounds. In Figure 3 is reported the bar charts of the quantified xanthones, iiridoids and secoiridoids by HPLC analysis of the methanol extract of radix, flowers and leaves of *Gentiana Lutea* L.

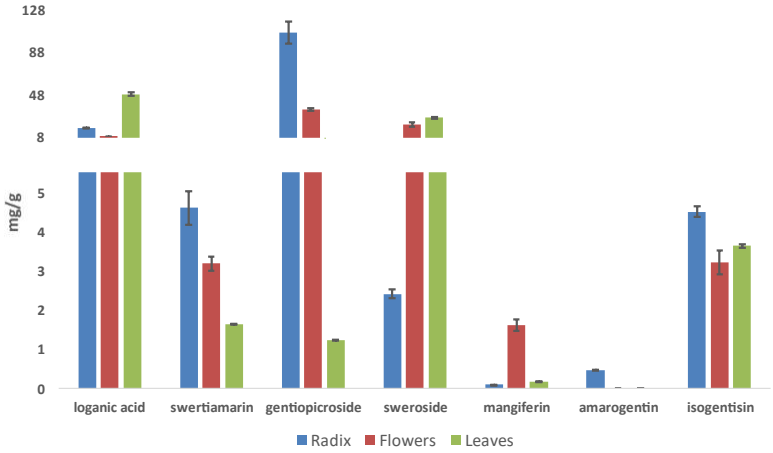


Figure 3. Bar charts of xanthones, iridoids and secoiridoids identified and quantified (mg/g of DW ± SD) in HPLC analysis of the methanol extract of radix, flowers and leaves of Gentiana Lutea L harvested in July 2021.

NMR metabolomic quantification of amino acids, organic acids and sugars distribution in Gentiana Lutea L. parts

First of all, the extraction and NMR parameters were optimized starting from our classical Bligh-Dyer extraction protocol adapted at food matrices (Di Matteo et al., 2021). Different combined solvents (methanol/chloroform/water or ethanol/ethyl acetate/water), extraction methods (sonicator or vortex) and extraction time were evaluated. Finally the extraction was realized with the sonicator and three cycles of extraction were performed to maximize the extraction yield.

This is the first NMR characterization of the Gentiana matrix. The identified metabolites by means of NMR spectroscopy were eleven amino acids (isoleucine, leucine, valine, threonine, alanine, GABA, glutamine, asparagine, tyrosine, phenylalanine, glutamine), seven organic acids (lactic acid, acetic acid, succinic acid, citric acid, malic acid, fumaric acid, formic acid), five sugars (fructose, sucrose, glucose, maltose, galactose) and uridine and choline. Moreover, loganic acid, sweroside and gentiopicroside were also assigned. In Figure 4-7 are reported the bar charts of the

quantified compounds by NMR analysis of the hydroalcoholic extract of radix, flowers and leaves of *Gentiana Lutea* L.

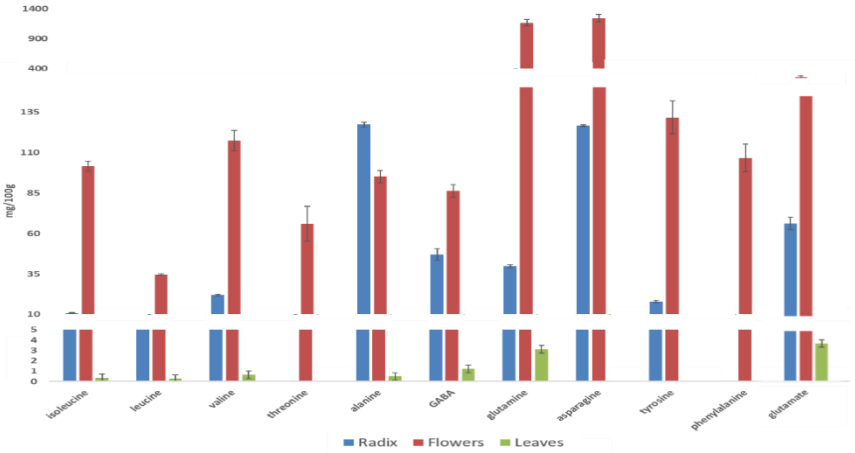


Figure 4. Bar charts of amino acids identified and quantified (mg/100g of DW ± SD) in ^{1}H NMR spectra of the hydroalcoholic extract of radix, flowers and leaves of Gentiana Lutea L harvested in July 2021.

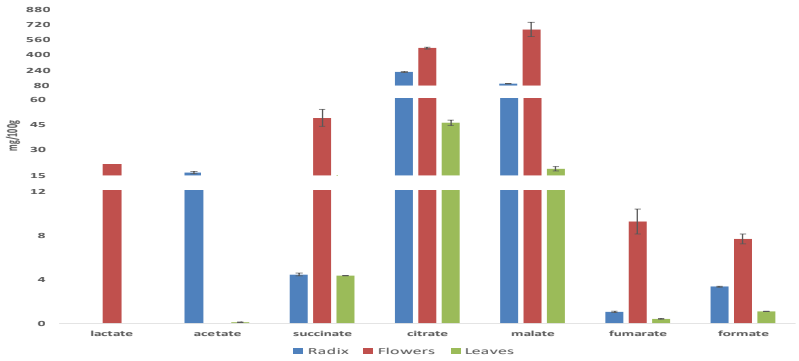


Figure 5. Bar charts of organic acids identified and quantified (mg/100g of DW ± SD) in ^{1}H NMR spectra of the hydroalcoholic extract of radix, flowers and leaves of Gentiana Lutea L harvested in July 2021.

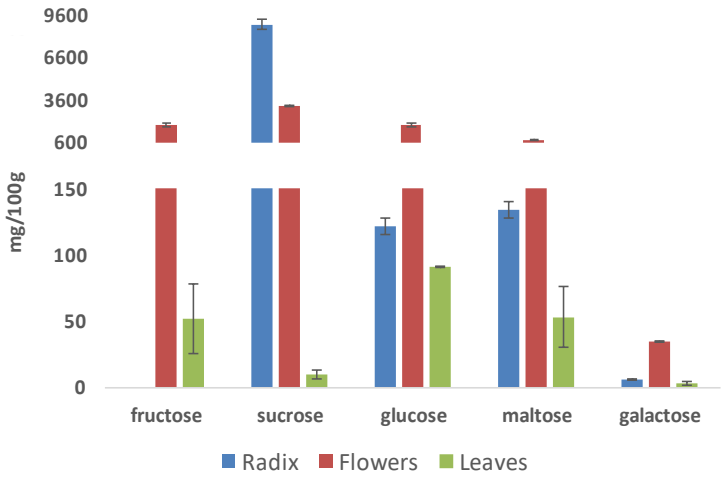


Figure 6. Bar charts of sugars identified and quantified (mg/100g of DW ± SD) in ^{1}H NMR spectra of the hydroalcoholic extract of radix, flowers and leaves of Gentiana Lutea L harvested in July 2021.

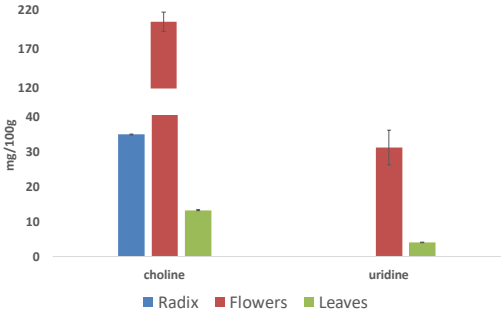


Figure 7. Bar charts of choline and uridine identified and quantified (mg/100g of DW ± SD) in ^{1}H NMR spectra of the hydroalcoholic extract of radix, flowers and leaves of Gentiana Lutea L harvested in July 2021.

Chemical composition of leaves of Gentiana Lutea L. and Gentiana Dinarica Beck collected at three harvesting stages

For the *Gentiana Lutea* L. leaves three harvesting stages were characterized and compared with the same collection of the leaves of *Gentiana Dinarica* Beck. In Figure 8-11 are reported the bar charts of the quantified compounds by NMR analysis of the hydroalcoholic extract of leaves of *Gentiana Lutea* L collected in three harvesting stage (July, August and September 2021). While, in Figure 12-15 are reported the bar charts of the quantified compounds by NMR analysis of the hydroalcoholic extract of leaves of *Gentiana Dinarica* Beck L collected in three harvesting stage (July, August and September 2021)

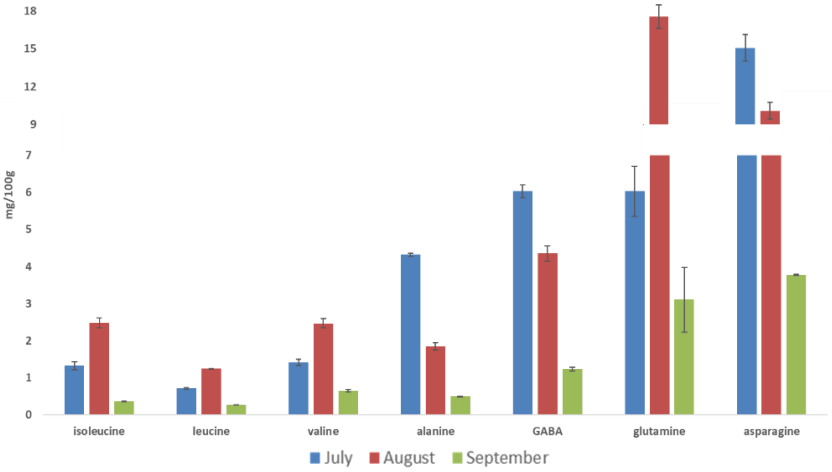


Figure 8. Bar charts of amino acids identified and quantified (mg/100g of DW ± SD) in ^{1}H NMR spectra of the hydroalcoholic extract of leaves of Gentiana Lutea L harvested in July, August and September 2021.

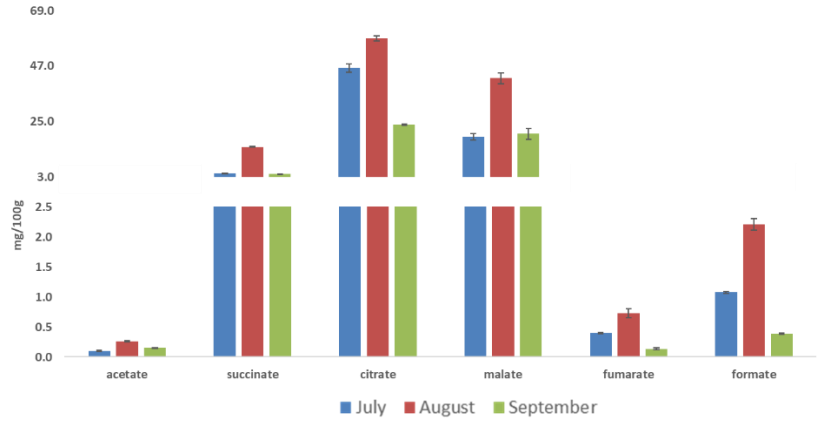


Figure 9. Bar charts of organic acids identified and quantified (mg/100g of DW ± SD) in ^{1}H NMR spectra of the hydroalcoholic extract of leaves of Gentiana Lutea L harvested in July, August and September 2021.

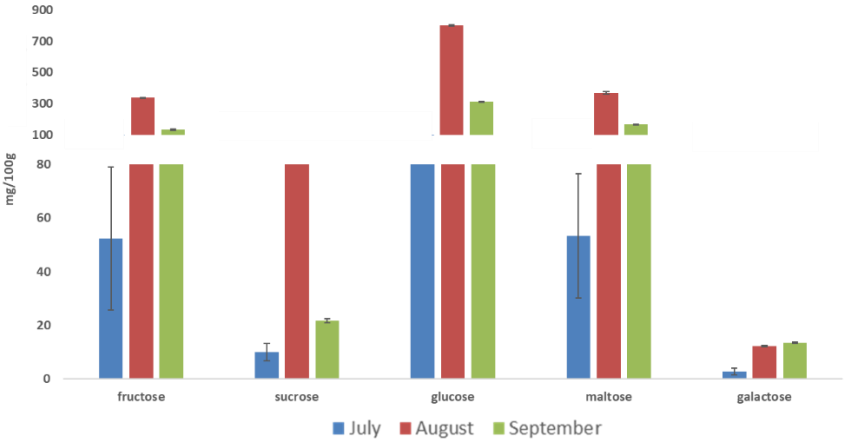


Figure 10. Bar charts of sugars identified and quantified (mg/100g of DW ± SD) in ^{1}H NMR spectra of the hydroalcoholic extract of leaves of Gentiana Lutea L harvested in July, August and September 2021.

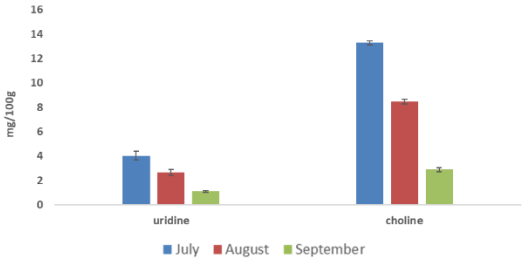


Figure 11. Bar charts of choline and uridine identified and quantified (mg/100g of DW ± SD) in ^{1}H NMR spectra of the hydroalcoholic extract of leaves of Gentiana Lutea L harvested in July, August and September 2021.

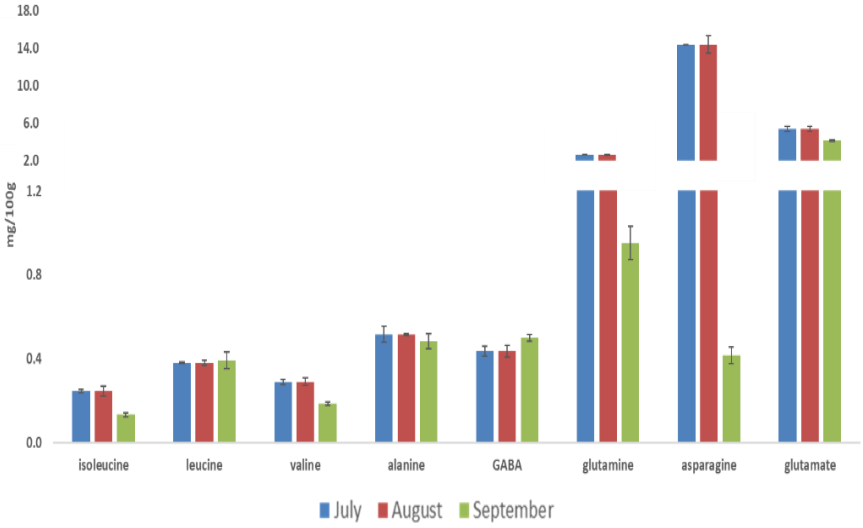


Figure 12. Bar charts of amino acids identified and quantified (mg/100g of DW ± SD) in ^{1}H NMR spectra of the hydroalcoholic extract of leaves of Gentiana Dinarica Beck harvested in July, August and September 2021.

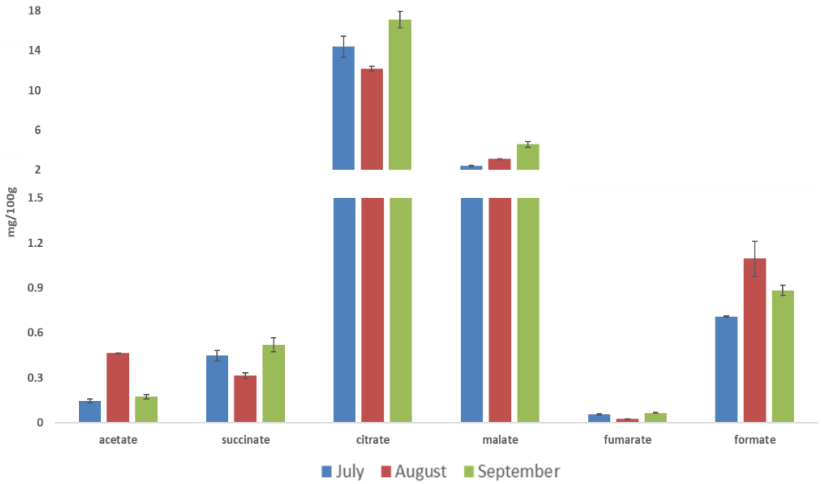


Figure 13. Bar charts of organic acids identified and quantified (mg/100g of DW ± SD) in ^{1}H NMR spectra of the hydroalcoholic extract of leaves of Gentiana Dinarica Beck harvested in July, August and September 2021.

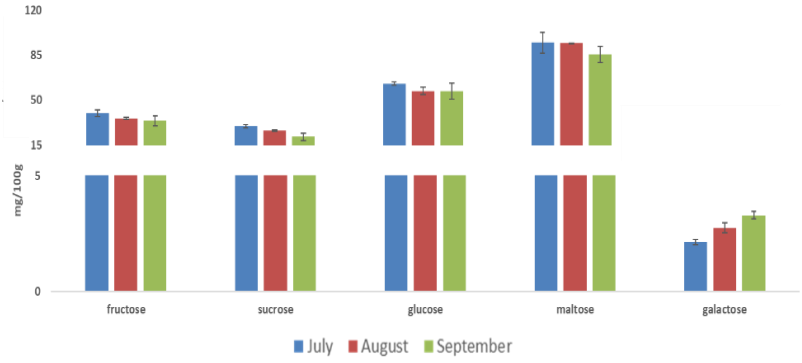


Figure 14. Bar charts of sugars identified and quantified (mg/100g of DW ± SD) in ^{1}H NMR spectra of the hydroalcoholic extract of leaves of Gentiana Dinarica Beck harvested in July, August and September 2021.

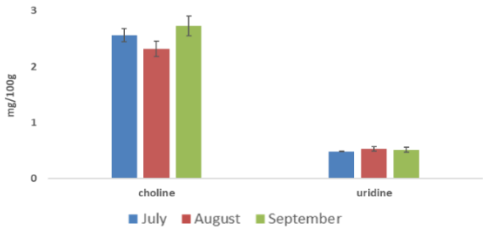


Figure 15. Bar charts of choline and uridine identified and quantified (mg/100g of DW ± SD) in ^{1}H NMR spectra of the hydroalcoholic extract of leaves of Gentiana Dinarica Beck harvested in July, August and September 2021.

A comparison of the quantified iridoids, secoiridoids and xanthones in *Gentiana Lutea* L. and *Gentiana Dinarica* Beck leaves collected in the three harvesting stages were provided in Figure 16.

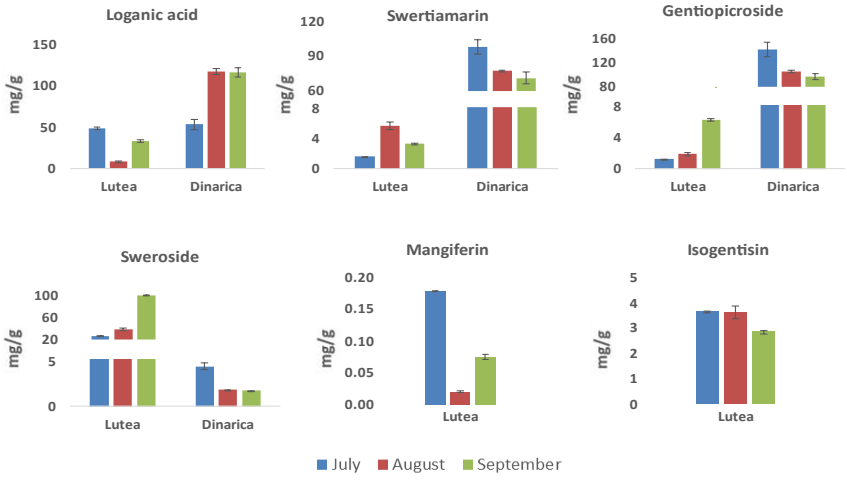


Figure 16. Bar charts comparison of loganic acids, swertiamarin, gentiopicroside and sweroside identified and quantified (mg/100g of DW ± SD) in HPLC analysis of the methanol extract of leaves of Gentiana Lutea L. and Gentiana Dinarica Beck harvested in July, August and September 2021. Mangiferin and Isogentisin were detected only in the Gentiana Lutea L. leaves.

PCA statistical analysis

The NMR and HPLC quantified metabolites were used as variables for the principal component analysis (PCA), Figure 17, by using MATLAB software (version R2020b). Before the analysis, the selected variables were processed using autoscaling and then mean centered. The first two PCs accounted for 86.5 % of the variability within the data.

PCs score plots showed a sample groping according to the type part of the Gentiana plant. In particular, regarding the iridoids, secoiridoids and xanthones contents, Gentiana Lutea L. radix was characterized by high levels of amarogentin, whereas Gentiana Lutea leaves by high levels of sweroside and the flowers by high amounts of mangiferin. The Gentiana Dinarica Beck leaves were characterize by the highest levels of loganic acid, swertiamarin and gentiopicroside. Regarding the other secondary metabolites quantified by NMR analysis, the radix presented the highest amounts of acetic acid and sucrose, whereas all the other metabolites were grouped around the flower samples of Gentiana, indicating the rich profile of the Gentiana flowers.

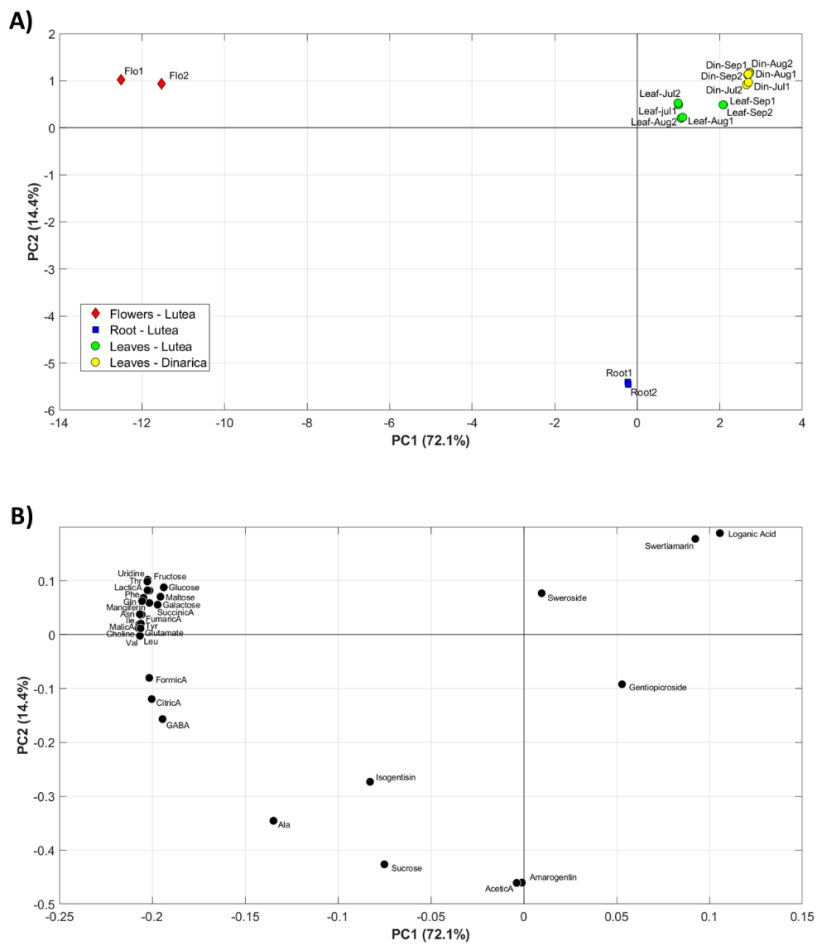


Figure 17. Principal components analysis (PCA) maps obtained using NMR and HPLC data of radix, leaves and flowers of Gentiana Lutea L. and leaves of Gentiana Dinarica Beck samples: (A) scores plot and (B) loadings plot relative to PC1 and PC2 (PCs). PC1 and PC2 represent 72.1% and 14.4%, of the total variance, respectively

Conclusion

Based on the realized chemical characterization of the *Gentiana Lutea* parts, it is possible to conclude that not only the roots are of interest but also the aerial part could have an application. Since the leaves of Gentiana show high amounts of some iridoids, secoiridoids and xanthones, they could be used for their isolation. While, as showed by the rich chemical abundance of secondary metabolites in the Gentiana flowers, it is possible to think about a food application as an ingredient for functional foods.

References

Aberham, A., Pieri, V., Croom, E. M., Ellmerer, E., & Stuppner, H. (2011). Analysis of iridoids, secoiridoids and xanthones in Centaurium erythraea, Frasera caroliniensis and Gentiana lutea using LC-MS and RP-HPLC. *Journal of Pharmaceutical and Biomedical Analysis*, *54*(3), 517–525. https://doi.org/10.1016/j.jpba.2010.09.030

Aberham, A., Schwaiger, S., Stuppner, H., & Ganzera, M. (2007). Quantitative analysis of iridoids, secoiridoids, xanthones and xanthone glycosides in Gentiana lutea L. roots by RP-HPLC and LC-MS. *Journal of Pharmaceutical and Biomedical Analysis*, *45*(3), 437–442. https://doi.org/10.1016/j.jpba.2007.07.001

Aiello, N., Bontempo, R., & Vender, C. (2013). L'utilisation de caractères morphologiques et de la teneur en amarogentine pour la caractèrisation de populations spontanées de gentiane jaune (Gentiana lutea L.) du Nord Est de l'Italie. *Acta Botanica Gallica*, *160*(1), 33–41. https://doi.org/10.1080/12538078.2013.772497

Bianco, A., Ramunno, A., & Melchioni, C. (2003). Iridoids from seeds of Gentiana lutea. *Natural Product Research*, *17*(4), 221–224. https://doi.org/10.1080/1057563021000040466

Bligh, E.G. and Dyer, W. J. (1959). A rapid method of total lipid extraction and purification. *Canadian Journal of Biochemistry and Physiology*, *37*(8).

Di Matteo, G., Spano, M., Esposito, C., Santarcangelo, C., Baldi, A., Daglia, M., Mannina, L., Ingallina, C., & Sobolev, A. P. (2021). NMR Characterization of Ten Apple Cultivars from the Piedmont Region. *Foods*, *10*(289). https://doi.org/https://doi.org/10.3390/foods10020289

Hou, S. B., Wang, X., Huang, R., Liu, H., Hu, H. M., Hu, W. Y., Lv, S. T., Zhao, H., & Chen, G. (2020). Seven new chemical constituents from the roots of Gentiana macrophylla pall. *Fitoterapia*, *141*(January), 104476. https://doi.org/10.1016/j.fitote.2020.104476

Ingallina, C., Sobolev, A. P., Circi, S., Spano, M., Fraschetti, C., Filippi, A., Di Sotto, A., Di Giacomo, S., Mazzoccanti, G., Gasparrini, F., Quaglio, D., Campiglia, E., Carradori, S., Locatelli, M., Vinci, G., Rapa, M., Ciano, S., Giusti, A. M., Botta, B., … Mannina, L. (2020). Cannabis sativa L. inflorescences from monoecious cultivars grown in central Italy: An untargeted chemical characterization from early flowering to ripening. *Molecules*, *25*(8). https://doi.org/10.3390/molecules25081908

Khan, I. A., & Abourashed, E. A. (2010). Gentian. In *Leung's Encyclopedia of Common Natural Ingredients Used in Food, Drugs, and Cosmetics* (Third edit). Wiley.

Lee, J., Sugawara, E., Yokoi, S., & Takahata, Y. (2010). Genotypic variation of volatile compounds from flowers of gentians. *Breeding Science*, *60*(1), 9–17. https://doi.org/10.1270/jsbbs.60.9

Li, W., Zhou, W., Kim, S., Koo, J. E., Kim, Y., Koh, Y. S., Shim, S. H., Ma, J. Y., & Ho Kim, Y. (2015). Three new secoiridoid glycosides from the rhizomes and roots of Gentiana scabra and their anti-inflammatory activities. *Natural Product Research*, *29*(20), 1920–1927. https://doi.org/10.1080/14786419.2015.1013955

Li, Y., Guo, S., Zhu, Y., Yan, H., Qian, D. W., Wang, H. Q., Yu, J. Q., & Duan, J. A. (2019). Comparative analysis of twenty-five compounds in different parts of Astragalus membranaceus var. mongholicus and Astragalus membranaceus by UPLC-MS/MS. *Journal of Pharmaceutical Analysis*, *9*(6), 392–399. https://doi.org/10.1016/j.jpha.2019.06.002

Lv, X., Sun, J. Z., Xu, S. Z., Cai, Q., & Liu, Y. Q. (2018). Rapid characterization and identification of chemical constituents in gentiana radix before and after wine-processed by UHPLC-LTQ-orbitrap MSn. *Molecules*, *23*(12). https://doi.org/10.3390/molecules23123222

Mustafa, A. M., Caprioli, G., Maggi, F., Vittori, S., & Sagratini, G. (2016). Comparative analysis of the volatile profiles from wild, cultivated, and commercial roots of Gentiana lutea L. By headspace solid phase microextraction (HS–SPME) coupled to gas chromatography mass spectrometry (GC–MS). *Food Analytical Methods*, *9*(2), 311–321. https://doi.org/10.1007/s12161-015-0196-5

Mustafa, A. M., Caprioli, G., Ricciutelli, M., Maggi, F., Marín, R., Vittori, S., & Sagratini, G. (2015). Comparative HPLC/ESI-MS and HPLC/DAD study of different populations of cultivated, wild and commercial Gentiana lutea L. *Food Chemistry*, *174*, 426–433. https://doi.org/10.1016/j.foodchem.2014.11.089

Qi, L. M., Zhang, J., Zhao, Y. L., Zuo, Z. T., Jin, H., & Wang, Y. Z. (2017). Quantitative and qualitative characterization of Gentiana rigescens Franch (Gentianaceae) on different parts and

cultivations years by HPLC and FTIR spectroscopy. *Journal of Analytical Methods in Chemistry*, *2017*. https://doi.org/10.1155/2017/3194146

Spano, M., Matteo, G. Di, Ingallina, C., Botta, B., Quaglio, D., Ghirga, F., Balducci, S., Cammarone, S., Campiglia, E., Giusti, A. M., Vinci, G., Rapa, M., Ciano, S., Mannina, L., & Sobolev, A. P. (2021). A Multimethodological Characterization of Cannabis sativa L . Inflorescences from Seven Dioecious Cultivars Grown in Italy : The Effect of Different Harvesting Stages. *Molecules*, *26*(10), 2912. https://doi.org/https://doi.org/10.3390/molecules26102912

Szucs, Z., Dános, B., & Nyiredy, S. (2002). Comparative analysis of the underground parts of Gentiana species by HPLC with diode-array and mass spectrometric detection. *Chromatographia*, *56*(SUPPL.), 19–23. https://doi.org/10.1007/bf02494108

Takahashi, H., Imamura, T., Miyagi, A., & Uchimiya, H. (2012). Comparative metabolomics of developmental alterations caused by mineral deficiency during in vitro culture of Gentiana triflora. *Metabolomics*, *8*(1), 154–163. https://doi.org/10.1007/s11306-011-0295-2

Tanaka, R., Hasebe, Y., & Nagatsu, A. (2014). Application of quantitative 1H-NMR method to determination of gentiopicroside in Gentianae radix and Gentianae scabrae radix. *Journal of Natural Medicines*, *68*(3), 630–635. https://doi.org/10.1007/s11418-014-0833-0

Tutin, T. G., Heywood, S. M., Burges, N. A., Moore, D. M., Valentine, D. H., Walters, S. M., & Webb, D. A. (1972). Gentiana L. In *Flora Europea, vol. 3*. Cambridge University Press.

Ullah, H., Sommella, E., Santarcangelo, C., Avino, D. D., Rossi, A., Dacrema, M., Di Minno, A., Di Matteo, G., Mannina, L., Campiglia, P., Magni, P., & Daglia, M. (2022). Hydroethanolic Extract of Prunus domestica L .: Metabolite Profiling and In Vitro Modulation of Molecular Mechanisms Associated to Cardiometabolic Diseases. *Nutrients*, *14*(2). https://doi.org/https://doi.org/10.3390/nu14020340

Venditti, A., Guarcini, L., Altieri, A., & Bianco, A. (2013). Phytochemical pattern of Gentiana species of Appennino in Central Italy. *Natural Product Research*, *27*(21), 2063–2065. https://doi.org/10.1080/14786419.2013.819863

Wu, Q. X., Chen, J., & Shi, Y. P. (2010). RP-HPLC and NMR study of antioxidant flavonoids in extract from Gentiana piasezkii. *Journal of Analytical Chemistry*, *65*(3), 298–304. https://doi.org/10.1134/S1061934810030159

Xu, Y., Li, Y., Maffucci, K. G., Huang, L., & Zeng, R. (2017). Analytical methods of phytochemicals from the genus gentiana. *Molecules*, *22*(12). https://doi.org/10.3390/molecules22122080

Yang, J. L., Liu, L. L., & Shi, Y. P. (2010). Phytochemicals and biological activities of Gentiana species.

Natural Product Communications, *5*(4), 649–664. https://doi.org/10.1177/1934578x1000500432

Zeng, H., Su, S., Xiang, X., Sha, X., Zhu, Z., Wang, Y., Guo, S., Yan, H., Qian, D., & Duan, J. (2017). Comparative analysis of the major chemical constituents in Salvia miltiorrhiza roots, stems, leaves and flowers during different growth periods by UPLC-TQ-MS/MS and HPLC-ELSD methods. *Molecules*, *22*(5), 1–16. https://doi.org/10.3390/molecules22050771

Zhao, S., Liu, Q., Chen, X., & Hu, Z. (2004). Separation and determination of gentiopicroside and swertiamarin in Tibetan medicine by micellar electrokinetic electrophoresis. *Biomedical Chromatography*, *18*(1), 10–15. https://doi.org/10.1002/bmc.285

Chapter 8: Review articles

8.1. Introduction

A review article is an article that summarizes the current state of understanding on a topic within a certain discipline. They offer a comprehensive analysis of the existing literature within a field of study, identifying current gaps or problems. They should be critical and constructive and provide recommendations for future research based on the available literature and without present unpublished new data.

In my PhD experience I was involved in the writing of the following review articles:

- Review 1: Role of food in the COVID-19 pandemic (Di Matteo et al., 2020)
- Review 2: Food bioactive compounds as NLRP3 inflammasome modulators (Spano et al., 2022)
- Review 3: NMR based approaches in the study of foods (Sobolev et al., 2022)

References

Di Matteo, G., Spano, M., Grosso, M., Salvo, A., Ingallina, C., Russo, M., Ritieni, A., & Mannina, L. (2020). Food and

COVID-19: Preventive/co-therapeutic strategies explored by current clinical trials and in silico studies. *Foods*, *9*(8). https://doi.org/10.3390/foods9081036

Sobolev, A. P., Ingallina, C., Spano, M., & Matteo, G. Di. (2022). NMR-Based Approaches in the Study of Foods. *Molecules*, *27*, 7906. https://doi.org/https://doi.org/10.3390/molecules27227906

Spano, M., Di Matteo, G., Ingallina, C., Ambroselli, D., Carradori, S., Gallorini, M., Giusti, A. M., Salvo, A., Grosso, M., & Mannina, L. (2022). Modulatory Properties of Food and Nutraceutical Components Targeting NLRP3 Inflammasome Activation. *Nutrient*, *14*(490), 1–44. https://doi.org/https://doi.org/10.3390/ nu14030490

8.2. Review 1: Role of food in the COVID-19 pandemic

In the lockdown due to the COVID-19 pandemic from March to May of 2020, our research group carried out a review article regarding the possible co-adjuvant / preventive effect of foods against the COVID-19 pandemic. After an extensive literature search related to food and COVID-19 in PubMed, Scopus, Google Scholar and ClinicalTrials.gov, we have identified two major research lines regarding foods in the early stages of the pandemic. A general approach regarding the role of micronutrients, food components and diet to strengthen the immune system studied through clinical trials and a targeted approach regarding the interaction between food components and proteins involved in the viral replication studied through in silico studies. From this work we expect that the results of the reported research lines could be extremely important in establishing the role of food in the COVID-19 pandemic and also in the possible future pandemics caused by viral infections.

foods

MDPI

Review

Food and COVID-19: Preventive/Co-therapeutic Strategies Explored by Current Clinical Trials and in Silico Studies

Giacomo Di Matteo [1,†], Mattia Spano [1,†], Michela Grosso [2], Andrea Salvo [1], Cinzia Ingallina [1], Mariateresa Russo [3], Alberto Ritieni [4,5,*] and Luisa Mannina [1]

1 Laboratory of Food Chemistry, Department of Chemistry and Technologies of Drugs, Sapienza University of Rome, 00185 Rome, Italy; giacomo.dimatteo@uniroma1.it (G.D.M.); mattia.spano@uniroma1.it (M.S.); andrea.salvo@uniroma1.it (A.S.); cinzia.ingallina@uniroma1.it (C.I.); luisa.mannina@uniroma1.it (L.M.)
2 Department of Molecular Medicine and Medical Biotechnology, School of Medicine, University of Naples Federico II, CEINGE-Biotecnologie Avanzate, 80131 Naples, Italy; michela.grosso@unina.it
3 Department of Agriculture, Food Chemistry Safety and Sensoromic Laboratory (FoCuSS Lab), University of Reggio Calabria, 89124 Reggio Calabria, Italy; mariateresa.russo@unirc.it
4 Department of Pharmacy, School of Medicine, University of Naples Federico II, 80131 Naples, Italy
5 UNESCO Chair of Health Education and Sustainable Development, University of Naples, 80131 Naples, Italy
* Correspondence: ritialb@unina.it; Tel.: +39-081-678652
† These authors gave an equal contribution to this work.

Received: 8 June 2020; Accepted: 29 July 2020; Published: 1 August 2020



Abstract: Foods, food ingredients, and their balanced consumption are recognized to have an important role in achieving or maintaining a state of wellbeing by acting as carriers of functional components and bioactive molecules. However, the potential contribution of foods to consumers' health has so far only been partially exploited. The rapidly evolving scenario of the coronavirus disease 2019 (COVID-19) pandemic is stimulating profound reflection on the relationships between food and the etiological agent, the severe acute respiratory syndrome coronavirus 2 (SARS-CoV-2). Here, the status of knowledge regarding food as a possible defense/co-therapeutic strategy against the SARS-CoV-2 coronavirus is considered through the discussion of two main current lines of research. One line of research relates to the role of micronutrients, food components, and diets in the strengthening of the immune system through clinical trials; formulations could be developed as immune system enhancers or as co-adjuvants in therapies. The other line of research relates to investigation of the chemical interactions that specific food compounds can have with host or virus targets so as to interfere with the viral infective cycle of SARS-CoV-2. This line requires, as a first step, an in silico evaluation to discover lead compounds, which may be further developed through drug-design studies, in vitro and in vivo tests, and, finally, clinical trials to obtain therapeutic molecules. All of these promising strategies promote the role of food in preventive/co-therapeutic strategies to tackle the COVID-19 pandemic.

Keywords: food; COVID-19; SARS-CoV-2; micronutrient Clinical trial; immune system; in silico study; protein interaction

1. Introduction

Foods are complex systems containing macro- and micronutrients, as well as plant secondary metabolites, that can take part in biochemical processes and help to achieve or maintain a state of wellbeing [1–3]. In the past few months, the potential contribution of foods to addressing the coronavirus

disease 2019 (COVID-19) pandemic has become a highly debated topic, fueled by misleading fake news that is not supported by scientific results [4].

Coronaviruses (CoVs) are positive-sense single-stranded RNA viruses (Group IV of the Baltimore classification). CoVs are part of the Coronaviridae family and fall into the Orthocoronavirinae subfamily, which includes four genera: Alphacoronavirus, Betacoronavirus, Gammacoronavirus, and Deltacoronavirus [5,6]. Until 2019, six coronaviruses capable of infecting humans were known. Two of these, both from the Betacoronavirus group, caused major epidemics characterized by fatal respiratory disease: SARS-CoV, responsible for severe acute respiratory syndrome (SARS) in 2002 in the province of Guangdong in China; and MERS-CoV, responsible for Middle-East respiratory syndrome (MERS) in 2012 in the Kingdom of Saudi Arabia [7]. Recently, a new CoV, called severe acute respiratory syndrome coronavirus 2 (SARS-CoV-2) [8], was responsible for the outbreak of the COVID-19 pandemic on 31 December 2019 in China [9]. The previous SARS and MERS outbreaks involved 29 and 27 countries, respectively, and, given that over 170 countries have been affected by the COVID-19 pandemic after only 3 months, the severity of the current infection is evident [10–12]. The most common symptoms and signs of SARS-CoV-2 infection are respiratory symptoms, fever, dry cough, fatigue, and dyspnea [13,14], whereas the clinical manifestations of infection range from asymptomatic to severe pneumonia. It is noteworthy that pneumonia, a lower respiratory tract infection, has occupied the first position in the communicable disease rank and the fourth position in the top ten causes of death globally [15].

Although the design and production of a vaccine and its safe use represent the best solution to control the pandemic, to date, no pharmaceutical treatments or vaccines are available for COVID-19 [16]. However, unlike bacterial infections, viral diseases are often not treated with drugs because of latency, viral resistance, high mutation rates, and several frequent adverse side effects of treatment [17–19]. Therefore, eradicating viral diseases is rather challenging, and many viruses remain without preventive vaccines or effective antiviral treatments. Currently, only a few therapeutic protocols are available to reduce symptoms such as fever, pain, and impaired breath functionality, or to reduce diffuse microclots in the lungs [20].

Without a definitive effective treatment, a large number of research groups from all over the world are contributing their efforts to exploration of novel prevention or co-therapeutic approaches [21–23]. On 29 April 2020, 4 months after the outbreak started, 1580 articles in Scopus included the keyword "COVID-19", and by 29 May 2020 the number had reached 4091 articles.

In this review, the role of food and food nutrients in the prevention and intervention of pathology is thoroughly reviewed. Two ways to tackle COVID-19 with food are discussed, namely the untargeted approach through immune enhancement, which is currently being investigated in clinical trials, and the targeted approach through the interaction with host or virus proteins (Figure 1), which is being investigated by in silico studies. The strengthening of immune systems has been deeply investigated for previous viral infections; this approach is a part of several ongoing studies related to the current COVID-19 outbreak and is particularly interesting for elderly or immunodepressed populations [24,25]. The other line of research is focused on investigation of the structure [26], the mode of action [27], and the possible targets [28] of SARS-CoV-2. Food and natural products are in fact excellent sources for discovering novel antiviral tools, revealing new structure–activity relationships, and developing effective preventive/co-therapeutic strategies against viral infections [29–31].

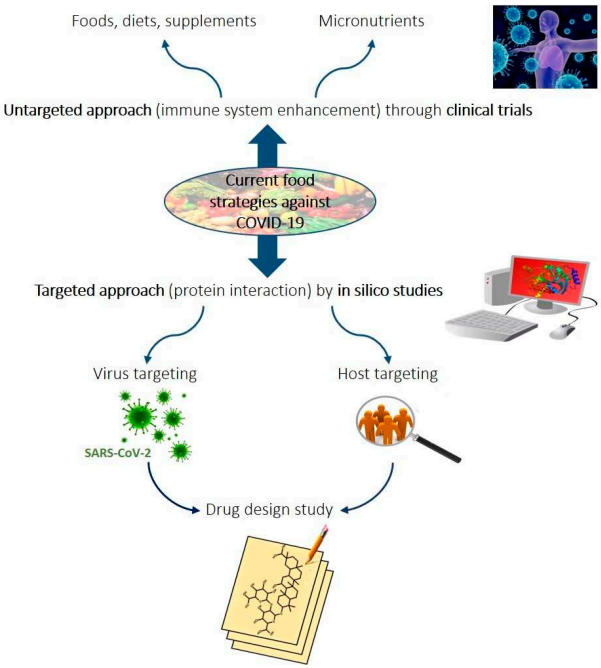


Figure 1. Scheme of current lines of research discussed in the present paper regarding food, food components, or diets used against coronavirus disease 2019 (COVID-19). The untargeted approach is based on immune system enhancement through food components and is being investigated in ongoing clinical trials, and the targeted approach is focused on the interaction between specific compounds and host or virus proteins and is being investigated by in silico studies.

2. Methodology

The clinical trials here reported were obtained using the Find Studies >New Search section in the U.S. National Library of Medicine Clinical Trials website [32]. The keywords "COVID-19" or "SARS-CoV-2" were searched in the "Condition or disease" field, with "All studies" selected in the "Status" field. Using these criteria with the two keywords, over 1800 studies were found on 24 May 2020. The twenty-three studies reported herein (see Table 1 and Supplementary Table S1) were selected by manually choosing only trials regarding food or nutrient topics and excluding all others in order to offer a comprehensive view of the current clinical trials on COVID-19 related to food as of 24 May 2020.

The in silico studies reported herein were obtained using the PubMed, Scopus, and Google Scholar databases. The keywords "in silico" or "docking" were paired with "SARS-CoV-2" or "COVID-19" to obtain articles published as of 4 July 2020. No language restriction was imposed. Some of the most relevant articles regarding food components were selected manually to give an overview of the current in silico studies on COVID-19 related to food. The selected articles are shown in Table 2.

3. Food as an Immune System Enhancer in Current Clinical Trials

The intake of some foods or food supplements can be extremely important for strengthening the immune system [33,34] and preventing the onset of pathologies such as respiratory infections.

This aspect may represent a new frontier in the field of functional foods and an important resource for elderly people, as well as for immunosuppressed individuals or high-risk communities such as those in hospitals or retirement homes. An appropriate intake of micronutrients is necessary at every stage of growth, and particularly in some physiological conditions (older age, severe nutritional deficiencies, and stressful situations). Vitamins and minerals take part in many human biological and biochemical processes and are involved in immune system fortification (reinforcement of epithelial barriers, activation of immune cells, and enhancement of cytokines and antibody production) [35] and the wellness state. The role of some micronutrients as supporting agents in the prevention and treatment of respiratory tract viral infection has been largely demonstrated [36,37].

In the case of COVID-19, some clinical trials investigating the effect of food components on COVID-19 prevention/treatment strategies are currently in progress (see Table 1). Other information regarding these studies is reported in Supplementary Table S1 in Supplementary Materials.

Table 1. List of the current clinical trials related to food (micronutrients, foods/diets, and other supplements) used for the prevention/treatment of COVID-19 as of 24 May 2020 [15]. A brief description reporting the trials' aims, enrolment, and interventions is also reported.

№.	Treatment	Brief Trial Description [1,5,*]	
Micronutrients			
1	Vitamin C Zinc gluconate	Aim	Reduce symptom duration
		Enrolment	18 years and older, COVID-19-positive, 520 participants
			- IG 1: vitamin C (8000 mg/day) - IG 2: zinc gluconate (50 mg/day)
		Intervention	- IG 3: vitamin C (8000 mg/day) and zinc gluconate (50 mg/day) - CG: standard care
			Duration: 10 days
2	Vitamin C	Aim	Reduce mortality and secondary symptoms
		Enrolment	All ages, COVID-19-positive, 500 participants
		Intervention	- IG: intravenous vitamin C (10 g/not specified)
			Duration: not specified
3	Zinc gluconate Vitamin D3	Aim	Reduce inflammatory reaction, which worsens acute respiratory distress syndrome
		Enrolment	60 years and older, COVID-19-positive, 3140 participants [¥]
			- IG: zinc gluconate (30 mg/day) and vitamin D3 (2000 IU (International Units)/day)
		Intervention	- CG: standard care
			Duration: 2 months
4	Vitamin D	Aim	Improve hard endpoints related to COVID-19 deleterious consequences
		Enrolment	40 years to 70 years, COVID-19-positive, 200 participants
			- IG: vitamin D (25,000 UI/day)
		Intervention	- CG: standard care
			Duration: not specified
5	Hydroxychloroquine Vitamin C Vitamin D Zinc	Aim	Determine whether the combined therapy prevents COVID-19 symptoms [†]
		Enrolment	18 years and older, FM, COVID-19-negative: high-risk individuals, 600 participants
		Intervention	- IG: hydroxychloroquine, vitamin C, vitamin D, zinc (not specified)
			Duration: not specified
6	Hydroxychloroquine Azithromycin Vitamin C Vitamin D Zinc	Aim	Determine whether the combined therapy can treat COVID-19 infection
		Enrolment	18 years and older, COVID-19-positive, 600 participants
		Intervention	- IG: hydroxychloroquine, azithromycin, vitamin C, vitamin D, zinc (not specified)
			Duration: 24 weeks
7	Vitamin C	Aim	Increase ventilator-free days, acute-inflammation-free days and organ-failure-free days
		Enrolment	18 years and older, FM, COVID-19-positive, 200 participants
			- IG: intravenous vitamin C (100 mg/kg/8 hours)
		Intervention	- CG: standard care
			Duration: 3 days
8	Vitamin D3	Aim	Improve the prognosis of older patients
		Enrolment	70 years and older, FM, COVID-19-positive, 260 participants [¥]
			- IG: vitamin D3 (400,000 IU/day)
		Intervention	- CG: standard dose of vitamin D3 (50,000 IU/day)
			Duration: not specified
9	Vitamin C	Aim	Improve the prognosis of patients
		Enrolment	18 years and older, COVID-19-positive, 140 participants
			- IG: intravenous vitamin C (24 g/day)
		Intervention	- CG: standard care
			Duration: 7 days
10	Vitamin C	Aim	Reduce the risk of respiratory failure requiring mechanical ventilation
		Enrolment	18 years to 99 years, FM, COVID-19-positive, 20 participants
			- IG 1: intravenous vitamin C (50 mg/kg/6 h) (mild deoxygenation)
		Intervention	- IG 2: intravenous vitamin C (50 mg/kg/6 h) (severe deoxygenation)
			Duration: 4 days

Table 1. *Cont.*

№.	Treatment		Brief Trial Description [1,$,*]
11	Vitamin C Active comparator treatment (hydroxychloroquine, azithromycin, zinc citrate, vitamin D3 and vitamin B12)	Aim	Prevent COVID-19 progression
		Enrolment	18 years and older, COVID-19-positive, 200 participants
		Intervention	- IG: vitamin C (200 mg/kg/day on day 1, 400 mg/kg/day from day 2) and active comparator treatment (hydroxychloroquine, azithromycin, zinc citrate, vitamin D3 and vitamin B12) - CG: active comparator treatment
			Duration: 7 days
12	Vitamin D2 Vitamin D3	Aim	Determine the efficacy of vitamin D in patients
		Enrolment	17 years and older, FM, COVID-19-positive, 64 participants
		Intervention	- IG 1: vitamin D2 (4 doses of 50000 IU in 3 weeks) - IG 2: vitamin D3 (1000 IU/day)
			Duration: 3 weeks
13	Calcifediol	Aim	Study the preventive and therapeutic effects of oral calcifediol [†]
		Enrolment	18 years to 75 years, COVID-19-negative and at high risk of acquiring COVID-19, or at risk for its morbidity and mortality, 1500 participants
		Intervention	- IG: oral calcifediol (25 μg/day) - CG: standard care
			Duration: 2 months
14	Calcifediol	Aim	Reduce the development of COVID-19 and the worsening of the various syndrome phases
		Enrolment	18 years to 90 years, COVID-19-positive, 1008 participants
		Intervention	- IG: oral calcifediol (266 μg/12 h on day 1, 266 μg/day on days 3, 7, 14, 21, 28) - CG: standard care
			Duration: 28 days
15	Vitamin C	Aim	Evaluate the safety and efficacy of ascorbic acid infusions in COVID-19 treatment
		Enrolment	18 years and older, COVID-19-positive, 66 participants
		Intervention	- IG: vitamin C infusion (0.3 g/kg on day 0, 0.6 g/kg on day 1, 0.9 g/kg on days 3–5) - CG: standard care
			Duration: 6 days
16	Aspirin Vitamin D	Aim	Test the hypothesis that treatment with aspirin and vitamin D in COVID-19 can mitigate the prothrombotic state and reduce hospitalization rates
		Enrolment	18 years and older, FM, COVID-19-positive, 1080 participants
		Intervention	- IG 1: aspirin (81 mg/day) - IG 2: aspirin (81 mg/day) and vitamin D (50000 IU/week) - CG: standard care
			Duration: 2 weeks
Foods/diets			
17	Natural honey	Aim	Study the efficacy of natural honey in patient treatment
		Enrolment	5 years to 75 years, COVID-19-positive, 1000 participants
		Intervention	- IG: natural honey (1 g/kg/day) - CG: standard care
			Duration: 14 days
18	Natural honey Black cumin	Aim	Reduce COVID-19 symptoms
		Enrolment	18 years and older, COVID-19-positive, 30 participants
		Intervention	- IG: natural honey and black cumin (1 g/kg/day) - CG: standard care
			Duration: 14 days
19	Ketogenic diet	Aim	Improve gas exchange, reduce inflammation and duration of mechanical ventilation
		Enrolment	18 years to 80 years, COVID-19-positive, 15 participants
		Intervention	- IG: ketogenic diet - CG: standard care
			Duration: 2 days
Other supplements			
20	Nutritional supplement enriched in eicosapentaenoic acid, gamma linolenic acid, and antioxidants	Aim	Reduce COVID-19 severity with more preservation of the nutritional status
		Enrolment	18 years to 65 years, COVID-19-positive, 30 participants
		Intervention	- IG: oral nutrition supplement (ONS) enriched in eicosapentaenoic acid, gamma linolenic acid, and antioxidants - CG: isocaloric/isonutrigenous ONS
			Duration: 14 days
21	Resistant potato starch Nonresistant corn starch	Aim	Determine the efficacy of resistant potato starch in reducing the need for hospitalization
		Enrolment	19 years and older, COVID-19-positive, 1300 participants
		Intervention	- IG: resistant potato starch (20 g/12 h) - CG: nonresistant corn starch (20 g/12 h)
			Duration: 14 days
22	Gum arabic Pectin	Aim	Study the efficacy of gum arabic as an immunomodulator and anti-inflammatory agent
		Enrolment	5 years to 90 years, COVID-19-positive, 110 participants
		Intervention	- IG: gum arabic (30 g/day) - CG: pectin (1 g/day)
			Duration: 4 weeks for IG and 12 weeks for CG
23	Quercetin	Aim	Evaluate the possible role of quercetin on prophylaxis and treatment of COVID-19 [†]
		Enrolment	18 years and older, COVID-19-negative and -positive, 50 participants
		Intervention	- IG 1: quercetin (1000 mg/day in COVID-19 patients) - IG 2: quercetin (500 mg/day in NO COVID-19 patients) - CG: no intervention (in NO COVID-19 patients)
			Duration: not specified

[1] IG = intervention group; CG = control group. [¥] The trial is being carried out on elderly participants. [†] Studies with prevention aim. [$]: All studies are ongoing. * Both sexes were recruited.

It is noteworthy that all of the studies are still ongoing, and that each study presents its own eligibility criteria. In particular, two studies (No. 3 and No. 8) specifically involve elderly patients (over 60 and over 70 years of age, respectively), whereas in the others, participants of different age ranges have been engaged. Three trials are focused on prevention (No. 5, 13, and 23, COVID-19-negative participants), whereas all the others have a co-therapeutic aim. In particular, in trial No. 5, the effect of a prophylactic treatment based on hydroxychloroquine, vitamin C, vitamin D, and zinc supplementations for 600 health workers of both sexes (18 years and older) at high risk of being infected by SARS-CoV-2 is reported.

In trial No. 13, 1500 people of both sexes (from 18 to 75 years old) both positive and negative for COVID-19 were enrolled. In particular the selected positive patients presented symptoms of acute respiratory tract infection (e.g. fever, cough, dyspnea) accompanied by computed tomography (CT) scan of the chest compatible with COVID-19 or by a COVID-19 positive test (polymerase chain reaction, PCR). The aim of the trial is to study the prophylactic and co-therapeutic effects of orally administered calcifediol supplementation.

Sixteen clinical trials relate to the supplementation of a single micronutrient or a micronutrient combination. Seven trials involve the co-therapeutic use of vitamin C (No. 1, 2, 7, 9, 10, 11, and 15) for different purposes, including symptom reduction, mortality reduction, increase in ventilator-free days, and prevention of COVID-19 progression. In clinical trial No. 1, vitamin C and zinc gluconate are being administered alone or in combination in 520 patients of both sexes (18 years and older, treated with the standard therapy) in order to evaluate the reduction of COVID-19 symptoms. In all other clinical trials on vitamin C, it is being administered alone. In clinical trial No. 2, 500 hospitalized COVID-19 patients with pneumonia (ranging from children to elderly patients, treated with standard therapy) are being treated with vitamin C intravenously to observe a possible reduction of mortality and symptoms. In clinical trial No. 7, 200 COVID-19 patients of both sexes (18 years and older, treated with standard therapy) with acute lung injury and hypoxemia have been recruited and are being treated with early infusion of vitamin C to evaluate reduction of the lung injury caused by SARS-CoV-2. In clinical trial No. 9, 140 SARS-CoV-2-infected patients of both sexes with severe acute respiratory infection (18 years and older, treated with the standard therapy) have been recruited to evaluate a coadjutant protocol based on daily intravenous infusion, with the aim of improving the prognosis of patients. In trial No. 10, the effect of vitamin C infusion is being evaluated in 20 COVID-19 patients with both mild and severe deoxygenation problems (18 years to 99 years) to evaluate the effect of vitamin C in reducing respiratory failure. Another clinical trial (No. 11) aims to study the effect of vitamin C supplementation, orally or intravenously administered, in addition to a comparative treatment (two drugs and three supplements), on 200 COVID-19 patients (18 years and older, both sexes), with the aim of reducing disease progression. Finally, in trial No. 15, 66 hospitalized COVID-19 patients of both sexes (18 years and older, treated with standard therapy) are being treated with vitamin C infusions to observe a possible improvement of health status.

The widespread use of vitamin C in the clinical trials considered is due to the well-recognized role of this micronutrient in the prevention and treatment of respiratory illness [38,39]. For instance, in a previous clinical case, the treatment of a respiratory syndrome with intravenous injection of ascorbic acid together with respiratory assistance turned out to be effective for the improvement of patient healing after 10 days of therapy [40].

Five studies (No. 4, 8, 12, 13, 14) concern the administration of vitamin D. In clinical trial No. 4, 200 COVID-19 patients of both sexes with mild symptoms (from 40 years to 70 years, treated with standard therapy) are receiving vitamin D supplements in order to improve their immune system and slow down the symptoms progression. In clinical trial No. 8, the potential role of two doses of vitamin D_3 (standard and high doses) as a supportive agent for COVID-19 treatment in 260 elderly patients (70 years and older, treated with standard therapy) of both sexes is being evaluated. In trial No. 12, 64 COVID-19 patients of both sexes (17 years and older) are being treated with low or high doses of vitamin D to study their eventual regression of symptoms. Finally, in trial No. 14, 1008 COVID-19

patients of both sexes (from 18 years to 90 years, treated with standard therapy) are receiving calcifediol with the aim of decelerate the syndrome progression. In two clinical trials (No. 3 and 16), vitamin D is being administered together with other supporting agents. In particular, in trial No. 3, vitamin D and zinc gluconate are being administered to 3140 COVID-19 elderly patients of both sexes (60 years and older, treated with standard therapy) in order to evaluate the reduction of inflammatory reactions. In trial No.16, vitamin D is being administered together with aspirin to 1080 COVID-19 patients of both sexes (18 years and older, treated with standard therapy) in order to mitigate the prothrombotic state and reduce hospitalization rates. In this case, the widespread use of vitamin D in clinical trials is also supported by literature data reporting the effectiveness of this micronutrient in the reduction of respiratory infection incidence. For instance, in a study by Urashima et al., vitamin D was administered to 167 schoolchildren via daily supplementation of 1200 IU (International Units), whereas another 167 schoolchildren were treated with a placebo for four months [41]. At the end of the trial, lower incidences of seasonal influenza A and asthma attack events were observed in the schoolchildren treated with vitamin D_3 supplementation.

It is noteworthy that in several of the clinical trials described above (No. 1, 3, 5 and 6), zinc is a component of the micronutrient mixture. The role of zinc in improving the immune system in several diseases, including respiratory infections, has been previously demonstrated [42]. For instance, a study carried out on two groups of children, treated with either placebo or zinc, showed a lower incidence (48%) of respiratory viral infections in the children treated with the zinc supplement [43].

In other clinical trials, the supplementation of other foods, food components, or diets has been proposed. In particular, trial No. 17 aims to evaluate the efficacy of natural honey in reducing the symptoms of 1000 COVID-19 patients of both sexes (from 5 years to 75 years, treated with standard therapy). Similarly, in trial No. 18, the efficacy of natural honey and black cumin seeds in reducing COVID-19 symptoms of 30 patients of both sexes (18 years and older, treated with standard care) is being investigated.

The efficacy of a ketogenic diet in mitigating COVID-19 symptoms is also being tested (No. 19). In particular, in this clinical study, 15 COVID-19 patients of both sexes (18 years to 80 years) with respiratory failure requiring intubation have been recruited in order to study the efficacy of a ketogenic diet (high-fat, low-carbohydrate, adequate-protein diet) in the reduction of respiratory problems. This trial is supported by data from previous studies on the efficacy of ketone bodies in reducing artificial ventilator duration [44] and inflammation events [45]. In trial No. 20, a supplement enriched in eicosapentaenoic acid, linolenic acid, and antioxidants is being administered to 30 patients (18 years to 65 years older, treated with standard therapy) of both sexes to preserve their nutritional status and to evaluate the improvement of their health state. The role of polysaccharide intake is also being investigated: in trial No. 21, resistant potato starch is being administrated to 1500 nonhospitalized patients of both sexes (19 years and older, treated with standard therapy) in order to evaluate the reduction of disease progression, whereas in trial No. 22, gum arabic is being administrated to 110 patients of both sexes (5 years to 90 years, treated with standard therapy) as an immunomodulator and anti-inflammatory agent.

Finally, in trial No. 23, 50 participants (from 18 years and older, treated with standard therapy) of both sexes have been enrolled in order to study quercetin's efficacy both as prophylaxis in COVID-19-negative participants and as treatment in COVID-19-positive patients.

In addition to the micronutrients, food components, and diets being used in the reported clinical trials, other micronutrients with a demonstrated modulation action on the immune system could also be useful in other immune-enhancing formulations to reduce the risks of respiratory tract infections in the case of COVID-19. For instance, the roles of vitamins A, B, and E in the reinforcement of the immune system are well ascertained. Vitamin A supplementation has been shown to reduce respiratory disease incidence only in subjects with malnutrition or, conversely, an increase in disease risks [46] in the case of normal nutritional intake [47,48]. A correlation between vitamin B deficiency and several diseases, including respiratory viral infections, has been observed [49]. In a clinical observational study

on 1176 children with acute lower respiratory tract infections, a relationship between an increase in disease incidence (44%) and low vitamin B_9 concentrations in serum was observed [50]. The effective role of vitamin E supplementation for the prevention of respiratory diseases is still debated, since it has not yet been demonstrated. However, in a clinical study, daily vitamin E supplementation improved the immune system activity of 33 elderly women and men with immune deficiencies; their immune system activity became comparable to that of the control healthy adult group [51].

Regarding minerals, low serum levels of Se are associated with higher risks of immune weakness. A clinical study reported that 83 patients with respiratory diseases presented low serum selenium levels compared with a control group [52]. A correlation between iron supplements in children and lower incidence of upper respiratory tract infections was highlighted by De Silva et al. [53].

Notably, an important aspect to consider in trying to understand the activities and the efficacy of bioactive compounds in food and food nutrients is their bioavailability. Many factors may affect bioavailability, such as: bioaccessibility from natural sources; food matrix effects from synergistic, additive, or antagonist interactions among complex matrix components; molecular structures; physicochemical conditions; and the general health condition, genetic profile, or previous diseases of the consumers [54,55]. The bioactive compounds present in a food may have greater or lesser bioavailability compared with supplements. However, it is important to underline that supplements are often administered at high concentrations to compensate for their low bioavailability, which is due to the absence of passive or active carriers that co-introduce bioactive compounds when they are present as food ingredients. In contrast, the bioaccessibility of some food supplement ingredients is very high because of the absence of interactions with food matrices that may interfere with the digestion process [56].

Finally, micronutrients and food compounds with other additional biological activities could be of interest for addressing other concerns related to COVID-19. For instance, vitamin E, garlic, selenium, fish oil, ginkgo biloba, ginger, and ginseng, all of which have anticoagulant activity [57,58], could be proposed as adjuvants in the thrombotic events that have been recently clinically correlated with SARS-CoV-2 disease progression in a high percentage of patients [59,60].

4. Food Compounds in Preliminary in Silico Studies

Although a vaccine is the most suitable solution to counteract the COVID-19 pandemic, its large-scale availability still requires the assessment of its toxicity, side effects, and efficiency in the population before allowing clinical trials [61]. Therefore, in this context, it may be of great relevance that some food components have adequate effects to be worth assessing with a targeted approach as potential candidates for treatment.

To better understand the potential roles of foods and their components in the fight against SARS-CoV-2, a brief description of the potential molecular targets already identified in the infection cycle [62] is needed. Considering the genomic similarities between SARS-CoV-2 and both MERS-CoV (50%) and SARS-CoV (79%) [63,64], some common features can be outlined in order to identify possible key factors for both drug discovery and food implications. It is well established that during the adsorption stage, the spike S-protein domain on the virus envelope is involved in binding with the human host angiotensin-converting enzyme (ACE2) to attack respiratory cells [65] in a very similar manner to that of the previous SARS-CoV. However, the much higher infectivity of this virus compared with that of the previous SARS-CoV and MERS-CoV infections could be explained by the recent finding of a region potentially involved in sialic-acid binding, which regulates host-cell infection [66]. Once SARS-CoV-2 is able to enter the cell and use the host translational machinery, the replication stage starts by expressing 16 nonstructural proteins (NSPs). Although not all of these proteins are well characterized yet, some of them may represent a potential target. In particular, viral papain-like protease (PL^{pro}) and main protease (M^{pro} or $3CL^{pro}$) (the COVID-19 virus M^{pro} is in the Protein Data Bank (PDB) with accession number 6LU7) enzymes that are responsible for the cleavage of several critical viral proteins are considered the Achille's heels of SARS-CoV-2, showing little structural variation

compared with their SARS-CoV counterparts [67]. The NSPs assemble into the replicase–transcriptase complex (RTC) and create a suitable environment for viral RNA synthesis. This process follows the translation and assembly of viral replicase complexes. SARS-CoV-2 then releases RNA into the host cell. Genomic RNA is translated into viral replicase polyproteins pp1a and pp1ab, which are then cleaved into small products by viral proteinases. Using a discontinuous transcription process, the polymerase produces a series of subgenomic mRNAs that are finally translated into key viral proteins. Viral proteins and genomic RNA are subsequently assembled into virions in the endoplasmic reticulum and Golgi apparatus, and then transported via vesicles and released from the cell.

Once molecular targets have been identified, studies to characterize potential drug candidates can be conducted in silico [28]. If the selected active compounds have good absorption, distribution, metabolism, excretion, and toxicity (ADMET) properties and respect "Lipinski's Rule of 5" (a series of four rules that suggest if a molecule can be properly orally administrated, if more than one rule is not respected the molecule is not suitable for oral administration), then in vitro and in vivo analyses are required in order to define their efficacy, safety, and toxicological profile. Finally, clinical trials will be necessary to investigate the potential therapeutic efficacy and tolerability of the selected molecules [68]. An important advantage of these approaches is the rapid assessment of efficiency and toxicity in cell lines or animal studies in order to optimize the final choice. This advantage is essential, considering the rapid infection spread and the virus' lethality.

The main recent in silico studies regarding the affinity of naturally-occurring compounds for either viral targets or host targets to counteract SARS-CoV-2 are discussed below. The selection of molecules as potential COVID-19 antagonists for in silico studies was based on their in vitro activity on other coronaviruses, as previously described. The compound affinity depends on the type and amount of bonding that occurs with the active site of the protein [69].

Many studies have been focused on the activity of compounds isolated from food sources, such as glycyrrhizin, glabridin, glycyrrhetinic acid, and many polyphenols, such as caffeic acid, resveratrol, kaempferol, curcumin, demetoxicurcumin, quercetin, catechin, epicatechin gallate, hesperetin, hesperidin, δ-viniferin, and myricitrin. The results described hereinafter are also summarized in Table 2. In particular, M^{pro} has become the main virus target studied in in silico studies, followed by the human ACE2 receptor, SARS-CoV-2 spike S protein and RNA polymerase. However, the examined molecules should also be tested against other human and/or virus targets, since some molecules, such as curcumin, hesperidin, catechin, and garlic and cinnamon compounds, have been shown to be potentially active against other targets as well. Multitarget antiviral molecules can have greater efficacy against SARS-CoV-2 pathogenesis than molecules targeting a single protein [70]. Several food compounds have been shown to be active against other coronaviruses (mainly SARS-CoV), whereas other molecules, such as demethoxycurcumin and epicatechingallate, have not been investigated against coronaviruses but are being investigated because of their chemical similarities to well-known antiviral analogs. Finally, mixtures of compounds derived from food matrices, such as garlic and cinnamon, were separated and then individually analyzed in silico.

Table 2. List of in silico studies related to food components. Details include the specific compound, chemical class, food source, anti-COVID-19 target, and previous studied activity on human coronaviruses (HCoVs). ACE2, angiotensin-converting enzyme; M^{pro}, main protease; SARS-CoV, severe acute respiratory syndrome coronavirus.

Compound	Chemical Class	Food Source	In Silico Anti-COVID-19 Target	Previous in Vitro Activity on Other HCoVs
Glycyrrhizin	Triterpene Saponin	Glycyrrhiza glabra	ACE2 [71]	SARS-CoV [72]
Glabridin	Isoflavane	Glycyrrhiza glabra	Spike S protein [73]	
Caffeic acid	Phenolic acid	Fruits, vegetables, coffee, propolis	M^{pro} [74]	NL63 [75]
Caffeic acid phenylethyl ester	Phenolic ester	Honey, propolis	M^{pro} [74]	
Chrysin	Flavone	Honey, propolis	M^{pro} [74]	
Galangin	Flavonol	Honey, propolis	M^{pro} [74]	
Resveratrol	Flavonol	Grapes, peanut, blueberry, bilberry, Cranberry	ACE2 [76]	SARS-CoV [77]
Kaempferol	Stilbenoid	Tea, spinach, broccoli, Cabbage	M^{pro} [78]	SARS-CoV [79]
Curcumin	Diarylheptanoid	Turmeric	M^{pro} [78] ACE2 [80] Spike S protein [80]	SARS-CoV [81]
Demethoxycurcumin	Diarylheptanoid	Turmeric	M^{pro} [78]	
Quercetin	Flavonol	Fruits, vegetables	M^{pro} [78]	SARS-CoV [82]
Catechin	Flavanol	Tea	M^{pro} [78] ACE2 [80] Spike S protein [80]	SARS-CoV [83]
Epicatechigallate	Flavanol	Tea	M^{pro} [78]	
Hesperetin	Flavanone	Citrus peel and albedo	ACE2 [71]	SARS-CoV [84]
Hesperidin	Flavanone	Citrus peel and albedo	M^{pro} [85] ACE2 [85] Spike S protein [85]	SARS-CoV [85]
diallyl tetrasulfide, trisulfide 2-propenyl propyl	Organosulfur	Garlic	M^{pro} [86] ACE2 [86]	
Tenufolin	Triterpene saponin	Cinnamomun verum	M^{pro} [87]	SARS-CoV [88]
Pavettanin C1	Lignin	Cinnamomun verum	Spike S protein [87]	SARS-CoV [88]
δ-Viniferin	Flavonol	Red wine	M^{pro} [89] ACE2 [89] RNA-dependent RNA polymerase [89]	
Myricitrin	Flavone	Myrica esculenta	M^{pro} [89] ACE2 [89]	SARS-CoV [78,90]

Hereinafter, the in silico studies related to isolated molecules from food sources are discussed.

Glycyrrhizin, a triterpene saponin, is the main compound of licorice root (*Glycyrrhiza glabra)*, a perennial herb used in traditional Chinese medicine [91]. The role of glycyrrhizin has long been studied in other viral infections, including HIV-1 and hepatitis C virus, in in vitro studies [92,93]. Moreover, the effect of glycyrrhizin was also studied against the SARS-CoV virus. It was found that glycyrrhizin inhibits viral replication and early steps of the replication cycle (adsorption and entry), with an unclear mode of action [72]. On the basis of these results, the effects against SARS-CoV-2 of glycyrrhizin was studied [71], although only in an in silico study, and a potential interaction of glycyrrhizin with a binding site near the hydrophobic site of the human ACE2 receptor was reported.

The importance of licorice as a source of active compounds was also confirmed by a study on glabridin, another triterpene from licorice root, which was tested against SARS-CoV-2. The compound was shown to have a high binding affinity with M^{pro} through one electrostatic and five hydrophobic interactions [73].

Glycyrrhetinic acid, another well-known triterpene in licorice root derived from the hydrolysis of saponin glycyrrhizic acid, showed the highest binding activity, among 2906 molecules tested, with a pocket of the SARS-CoV-2 spike S-protein that contributes to inhibiting the interaction with the ACE2 protein. This binding is based on hydrophobic and polar interactions with the steroidal scaffold of glycyrrhetinic acid and further reinforced by many ion and hydrogen interactions. The ability of the

most active compounds to prevent virus entry in the case of low viral load was further confirmed in an in vitro study [94].

Polyphenols are a very large class of compounds known not only for their antioxidant properties but also for several other biological activities (antitumor, antibacterial, antiviral) [95]. Here, some previous studies about polyphenol activity against respiratory viruses and the current evidence related to SARS-CoV-2 from in silico studies are discussed.

Caffeic acid is a phenolic acid widely present in a variety of foods (such as fruits, vegetables, coffee, and propolis) [96]. A recent in vitro study showed that caffeic acid had powerful antagonist activity against human coronavirus (HCoV) NL63 [75], inhibiting the virus' interaction with the ACE2 receptor. The potential antagonistic activity of caffeic acid toward SARS-CoV-2 was highlighted in a recent molecular-docking study in which the binding capacities of some propolis compounds against the virus M^{pro} were investigated [74]. This study showed that caffeic acid and its phenethyl ester have a good affinity for the active site of the enzyme, making these molecules potential virus antagonists. In the same study, two other propolis polyphenolic compounds, chrysin and galangin, were defined as potential anti-SARS-CoV-2 agents.

Resveratrol is a stilbenoid compound that exists in cis- and trans-isomeric forms, with the second being the predominant and biologically more active form [97], present in many nutritional foods such as grapes, peanut, blueberry, bilberry, cranberry, purple grapes, and grape juice [98]. Resveratrol has shown activity against many respiratory tract viruses [99] and also against SARS-CoV in an in vitro study [77]. This molecule also demonstrated a high binding affinity and the highest selectivity for the ACE2 complex, compared with the other stilbenoid compounds tested in a recent in silico study [76].

Additionally, δ-viniferin, a dehydrodimer of resveratrol produced along with other stilbenoids by stressed grapevine leaves, was also tested in in silico studies against SARS-CoV-2 to combat the cough symptoms of SARS-CoV-2 infection. δ-Viniferin, present in red wine [100] and used as an antitussive treatment in Indian medicine, has shown potent antiviral activity against a variety of viruses [101]. δ-Viniferin has been proven to be a multitargeted antiviral molecule against SARS-CoV-2, with a high binding affinity to M^{pro} through many interactions, such as polar, Pi-Pi, Pi-sulfur, and van der Waals interactions. In addition, this molecule also showed a high binding affinity with the RNA-dependent RNA polymerase (RdRp) target and with the ACE2 receptor [89].

The same study demonstrated the potential inhibitor activity of myricitrin, another antitussive molecule from Indian medicine present in *Myrica esculenta*, against SARS-CoV-2. This molecule presents a high binding affinity with M^{pro} through Pi–alkyl, Pi–sulfur, and van der Waals interactions and hydrogen bonds and, in addition, with the RdRp target and the ACE2 protein [89]. The interest in this molecule was also due to previous in vitro studies on SARS [78,90].

In a recent molecular-docking study [91], different polyphenols present in food matrices, namely kaempferol, curcumin, demetoxicurcumin, quercetin, catechin, and epicatechigallate, were investigated as potential COVID-19 inhibitors, having shown inhibitory activity against SARS in in vitro studies [79,81–83]. These molecules showed a high binding affinity to COVID-19 M^{pro}, with low binding energies and inhibition constants. Kaempferol, a flavonol mainly present in tea and some vegetables (e.g., spinach, broccoli, cabbage) [102], showed the highest activity.

In another molecular-docking study, curcumin, present in turmeric, and catechin, present in tea, were found to be good potential antagonists against the human ACE2 receptor and the spike S protein of SARS-CoV-2 [80], as a result of their strong interactions with their binding sites.

Finally, hesperetin, a flavonoid present in citrus pericarp and albedo (*Citrus aurantium*, *Citrus reticulata*), showed dose-dependent inhibition of SARS M^{pro} in a recent in vitro study [98]. In a recent in silico study, it was shown that hesperetin has the potential to inhibit the ACE2 receptor, suggesting that this molecule might bind ACE2 and might interfere with SARS-CoV-2 infection [71]. Furthermore, hesperidin, a hesperitin glycoside, showed the potential to inhibit many proteins related to SARS-CoV-2 by interfering with their viral cycle [85]. These results underline the importance of further studies regarding this molecule and its industrial extraction process from citrus peel.

The second part of this section is focused on in silico studies on compound mixtures derived from food matrices to find the components with the highest binding affinity.

Garlic is a foodstuff known in many cultures for a variety of pharmaceutical properties [103]. Since ancient times, essential oils obtained from foods or natural material have played significant roles in pharmaceutics for the presence of potential therapeutic agents [104]. Because of the high chemical diversity of secondary metabolites, the use of natural essential oils in order to tackle the current SARS-CoV-2 pandemic has been extensively investigated. Many studies have demonstrated that garlic extracts possess in vitro biological activities, including antiviral activity against respiratory viruses [105]. Recently, Thuy et al. [86] characterized garlic essential oils via GC–MS (Gas Chromatography Mass Spectrometry) analysis and docking simulation, finding 17 organosulfur compounds (representing 99.4% of the garlic's essential oil composition) capable of simultaneously inhibiting both the ACE2 host receptor and SARS-CoV-2 M^{pro} through noncovalent binding interactions. In particular, allyl disulfide, allyl trisulfide, diallyl tetrasulfide and trisulfide, and 2-propenyl propyl, which represent the major compounds of garlic essential oils, accounting for 59% of the entire composition, showed the highest affinity toward M^{pro}. Surprisingly, the same four compounds showed the highest affinity values with the lowest docking score energies toward the ACE2 receptor. The multitargeted activity of these compounds is very promising, blocking the SARS-CoV-2 at two levels; at the entry stage by interacting with the ACE2 host receptor, and during the replication and transcription steps by interacting with M^{pro}.

Cinnamon, a compound obtained from different plant species from the genus *Cinnamomum*, is a source of many antiviral compounds in traditional Indian medicine [106]. Cinnamon extracts showed moderate inhibitory activity in wild-type severe acute respiratory syndrome coronavirus (SARS-CoV) and HIV/SARS-CoV S pseudovirus infections [88]. In a preliminary in silico study, 48 isolated compounds across all cinnamon species were subjected to docking analysis with the spike S protein and M^{pro} of SARS-CoV-2. Teinufolin showed the highest binding affinity with M^{pro} through six hydrogen interactions and hydrophobic interactions with two amino acids, and pavettanin C1 showed the highest binding affinity with the spike S protein through nine hydrogen and hydrophobic interactions with four amino acids [87].

5. Conclusions

The potential contribution of food to consumers' health and wellbeing has so far been only partially exploited by food science. We expect that the pandemic health emergency and the urgent need to strengthen prevention and control strategies will contribute to the mobilization of research efforts in innovative topics including nutraceutical activities, food/drug interactions, improved bioavailability, and novel formulations of natural food components. Food-based approaches generally offer the advantage of reduced adverse side effects with respect to conventional pharmacology approaches.

A promising approach that involves food chemistry could be the formulation of food-based immune enhancers for COVID-19 patients to allow the proper intake of macro- and micronutrients and, at the same time, to help reduce infection severity.

Although micronutrients are safe compounds with important preventive and co-therapeutic activity for the treatment of many viruses, potentially including SARS-CoV-2, it should be considered that these molecules act on our biological system, and therefore, it is important to take food supplements in the correct doses, following expert advice, and only when it is necessary. It has been widely demonstrated that excessive doses of vitamins, mainly lipophilic ones, or minerals can provoke side effects that are harmful to human health. As confirmed by the Food and Agriculture Organization of the United Nations (FAO), the main preventive strategy against COVID-19 disease is the consumption of a healthy and balanced diet [107], whereas the use of supplements should be recommended only when really necessary.

In this context, the ongoing clinical trials discussed herein will give useful indications of the efficacy of the proposed protocols (compounds, dose, administration, etc.) and direct research toward new strategies.

The other strategic approach reported herein involves the discovery of lead compounds from food matrices through in silico studies; selected compounds can then be developed in drug-design studies, evaluated further in vitro and in vivo studies, and finally tested in clinical trials. Therefore, the food-science community could provide the most challenging and qualified contributions to investigation of the role of food both in the normal context and in the health emergency phase as it stands today.

In conclusion, many eating habits and beliefs about the role of food in human health have been shaken like an earthquake. At the end of the two-phase emergency, all of the main institutions, governments, and international agencies involving food and health consumers and the entire food chain are expected to kick-start and modify the global approach to food and its consumption, production, or transformation. In the remote past, humans used food as unique medicine; food-processing industrialization has reduced the natural value of their components, and the excessive use of ultraprocessed food has also favored morbidity conditions such as obesity, diabetes, and so on, that make individuals more susceptible to infective diseases. Therefore, it is arguable that the COVID-19 pandemic may be the first of many other global health crises that could be further exacerbated by progressively weakened immune systems.

Supplementary Materials: The following are available online at http://www.mdpi.com/2304-8158/9/8/1036/s1, Table S1. List of the current clinical trials related to food (micronutrients, foods/diets, and other supplements) used for the prevention/treatment of COVID-19 with NTC identifier number, study name, treatment, aim, number of participants, study responsible, phase, and start and estimated completion dates.

Funding: This research received no external funding.

Acknowledgments: Grants: Italian Ministry of Education, Universities and Research-Dipartimenti di Eccellenza-L. 232/2016; LOTTA CONTRO COVID-TASK FORCE CEINGE, Decreto Dirigenziale n. 672020—Regione Campania.

Conflicts of Interest: The authors declare no conflict of interest.

References

1. Rock, C.L.; Jacob, R.; Bowen, P.E. Update on the biological characteristics of the antioxidant micronutrients: Vitamin C, vitamin E, and the carotenoids. *J. Am. Diet. Assoc.* **1996**, *96*, 693–702. [CrossRef]
2. Hänsch, R.; Mendel, R.R. Physiological functions of mineral micronutrients (Cu, Zn, Mn, Fe, Ni, Mo, B, Cl). *Curr. Opin. Plant Biol.* **2009**, *12*, 259–266. [CrossRef] [PubMed]
3. Shahidi, F.; Ambigaipalan, P. Phenolics and polyphenolics in foods, beverages and spices: Antioxidant activity and health effects—A review. *J. Funct. Foods* **2015**, *18*, 820–897. [CrossRef]
4. Brennen, A.J.S.; Simon, F.M.; Howard, P.N.; Nielsen, R.K. *Types, Sources, and Claims of COVID-19 Misinformation*; Oxford Univ. Press: Oxford, UK, 2020.
5. Banerjee, A.; Kulcsar, K.; Misra, V.; Frieman, M.; Mossman, K. Bats and coronaviruses. *Viruses* **2019**, *11*, 41. [CrossRef] [PubMed]
6. Woo, P.C.Y.; Huang, Y.; Lau, S.K.P.; Yuen, K.Y. Coronavirus genomics and bioinformatics analysis. *Viruses* **2010**, *2*, 1805–1820. [CrossRef] [PubMed]
7. Su, S.; Wong, G.; Shi, W.; Liu, J.; Lai, A.C.K.; Zhou, J.; Liu, W.; Bi, Y.; Gao, G.F. Epidemiology, Genetic Recombination, and Pathogenesis of Coronaviruses. *Trends Microbiol.* **2016**, *24*, 490–502. [CrossRef]
8. World Health Organization. Naming the Coronavirus Disease (COVID-19) and the Virus That Causes It. Available online: https://www.who.int/emergencies/diseases/novel-coronavirus-2019/technical-guidance/naming-the-coronavirus-disease-(covid-2019)-and-the-virus-that-causes-it (accessed on 14 April 2020).
9. Amodio, E.; Vitale, F.; Cimino, L.; Casuccio, A.; Tramuto, F. Outbreak of Novel Coronavirus (SARS-CoV-2): First Evidences From International Scientific Literature and Pending Questions. *Healthcare* **2020**, *8*, 51. [CrossRef]
10. World Health Organization. Middle East respiratory Syndrome Coronavirus (MERS-CoV). Available online: https://www.who.int/emergencies/mers-cov/en/ (accessed on 23 April 2020).
11. World Health Organization. Consensus Document on the Epidemiology of Severe Acute Respiratory Syndrome (SARS). Available online: https://apps.who.int/iris/handle/10665/70863 (accessed on 23 April 2020).

12. World Health Organization. Coronavirus Disease (COVID-2019) Situation Reports. Available online: https://www.who.int/emergencies/diseases/novel-coronavirus-2019/situation-reports (accessed on 23 April 2020).
13. Huang, C.; Wang, Y.; Li, X.; Ren, L.; Zhao, J.; Hu, Y.; Zhang, L.; Fan, G.; Xu, J.; Gu, X.; et al. Clinical features of patients infected with 2019 novel coronavirus in Wuhan, China. *Lancet* **2020**, *395*, 497–506. [CrossRef]
14. Lupia, T.; Scabini, S.; Mornese Pinna, S.; Di Perri, G.; De Rosa, F.G.; Corcione, S. 2019 novel coronavirus (2019-nCoV) outbreak: A new challenge. *J. Glob. Antimicrob. Resist.* **2020**, *21*, 22–27. [CrossRef]
15. World Health Organization. The Top 10 Causes of Death. Available online: https://www.who.int/en/news-room/fact-sheets/detail/the-top-10-causes-of-death (accessed on 18 April 2020).
16. Zhang, L.; Liu, Y. Potential interventions for novel coronavirus in China: A systematic review. *J. Med. Virol.* **2020**, *92*, 479–490. [CrossRef]
17. Battistini, R.; Rossini, I.; Ercolini, C.; Goria, M.; Callipo, M.R.; Maurella, C.; Pavoni, E.; Serracca, L. Antiviral Activity of Essential Oils Against Hepatitis A Virus in Soft Fruits. *Food Environ. Virol.* **2019**, *11*, 90–95. [CrossRef] [PubMed]
18. Li, J.; Xu, Y.; Liu, J.; Yang, B.; Yang, C.; Zhang, M.; Dong, X. Drug resistance evolution in patients with human immunodeficiency virus-1 under long-term antiretroviral treatment-failure in Yunnan Province, China. *Virol. J.* **2019**, *16*, 5. [CrossRef] [PubMed]
19. Pawlotsky, J.M. Hepatitis C Virus Resistance to Direct-Acting Antiviral Drugs in Interferon-Free Regimens. *Gastroenterology* **2016**, *151*, 70–86. [CrossRef]
20. Wu, R.; Wang, L.; Kuo, H.C.D.; Shannar, A.; Peter, R.; Chou, P.J.; Li, S.; Hudlikar, R.; Liu, X.; Liu, Z.; et al. An Update on Current Therapeutic Drugs Treating COVID-19. *Curr. Pharmacol. Rep.* **2020**, *6*, 56–70. [CrossRef] [PubMed]
21. Islam, M.T.; Sarkar, C.; El-Kersh, D.M.; Jamaddar, S.; Uddin, S.J.; Shilpi, J.A.; Mubarak, M.S. Natural products and their derivatives against coronavirus: A review of the non-clinical and pre-clinical data. *Phyther. Res.* **2020**. [CrossRef] [PubMed]
22. Orhan, I.E.; Senol Deniz, F.S. Natural Products as Potential Leads Against Coronaviruses: Could They be Encouraging Structural Models Against SARS-CoV-2? *Nat. Prod. Bioprospect.* **2020**. [CrossRef]
23. Stahlmann, R.; Lode, H. Medication for COVID-19-an Overview of Approaches Currently Under Study. *Dtsch. Arztebl. Int.* **2020**, *117*, 213–219. [CrossRef]
24. Franquet, T. Respiratory infection in the AIDS and immunocompromised patient. *Eur. Radiol. Suppl.* **2004**, *14*, 21–33. [CrossRef]
25. Simon, A.K.; Hollander, G.A.; McMichael, A. Evolution of the immune system in humans from infancy to old age. *Proc. R. Soc. B Biol. Sci.* **2015**, *282*, 20143085. [CrossRef]
26. Zhang, L.; Lin, D.; Sun, X.; Curth, U.; Drosten, C.; Sauerhering, L.; Becker, S.; Rox, K.; Hilgenfeld, R. Crystal structure of SARS-CoV-2 main protease provides a basis for design of improved α-ketoamide inhibitors. *Science* **2020**, eabb3405. [CrossRef]
27. Vellingiri, B.; Jayaramayya, K.; Iyer, M.; Narayanasamy, A.; Govindasamy, V.; Giridharan, B.; Ganesan, S.; Venugopal, A.; Venkatesan, D.; Ganesan, H.; et al. COVID-19: A promising cure for the global panic. *Sci. Total Environ.* **2020**, *725*, 138277. [CrossRef] [PubMed]
28. Wu, C.; Liu, Y.; Yang, Y.; Zhang, P.; Zhong, W.; Wang, Y.; Wang, Q.; Xu, Y.; Li, M.; Li, X.; et al. Analysis of therapeutic targets for SARS-CoV-2 and discovery of potential drugs by computational methods. *Acta Pharm. Sin. B* **2020**. [CrossRef] [PubMed]
29. Lin, L.T.; Hsu, W.C.; Lin, C.C. Antiviral natural products and herbal medicines. *J. Tradit. Complement. Med.* **2014**, *4*, 24–35. [CrossRef] [PubMed]
30. Naithani, R.; Huma, L.; Holland, L.; Shukla, D.; McCormick, D.; Mehta, R.; Moriarty, R. Antiviral Activity of Phytochemicals: A Comprehensive Review. *Mini-Rev. Med. Chem.* **2008**, *8*, 1106–1133. [CrossRef]
31. Falcó, I.; Randazzo, W.; Rodríguez-Díaz, J.; Gozalbo-Rovira, R.; Luque, D.; Aznar, R.; Sánchez, G. Antiviral activity of aged green tea extract in model food systems and under gastric conditions. *Int. J. Food Microbiol.* **2019**, *292*, 101–106. [CrossRef]
32. U.S. National Library of Medicine. ClinicalTrials.gov. Available online: https://clinicaltrials.gov/ct2/home (accessed on 24 May 2020).
33. Maggini, S.; Pierre, A.; Calder, P.C. Immune function and micronutrient requirements change over the life course. *Nutrients* **2018**, *10*, 1531. [CrossRef]

34. Gombart, A.F.; Pierre, A.; Maggini, S. A review of micronutrients and the immune system–working in harmony to reduce the risk of infection. *Nutrients* **2020**, *12*, 236. [CrossRef]
35. Maggini, S.; Wintergerst, E.S.; Beveridge, S.; Hornig, D.H. Selected vitamins and trace elements support immune function by strengthening epithelial barriers and cellular and humoral immune responses. *Proc. Br. J. Nutr.* **2007**, *98*, 29–35. [CrossRef]
36. Martineau, A.R.; Jolliffe, D.A.; Hooper, R.L.; Greenberg, L.; Aloia, J.F.; Bergman, P.; Dubnov-Raz, G.; Esposito, S.; Ganmaa, D.; Ginde, A.A.; et al. Vitamin D supplementation to prevent acute respiratory tract infections: Systematic review and meta-analysis of individual participant data. *BMJ* **2017**, *356*. [CrossRef]
37. Taylor, C.E.; Camargo, C.A. Impact of micronutrients on respiratory infections. *Nutr. Rev.* **2011**, *69*, 259–269. [CrossRef]
38. Hemilä, H.; Douglas, R.M. Vitamin C and acute respiratory infections. *Int. J. Tuberc. Lung Dis.* **1999**, *3*, 756–761. [PubMed]
39. Hemilä, H. Vitamin C Supplementation and Respiratory Infections: A Systematic Review. *Mil. Med.* **2004**, *169*, 920–925. [CrossRef] [PubMed]
40. Fowler, A.A., III; Kim, C.; Lepler, L.; Malhotra, R.; Debesa, O.; Natarajan, R.; Fisher, B.J.; Syed, A.; DeWilde, C.; Priday, A.; et al. Intravenous vitamin C as adjunctive therapy for enterovirus/rhinovirus induced acute respiratory distress syndrome. *World J. Crit. Care Med.* **2017**, *6*, 85. [CrossRef] [PubMed]
41. Urashima, M.; Segawa, T.; Okazaki, M.; Kurihara, M.; Wada, Y.; Ida, H. Randomized trial of vitamin D supplementation to prevent seasonal influenza A in schoolchildren. *Am. J. Clin. Nutr.* **2010**, *91*, 1255–1260. [CrossRef] [PubMed]
42. World Health Organization. Zinc Supplementation to Improve Treatment Outcomes Among Children Diagnosed with Respiratory Infections. Available online: https://www.who.int/elena/titles/bbc/zinc_pneumonia_children/en/ (accessed on 3 July 2020).
43. Sazawal, S.; Black, R.E.; Jalla, S.; Mazumdar, S.; Sinha, A.; Bhan, M.K. Zinc supplementation reduces the incidence of acute lower respiratory infections in infants and preschool children: A double-blind, controlled trial. *Pediatrics* **1998**, *102*, 1–5. [CrossRef]
44. Al-Saady, N.M.; Blackmore, C.M.; Bennett, E.D. High fat, low carbohydrate, enteral feeding lowers PaCO2 and reduces the period of ventilation in artificially ventilated patients. *Intensive Care Med.* **1989**, *15*, 290–295. [CrossRef]
45. Yamanashi, T.; Iwata, M.; Kamiya, N.; Tsunetomi, K.; Kajitani, N.; Wada, N.; Iitsuka, T.; Yamauchi, T.; Miura, A.; Pu, S.; et al. Beta-hydroxybutyrate, an endogenic NLRP3 inflammasome inhibitor, attenuates stress-induced behavioral and inflammatory responses. *Sci. Rep.* **2017**, *7*, 1–11.
46. Chen, H.; Zhuo, Q.; Yuan, W.; Wang, J.; Wu, T. Vitamin A for preventing acute lower respiratory tract infections in children up to seven years of age. *Cochrane Database Syst. Rev.* **2008**, 1–46. [CrossRef]
47. Sempértegui, F.; Estrella, B.; Camaniero, V.; Betancourt, V.; Izurieta, R.; Ortiz, W.; Fiallo, E.; Troya, S.; Rodríguez, A.; Griffiths, J.K. The beneficial effects of weekly low-dose vitamin A supplementation on acute lower respiratory infections and diarrhea in Ecuadorian children. *Pediatrics* **1999**, *104*. [CrossRef]
48. Griffiths, J.K. The vitamin A paradox. *J. Pediatr.* **2000**, *137*, 604–607. [CrossRef]
49. Gay, R.; Meydani, S.N. The Effects of Vitamin E, Vitamin B6, and Vitamin B12 on Immune Function. *Nutr. Clin. Care* **2001**, *4*, 188–198. [CrossRef]
50. Strand, T.A.; Taneja, S.; Bhandari, N.; Refsum, H.; Ueland, P.M.; Gjessing, H.K.; Bahl, R.; Schneede, J.; Bhan, M.K.; Sommerfelt, H. Folate, but not vitamin B-12 status, predicts respiratory morbidity in north Indian children. *Am. J. Clin. Nutr.* **2007**, *86*, 139–144. [CrossRef] [PubMed]
51. De la Fuente, M.; Hernanz, A.; Guayerbas, N.; Victor, V.M.; Arnalich, F. Vitamin E ingestion improves several immune functions in elderly men and women. *Free Radic. Res.* **2008**, *42*, 272–280. [CrossRef] [PubMed]
52. Lee, Y.H.; Lee, S.J.; Lee, M.K.; Lee, W.Y.; Yong, S.J.; Kim, S.H. Serum selenium levels in patients with respiratory diseases: A prospective observational study. *J. Thorac. Dis.* **2016**, *8*, 2068–2078. [CrossRef]
53. De Silva, A.; Atukorala, S.; Weerasinghe, I.; Ahluwalia, N. Iron supplementation improves iron status and reduces morbidity in children with or without upper respiratory tract infections: A randomized controlled study in Colombo, Sri Lanka. *Am. J. Clin. Nutr.* **2003**, *77*, 234–241. [CrossRef]
54. Parada, J.; Aguilera, J.M. Food microstructure affects the bioavailability of several nutrients. *J. Food Sci.* **2007**, *72*, 21–32. [CrossRef]

55. Gayoso, L.; Claerbout, A.S.; Calvo, M.I.; Cavero, R.Y.; Astiasarán, I.; Ansorena, D. Bioaccessibility of rutin, caffeic acid and rosmarinic acid: Influence of the in vitro gastrointestinal digestion models. *J. Funct. Foods* **2016**, *26*, 428–438. [CrossRef]
56. Pressman, P.; Clemens, R.A.; Hayes, A.W. Bioavailability of micronutrients obtained from supplements and food. *Toxicol. Res. Appl.* **2017**, *1*, 239784731769636. [CrossRef]
57. Stanger, M.J.; Thompson, L.A.; Young, A.J.; Lieberman, H.R. Anticoagulant activity of select dietary supplements. *Nutr. Rev.* **2012**, *70*, 107–117. [CrossRef]
58. Olas, B. Anti-Aggregatory Potential of Selected Vegetables—Promising Dietary Components for the Prevention and Treatment of Cardiovascular Disease. *Adv. Nutr.* **2019**, *10*, 280–290. [CrossRef]
59. Tang, N.; Bai, H.; Chen, X.; Gong, J.; Li, D.; Sun, Z. Anticoagulant treatment is associated with decreased mortality in severe coronavirus disease 2019 patients with coagulopathy. *J. Thromb. Haemost.* **2020**, *18*, 1094–1099. [CrossRef] [PubMed]
60. Driggin, E.; Madhavan, M.V.; Bikdeli, B.; Chuich, T.; Laracy, J.; Biondi-Zoccai, G.; Brown, T.S.; Der Nigoghossian, C.; Zidar, D.A.; Haythe, J.; et al. Cardiovascular Considerations for Patients, Health Care Workers, and Health Systems During the COVID-19 Pandemic. *J. Am. Coll. Cardiol.* **2020**, *75*, 2352–2371. [CrossRef] [PubMed]
61. World Health Organization. Pandemic Influenza Vaccine Manufacturing Process and Timeline. Available online: https://www.who.int/csr/disease/swineflu/notes/h1n1_vaccine_20090806/en/ (accessed on 3 July 2020).
62. Ostaszewski, M.; Mazein, A.; Gillespie, M.E.; Kuperstein, I.; Niarakis, A.; Hermjakob, H.; Pico, A.R.; Willighagen, E.L.; Evelo, C.T.; Hasenauer, J.; et al. COVID-19 Disease Map, building a computational repository of SARS-CoV-2 virus-host interaction mechanisms. *Sci. Data* **2020**, *7*, 8–11. [CrossRef]
63. Lu, R.; Zhao, X.; Li, J.; Niu, P.; Yang, B.; Wu, H.; Wang, W.; Song, H.; Huang, B.; Zhu, N.; et al. Genomic characterisation and epidemiology of 2019 novel coronavirus: Implications for virus origins and receptor binding. *Lancet* **2020**, *395*, 565–574. [CrossRef]
64. Fani, M.; Teimoori, A.; Ghafari, S. Comparison of the COVID-2019 (SARS-CoV-2) pathogenesis with SARS-CoV and MERS-CoV infections. *Future Virol.* **2020**, *10*, 280–290. [CrossRef]
65. Hoffmann, M.; Kleine-Weber, H.; Schroeder, S.; Krüger, N.; Herrler, T.; Erichsen, S.; Schiergens, T.S.; Herrler, G.; Wu, N.H.; Nitsche, A.; et al. SARS-CoV-2 Cell Entry Depends on ACE2 and TMPRSS2 and Is Blocked by a Clinically Proven Protease Inhibitor. *Cell* **2020**, *181*, 271–280. [CrossRef]
66. Milanetti, E.; Miotto, M.; Di Rienzo, L.; Monti, M.; Gosti, G.; Ruocco, G. In-Silico evidence for two receptors based strategy of SARS-CoV-2. *BioRxiv* **2020**, 11107, under review. [CrossRef]
67. Huynh, T.; Wang, H.; Luan, B. In Silico Exploration of Molecular Mechanism of Clinically Oriented Drugs for Possibly Inhibiting SARS-CoV-2's Main Protease. *J. Phys. Chem. Lett.* **2020**. [CrossRef]
68. U.S. Food and Drog Administration. The Drug Development Process. Available online: https://www.fda.gov/patients/learn-about-drug-and-device-approvals/drug-development-process (accessed on 3 July 2020).
69. Öztürk, H.; Özgür, A.; Ozkirimli, E. DeepDTA: Deep drug-target binding affinity prediction. *Proc. Bioinf.* **2018**, *34*, 821–829. [CrossRef]
70. Joshi, R.S.; Jagdale, S.S.; Bansode, S.B.; Shankar, S.S.; Tellis, M.B.; Pandya, V.K.; Chugh, A.; Giri, A.P.; Kulkarni, M.J. Discovery of Potential Multi-Target-Directed Ligands by Targeting Host-specific SARS-CoV-2 Structurally Conserved Main Protease. *J. Biomol. Struct. Dyn.* **2020**, 1–16. [CrossRef]
71. Chen, H.; Du, Q. Potential natural compounds for preventing SARS-CoV-2 (2019-nCoV) infection. *Preprints* **2020**, 2020010358, under review. [CrossRef]
72. Cinatl, J.; Morgenstern, B.; Bauer, G.; Chandra, P.; Rabenau, H.; Doerr, H.W. Glycyrrhizin, an active component of liquorice roots, and replication of SARS-associated coronavirus. *Lancet* **2003**, *361*, 2045–2046. [CrossRef]
73. Islam, R.; Parves, M.R.; Paul, A.S.; Uddin, N.; Rahman, M.S.; Al Mamun, A.; Hossain, M.N.; Ali, M.A.; Halim, M.A. A molecular modeling approach to identify effective antiviral phytochemicals against the main protease of SARS-CoV-2. *J. Biomol. Struct. Dyn.* **2020**. [CrossRef] [PubMed]
74. Hashem, H.E. IN Silico Approach of Some Selected Honey Constituents as SARS-CoV-2 Main Protease (COVID-19) Inhibitors. *Eurasian J. Med. Oncol.* **2020**. [CrossRef]
75. Weng, J.R.; Lin, C.S.W.S.W.; Lai, H.C.; Lin, Y.P.; Wang, C.Y.; Tsai, Y.C.; Wu, K.C.; Huang, S.H.; Lin, C.S.W.S.W. Antiviral activity of Sambucus FormosanaNakai ethanol extract and related phenolic acid constituents against human coronavirus NL63. *Virus Res.* **2019**, *273*, 197767. [CrossRef] [PubMed]

76. Wahedi, H.M.; Ahmad, S.; Abbasi, S.W. Stilbene-based natural compounds as promising drug candidates against COVID-19. *J. Biomol. Struct. Dyn.* **2020**, 1–10. [CrossRef] [PubMed]
77. Li, Y.Q.; Li, Z.L.; Zhao, W.J.; Wen, R.X.; Meng, Q.W.; Zeng, Y. Synthesis of stilbene derivatives with inhibition of SARS coronavirus replication. *Eur. J. Med. Chem.* **2006**, *41*, 1084–1089. [CrossRef]
78. Khaerunnisa, S.; Kurniawan, H.; Awaluddin, R.; Suhartati, S. Potential Inhibitor of COVID-19 Main Protease (M pro) from Several Medicinal Plant Compounds by Molecular Docking Study. *Preprints* **2020**, 1–14, under review. [CrossRef]
79. Schwarz, S.; Sauter, D.; Wang, K.; Zhang, R.; Sun, B.; Karioti, A.; Bilia, A.R.; Efferth, T.; Schwarz, W. Kaempferol derivatives as antiviral drugs against the 3a channel protein of coronavirus. *Planta Med.* **2014**, *80*, 177–182. [CrossRef]
80. Jena, A.B. Catechin and Curcumin interact with corona (2019-nCoV/SARS-CoV2) viral S protein and ACE2 of human cell membrane. *Insights Comput. Study Implic. Interv.* **2020**, 1–19, under review. [CrossRef]
81. Park, J.Y.; Jeong, H.J.; Kim, J.H.; Kim, Y.M.; Park, S.J.; Kim, D.; Park, K.H.; Lee, W.S.; Ryu, Y.B. Diarylheptanoids from Alnus japonica inhibit papain-like protease of severe acute respiratory syndrome coronavirus. *Biol. Pharm. Bull.* **2012**, *35*, 2036–2042. [CrossRef] [PubMed]
82. Lee, C.; Lee, J.M.; Lee, N.R.; Kim, D.E.; Jeong, Y.J.; Chong, Y. Investigation of the pharmacophore space of Severe Acute Respiratory Syndrome coronavirus (SARS-CoV) NTPase/helicase by dihydroxychromone derivatives. *Bioorganic Med. Chem. Lett.* **2009**, *19*, 4538–4541. [CrossRef] [PubMed]
83. Chang, C.K.; Lo, S.C.; Wang, Y.S.; Hou, M.H. Recent insights into the development of therapeutics against coronavirus diseases by targeting N protein. *Drug Discov. Today* **2016**, *21*, 562–572. [CrossRef] [PubMed]
84. Lin, C.W.; Tsai, F.J.; Tsai, C.H.; Lai, C.C.; Wan, L.; Ho, T.Y.; Hsieh, C.C.; Chao, P.D.L. Anti-SARS coronavirus 3C-like protease effects of Isatis indigotica root and plant-derived phenolic compounds. *Antivir. Res.* **2005**, *68*, 36–42. [CrossRef] [PubMed]
85. Meneguzzo, F.; Ciriminna, R.; Zabini, F.; Pagliaro, M. Review of evidence available on hesperidin-rich products as potential tools against COVID-19 and hydrodynamic cavitation-based extraction as a method of increasing their production. *Processes* **2020**, *8*, 549. [CrossRef]
86. Thuy, B.T.P.; My, T.T.A.; Hai, N.T.T.; Hieu, L.T.; Hoa, T.T.; Thi Phuong Loan, H.; Triet, N.T.; Van Anh, T.T.; Quy, P.T.; Van Tat, P.; et al. Investigation into SARS-CoV-2 Resistance of Compounds in Garlic Essential Oil. *ACS Omega* **2020**, *5*, 8312–8320. [CrossRef]
87. Prasanth, D.S.N.B.K.; Murahari, M.; Chandramohan, V.; Panda, P.; Atmakuri, L.R.; Guntupalli, C. In silico identification of potential inhibitors from Cinnamon against main protease and spike glycoprotein of SARS CoV-2. *J. Biomol. Struct. Dyn.* **2020**, 1–15. [CrossRef]
88. Zhuang, M.; Jiang, H.; Suzuki, Y.; Li, X.; Xiao, P.; Tanaka, T.; Ling, H.; Yang, B.; Saitoh, H.; Zhang, L.; et al. Procyanidins and butanol extract of Cinnamomi Cortex inhibit SARS-CoV infection. *Antivir. Res.* **2009**, *82*, 73–81. [CrossRef]
89. Yu, M.S.; Lee, J.; Lee, J.M.; Kim, Y.; Chin, Y.W.; Jee, J.G.; Keum, Y.S.; Jeong, Y.J. Identification of myricetin and scutellarein as novel chemical inhibitors of the SARS coronavirus helicase, nsP13. *Bioorganic Med. Chem. Lett.* **2012**, *22*, 4049–4054. [CrossRef]
90. Keum, Y.S.; Jeong, Y.J. Development of chemical inhibitors of the SARS coronavirus: Viral helicase as a potential target. *Biochem. Pharmacol.* **2012**, *84*, 1351–1358. [CrossRef]
91. Wang, X.; Zhang, H.; Chen, L.; Shan, L.; Fan, G.; Gao, X. Liquorice, a unique "guide drug" of traditional Chinese medicine: A review of its role in drug interactions. *J. Ethnopharmacol.* **2013**, *150*, 781–790. [CrossRef]
92. Fiore, C.; Eisenhut, M.; Krausse, R.; Ragazzi, E.; Pellati, D.; Armanini, D.; Bielenberg, J. Antiviral effects of Glycyrrhiza species. *Phyther. Res.* **2008**, *22*, 141–148. [CrossRef]
93. Wang, L.; Yang, R.; Yuan, B.; Liu, Y.; Liu, C. The antiviral and antimicrobial activities of licorice, a widely-used Chinese herb. *Acta Pharm. Sin. B* **2015**, *5*, 310–315. [CrossRef] [PubMed]
94. Carino, A.; Moraca, F.; Fiorillo, B.; Marcanó, S.; Sepe, V.; Biagioli, M.; Finamore, C.; Bozza, S.; Francisci, D.; Distrutti, E.; et al. Hijacking SARS-Cov-2/ACE2 receptor interaction by natural and semi-synthetic steroidal agents acting on functional pockets on receptor binding region. *BioRxiv* **2020**. [CrossRef]
95. Koech, R.K.; Wanyoko, J.; Wachira, F. Antioxidant, antimicrobial and synergistic activities of tea polyphenols. *Int. J. Infect. Dis.* **2014**, *21*, 98. [CrossRef]

96. Meinhart, A.D.; Damin, F.M.; Caldeirão, L.; de Jesus Filho, M.; da Silva, L.C.; da Silva Constant, L.; Filho, J.T.; Wagner, R.; Godoy, H.T. Chlorogenic and caffeic acids in 64 fruits consumed in Brazil. *Food Chem.* **2019**, *286*, 51–63. [CrossRef]
97. Francioso, A.; Mastromarino, P.; Masci, A.; d'Erme, M.; Mosca, L. Chemistry, Stability and Bioavailability of Resveratrol. *Med. Chem.* **2014**, *10*, 237–245. [CrossRef]
98. Tian, B.; Liu, J. Resveratrol: A review of plant sources, synthesis, stability, modification and food application. *J. Sci. Food Agric.* **2020**, *100*, 1392–1404. [CrossRef]
99. Filardo, S.; Di Pietro, M.; Mastromarino, P.; Sessa, R. Therapeutic potential of resveratrol against emerging respiratory viral infections. *Pharmacol. Ther.* **2020**, *214*, 107613. [CrossRef]
100. Pezet, R.; Perret, C.; Jean-Denis, J.B.; Tabacchi, R.; Gindro, K.; Viret, O. δ-viniferin, a resveratrol dehydrodimer: One of the major stilbenes synthesized by stressed grapevine leaves. *J. Agric. Food Chem.* **2003**. [CrossRef]
101. Lee, S.; Mailar, K.; Il Kim, M.; Park, M.; Kim, J.; Min, D.H.; Heo, T.H.; Bae, S.K.; Choi, W.; Lee, C. Plant-derived purification, chemical synthesis, and in vitro/in vivo evaluation of a resveratrol dimer, viniferin, as an HCV Replication inhibitor. *Viruses* **2019**, *11*, 890. [CrossRef] [PubMed]
102. Hossen, M.J.; Uddin, M.B.; Ahmed, S.S.U.; Yu, Z.L.; Cho, J.Y. Kaempferol: Review on natural sources and bioavailability. In *Kaempferol: Biosynthesis, Food Sources and Therapeutic Uses*; Nova Science Publishers: New York, NY, USA, 2016; pp. 101–150. ISBN 9781634858588.
103. Dixit, P. *Medicinal Properties of Garlic: A Review*; Anusandhaan-Vigyaan Shodh Patrika, B.S.N.V. Post Graduate College: Lucknow, India, 2018; Volume 6.
104. Swamy, M.K.; Akhtar, M.S.; Sinniah, U.R. Antimicrobial properties of plant essential oils against human pathogens and their mode of action: An updated review. Evidence-based Complement. *Altern. Med.* **2016**, *2016*, 1–21.
105. Bayan, L.; Koulivand, P.H.; Gorji, A. Garlic: A review of potential therapeutic effects. *Avicenna J. Phytomed.* **2014**, *4*, 1–14. [CrossRef] [PubMed]
106. Kumar, S.; Kumari, R.; Mishra, S. Pharmacological properties and their medicinal uses of Cinnamomum: A review. *J. Pharm. Pharmacol.* **2019**, *71*, 1735–1761. [CrossRef]
107. Food and Agriculture Organization of the United Nations (FAO). Maintaining a Healthy Diet during the COVID-19 Pandemic. Available online: http://www.fao.org/documents/card/en/c/ca8380en/ (accessed on 2 July 2020).



© 2020 by the authors. Licensee MDPI, Basel, Switzerland. This article is an open access article distributed under the terms and conditions of the Creative Commons Attribution (CC BY) license (http://creativecommons.org/licenses/by/4.0/).

8.3. Review 2: Food bioactive compounds as NLRP3 inflammasome modulators

Inflammasomes are key intracellular multimeric proteins able to initiate the cellular inflammatory signaling pathway. NLRP3 inflammasome represents one of the main protein complexes involved in the development of inflammatory events, and its activity has been largely demonstrated to be connected with inflammatory or autoinflammatory disorders, including diabetes, gouty arthritis, liver fibrosis, Alzheimer's disease, respiratory syndromes, atherosclerosis, and cancer initiation. In recent years, it has been demonstrated how dietary intake and nutritional status represent important environmental elements that can modulate metabolic inflammation, since food matrices are an important source of several bioactive compounds. In this review, an updated status of knowledge regarding food bioactive compounds as NLRP3 inflammasome modulators is discussed. Several chemical classes, namely polyphenols, organosulfurs, terpenes, fatty acids, proteins, amino acids, saponins, sterols, polysaccharides, carotenoids, vitamins, and probiotics, have been shown to

possess NLRP3 inflammasome-modulating activity through in vitro and in vivo assays, mainly demonstrating an anti-NLRP3 inflammasome activity. Plant foods are particularly rich in important bioactive compounds, each of them can have different effects on the pathway of inflammatory response, confirming the importance of the nutritional pattern (food model) as a whole rather than any single nutrient or functional compoun

nutrients

MDPI

Review

Modulatory Properties of Food and Nutraceutical Components Targeting NLRP3 Inflammasome Activation

Mattia Spano [1], Giacomo Di Matteo [1], Cinzia Ingallina [1], Donatella Ambroselli [1], Simone Carradori [2,*], Marialucia Gallorini [2], Anna Maria Giusti [3], Andrea Salvo [1], Michela Grosso [4] and Luisa Mannina [1]

[1] Department of Chemistry and Technology of Drugs, Sapienza University of Rome, Piazzale Aldo Moro 5, 00185 Rome, Italy; mattia.spano@uniroma1.it (M.S.); giacomo.dimatteo@uniroma1.it (G.D.M.); cinzia.ingallina@uniroma1.it (C.I.); donatella.ambroselli@uniroma1.it (D.A.); andrea.salvo@uniroma1.it (A.S.); luisa.mannina@uniroma1.it (L.M.)
[2] Department of Pharmacy, "G. d'Annunzio" University of Chieti-Pescara, Via dei Vestini 31, 66100 Chieti, Italy; marialucia.gallorini@unich.it
[3] Department of Experimental Medicine, Sapienza University of Rome, Piazzale Aldo Moro 5, 00185 Rome, Italy; annamaria.giusti@uniroma1.it
[4] Department of Molecular Medicine and Medical Biotechnology, School of Medicine, University of Naples Federico II, CEINGE-Biotecnologie Avanzate, 80131 Naples, Italy; michela.grosso@unina.it
* Correspondence: simone.carradori@unich.it

Abstract: Inflammasomes are key intracellular multimeric proteins able to initiate the cellular inflammatory signaling pathway. NLRP3 inflammasome represents one of the main protein complexes involved in the development of inflammatory events, and its activity has been largely demonstrated to be connected with inflammatory or autoinflammatory disorders, including diabetes, gouty arthritis, liver fibrosis, Alzheimer's disease, respiratory syndromes, atherosclerosis, and cancer initiation. In recent years, it has been demonstrated how dietary intake and nutritional status represent important environmental elements that can modulate metabolic inflammation, since food matrices are an important source of several bioactive compounds. In this review, an updated status of knowledge regarding food bioactive compounds as NLRP3 inflammasome modulators is discussed. Several chemical classes, namely polyphenols, organosulfurs, terpenes, fatty acids, proteins, amino acids, saponins, sterols, polysaccharides, carotenoids, vitamins, and probiotics, have been shown to possess NLRP3 inflammasome-modulating activity through in vitro and in vivo assays, mainly demonstrating an anti-NLRP3 inflammasome activity. Plant foods are particularly rich in important bioactive compounds, each of them can have different effects on the pathway of inflammatory response, confirming the importance of the nutritional pattern (food model) as a whole rather than any single nutrient or functional compound.

Keywords: NLRP3 inflammasome; modulation activity; food; nutrients

Citation: Spano, M.; Di Matteo, G.; Ingallina, C.; Ambroselli, D.; Carradori, S.; Gallorini, M.; Giusti, A.M.; Salvo, A.; Grosso, M.; Mannina, L. Modulatory Properties of Food and Nutraceutical Components Targeting NLRP3 Inflammasome Activation. *Nutrients* **2022**, *14*, 490. https://doi.org/10.3390/nu14030490

Academic Editor: Francesca Giampieri

Received: 30 November 2021
Accepted: 20 January 2022
Published: 23 January 2022

Publisher's Note: MDPI stays neutral with regard to jurisdictional claims in published maps and institutional affiliations.

Copyright: © 2022 by the authors. Licensee MDPI, Basel, Switzerland. This article is an open access article distributed under the terms and conditions of the Creative Commons Attribution (CC BY) license (https://creativecommons.org/licenses/by/4.0/).

1. Introduction

1.1. The NLRP3 Inflammasome

Inflammasomes are key intracellular multimeric protein complexes, able to initiate inflammatory signaling through sensor receptors, defined as pattern-recognition receptors (PPR). PPRs recognize pathogen-associated molecular patterns (PAMPs), or damage-associated molecular patterns (DAMPs) generated by endogenous stress stimuli. The signal transduction continues intracellularly through an adaptor protein and an effector enzyme that cause the maturation and the secretion of pro-inflammatory cytokines. As a result, the inflammasome activation ends up with the production of caspase-1, a major mediator in the inflammatory adaptive immune cell response [1]. Pro-interleukin 1β (pro-IL-1β) and pro-IL-18 are cleaved by active caspase-1 into their

biologically active form to trigger endothelial cell responses, such as vasodilatation, which allows the extravasation of immune cells, or acts to control hypotension, fever, and pain threshold. In particular, IL-18 is crucial for interferon-gamma (IFN-γ) production and thus for adaptive immunity [2]. Finally, caspase-1 activation stimulates a unique pro-inflammatory cell death process, namely pyroptosis. Pyroptosis triggers intracellular pathogens to escape from their replicative environment, leading to their exposition to immune factors and thus allowing the immune system to face infections (Figure 1) [3].

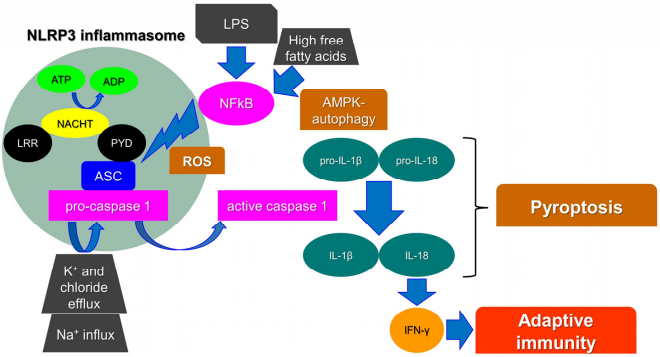


Figure 1. NLRP3 activation and the main players involved in pyroptosis. Leucine-rich repeat (LRR), pyrin domain (PYD), interferon-gamma (IFN-γ), interleukin (IL), reactive oxygen species (ROS), lipopolysaccharide (LPS), NOD-, LRR- and pyrin domain-containing protein 3 (NLRP3), caspase-recruitment domain (ASC), nuclear factor kappa-light-chain-enhancer of activated B cells (NF-kB), AMP-activated protein kinase (AMPK), adenosine diphosphate (ADP), adenosine triphosphate (ATP).

Among other PPRs, leucine-rich repeat (LRR)-containing proteins (NLR) family members (NLRP1 and 3) are widely known as components of inflammasomes. In particular, it has been reported that the NLRP3 inflammasome is crucial for adaptive cell responses towards viral, bacterial, and fungal infections. Nevertheless, when dysregulated, it has been associated with a variety of inflammatory or autoinflammatory disorders, such as diabetes, gouty arthritis, liver fibrosis, Alzheimer's disease (AD), respiratory syndromes, atherosclerosis, and cancer initiation [4]. The NLRP3 protein consists of a C-terminal leucine-rich repeat (LRR) domain and an amino-terminal pyrin domain (PYD). The central domain is a nucleotide-binding, oligomerization domain (NACHT domain). The interaction between the PYD domain with the caspase-recruitment domain (ASC) facilitates the initiation of the inflammasome assembly. In parallel, the NACHT domain functions as an ATPase and the amount of ADP produced allows NLRP3 oligomerization and activation [5]. Finally, the LRR domain functions as a signal effector; although, its role is still not fully understood. It has been highlighted that the NLRP3, lacking the LRR domain, can be fully activated via the canonical inflammasome pathway. It has been therefore hypothesized that it may act as an auto-inhibitor, thus controlling aberrant signal amplification and participating in a protective mechanism, avoiding autoinflammation [6].

Many molecular mechanisms/compounds have been widely proposed for the activation of NLRP3, involving, among others, biological, physical, chemical, and metabolic agents, such as uric acid crystals, cholesterol, free fatty acids and lipids, β-amyloid (BA) protein, aluminum hydroxide, high intracellular glucose, and high levels of reactive oxygen species (ROS). Others factors, such as heme, ionic flux, lipopolysaccharide (LPS) toxin, pathogen-associated RNA, and ceramides, are also included [7]. Likewise,

Ca^{2+}-related signaling, Na^{+} influx, and K^{+} and chloride efflux have been reported as crucial events in the NLRP3 inflammasome [8]. As a matter of fact, a recently identified component of the NLRP3 inflammasome, namely NEK7 (NIMA-related kinase 7), requires K^{+} efflux for inflammasome assembly. It has been proposed that the activation of NLRP3 requires two steps. Firstly, the mitotic kinase NEK7 binds to NLRP3; although, this complex could not be sufficient for NLRP3 activation. Indeed, the inflammasome oligomerization requires ATP binding and thus the conversion of NACHT from an inactive to an active conformation [9]. Reactive oxygen species (ROS) production, mainly from mitochondria, has also been reported as an initiator of the activation of the NLRP3 inflammasome. Many studies have shown that NLRP3 agonists generate ROS in different cell types. As an example, fatty acid caused by a high-fat diet activates the NLRP3 inflammasome through the molecular axis AMPK–autophagy–NF-kB-ROS [7]. Moreover, Amyloid β, post-translational modifications of NLRP3, and non-canonical inflammasome activations have been reported as triggers for the NLRP3 inflammasome [10–12].

1.2. Food and Inflammation (Diet and Inflammation)

The emerging role of chronic inflammation as a determinant in the progress of the major degenerative diseases typical of modern society has promoted research to comprehend the influence of nutrition and dietary patterns on inflammatory markers. Dietary intake and nutritional status represent important environmental factors, which can modulate metabolic inflammation. In recent years, research has advanced significantly to achieve understanding of the impact of dietary components on metabolic inflammation, in the context of chronic infirmities, such as obesity, type-2 diabetes (T2D), cardiovascular diseases (CVD), and cancer [13]. Inflammatory and innate immune responses, provoked by pathogen-associated and other danger-associated signals, appearing during infections, result in the activation of cytosolic inflammasomes. Inflammasome signaling mainly furnishes a host innate immune defense against a broad range of microbial infections, including influenza virus [14,15]. Furthermore, NLRP3 inflammasome can also be activated by different endogenous risk agents, such as palmitic acid, amyloid β, and cholesterol crystals [16]. So, NLRP3 inflammasome intervening in such responses is associated with the development of several lifestyle-related chronic diseases, characterized by persistent inflammation [17].

In the mid-1900s, an important concept was emerging about the relationship between the immune and metabolic response systems, indicating that insulin resistance (IR), glucose intolerance, dyslipidemia, and other metabolic abnormalities occur in the course of an infection. Later, in the 1980s, a reduced binding capacity of insulin to its receptor in isolated blood cells was found in human patients affected by acute infection [18]. The network that connects metabolic and immune functions has been structured in relation to a lifestyle that was quite different from that of today, so that the current metabolic overload induces a low-grade chronic inflammatory state, for which some authors have recently proposed the term “metaflammation”. This term is used to describe the chronic low-grade inflammation orchestrated by metabolic cells in response to excess nutrients and energy. Metaflammation plays a pivotal role in the development and systemic expansion of the metabolic disease. White adipose tissue is likely to be the primary site of the metaflammation development; although, progressively, other metabolic tissues, such as liver, pancreas, and gut cells, get involved, affecting the metabolic homeostasis [13,19,20].

The strong link between nutrient sensing and immune signaling is justified by an evolutionarily conserved crosstalk pathway between immune and metabolic mediators. The functional units that control key metabolic and immune functions in higher organisms have evolved from common ancestral structures. Some invertebrates, such as the fruit fly *Drosophila melanogaster* or the nematode *Caenorhabditis elegans*, gave similar evidence of a conventional cellular crosstalk between immune and metabolic organs. Basically, cytokines act as metabolic hormones in the adaptation to nutrient fluctuations

[13]. In *Drosophila*, for example, the body fat acts as the liver, adipose, and immune system, serving both the functions of nutrient storage and body defense [20]. During the course of evolution, a conservative, similar structure in an ancient mammalian ancestor differentiated into distinct metabolic organs and immune ones, as we essentially have in modern mammals, including humans. The principal framework of this translation from an adaptative to a maladaptive state is resumed by three integrated systems—Eiger, the *Drosophila* orthologue of TNF, and its receptor Wengen (in *Drosophila*) or TNFR (human); insulin and its receptors (dILP in *Drosophila*, insulin receptor insR in human); the TLR signaling pathways (Toll receptor in *Drosophila*). TNF and TLR signaling block insulin pathway or production through JNK activation and MyD88, from flies to humans, whereas activation results in abnormal metabolic homeostasis adaptation, which leads to a chronic metabolic inflammation. As a result, immunometabolic diseases often appear as clusters and promote ageing, disability, and premature death [13].

It has been shown that an excess of fat mass, especially the visceral type, associated with a diet rich in saturated fats and simple sugars and low in fiber and micronutrients (minerals and vitamins), which is the current Western diet, is able to promote a chronic low-grade inflammatory state, which, albeit involving molecules and signals common to the classic inflammatory response, recognizes the primary trigger in the metabolic overload [21]. Conversely, obesity, by inducing chronic low-grade activation of inflammatory pathways, is linked to the development of IR and T2D [22]. In relation to the different organ meiopragia, genetically determined, the metaflammation can manifest itself in pathologies, such as tumors, neuro- and cardio-vascular diseases, neurodegenerative diseases (AD), or metabolic diseases (metabolic syndrome, T2D, non-alcoholic fatty liver disease (NAFLD)). These pathologies are characterized by a variable increase in serum biomarkers level of inflammation, especially TNF-α, IL-1β, IL-6, PCR, fibrinogen, intercellular (ICAM1), and vascular (VCAM1) adhesion molecules, etc. These biomarkers were also shown to be significantly related to the risk of T2D, cardiovascular disease and cancers in healthy subjects [23].

Moreover, particular interest has been directed to IL-1β-mediated inflammation because of the strong inter-relationship between dietary fats, metabolic stressors, and NLRP3-mediated inflammation [24]. Metabolic stress, in the form of obesity, saturated fatty acids (SFAs), cholesterol, reactive oxygen species, and/or uric acid promote IL-1β signaling [25]. IL-1β disrupts cellular metabolism by interrupting a range of signaling pathways, including insulin sensitivity, lipid metabolism, and adipogenesis [26]. It is now widely accepted that IL-1β signaling plays a key role in the development of obesity, IR, and T2D risk [27–31].

1.3. Role of Diet in Inflammatory Response

During the feeding/fasting cycle, in physiological conditions, an intermittent, non-specific, low-grade inflammatory response occurs at the level of "metabolic tissues" (adipose, muscle, and liver tissue), which results in a transient increase in some inflammatory proteins/cytokines in the serum. This increment reaches its maximum peak during the absorption phase (post-prandial) and then gradually decreases in about 2 h, when the nutrients have been distributed, metabolized, and/or accumulated in the respective cellular sites [32]. The inflammatory response is amplified in overeating conditions (hyperlipidic diet, excess of saturated fats and simple carbohydrates, and low intake of fiber, vitamins, and antioxidant compounds), in obesity, and in diabetes—when the metabolic overload generates a "traffic jam" of the physiological metabolic pathways, progressive recruitment and activation of immune-competent cells, such as macrophages, mast cells, and T lymphocytes, occurs [33]. This results in the establishment of a vicious circle in which the physiological quiescent phase of the inflammatory response is incomplete and generates a pro-inflammatory milieu that impairs the metabolic functions [34]. On the contrary, a food pattern adherent to the Mediterranean dietary model is associated with a reduction in serum concentration of inflammatory biomarkers [35]. The complex mechanisms

through which this inflammatory response is induced by the diet are gradually emerging. It was found that both stages of IL-1β priming and NLRP3-mediated IL-1β activation may be affected by the nutritional environment. One of these mechanisms appears to be associated with the quality of the diet, that is, the excess or lack of specific nutrients intake [28,36].

1.4. Fatty Acids and Inflammatory Response

Experimental data showed that the quantity and quality of fats influences the acute inflammatory response to a single meal. The study revealed that SFAs content and the ratio among polyunsaturated fatty acids (PUFAs) from ω-3 to ω-6 have proved to be the major determinants of the extent of postprandial inflammatory response [36,37]. In particular, it has been observed that high meal SFA increased inflammatory indices; contrarily, high ω-3/ω-6 PUFA ratio decreased them [36,37].

Fatty acids can affect the inflammatory response either through the synthesis of eicosanoids that regulate the transduction of signals at cell membrane or cytoplasmic level, by modulating the activity of transcription factors involved in the inflammatory process.

An examination of data from the National Health and Nutrition Examination Survey (NHANES 99-00) found that levels of SFAs in serum phospholipids of male civil servant workers (40–69 years) positively correlated with some inflammatory markers, such as HS-CRP (high sensitivity C-reactive protein) and fibrinogen; by contrast, phospholipid PUFA levels were inversely associated with HS-CRP [32,36]. It has been recently shown in a C57BL/6 male mice model that consuming a high-fat diet, enriched with SFAs, induces especially adipose IL-1β inflammation and insulin resistance. However, if SFAs are replaced with monounsaturated fatty acids (MUFAs), an attenuation of NLRP3-mediated inflammation is observed [16,28].

In vitro studies have shown that SFAs, such as lauric, myristic, and palmitic acids, are able to activate the Toll-like receptors (TLR) of adipocytes and macrophages [28]. The SFA-TLR interaction determines the activation of c-jun N-terminal kinase (JNK), the inhibitor of kappa B kinase (IKK), and protein kinase R (PKR), to which it follows that:

- Phosphorylation of insulin receptor substrate-1 (IRS-1) in serine and its degradation and elimination through the ubiquitin pathway, thus blocking insulin signal transmission;
- Activation of the transcription factor NF-kB, by its dissociation from the cytoplasmic inhibitor (IkB) and transfer to the nucleus, with over-regulation of the pro-inflammatory gene expression.

In conclusion, SFAs impair insulin signaling through TLR4, activating the NF-κB pathway and NLRP3 inflammasome that promotes the conversion of pro-IL-1β into mature IL-1β [16,31,32]. In a clinical study, the relationship between SFAs and inflammation biomarkers has been demonstrated in subjects with excess weight, in which the ω6:ω3 ratio is directly related to the concentrations of IL-6, CRP, and adhesion molecules; in addition, the inhibition of IRS-1 and the reduction in adiponectin levels induce IR, thus increasing the risk of the metabolic syndrome [21]. Additionally, trans-fatty acid (TFA) consumption has been found to be positively associated with markers of systemic inflammation. In the Harvard Nurses' Health Study, it emerged that TFA intake was positively associated with IL-6 and HS-CRP in women with higher BMI (body mass index) and serum HS-CRP level [38]. Partially hydrogenated oils (PHO) are the main source of industrially produced TFA. PHO is an ingredient in different foods, including margarine and vegetable shortening, but also in baked foods (crackers, biscuits, pies), or in those fried in semi-hydrogenated oils/fats. However, there are also many foods that naturally contain TFA, such as dairy products and meat from ruminant animals. A review of observational and interventional data concluded that the TFA pro-inflammatory effects (increased TNF-α, IL-6, and HS-CRP) were associated with markers of vascular endothelial dysfunction and were most evident when compared with the effects of cis-unsaturated fatty acids [38].

Controlled trials and observational studies provide concordant demonstration that the TFA intake from PHO adversely affects multiple cardiovascular risk factors and contributes significantly to increased risk of CHD events [39]. Several experimental and observational studies in humans have demonstrated the potential benefits of replacing SFAs with unsaturated fatty acids, such as oleic acid and PUFAs. These studies have shown an inverse association between consumption of ω-3 PUFA and systemic markers of inflammation, such as TNFs and ILs [40]. ω-6 PUFA consumption shows variable effects on inflammation. Both anti-inflammatory and pro-inflammatory effects have been described [41], suggesting how the interaction of ω-6 PUFAs and their lipid mediator derivatives in the context of inflammation is complex and still not properly understood. For example, in overweight subjects, the serum concentration of ω-6 PUFAs (α-linoleic acid (ALA), AL, and AA) has been shown to be inversely related to IL-6 levels [41]. ω-3 PUFAs (ALA, eicosapentaenoic acid (EPA) and especially docosahexaenoic acid (DHA)) have much more marked effects than ω-6 PUFAs in reducing the expression of numerous pro-inflammatory cytokines, such as IL-6, TNF-α, IL-18, sICAM-1, sVCAM-1, sE-selectin, and HS-CRP. ω-3 PUFAs suppress NLRP3 inflammasome in obese subjects through downregulation of inflammasome gene expression in adipocytes and macrophages [28]. It has been shown that stimulation of macrophages with ω-3 PUFAs (at a dose of 20 μM) was able to suppress NLRP3 inflammasome activation and to inhibit subsequent caspase-1 activation and IL-1β secretion [42,43].

Furthermore, the ω-3 PUFAs, by binding to the G-protein-coupled receptor 120 (GRP120—a membrane receptor sensitive to fatty acids, expressed at the level of macrophages), block the NFκB activation pathway. Finally, EPA would be able to inhibit the activity of the Δ-6 desaturase enzyme, thus reducing AA formation [42,44]. Some studies indicate that dietary consumption of MUFAs, oleic acid in particular, may have anti-inflammatory effects. Studies suggest that dietary MUFAs can reduce IL-1β-mediated adipose dysfunction and insulin resistance via preservation of AMP-activated protein kinase (AMPK) activity which, in turn, quenches NLRP3 inflammasome activation [30,45,46].

1.5. Carbohydrates and Inflammatory Response

Diets with relatively high glycemic index (GI) and glycemic load (GL) have been linked to elevated risk of T2D, coronary heart disease, and stroke, particularly among overweight individuals [47]. GI and GL are associated with an increase in the plasma concentration of inflammatory biomarkers, such as IL-6, HS-CRP, and IL-18 [36]. There are convincing data suggesting that NLRP3 inflammasome is fundamental in the deleterious effect observed in chronic hyperglycemia and oxidative stress. Hyperglycemia is associated with both conditions of oxidative stress and inflammatory state and promotes mitochondrial metabolism in β cells which enhances the production of ROS, thus inducing NLRP3 inflammasome activation and then IL-1β production [48].

Recent clinical trials indicate that targeting the prototypic pro-inflammatory cytokine IL-1β ameliorates the outcomes of cardiovascular disease, which is the first cause of death in T2D patients. Several T2D-related metabolic factors, including reactive oxygen species, glyco/lipoxidation end products, and cholesterol crystals, have been involved in the pathogenesis of diabetes complications (diabetic kidney disease and diabetic retinopathy) and in the progression of atherosclerosis and NAFLD [49].

High levels of glucose and non-esterified fatty acids (NEFAs) can cause oxidative stress due to both the decoupling of oxidative phosphorylation and to the increased mitochondrial β-oxidation. Lee et al. found that hyperglycemia-induced elevated mitochondrial reactive oxygen species in myeloid cells of T2D patients are associated with increased production of inflammasome-dependent cytokines IL-1β and IL-18 [50]. Some data also showed that inhibition of AMP-activated protein kinase can exacerbate ROS-dependent NLRP3 activation [50]. It was recently pointed out that NLRP3 might directly sense the presence of increased ROS production (mitochondrial superoxide anion radical

($O_2^{\bullet-}$), hydrogen peroxide (H_2O_2)) by normal or malfunctioning mitochondria, or indirectly by other activators of NLRP3. In particular, it was suggested that increased ROS are sensed by a complex of redox-dependent inhibition of thioredoxin (TRX) and TRX-interacting protein (TXNIP) and cause the dissociation of the complex described above. Following an increase in cellular ROS concentration, this complex dissociates and TXNIP binds to the LRR region of NLRP3, with the consequent NLRP3 activation [51].

Chronic hyperglycemia (associated or not with increased triglycerides and NEFAs) promotes the formation of advanced glycation end-products (AGEs). The interaction between AGEs and receptors for advanced glycation end-products (RAGEs), the activation of the polyols pathway and the auto-oxidation of glucose lead to increased production of ROS which, in turn, induce the activation of transcription factors, such as NF-kB [52]. The result is an increase in inflammatory biomarkers, such as HS-CRP, IL-6, IL-1β, IL-8, IL-18, and TNF-α, matrix metalloproteinases, and markers of endothelial dysfunction (VCAM-1, ICAM-1 and E-selectin). Redox signaling molecules, such as ROS, mediate NLRP3 inflammasome activation, while ROS inhibitors suppress NLRP3 inflammasome-mediated inflammation [52], indicating the vital role of oxidative stress on inflammasome activation that can be prevented by supplementation with antioxidants, such as vitamin C, E, lipoic acid, phenolic compounds, and other bioactive compounds found in plant foods [48,53].

Consumption of whole grains, through increased fiber intake, is associated with a reduction in serum concentrations of inflammation biomarkers (HS-CRP, IL-6, Il-1 β); although, the mechanisms still need to be elucidated, and a synergistic effect of fiber, minerals, vitamins, or phytochemicals, such as lignans and phenolic acids, could take place [21,36].

Several studies in recent years have demonstrated the role of specific nutrients in the primary or secondary prevention of inflammation-related diseases, such as metabolic syndrome and diabetes. In this regard, some nutraceuticals and bioactive compounds (polyphenols, flavonoids, carotenoids, curcumin, resveratrol, etc.) have been widely studied and have been recognized for their ability to inhibit the synthesis of TNF-α in monocytes and macrophages and downregulate the expression of TLR2 and TLR4 in human monocytes [1].

However, due to the reciprocal synergistic or antagonistic interactions between nutrients and/or other food compounds (antinutrients and/or phytochemicals), it is clear that, in order to understand the role of diet in the modulation of the inflammatory state and oxidative stress, it is necessary to evaluate the nutritional pattern in its entirety. It was found that diet characterized by an abundant consumption of vegetables, fruit, nuts, olive oil, legumes, and fish, with moderate amounts of alcohol and low intake of red meat, processed meats, refined grains, and dairy products, has a protective effect against immunometabolic diseases [49]. These aspects correspond to the characteristics of the Mediterranean dietary pattern. Indeed, several studies have shown an inverse association between the degree of adherence to the diet Mediterranean and serum levels of IL-6, CRP, and TNF-α [35].

2. Materials and Methods

The literature search was carried out in August 2021 in official scientific databases, using combinations of keywords "NLRP3", "NLRP3 inflammasome", "food", "nutrients", and "bioactive compound" in the literature published during the last five years. Study selection and data were collected according to the 2009 Preferred Reporting Items for Systematic Reviews and Meta-Analyses (PRISMA) guidelines [54], Figure 2.

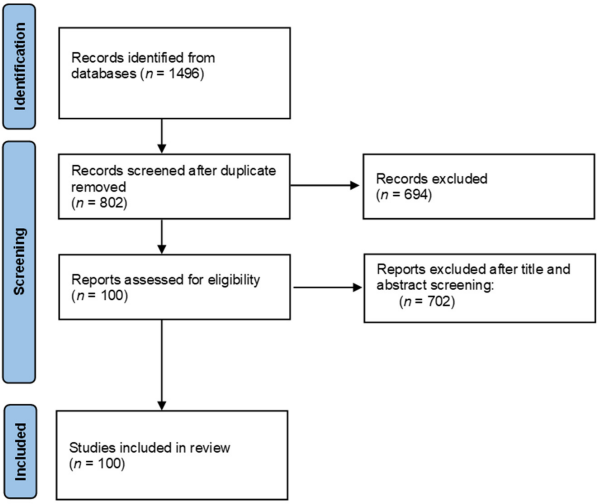


Figure 2. Preferred Reporting Items for Systematic Reviews and Meta-Analyses (PRIMSA) flow chart.

3. Food Components as NLPR3 Modulators

3.1. Polyphenols

Polyphenols are secondary metabolites produced by the metabolic processes of plants. Although more than 8000 polyphenols have been identified up to now, all these compounds arise from a common intermediate—phenylalanine or shikimic acid. Generally, they occur in conjugated forms, with one or more sugar residues, organic acids, amines, lipids, and other phenols [55]. Polyphenols may be classified into different groups based on their phenol rings number or on the structural elements that bind these rings to one another. The main classes include phenolic acids, flavonoids, stilbenes, and lignans. In recent years, a great interest on the potential health effects of polyphenols has been developed, since these molecules have shown to be mainly characterized by antioxidant and anti-inflammatory activities, proving to be very effective in the prevention and reduction in tumors, chronic inflammations, diabetes, aging, and infections [56]. The anti-inflammatory activity of polyphenols has also been demonstrated with the inhibition of the NLRP3 inflammasome activation. In the present paragraph, the anti-NLRP3 inflammasome activity of several polyphenols is discussed, by dividing the discussed compounds basing on their polyphenol class. A summary list of all the discussed food derived molecules is presented in Table 1.

Table 1. Summary list of all the discussed food-derived molecules with a NLRP3 inflammasome modulatory activity. Compound name, food source, considered experimental model, dose, treatment duration, and main outcome are described.

Chemical Class	Compound	Food Source	Experimental Model	Dose	Treatment (Duration)	Main Outcome	References
Phenolic acids	Sinapic acid	Vegetables, spices, fruits, cereals, oilseed wine, vinegar	Male Kunming mice (induced colitis)	10, 50 mg/kg	7 days	Dose-dependent reduction in the NLRP3 inflammasome proteins expression.	[57]
	Ferulic acid	Fruits, vegetables, grains, beans, seeds, nuts, grasses, corn, wheat, turmeric	Male Wistar rat (induced kidney injury)	25, 50 mg/kg	15 days	Both doses of ferulic acid administration have produced an amelioration of NLRP3 and caspase-1 proteins expression.	[58]
	Chlorogenic acid	Fruit, coffee beans, eggplants	1. Male and female BALB/c mice (colon tissue)	1. 20, 40 mg/kg	1. 7 days	1. Decrease in NLRP3, ASC, caspase-1 p45, and caspase-1 p20 protein levels.	[59]
			2. RAW264.7 cells	2. Many concentrations of chlorogenic acid	2. Not reported	2. Decrease secretion of IL-1β and IL-18.	
Flavones and flavonones	Apigenin	Parsley, onions, oranges, tea	1. Male C57BL/6 J mice (induced NAFLD)	1. 50 mg/kg of BW per day	1. 7 days	1., 2.: Reduction in NLRP3, ASC, pro-caspase-1, caspase-1, together with a reduction in ROS production. 3. Reduced NLRP3 protein expression.	1 and 2. [60] 3. [61]
			2. Hepa1–6 cells	2. 16 and 32 µM	2. 24 h		
			3. ISO-HAS human endothelial cells	3. 30 and 50 µM	3. 24 h		
	Isoorientin	Gentiana	1. Male ICR mice (induced hyperuricemia)	1. 5 and 10 mg/kg of BW	1. Single dose	Dose-dependent inhibition of xanthine oxidase activity and interleukin release.	[62]

			2. MXC207 cells	2. 25, 50, 100, 200, and 400 μM	2. 24 h		
	Chrysin	Honey, propolis, carrots, chamomile, fruits, mushrooms	Male Sprague Dawley rats (induced hyperuricemia)	50, 100, and 150 mg/kg of BW	4 weeks	Reduction in IL-1β expression and ROS activity.	[63]
	Luteolin	Chamomile, carrots, olive oil, species	Male Sprague Dawley rats (induced SCII)	50 and 100 mg/kg of BW	14 days	Reduction in NLRP3, IL-1β, and IL-18 expression.	[64]
	Hesperidin methylchalcone	Citrus	Swiss mice (induced gout arthritis)	30 mg/kg of BW	Single dose	Reduction in NLRP3, ASC, pro-caspase-1, and pro-IL-1β mRNA expression.	[65]
	Naringin	Citrus	Male C57BL/6 mice (induced ulcerative colitis)	25, 50, and 100 mg/kg of BW	7 days	Dose-dependent reduction in NLRP3, ASC, caspase-1, and IL-1β expression.	[66]
Flavonols	Quercetin	Fruits, vegetables, seeds, grains	1. Male SPF-Wistar rats (induced liver injury)	1. 100 mg/kg of BW	1. 14 days	1. Reduction in ROS, NF-κB, NLRP3, IL-1β, and IL-18 expression.	1. [67]
			2. ApoE-/- mice (induced atherosclerotic inflammation)	2. 100 mg/kg of BW	2. 16 days	2. Decrease in pro-IL-1β and IL-1β production.	2. [68]
			3. Senescence accelerated mouse P8 and R1	3. 35 and 70 mg/kg of BW	3. 4 weeks	3. Increase in cognitive functions and reduction in NLRP3 activation factors expression.	3. [69]
			4. Caco-2 cell triggered with E.coli	4. 200 μM	4. 12 h	4. Reduction in NLRP3, caspase-1, and IL-1β expression, together with an enhanced ROS scavenger activity.	4. [70]
	Dihydroquercetin	Onions, milk thistle, Douglas fir bark	1. Male C57BL/6 mice (induced liver steatosis)	1. 1, 5, and 25 mg/kg of BW	1. Single dose	Inhibition of NLRP3, caspase-1 cleavage, and IL-1β production.	[71]

			2. Human hepatoma cells HepG2	2. 6.25, 25, and 100 μM	2. 1 h		
	Kaempferol	Tea, vegetables, oranges, wine	Male C57BL/6 mice (induced hepatotoxicity)	30 and 60 mg/kg of BW	7 days	Dose-dependent reduction in IL-1β, TNF-α, and IL-6 expression.	[72]
	Myricetin	Vegetables, fruits, nuts, berries, tea, red wine	Male Wistar rats (induced diabetes)	20 mg/kg of BW	4 weeks	Reduced NLRP3 inflammasome activation.	[73]
Other phenolics	Curcumin	Turmeric	1. Male Sprague Dawley rats (chronic unpredictable mild stress)	1. 100 mg/kg of BW	1. 4 weeks	1. Reduction in IL-1β, IL-6 and TNF-α expression.	1. [74]
			2. Hemodialysis patients	2. 2.5 g of turmeric (95% curcumin) after dialysis	2. 12 weeks	2. Lower expression levels of NLRP3 inflammasome markers (NF-kB, NLRP3 and IL-1β.	2. [75]
	6-shogaol	Ginger roots	1. Human artery smooth muscle cells (induced calcification)	1. Not indicated	1. Not indicated	1. Reduction in NLRP3, caspase-1 and IL-1β expression.	1. [76]
			2. Human THP-1 monocytes	2. 5, 10, 20 and 40 μM	2. 1 h	2. Reduction in the canonical NLRP3 inflammasome-mediated IL-1β secretion.	2. [77]
	Pterostilbene	Grapes, blueberries	1. Female BALB/c mice (induced acute liver failure)	1. 50 mg/kg/12 h of BW	1. 24 h	1., 2.: Decrease in IL-1β, IL-6, caspase-1, TNF-α, and NLRP3 protein expression. 3. Increased autophagy, resulting in a decrease in NLRP3 and caspase-1.	1. [78]
			2. Female C57BL/6 mice (allergic contact dermatitis)	2. 500 mg/kg of BW	2. 5 weeks		2. [79]
			3. NRK-52E cells	3. 2 μM	3. 24, 48, and 72 h		3. [80]
	Polydatin	Grapes juice	1. Male Sprague Dawley rats	1. 25 and 50 mg/kg of BW	1. 7 days	1. Dose-dependent decrease in IL-1β, TNF-α, IL-6, NLRP3, and caspase-1.	1. [81] 2 and 3. [82]

			(induced hyperuricemia)				
			2. Male Wistar rats (induced dry-eye disease)	2. 0.05 and 0.5% ocular solution	2. 4 days	2. Dose-dependent decrease in IL-1β, IFN-α, TNF-α, and IL-6.	
			3. Human conjunctival cell line HCC	3. 0.1, 1 and 10 μM	3. 8 h	3. Dose-dependent decrease in NLRP3 and caspase-1.	
	Cyanidin-3-O-β-glucoside	Red-violet fruits	1. Human retinal pigment epithelium cells, ARPE-19	1. 50 and 100 μM	1. 2 h	1. Dose-dependent decrease in NLRP3, IL-18, IL-β and caspase-1.	1. [83]
			2. Male C57BL/6 J mice (induced hepatic inflammation)	2. 200 mg/kg of BW	2. 8 weeks	2. Decrease in NLRP3, IL-18, IL-1β, and caspase-1 expression, together with the block of NF-κB signaling pathway.	2. [84]
	Epigallocatechin-3-gallate	Green tea	1. Male Balb/C mice (induced acute pancreatitis) 2. Balb/C adherent cells 3. APP/PS1 transgenic mice 4. Mouse microglial cell line BV2	1. 5, 10, 20, 40, and 80 mg/kg of BW 2. 2.5, 5, and 10 μM 3. 2 mg/kg of BW 4. 10 μM	1. 4 weeks 2. 24 h 3. 4 weeks 4. 1 h	1. Dose-dependent decrease in IL-1β. 2. Dose-dependent decrease in caspase-1, IL-1β, and ROS. 3., 4.: Suppressed activation of NLRP3 inflammasome via TLR4/NF-κB pathway.	1. and 2. [85] 3. and 4. [86]
	Resveratrol (encapsulated in poly(lactic-co-glycolic acid) nanoparticles)	Grapes, blueberries, raspberries, mulberries, peanuts	1. Male C57BL/6 mice (induced kidney injury) 2. Epithelial cell line HK-2	1. 2 and 4 mg/kg 2. 25, 50, and 100 μM	1. 2 weeks 2. 24 h	1., 2.: Dose-dependent reduction in NLRP3, pro-caspase-1, cleaved-caspase-1, and IL-1β expression.	1, and 2. [87]
Polyphenols mixture	1. Fermented non-digestible fraction of baked corn and	Zea mays L., Phaseolus vulgaris L.	Caco-2 cells, THP-1 cells	1. 40, 200, and 300 μg/mL	48 h	Inhibition of the NLRP3 assemblage, decreasing caspase-1 activity, IL-1β, and apoptosis.	[88]

	common bean snacks (FNDF) 2. FNDF pure components (include gallic acid)			2. Gallic acid 38.85 μM			
	1. Green tea polyphenols (GTPs) 2. Epigallocatechin-3-gallate (EGCG)	Green tea	Male ICR mice (liver tissue)	1. 0.32% GTPs (*w*/*v*) 2. 0.32% EGCG (*w*/*v*)	12 days	Downregulation of NLRP3, ASC, caspase-1, and IL-1β proteins expression.	[89]
	Green tea polyphenols (GTPs)	Green tea	Male ICR mice (liver tissue)	100, 200 mg/kg of BW	7 days	Inhibition of NLRP3, ASC, and caspase-1 (p20) expression in a dose-dependent manner.	[90]
	Soy isoflavones	Soybeans	Male C57BL/6 mice (colon tissue)	50, 100 mg/kg of BW	5 days	Reduction in NLRP3, Caspase-1 p20 and ASC protein levels and suppression of IL-1β and IL-18 secretion.	[91]
	Red raspberry polyphenols	*Rubus idaeus L.*	1. Male C57BL/6 mice (adipose tissue) 2. C3H10T1/2 cells	1. 120 mg/kg of BW per day 2. 10 μg mL^{-1}	1. 16 weeks 2. 2 days	1. Attenuation of NLRP3 inflammasome activation in adipose tissue macrophages and epididymal white adipose tissue. 2. Reducing of IL-1β, IL-18, and NLRP3 protein levels expression.	[92]
Organosulfur compounds	Allicin	Garlic	1. Male Sprague Dawley rats (acrylamide treated) 2. Kupffer cells (BNCC341160)	1. 25 and 50 mg/kg of BW 2. 3.75, 7.5, and 15 μM	1. 4 weeks 2. 2 h	1., 2.: Reduced NLRP3 inflammasome activation, decreasing cleaved-caspase-1, IL-1β, IL-18, IL-6, and TNF-α secretion.	1. and 2. [93]
	Benzyl isothiocyanate	Cruciferous vegetables	1. Male C57BL/6 J mice (induced	1. 1 g/kg of BW 2. 2.5 and 5.0 μM	1. 9 weeks 2. 4 h	1., 2.: Reduction in NLRP3, p20 caspase-1, and IL1-β expression.	1. and 2. [94]

			nonalcoholic steatohepatitis) 2. Mice Kupffer cells				
	Sulforaphane	Cruciferous vegetables	BALB/c mice (induced pancreatic injury)	5 mg/kg of BW	3 days	Reduced expression of NLRP3, p20 caspase-1, and IL1-β.	[95]
	Methylsulfonylmethane	Garlic	Bone marrow-derived macrophages	0.3, 0.5, 1.0, 2.0, 4.0, and 8.0%	6 h	Blocking the NF-κB signaling and pro IL1-β expression.	[96]
Terpenes and terpenoids	Carnosic acid	*Rosmarinus* and *Salvia*	Male Balb/c mice (induced acute colitis)	50 or 100 mg/kg of BW	10 days	Reduced release of caspase-2 and ROS.	[97]
	Geranylgeraniol	Flax, sunflower, and olive oils	Daoy cells	50 μM	24 h	Inhibition of NLRP3 gene expression.	[98]
	Kaurenoic Acid	*X. aethiopica* fruits	BALB/c mice macrophages	10, 30, 50, 70, and 90 μM	24 h	Increased the production of NO and IL-1β.	[99]
Fatty acids	Saturated fatty acids	Palmitate acid	LPS-primed bone marrow-derived macrophages generated from wild-type (WT), *Nlrp3*$^{-/-}$, *Pycard*$^{-/-}$, or *Nlrc4*$^{-/-}$	200 or 500 μM	24 h	Inhibition of AMP-activated protein kinase followed by the accumulation of mitochondrial ROS, thus activating the NLRP3-ASC inflammasome and causing caspase-1, IL-1β, and IL-18 increased production.	[16]
		Stearate acid	LPS-primed bone marrow-derived dendritic cells	250 μM	5, 20 h	NLRP3 inflammasome activation mediated by IRE1α activation (inositol-requiring enzyme 1-α) through the saturated phosphatidylcholine accumulation.	[100]
		Virgin coconut oil	Male *Wistar* rats AD (receiving Amyloid-β) and high-fat diet (HFD)	8 and 10%	8 weeks	Reduction in IL-1β protein, caspase-1, and NLRP3 genes expression.	[101]

			models both in vitro and in vivo				
	PUFA	Fish oil	Obesity male *Wistar* rat models	Intragastrically 1 mL/kg per day	8 weeks	Reduction in IL-1β protein, caspase-1, and NLRP3 genes expression.	[102]
		Safflower oil	A. Fat-1 transgenic mice generated onto a C57BL/6 background B. Wild-type mice	10 g safflower oil (per 100 g of diet)	80 days	Caspase-1, IL-1β, and IL-18 reduction. Blockade of high glucose-induced TXNIP via the PI3K/Akt pathway in pre-adipocytes.	[103]
		Walnut oil	DSS-induced colitis in Kunming (KM) male mice	2.5 mL/kg·d Walnut oil	27 days	inhibition of ROS production, mediation of NLRP3/ASC/caspase-1 signaling pathway, regulation of gut microbiota and SCFAs levels.	[104]
		DHA	A. ASH-associated mouse LPS-induced Kupffer cell lines B. C57BL/6 J mice	1. 50 μM 2. Intragastrally DHA 50 mg/kg once per day	1. 4 h 2. 7 days	Mechanisms through which ω-3 PUFAs reduce metabolic inflammation may include the G protein-coupled receptor 120 (GPR120) and GPR40 which interact with NLRP3 and inhibited the NLRP3 inflammasome complex assembly.	[105]
		Fish oil	Male Sprague Dawley rats (prefrontal cortex and hippocampus of rats)	1.5 g/kg of BW	3 weeks	Reduced MDA level and mRNA levels of pro-inflammatory cytokines 1 L-1β, IL-6. Mitigation of the LPS-induced P2X7R and NLRP3 activation, downregulated LPS-induced iNOS and NF-κB expression in both prefrontal cortex and hippocampus.	[106]
Proteins and amino acid derivatives	RDP2	*Oryza Sativa*	Kunming mice (induced hyperuremia)	Allopurinolo: 10 mg/kg of BW Benzbromaron: 8 mg/kg of BW RDP2: 5, 10, 100 μg/kg of BW	7 days	1. Reduction serum uric acid levels 2. Reduction in NLRP3, ASC, and caspase-1 expression in the kidneys.	[107]

RDP3	*Oryza Sativa*	Kunming mice (induced hyperuremia)	Allopurinol: 10 mg/kg of BW Benzbromaron: 8 mg/kg of BW RDP3: 100 μg/kg, 500 μg/kg and 1 mg/kg of BW	7 days	1. Serum uric acid concentrations in the RDP3 group were significantly lower than in the other treatments. 2. RDP3 reduced inflammation by inhibiting the expression of the NLRP3 inflammasome.	[108]
TMOP (Tuna meat oligopeptides)	Tuna	ICR mice (induced hyperuremia)	50 mg/kg and 300 mg/kg of BW	8 weeks	Dose-dependent reduction in hyperuricaemia, due to the inhibition of NLRP3 inflammasome complex.	[109]
Soy protein concentrate (SPC)	Soy	CF-1 mice (induced acute ulcerative colitis)	DSS (1.5% DSS in drinking fluid and AIN93G), DS6 (1.5% DSS and 6% dietary SPC), and DS12 (1.5% DSS and 12% dietary SPC)	7 days	Prevent increased pro-inflammatory signaling and thereby moderate colitis severity.	[110]
α-gliadin 31–43	Gluten	C57BL/6 mice intestinal samples	200 μl	4/16 h	1. Formation of oligomers that activate the inflammasome. 2. Stimulation of IL-1β release.	[111]
N-acetyl-cysteine (NAC)	Garlic, onions, and leeks	Raised and pregnant sows	500 mg/kg of BW	From day 85 until delivery	Reduction maternal and placental inflammatory cytokines through inhibition of the NLRP3 inflammasome.	[112]
Glycine	Fish, meat, spirulina algae, soy protein, egg whites	C57BL/6 male mice (induced lung injury)	1000 mg in 5 mL of 0.9% saline	7 days	Prevent mucin reduction and upregulation of pro-inflammatory cytokines.	[113]
Carnosine	Fish and meat	SAMP8 mice	100–200 mg/kg of BW	6 weeks	Decreased levels of malondialdehyde and reactive oxygen species (ROS), increased activity of superoxide dismutase (SOD) and the level of adenosine triphosphate;	[114]

						NLRP3 inflammasome reduction.	
	L-Homocarnosine	Meat	Ischemic albino Wistar rats	0,5 mM and 1 mM	45 days	Reduction in NLRP3 inflammasome levels to near normal levels.	[115]
	Choline	Eggs, meat, fish, legumes	APP/PS1 transgenic mice	1.10 g/kg and 4.95 g/kg of BW	9 mounths	Reduction Aβ deposition, microgliosis, and pro-inflammatory cytokine production.	[116]
Saponins and sterols	25-OCH_3-PPD ginsenoside	*Panax ginseng*	C57BL/6 mice (induced TAA)	5, 10, or 20 mg/kg of BW	5 weeks	Reduction inflammation by regulating P2X7R-mediated NLRP-3 inflammasome.	[117]
	Rh1 and Rg2 ginsenosides	*Panax notoginseng*	C57BL/6 mice (induced NAFLD)	50 or 150 mg/kg of BW	9 weeks	Inhibition NLRP3 inflammasome, promoting mitophagy, and reduction mtROS production.	[118]
	Ginsenoside compound K (CK)	*Panax ginseng*	Diabetic db/db and db/m mice	10 mg/kg of BW	12 weeks	Downregulation inflammatory cytokines and mediator production by suppressing the NLRP3 inflammasome pathway.	[119]
	Magnesium isoglycyrrhizinate	*Glycyrrhiza glabra*	Sprague Dawley mice	10, 20, and 40 mg/kg of BW	11 weeks	Inhibition the activation of the NF-κB/inflammasome NLRP3 and reduction the immunological–inflammatory response.	[120]
	Physalin B	*Physalis alkekengi L.*	BALB/c mice	250 μL	7 days	Reduction the pro-inflammatory cytokine levels, suppression the NF-κB cascade and pathway STAT3 and arrestin1 signaling, and inhibition NLRP3 inflammasome activation.	[121]
	β-sitosterol	*Moringa oleifera*	HaCaT keratinocytes and J774A.1 macrophages	7.5 to 30 μM	24 h	Significant reduction in NLRP3 expression, inhibition of caspase-1, and NF-KB activation in macrophages.	[122]
Polysaccharides	Polysaccharide composed of galactose, glucose, mannose, and arabinose with molar ratios of	*Trametes orientalis*	Male Kunming mice (induced lung injury)	Intragastrally 50, 100, 200 mg/kg of BW	21 days	Suppression of IL-1β expression and blockage of NLRP3, ASC, and caspase-1 increases in a dose-dependent manner.	[123]

5.79:5.77:3.45:1.20 (average MW 63000)						
Polysaccharides extracted from *Dendrobium officinale*	*Dendrobium officinale*	1. DSS male BalB/c mice (induced induced acute ulcerative colitis) 2. LPS-stimulated NCM460 cells	1. 50, 100, and 200 mg/kg of BW 2. 50, 100, and 200 mg/mL	1. 7 days 2. 24 h	Suppression of NLRP3, ASC, caspase-1, IL-1β, and IL-18 mRNA expression.	[124]
CYP-1 mannoglucan	*Chinese yam*	1. In vitro RAW 264.7 murine macrophage cells 2. In vivo DDS-induced colitis male C57BL/6 J mice	1. 31.25, 62.5, 125, 250, and 500 μg/mL 2. Intragastrically 300 mg/kg of BW	1. 24 h 2. 7 days	Suppress the expression of several key genes involved in colonic inflammatory signaling pathways (such as NF-κB and NLRP3).	[125]
Ganoderma lucidum polysaccharides	*Ganoderma lucidum*	Male Kun-Ming mice	50, 100, 150 mg/kg of BW	7 days	Decreased protein expression levels of NLRP3, ASC, and caspase-1 in liver tissue.	[126]
Mannose, arabinose, and fucose at a molar ratio of 1.6:1.0:2.7	*Armillariella tabescens,*	Male C57BL/6 J mice	100, 200, and 400 mg/kg Per day	4 weeks	Reduction in MDA, pro-inflammatory factors (TNF-α, IL-18, and IL-1β) and FAS, G6Pase, and PEPCK levels in a dose-dependent manner. Decreased TXNIP and NLRP3 expression levels.	[127]
Low methoxyl pectin		4-week-old female non-obese diabetic (NOD) mice	Diets with 5% (wt/wt) LMP	1. 36 weeks 2. 18 weeks	Suppression of NLRP3 and associated proteins expression (NLRP3, caspase-1-p20, cleaved IL-1β, and cleaved IL-18) in cecum; increase in the SCFAs (short chain fatty acids) by gut microbiota.	1. [128] 2. [129]
Non-digestible carbohydrates (NDCs) consisting	Chayote fruit	Human THP-1 macrophage-like cells	100, 200, and 400 μg/mL	24 h	Inhibition of CC-induced active caspase-1 (400 μg/mL), reduction in ROS accumulation and IL-1β. mRNA expression	[130]

of pectic homogalacturonan and highly branched rhamnogalacturonan-II, as well as hemicellulosic material including glucomannan, xyloglucan, and glucurono(arabino) xylan		Human monocytic cell line THP-1			of IL-1β and NLRP3 in macrophage-like cells. Inhibition of NLRP3 and IL-1β gene expression in both CC-pretreated macrophage-like cells LPS-induced cells.	
Mannoglucan sulfate SF-2	Starfish (*A. rollestoni*)	1. RAW 264.7 cells murine macrophages 2. Primary peritoneal macrophages isolated form male ICR mice 3. ICR mice	1. and 2. 80 μg/mL 3. 30 and 60 mg/kg of BW	1. and 2. 0 h, 0.5 h, 1 h, 3 h, 6 h, and 9 h. C. 14 days	Improved release of cytokines and NLRP3 expression by the elevated expression of NLRP3, cleaved caspase-1, and ASC proteins.	[131]

Abbreviations: NLR family pyrin domain containing 3 (NLRP3), caspase-recruitment domain (ASC), interleukin (IL), reactive oxygen species (ROS), tumor necrosis factor (TNF).

3.1.1. Phenolic Acids

Phenolic acids are one of the main compounds of polyphenol class. Phenolic acids are characterized by a phenolic ring with a carboxylic acid function and can be further divided into two main groups, benzoic acid or cinnamic acid derivatives, based on the C1–C6 or C3–C6 backbones [132]. Several compounds belonging to the phenolic acids family have shown to possess interesting antioxidative and anti-inflammatory properties [56,133]. The modulating activity against the NLRP3 inflammasome complex has also been widely studied [1].

Sinapic acid is a hydroxycinnamic acid widely found in many foodstuffs, such as vegetables, spices, citrus, berry fruits, cereals, oilseed crops, wine, and vinegar. Sinapic acid has shown antioxidant and anti-inflammatory properties [134], as well as a modulating activity against the NLRP3 inflammasome complex in mouse models with chemically induced colitis [57]. The monitoring of NLRP3 inflammasome protein levels in the inflamed colon tissue of Kunming mice (colitis model), by Western blot analysis, after sinapic acid treatment for 7 days, have shown a reduction in the amounts of NLRP3, ASC, IL-1β, and caspase-1 proteins. In particular, the administration of 50 mg/kg of sinapic acid had a higher effect than 10 mg/kg.

Ferulic acid is an another hydroxycinnamic acid commonly found in fruits, vegetables, grains, beans, leaves, seeds, nuts, grasses, flowers, and in some plants, such as corn and wheat, and in the spice turmeric [135]. A total of 24 adult male Wistar rats with kidney injury induced by methotrexate were treated with 25 or 50 mg/kg of ferulic acid for 15 days [58]. Both doses of ferulic acid have produced an amelioration of NLRP3 and caspase-1 proteins expression, and subsequently a reduction in the IL-1β levels in the rat kidneys.

Chlorogenic acid is another phenolic acid, widely studied for its anti-inflammatory properties [136]. Chlorogenic acid can be found in foods, such as apples, coffee beans, eggplants, grapes, kiwi fruits, pears, plums, potatoes, tea, and tomatoes. This molecule has demonstrated an inhibitory effect against the NLRP3 signaling pathway, decreasing the protein levels of NLRP3, ASC, caspase-1 p45, and caspase-1 p20 in the colon tissue of BALB/c mice with induced colitis [59]. The NLRP3 expression reduction in RAW264.7 cells stimulated by LPS and adenosine triphosphate, resulting in the decreased secretion of IL-1β and IL-18, was also observed.

Lastly, among cinnamaldehyde-related compounds, only cinnamaldehyde and 2-methoxycinnamaldehyde limited the expression of NLRP3 and pro-IL-1β at 25–100 μM, whereas cinnamic acid, cinnamyl alcohol, cinnamyl acetate, and α-methylcinnamaldehyde were ineffective, thus demonstrating the importance of the propenal group in the side chain [137,138].

3.1.2. Flavones and Flavanones

Among flavones, apigenin, largely present in common fruits and vegetables, such as parsley, onions, oranges, tea, etc., has shown to be effective in reducing NLRP3 inflammasome activation in two different studies. In the first one, in vivo and in vitro models of high-fat diet-induced non-alcoholic fatty liver disease (HFD-induced NAFLD) have been treated with apigenin [60]. In particular, mice were administered by gavage with 50 mg/kg apigenin (4 mg/kg HED); whereas, for in vitro studies, Hepa1–6 cells were exposed for 24 h with 16 and 32 μM apigenin. In both assays, an important liver reduction in NLRP3, ASC, pro-caspase-1, and caspase-1 (measured by PCR), together with a reduction in ROS production was obtained by inhibiting xanthine oxidase. In the second study [61], 30 and 50 μM apigenin showed to be effective in reducing NLRP3 protein expression in ISO-HAS human endothelial cells treated with the pro-inflammatory agent TMAO (trimethylamine *N*-oxide). Isoorientin, a flavone identified in Gentiana roots, has shown to possess anti-NLRP3 inflammasome activation in in vivo and in vitro models of hyperuricemia by using 5 and 10 mg/kg (0.4 and 0.8 mg/kg HED) dosages in male ICR mice for in vivo studies and

25, 50, 100, 200, and 400 μM isoorientin for in vitro assays (MXC207 cells). In both cases, a dose-dependent reduction in inflammasome expression was observed, through the inhibition of xanthine oxidase activity and interleukin release [62]. In a very similar way, the anti-inflammasome activity in hyperuricemia male Sprague Dawley mice model has also been demonstrated for chrysin flavone, used at 50, 100, and 150 mg/kg oral doses (4, 8, and 12 mg/kg HED) for 4 weeks [63]. Luteolin preventive effects in spinal cord ischemia–reperfusion injury (SCII) have been demonstrated in an in vivo study where the treatment of male Sprague Dawley mice with intragastric injections of 50 and 100 mg/kg doses (4 and 8 mg/kg HED) of the considered flavone for 14 days has shown to reduce, with respect to non-treated mice, the incoming of induced SCII. In particular, the reduction in this event has been associated with the reduction in NLRP3, IL-1β, and IL-18 expression by ELISA assay [64].

Regarding flavanones, hesperidin methylchalcone and naringin have been demonstrated to be effective in reducing NLRP3 inflammasome activation. In particular, hesperidin methylchalcone, particularly present in citrus fruits, has shown to reduce the NLRP3, ASC, pro-caspase-1, and pro-IL-1β mRNA expression in induced gout arthritis Swiss mice models when orally administrated at 30 mg/kg (2.4 mg/kg HED) [65]. In a model of DSS-induced ulcerative colitis in male C57BL/6 mice [66], naringin has shown to reduce NLRP3, ASC, caspase-1, and IL-1β expression in the colon tissue in a dose-dependent way, when administrated at 25, 50, and 100 mg/kg (2, 4, and 8 mg/kg HED) for 7 days.

3.1.3. Flavonols

Among polyphenols, quercetin, largely present in several vegetables and fruits, has been the most considered compound for the study of its anti-NLRP3 inflammasome activity. In particular, in an alcohol-induced acute liver injury in male SPF-Wistar mice, the oral administration of 100 mg/kg quercetin (8 mg/kg HED) for 14 days caused a reduction in the injury evolution, thanks to a lower expression of inflammasome factors including ROS, NF-κB, NLRP3 inflammasome, IL-1β, and IL-18, measured by ELISA assays in the liver tissue [67]. The same quercetin dosage described in the previous study has been applied for 16 days in high fat treated ApoE$^{-/-}$ mice to observe the potential reduction in atherosclerotic inflammation, where NLRP3 inflammasome is largely involved. In the study, an important decrease in pro-IL-1β and IL-1β was registered [68]. The effect of quercetin in reducing inflammasome activation has also been demonstrated for neurodegenerative models [69], since aging mice treated with 35 and 70 mg/kg (2.8 and 5.6 mg/kg HED) of quercetin for 4 weeks have shown a dose-dependent increase in the cognitive functions, together with an important reduction in NLRP3 activation factors expression by Western blot analysis. An in vitro assay on *E. coli*-infected cells has also been carried out to demonstrate the anti-inflammasome activity of quercetin during infection. In particular, the 12 h treatment with 200 μM quercetin before infection has shown to strongly reduce NLRP3, caspase-1, and IL-1β expression, together with an enhanced ROS scavenger activity [70]. Similarly, a quercetin saturated derivative, dihydroquercetin, has shown to be active against NLRP3 inflammasome in alcoholic liver steatosis in vivo (male C57BL/6 mice) and in vitro (human hepatoma cells HepG2) models [71]. Other two flavonols largely present in tea, vegetables, oranges and wine, namely kaempferol and myricetin, have been shown to be effective in reducing NLRP3 inflammasome. In particular, kaempferol has been used in an in vivo induced hepatotoxicity male C57BL/6 mice model, causing a dose-dependent decrease in NLRP3 inflammasome activation factors (IL-1β, TNF-α, IL-6) in the liver and in the blood when administrated at 30 and 60 mg/kg (2.4 and 4.8 mg/kg HED) dosages for 7 days [72]. It is noteworthy that, in this work, kaempferol has been extracted from a Chinese medical plant but, since its purity has been measured >98%, the activity can be asserted to the single molecule as it is. The same inflammasome inhibition has been observed for myricetin, when its activity has been considered in a high-fat diet model for the simulation of human T2D symptoms in male Wistar mice treated with oral doses of 20 mg/kg (1.6 mg/kg HED) myricetin for 4 weeks [73].

3.1.4. Other Phenolics

Curcumin is the main active compound of turmeric and its anti-inflammatory activities have been largely demonstrated in many inflammatory diseases, in which the inhibition of NLRP3 inflammasome represents an important mechanism of action [139]. This activity has also been observed in a chronic unpredictable mild stress (CUMS) mice model for the simulation of depression pathology, that also involves inflammatory process. In particular, during inducing CUMS in mice, the treatment with 100 mg/kg (8 mg/kg HED) curcumin daily dosages for 4 weeks has caused a reduction in CUMS symptoms in curcumin-treated mice, with respect to untreated ones. This symptom reduction has been accompanied by a strong decrease in NLRP3 inflammasome factors in the hippocampus, namely IL-1β, IL-6, and TNF-α, measured with Western blotting analysis [74]. Interestingly, curcumin supplementation has also been studied in a randomized double-blind clinical study to investigate its anti-inflammatory effects in hemodialysis patients [75]. In this study, half of the considered hemodialysis patients have received, 3 times a week for 12 weeks, a beverage containing 2.5 g of turmeric (95% curcumin) after dialysis. At the end of the trial, patients who received curcumin supplementation have shown lower expression levels of blood NLRP3 inflammasome markers (NF-kB, NLRP3, and IL-1β) with respect to non-curcumin-treated ones, underlining the potential anti-inflammasome activity. 6-Shogaol is one of the main pungent chemical constituents of ginger roots and its anti-NLRP3 activation has been demonstrated in an in vitro assay where cell calcification has been induced in human artery smooth muscle cells with high dosage of glucose. The 14-day treatment of cell cultures with 6-shogaol drastically reduced the expression of NLRP3, caspase-1, and IL-1β [76]. The potent anti-inflammatory activity of 6-shogaol has also been demonstrated when the NLRP3 inflammasome has been activated in human THP-1 monocytes [77]. In this study, 5, 10, 20, and 40 μM of 6-, 8-, and 10-shoagol/gingerol (all present in ginger roots) have been used to treat cell cultures, resulting in a higher dose-dependent decrease in NLRP3 and IL-1β levels when 6-shoagol was used. Pterostilbene, a stilbenoid compound largely present in grapes and blueberries, has shown to be largely effective in inhibiting inflammasome in acute liver failure, allergic contact dermatitis, and hyperuricemia models. In particular, in an acute liver failure model obtained by treating female BALB/c mice with lipopolysaccharide and D-galactosamine, the concurrent intraperitoneal administration of 50 mg/kg/12 h (4 mg/kg HED) pterostilbene for 1 day determined an important decrease in IL-1β, IL-6, caspase-1, TNF-α, and NLRP3 protein [78]. Similar effects, together with ROS reduction, have been observed when 500 mg/kg (40 mg/kg HED) dosage of pterostilbene were injected for 2 weeks and then orally for 3 weeks in female C57BL/6 mice with chromium-induced allergic contact dermatitis [79]. The anti-inflammasome activity of pterostilbene in hyperuricemia model has been demonstrated by an in vitro assay where NLRP3 inflammasome and epithelial–mesenchymal transition in renal cells have been stimulated by TGF-β [80]. The cells treatment with 2 μM pterostilbene caused a reduction in NLRP3 inflammasome by inducing autophagy, a cellular process that is activated when cellular stress events, such as inflammatory factors release, occur [140]. Hyperuricemia disease has also been considered to demonstrate the anti-inflammasome activity of the stilbenoid glucoside polydatin present in grape juice. In the considered in vivo model [81], male Sprague Dawley mice with potassium oxidate-induced hyperuricemia and daily treated with oral 25 and 50 mg/kg (2 and 4 mg/kg) polydatin for 7 days have shown a dose-dependent decrease in IL-1β, TNF-α, IL-6, NLRP3, and caspase-1, measured in the kidney tissues, with respect to non-treated mice. Polydatin has also shown to be effective in reducing NLRP3 inflammasome in both in vivo and in vitro dry-eye disease models when used at 0.05/0.5% ocular solution and 0.1/1/10 μM solution, respectively [82]. Again, an eye inflammation event has been simulated for the anti-inflammasome activity study of cyanidin-3-*O*-β-glucoside (C3G), a phenolic molecule mainly present in red–violet fruits. In particular, 4-hydroxyhexenal-induced inflammation in human retinal pigment epithelial cells has shown to be less severe when cells have been pre-treated for 2 h with 50 and 100 μM C3G, showing a dose-dependent decrease in

NLRP3, IL-18, IL-β, and caspase-1 [83]. C3G has also been effective in reducing NLRP3 inflammasome activation in an in vivo hepatic inflammation model in male C57BL/6 J mice, where the administration of a 200 mg/kg/day (16 mg/kg HED) C3G dosage for 8 weeks caused a decrease in NLRP3, IL-18, IL-1β, and caspase-1 expression in serum and liver, together with blocking the NF-κB signaling pathway [84]. Green tea is characterized by the presence of several bioactive polyphenols, of which epigallocatechin-3-gallate is the most abundant. This molecule has shown to be very effective in attenuating NLRP3 inflammasome in both in vivo and in vitro lung injury models [85]. In particular, a male Balb/C mice model of acute pancreatitis induced lung injury has been treated with several epigallocatechin-3-gallate dosages (5, 10, 20, 40, and 80 mg/kg) (0.4, 0.8, 1.6, and 3.2 mg/kg HED) for 4 weeks, and a notably dose-dependent decrease in IL-1β inflammation factor has been observed after treatment. Similarly, the in vitro treatment of injured adherent cells with 2.5, 5, and 10 μM epigallocatechin-3-gallate has shown a dose-dependent decrease in caspase-1, IL-1β, and ROS. The same results have been observed in both in vivo and in vitro models of microglial inflammation and neurotoxicity where the use of 2 mg/kg/day (0.16 mg/kg HED) and 10 μM of epigallocatechin-3-gallate has reduced the NLRP3 inflammasome factors expression [86]. Resveratrol has shown to be very effective in reducing NLRP3 inflammasome when encapsulated in poly(lactic-co-glycolic acid) nanoparticles (Res NPs), in both in vitro and in vivo kidney injury models [87]. In particular, kidney cells with LPS/ATP-induced inflammation have shown a dose-dependent reduction in NLRP3, pro-caspase-1, cleaved-caspase-1, and IL-1β expression when treated with 25, 50, and 100 μM Res NPs. The same dose-dependent results have been observed by treating mice injured kidney with 2 and 4 mg/kg 2 times a week for 4 weeks.

3.1.5. Polyphenols Mixtures

Food extracts characterized by the presence of polyphenols mixtures have also shown to be effective in the inhibition of NLRP3 inflammasome. In this case, it is not possible to have an idea about the contribute of single molecules that are present in the mixture, also in consideration of the synergistic, additive, and antagonistic effects that can occur [141]. Anyway, the study of food-derived mixtures is also important, considering that whole foods, food supplements, and nutraceutical products are generally a mixture of several compounds.

Fermented non-digestible fraction (FNDF) of baked corn (*Zea mays* L.) and common bean (*Phaseolus vulgaris* L.) snacks are food products, rich in polyphenols, such as gallic acid and other compounds, such as butyric acid and verbascose, that present an in vitro anti-inflammatory activity. Regarding the NLRP3 inflammasome complex, the FNDF pure components inhibited the NLRP3 assemblage, decreasing caspase-1 activity, IL-1β, and apoptosis in THP-1 cells and differentiated Caco-2 cells after NLRP3 inflammasome activation [88].

Green tea is a plant with well-known antioxidant and anti-inflammatory activities based on the high polyphenol contents, with epigallocatechin-3-gallate (EGCG) being the most abundant one. In a recent work, the green tea polyphenols (GTPs) have reported a modulating activity against the NLRP3 inflammasome activation [89]. In particular, GTPs and EGCG were administered at ICR mice with induced liver damage and the expression levels of NLRP3 inflammasome proteins were determined by Western blot analysis. The results showed a significant down-regulation of NLRP3, ASC, caspase-1, and IL 1β protein expressions, indicating a reduction in NLRP3 signaling in mice.

In another study, the GTPs were administrated to the same mice, in a dose (100–200 mg/kg) (8 and 16 mg/kg HED) comparable with the normal drinking tea levels consumed by humans, in order to determine their protective effects against the inflammasome activation. The results confirmed that GTPs inhibited the NLRP3, ASC, and caspase-1 p20 expression in a dose-dependent manner [90].

Soy isoflavones represent an interesting flavonoid choice for the treatment of many inflammation disorders. A recent study conducted on dextran sodium sulphate (DSS)-

treated mice reported the inhibiting capacity of soy isoflavones on NLRP3 inflammasome complex expression, reducing the NLRP3, caspase-1 p20, and ASC protein levels and suppressing the release of IL-1β and IL-18 [91].

Red raspberry polyphenol extracts are rich in anthocyanins, ellagic acid, myricetin, (−)-epicatechin, and (+)-catechin. The extract was administrated to C57BL/6 mice revealing the attenuation of NLRP3 inflammasome activation in adipose tissue macrophages and epididymal white adipose tissue. The downregulation of NLRP3 inflammasome activation, leading to reduced expression levels of IL-1β, IL-18, and NLRP3 proteins, was also observed in vitro on C3H10T1/2 cells [92].

3.2. Organosulfur Compounds

Organosulfur compounds (OSCs) are a class of molecules usually present in several food sources, such as cereals, legumes, vegetables, and fruits. However, the main food sources of OSCs belong to the *Allium* (garlic, onion) and *Brassica* (broccoli, cabbage, cauliflower) genera [142] and are responsible for the typical flavor of these matrices. This group, that mainly includes isothiocyanates, indoles, allylic sulfur compounds, and sulfones, is well known to possess several biological activities, such as antioxidant, anticancer, antimicrobial, and anti-inflammatory [143,144]. Among the possible mechanisms considered to be involved in the anti-inflammatory activity, inhibition of NLRP3 activation has been demonstrated to be the action mode of some OSCs. Allicin, an isothiocyanate compound very abundant in garlic, has shown to reduce the acrylamide induced inflammation in both Kupffer and Sprague Dawley rat liver cells by inhibiting several inflammation pathways that activate the NLRP3 inflammasome in liver [93]. In both in vitro (1 mM acrylamide and 3.75, 7.5, 15 μM allicin) and in vivo (30 mg/kg/d acrylamide and 25 or 50 mg/kg/d of allicin) (2 or 4 mg/kg HED) studies, by comparing the cells treated with acrylamide and allicin/acrylamide, a decrease in several inflammation factors involved in the activation of NLRP3 inflammasome was observed in allicin groups. In particular, allicin has shown to reduce the release of ROS and ERS (endoplasmic reticulum stress) factors that represent the activation signals for NLRP3 inflammasome. Another study has been carried out on Kupffer and liver cells in order to observe the effect of benzyl isothiocyanate, an isothiocyanate compound present in cruciferous vegetables, in reducing the inflammation events in diet-induced NASH [94]. When benzyl isothiocyanate was administrated to Kupffer cell cultures (2.5 or 5.0 μM benzyl isothiocyanate) or male C57BL/6 J mice with induced NASH (1 g/kg/d benzyl isothiocyanate for 9 weeks) (80 mg/kg HED), a reduction in NLRP3 inflammasome activation was observed, through a reduction in NLRP3, p20 caspase-1, and IL1-β expression in blood and liver; moreover, benzyl isothiocyanate has shown to reduce the release of cathepsin β, an inflammasome assembler, and the interaction of cathepsin B with NLRP3. Similar to what described in the previous study, sulforaphane, an allylic sulfur molecule typical of broccoli and other cruciferous vegetables, has shown to reduce the expression of NLRP3, p20 caspase-1, and IL1-β in cerulean-induced acute pancreatitis in BALB/c mice, through a 3-day treatment with 5 mg/kg (0.4 mg/kg HED) of sulforaphane [95]. Finally, another OSC typical of *Allium* genus vegetables, methylsulfonylmethane, has shown to have anti-NLRP3 inflammasome activity in in vitro assays on human and mouse macrophages by using different methylsulfonylmethane solution concentrations (0.3, 0.5, 1.0, 2.0, 4.0, and 8.0%) [96]. In particular, the inhibition of NLRP3 inflammasome was demonstrated to occur at several steps, namely by blocking the NF-κB signaling and pro IL1-β expression and by reducing IL-1β production and inhibiting mitochondrial ROS production.

3.3. Terpenes and Terpenoids

Terpenes are a class of volatile hydrocarbon compounds derived from two or more isoprene units and represent the main components of vegetable essential oils. In recent years, a paramount interest for these molecules has emerged, since several biological activities, such as antitumoral, anti-inflammatory, antibacterial, antiviral, antimalarial, and

cardiovascular modulation have been demonstrated [145]. In particular, among the different proposed anti-inflammatory modes of action, the inhibition of NLRP3 inflammasome has shown to be the typical mechanism of action of these compounds. Carnosic acid, a diterpenoid mainly present in *Rosmarinus* and *Salvia* plants, has been demonstrated to reduce the evolution of DSS-induced colitis in male Balb/c mice daily gavaged with 50 or 100 mg/kg (4 and 8 mg/kg HED) of carnosic acid for 10 days by inhibiting the activation of caspase-2 and the release of pro-inflammatory cytokines and ROS in the colon tissue [97]. Moreover, in this study, the anti-NLRP3 inflammasome activity of carnosic acid has shown to be comparable with those of 5-aminosalicylic acid, a standard of care for the treatment of colitis disease. The anti-NLRP3 inflammasome effect of geranylgeraniol, a diterpenoid naturally occurred in vegetable oils such as flax, sunflower, and olive, has been studied in an in vitro model of programmed cell death induced in Daoy cell lines after treatment with 10 μM statins or mevalonate for 24 h [98]. The addition of 50 μM geranylgeraniol, following the treatment with statins or mevalonate, has shown to be effective in the reduction in cell death by inhibiting the expression of NLRP3 gene after 24 h. Conversely to what observed in the previous studies, in the following work the beneficial effect of a terpene (kaurenoic acid) has been associated with a stimulation of the NLRP3 inflammasome activation. In particular, kaurenoic acid, a diterpenoid found in several natural spices, such as the fruits of *X. aethiopica*, has shown to possess a dose-dependent (at 10, 30, 50, 70, and 90 μM) triggering effect of NLRP3 inflammasome in BALB/c mice macrophages infected with *L. amazonensis* promastigotes by increasing the production of the inflammatory mediators NO and IL-1β [99].

Although not present in natural sources used as foods, other diterpenoids, sesquiterpenes, iridoids, phytocannabinoids, and derivatives typical of plants used in Eastern and Western medicine, namely α-bisabolol, aucubin, abscisic acid (phytohormone), cannabidiol, phytanyl amine, triptolide, tanshinone IIA, sodium tanshinone IIA sulfonate, paclitaxel, phorbol myristate acetate, andrographolide, oridonin, glaucocalyxin A, and teuvincenone F have shown to be effective in the prevention of NLRP3 inflammasome activation by blocking the release of inflammasome enhancers, mainly IL-1β, IL-4, IL-6, IL-12, IL-18, caspase-1, and ROS [146–153]. Similarly, other terpenoids, such as the triterpenoid celastrol [154] and the sesquiterpenoids of *Ainsliaea yunnanensis* [155], have shown to be involved in the modulation of NLRP3.

3.4. Fatty Acids

In general, most of the evidence highlighted that SFAs acted as priming signals of inflammasome activation, whereas MUFAs and PUFAs have been shown to impair this activation, but these assumptions have frequently been challenged [31]. To better understand the FA implication in NLRP3 inflammasome, data reported in the literature will be described according two categories: SFAs and UFAs.

3.4.1. Saturated Fatty Acids

Different research groups attempted to investigate the mechanisms underlying SFA-mediated NLRP3 inflammasome activation. Wen et al. demonstrated palmitate acid inhibits AMP-activated protein kinase in LPS-primed bone marrow-derived macrophages followed by the accumulation of mitochondrial ROS, thus activating the NLRP3-ASC inflammasome and causing caspase-1, IL-1β, and IL-18 production [16]. According to Robblee et al., palmitate and stearate acids could induce activation of one of the three endoplasmic reticulum stress sensors, IRE1α (inositol-requiring enzyme 1-α), through the saturated phosphatidylcholine accumulation, and mediate the NLRP3 inflammasome activation in LPS-primed bone marrow-derived dendritic cells [100]. More recently, Gianfrancesco et al. suggested that the accumulation of saturated phosphatidylcholine induced by SFAs led to the loss of membrane fluidity and the disruption of Na^+, K^+-ATPase transmembrane protein, resulting in an increase in K^+ efflux, which is considered a NLRP3 activator [156].

However, few studies reported the anti-inflammatory effects displayed by different SFAs. As an example, virgin coconut oil (VOC), mainly composed of medium chain saturated fatty acids (6–12 carbons), reduced IL-1β protein, caspase-1, and NLRP3 genes expression at different doses in AD (receiving Amyloid-β) and in high-fat diet (HFD) models both in vitro and in vivo [101]. The anti-inflammatory properties of VOC might be ascribed to lauric acid (which represents up to 55% of the total) that is considered the precursor of monolaurin, which has been shown to modulate immune cell proliferation and, through this, it can control inflammasome [157].

3.4.2. Unsaturated Fatty Acids

In the literature, most of the studies on NLRP3 inflammasome and fatty acids are focused on PUFAs. In particular, fish oil, a matrix particularly enriched in ω-3 DHA and EPA, has been extensively studied. All data reported the anti-inflammatory properties of EPA and DHA resulting in a downregulation of NLRP3 gene expression and in a decreased secretion of pro-inflammatory cytokines (IL-1β and IL-18) in obesity models [102,103], in DSS-induced colitis in mice [104], in LPS-induced Kupffer cells [105], and in both prefrontal cortex and hippocampus of rats [106]. Nevertheless, numerous studies have explored the anti-inflammatory mechanisms of PUFAs. Dang et al. suggested fish oil could attenuate the LPS-induced neuroinflammation and oxidative through modulation of P2X7R/NLRP3 inflammasome axis [106]. Miao et al. underlined that the mechanisms involve inhibition of ROS production, mediation of NLRP3/ASC/caspase-1 signaling pathway, regulation of gut microbiota, and SCFAs levels [104]. More recently, Quingyao et al. assumed that DHA-mediated NLRP3 inflammasome inhibition was due to the blockade of high glucose-induced TXNIP via the PI3K/Akt pathway in pre-adipocytes [103]. Other mechanisms through which ω-3 PUFAs reduce metabolic inflammation may include the G protein-coupled receptor 120 (GPR120) and GPR40, which interact with NLRP3 and inhibited the NLRP3 inflammasome complex assembly [42,105].

Interestingly, different properties have been reported between ω-3 and ω-6 PUFAs. Schuster et al. investigated the anti-inflammatory activity of different fatty acids (SFAs, MUFAs and PUFAs) in macrophages, blood monocytes, and hepatocytes, confirming the data described above. Nevertheless, when compared with ω-6 PUFAs, ω-3 were more potent in inhibiting ATP-mediated NLRP3 inflammasome [158]. Conversely, Yan et al. found out that ω-6 PUFAs failed to block IL-1β secretion induced by nigericin [42]. All these findings suggest that fatty acids should be considered individually in terms of defining potential differences with respect to metabolic or inflammatory properties, or both.

3.5. Carotenoids

Recently, only two carotenoids were studied in vivo for the modulation of NLPR3 inflammasome. Zeaxanthin dipalmitate, a lipophilic antioxidant whose primary presence in some functional fruits (e.g., *Lycium barbarum*) has been confirmed, demonstrated the ability to counteract ethanol-induced hepatic damage in a murine model of AFLD targeting the converged AMPK-FoxO3a mitophagy and NPLR3 pathway combined to P2X7 and adiponectin receptor 1 on the hepatocyte membrane [159]. Since the role of NLRP3 in virtually all liver diseases has been demonstrated, this compound or foods containing it can have a positive impact or a preventive effect against a large range of human pathologies. Conversely, astaxanthin, which is poorly represented in typical Western diet but is rich in seafood, exerted an indirect NPLR3 modulation (−23%) via the modification of the gut microbiota in a murine model of inflammation and metabolic homeostasis when administered as a supplementation (0.04% *w*/*w*) to the normal diet [160].

3.6. Proteins and Amino Acid Derivatives

Proteins, peptides, and amino acids appear to be involved in the inhibition of the inflammasome pathway. Two short peptides, RDP2, RDP3 (rice-derived-peptide-2,

AAAAGAMPK-NH2, 785,97 Da), and RDP3 (rice-derived-peptide-3, AAAAMAGPK-NH2, 785,97 Da), were identified and isolated from the aqueous extract of the shelled fruits of *Oryza sativa* and studied to verify the antigout effects [107,108]. The RDP2 peptide [107] study was conducted on hyperuremic mice, that were injected intraperitoneally once a day for 7 days, and divided into 7 groups: control, model, allopurinol (Allo, 10 mg/kg, 0.8 mg/kg HED), benzbromarone (Benz, 8 mg/kg, 0.6 mg/kg HED), and 3 RDP2 groups (5, 10, and 100 μg/kg, 0.4, 0.8, and 8 μg/kg HED). The RDP2 groups induced a reduction in serum uric acid levels by decreasing renal inflammation. Indeed, the content of serum IL-1β, the production of which depended on NLRP3 inflammasome, was significantly decreased in hyperuricemic mice treated with the RDP2 peptide, and the expression of NLRP3, ASC, and caspase-1 in the kidneys was reduced. A model of hyperuremic mice was established to explore the mechanism and function of the RDP3 peptide [108] and animal tests were performed by dividing mice into various groups: control, model, allopurinol, benzbromarone, and RDP3. Mice were injected with uric acid intraperitoneally to induce hyperuricemia; then, for 7 days, the groups were treated with intraperitoneal injection of standard drugs allopurinol (10 mg/kg, 0.8 mg/kg HED) or with benzbromarone (8 mg/kg, 0.6 mg/kg HED); instead, the RDP3 groups were treated with intraperitoneal injection of different doses of RDP3 (100 μg/kg, 500 μg/kg and 1 mg/kg, 8 μg/kg, 40 μg/kg, and 0.08 mg/kg). The results showed that serum uric acid concentrations in the RDP3 group were significantly lower than in the other treatments. Furthermore, Western blot analysis was performed to detect NLRP3 inflammasome expression in the kidneys of mice and it was observed that NLRP3 contents in the model group kidneys were higher than those of the allopurinol group, suggesting that NLRP3 was activated. Contrariwise, the expression of the NLRP3 inflammasome was significantly decreased in the RDP3 group, demonstrating that RDP3 reduced inflammation by inhibiting the expression of the NLRP3 inflammasome.

Regarding the hyperuricemia and its associated kidney inflammation, the effects and biological mechanisms of tuna meat oligopeptides (TMOP) were investigated in mice [109]. The conducted experiments indicated that TMOP relieved hyperuricemia dose-dependently and regulated uric acid metabolism in mice with diet-induced hyperuricemia. The administration of TMOP inhibited the activation of the NLRP3 inflammasome complex, and intestinal microbiota-mediated beneficial effects of TMOP were explored by fecal microbiota transplantation.

Concerning the intestinal diseases, the ability of an isoflavone-free soy protein concentrate (SPC) to prevent inflammation and loss of intestinal barrier function have been examined [110]. The cytoprotective effects of soy protein concentrate were analyzed in vitro, and its anti-inflammatory effects in the mouse model of acute ulcerative colitis treated with DSS. In particular, the experiments were conducted on mice fed in the basic diet with the components present in the SPC powder for 7 days a randomized based on weight into control (water and AIN93G diet), DSS (1.5% DSS in drinking fluid and AIN93G), DS6 (1.5% DSS and 6% dietary SPC), and DS12 (1.5% DSS and 12% dietary SPC). SPC mice had lower NLRP3 mRNA levels than DSS-treated control mice, demonstrating that SPC is able to prevent increased pro-inflammatory signaling and thereby moderate colitis severity. Overall, the findings support the efficacy of dietary SPC as a means of preventing colonic inflammation and loss of gut barrier function.

Otherwise, a gluten-derived peptide with high content of glutamine and proline residues, α-gliadin 31–43, has been identified, which appears to induce an innate immune response in the gut [111]. Mice intestinal samples, treated for 4 or 16 h with 200 μL of p31–43 using a curved oral gavage needle, were collected for mRNA evaluation and for histological analysis. The results showed that p31–43 gliadin has an inherent propensity to form oligomers that activate NLRP3 inflammasome and that this pathway is required for intestinal inflammation and pathology when p31–43 is administered orally to mice.

By considering that the redox state of the cell can mediate the production of placental cytokines, which are responsible for the function and development of the placenta and

that the NLRP3 inflammasome represents the first line of innate immunity [161], the NLRP3 placental inflammasome was investigated in a study regarding the integration of N-acetyl-cysteine (NAC) in the late gestational diet of sows [112]. A total of 16 sows at day 85 of gestation were selected based on body weight and assigned into 2 groups: the control group (7 sows) and NAC group (9 sows; the basal diet supplemented with 500 mg/kg NAC, 40 mg/kg HED). The effects of NAC on placental redox status, function, inflammasome, and fecal microbiota in sows were explored to elucidate the relationship between the fecal microbiota and the placenta. The results obtained showed that NAC significantly reduced maternal and placental inflammatory cytokines through inhibition of the NLRP3 inflammasome in sows during late pregnancy; suppression of oxidative stress and inflammatory response in sows and placenta can therefore reduce fetal exposure to inflammatory mediators and improve fetal growth.

NLRP3 inflammasome has been reported to play an essential role in the inflammation responses during acute lung injury [162]. Regarding this point, glycine supplementation in lipopolysaccharide-induced acute lung injury in mice was investigated [113]. Indeed, after being treated with aerosolized glycine (1000 mg in 5 mL of 0.9% saline) or vehicle (0.9% saline) once daily for 7 continuous days, the male mice were exposed to aerosolized lipopolysaccharide to induced lung injury in mice. The glycine prevents mucin reduction and upregulation of pro-inflammatory cytokines in lung tissue; this beneficial effect of glycine was associated with modulation of the NLRP3 inflammasome and NRF2 signaling. Carnosine (β-alanyl-histidine) and L-homocarnosine (γ-aminobutyryl-histidine) are the major endogenous constituents of excitable tissues—the brain and skeletal muscles [163]. Their supplementation was also studied in terms of modulation of NLRP3. The neuroprotective and anti-aging carnosine was shown to improve cognitive dysfunction in SAMP8 mice after a 6-week oral administration (100–200 mg/Kg/day) via NLRP3 inactivation and amelioration of the oxidative stress [114]. The effects of L-Homocarnosine against inflammation induced by cerebral ischemia in male albino rats were also analyzed [115]. In this study rats were grouped into control, middle cerebral artery occlusion (MCAO), 0.5 mM L-Homocarnosine + MCAO, and 1 mM L-Homocarnosine + MCAO treatment groups and treated for 45 days. NLRP3 inflammasome levels were substantially elevated in MCAO rats, whereas supplementation with 1 mM L-homocarnosine significantly reduced NLRP3 inflammasome levels to near normal levels.

Since cholinergic degeneration plays a major role in the pathophysiology of AD, it has been investigated whether choline supplementation during adulthood delays the progression of this disease [116]. The study was conducted on the APP/PS1 model of double transgenic mice expressing a chimeric mouse/human amyloid precursor protein (Mo/HuAPP695swe) and a mutant human presenilin 1 (PS1-dE9), both directed to CNS neurons; APP/PS1 transgenic mice were divided into a control group (1.10 g choline chloride per kg, 0.09 mg/kg) and a group supplemented with choline (4.95 g choline chloride kg, 0.4 mg/kg HED). Firstly, it was shown that choline supplementation improves the cognitive and non-cognitive behavioral effects of AD; furthermore, from the results, both an increase in the formation of the synaptic membrane and the inhibition of the NLRP3 inflammasome were observed. Inhibition of inflammasome activation explained the reduced Aβ deposition, microgliosis, and pro-inflammatory cytokine production observed in the brains of APP/PS1 mice after 9 months of choline supplementation.

3.7. Saponins and Sterols

Ginseng is considered as a highly valued herb and widely used in dietary supplements and herbal medicines, as it exerts a regulation on endocrine system, nerves, metabolism, and other physiological functions [164,165]. The effectiveness of ginseng is attributable to its main active components, ginsenosides, a class of triterpene saponins with a steroid structure.

It has been confirmed that 25-OCH_3-PPD (20*S*,25-methoxyldammarane-3β,12β,20-triol), a ginsenoside isolated from *Panax ginseng*, relieves liver damage, by inducing apoptosis of activated hepatic stellate cells [166]. Considering the correlation between inflammation and liver fibrosis, a study evaluated the regulation of 25-OCH_3-PPD (5, 10, or 20 mg/kg for 5 weeks, 0.4, 0.8, or 1.6 mg/kg HED) against hepatic fibrosis and inflammation in thioacetamide (TAA)-stimulated mice by activating the LXRs (liver X receptors) pathway [117]. Study results demonstrated that 25-OCH_3-PPD has a hepatoprotective effect against liver fibrosis and reduces inflammation by regulating P2X7R-mediated NLRP3 inflammasome.

Wang et al. [118] analyzed the effects of saponins isolated from *Panax notoginseng* in ameliorating NLFD through inhibition of inflammasome activation. The saponin extract, compared with conventional red ginseng, contained significantly increased amounts of ginsenosides Rh1 (10.34-fold) and Rg2 (7.1-fold), which are the main components highlighting the pharmacological activity of ginseng. In this study mice were fed a fast-food diet for 16 weeks to induce NLFD and then treated with saponin extract (50 or 150 mg/kg) for 9 weeks to determine the effects of the saponin. Particularly, it has been observed that Rh1 and Rg2 ginsenosides exerted anti-inflammatory effects and inhibited NLRP3 inflammasome by promoting mitophagy and alleviating mtROS production.

The characteristics of the ginsenoside compound K (CK) are peculiar, a final metabolite of panaxadiol ginsenosides. CK seems to be involved in the stimulation of insulin secretion and its protective effect against diabetic nephropathy has been elucidated in inhibiting the oxidative stress, NLRP3 inflammasome, and NF-κB/p38 [167,168].

Numerous studies have demonstrated the neuroprotective action and antidiabetic properties of CK, indicating its potential in the treatment of memory disorders and cognitive dysfunctions related to diabetes mellitus; in particular, a study tried to assess the effects of CK against memory impairment and cognitive dysfunction in diabetic db/db mice treated with 10 mg/kg of CK for 12 weeks [119]. The results showed that the CK treatment improved insulin resistance, alleviated cognitive dysfunctions, relieved oxidative stress, attenuated inflammatory responses in the hippocampus, and inhibited NLRP3 activation. Specifically, CK downregulates inflammatory cytokines and mediator production by suppressing the NLRP3 inflammasome pathway.

Magnesium isoglycyrrhizinate, a magnesium salt of 18α-glycyrrhizic acid stereoisomer extracted from the roots of the plant *Glycyrrhiza glabra*, acts as a hepatoprotective agent in the immune and anti-inflammatory modulation of liver disease [169]. The effects of magnesium isoglycyrrhizinate on the characteristics of the metabolic syndrome in fructose fed rats were investigated [170]. Rats were given 100 mL of water containing 10% fructose for 6 weeks, followed by treatment with saline injection, 10, 20, and 40 mg/kg (0.8, 1.6, and 3.2 mg/kg HED) of magnesium isoglycyrrhizinate (by intraperitoneal injection) or 4 mg/kg (0.3 mg/kg HED) of pioglitazone (for intragastric administration) for an additional 11 weeks. The data showed that magnesium isoglycyrrhizinate inhibited the activation of the NF-κB/NLRP3 and thus reduced the immunological–inflammatory response, preventing hepatic lipid metabolic disorder and accumulation in high fructose conditions [120].

Physalin B, one of the main active withanolides existing in *Physalis alkekengi* L. var. *franchetii*, displayed anti-inflammatory activity in intestinal ischemia [171]. The Physalin B antiulcer effects in mice with ulcerative colitis DSS-induced were evaluated [121]; mice were injected intraperitoneally with Physalin B (250 μL) once daily for 7 days. Body

weight, colonic length, disease activity index, pathological changes in colonic tissue, cytokine levels, NF-κB pathway, protein levels of related pathways, and NLRP3 activation were measured. The results of this study provided evidence that Physalin B could significantly inhibit the production and secretion of various inflammatory factors: Physalin B reduced the pro-inflammatory cytokine levels of mice with colitis, suppressed the NF-κB cascade, STAT3-arrestin1 signaling, and inhibited NLRP3 inflammasome activation.

A plant phytosterol isolated from *Moringa oleifera*, β-sitosterol, was studied to evaluate its anti-inflammatory activity in two cell lines [122]. Tween 80 surfactant was used to produce a dispersion of small particles of β-sitosterol dissolved in dimethyl sulfoxide and applied to macrophages to evaluate the anti-inflammatory activity of β−sitosterol. Cells were incubated with BSS (7.5–60 μM). An increase in the solubility of water-insoluble phytosterols has been reported thanks to the formation of nanoparticles, the formulation of which is able to inhibit the signal transduction pathways of inflammation in macrophages. The results indicated that β-sitosterol dispersed well in the medium as nanoparticles, suppressed the secretion of inflammatory factors from keratinocytes and macrophages induced by PGN, TNF-α, or LPS (such as TNF-α, IL-1β, IL-6, IL-8, and ROS), significantly reduced NLRP3 expression and inhibited caspase-1 activation.

3.8. Polysaccharides

Polysaccharides from different sources (mushroom, herbs, plant, seaweed) have proved to exert an anti-inflammatory role via affecting the NLRP3 inflammasome pathway. However, a detailed mechanistic study on how polysaccharides modulate NLRP3 activation remained to be explored. In particular, several polysaccharides involved in the modulation of NLRP3 inflammasome belong to traditional Chinese medicine, but they are also present in dietary plants. As an example, the major bioactive component of *Trametes orientalis*, used for the treatment of pulmonary disease, is a polysaccharide composed of galactose, glucose, mannose, and arabinose with molar ratios of 5.79:5.77:3.45:1.20 (average MW 63000), which proved to inhibit the activation of NLRP3 inflammasome and the release of pro-inflammatory cytokines, including TNF-α, IL-1β, and IL-6, by the detection of expression levels of proteins in lung tissue involved in the NLRP3 inflammatory pathway [123]. Liang et al. found out the anti-inflammatory activity of polysaccharides extracted from *Dendrobium officinale* (DOPS) was likely to via suppressing mRNA expression of NLRP3, ASC, caspase-1, IL-1β, and IL-18 both in vivo, in DSS-induced acute ulcerative colitis mice, and in vitro, in LPS-stimulated NCM460 cells model, through a possible downregulation of β-arrestin1 expression (which could positively regulate NLRP3) [124]. A recent work by Li et al. reported CYP-1, a newly characterized mannoglucan from Chinese yam was able to suppress the expression of several key genes involved in colonic inflammatory signaling pathways (such as NF-κB and NLRP3) in DDS-induced colitis mice [125]. *Ganoderma lucidum* polysaccharides (GLPS), isolated from a Chinese medicinal mushroom, proved to markedly inhibit liver inflammatory factors via suppression of NLRP3 in liver tissue. Indeed, GPLS-treated acute liver injury mice exhibited a significantly decreased protein expression levels of NLRP3, ASC, and caspase-1 [126]. *Armillariella tabescens* (AT), that belongs to the family of *Tricholomataceae*, is a well-known traditional medicinal mushroom, characterized by 86.52% of polysaccharides (mannose, arabinose, and fucose at a molar ratio of 1.6:1.0:2.7.). AT possesses potent antioxidant and anti-inflammatory properties by possibly involving the repression of the TXNIP/NLRP3 inflammasome pathway in the liver of T2D mice [127]. Among the plant-derived polysaccharides, low methoxyl pectin (LMP) showed an important role in the autoimmune diabetes through suppression of NLRP3 and associated proteins expression in cecum (NLRP3, caspase-1-p20, cleaved IL-1*β*, and cleaved IL-18) [128]. The NLRP3 inhibition could be ascribed to the increase in the SCFAs (short chain fatty acids) by gut microbiota, induced by LMP supplementation, which act as histone-deacetylase (HDAC) inhibitors towards the NLRP3 inflammasome. Furthermore, Wu et al. pointed out that LMP supplementation also suppressed NLRP3 activation in pancreas, but a detailed mechanistic

study on how LMP modulates NLRP3 inflammasome activation in pancreas has not yet been performed [129].

Recently, Castro-Alves et al. investigated the activity of non-digestible carbohydrates (NDCs) from chayote fruit, which consist mainly of pectic homogalacturonan and highly branched rhamnogalacturonan-II, as well as hemicellulosic material including glucomannan, xyloglucan, and glucurono(arabino)xylan, in human THP-1 macrophage-like cells. Results showed that NDCs indirectly inhibit NLRP3 activation through the interaction between the NDCs and other pattern-recognition receptors that are essential to induce priming signals required for NLRP3 activation [130].

Several papers highlighted the anti-inflammatory activity of different polysaccharides probably ascribed to NLRP3 inhibition by decreased protein levels of NLRP3, ASC, caspase-1, and IL-1β [172–174]; however, few works assessed the pro-inflammatory efficacy of some polysaccharides towards the NLRP3 inflammasome. In particular, Liu et al. found out that the polysaccharide SF-2, a mannoglucan sulfate isolated from starfish (*A. rollestoni*), could improve the release of cytokines and the expression of NLRP3 in primary macrophages, confirmed by the elevated expression of NLRP3, cleaved caspase-1, and ASC proteins [131].

3.9. Vitamins and Derivatives

The importance of lipophilic vitamin E and its derivatives, which mainly occur as abundant nutrients in oily nuts and seeds, in inflammation and oxidation processes has been elegantly reviewed by Wallert and collaborators [175]. Different forms of vitamin E or their long-chain metabolites can interfere with ROS production, NF-kB priming, or NLRP3 activation. Recently, further studies confirmed these results in two different murine models of HFD and alloxan-induced diabetes, especially regarding γ-tocopherol supplementation, as such, or in more complex extracts (e.g., Rosa mosqueta oil contains about 74 g/100 g oil of α-tocopherol and 359 g/100 g oil of γ-tocopherol, stripped corn oil) [176,177].

Vitamin D and its derivatives were also studied, alone or in association with probiotics and microelements as food supplements, for their effects on the modulation of inflammasome halting the priming step required for NLRP3 (and NLRP1) activation in immune cells, in placental explants from preeclamptic and normotensive pregnant women, in clinical trials involving COVID-19 patients [178], in the proliferative diabetic retinopathy pathogenesis, in diabetic corneal wound healing and reinnervation, in non-alcoholic fatty liver disease, and in acute kidney injury.

3.10. Probiotics, Symbiotics, and Their Main Components

Lactic acid bacteria (LAB) are currently used as food supplements for human health as probiotics due to their modulatory effects on intestinal conditions, immunomodulatory function, and host metabolism. The effect of each probiotic is dependent on the cell line and species used. To test the anti-inflammatory action of LAB or their main components (e.g., butyrate at 200 mg/kg, 16.3 mg/kg HED) via the inhibition of inflammasome activation, *Lactobacillus paracasei* KW3110 (1×10^6 cells/mL), *Bifidobacterium infantis* (2×10^8 CFU/mL) in combination with the prebiotic xylooligosaccharide (XOS, 230 mg/kg, 18.7 mg/kg HED), *Enterococcus faecium* NCIMB 10415 (1×10^7 CFU/mL), and heat-killed cells of *Enterococcus faecalis* (17 mg/kg, 1.4 mg/kg HED) were recently proposed in different in vitro and in vivo disease models of DSS-induced ulcerative colitis [179], HFD-induced T2D [180], cerulein-induced acute pancreatitis [181], and colitis-associated colorectal cancer [182], as well as on porcine dendritic cells [183]. The beneficial effects of a direct modulation of NLRP3 were also confirmed by a downregulation of pro-inflammatory cytokines, upregulation of anti-inflammatory players. These results have been also described feeding animals or treating cells derived from livestock with probiotics (1×10^5 CFU of *Lactobacillus rhamnosus* GR-1 and 3×10^5–2×10^7 CFU of *Lactobacillus johnsonii* L531) with the aim of limiting the inflammatory damage of bacterial infections induced by *Escherichia*

coli in porcine mammary epithelial cells, MAC-T cells and in a mouse mastitis model, or *Salmonella typhimurium* in IPEC-J2 cells [184–186]. The administration of these probiotics allowed limited bacterial adhesion to cells and bacterial alteration of cellular morphology, thus removing the first cause of ROS production and immune system activation. The NLRP3 attenuation downregulated ILs, TNF-α, and chemokine Cxcl2 expression and, concurrently, decreased the expression of autophagic receptor SQSTM1/p62 and induced tight junction injury.

4. Food and Nutraceuticals Components Bioavailability and Toxicity

Apart from table sugar, foods are "complex matrices" made up of different components, divided into macronutrients (proteins, carbohydrates, and fats), micronutrients (vitamins and minerals), and water. The presence of other minority components also increases the complexity of food matrices. Some of them are defined as "bioactive compounds" because, based on scientific evidence, it is assumed that they can have a positive effect on our organism and can play a fundamental and important role in modulating inflammasomes [12,30,35].

The "bioactive compounds" belong to many different categories based on their chemical nature and on the type of positive effect they could exert on human health. Commonly, they are not considered nutrients and are referred as "essential and non-essential compounds" that occur in nature, are part of the food chain, and can help to protect ourselves from illnesses and improve our quality life [1,187]. Although the most known and studied "bioactive compounds" are of plant origin, it is wrong to think that they are not present in foods of animal origin. Conjugated linoleic acid, taurine, carnitine, carnosine, glutathione, and lipoic acid are some examples, together with bioactive peptides, which confirm the importance of all food types in our diet [188,189].

Certainly, the most numerous classes of "bioactive compounds" are represented by phytochemicals: molecules of various kinds such as carotenoids, tocopherols, phytosterols, phenolic compounds, etc., but, in any case, these are of vegetable origin. Among all these different metabolites that are important for their health benefits, the phenolic compounds have been studied most extensively [190,191]. These constituents, with more than 5000 structurally diverse molecules of various types, are the most numerous, abundant, and widely distributed "bioactive compounds", very important for their potential beneficial effects, which are also associated with inflammasome disorder in diseases [1,17,53,190,192]. Many of these positive effects on safety and efficacy have been studied in vitro and on animal models and have yet to be confirmed with absolute certainty on humans with clinical trials [193–195]. It is well known that the "bioactive compounds", whatever their origin (from animals or plants source), due to the food complexity and in order to exert their beneficial health action, need to be released from the food matrix after ingestion, and then metabolized [196]. As different researchers highlighted, the global food matrix composition, with the presence of nutrient interaction, has a crucial role on the health benefit of "bioactive compounds"; however, some other specific characteristics can determine the biological activity of these metabolites [17,197]. The factors that influence the absorption and bioavailability of "bioactive compounds" are numerous, one of these is represented by the cell wall structure and properties, since, often, they are resistant to degradation in the upper gut [196]. In addition, the in vivo biological activity of many high molecular weight compounds, such as flavonoids, is influenced considerably by molecular structure, binding to other molecules (i.e., by esterification or glycosylation), different isomeric configuration and their interaction with macromolecules, such as proteins and dietary fibers [196,198–201]. Among these factors, we must include different transport and diffusion mechanisms of ingested food "bioactive compounds" because their bioavailability can be blocked and/or modified significantly by certain nutrients [202]. Moreover, as many drugs, also bioactive food compounds are subjected to several metabolic and enzymatic processes that modify the structure and could be responsible for molecular forms, which are different from the original constituent of the ingested food

and can show a different effect (increase, decrease, or toxic) in presence of specific nutrients (i.e., lipids) [196].

The intake of "bioactive compounds" in the human diet varies enormously in relation to the type, quantity, and quality of foods consumed. Generally, the most important food sources of bioactive nutrients are vegetable, fruits, chocolate, tea, wine, olives, and spices; however, their concentration in the same food varies, often significantly, in relation to the cultivation techniques and food processing, the degree of ripeness, and the time elapsed between harvesting and consumption [198,203]. Thus, because different foods contain a huge variety of bioactive compounds and a lot of them often are poorly absorbed in our intestine, there is great difficulty in establishing the "effective dose", which is the amount of this substance that we must take to have the expected effect. Furthermore, the "bioactive compounds" stability and, consequently, their antioxidant, anti-inflammatory, and immunomodulatory properties, may be lost during digestion [1,190].

Usually, to improve the sensory attributes and make a product more attractive for taste, consistency, and appearance, many foods are submitted to culinary treatments. Different domestic practice and cooking techniques (i.e., boiling, roasting, stir-frying, microwaving, and streaming) have been compared to define the optimal process to reduce the degradation of the "bioactive compounds". It was observed that food nature, cooking time, temperature, addition of acidulant, spices, or other condiments might influence both the amount of water-soluble "bioactive compounds" and of those fixed to the lipidic matrix [204]. Each food contains a characteristic composition, and the chemical structure of each bioactive metabolite strongly influences the loss extent of individual component. Generally, food processing and even storage frequently cause losses in phenolic compounds [205]. Overall, high-temperature food processing (i.e., roasting, blanching, drying, and pasteurization) considerably reduces the concentration of phenolic compounds in foods. To ensure the greatest phenolic amounts, it is recommended to consume fresh food or use steam cooking with almost no osmotic processes. Other methods, such as microwave cooking, that imply low water and short cooking time, are more recommended to maintain high levels of these compounds inside foods. In fact, when subject to boiling (commonly used for vegetable) or too high temperatures, foods suffer considerable losses of most phenolic compounds, especially flavonol glucosides [204–206]. For other bioactive compounds that are part of lipidic membrane or oil fraction of foods (i.e., carotenoids and tocopherols), cooking methods involving water are less aggressive than those using oils for stir-frying [204]. Innovative non-thermal procedures (UV, high hydrostatic pressure, and pulsed electric fields treatments) do not significantly deteriorate bioactive compounds, preserve their antioxidant activity, and provide promising alternative to thermal processing commonly used for food disinfection or to inactivate microbes and enzymes in foods [206].

Although there is evidence showing the beneficial effects of "bioactive compounds" present in foods, more studies suggest that their health benefits instead depend on the synergy and interactions among different molecules [207]. Therefore, in drafting the anti-inflammatory diet it must be considered that bioactive nutrients cannot be from a single food but rather it is the result from the synergy between foods that provide different antioxidant molecules to counteract the inflammatory processes that occur. In addition, as stated above, it is not only important to know how much a nutrient is present in a specific food, but it is even more important to know how much of it is bioavailable.

Despite the growing amounts of studies, definitive conclusions supporting the bioavailability of most "bioactive compounds" from a wide variety of food for optimal nutrition and health well-being are difficult to obtain. Consumers' demand for well-being pushes towards an increasing request for food supplements and innovative new market segments have been developed to meet their needs. Alternatively, dietary supplements, also differentiated into nutraceutical or functional foods, can be supplied to consumers to deliver a specific bioactive compound or a group of them [1,189]. Generally, nutraceuticals

are bioactive compounds derived from food sources. They can include one or more substances that are purported to provide extra health benefits and are considered as a pharmaceutical alternative [208]. They are supplied to consumers in a concentrated form and the ingredients are in higher dose than in normal foods. Therefore, as a drug, the food supplement should be used as a necessary complement in diets that are poor in nutrients and foods, in order to provide more energy and nutrients to our body to properly support its physiological processes. On the other hand, functional foods are foods fortified with an extensive array of bioactive compounds which provide a clinically proven health benefit, beyond their natural properties, when consumed in a regular and consistent manner through diet [189,209]. Therefore, as a drug, nutritional supplementation of nutrients in order to increase the functionality of the immune system has no indication in case of adequate intake; on the contrary, it can be even harmful if it involves exceeding the maximum daily doses.

Nowadays, a great variety of nutraceuticals and functional foods are provided to the consumers; however, their use is largely unregulated, or they are treated differently according to local jurisdictions. Generally, they are more the subject of marketing hype, and for many of these "supplements", it is not even yet known whether they provide more benefits than risks to consumers. Currently the term "bioactive compound" is not defined in the European regulations; however, the European Food Safety Authority (EFSA) is carrying out scientific evaluations to assess the safety and the toxicity of "bioactive compounds" that can be found in foods [210]. Due to the great number of compounds that can have a potentially positive effect on health, the European Commission has not produced a list of authorized ones, but it has tried to put order for "borderline" products, by identifying the criteria to define a dietary supplement. At present, among food supplement phytochemicals, EFSA claims for hydroxytyrosol, its derivatives (i.e., oleuropein complex and tyrosol), and olive oil polyphenols as substances able to protect the blood lipids from the harmful effects of oxidative stress [211]. With this background, we highlighted that the "bioactive compounds" present in foods can possess a potential therapeutic effect on different diseases associated with the activation of inflammasomes. Anyhow, due to different food matrix effects and compositions, the outcome obtained from concentrations used in in vitro tests are often not achievable through a targeted diet. Currently there is insufficient information available on the safety of supplements or functional foods. They cannot be considered as the emergency remedy and are not intended as a substitute for a varied and balanced diet and a correct lifestyle.

Finally, food consumed as such, or after cooking processes, as well as water, may also contain internal or accidental components with a stimulating effect on NLRP3 inflammasome. Among these, mycotoxins (zearalenone, patulin, deoxynivalenol), trace metals (arsenic, cadmium), environmental and food contaminants (acrolein, 3-monochloropropane-1,2-diol, glycidol, and its esters), and acrylamide are few examples of NLRP3 activators, endowed with harmful inflammatory effects [212–220].

5. Conclusions

Eating is something we have always done and which, from birth to old age, strongly affects life quality and physical and psychological well-being. Nowadays, consumers are increasingly interested in lifestyles and nutritional habits that can prevent diseases since different studies have evidenced that a relationship occurs between these factors and pathological consequences based on inflammatory processes. In this regard, it should be emphasized that these effects are related, not only to the quantity, but, above all, to the variety of food choices and, in particular, to the inclusion of fruit and vegetables. Plant foods are particularly rich in important bioactive compounds, each of them can produce different effects on the pathway of inflammatory response, confirming the importance of the nutritional pattern (food model) as a whole, rather than the single nutrient or functional compound.

Author Contributions: All authors have participated in the elaboration of the manuscript, have read the final version, and agreed with the contents. All authors have read and agreed to the published version of the manuscript.

Funding: This research received no external funding.

Institutional Review Board Statement: Not applicable.

Informed Consent Statement: Not applicable.

Data Availability Statement: Not applicable.

Acknowledgments: Grants: Italian Ministry of Education, Universities and Research-Dipartimenti di Eccellenza-L. 232/2016

Conflicts of Interest: The authors declare no conflict of interest.

References

1. Castejón-Vega, B.; Giampieri, F.; Alvarez-Suarez, J.M. Nutraceutical compounds targeting inflammasomes in human diseases. *Int. J. Mol. Sci.* **2020**, *21*, 4829.
2. Martinon, F.; Burns, K.; Tschopp, J. The Inflammasome: A molecular platform triggering activation of inflammatory caspases and processing of proIL-β. *Mol. Cell* **2002**, *10*, 417–426. https://doi.org/10.1016/S1097-2765(02)00599-3.
3. Kelley, N.; Jeltema, D.; Duan, Y.; He, Y. The NLRP3 inflammasome: An overview of mechanisms of activation and regulation. *Int. J. Mol. Sci.* **2019**, *20*, 3328.
4. Fusco, R.; Siracusa, R.; Genovese, T.; Cuzzocrea, S.; Paola, R. Di Focus on the role of NLRP3 inflammasome in diseases. *Int. J. Mol. Sci.* **2020**, *21*, 4223.
5. Duncan, J.A.; Bergstralh, D.T.; Wang, Y.; Willingham, S.B.; Ye, Z.; Zimmermann, A.G.; Ting, J.P.Y. Cryopyrin/NALP3 binds ATP/dATP, is an ATPase, and requires ATP binding to mediate inflammatory signaling. *Proc. Natl. Acad. Sci. USA* **2007**, *104*, 8041–8046. https://doi.org/10.1073/pnas.0611496104.
6. Hafner-Bratkovič, I.; Sušjan, P.; Lainšček, D.; Tapia-Abellán, A.; Cerović, K.; Kadunc, L.; Angosto-Bazarra, D.; Pelegrín, P.; Jerala, R. NLRP3 lacking the leucine-rich repeat domain can be fully activated via the canonical inflammasome pathway. *Nat. Commun.* **2018**, *9*, 5182. https://doi.org/10.1038/s41467-018-07573-4.
7. Yang, Y.; Wang, H.; Kouadir, M.; Song, H.; Shi, F. Recent advances in the mechanisms of NLRP3 inflammasome activation and its inhibitors. *Cell Death Dis.* **2019**, *10*, 182.
8. Gong, T.; Yang, Y.; Jin, T.; Jiang, W.; Zhou, R. Orchestration of NLRP3 Inflammasome Activation by Ion Fluxes. *Trends Immunol.* **2018**, *39*, 393–406.
9. Sharif, H.; Wang, L.; Wang, W.L.; Magupalli, V.G.; Andreeva, L.; Qiao, Q.; Hauenstein, A.V.; Wu, Z.; Núñez, G.; Mao, Y.; et al. Structural mechanism for NEK7-licensed activation of NLRP3 inflammasome. *Nature* **2019**, *570*, 338–343. https://doi.org/10.1038/s41586-019-1295-z.
10. Kuwar, R.; Rolfe, A.; Di, L.; Blevins, H.; Xu, Y.; Sun, X.; Bloom, G.S.; Zhang, S.; Sun, D. A novel inhibitor targeting NLRP3 inflammasome reduces neuropathology and improves cognitive function in alzheimer's disease transgenic mice. *J. Alzheimer's Dis.* **2021**, *82*, 1769–1783. https://doi.org/10.3233/JAD-210400.
11. Liang, Z.; Damianou, A.; Di Daniel, E.; Kessler, B.M. Inflammasome activation controlled by the interplay between post-translational modifications: Emerging drug target opportunities. *Cell Commun. Signal.* **2021**, *19*, 23.
12. McCarty, M.F.; Assanga, S.B.I.; Luján, L.L.; O'keefe, J.H.; Dinicolantonio, J.J. Nutraceutical strategies for suppressing nlrp3 inflammasome activation: Pertinence to the management of covid-19 and beyond. *Nutrients* **2021**, *13*, 47.
13. Hotamisligil, G.S. Inflammation, metaflammation and immunometabolic disorders. *Nature* **2017**, *542*, 177–185.
14. Allen, I.C.; Scull, M.A.; Moore, C.B.; Holl, E.K.; McElvania-TeKippe, E.; Taxman, D.J.; Guthrie, E.H.; Pickles, R.J.; Ting, J.P.Y. The NLRP3 Inflammasome Mediates In Vivo Innate Immunity to Influenza A Virus through Recognition of Viral RNA. *Immunity* **2009**, *30*, 556–565. https://doi.org/10.1016/j.immuni.2009.02.005.
15. Son, S.; Hwang, I.; Hyeokhan, S.; Shin, J.S.; Shin, O.S.; Yu, J.W. Advanced glycation end products impair NLRP3 inflammasome-mediated innate immune responses in macrophages. *J. Biol. Chem.* **2017**, *292*, 20437–20448. https://doi.org/10.1074/jbc.M117.806307.
16. Wen, H.; Gris, D.; Lei, Y.; Jha, S.; Zhang, L.; Huang, M.T.H.; Brickey, W.J.; Ting, J.P.Y. Fatty acid-induced NLRP3-ASC inflammasome activation interferes with insulin signaling. *Nat. Immunol.* **2011**, *12*, 408–415. https://doi.org/10.1038/ni.2022.
17. Alvarenga, L.; Cardozo, L.F.M.F.; Borges, N.A.; Lindholm, B.; Stenvinkel, P.; Shiels, P.G.; Fouque, D.; Mafra, D. Can nutritional interventions modulate the activation of the NLRP3 inflammasome in chronic kidney disease? *Food Res. Int.* **2020**, *136*, 109306.
18. Drobny, E.C.; Abramson, E.C.; Baumann, G. Insulin receptors in acute infection: A study of factors conferring insulin resistance. *J. Clin. Endocrinol. Metab.* **1984**, *58*, 710–716. https://doi.org/10.1210/jcem-58-4-710.
19. Caputo, T.; Gilardi, F.; Desvergne, B. From chronic overnutrition to metaflammation and insulin resistance: Adipose tissue and liver contributions. *FEBS Lett.* **2017**, *591*, 3061–3088.

20. Hotamisligil, G.S. Inflammation and metabolic disorders. *Nature* **2006**, *444*, 860–867.
21. Calder, P.C.; Ahluwalia, N.; Brouns, F.; Buetler, T.; Clement, K.; Cunningham, K.; Esposito, K.; Jönsson, L.S.; Kolb, H.; Lansink, M.; et al. Dietary factors and low-grade inflammation in relation to overweight and obesity. *Br. J. Nutr.* **2011**, *106*, S1–S78. https://doi.org/10.1017/s0007114511005460.
22. Lumeng, C.N.; Saltiel, A.R. Inflammatory links between obesity and metabolic disease. *J. Clin. Investig.* **2011**, *121*, 2111–2117.
23. Barbaresko, J.; Koch, M.; Schulze, M.B.; Nöthlings, U. Dietary pattern analysis and biomarkers of low-grade inflammation: A systematic literature review. *Nutr. Rev.* **2013**, *71*, 511–527. https://doi.org/10.1111/nure.12035.
24. Schroder, K.; Tschopp, J. The Inflammasomes. *Cell* **2010**, *140*, 821–832.
25. Tack, C.J.; Stienstra, R.; Joosten, L.A.B.; Netea, M.G. Inflammation links excess fat to insulin resistance: The role of the interleukin-1 family. *Immunol. Rev.* **2012**, *249*, 239–252. https://doi.org/10.1111/j.1600-065X.2012.01145.x.
26. Lagathu, C.; Yvan-Charvet, L.; Bastard, J.P.; Maachi, M.; Quignard-Boulangé, A.; Capeau, J.; Caron, M. Long-term treatment with interleukin-1β induces insulin resistance in murine and human adipocytes. *Diabetologia* **2006**, *49*, 2162–2173. https://doi.org/10.1007/s00125-006-0335-z.
27. Stienstra, R.; Van Diepen, J.A.; Tack, C.J.; Zaki, M.H.; Van De Veerdonk, F.L.; Perera, D.; Neale, G.A.; Hooiveld, G.J.; Hijmans, A.; Vroegrijk, I.; et al. Inflammasome is a central player in the induction of obesity and insulin resistance. *Proc. Natl. Acad. Sci. USA* **2011**, *108*, 15324–15329. https://doi.org/10.1073/pnas.1100255108.
28. Roche, H.M. Dietary modulation of energy homoeostasis and metabolic-inflammation. *Proc. Nutr. Soc.* **2019**, *78*, 313–318.
29. McGillicuddy, F.C.; Harford, K.A.; Reynolds, C.M.; Oliver, E.; Claessens, M.; Mills, K.H.G.; Roche, H.M. Lack of interleukin-1 receptor I (IL-1RI) protects mice from high-fat diet-induced adipose tissue inflammation coincident with improved glucose homeostasis. *Diabetes* **2011**, *60*, 1688–1698. https://doi.org/10.2337/db10-1278.
30. Kirwan, A.M.; Lenighan, Y.M.; O'Reilly, M.E.; McGillicuddy, F.C.; Roche, H.M. Nutritional modulation of metabolic inflammation. *Biochem. Soc. Trans.* **2017**, *45*, 979–985.
31. Ralston, J.C.; Lyons, C.L.; Kennedy, E.B.; Kirwan, A.M.; Roche, H.M. Fatty Acids and NLRP3 Inflammasome-Mediated Inflammation in Metabolic Tissues. *Annu. Rev. Nutr.* **2017**, *37*, 77–102.
32. Dewhurst-Trigg, R.; Hulston, C.J.; Markey, O. The effect of quantity and quality of dietary fat intake on subcutaneous white adipose tissue inflammatory responses. *Proc. Nutr. Soc.* **2020**, *79*, 542–556.
33. Nishimura, S.; Manabe, I.; Nagasaki, M.; Eto, K.; Yamashita, H.; Ohsugi, M.; Otsu, M.; Hara, K.; Ueki, K.; Sugiura, S.; et al. CD8+ effector T cells contribute to macrophage recruitment and adipose tissue inflammation in obesity. *Nat. Med.* **2009**, *15*, 914–920. https://doi.org/10.1038/nm.1964.
34. Gregor, M.F.; Hotamisligil, G.S. Inflammatory mechanisms in obesity. *Annu. Rev. Immunol.* **2011**, *29*, 415–445. https://doi.org/10.1146/annurev-immunol-031210-101322.
35. Roncero-Ramos, I.; Rangel-Zuñiga, O.A.; Lopez-Moreno, J.; Alcala-Diaz, J.F.; Perez-Martinez, P.; Jimenez-Lucena, R.; Castaño, J.P.; Roche, H.M.; Delgado-Lista, J.; Ordovas, J.M.; et al. Mediterranean Diet, Glucose Homeostasis, and Inflammasome Genetic Variants: The CORDIOPREV Study. *Mol. Nutr. Food Res.* **2018**, *62*, 1700960. https://doi.org/10.1002/mnfr.201700960.
36. Galland, L. Diet and inflammation. *Nutr. Clin. Pract.* **2010**, *25*, 634–640.
37. Margioris, A.N. Fatty acids and postprandial inflammation. *Curr. Opin. Clin. Nutr. Metab. Care* **2009**, *12*, 129–137.
38. Mozaffarian, D.; Aro, A.; Willett, W.C. Health effects of trans-fatty acids: Experimental and observational evidence. *Eur. J. Clin. Nutr.* **2009**, *63*, S5–S21. https://doi.org/10.1038/sj.ejcn.1602973.
39. World Health Organization Nutrition: Trans fat. https://www.who.int/news-room/questions-and-answers/item/nutrition-trans-fat. (accessed on 10 January 2022)
40. Riediger, N.D.; Othman, R.A.; Suh, M.; Moghadasian, M.H. A Systemic Review of the Roles of n-3 Fatty Acids in Health and Disease. *J. Am. Diet. Assoc.* **2009**, *109*, 668–679. https://doi.org/10.1016/j.jada.2008.12.022.
41. Innes, J.K.; Calder, P.C. Omega-6 fatty acids and inflammation. *Prostaglandins Leukot. Essent. Fat. Acids* **2018**, *132*, 41–48.
42. Yan, Y.; Jiang, W.; Spinetti, T.; Tardivel, A.; Castillo, R.; Bourquin, C.; Guarda, G.; Tian, Z.; Tschopp, J.; Zhou, R. Omega-3 Fatty Acids Prevent Inflammation and Metabolic Disorder through Inhibition of NLRP3 Inflammasome Activation. *Immunity* **2013**, *38*, 1154–1163. https://doi.org/10.1016/j.immuni.2013.05.015.
43. Lee, K.R.; Midgette, Y.; Shah, R. Fish oil derived omega 3 fatty acids suppress adipose NLRP3 inflammasome signaling in human obesity. *J. Endocr. Soc.* **2019**, *3*, 504–515. https://doi.org/10.1210/js.2018-00220.
44. Sears, B. Anti-inflammatory diets for obesity and diabetes. *J. Am. Coll. Nutr.* **2009**, *28*, 482S–491S. https://doi.org/10.1080/07315724.2009.10718115.
45. Basu, A.; Devaraj, S.; Jialal, I. Dietary factors that promote or retard inflammation. *Arterioscler. Thromb. Vasc. Biol.* **2006**, *26*, 995–1001.
46. Finucane, O.M.; Lyons, C.L.; Murphy, A.M.; Reynolds, C.M.; Klinger, R.; Healy, N.P.; Cooke, A.A.; Coll, R.C.; Mcallan, L.; Nilaweera, K.N.; et al. Monounsaturated fatty acid-enriched high-fat diets impede adipose NLRP3 inflammasome-mediated IL-1β secretion and insulin resistance despite obesity. *Diabetes* **2015**, *64*, 2116–2128. https://doi.org/10.2337/db14-1098.

47. Levitan, E.B.; Cook, N.R.; Stampfer, M.J.; Ridker, P.M.; Rexrode, K.M.; Buring, J.E.; Manson, J.A.E.; Liu, S. Dietary glycemic index, dietary glycemic load, blood lipids, and C-reactive protein. *Metabolism* **2008**, *57*, 437–443. https://doi.org/10.1016/j.metabol.2007.11.002.
48. Zhou, R.; Yazdi, A.S.; Menu, P.; Tschopp, J. A role for mitochondria in NLRP3 inflammasome activation. *Nature* **2011**, *469*, 221–226. https://doi.org/10.1038/nature09663.
49. Pavillard, L.E.; Marín-Aguilar, F.; Bullon, P.; Cordero, M.D. Cardiovascular diseases, NLRP3 inflammasome, and western dietary patterns. *Pharmacol. Res.* **2018**, *131*, 44–50.
50. Lee, H.M.; Kim, J.J.; Kim, H.J.; Shong, M.; Ku, B.J.; Jo, E.K. Upregulated NLRP3 inflammasome activation in patients with type 2 diabetes. *Diabetes* **2013**, *62*, 194–204. https://doi.org/10.2337/db12-0420.
51. Tschopp, J.; Schroder, K. NLRP3 inflammasome activation: The convergence of multiple signalling pathways on ROS production? *Nat. Rev. Immunol.* **2010**, *10*, 210–215.
52. Martinon, F. Signaling by ROS drives inflammasome activation. *Eur. J. Immunol.* **2010**, *40*, 616–619.
53. Jhang, J.J.; Lin, J.H.; Yen, G.C. Beneficial Properties of Phytochemicals on NLRP3 Inflammasome-Mediated Gout and Complication. *J. Agric. Food Chem.* **2018**, *66*, 765–772.
54. Moher, D.; Liberati, A.; Tetzlaff, J.; Altman, D.G.; Altman, D.; Antes, G.; Atkins, D.; Barbour, V.; Barrowman, N.; Berlin, J.A.; et al. Preferred reporting items for systematic reviews and meta-analyses: The PRISMA statement. *PLoS Med.* **2009**, *6*, e1000097.
55. Pandey, K.B.; Rizvi, S.I. Plant polyphenols as dietary antioxidants in human health and disease. *Oxid. Med. Cell. Longev.* **2009**, *2*, 270–278.
56. Li, A.N.; Li, S.; Zhang, Y.J.; Xu, X.R.; Chen, Y.M.; Li, H. Bin Resources and biological activities of natural polyphenols. *Nutrients* **2014**, *6*, 6020–6047.
57. Qian, B.; Wang, C.; Zeng, Z.; Ren, Y.; Li, D.; Song, J. Le Ameliorative effect of sinapic acid on dextran sodium sulfate-(DSS-) induced ulcerative colitis in kunming (km) mice. *Oxid. Med. Cell. Longev.* **2020**, *2020*, 8393504. https://doi.org/10.1155/2020/8393504.
58. Mahmoud, A.M.; Hussein, O.E.; Abd El-Twab, S.M.; Hozayen, W.G. Ferulic acid protects against methotrexate nephrotoxicity: Via activation of Nrf2/ARE/HO-1 signaling and PPARγ, and suppression of NF-κB/NLRP3 inflammasome axis. *Food Funct.* **2019**, *10*, 4593–4607. https://doi.org/10.1039/c9fo00114j.
59. Zeng, J.; Zhang, D.; Wan, X.; Bai, Y.; Yuan, C.; Wang, T.; Yuan, D.; Zhang, C.; Liu, C. Chlorogenic Acid Suppresses miR-155 and Ameliorates Ulcerative Colitis through the NF-κB/NLRP3 Inflammasome Pathway. *Mol. Nutr. Food Res.* **2020**, *64*, e2000452. https://doi.org/10.1002/mnfr.202000452.
60. Lv, Y.; Gao, X.; Luo, Y.; Fan, W.; Shen, T.; Ding, C.; Yao, M.; Song, S.; Yan, L. Apigenin ameliorates HFD-induced NAFLD through regulation of the XO/NLRP3 pathways. *J. Nutr. Biochem.* **2019**, *71*, 110–121. https://doi.org/10.1016/j.jnutbio.2019.05.015.
61. Yamagata, K.; Hashiguchi, K.; Yamamoto, H.; Tagami, M. Dietary Apigenin Reduces Induction of LOX-1 and NLRP3 Expression, Leukocyte Adhesion, and Acetylated Low-Density Lipoprotein Uptake in Human Endothelial Cells Exposed to Trimethylamine-N-Oxide. *J. Cardiovasc. Pharmacol.* **2019**, *74*, 558–565. https://doi.org/10.1097/FJC.0000000000000747.
62. An, M.F.; Wang, M.Y.; Shen, C.; Sun, Z.R.; Zhao, Y.L.; Wang, X.J.; Sheng, J. Isoorientin exerts a urate-lowering effect through inhibition of xanthine oxidase and regulation of the TLR4-NLRP3 inflammasome signaling pathway. *J. Nat. Med.* **2021**, *75*, 129–141. https://doi.org/10.1007/s11418-020-01464-z.
63. Chang, Y.H.; Chiang, Y.F.; Chen, H.Y.; Huang, Y.J.; Wang, K.L.; Hong, Y.H.; Ali, M.; Shieh, T.M.; Hsia, S.M. Anti-inflammatory and anti-hyperuricemic effects of chrysin on a high fructose corn syrup-induced hyperuricemia rat model via the amelioration of urate transporters and inhibition of nlrp3 inflammasome signaling pathway. *Antioxidants* **2021**, *10*, 564. https://doi.org/10.3390/antiox10040564.
64. Fu, J.; Sun, H.; Zhang, Y.; Xu, W.; Wang, C.; Fang, Y.; Zhao, J. Neuroprotective Effects of Luteolin Against Spinal Cord Ischemia-Reperfusion Injury by Attenuation of Oxidative Stress, Inflammation, and Apoptosis. *J. Med. Food* **2018**, *21*, 13–20. https://doi.org/10.1089/jmf.2017.4021.
65. Ruiz-Miyazawa, K.W.; Pinho-Ribeiro, F.A.; Borghi, S.M.; Staurengo-Ferrari, L.; Fattori, V.; Amaral, F.A.; Teixeira, M.M.; Alves-Filho, J.C.; Cunha, T.M.; Cunha, F.Q.; et al. Hesperidin Methylchalcone Suppresses Experimental Gout Arthritis in Mice by Inhibiting NF-κB Activation. *J. Agric. Food Chem.* **2018**, *66*, 6269–6280. https://doi.org/10.1021/acs.jafc.8b00959.
66. Cao, H.; Liu, J.; Shen, P.; Cai, J.; Han, Y.; Zhu, K.; Fu, Y.; Zhang, N.; Zhang, Z.; Cao, Y. Protective Effect of Naringin on DSS-Induced Ulcerative Colitis in Mice. *J. Agric. Food Chem.* **2018**, *66*, 13133–13140. https://doi.org/10.1021/acs.jafc.8b03942.
67. Liu, S.; Tian, L.; Chai, G.; Wen, B.; Wang, B. Targeting heme oxygenase-1 by quercetin ameliorates alcohol-induced acute liver injury via inhibiting NLRP3 inflammasome activation. *Food Funct.* **2018**, *9*, 4184–4193. https://doi.org/10.1039/c8fo00650d.
68. Li, H.; Xiao, L.; He, H.; Zeng, H.; Liu, J.; Jiang, C.; Mei, G.; Yu, J.; Chen, H.; Yao, P.; et al. Quercetin Attenuates Atherosclerotic Inflammation by Inhibiting Galectin-3-NLRP3 Signaling Pathway. *Mol. Nutr. Food Res.* **2021**, *65*, 2000746. https://doi.org/10.1002/mnfr.202000746.
69. Li, H.; Chen, F.J.; Yang, W.L.; Qiao, H.Z.; Zhang, S.J. Quercetin improves cognitive disorder in aging mice by inhibiting NLRP3 inflammasome activation. *Food Funct.* **2021**, *12*, 717–725. https://doi.org/10.1039/d0fo01900c.
70. Xue, Y.; Du, M.; Zhu, M.J. Quercetin suppresses NLRP3 inflammasome activation in epithelial cells triggered by Escherichia coli O157:H7. *Free Radic. Biol. Med.* **2017**, *108*, 760–769. https://doi.org/10.1016/j.freeradbiomed.2017.05.003.

71. Zhang, Y.; Jin, Q.; Li, X.; Jiang, M.; Cui, B.W.; Xia, K.L.; Wu, Y.L.; Lian, L.H.; Nan, J.X. Amelioration of Alcoholic Liver Steatosis by Dihydroquercetin through the Modulation of AMPK-Dependent Lipogenesis Mediated by P2X7R-NLRP3-Inflammasome Activation. *J. Agric. Food Chem.* **2018**, *66*, 4862–4871. https://doi.org/10.1021/acs.jafc.8b00944.
72. Du, Y.C.; Lai, L.; Zhang, H.; Zhong, F.R.; Cheng, H.L.; Qian, B.L.; Tan, P.; Xia, X.M.; Fu, W.G. Kaempferol from: Penthorum chinense Pursh suppresses HMGB1/TLR4/NF-?B signaling and NLRP3 inflammasome activation in acetaminophen-induced hepatotoxicity. *Food Funct.* **2020**, *11*, 7925–7934. https://doi.org/10.1039/d0fo00724b.
73. Lalitha, N.; Sadashivaiah, B.; Ramaprasad, T.R.; Singh, S.A. Anti-hyperglycemic activity of myricetin, through inhibition of DPP-4 and enhanced GLP-1 levels, is attenuated by co-ingestion with lectin-rich protein. *PLoS ONE* **2020**, *15*, e0231543. https://doi.org/10.1371/journal.pone.0231543.
74. Zhang, W.-Y.; Guo, Y.-J.; Han, W.-X.; Yang, M.-Q.; Wen, L.-P.; Wang, K.-Y.; Jiang, P. Curcumin relieves depressive-like behaviors via inhibition of the NLRP3 inflammasome and kynurenine pathway in rats suffering from chronic unpredictable mild stress. *Int. Immunopharmacol.* **2019**, *67*, 138–144. https://doi.org/10.1016/j.intimp.2018.12.012.
75. Alvarenga, L.; Salarolli, R.; Cardozo, L.F.M.F.; Santos, R.S.; de Brito, J.S.; Kemp, J.A.; Reis, D.; de Paiva, B.R.; Stenvinkel, P.; Lindholm, B.; et al. Impact of curcumin supplementation on expression of inflammatory transcription factors in hemodialysis patients: A pilot randomized, double-blind, controlled study. *Clin. Nutr.* **2020**, *39*, 3594–3600. https://doi.org/10.1016/j.clnu.2020.03.007.
76. Chen, T.C.; Yen, C.K.; Lu, Y.C.; Shi, C.S.; Hsieh, R.Z.; Chang, S.F.; Chen, C.N. The antagonism of 6-shogaol in high-glucose-activated NLRP3 inflammasome and consequent calcification of human artery smooth muscle cells. *Cell Biosci.* **2020**, *10*, 5–10. https://doi.org/10.1186/s13578-019-0372-1.
77. Ho, S.C.; Chang, Y.H. Comparison of inhibitory capacities of 6-, 8- and 10-gingerols/shogaols on the canonical NLRP3 inflammasome-mediated IL-1β secretion. *Molecules* **2018**, *23*, 466. https://doi.org/10.3390/molecules23020466.
78. Zhang, E.; Huang, J.; Wang, K.; Yu, Q.; Zhu, C.; Ren, H. Pterostilbene Protects against Lipopolysaccharide/D-Galactosamine-Induced Acute Liver Failure by Upregulating the Nrf2 Pathway and Inhibiting NF-κB, MAPK, and NLRP3 Inflammasome Activation. *J. Med. Food* **2020**, *23*, 952–960. https://doi.org/10.1089/jmf.2019.4647.
79. Wang, B.J.; Chiu, H.W.; Lee, Y.L.; Li, C.Y.; Wang, Y.J.; Lee, Y.H. Pterostilbene attenuates hexavalent chromium-induced allergic contact dermatitis by preventing cell apoptosis and inhibiting IL-1β-related NLRP3 inflammasome activation. *J. Clin. Med.* **2018**, *7*, 489. https://doi.org/10.3390/jcm7120489.
80. Wang, Y.J.; Chen, Y.Y.; Hsiao, C.M.; Pan, M.H.; Wang, B.J.; Chen, Y.C.; Ho, C.T.; Huang, K.C.; Chen, R.J. Induction of Autophagy by Pterostilbene Contributes to the Prevention of Renal Fibrosis via Attenuating NLRP3 Inflammasome Activation and Epithelial-Mesenchymal Transition. *Front. Cell Dev. Biol.* **2020**, *8*, 436. https://doi.org/10.3389/fcell.2020.00436.
81. Chen, L.; Lan, Z. Polydatin attenuates potassium oxonate-induced hyperuricemia and kidney inflammation by inhibiting NF-κB/NLRP3 inflammasome activation via the AMPK/SIRT1 pathway. *Food Funct.* **2017**, *8*, 1785–1792. https://doi.org/10.1039/c6fo01561a.
82. Park, B.; Jo, K.; Lee, T.G.; Hyun, S.W.; Kim, J.S.; Kim, C.S. Polydatin inhibits NLRP3 inflammasome in dry eye disease by attenuating oxidative stress and inhibiting the nf-κb pathway. *Nutrients* **2019**, *11*, 2792. https://doi.org/10.3390/nu11112792.
83. Jin, X.; Wang, C.; Wu, W.; Liu, T.; Ji, B.; Zhou, F. Cyanidin-3-glucoside alleviates 4-Hydroxyhexenal-induced NLRP3 inflammasome activation via JNK-c-Jun/AP-1 pathway in human retinal pigment epithelial cells. *J. Immunol. Res.* **2018**, *2018*, 5604610, https://doi.org/10.1155/2018/5604610.
84. Zhou, Y.; Wang, S.; Wan, T.; Huang, Y.; Pang, N.; Jiang, X.; Gu, Y.; Zhang, Z.; Luo, J.; Yang, L. Cyanidin-3-O-β-glucoside inactivates NLRP3 inflammasome and alleviates alcoholic steatohepatitis via SirT1/NF-κB signaling pathway. *Free Radic. Biol. Med.* **2020**, *160*, 334–341. https://doi.org/10.1016/j.freeradbiomed.2020.08.006.
85. Luo, Z.L.; Sun, H.Y.; Wu, X.B.; Cheng, L.; Ren, J.D. Epigallocatechin-3-gallate attenuates acute pancreatitis induced lung injury by targeting mitochondrial reactive oxygen species triggered NLRP3 inflammasome activation. *Food Funct.* **2021**, *12*, 5658–5667. https://doi.org/10.1039/d1fo01154e.
86. Zhong, X.; Liu, M.; Yao, W.; Du, K.; He, M.; Jin, X.; Jiao, L.; Ma, G.; Wei, B.; Wei, M. Epigallocatechin-3-Gallate Attenuates Microglial Inflammation and Neurotoxicity by Suppressing the Activation of Canonical and Noncanonical Inflammasome via TLR4/NF-κB Pathway. *Mol. Nutr. Food Res.* **2019**, *63*, 1801230. https://doi.org/10.1002/mnfr.201801230.
87. Lin, Y.F.; Lee, Y.H.; Hsu, Y.H.; Chen, Y.J.; Lin, Y.F.; Cheng, F.Y.; Chiu, H.W. Resveratrol-loaded nanoparticles conjugated with kidney injury molecule-1 as a drug delivery system for potential use in chronic kidney disease. *Nanomedicine* **2017**, *12*, 2741–2756. https://doi.org/10.2217/nnm-2017-0256.
88. Luzardo-Ocampo, I.; Loarca-Piña, G.; Gonzalez de Mejia, E. Gallic and butyric acids modulated NLRP3 inflammasome markers in a co-culture model of intestinal inflammation. *Food Chem. Toxicol.* **2020**, *146*, 111835. https://doi.org/10.1016/j.fct.2020.111835.
89. Wang, D.; Gao, Q.; Wang, T.; Kan, Z.; Li, X.; Hu, L.; Peng, C.-Y.; Qian, F.; Wang, Y.; Granato, D. Green tea polyphenols and epigallocatechin-3-gallate protect against perfluorodecanoic acid induced liver damage and inflammation in mice by inhibiting NLRP3 inflammasome activation. *Food Res. Int.* **2020**, *127*, 108628. https://doi.org/10.1016/j.foodres.2019.108628.
90. Wang, D.; Zhang, M.; Wang, T.; Cai, M.; Qian, F.; Sun, Y.; Wang, Y. Green tea polyphenols prevent lipopolysaccharide-induced inflammatory liver injury in mice by inhibiting NLRP3 inflammasome activation. *Food Funct.* **2019**, *10*, 3898–3908. https://doi.org/10.1039/c9fo00572b.

91. Gao, X.; Fan, W.; Tan, L.; Shi, Y.; Ding, C.; Liu, S.; Miao, Y.; Luo, Y.; Shi, X.; DeSaeger, S.; et al. Soy isoflavones ameliorate experimental colitis by targeting ERα/NLRP3 inflammasome pathways. *J. Nutr. Biochem.* **2020**, *83*, 108438. https://doi.org/10.1016/j.jnutbio.2020.108438.
92. Fan, R.; You, M.; Toney, A.M.; Kim, J.; Giraud, D.; Xian, Y.; Ye, F.; Gu, L.; Ramer-Tait, A.E.; Chung, S. Red Raspberry Polyphenols Attenuate High-Fat Diet–Driven Activation of NLRP3 Inflammasome and its Paracrine Suppression of Adipogenesis via Histone Modifications. *Mol. Nutr. Food Res.* **2020**, *64*, e1900995. https://doi.org/10.1002/mnfr.201900995.
93. Nan, B.; Yang, C.; Li, L.; Ye, H.; Yan, H.; Wang, M.; Yuan, Y. Allicin alleviated acrylamide-induced NLRP3 inflammasome activation via oxidative stress and endoplasmic reticulum stress in Kupffer cells and SD rats liver. *Food Chem. Toxicol.* **2021**, *148*, 111937, https://doi.org/10.1016/j.fct.2020.111937.
94. Chen, H.W.; Yen, C.C.; Kuo, L.L.; Lo, C.W.; Huang, C.S.; Chen, C.C.; Lii, C.K. Benzyl isothiocyanate ameliorates high-fat/cholesterol/cholic acid diet-induced nonalcoholic steatohepatitis through inhibiting cholesterol crystal-activated NLRP3 inflammasome in Kupffer cells. *Toxicol. Appl. Pharmacol.* **2020**, *393*, 114941. https://doi.org/10.1016/j.taap.2020.114941.
95. Dong, Z.; Shang, H.; Chen, Y.Q.; Pan, L.L.; Bhatia, M.; Sun, J. Sulforaphane Protects Pancreatic Acinar Cell Injury by Modulating Nrf2-Mediated Oxidative Stress and NLRP3 Inflammatory Pathway. *Oxid. Med. Cell. Longev.* **2016**, *2016*, 4916497. https://doi.org/10.1155/2016/7864150.
96. Ahn, H.; Kim, J.; Lee, M.J.; Kim, Y.J.; Cho, Y.W.; Lee, G.S. Methylsulfonylmethane inhibits NLRP3 inflammasome activation. *Cytokine* **2015**, *71*, 223–231. https://doi.org/10.1016/j.cyto.2014.11.001.
97. Yang, N.; Xia, Z.; Shao, N.; Li, B.; Xue, L.; Peng, Y.; Zhi, F.; Yang, Y. Carnosic acid prevents dextran sulfate sodium-induced acute colitis associated with the regulation of the Keap1/Nrf2 pathway. *Sci. Rep.* **2017**, *7*, 12117. https://doi.org/10.1038/s41598-017-11408-5.
98. Marcuzzi, A.; Piscianz, E.; Zweyer, M.; Bortul, R.; Loganes, C.; Girardelli, M.; Baj, G.; Monasta, L.; Celeghini, C. Geranylgeraniol and neurological impairment: Involvement of apoptosis and mitochondrial morphology. *Int. J. Mol. Sci.* **2016**, *17*, 365. https://doi.org/10.3390/ijms17030365.
99. Miranda, M.M.; Panis, C.; Da Silva, S.S.; Macri, J.A.; Kawakami, N.Y.; Hayashida, T.H.; Madeira, T.B.; Acquaro, V.R.; Nixdorf, S.L.; Pizzatti, L.; et al. Kaurenoic acid possesses leishmanicidal activity by triggering a NLRP12/IL-1 β/cNOS/NO Pathway. *Mediat. Inflamm.* **2015**, *2015*, 392918. https://doi.org/10.1155/2015/392918.
100. Robblee, M.M.; Kim, C.C.; Abate, J.P.; Valdearcos, M.; Sandlund, K.L.M.; Shenoy, M.K.; Volmer, R.; Iwawaki, T.; Koliwad, S.K. Saturated Fatty Acids Engage an IRE1α-Dependent Pathway to Activate the NLRP3 Inflammasome in Myeloid Cells. *Cell Rep.* **2016**, *14*, 2611–2623. https://doi.org/10.1016/j.celrep.2016.02.053.
101. Mirzaei, F.; Khazaei, M.; Komaki, A.; Amiri, I.; Jalili, C. Virgin coconut oil (VCO) by normalizing NLRP3 inflammasome showed potential neuroprotective effects in Amyloid-β induced toxicity and high-fat diet fed rat. *Food Chem. Toxicol.* **2018**, *118*, 68–83. https://doi.org/10.1016/j.fct.2018.04.064.
102. López-Tenorio, I.I.; Domínguez-López, A.; Miliar-García, Á.; Escalona-Cardoso, G.N.; Real-Sandoval, S.A.; Gómez-Alcalá, A.; Jaramillo-Flores, M.E. Modulation of the mRNA of the Nlrp3 inflammasome by Morin and PUFAs in an obesity model induced by a high-fat diet. *Food Res. Int.* **2020**, *137*, 109706. https://doi.org/10.1016/j.foodres.2020.109706.
103. Yu, Q.; Wang, T.; Wang, F.; Yang, Y.; He, C.; Yang, W.; Zhang, J.; Zou, Z. High n-3 fatty acids counteract hyperglycemia-induced insulin resistance in fat-1 mice: Via pre-adipocyte NLRP3 inflammasome inhibition. *Food Funct.* **2021**, *12*, 230–240. https://doi.org/10.1039/d0fo02092c.
104. Miao, F.; Shan, C.; Ma, T.; Geng, S.; Ning, D. Walnut oil alleviates DSS–induced colitis in mice by inhibiting NLRP3 inflammasome activation and regulating gut microbiota. *Microb. Pathog.* **2021**, *154*, 104866. https://doi.org/10.1016/j.micpath.2021.104866.
105. Fan, G.; Li, Y.; Chen, J.; Zong, Y.; Yang, X. DHA/AA alleviates LPS-induced Kupffer cells pyroptosis via GPR120 interaction with NLRP3 to inhibit inflammasome complexes assembly. *Cell Death Dis.* **2021**, *12*, 73. https://doi.org/10.1038/s41419-020-03347-3.
106. Dang, R.; Zhou, X.; Tang, M.; Xu, P.; Gong, X.; Liu, Y.; Jiao, H.; Jiang, P. Fish oil supplementation attenuates neuroinflammation and alleviates depressive-like behavior in rats submitted to repeated lipopolysaccharide. *Eur. J. Nutr.* **2018**, *57*, 893–906. https://doi.org/10.1007/s00394-016-1373-z.
107. Liu, N.; Meng, B.; Zeng, L.; Yin, S.; Hu, Y.; Li, S.; Fu, Y.; Zhang, X.; Xie, C.; Shu, L.; et al. Discovery of a novel rice-derived peptide with significant anti-gout potency. *Food Funct.* **2020**, *11*, 10542–10553. https://doi.org/10.1039/d0fo01774d.
108. Liu, N.; Wang, Y.; Zeng, L.; Yin, S.; Hu, Y.; Li, S.; Fu, Y.; Zhang, X.; Xie, C.; Shu, L.; et al. RDP3, A Novel Antigout Peptide Derived from Water Extract of Rice. *J. Agric. Food Chem.* **2020**, *68*, 7143–7151. https://doi.org/10.1021/acs.jafc.0c02535.
109. Han, J.; Wang, X.; Tang, S.; Lu, C.; Wan, H.; Zhou, J.; Li, Y.; Ming, T.; Wang, Z.J.; Su, X. Protective effects of tuna meat oligopeptides (TMOP) supplementation on hyperuricemia and associated renal inflammation mediated by gut microbiota. *FASEB J.* **2020**, *34*, 5061–5076. https://doi.org/10.1096/fj.201902597RR.
110. Bitzer, Z.T.; Wopperer, A.L.; Chrisfield, B.J.; Tao, L.; Cooper, T.K.; Vanamala, J.; Elias, R.J.; Hayes, J.E.; Lambert, J.D. Soy protein concentrate mitigates markers of colonic inflammation and loss of gut barrier function in vitro and in vivo. *J. Nutr. Biochem.* **2017**, *40*, 201–208. https://doi.org/10.1016/j.jnutbio.2016.11.012.

111. Gómez Castro, M.F.; Miculán, E.; Herrera, M.G.; Ruera, C.; Perez, F.; Prieto, E.D.; Barrera, E.; Pantano, S.; Carasi, P.; Chirdo, F.G. P31-43 gliadin peptide forms oligomers and induces NLRP3 inflammasome/caspase 1-dependent mucosal damage in small intestine. *Front. Immunol.* **2019**, *10*, 31. https://doi.org/10.3389/fimmu.2019.00031.
112. Luo, Z.; Xu, X.; Sho, T.; Luo, W.; Zhang, J.; Xu, W.; Yao, J.; Xu, J. Effects of n-acetyl-cysteine supplementation in late gestational diet on maternal-placental redox status, placental NLRP3 inflammasome, and fecal microbiota in sows. *J. Anim. Sci.* **2019**, *97*, 1757–1771. https://doi.org/10.1093/jas/skz058.
113. Zhang, Y.; Ma, X.; Jiang, D.; Chen, J.; Jia, H.; Wu, Z.; Kim, I.H.; Yang, Y. Glycine attenuates lipopolysaccharide-induced acute lung injury by regulating NLRP3 inflammasome and NRF2 signaling. *Nutrients* **2020**, *12*, 611. https://doi.org/10.3390/nu12030611.
114. Dai, Z.; Lu, X.Y.; Zhu, W.L.; Liu, X.Q.; Li, B.Y.; Song, L.; Liu, H.F.; Cai, W.W.; Deng, Y.X.; Xu, T.T.; et al. Carnosine ameliorates age-related dementia: Via improving mitochondrial dysfunction in SAMP8 mice. *Food Funct.* **2020**, *11*, 2489–2497. https://doi.org/10.1039/c9fo02453k.
115. Huang, J.; Wang, T.; Yu, D.; Fang, X.; Fan, H.; Liu, Q.; Yi, G.; Yi, X.; Liu, Q. L-Homocarnosine attenuates inflammation in cerebral ischemia–reperfusion injury through inhibition of nod-like receptor protein 3 inflammasome. *Int. J. Biol. Macromol.* **2018**, *118*, 357–364. https://doi.org/10.1016/j.ijbiomac.2018.06.032.
116. Wang, Y.; Guan, X.; Chen, X.; Cai, Y.; Ma, Y.; Ma, J.; Zhang, Q.; Dai, L.; Fan, X.; Bai, Y. Choline Supplementation Ameliorates Behavioral Deficits and Alzheimer's Disease-Like Pathology in Transgenic APP/PS1 Mice. *Mol. Nutr. Food Res.* **2019**, *63*, 1801407, https://doi.org/10.1002/mnfr.201801407.
117. Han, X.; Song, J.; Lian, L.H.; Yao, Y.L.; Shao, D.Y.; Fan, Y.; Hou, L.S.; Wang, G.; Zheng, S.; Wu, Y.L.; et al. Ginsenoside 25-OCH3-PPD Promotes Activity of LXRs to Ameliorate P2X7R-Mediated NLRP3 Inflammasome in the Development of Hepatic Fibrosis. *J. Agric. Food Chem.* **2018**, *66*, 7023–7035. https://doi.org/10.1021/acs.jafc.8b01982.
118. Wang, F.; Park, J.S.; Ma, Y.; Ma, H.; Lee, Y.J.; Lee, G.R.; Yoo, H.S.; Roh, Y.S.; Hong, J.T. Ginseng saponin enriched in rh1 and rg2 ameliorates nonalcoholic fatty liver disease by inhibiting inflammasome activation. *Nutrients* **2021**, *13*, 856. https://doi.org/10.3390/nu13030856.
119. Li, C.W.; Deng, M.Z.; Gao, Z.J.; Dang, Y.Y.; Zheng, G.D.; Yang, X.J.; Chao, Y.X.; Cai, Y.F.; Wu, X.L. Effects of compound K, a metabolite of ginsenosides, on memory and cognitive dysfunction in db/db mice involve the inhibition of ER stress and the NLRP3 inflammasome pathway. *Food Funct.* **2020**, *11*, 4416–4427. https://doi.org/10.1039/c9fo02602a.
120. Zhao, X.J.; Yang, Y.Z.; Zheng, Y.J.; Wang, S.C.; Gu, H.M.; Pan, Y.; Wang, S.J.; Xu, H.J.; Kong, L.D. Dataset on assessment of magnesium isoglycyrrhizinate injection for dairy diet and body weight in fructose-induced metabolic syndrome of rats. *Data Br.* **2018**, *18*, 69–75. https://doi.org/10.1016/j.dib.2018.03.016.
121. Zhang, Q.; Xu, N.N.; Hu, X.; Zheng, Y. Anti-colitic effects of Physalin B on dextran sodium sulfate-induced BALB/c mice by suppressing multiple inflammatory signaling pathways. *J. Ethnopharmacol.* **2020**, *259*, 112956. https://doi.org/10.1016/j.jep.2020.112956.
122. Liao, P.C.; Lai, M.H.; Hsu, K.P.; Kuo, Y.H.; Chen, J.; Tsai, M.C.; Li, C.X.; Yin, X.J.; Jeyashoke, N.; Chao, L.K.P. Identification of β-Sitosterol as in Vitro Anti-Inflammatory Constituent in Moringa oleifera. *J. Agric. Food Chem.* **2018**, *66*, 10748–10759. https://doi.org/10.1021/acs.jafc.8b04555.
123. Zheng, Y.; Fan, J.; Chen, H.W.; Liu, E.Q. Trametes orientalis polysaccharide alleviates PM2.5-induced lung injury in mice through its antioxidant and anti-inflammatory activities. *Food Funct.* **2019**, *10*, 8005–8015. https://doi.org/10.1039/c9fo01777a.
124. Liang, J.; Chen, S.; Chen, J.; Lin, J.; Xiong, Q.; Yang, Y.; Yuan, J.; Zhou, L.; He, L.; Hou, S.; et al. Therapeutic roles of polysaccharides from Dendrobium Officinaleon colitis and its underlying mechanisms. *Carbohydr. Polym.* **2018**, *185*, 159–168. https://doi.org/10.1016/j.carbpol.2018.01.013.
125. Li, P.; Xiao, N.; Zeng, L.; Xiao, J.; Huang, J.; Xu, Y.; Chen, Y.; Ren, Y.; Du, B. Structural characteristics of a mannoglucan isolated from Chinese yam and its treatment effects against gut microbiota dysbiosis and DSS-induced colitis in mice. *Carbohydr. Polym.* **2020**, *250*, 116958. https://doi.org/10.1016/j.carbpol.2020.116958.
126. Chen, Y.S.; Chen, Q.Z.; Wang, Z.J.; Hua, C. Anti-inflammatory and hepatoprotective effects of ganoderma lucidum polysaccharides against carbon tetrachloride-induced liver injury in Kunming Mice. *Pharmacology* **2019**, *103*, 143–150. https://doi.org/10.1159/000493896.
127. Yang, R.; Li, Y.; Cai, J.; Ji, J.; Wang, Y.; Zhang, W.; Pan, W.; Chen, Y. Polysaccharides from: Armillariella tabescens mycelia ameliorate insulin resistance in type 2 diabetic mice. *Food Funct.* **2020**, *11*, 9675–9685. https://doi.org/10.1039/d0fo00728e.
128. Wu, C.; Pan, L.L.; Niu, W.; Fang, X.; Liang, W.; Li, J.; Li, H.; Pan, X.; Chen, W.; Zhang, H.; et al. Modulation of Gut Microbiota by Low Methoxyl Pectin Attenuates Type 1 Diabetes in Non-obese Diabetic Mice. *Front. Immunol.* **2019**, *10*, 1733. https://doi.org/10.3389/fimmu.2019.01733.
129. Wu, C.; Pan, L.L.; Luo, Y.; Niu, W.; Fang, X.; Liang, W.; Li, J.; Li, H.; Pan, X.; Yang, G.; et al. Low Methoxyl Pectin Protects against Autoimmune Diabetes and Associated Caecal Dysfunction. *Mol. Nutr. Food Res.* **2019**, *63*, e1900307. https://doi.org/10.1002/mnfr.201900307.
130. Castro-Alves, V.C.; Shiga, T.M.; Nascimento, J.R.O. do Polysaccharides from chayote enhance lipid efflux and regulate NLRP3 inflammasome priming in macrophage-like THP-1 cells exposed to cholesterol crystals. *Int. J. Biol. Macromol.* **2019**, *127*, 502–510. https://doi.org/10.1016/j.ijbiomac.2019.01.048.

131. Liu, Y.; Wu, X.; Wang, Y.; Jin, W.; Guo, Y. The immunoenhancement effects of starfish: Asterias rollestoni polysaccharides in macrophages and cyclophosphamide-induced immunosuppression mouse models. *Food Funct.* **2020**, *11*, 10700–10708. https://doi.org/10.1039/d0fo01488e.
132. Tsao, R. Chemistry and biochemistry of dietary polyphenols. *Nutrients* **2010**, *2*, 1231–1246.
133. Zhang, H.; Tsao, R. Dietary polyphenols, oxidative stress and antioxidant and anti-inflammatory effects. *Curr. Opin. Food Sci.* **2016**, *8*, 33–42.
134. Chen, C. Sinapic acid and its derivatives as medicine in oxidative stress-induced diseases and aging. *Oxid. Med. Cell. Longev.* **2016**, *2016*, 3571614.
135. Rosazza, J.P.N.; Huang, Z.; Dostal, L.; Volm, T.; Rousseau, B. Review: Biocatalytic transformations of ferulic acid: An abundant aromatic natural product. *J. Ind. Microbiol.* **1995**, *15*, 457–471.
136. Santana-Gálvez, J.; Cisneros-Zevallos, L.; Jacobo-Velázquez, D.A. Chlorogenic Acid: Recent advances on its dual role as a food additive and a nutraceutical against metabolic syndrome. *Molecules* **2017**, *22*, 358.
137. Ho, S.C.; Chang, Y.H.; Chang, K.S. Structural moieties required for cinnamaldehyde-related compounds to inhibit canonical IL-1β secretion. *Molecules* **2018**, *23*, 3241. https://doi.org/10.3390/molecules23123241.
138. Liu, P.; Wang, J.; Wen, W.; Pan, T.; Chen, H.; Fu, Y.; Wang, F.; Huang, J.H.; Xu, S. Cinnamaldehyde suppresses NLRP3 derived IL-1β via activating succinate/HIF-1 in rheumatoid arthritis rats. *Int. Immunopharmacol.* **2020**, *84*, 106570. https://doi.org/10.1016/j.intimp.2020.106570.
139. Hassanzadeh, S.; Read, M.I.; Bland, A.R.; Majeed, M.; Jamialahmadi, T.; Sahebkar, A. Curcumin: An inflammasome silencer. *Pharmacol. Res.* **2020**, *159*, 104921.
140. Netea-Maier, R.T.; Plantinga, T.S.; van de Veerdonk, F.L.; Smit, J.W.; Netea, M.G. Modulation of inflammation by autophagy: Consequences for human disease. *Autophagy* **2016**, *12*, 245–260.
141. Wang, S.; Meckling, K.A.; Marcone, M.F.; Kakuda, Y.; Tsao, R. Synergistic, additive, and antagonistic effects of food mixtures on total antioxidant capacities. *J. Agric. Food Chem.* **2011**, *59*, 960–968. https://doi.org/10.1021/jf1040977.
142. Ruhee, R.T.; Roberts, L.A.; Ma, S.; Suzuki, K. Organosulfur Compounds: A Review of Their Anti-inflammatory Effects in Human Health. *Front. Nutr.* **2020**, *7*, 64.
143. Osipova, V.; Polovinkina, M.; Gracheva, Y.; Shpakovsky, D.; Osipova, A.; Berberova, N. Antioxidant activity of some organosulfur compounds in vitro. *Arab. J. Chem.* **2021**, *14*, 103068. https://doi.org/10.1016/j.arabjc.2021.103068.
144. Putnik, P.; Gabrić, D.; Roohinejad, S.; Barba, F.J.; Granato, D.; Mallikarjunan, K.; Lorenzo, J.M.; Bursać Kovačević, D. An overview of organosulfur compounds from Allium spp.: From processing and preservation to evaluation of their bioavailability, antimicrobial, and anti-inflammatory properties. *Food Chem.* **2019**, *276*, 680–691.
145. Yang, W.; Chen, X.; Li, Y.; Guo, S.; Wang, Z.; Yu, X. Advances in Pharmacological Activities of Terpenoids. *Nat. Prod. Commun.* **2020**, *15*, 1934578X20903555.
146. Islam, M.T.; Bardaweel, S.K.; Mubarak, M.S.; Koch, W.; Gaweł-Beben, K.; Antosiewicz, B.; Sharifi-Rad, J. Immunomodulatory Effects of Diterpenes and Their Derivatives Through NLRP3 Inflammasome Pathway: A Review. *Front. Immunol.* **2020**, *11*, 572136.
147. Zhao, X.; Pu, D.; Zhao, Z.; Zhu, H.; Li, H.; Shen, Y.; Zhang, X.; Zhang, R.; Shen, J.; Xiao, W.; et al. Teuvincenone F suppresses LPS-induced inflammation and NLRP3 inflammasome activation by attenuating NEMO ubiquitination. *Front. Pharmacol.* **2017**, *8*, 565. https://doi.org/10.3389/fphar.2017.00565.
148. Aachoui, Y.; Chowdhury, R.R.; Fitch, R.W.; Ghosh, S.K. Molecular signatures of phytol-derived immunostimulants in the context of chemokine-cytokine microenvironment and enhanced immune response. *Cell. Immunol.* **2011**, *271*, 227–238. https://doi.org/10.1016/j.cellimm.2011.07.001.
149. Liu, D.; Qin, H.; Yang, B.; Du, B.; Yun, X. Oridonin ameliorates carbon tetrachloride-induced liver fibrosis in mice through inhibition of the NLRP3 inflammasome. *Drug Dev. Res.* **2020**, *81*, 526–533. https://doi.org/10.1002/ddr.21649.
150. Duan, M.X.; Yuan, Y.; Liu, C.; Cai, Z.; Xie, Q.; Hu, T.; Tang, Q.; Wu, Q.Q. Indigo fruits ingredient, aucubin, protects against LPS-induced cardiac dysfunction in mice. *J. Pharmacol. Exp. Ther.* **2019**, *371*, 348–359. https://doi.org/10.1124/jpet.119.259069.
151. Zhao, C.C.; Xu, J.; Xie, Q.M.; Zhang, H.Y.; Fei, G.H.; Wu, H.M. Abscisic acid suppresses the activation of NLRP3 inflammasome and oxidative stress in murine allergic airway inflammation. *Phyther. Res.* **2021**, *35*, 3298–3309. https://doi.org/10.1002/ptr.7051.
152. Huang, Y.; Wan, T.; Pang, N.; Zhou, Y.; Jiang, X.; Li, B.; Gu, Y.; Huang, Y.; Ye, X.; Lian, H.; et al. Cannabidiol protects livers against nonalcoholic steatohepatitis induced by high-fat high cholesterol diet via regulating NF-κB and NLRP3 inflammasome pathway. *J. Cell. Physiol.* **2019**, *234*, 21224–21234. https://doi.org/10.1002/jcp.28728.
153. Nagoor Meeran, M.F.; Azimullah, S.; Laham, F.; Tariq, S.; Goyal, S.N.; Adeghate, E.; Ojha, S. α-Bisabolol protects against β-adrenergic agonist-induced myocardial infarction in rats by attenuating inflammation, lysosomal dysfunction, NLRP3 inflammasome activation and modulating autophagic flux. *Food Funct.* **2020**, *11*, 965–976.
154. Yang, X.; Wu, F.; Li, L.; Lynch, E.C.; Xie, L.; Zhao, Y.; Fang, K.; Li, J.; Luo, J.; Xu, L.; et al. Celastrol alleviates metabolic disturbance in high-fat diet-induced obese mice through increasing energy expenditure by ameliorating metabolic inflammation. *Phyther. Res.* **2021**, *35*, 297–310. https://doi.org/10.1002/ptr.6800.
155. Li, J.; Li, X.; Wang, X.; Zhong, X.; Ji, L.; Guo, Z.; Liu, Y.; Shang, X. Sesquiterpenoids and their anti-inflammatory activity: Evaluation of ainsliaea yunnanensis. *Molecules* **2019**, *24*, 1701. https://doi.org/10.3390/molecules24091701.

156. Gianfrancesco, M.A.; Dehairs, J.; L'homme, L.; Herinckx, G.; Esser, N.; Jansen, O.; Habraken, Y.; Lassence, C.; Swinnen, J.V.; Rider, M.H.; et al. Saturated fatty acids induce NLRP3 activation in human macrophages through K + efflux resulting from phospholipid saturation and Na, K-ATPase disruption. *Biochim. Biophys. Acta-Mol. Cell Biol. Lipids* **2019**, *1864*, 1017–1030. https://doi.org/10.1016/j.bbalip.2019.04.001.
157. Witcher, K.J.; Novick, R.P.; Schlievert, P.M. Modulation of immune cell proliferation by glycerol monolaurate. *Clin. Diagn. Lab. Immunol.* **1996**, *3*, 10–13. https://doi.org/10.1128/cdli.3.1.10-13.1996.
158. Shen, L.; Yang, Y.; Ou, T.; Key, C.C.C.; Tong, S.H.; Sequeira, R.C.; Nelson, J.M.; Nie, Y.; Wang, Z.; Boudyguina, E.; et al. Dietary PUFAs attenuate NLRP3 inflammasome activation via enhancing macrophage autophagy. *J. Lipid Res.* **2017**, *58*, 1808–1821. https://doi.org/10.1194/jlr.M075879.
159. Gao, H.; Lv, Y.; Liu, Y.; Li, J.; Wang, X.; Zhou, Z.; Tipoe, G.L.; Ouyang, S.; Guo, Y.; Zhang, J.; et al. Wolfberry-Derived Zeaxanthin Dipalmitate Attenuates Ethanol-Induced Hepatic Damage. *Mol. Nutr. Food Res.* **2019**, *63*, e1801339. https://doi.org/10.1002/mnfr.201801339.
160. Wu, L.; Lyu, Y.; Srinivasagan, R.; Wu, J.; Ojo, B.; Tang, M.; El-Rassi, G.D.; Metzinger, K.; Smith, B.J.; Lucas, E.A.; et al. Astaxanthin-Shifted gut microbiota is associated with inflammation and metabolic homeostasis in mice. *J. Nutr.* **2020**, *150*, 2687–2698. https://doi.org/10.1093/jn/nxaa222.
161. Latz, E.; Xiao, T.S.; Stutz, A. Activation and regulation of the inflammasomes. *Nat. Rev. Immunol.* **2013**, *13*, 397–411.
162. Dolinay, T.; Kim, Y.S.; Howrylak, J.; Hunninghake, G.M.; An, C.H.; Fredenburgh, L.; Massaro, A.F.; Rogers, A.; Gazourian, L.; Nakahira, K.; et al. Inflammasome-regulated cytokines are critical mediators of acute lung injury. *Am. J. Respir. Crit. Care Med.* **2012**, *185*, 1225–1234. https://doi.org/10.1164/rccm.201201-0003OC.
163. Bauer, K. Carnosine and homocarnosine, the forgotten, enigmatic peptides of the brain. *Neurochem. Res.* **2005**, *30*, 1339–1345. https://doi.org/10.1007/s11064-005-8806-z.
164. Huang, Y.C.; Lin, C.Y.; Huang, S.F.; Lin, H.C.; Chang, W.L.; Chang, T.C. Effect and mechanism of ginsenosides CK and Rg1 on stimulation of glucose uptake in 3T3-L1 adipocytes. *J. Agric. Food Chem.* **2010**, *58*, 6039–6047. https://doi.org/10.1021/jf9034755.
165. Wang, Z.; Hu, J.N.; Yan, M.H.; Xing, J.J.; Liu, W.C.; Li, W. Caspase-Mediated Anti-Apoptotic Effect of Ginsenoside Rg5, a Main Rare Ginsenoside, on Acetaminophen-Induced Hepatotoxicity in Mice. *J. Agric. Food Chem.* **2017**, *65*, 9226–9236. https://doi.org/10.1021/acs.jafc.7b03361.
166. Wu, Y.L.; Wan, Y.; Jin, X.J.; Ouyang, B.Q.; Bai, T.; Zhao, Y.Q.; Nan, J.X. 25-OCH3-PPD induces the apoptosis of activated t-HSC/Cl-6 cells via c-FLIP-mediated NF-κB activation. *Chem. Biol. Interact.* **2011**, *194*, 106–112. https://doi.org/10.1016/j.cbi.2011.08.010.
167. Han, G.C.; Ko, S.K.; Sung, J.H.; Chung, S.H. Compound K enhances insulin secretion with beneficial metabolic effects in db/db mice. *J. Agric. Food Chem.* **2007**, *55*, 10641–10648. https://doi.org/10.1021/jf0722598.
168. Song, W.; Wei, L.; Du, Y.; Wang, Y.; Jiang, S. Protective effect of ginsenoside metabolite compound K against diabetic nephropathy by inhibiting NLRP3 inflammasome activation and NF-κB/p38 signaling pathway in high-fat diet/streptozotocin-induced diabetic mice. *Int. Immunopharmacol.* **2018**, *63*, 227–238. https://doi.org/10.1016/j.intimp.2018.07.027.
169. Mao, Y.M.; Zeng, M.D.; Chen, Y.; Chen, C.W.; Fu, Q.C.; Cai, X.; Wu, S.M.; Chen, Y.G.; Sun, Y.; Li, J.; et al. Magnesium isoglycyrrhizinate in the treatment of chronic liver diseases: A randomized, double-blind, multi-doses, active drug controlled, multi-center study. *Chin. J. Hepatol.* **2009**, *17*, 847–851.
170. Zhao, X.J.; Yang, Y.Z.; Zheng, Y.J.; Wang, S.C.; Gu, H.M.; Pan, Y.; Wang, S.J.; Xu, H.J.; Kong, L.D. Magnesium isoglycyrrhizinate blocks fructose-induced hepatic NF-κB/NLRP3 inflammasome activation and lipid metabolism disorder. *Eur. J. Pharmacol.* **2017**, *809*, 141–150. https://doi.org/10.1016/j.ejphar.2017.05.032.
171. Vieira, A.T.; Pinho, V.; Lepsch, L.B.; Scavone, C.; Ribeiro, I.M.; Tomassini, T.; Ribeiro-Dos-Santos, R.; Soares, M.B.P.; Teixeira, M.M.; Souza, D.G. Mechanisms of the anti-inflammatory effects of the natural secosteroids physalins in a model of intestinal ischaemia and reperfusion injury. *Br. J. Pharmacol.* **2005**, *146*, 244–251. https://doi.org/10.1038/sj.bjp.0706321.
172. Xu, J.; Zhang, Q.; Li, Z.; Gao, Y.; Pang, Z.; Wu, Y.; Li, G.; Lu, D.; Zhang, L.; Li, D. Astragalus Polysaccharides Attenuate Ovalbumin-Induced Allergic Rhinitis in Rats by Inhibiting NLRP3 Inflammasome Activation and NOD2-Mediated NF-?B Activation. *J. Med. Food* **2021**, *24*, 1–9. https://doi.org/10.1089/jmf.2020.4750.
173. Zong, S.; Ye, Z.; Zhang, X.; Chen, H.; Ye, M. Protective effect of: Lachnum polysaccharide on dextran sulfate sodium-induced colitis in mice. *Food Funct.* **2020**, *11*, 846–859.
174. Zhang, R.; Han, S.; Zhang, Z.; Zhang, W.; Yang, J.; Wan, Z.; Qin, L. Cereal Fiber Ameliorates High-Fat/Cholesterol-Diet-Induced Atherosclerosis by Modulating the NLRP3 Inflammasome Pathway in ApoE-/- Mice. *J. Agric. Food Chem.* **2018**, *66*, 4827–4834. https://doi.org/10.1021/acs.jafc.8b00380.
175. Wallert, M.; Börmel, L.; Lorkowski, S. Inflammatory Diseases and Vitamin E—What Do We Know and Where Do We Go? *Mol. Nutr. Food Res.* **2021**, *65*, 2000097.
176. Tapia, G.; Silva, D.; Romero, N.; Pettinelli, P.; Dossi, C.G.; de Miguel, M.; González-Mañán, D. Role of dietary α- and γ-tocopherol from Rosa mosqueta oil in the prevention of alterations induced by high-fat diet in a murine model. *Nutrition* **2018**, *53*, 1–8. https://doi.org/10.1016/j.nut.2018.01.012.
177. Lee, H.; Lim, Y. Gamma-tocopherol ameliorates hyperglycemia-induced hepatic inflammation associated with NLRP3 inflammasome in alloxan-induced diabetic mice. *Nutr. Res. Pract.* **2019**, *13*, 377–383. https://doi.org/10.4162/nrp.2019.13.5.377.

178. Mullin, G.E.; Limektkai, B.; Wang, L.; Hanaway, P.; Marks, L.; Giovannucci, E. Dietary Supplements for COVID-19. In *Advances in Experimental Medicine and Biology*; Springer, Berlin: 2021; Volume 1318, pp. 499–515.
179. Sheng, K.; He, S.; Sun, M.; Zhang, G.; Kong, X.; Wang, J.; Wang, Y. Synbiotic supplementation containing: Bifidobacterium infantis and xylooligosaccharides alleviates dextran sulfate sodium-induced ulcerative colitis. *Food Funct.* **2020**, *11*, 3964–3974. https://doi.org/10.1039/d0fo00518e.
180. Suzuki, H.; Yamazaki, T.; Ohshio, K.; Sugamata, M.; Yoshikawa, M.; Kanauchi, O.; Morita, Y. A Specific Strain of Lactic Acid Bacteria, Lactobacillus paracasei , Inhibits Inflammasome Activation In Vitro and Prevents Inflammation-Related Disorders. *J. Immunol.* **2020**, *205*, 811–821. https://doi.org/10.4049/jimmunol.1900657.
181. Pan, X.; Fang, X.; Wang, F.; Li, H.; Niu, W.; Liang, W.; Wu, C.; Li, J.; Tu, X.; Pan, L.L.; et al. Butyrate ameliorates caerulein-induced acute pancreatitis and associated intestinal injury by tissue-specific mechanisms. *Br. J. Pharmacol.* **2019**, *176*, 4446–4461. https://doi.org/10.1111/bph.14806.
182. Chung, I.C.; Ouyang, C.N.; Yuan, S.N.; Lin, H.C.; Huang, K.Y.; Wu, P.S.; Liu, C.Y.; Tsai, K.J.; Loi, L.K.; Chen, Y.J.; et al. Pretreatment with a heat-killed probiotic modulates the NLRP3 inflammasome and attenuates colitis-associated colorectal cancer in mice. *Nutrients* **2019**, *11*, 516. https://doi.org/10.3390/nu11030516.
183. Loss, H.; Aschenbach, J.R.; Ebner, F.; Tedin, K.; Lodemann, U. Effects of a pathogenic ETEC strain and a probiotic Enterococcus faecium strain on the inflammasome response in porcine dendritic cells. *Vet. Immunol. Immunopathol.* **2018**, *203*, 78–87. https://doi.org/10.1016/j.vetimm.2018.08.004.
184. Zou, Y.J.; Xu, J.J.; Wang, X.; Zhu, Y.H.; Wu, Q.; Wang, J.F. Lactobacillus johnsonii l531 ameliorates Escherichia coli-induced cell damage via inhibiting NLRP3 inflammasome activity and promoting ATG5/ATG16L1-mediated autophagy in porcine mammary epithelial cells. *Vet. Sci.* **2020**, *7*, 112. https://doi.org/10.3390/VETSCI7030112.
185. Chen, S.; Li, Y.; Chu, B.; Yuan, L.; Liu, N.; Zhu, Y.; Wang, J. Lactobacillus johnsonii l531 alleviates the damage caused by salmonella typhimurium via inhibiting tlr4, nf-κb, and nlrp3 inflammasome signaling pathways. *Microorganisms* **2021**, *9*, 1983. https://doi.org/10.3390/microorganisms9091983.
186. Li, Y.; Zhu, Y.; Chu, B.; Liu, N.; Chen, S.; Wang, J. Lactobacillus rhamnosus GR-1 Prevents Escherichia coli-Induced Apoptosis Through PINK1/Parkin-Mediated Mitophagy in Bovine Mastitis. *Front. Immunol.* **2021**, *12*, 3743. https://doi.org/10.3389/fimmu.2021.715098.
187. Biesalski, H.K.; Dragsted, L.O.; Elmadfa, I.; Grossklaus, R.; Müller, M.; Schrenk, D.; Walter, P.; Weber, P. Bioactive compounds: Definition and assessment of activity. *Nutrition* **2009**, *25*, 1202–1205. https://doi.org/10.1016/j.nut.2009.04.023.
188. Zhang, X.; Chen, F.; Wang, M. Bioactive Substances of Animal Origin. In *Handbook of Food Chemistry*; Springer, Berlin: 2015; pp. 1009–1033, ISBN 9783642366055.
189. Zhao, Y.; Wu, Y.Z.; Wang, M. Bioactive Substances of Plant Origin. In *Handbook of Food Chemistry*; Springer, Berlin: 2015; pp. 967–1008, ISBN 9783642366055.
190. Abbas, M.; Saeed, F.; Anjum, F.M.; Afzaal, M.; Tufail, T.; Bashir, M.S.; Ishtiaq, A.; Hussain, S.; Suleria, H.A.R. Natural polyphenols: An overview. *Int. J. Food Prop.* **2017**, *20*, 1689–1699.
191. Ditu, L.M.; Grigore, M.E.; Camen-Comanescu, P.; Holban, A.M. Introduction in Nutraceutical and Medicinal Foods. In *Therapeutic, Probiotic, and Unconventional Foods*; Elsevier, Amsterdam: 2018; pp. 1–12, ISBN 9780128146262.
192. Hung, W.L.; Ho, C.T.; Pan, M.H. Targeting the NLRP3 Inflammasome in Neuroinflammation: Health Promoting Effects of Dietary Phytochemicals in Neurological Disorders. *Mol. Nutr. Food Res.* **2020**, *64*, 1900550.
193. Bagherniya, M.; Khedmatgozar, H.; Fakheran, O.; Xu, S.; Johnston, T.P.; Sahebkar, A. Medicinal plants and bioactive natural products as inhibitors of NLRP3 inflammasome. *Phyther. Res.* **2021**, *35*, 4804–4833.
194. Oliviero, F.; Scanu, A.; Zamudio-Cuevas, Y.; Punzi, L.; Spinella, P. Anti-inflammatory effects of polyphenols in arthritis. *J. Sci. Food Agric.* **2018**, *98*, 1653–1659.
195. Qiu, W.Q.; Pan, R.; Tang, Y.; Zhou, X.G.; Wu, J.M.; Yu, L.; Law, B.Y.K.; Ai, W.; Yu, C.L.; Qin, D.L.; et al. Lychee seed polyphenol inhibits Aβ-induced activation of NLRP3 inflammasome via the LRP1/AMPK mediated autophagy induction. *Biomed. Pharmacother.* **2020**, *130*, 110575. https://doi.org/10.1016/j.biopha.2020.110575.
196. Rein, M.J.; Renouf, M.; Cruz-Hernandez, C.; Actis-Goretta, L.; Thakkar, S.K.; da Silva Pinto, M. Bioavailability of bioactive food compounds: A challenging journey to bioefficacy. *Br. J. Clin. Pharmacol.* **2013**, *75*, 588–602. https://doi.org/10.1111/j.1365-2125.2012.04425.x.
197. Roth-Walter, F.; Moskovskich, A.; Gomez-Casado, C.; Diaz-Perales, A.; Oida, K.; Singer, J.; Kinaciyan, T.; Fuchs, H.C.; Jensen-Jarolim, E. Immune suppressive effect of cinnamaldehyde due to inhibition of proliferation and induction of apoptosis in immune cells: Implications in cancer. *PLoS ONE* **2014**, *9*, e108402. https://doi.org/10.1371/journal.pone.0108402.
198. Haminiuk, C.W.I.; Maciel, G.M.; Plata-Oviedo, M.S.V.; Peralta, R.M. Phenolic compounds in fruits—An overview. *Int. J. Food Sci. Technol.* **2012**, *47*, 2023–2044.
199. Hollman, P.C.H.; Katan, M.B. Dietary flavonoids: Intake, health effects and bioavailability. *Food Chem. Toxicol.* **1999**, *37*, 937–942.
200. Ottaviani, J.I.; Momma, T.Y.; Heiss, C.; Kwik-Uribe, C.; Schroeter, H.; Keen, C.L. The stereochemical configuration of flavanols influences the level and metabolism of flavanols in humans and their biological activity in vivo. *Free Radic. Biol. Med.* **2011**, *50*, 237–244. https://doi.org/10.1016/j.freeradbiomed.2010.11.005.

201. Scholz, S.; Williamson, G. Interactions affecting the bioavailability of dietary polyphenols in vivo. *Int. J. Vitam. Nutr. Res.* **2007**, *77*, 224–235.
202. Di, L.; Kerns, E.H. Drug-Like Properties: Concepts, Structure Design and Methods from ADME to Toxicity Optimization; Academic Press, Cambridge: 2016; ISBN 9780128010761.
203. Giada, M.D.L.R. Food Phenolic Compounds: Main Classes, Sources and Their Antioxidant Power. In *Oxidative Stress and Chronic Degenerative Diseases—A Role for Antioxidants*; Elsevier, Amsterdam: 2013.
204. Ruiz-Rodriguez, A.; Marín, F.R.; Ocaña, A.; Soler-Rivas, C. Effect of domestic processing on bioactive compounds. *Phytochem. Rev.* **2008**, *7*, 345–384.
205. Rothwell, J.A.; Medina-Remón, A.; Pérez-Jiménez, J.; Neveu, V.; Knaze, V.; Slimani, N.; Scalbert, A. Effects of food processing on polyphenol contents: A systematic analysis using Phenol-Explorer data. *Mol. Nutr. Food Res.* **2015**, *59*, 160–170. https://doi.org/10.1002/mnfr.201400494.
206. Al-juhaimi, F.; Ghafoor, K.; Özcan, M.M.; Jahurul, M.H.A.; Babiker, E.E.; Jinap, S.; Sahena, F.; Sharifudin, M.S.; Zaidul, I.S.M. Effect of various food processing and handling methods on preservation of natural antioxidants in fruits and vegetables. *J. Food Sci. Technol.* **2018**, *55*, 3872–3880.
207. Carlsen, M.H.; Halvorsen, B.L.; Holte, K.; Bøhn, S.K.; Dragland, S.; Sampson, L.; Willey, C.; Senoo, H.; Umezono, Y.; Sanada, C.; et al. The total antioxidant content of more than 3100 foods, beverages, spices, herbs and supplements used worldwide. *Nutr. J.* **2010**, *9*, 3. https://doi.org/10.1186/1475-2891-9-3.
208. Gul, K.; Singh, A.K.; Jabeen, R. Nutraceuticals and Functional Foods: The Foods for the Future World. *Crit. Rev. Food Sci. Nutr.* **2016**, *56*, 2617–2627.
209. Martirosyan, D.; von Brugger, J.; Bialow, S. Functional food science: Differences and similarities with food science. *Funct. Foods Health Dis.* **2021**, *11*, 408–430.
210. Vettorazzi, A.; de Cerain, A.L.; Sanz-Serrano, J.; Gil, A.G.; Azqueta, A. European regulatory framework and safety assessment of food-related bioactive compounds. *Nutrients* **2020**, *12*, 613.
211. Bellumori, M.; Cecchi, L.; Innocenti, M.; Clodoveo, M.L.; Corbo, F.; Mulinacci, N. The EFSA health claim on olive oil polyphenols: Acid hydrolysis validation and total hydroxytyrosol and tyrosol determination in Italian virgin olive oils. *Molecules* **2019**, *24*, 2179. https://doi.org/10.3390/molecules24112179.
212. Liu, P.W.; Li, C.I.; Huang, K.C.; Liu, C.S.; Chen, H.L.; Lee, C.C.; Chiou, Y.Y.; Chen, R.J. 3-MCPD and glycidol coexposure induces systemic toxicity and synergistic nephrotoxicity via NLRP3 inflammasome activation, necroptosis, and autophagic cell death. *J. Hazard. Mater.* **2021**, *405*, 124241. https://doi.org/10.1016/j.jhazmat.2020.124241.
213. Jia, X.; Qiu, T.; Yao, X.; Jiang, L.; Wang, N.; Wei, S.; Tao, Y.; Pei, P.; Wang, Z.; Zhang, J.; et al. Arsenic induces hepatic insulin resistance via mtROS-NLRP3 inflammasome pathway. *J. Hazard. Mater.* **2020**, *399*, 123034. https://doi.org/10.1016/j.jhazmat.2020.123034.
214. Li, X.; Li, H.; Cai, D.; Li, P.; Jin, J.; Jiang, X.; Li, Z.; Tian, L.; Chen, G.; Sun, J.; et al. Chronic oral exposure to cadmium causes liver inflammation by NLRP3 inflammasome activation in pubertal mice. *Food Chem. Toxicol.* **2021**, *148*, 111944. https://doi.org/10.1016/j.fct.2020.111944.
215. Liu, Y.; Zhang, X.; Yan, D.; Wang, Y.; Wang, N.; Liu, Y.; Tan, A.; Chen, X.; Yan, H. Chronic acrylamide exposure induced glia cell activation, NLRP3 inflammasome upregulation and cognitive impairment. *Toxicol. Appl. Pharmacol.* **2020**, *393*, 114949. https://doi.org/10.1016/j.taap.2020.114949.
216. Bo, N.; Yilin, H.; Chaoyue, Y.; Lu, L.; Yuan, Y. Acrylamide induces NLRP3 inflammasome activation via oxidative stress- and endoplasmic reticulum stress-mediated MAPK pathway in HepG2 cells. *Food Chem. Toxicol.* **2020**, *145*, 111679. https://doi.org/10.1016/j.fct.2020.111679.
217. Lee, P.Y.; Liu, C.C.; Wang, S.C.; Chen, K.Y.; Lin, T.C.; Liu, P.L.; Chiu, C.C.; Chen, I.C.; Lai, Y.H.; Cheng, W.C.; et al. Mycotoxin zearalenone attenuates innate immune responses and suppresses nlrp3 inflammasome activation in lps-activated macrophages. *Toxins* **2021**, *13*, 593. https://doi.org/10.3390/toxins13090593.
218. Wang, X.; Jiang, L.; Shi, L.; Yao, K.; Sun, X.; Yang, G.; Jiang, L.; Zhang, C.; Wang, N.; Zhang, H.; et al. Zearalenone induces NLRP3-dependent pyroptosis via activation of NF-κB modulated by autophagy in INS-1 cells. *Toxicology* **2019**, *428*, 152304. https://doi.org/10.1016/j.tox.2019.152304.
219. Chu, Q.; Wang, S.; Jiang, L.; Jiao, Y.; Sun, X.; Li, J.; Yang, L.; Hou, Y.; Wang, N.; Yao, X.; et al. Patulin induces pyroptosis through the autophagic-inflammasomal pathway in liver. *Food Chem. Toxicol.* **2021**, *147*, 111867. https://doi.org/10.1016/j.fct.2020.111867.
220. Molagoda, I.M.N.; Lee, S.; Jayasooriya, R.G.P.T.; Jin, C.Y.; Choi, Y.H.; Kim, G.Y. Deoxynivalenol enhances IL-1ß expression in bv 2. Microglial cells through activation of the NF-KB pathway and the ASC/NLRP 3. inflammasome. *EXCLI J.* **2019**, *18*, 356–369. https://doi.org/10.17179/excli2018-1974.

8.4. Review 3: NMR based approaches in the study of foods

In the last decades the NMR spectroscopy has been largely used in the study of foods. Studying the different approaches used in the investigation of foods by the NMR methodologies, three main starting points have been identified. One starting point focuses on the food that needs to be analyzed. Farmers, companies, and consumers are interested in getting to know the product in depth in order to improve cultivation conditions, processes and for safety reasons. In this case, the combination of different NMR methodologies can be useful to describe different aspects of the product. Another approach starts from common challenges regarding foods such as frauds, geographical and botanical origins, etc. In this case, consumers and specific research programs constantly stimulate the world of research to propose new solutions. Finally, it is possible to start from a single specific NMR methodology developing a broad range of its applications to tackle common food-related challenges and different aspects.

molecules

MDPI

Review

NMR-Based Approaches in the Study of Foods

Anatoly P. Sobolev [1], Cinzia Ingallina [2], Mattia Spano [2], Giacomo Di Matteo [2] and Luisa Mannina [2,*]

[1] Magnetic Resonance Laboratory "Segre-Capitani", Institute for Biological Systems, CNR, Via Salaria, Km 29.300, 00015 Monterotondo, Italy
[2] Laboratory of Food Chemistry, Department of Chemistry and Technology of Drugs, Sapienza University of Rome, P.le Aldo Moro 5, 00185 Rome, Italy
* Correspondence: luisa.mannina@uniroma1.it; Tel.: +39-06-49913735

Abstract: In this review, the three different NMR-based approaches usually used to study foodstuffs are described, reporting specific examples. The first approach starts with the food of interest that can be investigated using different complementary NMR methodologies to obtain a comprehensive picture of food composition and structure; another approach starts with the specific problem related to a given food (frauds, safety, traceability, geographical and botanical origin, farming methods, food processing, maturation and ageing, etc.) that can be addressed by choosing the most suitable NMR methodology; finally, it is possible to start from a single NMR methodology, developing a broad range of applications to tackle common food-related challenges and different aspects related to foods.

Keywords: NMR methodology; food structure; food composition

check for updates

Citation: Sobolev, A.P.; Ingallina, C.; Spano, M.; Di Matteo, G.; Mannina, L. NMR-Based Approaches in the Study of Foods. *Molecules* **2022**, *27*, 7906. https://doi.org/10.3390/molecules27227906

Academic Editor: Francesco Cacciola

Received: 7 October 2022
Accepted: 14 November 2022
Published: 15 November 2022

Publisher's Note: MDPI stays neutral with regard to jurisdictional claims in published maps and institutional affiliations.

Copyright: © 2022 by the authors. Licensee MDPI, Basel, Switzerland. This article is an open access article distributed under the terms and conditions of the Creative Commons Attribution (CC BY) license (https://creativecommons.org/licenses/by/4.0/).

1. Introduction

The study of food structure and chemical composition requires adequate analytical methods that have to be comprehensive and as unintrusive as possible. These criteria are largely satisfied by the combination of different NMR methodologies that represents a powerful tool for the study of food matrixes, being recognized as one of the best performing approaches in food analysis [1].

In this review, we want to show how the topic of food can be addressed using NMR methodologies. In the literature, a number of reviews regarding NMR and foods have been already reported. Some reviews relate to specific foods such as wine [2] or honey [3]; others are focused on the application of specific NMR methodologies for food investigation such as HR-MAS [4], NMR relaxometry/MRI [5], and high-resolution NMR in liquids [6,7]. Additional methodologies deal with common food-related challenges such as food frauds [8], authentication, and quality [9]. Taking into account the complexity and richness of this scenario, we tried to aggregate the different approaches into three principal starting points usually used to investigate foods. These three starting points reflect the often converging but sometimes different interests of food producers, retailers, consumers, and researchers.

One starting point focuses on the food that needs to be analyzed. Farmers, companies, and consumers are interested in getting to know the product in depth in order to improve cultivation conditions and processes and for safety reasons. In this case, the combination of different NMR methodologies can be useful to describe different aspects of the product.

Another approach starts from common challenges regarding foods such as frauds, geographical and botanical origins, etc. In this case, consumers and specific research programs constantly stimulate the world of research to propose new solutions.

Finally, it is possible to start from a single specific NMR methodology, developing a broad range of applications to tackle common food-related challenges and different aspects.

These three starting points make use of the information that can be obtained from the different NMR methodologies, namely high-resolution NMR of liquid samples, high-resolution magic-angle spinning (HR-MAS) of semisolid samples, cross-polarization magic-

angle spinning (CP-MAS) of solids, low-field relaxometry, and magnetic resonance imaging (MRI). These methodologies can be explained in more detail as follows:

- High-resolution NMR of liquid samples [6] is used to define the chemical structure of isolated compounds or compounds in complex mixtures. It can be applied also to solid and semisolid food samples after extraction of soluble components;
- High-resolution magic-angle spinning (HR-MAS) NMR methodology has been developed to analyze mobile molecular components in all types of matrixes and it is particularly useful in analyzing intact semisolid samples without any extraction. The rotation of the sample around an axis forming an angle of 54.7° (magic angle) with respect to the applied magnetic field B_0 drastically reduces the broadening of signals due to magnetic susceptibility variations and makes it possible to obtain high-resolution spectra of all mobile molecular components;
- Cross-polarization magic-angle spinning (CP-MAS) is the most frequently used methodology for the NMR analysis of solids. It combines three techniques: fast magic-angle rotation of the sample, high-power decoupling of protons, and cross-polarization (transferring part of the hydrogen magnetization to a heteronucleus to improve its sensitivity) [10]. Generally, in food samples, CP-MAS is applied to study the insoluble fraction (fibers, proteins, etc.), observing ^{13}C as the heteronucleus. Moreover, ^{31}P and ^{2}H solid-state NMR spectroscopic techniques were largely employed to examine the interaction among lipids and many bioactive compounds from foods [11–14];
- Low-field ^{1}H NMR relaxometry [15] is a suitable tool to study the most abundant components of intact foodstuffs by measurement of relaxation parameters (longitudinal relaxation time, T_1, water self-diffusion (D_w), T_2) and amplitudes of the NMR signal. Information on food microstructure such as water compartments and diffusion can be obtained by detecting proton signals dominated by H_2O contained in foodstuffs. Sample pretreatment is not required, and the method can be easily used for quality control applications;
- MRI allows one to obtain detailed morphological images of internal sections of intact tissues [16]. Furthermore, using specific data acquisition protocols, it is able to provide multiple pieces of complementary information also relating to the composition and dynamics of the molecules that form the investigated tissue.

2. First Starting Point: Food

The three different starting points usually used to study foodstuffs by means of NMR methodologies are discussed here, reporting specific examples.

This approach starts with the food that needs to be investigated. It is possible to describe specific and complementary aspects of the product using different NMR methodologies. The chemical-nutritional composition of the investigated food is obtained by means of NMR in the liquid state, HRMAS, and CPMAS methodologies. Using different 1D and 2D sequences, it is possible to obtain the chemical profile of the food or the food extracts. On the other hand, morphological and physico-chemical aspects of the food can be investigated by means of low-field ^{1}H NMR relaxometry and MRI.

In the case of vegetables/fruits, the chemical profile and the morphological aspects have often been investigated to obtain information regarding fruit quality and nutritional properties and to monitor fruit changes over the time.

The chemical-nutritional profile of vegetables and fruits is strongly related to their harvesting and post-harvesting time-depending changes. Therefore, the monitoring of metabolite profiling over time allows information on the chemical composition of the samples in specific periods to be obtained. This type of investigation also enables one to detect compounds present only in specific stages of development. This information can be useful in choosing the best harvesting period for direct sales or conservation of the product, but also for obtaining specific nutrients and nutraceuticals.

Ripeness, post-harvesting changes, and shelf-life evaluation can be also investigated by means of MRI and low-field relaxometry that provide complementary information related to the composition and dynamics of the molecules that form the food tissue.

In the case of other products, other aspects can be of interest. For instance, in the case of processed food, the different process phases as well as product storage can be monitored using the most appropriate NMR methodologies.

Here, the case study of kiwifruit is reported. Kiwifruit is a fruit belonging to the family of Actinidiaceae (*Actinidia chinensis* and *Actinidia deliciosa*) native to China. It grows spontaneously in humid environments and is characterized by peculiar flavor, fragrance, and healthful properties. Today, New Zealand and Italy are respectively the first and second largest producers of kiwifruit in the world.

2.1. Kiwifruit: Chemical Profile and Morphological Aspects

The chemical profile of kiwifruit's aqueous and organic extracts has been determined using 1D and 2D high-resolution NMR experiments [17]. Sugars (glucose, fructose, sucrose, myo-inositol, galactose, xylose, raffinose, and mannose), organic acids (malic, citric, quinic, ascorbic, lactic, and shikimic acids), amino acids (alanine, glutamine, threonine, arginine, glutamate, aspartate, valine, leucine, isoleucine, lysine, tryptophane, γ-aminobutyrate, histidine, and phenylalanine), and other compounds (choline, adenosine triphosphate, O^3-β-d-glucopyranosyl-*trans*/*cis*-caffeic acid, uridine, quercetin 3-rhamnoside, and epicatechin) have been identified and quantified in the ^{1}H NMR spectra of kiwifruit aqueous extracts. In the ^{1}H spectra of kiwifruit organic extract, fatty acids, phospholipids, sterols, and galactolipids have been identified [18].

Information on water content and water distribution in the sample has been obtained by low-field NMR relaxometry and NMR imaging. Three components of T_2 relaxation time have been detected and associated with protons in the cell walls, in cytoplasm and in extracellular space, and in the vacuole [19]. The internal morphologies of kiwifruit have been investigated by MRI, which provided informative images regarding the spin density distribution of water molecules and the relationship between water and cellular tissues [20].

2.2. Kiwifruit Ripeness

2.2.1. Chemical Profile over the Time (Ripeness and Postharvest Period)

The chemical profile has been monitored over the season, typically from June to December, showing characteristic temporal trends of several compounds. For instance, in the case of organic acids, the content of quinic and ascorbic acids decreases over the season, whereas citric and malic acids have shown the highest level in August. It has been also possible to detect the shikimic acid present only in June and July [21].

Regarding sugars (sucrose, fructose, and glucose), a general increment in their content has been observed, reaching the highest value in December. Furthermore, amino acids have shown specific temporal trends: as an example, the level of valine, leucine, and isoleucine—important essential ramified amino acids—and threonine, glutamine, and asparagine have shown the highest value in July and in August.

It is well-known that in the case of kiwifruits, before commercialization, a postharvest period is required to obtain the best edible conditions. Different postharvest treatments can be used (cold storage for a long time, exposition to C_2H_4, etc.). The chemical profiles of kiwifruits stored in a controlled chamber (at 4 °C, with 85% relative humidity) and removed after 0 (T0), 30 (T1), 60 (T2), and 90 (T3) days of cold storage have been investigated [18]. About 42 metabolites have been identified and quantified in the ^{1}H spectra of aqueous extracts (free amino acids, organic acids, sugars, and others) and organic extracts (fatty acids, phospholipids, sterols, and galactolipids). NMR data submitted to chemometric analysis, namely to PCA (Figure 1), provide a general view of metabolite changes associated with postharvest cold storage of fruits at four postharvest stages: from fruit harvest to pre-commercialization. Sugars, ascorbic acid, threonine, isoleucine, valine, and di-unsaturated fatty acids present at the highest level during the final stages of postharvest, whereas

alanine and digalactosyl diacylglycerol showed the highest level just after the harvest. Sucrose showed a constant increment during the postharvest period, whereas glucose and fructose increased only during the first stage, remaining relatively constant in the later stages. The level of lactic, quinic, and citric acids remained unchanged in the T0–T3 range, whereas a slight increment in ascorbic acid concentration was observed at the T3 stage. Regarding the organic extracts, a constant increment and a decrement in di-unsaturated fatty acids and digalactosyl diacylglycerol were observed, respectively, whereas the other metabolites remained unchanged.

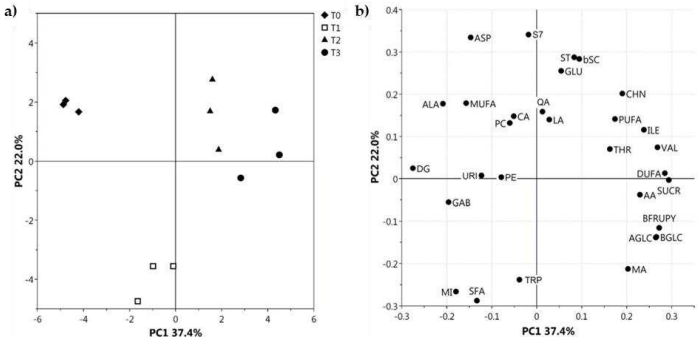


Figure 1. (**a**) PCA score (**b**) and loading plots of metabolite profiles (30 metabolites/metabolite classes) obtained from NMR data related to hydroalcoholic and organic extracts of kiwifruit at different postharvest stages (T0–T3). Results associated with malic acid (MA), citric acid (CA), ascorbic acid (AA), lactic acid (LA), quinic acid (QA), α- and β-glucose (AGLC and BGLC), sucrose (SUCR), β-fructopyranose (BFRUPY), Ala, Thr, Glu, Asp, Val, Ile, Trp and γ-aminobutyric acid (GAB), choline (CHN), uridine (URI), myo-inositol (MI), phosphatidylcholine (PC), phosphatidylethanolamine (PE), digalactosyl diacylglycerol (DG), stigmast-7-en-3β-ol (S7), stigmasterol (ST), poly-unsaturated fatty acids (PUFA), di-unsaturated fatty acids (DUFA), mono-unsaturated fatty acids (MUFA), saturated fatty acids (SFA), and β-sitosterol plus campesterol (bSC) are shown (Reprinted from [18] with permission from Frontiers).

2.2.2. Morphological Changes over the Time

Information regarding the degree of ripeness has been also obtained by means of low-field relaxometry due to the correlation between the changes in T_2 relaxation time and the increment in kiwifruit "softness" during storage. The results indicate that quantitative MRI is able to measure temporal trends and tissue differences in MR properties of kiwifruit [20]. Measurements were made at a magnetic field strength of 2.0 T (85 MHz). Distinct differences between the relaxation properties of the flesh, locule, and core tissues at particular sampling dates as well as trends during the season (for example, the tendency towards longer relaxation times later in the season in locular tissue) were reported (Figure 2).

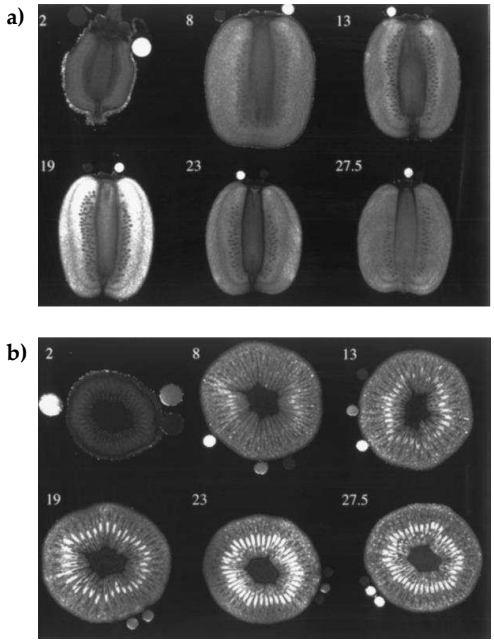


Figure 2. The spin–lattice relaxation (T1) images (**a**) through a longitudinal equatorial plane and spin–spin relaxation (T2) images (**b**) through a transverse equatorial plane of kiwifruit (*A. deliciosa*) during development and ripening. Numbers correspond to weeks from fruitset, with commercial harvest occurring at week 23. Images at 23 and 27.5 weeks are of the same fruit at harvest and after 4.5 weeks ripening. Image resolution varies from 0.12 in the youngest fruit to 0.33 mm in the older samples (256 × 256 pixel data arrays). The circular internal standard tubes (4 mm inner diameter) serve as a scale marker for each panel. Image intensity is based on a continuous grey-scale setting ranging from 0 ms = black to 2500 ms = white (Adapted from [20] with permission from Elsevier, Copyright 1999).

In order to study kiwifruit ripeness, T_2 relaxation times have also been measured directly on the fruit, without cutting it, on pre-harvest kiwifruits by means of a portable single-sided NMR instrument (Figure 3a,b). The experimental condition used to carry out this experiment has allowed only the detection of the two longest T_2 relaxation times, not detecting the shortest one due to the water signal strictly associated with cell wall compartments. During the ripening phase, an increase in the two T_2 relaxation times (attributed to water in the cytoplasm and extracellular space, reported as T_{2a}, and to water in the vacuole, reported as T_{2b}) has been observed. This trend towards longer T_2 relaxation times over the season reflects a change in the fruit structure (Figure 3 c,d) [17,21].

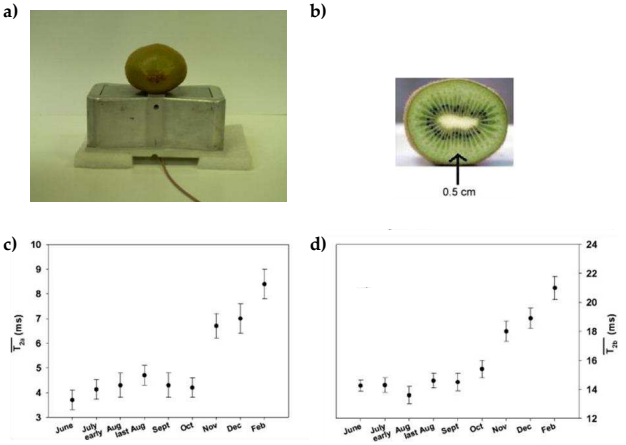


Figure 3. (**a**) Measurement of intact kiwifruit with a portable unilateral NMR instrument. (**b**) Section of kiwifruit showing the depth of measurement with a portable NMR instrument. Average T_{2a} (**c**) and T_{2b} (**d**) were measured on nine kiwifruits vs. the harvesting month; the error bars represent the maximum error calculated with the error propagation theory (Adapted from [17] with permission from Elsevier, Copyright 2010).

In kiwifruit, effects of water loss on the water status were investigated using MRI [22], which provides informative images regarding the spin density distribution of water molecules and the relationship between water and cellular tissues. The organization and mobility of water change, thus, induces textural changes and kiwifruit softening. T_2-weighted images are extremely effective for describing these phenomena.

2.3. Comparison among Cultivars

Comparison among the metabolite profiles of different kiwifruit cultivars can be performed. The ^{1}H spectra of kiwifruit extracts from different cultivars have shown the same compounds at different concentrations in the same harvesting period. This confirms that every cultivar has a specific time of maturation. For instance, comparison among the ^{1}H metabolite profiles of Hayward, CI. GI, and Zespri cultivars at different time points indicates that the maturation of the Zespri cultivar precedes the other two varieties [21].

2.3.1. MRI for Morphological and Physico-Chemical Aspects

MRI high-resolution images are a reliable tool for appreciating morphological differences in fruits. New kiwifruit selections have been investigated by means of MRI: the internal morphologies of these selections have been compared to fruits of the commercial Hayward cultivar [23]. The MRI images show clear morphological differences concerning, for example, the distribution of seeds, the compartmentalization of tissues, and the position of columella. This information can be also useful in suggesting the most promising selections for commercial purposes.

2.3.2. Comparison among Healthy and Non-Healthy Kiwifruit

The metabolite profile has been also useful to discriminate between kiwifruit collected from healthy plants and plants affected by elephantiasis. Elephantiasis causes the progressive degradation of woody tissues and an anomalous diametrical growth of the trunk, making kiwifruits non-compliant with commercial quality standards. The ^{1}H NMR spectra

of aqueous extract of kiwifruits affected by elephantiasis show a higher number of small oligosaccharides with respect to healthy fruits [24].

3. Second Starting Point: Common Food-Related Challenges

The world of food has to face different challenges. Some challenges, such as fraud detection, shelf-life determination, monitoring the geographical origin, etc., are common to many foods, whereas others refer only to specific foods. However, since each food has a specific chemical composition, micro- and macrostructure, texture, etc., the same challenge often requires specific solutions according to the type of food. The NMR methodology has proved to be a sufficiently versatile tool for addressing different specific problems, therefore representing a method of great interest for safeguarding the entire food production chain from manufacturers to consumers.

One of the common food-related challenges of great interest is food fraud detection. Frauds often concern foods of high economic value, which, for example, are substituted or mixed with products of lower economic value, giving a product with poor sensory and nutritional characteristics. Sometimes the fraud may constitute a serious risk to human health and, therefore, it has to be revealed quickly.

Here, some examples of frauds are reported, focusing on cases that cause a change in the chemical composition of the product.

3.1. Olive Oils: Addition of Hazelnut Oils to Olive Oils

One of the frauds involving the olive oil sector is the addition of hazelnut oils to olive oils. It is important to clarify that a good-quality hazelnut oil would be more expensive than olive oil: the fraud concerns hazelnut oil made with poor-quality hazelnuts. The composition of the two oils is very similar. However, using the NMR methodology, it is possible to distinguish the two types of oils since, in hazelnut oils, linolenic fatty chains and squalene are almost absent and, therefore, in the ^{1}H NMR spectrum, the corresponding signals are almost lacking [25]. On the other hand, the challenge is represented by the difficulty to detect the addition of hazelnut oil to olive oil. A methodology has been proposed: by measuring the intensity of six NMR signals, namely saturated, di-unsaturated, tri-unsaturated fatty chains, squalene, and β-sitosterol, hazelnut oil addition as low as 10% in refined olive oils can be revealed (Figure 4). The ^{1}H NMR protocol described according to ISO format has been tested on different NMR instruments operating at different magnetic fields (proton frequency of 600, 500, and 400 MHz) and has been tested by independent laboratories [26]. The issue was also addressed by means of low-field NMR, firstly by Parker et al. [27] and recently by Gouilleux et al. [28,29], demonstrating the efficacy of a profiling strategy based on fast 2D NMR spectra for the detection of hazelnut oil addition into olive oil.

3.2. Honey: Fraudulent Designation of Botanical Origin and Addition of Sugars

Honey is a well-appreciated food product. The recognized properties of honey as well as its sensory characteristic depend strongly on the botanical origin. Monofloral honeys have distinct sensory profiles and are more expensive than polyfloral products, giving rise to fraudulent mislabeling and adulterations with honey of lower value or with the addition of sugars. To adulterate honey, different sugary substances have been used: the majority of which are derived from corn, wheat, beets, cane sugar, and rice. One syrup often used as an adulterant is high-fructose corn syrup, known as HFCS. It is a low-cost product and it has a composition of glucose and fructose similar to that of honey. Frauds are more and more frequent and the fraud detection tools available to consumers are few: the problem is open and constantly evolving.

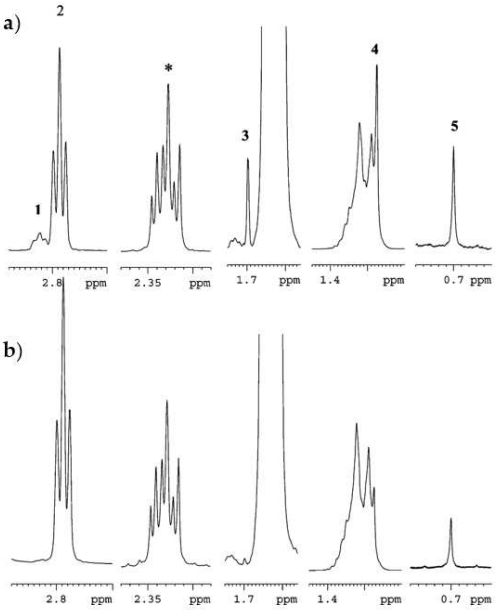


Figure 4. ^{1}H NMR resonances selected for statistical analyses in the 600.13 MHz ^{1}H spectrum of an (**a**) olive oil (top trace) and (**b**) a hazelnut oil. Peaks: 1, diallylic protons of linolenic acid, 2.82 ppm; 2, diallylic protons of linoleic acid, 2.78 ppm; 3, a signal due to squalene, 1.69 ppm; 4, methylenic protons of palmitic and stearic fatty chains, 1.27 ppm; 5, methyl-18 of β-sitosterol, 0.70 ppm. The reference peak at 2.32 ppm is also reported (∗) (Reprinted with permission [26] from American Chemical Society, Copyright 2009).

The botanical designation of honey can be put on the label when honey "comes wholly or mainly from that particular source and has the organoleptic, physical-chemical and microscopic properties corresponding with that origin." [30]. However, clear analytical parameters to define monofloral honey do not exist. To date, melissopalynological analysis is the only technique used to characterize monofloral and polyfloral samples as well as to determine the geographical origin. However, the results of this analysis can be strongly influenced by possible contaminations and the development of suitable analytical methodologies is strongly required.

Among the frauds mentioned before, the NMR methodology has provided an important contribution to the detection of sugars' addition in honey samples and to the determination of incorrect labeling that does not reflect the exact geographical or botanical origin. The NMR methodology is also useful in determining the presence of adulterants, in quantifying them, and in building high-performance prediction models that can establish the origin and genuineness of commercial samples.

3.2.1. Addition of Sugars in Honey Samples

The aqueous ^{1}H spectra of honey samples are dominated by strong signals of sugars [31]. The ^{1}H spectrum of honey in DMSO-d_6 reveals the presence of exogenous sugars (up to 10% by weight), through the identification of hydroxyl groups of maltose, sucrose, and other minority oligosaccharides, completely absent or present only in very small amounts in unadulterated samples. Therefore, in the adulterated honey samples, groups of

signals due generally to maltose and other polysaccharides absent in the genuine product are clearly visible. In some cases, the adulteration is more sophisticated and it is necessary to determine the complete sugar profile of the investigated product and compare the profile with that of authentic honey. The saccharides identified in the ^{1}H spectrum can be divided into three categories: endogenous sugars typical of honey, not detected or present only in traces in commercial sugar syrups; exogenous sugars present only in syrups; and sugars determined both in authentic honey and in some commercial sugar syrups. The sugar profile has been investigated in the case of acacia honey. The concentration range of endogenous sugars in genuine European acacia honey has been taken as a reference to evaluate the authenticity of a sample of the same botanical origin. Concentration levels significantly lower than the reference values could be indicative of adulteration of the honey by, for instance, dilution with sugar syrup. On the other hand, the presence of exogenous saccharides is strong evidence of adulteration.

A comparison between European and Chinese acacia honey samples has been reported [32]. In this case, principal component analysis (PCA) has been applied: samples were divided into two clusters as shown by the score plot (Figure 5). Chinese honey samples were characterized by a higher content of monosaccharides (glucose, fructose, and mannose) and a lower content of oligosaccharides. Several Chinese honey samples circulating in the European market showed a relevant presence of mannose, absent in genuine acacia honeys and a lower content of endogenous disaccharides typical for European ones. Mannose is instead present in rice syrups and in those with a high fructose content. The sugar NMR profile of a certainly genuine acacia sample from China falls within that of European honeys; this makes us assume that the different values do not depend on geographical origin but on adulteration. It is important to underline that both the melissopalynological analysis and the EA/LC–IRMS did not reveal particular anomalies in these Chinese samples, confirming their declared botanical origin. This further underlines the importance of NMR analysis and the great potential of the CSSF–TOCSY method in validating the authenticity of honey [32].

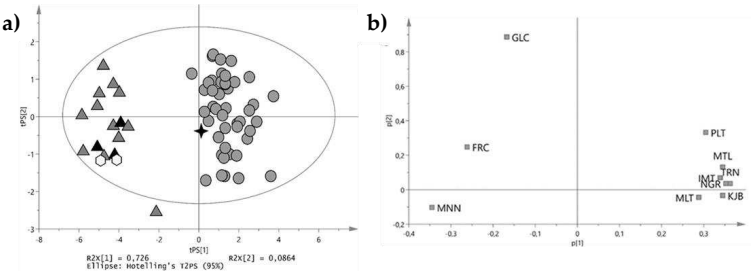


Figure 5. (**a**) Score plot of PCA performed on the sugars matrix. Sucrose and erlose were not considered in this analysis because of their large concentration variability. PC1 and PC2 accounts for 81% of the total variance (i.e., 72.6% + 8.64%). Grey circles: European honey; grey triangles: commercial Chinese honey; black triangles: Chinese honey analyzed with SCIRA; black star: Chinese honey purchased in China; white hexagons: honey from bee-feeding experiments. (**b**) Loading plot that highlights the metabolites responsible for the cluster separation (Reprinted from [32], with permission from Elsevier, Copyright 2020).

3.2.2. Fraudulent Designation of Botanical Origin

The NMR methodology addresses the problem of honey's botanical origin by proposing various solutions. Here, only a few significant examples are reported. One NMR approach is based on the observation that organic honey extracts of different botanical origins show a distinct chemical profile and, in several cases, some molecules can be considered as

specific markers, being present only in specific honey samples [33,34]. Here, the markers identified in the ^{1}H spectra of several honey samples (organic extracts) are reported:

Linden honey:

- 4-(1-hydroxy-1-methylethyl)cyclohexa-1,3-diencarboxyl methyl ester
- 4-(1-hydroxy-1-methylethyl)cyclohexa-1,3-dienecarboxylic acid
- 4-(1-methylethenyl)cyclohexa-1,3-diencarboxylic acid
- 4-(1-hydroxy-1-methylethyl) benzoic acid
- (E)-2,6-dimethyl-3,7-octadiene-2,6-diol;

Chestnut honey:

- deoxyvasicinone
- γ-lactam derivative of 3-(2′-pyrrolidinyl)-kinurenic acid
- γ-LACT-3-PKA
- 2-quinolone
- 4-quinolone;

Acacia honey:

- pinocembrin
- chrysin
- alpinone
- (Z, E)-abscissic acid;

Orange honey:

- caffeine
- (E)-2,6-dimethylotta-2,7-dien-1,6-diol (8-hydroxylinalol);

Eucalyptus honey:

- dehydrovomifoliol
- 3-oxo-α-ionone;

Strawberry tree honey:

- unedone homogenistic acid.

In some easy cases, it is possible to identify the co-presence of several botanical species in the same honey samples thanks to the presence in the ^{1}H spectra of the signals of the specific markers. For instance, the ^{1}H spectrum of honey samples from two botanical species, namely ailanthus and linden, clearly shows the presence of the signals due to specific markers of the two botanical species, as shown in Figure 6 [35].

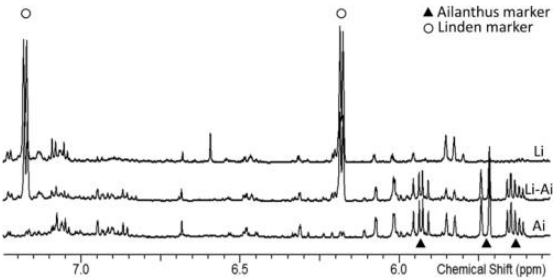


Figure 6. A region of the ^{1}H NMR spectra of chloroform extracts where the linden and ailanthus markers resonate: (from top to bottom) monofloral linden honey; honey containing both linden and ailanthus; monofloral ailanthus honey (Reprinted with permission from [35]. Copyright 2016 American Chemical Society).

However, it is possible to build classification models considering each type of honey as a single class. To identify the different floral contributions in honey, a statistical approach that considers all types of honey has been developed. This approach is based on *n* models of the OPLS-DA type (one for each botanical type), in which each botanical type is compared with all the others. It allows us to highlight the floral contributions in a given honey [36]. For instance, if you have 20 different flower varieties, 20 models called "one vs. all" are built. Given an unknown honey, each model returns the probability of belonging to a certain type. In this way, it is possible to identify the main floral contributions in the honey.

3.3. Coffee

3.3.1. Fraudulent Addition of Robusta to Arabica Coffee

Coffee from Arabica species is the most valuable and expensive type of coffee. The problem of adulteration of Arabica coffee with the less valuable Robusta coffee can be addressed by measuring the amount of specific fat-soluble markers belonging to the class of diterpenes. Kahweol is characteristic of the Arabica variety and is present only in trace amounts in Robusta coffee samples; on the other hand, 16-O-methylcafestol is present only in Robusta coffee. To date, the official method for authenticity testing is the German standard method DIN 10,779 [37], which provides the quantification of 16-O-methylcafestol in coffee through a lipid extraction and a high-performance liquid chromatography (HPLC) analysis. The marker of Robusta coffee, 16-O-methylcafestol, can be detected in the ^{1}H NMR spectrum of the chloroform extract of the roasted coffee powder thanks to the characteristic signal of the methoxide group at 3.17 ppm, as shown in Figure 7 [38,39]. In this way, by means of ^{1}H NMR, the presence of Robusta coffee traces (with an approximate limit of detection of 1–3%) in Arabica coffee is detectable. However, a common problem of the method that exploits the 16-O-methylcafestol is its wide range of concentration in different Robusta samples, which acts as an obstacle to the quantification of Robusta percentage in roasted coffee blends. Another issue regarding the coffee discrimination based only on the 16-O-methylcafestol quantification was reported by Gunning et al. [40], who found a small marker peak at 3.17 ppm in 30 Arabica coffees of assured origin. They have also established that the investigated signal arises not only from 16-O-methylcafestol, but likely from both 16-O-methylcafestol and 16-O-methylkahweol. The article concludes that the usage of other methods may not need to be affected if their detection limit for 16-O-methylcafestol is above the levels observed in authentic Arabica coffees, as appears to be the case for the DIN official method. However, regarding NMR application in the coffee fraud issue, the 3.17 ppm peak area can be used as a reasonable proxy for the Robusta content in mixture samples by defining a threshold, marking the upper limit of the normal Arabica range. Moreover, the researchers have established the possibility of using a 60 MHz low-field NMR method to assess the coffee's authenticity, since for the quantification of a single, well-resolved spectral peak, there is no advantage in using the higher-field-strength NMR. Other studies regarding the discrimination of Arabica and Robusta coffee were focused on the aqueous extract and take into account the entire metabolic profile [41]. In this case, the NMR spectra were used as input to create an OPLS model, using the different metabolite amounts of the two cultivars. This approach could prevent frauds and erroneous evaluations, providing discrimination that takes into account several chemical compounds simultaneously instead of a single marker.

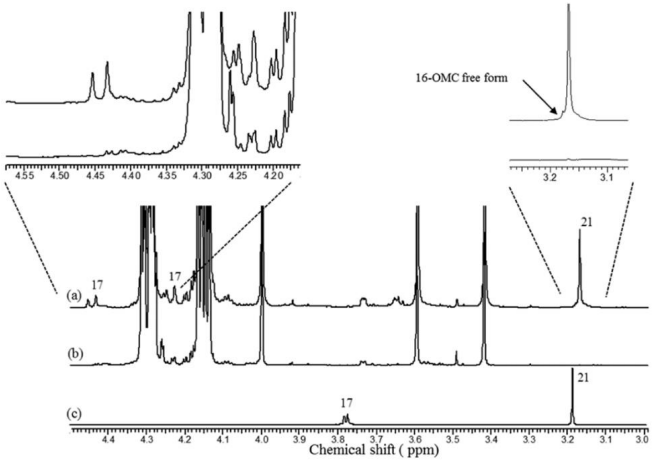


Figure 7. Expanded region of the ^{1}H NMR spectrum showing the diagnostic resonances of protons 17 and 21: (**a**) 100% *Robusta* sample, (**b**) 100% Arabica sample, and (**c**) 16-OMC standard. In the insets on the top of the figure, the signals of protons 17 and 21 of 16-OMC ester are enlarged. They are clearly visible in the *Robusta* sample (top), but they are absent from the Arabica sample. The arrow shows the weak methyl signals in position 21 of 16-OMC in its free form (Adapted with permission from [39]. Copyright 2014, American Chemical Society).

3.3.2. Geographical Origin

Another issue regarding coffee chain production addressed by means of NMR is the determination of the geographical origin from the perspective of fraud detection. Presently, the geographical origin of coffee is not determined analytically, whereas NMR spectroscopy combined with chemometrics resulted in a powerful and objective tool to trace the authenticity of roasted coffee. This kind of determination could be very useful for the trade sectors that require a high level of traceability to ensure quality and geographical origin. Here, some significant examples are reported. One NMR approach has been based on the discrimination of aqueous extracts of roasted coffee from three main production areas: America, Africa, and Asia [42]. The resulting NMR data analyzed with an OPLS-DA model indicated that American roasted coffee samples are characterized by a higher level of fatty acid chains, the African samples contain more chlorogenic acids and lactate, and the Asian ones are characterized by a high content of acetate and trigonelline, leading to a clear discrimination of roasted coffee samples according to their continent of origin. In another study, coffee samples (methanol coffee extracts) from Colombia, one of the main producers of coffee in the world, have been well-distinguished with respect to the coffee of other countries, including Colombia's closest neighbors, using NMR fingerprinting combined with chemometric analysis, namely PLS-DA [43]. Discrimination of coffees from Colombia is based mainly on a different content of fatty acids, acetate, and caffeine. This approach could represent a relevant opportunity to protect national productions.

A further NMR study has investigated the effect of different manufacturing process on the chemical composition of coffee. NMR data regarding instant coffee aqueous extracts (soluble extracts prepared industrially from coffee blends of different origins and varieties) from three different producers have been subjected to principal component analysis (PCA) followed by linear discriminant analysis (LDA). Coffee samples have been grouped according to their manufacturer, suggesting that NMR analysis can be useful to monitor the reproducibility and variations in industrial products. Moreover, it is possible to monitor

coffee authenticity and quality assurance, allowing the discovery of possible frauds due to the sale of low-quality products marked as high-quality ones [44].

3.4. Saffron

Saffron is one of the most used spices in the world and is well-known for its characteristic color, aroma, and flavor, respectively owing to the presence of crocins, safranal, and picrocrocin [45]. The collection and production of this spice are very laborious processes and, considering that the number of stigmas per flower is very low, a great number of flowers are needed—about 450,000—to obtain 1 kg of product. All these aspects have made saffron a very expensive spice and, consequently, this product is subjected to several fraud actions, represented by the addiction of plant-derived materials (*C. sativus* stamens, arnica, calendula, cayenne pepper, sandalwood, safflower, turmeric, and gardenia) or artificial colorants as bulking agents [46]. High-resolution ^{1}H NMR combined with chemometrics has shown to be very effective in tracing this kind of fraud by developing predictive models able to discriminate original saffron from adulterated samples with a minimum of 20% *w/w* bulking agents [47,48]. In a recent study, an improvement of this sensitivity has been obtained, detecting a 5% *w/w* saffron adulteration with safflower and turmeric [49]. In particular, the application of both unsupervised (PCA, HCD) and supervised (PLS-DA) chemometric models on ^{1}H NMR spectra of pure and adulterated saffron aqueous extracts allowed the detection of statistically significant variability, mainly due to sugars (positively related to adulterated samples), crocin, and formic acid (positively related to pure saffron). The application of the same protocol on ^{1}H NMR spectra of DMSO-d_6 organic extracts resulted in a discrimination between pure and adulterated saffron samples mainly due to curcuminoids (positively related to turmeric-adulterated saffron), linoleic acid (positively related to safflower-adulterated saffron), crocins, and safranal (positively related to pure saffron).

Recently, saffron adulterations with arnica, calendula, safflower, turmeric, cayenne pepper, sandalwood, and tartrazine have been analyzed using benchtop 60 MHz NMR analysis proposed as an alternative to the high-field NMR approach [50]. In particular, the benchtop 60 MHz NMR analysis of DMSO-d_6 organic extracts of pure saffron has been able to detect some typical signals of crocins and picrocrocin (Figure 8), making it possible to use these signals as elements of distinction between pure and adulterated saffron.

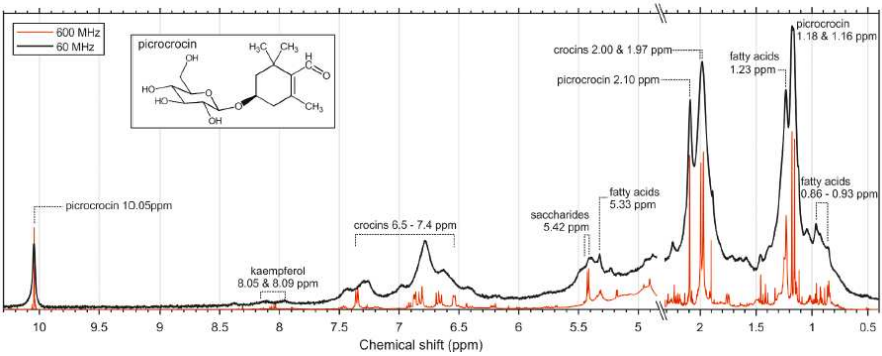


Figure 8. Comparison of 60 MHz (benchtop) and 600 MHz (high-field) ^{1}H NMR spectra obtained from an extract of saffron in DMSO-d6, with annotations of the main features identified in the 60 MHz spectrum. The benchtop spectral profile is dominated by resonances attributed to picrocrocin, a major saffron metabolite, the structure of which is given in the inset panel. The isolated peak at 10.05 ppm is in a generally uncrowded region of the spectrum and provides a useful indicator of the presence of saffron in a sample. Reprinted from [50], with permission from Elsevier, Copyright 2020.

The analysis of pure and adulterated saffron samples at different bulking percentages (5, 10, 20, 30, 40, 50%) has allowed the detection of, through the application of DD-SIMCA, OCC-NN, and IF one-class classification approaches, statistically significant differences between analyzed samples, although the minimum detectable bulking percentage was 30%. Additionally, this approach can offer a low-cost routine method for authenticity screening.

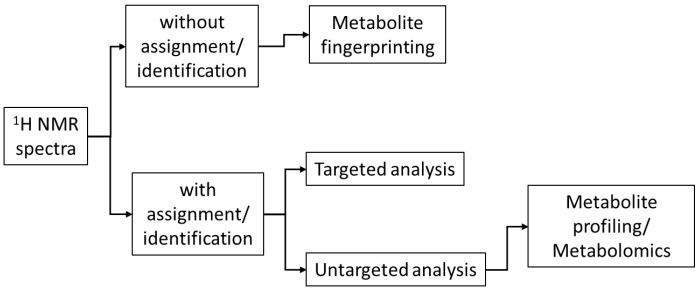
3.5. Milk

Milk is a very complex and nutritionally rich foodstuff whose study through NMR spectroscopy has allowed researchers to solve several issues related to origin, production practices, and adulteration [51–54]. Here, two representative examples related to milk adulteration detected by applying different NMR approaches are discussed. In the first study, high-resolution ^{1}H NMR spectroscopy has been applied to detect adulteration of caprine milk with cheaper bovine milk [55]. In particular, the application of PCA and OPLS-DA chemometrics approaches on ^{1}H binned spectra of aqueous extract of pure and adulterated (1, 5, and 10%) caprine milk has facilitated predictive models able to detect this kind of adulteration through the identification of specific markers, namely N-acetyl carbohydrates, typical of bovine milk.

Interestingly, ^{1}H TD-NMR has also been successfully applied to detect milk adulterations in a study where bovine milk was spiked with known levels (from 5 to 50% *v*/*v*) of whey, urea, hydrogen peroxide, synthetic urine, and synthetic milk [56]. In particular, T_2 relaxation time was significantly affected by adulteration, showing, with respect to the T_2 value of pure milk, an increase in its value depending on the adulterant percentage. This significant difference has also been confirmed by exploratory analysis (PCA), classification (SIMCA and kNN), and proposition of regression models (PLSR), thus confirming the potential use of ^{1}H TD-NMR as an alternative rapid method for detecting and quantifying milk adulteration.

4. Third Starting Point: NMR Methodology

As previously reported, each NMR methodology can be useful in investigating specific aspects related to foods. In particular, high-resolution ^{1}H-NMR spectroscopy in solutions can be applied to the study of foods, following different approaches that can be classified as metabolite fingerprinting, target analysis, and untargeted analysis (Scheme 1).



Scheme 1. Classification of high-resolution ^{1}H NMR spectroscopy's application types for food analysis.

Both targeted and untargeted analysis required the compounds' identification. In fact, the NMR methodology is well-known to be suitable for the identification of the chemical structure of compounds in solutions, especially those with relatively low molecular weight (less than 1 kDa). The high resolution of NMR spectra makes it also possible to study complex mixtures, such as liquid foods and food extracts, without physical separation of the components. However, due to the extreme signal overlapping in the spectra of

foodstuffs and in order to realize a complete signal assignment, 2D NMR experiments [7], 1D selective pulse experiments [57,58], and the DOSY experiment [59] are usually performed. The 2D experiments give us a plane surface with a series of cross-peaks that represent correlations between two frequencies. The most common 2D experiments are ^{1}H-^{1}H TOCSY, ^{1}H-^{1}H COSY, ^{1}H-^{13}C HSQC, and ^{1}H-^{13}C HMBC. They are powerful experiments for the identification of all the correlations ^{1}H-^{1}H and ^{1}H-^{13}C for each metabolite in complex mixtures in order to realize a complete structure assignment of the majority of the present compounds. Among the various types of 1D selective NMR experiments that are available, one of the most useful is the 1D TOCSY selective pulse sequence, in which a single resonance is selectively irradiated, and the magnetization propagates through the ^{1}H coupling network [57]. It is a powerful experiment for distinct spin systems within the molecule, potentially revealing multiple structures that were otherwise overlapped or buried. The DOSY experiment is recorded as a series of 1D NMR spectra with an increasing magnetic field strength gradient, finally combined to obtain a 2D NMR spectrum, showing NMR chemical shifts and self-diffusion coefficients on the horizontal and vertical axes, respectively. The DOSY experiment is particularly useful in the case of mixtures of compounds with different molecular weights. It is also helpful in spiking experiments and databases containing NMR data of metabolites (HMDB, MMCD, TOCCATA) [60,61]. Identification of components can be followed by their quantification (qNMR).

When absolute metabolite quantification is required, the duration of recycle time and the number of scans to reach a suitable signal-to-noise ratio have to be optimized in each experiment. The traditional quantification method is represented by the integration of a specific signal area vs. the signal area of a reference compound. In aqueous solutions, trimethylsilylpropanoic acid sodium salt (TSP) and sodium trimethylsilyl propanesufonate (DSS) have been widely used, whereas hexamethyldisiloxane (HMDSO) has been proposed for organic solutions. An alternative to the use of the internal standard is represented by the Electronic REference To access In vivo Concentrations (ERETIC) and QUANTification by Artificial Signal (QUANTAS) methods that provide a reference signal synthesized by an electronic device. Particular attention must be paid to the integration procedure when the water peak dominates the ^{1}H spectrum of a foodstuff sample. In this case, it is difficult to perform a correct quantitative analysis of the signals close to the water signal tail. Moreover, water suppression procedures can also partially saturate the resonances near the water signal, affecting their quantification. So, experimental water suppression parameters must be accurately calibrated. Finally, in another quantification method, the measure of the signal height, reported as signal intensity, is used instead of the integral for quantitative measurements since, as in the case of the integral, signal intensity is proportional to the compound concentration. In order to use this approach, the linewidth of each specific resonance has to be the same in all compared spectra. The measurement of the intensity can be performed manually or, in the case of many signals, by using an automatic peak-peaking procedure. Once the metabolite identification has been realized, the targeted or untargeted approach can be applied.

In the targeted analysis, the identification and quantification of single or a few marker compounds, chosen according to previous knowledge about the food under investigation, are performed. Metabolite extraction and other preparation procedures are carried out in order to concentrate the selected metabolite and to remove interference from other compounds. This approach is mainly applied to identify compounds that are responsible for some peculiar characteristic of the analyzed foodstuff, thus characterizing its origin, variety, or identifying adulterations. An example is the reported case regarding coffee in Section 3.3.1, in which the quantification of only 16-O-methylcafestol [38] or a few characteristic metabolites [62,63] in coffee samples allows the discrimination between Arabica and Robusta coffee varieties and the fraudulent addition of Robusta to Arabica coffee. Another example is the protocol of targeted ^{1}H NMR quantitative analysis of six common sugars in food and beverages developed by Yang et al. [64]. Fructose, galactose, glucose, lactose, maltose, and sucrose were simultaneously quantified in a single

high-resolution ^{1}H NMR experiment. The sample preparation procedure for the analysis was very simple: an aliquot of a liquid sample was diluted in D_2O followed by direct NMR analysis, whereas solid samples were suspended in H_2O, then the soluble fraction was filtered, concentrated in vacuum, and dissolved in D_2O. The quantification procedure was based on the integration areas of the characteristic proton signals. The method was successfully applied to a wide range of food and beverages including black tea, fruit juices, vinegar, wine, sake, soy milk and soy sauce, chocolate, honey, cookie, sauce paste, etc. The targeted NMR approach has been mainly used in food authentication, e.g., to distinguish between the two marketable oregano species with apigenin and p-cymene as biomarkers of *Origanum onites* and salvianolic acid B of *Origanum vulgare* [65]; to identify fraudulent processing techniques (with phlorin as marker) [66] or adulteration (with coumarins and psoralens as markers) [67] of Citrus juices; to evaluate saccharide adulteration in honey [68]; to detect illegal adulterants in herbal medicines [69]; and to quantify compound markers of quality in spirit drinks [70]. The targeted approach has been also used for the quantification of chosen metabolites in food matrices, e.g., in the quantification of polyols in sugar-free foodstuffs by the Chemical Shift Selective Filter–Total Correlation Spectroscopy (CSSF–TOCSY) NMR experiment [71]; the analysis of fatty acids in walnut oil [72]; the quantification of methylglyoxal in manuka honey [73]; and the quantification of cannabinoids in hempseeds [74] and hempseed oils [75]. Targeted analysis with quantification of the two best known cannabinoids (Δ9-tetrahydrocannabinol and cannabidiol) has been also realized by Araneda et al. [76] using a benchtop NMR instrument.

Untargeted analysis consists in the identification and quantification of a number of metabolites belonging to various classes of compounds in a given sample, often without any separation procedure. The untargeted or bottom–up approach does not rely on a predetermined hypothesis and, therefore, the solution to a problem may require the identification and quantification of as many metabolites as possible. All the quantified metabolites are then normally used as input for the chemometric analysis. Here, the case study of sea bass is discussed as an example of untargeted analysis. In this study, a mixed metabolic profiling–metabolomics approach was followed [77]. High-resolution NMR spectroscopy was used as an analytical tool to determine the complete metabolic profiling of sea bass extracts: the ^{1}H spectra of sea bass extracts in aqueous and organic solvents were analyzed, all the NMR signals were assigned using 2D NMR spectra, and finally, the content of the identified metabolites was measured and submitted to chemometric analysis. Water-soluble metabolites belonging to different classes such as sugars, amino acids, dipeptides, and organic acids as well as metabolites soluble in organic solvents such as lipids, sterols, and fatty acids were identified. Metabolite profiling and suitable statistical analysis were used to discriminate between wild and cultured sea bass samples. Preliminary results showed that discrimination between wild and cultured sea bass was obtained not only using fatty acid composition, but also cholesterol and phosphatidylethanolamine and some water-soluble metabolites such as choline, trimethylamine oxide, glutamine, and fumaric and malic acids. This type of approach has been frequently used to study various aspects of foods, such as pedoclimatic factors (olive oil [78–80]), geographical origin (wines [81–83], olive oils [84–86]), botanical origin (honey [34,87]), ripening (kiwi [21], tomatoes [88,89], pistachio [90]), postharvest changes (kiwi [18], banana [91]), and the manufacturer (beer [92]). Food authenticity (wine [93–95], honey [32,96], coffee [97]) has been also studied with the described untargeted approach.

Unlike the targeted and untargeted approaches, metabolic fingerprinting does not require metabolite identification. In fact, even without identification, an ^{1}H NMR spectrum represents a kind of fingerprint, reflecting the metabolic composition of a given foodstuff that can be used as such for traceability monitoring and other purposes. Although identification is preferable, it requires additional time, effort, and costs that are not always justified. In this approach, all the NMR resonances are measured without any identification. Then, the whole spectra (keeping the original number of data points) or the spectra divided in buckets (or bins) are used as input for the chemometric analysis. Metabolite fingerprinting

(namely the entire ^{1}H NMR spectrum) is used for rapid screening of a set of food samples to compare the samples of different origins, for traceability purposes, and for monitoring the possible changes in the same matrix with time or during a specific process. It is the case of wheat grain flour characterization by ^{1}H NMR that aimed to compare three fractions (bran, germ, and refined wheat) and whole-grain flour of two wheat varieties [98]. The entire ^{1}H NMR spectra of wheat flour polar (with methanol) and apolar (with chloroform) extracts were acquired and binned to reduce the number of variables (from 32,000 down to 700–90, depending on the size of the binning interval). Multivariate statistics (PCA) of NMR spectrum-derived variables enabled authors to clearly distinguish the three fractions and the whole-grain flour samples. The NMR profiling approach has been largely used to study the same food aspects described for the untargeted NMR analysis: pedoclimatic factors (olive oil [99,100]), geographical origin (wines [101,102], olive oils [103–105], cocoa beans [106], coffee [41], saffron [107], asparagus [108], walnuts [109], hazelnut [110], honey [111]), botanical origin (honey [112]), ripening (tomatoes (64), passion fruit (69)), post-harvesting (peaches, tomatoes, and plums [113]), and the manufacturer (beer [114], coffee [44]). Food authenticity (seeds [115], olive oil [116], beer [117], honey [118], avocado oil [119]) has been also studied with the described untargeted approach.

It is also common to combine the NMR profiling approach with the untargeted approach: the whole NMR spectra or bins (buckets) of the spectra are used as input for the chemometric analysis, and then the identification of some signals of interest is performed. However, both untargeted NMR analysis and metabolite fingerprinting generate a large amount of data from which it is necessary to extract the desired information using chemometric methods that can identify possible patterns among samples. In fact, since the number of identified metabolites and the number of studied samples can be very consistent, the only possibility of generating some final consideration or hypothesis from the obtained data is represented by the application of proper statistical approaches. The nature of quantitative data extracted from an NMR spectrum influences the choice of the statistical approach for their elaboration. Two types of statistical approaches can be used for data analysis, namely univariate and multivariate [120]. Among these, multivariate statistical analysis is generally applied for processing NMR data from complex matrices such as foodstuffs by means of unsupervised and supervised approaches. Explorative unsupervised analysis such as principal component analysis (PCA) and tree clustering analysis (TCA) is often the first step of statistical treatment. The structure of data, presence of outliers, and natural grouping of samples can be revealed at this step and in many cases, the obtained results are sufficient to distinguish different groups of samples according to metabolic differences. However, in the case of classification and prediction problems, the application of supervised multivariate techniques (PLS, LDA, PLS-DA, OPLS-DA, SIMCA) is necessary.

To date, together with these conventional statistic approaches, machine learning and neural networks are applied to gain useful insights and a corresponding interpretation of NMR outcomes [121,122]. Machine learning is a branch of artificial intelligence that is involved in finding links among complex patterns of molecular data through classification, clustering, features discovery, and integration [123]. Machine learning applied to NMR data is a useful tool for the dimensional reduction of the spectral data and the classification and clustering of the spectral data in latent feature spaces. Machine learning has been successfully applied to solve many food issues, including fraud detection, geographical origin, production/processing procedures, and food safety [122].

5. Conclusions

The three starting points reported suggest that the combination of food-related challenges and NMR methodologies' capacity to cope with them still has infinite possibilities to be explored. All three approaches will benefit from the development of the NMR sector, which includes advancements in methodologies and techniques (new NMR pulse sequences, new instrumentation, etc.). New trends concern the automation of NMR analy-

sis to exclude human error and lower the analysis cost, making this methodology more accessible for widespread applications in industry and in food control companies. Until a few years ago, the technological trend in NMR-related instrumentation was to go towards higher magnetic fields to increase the sensitivity and spectral resolution. Now, in parallel, there is a growing tendency to obtain better performances for spectrometers operating at medium and low magnetic fields generated by permanent magnets instead of superconductive ones [124–126]. Since, unlike superconductive magnets, permanent magnets do not need costly cryogenic liquids (liquid helium and nitrogen) for maintenance, lower costs make them more suitable for extended use in companies and research centers. So, the idea is to adapt the solutions found with high-field NMR spectrometers to low-field ones.

A further aspect of great interest to the NMR community is the unification of the analytical protocols used to investigate foods. Many foods have been analyzed using different experimental methods (extraction procedures, solvents, magnetic fields, etc.). This lack of uniformity often yields results that cannot be compared and, in any case, cannot be proposed as official methods. A great effort expected from the NMR scientific community is, therefore, to standardize specific analytical procedures for each food.

Finally, the scientific community is apt to create a food NMR database sharable not only among the scientific world but also with companies to provide an in-depth knowledge of the products.

Author Contributions: Conceptualization, L.M. and A.P.S.; resources, L.M.; writing—original draft preparation, L.M., A.P.S., C.I., M.S. and G.D.M.; writing—review and editing, L.M., A.P.S., C.I., M.S. and G.D.M.; supervision, L.M.; project administration, L.M.; funding acquisition, L.M. and A.P.S. All authors have read and agreed to the published version of the manuscript.

Funding: This research was in part supported by Ri-cicloHorto Project (POR FESR Lazio 2014–2020. Progetto T0002E0001. "Progetti di Gruppi di Ricerca 2020" Protocol A0375-2020-36541 CUP: B85F21001170002).

Institutional Review Board Statement: Not applicable.

Informed Consent Statement: Not applicable.

Data Availability Statement: Not applicable.

Conflicts of Interest: The authors declare no conflict of interest.

References

1. Mannina, L.; Sobolev, A.P.; Aru, V.; Bellomaria, A.; Bertocchi, F.; Botta, B.; Cagliani, L.R.; Caligiani, A.; Capozzi, F.; Çela, D. *NMR Methodologies in Food Analysis*; Nova Science Publishers, Inc.: Hauppauge, NY, USA, 2017; ISBN 9781536122824.
2. Solovyev, P.A.; Fauhl-Hassek, C.; Riedl, J.; Esslinger, S.; Bontempo, L.; Camin, F. NMR spectroscopy in wine authentication: An official control perspective. *Compr. Rev. Food Sci. Food Saf.* **2021**, *20*, 2040–2062. [CrossRef] [PubMed]
3. Siddiqui, A.J.; Musharraf, S.G.; Choudhary, M.I.; Rahman, A. Application of analytical methods in authentication and adulteration of honey. *Food Chem.* **2017**, *217*, 687–698. [CrossRef] [PubMed]
4. Santos, A.D.C.; Fonseca, F.A.; Lião, L.M.; Alcantara, G.B.; Barison, A. High-resolution magic angle spinning nuclear magnetic resonance in foodstuff analysis. *TrAC-Trends Anal. Chem.* **2015**, *73*, 10–18. [CrossRef]
5. Kirtil, E.; Cikrikci, S.; McCarthy, M.J.; Oztop, M.H. Recent advances in time domain NMR & MRI sensors and their food applications. *Curr. Opin. Food Sci.* **2017**, *17*, 9–15.
6. Mannina, L.; Sobolev, A.P.; Viel, S. Liquid state 1H high field NMR in food analysis. *Prog. Nucl. Magn. Reson. Spectrosc.* **2012**, *66*, 1–39. [CrossRef]
7. Hatzakis, E. Nuclear Magnetic Resonance (NMR) Spectroscopy in Food Science: A Comprehensive Review. *Compr. Rev. Food Sci. Food Saf.* **2019**, *18*, 189–220. [CrossRef]
8. Sobolev, A.P.; Thomas, F.; Donarski, J.; Ingallina, C.; Circi, S.; Cesare Marincola, F.; Capitani, D.; Mannina, L. Use of NMR applications to tackle future food fraud issues. *Trends Food Sci. Technol.* **2019**, *91*, 347–353. [CrossRef]
9. Marcone, M.F.; Wang, S.; Albabish, W.; Nie, S.; Somnarain, D.; Hill, A. Diverse food-based applications of nuclear magnetic resonance (NMR) technology. *Food Res. Int.* **2013**, *51*, 729–747. [CrossRef]
10. Mao, J.; Cao, X.; Olk, D.C.; Chu, W.; Schmidt-Rohr, K. Advanced solid-state NMR spectroscopy of natural organic matter. *Prog. Nucl. Magn. Reson. Spectrosc.* **2017**, *100*, 17–51. [CrossRef]
11. Khodov, I.A.; Musabirova, G.S.; Klochkov, V.V.; Karataeva, F.K.; Huster, D.; Scheidt, H.A. Structural details on the interaction of fenamates with lipid membranes. *J. Mol. Liq.* **2022**, *367*, 120502. [CrossRef]

12. Saad, A.; Bousquet, J.; Fernandez-Castro, N.; Loquet, A.; Géan, J. New Insights into Wine Taste: Impact of Dietary Lipids on Sensory Perceptions of Grape Tannins. *J. Agric. Food Chem.* **2021**, *69*, 3165–3174. [CrossRef] [PubMed]
13. Huster, D.; Arnold, K.; Gawrisch, K. Influence of docosahexaenoic acid and cholesterol on lateral lipid organization in phospholipid mixtures. *Biochemistry* **1998**, *37*, 17299–17308. [CrossRef] [PubMed]
14. Yu, X.; Chu, S.; Hagerman, A.E.; Lorigan, G.A. Probing the interaction of polyphenols with lipid bilayers by solid-state nmr spectroscopy. *J. Agric. Food Chem.* **2011**, *59*, 6783–6789. [CrossRef]
15. Van Duynhoven, J.; Voda, A.; Witek, M.; van As, H. Time-Domain NMR Applied to Food Products. *Annu. Rep. NMR Spectrosc.* **2010**, *69*, 145–197.
16. Hills, B.P.; Godward, J.; Manning, C.E.; Biechlin, J.L.; Wright, K.M. Microstructural characterization of starch systems by NMR relaxation and Q-space microscopy. *Magn. Reson. Imaging* **1998**, *16*, 557–564. [CrossRef]
17. Capitani, D.; Mannina, L.; Proietti, N.; Sobolev, A.P.; Tomassini, A.; Miccheli, A.; Di Cocco, M.E.; Capuani, G.; De Salvador, R.; Delfini, M. Monitoring of metabolic profiling and water status of Hayward kiwifruits by nuclear magnetic resonance. *Talanta* **2010**, *82*, 1826–1838. [CrossRef]
18. Salzano, A.M.; Renzone, G.; Sobolev, A.P.; Carbone, V.; Petriccione, M.; Capitani, D.; Vitale, M.; Novi, G.; Zambrano, N.; Pasquariello, M.S.; et al. Unveiling kiwifruit metabolite and protein changes in the course of postharvest cold storage. *Front. Plant Sci.* **2019**, *10*, 71. [CrossRef]
19. Panarese, V.; Laghi, L.; Pisi, A.; Tylewicz, U.; Rosa, M.D.; Rocculi, P. Effect of osmotic dehydration on Actinidia deliciosa kiwifruit: A combined NMR and ultrastructural study. *Food Chem.* **2012**, *132*, 1706–1712. [CrossRef]
20. Clark, C.J.; Drummond, L.N.; MacFall, J.S. Quantitative NMR imaging of kiwifruit (Actinidia deliciosa) during growth and ripening. *J. Sci. Food Agric.* **1998**, *78*, 349–358. [CrossRef]
21. Capitani, D.; Mannina, L.; Proietti, N.; Sobolev, A.P.; Tomassini, A.; Miccheli, A.; Di Cocco, M.E.; Capuani, G.; De Salvador, F.R.; Delfini, M. Metabolic profiling and outer pericarp water state in zespri, CI.GI, and hayward kiwifruits. *J. Agric. Food Chem.* **2013**, *61*, 1727–1740. [CrossRef]
22. Burdon, J.; Clark, C. Effect of postharvest water loss on "hayward" kiwifruit water status. *Postharvest Biol. Technol.* **2001**, *22*, 215–225. [CrossRef]
23. Taglienti, A.; Ritota, M.; Cozzolino, S.; Sequi, P.; Valentini, M.; Conte, L.; Terlizzi, M. MRI characterization of new kiwifruit selections. *Proc. Acta Hortic.* **2011**. [CrossRef]
24. Bonora, S.; Francioso, O.; Tugnoli, V.; Prodi, A.; Di Foggia, M.; Righi, V.; Nlpoti, P.; Filippini, G.; Pisi, A. Structural characteristics of "hayward" kiwifruits from elephantiasis-affected plants studied by drift, ft-raman, nmr, and sem techniques. *J. Agric. Food Chem.* **2009**, *57*, 4827–4832. [CrossRef] [PubMed]
25. Maestrello, V.; Solovyev, P.; Bontempo, L.; Mannina, L.; Camin, F. Nuclear magnetic resonance spectroscopy in extra virgin olive oil authentication. *Compr. Rev. Food Sci. Food Saf.* **2022**. [CrossRef] [PubMed]
26. Mannina, L.; D'Imperio, M.; Capitani, D.; Rezzi, S.; Guillou, C.; Mavromoustakos, T.; Vilchez, M.D.M.; Fernández, A.H.; Thomas, F.; Aparicio, R. 1H NMR-based protocol for the detection of adulterations of refined olive oil with refined hazelnut oil. *J. Agric. Food Chem.* **2009**, *57*, 11550–11556. [CrossRef] [PubMed]
27. Parker, T.; Limer, E.; Watson, A.D.; Defernez, M.; Williamson, D.; Kemsley, E.K. 60 MHz 1H NMR spectroscopy for the analysis of edible oils. *TrAC-Trends Anal. Chem.* **2014**, *57*, 147–158. [CrossRef] [PubMed]
28. Gouilleux, B.; Charrier, B.; Akoka, S.; Felpin, F.X.; Rodriguez-Zubiri, M.; Giraudeau, P. Ultrafast 2D NMR on a benchtop spectrometer: Applications and perspectives. *TrAC-Trends Anal. Chem.* **2016**, *83*, 65–75. [CrossRef]
29. Gouilleux, B.; Marchand, J.; Charrier, B.; Remaud, G.S.; Giraudeau, P. High-throughput authentication of edible oils with benchtop Ultrafast 2D NMR. *Food Chem.* **2018**, *244*, 153–158. [CrossRef] [PubMed]
30. FAO. *Codex Alimentarius Commission Revised Codex Standard for Honey Codex Stan 12-1981, Rev. 1 (1987), Rev. 2 (2001)*; FAO (Food and Agriculture Organization of the United Nations): Rome, Italy, 1981; pp. 1–7.
31. Schwarzinger, S.; Brauer, F.; Rösch, P.; Kämpf, B. Large-Scale Screening of Food Products for Quality and Authenticity. *New Food Magazine* **2015**.
32. Schievano, E.; Sbrizza, M.; Zuccato, V.; Piana, L.; Tessari, M. NMR carbohydrate profile in tracing acacia honey authenticity. *Food Chem.* **2020**, *309*, 125788. [CrossRef]
33. Schievano, E.; Mammi, S.; Menegazzo, I. Nuclear Magnetic Resonance as a Method to Predict the Geographical and Entomological Origin of Pot-Honey. In *Pot-Honey a Leg. Stingless Bees*; Springer Science & Business Media: New York, NY, USA, 2013; pp. 429–445.
34. Schievano, E.; Morelato, E.; Facchin, C.; Mammi, S. Characterization of markers of botanical origin and other compounds extracted from unifloral honeys. *J. Agric. Food Chem.* **2013**, *61*, 1747–1755. [CrossRef]
35. Schievano, E.; Finotello, C.; Uddin, J.; Mammi, S.; Piana, L. Objective Definition of Monofloral and Polyfloral Honeys Based on NMR Metabolomic Profiling. *J. Agric. Food Chem.* **2016**, *64*, 3645–3652. [CrossRef] [PubMed]
36. Schievano, E.; Stocchero, M.; Morelato, E.; Facchin, C.; Mammi, S. An NMR-based metabolomic approach to identify the botanical origin of honey. *Metabolomics* **2012**, *8*, 679–690. [CrossRef]
37. Analysis of Coffee and Coffee Products—Determination of 16-O-Methyl Cafestol Content of Roasted Coffee—HPLC-Method. Available online: https://www.en-standard.eu/din-10779-analysis-of-coffee-and-coffee-products-determination-of-16-o-methyl-cafestol-content-of-roasted-coffee-hplc-method/ (accessed on 6 October 2022).

38. Monakhova, Y.B.; Ruge, W.; Kuballa, T.; Ilse, M.; Winkelmann, O.; Diehl, B.; Thomas, F.; Lachenmeier, D.W. Rapid approach to identify the presence of Arabica and Robusta species in coffee using 1H NMR spectroscopy. *Food Chem.* **2015**, *182*, 178–184. [CrossRef] [PubMed]
39. Schievano, E.; Finotello, C.; De Angelis, E.; Mammi, S.; Navarini, L. Rapid authentication of coffee blends and quantification of 16-O-methylcafestol in roasted coffee beans by nuclear magnetic resonance. *J. Agric. Food Chem.* **2014**, *62*, 12309–12314. [CrossRef]
40. Gunning, Y.; Defernez, M.; Watson, A.D.; Beadman, N.; Colquhoun, I.J.; Le Gall, G.; Philo, M.; Garwood, H.; Williamson, D.; Davis, A.P.; et al. 16-O-methylcafestol is present in ground roast Arabica coffees: Implications for authenticity testing. *Food Chem.* **2018**, *248*, 52–60. [CrossRef]
41. Consonni, R.; Cagliani, L.R.; Cogliati, C. NMR based geographical characterization of roasted coffee. *Talanta* **2012**, *88*, 420–426. [CrossRef]
42. Cagliani, L.R.; Pellegrino, G.; Giugno, G.; Consonni, R. Quantification of Coffea arabica and Coffea canephora var. robusta in roasted and ground coffee blends. *Talanta* **2013**, *106*, 169–173. [CrossRef]
43. Arana, V.A.; Medina, J.; Alarcon, R.; Moreno, E.; Heintz, L.; Schäfer, H.; Wist, J. Coffee's country of origin determined by NMR: The Colombian case. *Food Chem.* **2015**, *175*, 500–506. [CrossRef]
44. Charlton, A.J.; Farrington, W.H.H.; Brereton, P. Application of 1H NMR and multivariate statistics for screening complex mixtures: Quality control and authenticity of instant coffee. *J. Agric. Food Chem.* **2002**, *50*, 3098–3103. [CrossRef]
45. Cardone, L.; Castronuovo, D.; Perniola, M.; Cicco, N.; Candido, V. Saffron (*Crocus sativus* L.), the king of spices: An overview. *Sci. Hortic.* **2020**, *272*, 109560. [CrossRef]
46. Koocheki, A.; Milani, E. Saffron adulteration. In *Saffron*; Woodhead Publishing: Sawston, UK, 2020.
47. Petrakis, E.A.; Cagliani, L.R.; Polissiou, M.G.; Consonni, R. Evaluation of saffron (*Crocus sativus* L.) adulteration with plant adulterants by1H NMR metabolite fingerprinting. *Food Chem.* **2015**, *173*, 890–896. [CrossRef] [PubMed]
48. Dowlatabadi, R.; Farshidfar, F.; Zare, Z.; Pirali, M.; Rabiei, M.; Khoshayand, M.R.; Vogel, H.J. Detection of adulteration in Iranian saffron samples by 1H NMR spectroscopy and multivariate data analysis techniques. *Metabolomics* **2017**, *13*, 1–11. [CrossRef]
49. Musio, B.; Todisco, S.; Antonicelli, M.; Garino, C.; Arlorio, M.; Mastrorilli, P.; Latronico, M.; Gallo, V. Non-Targeted NMR Method to Assess the Authenticity of Saffron and Trace the Agronomic Practices Applied for Its Production. *Appl. Sci.* **2022**, *12*, 2583. [CrossRef]
50. Gunning, Y.; Davies, K.S.; Kemsley, E.K. Authentication of saffron using 60 MHz 1H NMR spectroscopy. *Food Chem.* **2023**, *404*, 134649. [CrossRef]
51. Erich, S.; Schill, S.; Annweiler, E.; Waiblinger, H.U.; Kuballa, T.; Lachenmeier, D.W.; Monakhova, Y.B. Combined chemometric analysis of 1H NMR, 13C NMR and stable isotope data to differentiate organic and conventional milk. *Food Chem.* **2015**, *188*, 1–7. [CrossRef]
52. Bruschetta, G.; Notti, A.; Lando, G.; Ferlazzo, A. A promising 31P NMR-multivariate analysis approach for the identification of milk phosphorylated metabolites and for rapid authentication of milk samples. *Biochem. Biophys. Rep.* **2021**, *27*, 101087. [CrossRef]
53. Mazzei, P.; Piccolo, A. NMR-based metabolomics of water-buffalo milk after conventional or biological feeding. *Chem. Biol. Technol. Agric.* **2018**, *5*, 3. [CrossRef]
54. Bergana, M.M.; Adams, K.M.; Harnly, J.; Moore, J.C.; Xie, Z. Non-targeted detection of milk powder adulteration by 1H NMR spectroscopy and conformity index analysis. *J. Food Compos. Anal.* **2019**, *78*, 49–58. [CrossRef]
55. Rysova, L.; Legarova, V.; Pacakova, Z.; Hanus, O.; Nemeckova, I.; Klimesova, M.; Havlik, J. Detection of bovine milk adulteration in caprine milk with N-acetyl carbohydrate biomarkers by using 1H nuclear magnetic resonance spectroscopy. *J. Dairy Sci.* **2021**, *104*, 9583–9595. [CrossRef]
56. Santos, P.M.; Pereira-Filho, E.R.; Colnago, L.A. Detection and quantification of milk adulteration using time domain nuclear magnetic resonance (TD-NMR). *Microchem. J.* **2016**, *124*, 15–19. [CrossRef]
57. Novoa-Carballal, R.; Fernandez-Megia, E.; Jimenez, C.; Riguera, R. NMR methods for unravelling the spectra of complex mixtures. *Nat. Prod. Rep.* **2011**, *28*, 78–98. [CrossRef] [PubMed]
58. Sandusky, P.; Raftery, D. Use of selective TOCSY NMR experiments for quantifying minor components in complex mixtures: Application to the metabonomics of amino acids in honey. *Anal. Chem.* **2005**, *77*, 2455–2463. [CrossRef] [PubMed]
59. Gil, A.M.; Duarte, I.; Cabrita, E.; Goodfellow, B.J.; Spraul, M.; Kerssebaum, R. Exploratory applications of diffusion ordered spectroscopy to liquid foods: An aid towards spectral assignment. *Anal. Chim. Acta* **2004**, *506*, 215–223. [CrossRef]
60. Bingol, K.; Zhang, F.; Bruschweiler-Li, L.; Brüschweiler, R. TOCCATA: A customized carbon total correlation spectroscopy NMR metabolomics database. *Anal. Chem.* **2012**, *84*, 9395–9401. [CrossRef]
61. Tulpan, D.; Léger, S.; Belliveau, L.; Culf, A.; Čuperlović-Culf, M. MetaboHunter: An automatic approach for identification of metabolites from 1H-NMR spectra of complex mixtures. *BMC Bioinform.* **2011**, *12*, 400. [CrossRef]
62. Okaru, A.O.; Scharinger, A.; De Rezende, T.R.; Teipel, J.; Kuballa, T.; Walch, S.G.; Lachenmeier, D.W. Validation of a quantitative proton nuclear magnetic resonance spectroscopic screening method for coffee quality and authenticity (NMR coffee screener). *Foods* **2020**, *9*, 47. [CrossRef]
63. Burton, I.W.; Martinez Farina, C.F.; Ragupathy, S.; Arunachalam, T.; Newmaster, S.; Berrué, F. Quantitative NMR Methodology for the Authentication of Roasted Coffee and Prediction of Blends. *J. Agric. Food Chem.* **2020**, *68*, 14643–14651. [CrossRef]
64. Yang, W.B.; Shu, H.W.; Yi, T.C. QNMR as a Tool for Determination of Six Common Sugars in Foods. In *Applications of NMR Spectroscopy: Volume 8*; Bentham Science: Sharjah, United Arab Emirates, 2020; pp. 1–24. ISBN 9789811439971.

65. Mandrone, M.; Marincich, L.; Chiocchio, I.; Petroli, A.; Gođevac, D.; Maresca, I.; Poli, F. NMR-based metabolomics for frauds detection and quality control of oregano samples. *Food Control* **2021**, *127*, 108141. [CrossRef]
66. Jungen, M.; Schütz, B.; Schweiggert, R. Influence of species and processing techniques on phlorin in Citrus juices as quantified by 1H-NMR spectroscopy. *LWT* **2020**, *134*, 109949. [CrossRef]
67. Jungen, M.; Lotz, P.; Patz, C.D.; Steingass, C.B.; Schweiggert, R. Coumarins, psoralens, and quantitative 1H-NMR spectroscopy for authentication of lemon (*Citrus limon* [L.] Burm.f.) and Persian lime (*Citrus* × *latifolia* [Yu.Tanaka] Tanaka) juices. *Food Chem.* **2021**, *359*, 129804. [CrossRef]
68. Cagliani, L.R.; Maestri, G.; Consonni, R. Detection and evaluation of saccharide adulteration in Italian honey by NMR spectroscopy. *Food Control* **2022**, *133*, 108574. [CrossRef]
69. Li, F.F.; Guo, C.C.; Zhang, Y.L.; Wang, N.; Shi, Y.; Wang, S.Q. A screening method based on 1D CSSF-TOCSY for the identification and quantification of 11 illegal adulterants in herbal medicines. *Microchem. J.* **2020**, *153*, 104495. [CrossRef]
70. Teipel, J.C.; Hausler, T.; Sommerfeld, K.; Scharinger, A.; Walch, S.G.; Lachenmeier, D.W.; Kuballa, T. Application of 1h nuclear magnetic resonance spectroscopy as spirit drinks screener for quality and authenticity control. *Foods* **2020**, *9*, 1355. [CrossRef] [PubMed]
71. Scettri, A.; Schievano, E. Quantification of polyols in sugar-free foodstuffs by qNMR. *Food Chem.* **2022**, *390*, 133125. [CrossRef] [PubMed]
72. Qian, J.; Zhao, C.; Zhu, H.; Tong, J.; Zhao, X.; Yang, H.; Guo, H. NMR detection of fatty acids content in walnut oil and compared with liquid chromatography. *J. Food Meas. Charact.* **2021**, *15*, 2716–2726. [CrossRef]
73. Donarski, J.A.; Roberts, D.P.T.; Charlton, A.J. Quantitative NMR spectroscopy for the rapid measurement of methylglyoxal in manuka honey. *Anal. Methods* **2010**, *2*, 1479–1483. [CrossRef]
74. Siciliano, C.; Bartella, L.; Mazzotti, F.; Aiello, D.; Napoli, A.; De Luca, P.; Temperini, A. 1H NMR quantification of cannabidiol (CBD) in industrial products derived from Cannabis sativa L. (hemp) seeds. In *Proceedings of the IOP Conference Series: Materials Science and Engineering*; IOP Publishing Ltd: Bristol, UK, 2019; Volume 572.
75. Barthlott, I.; Scharinger, A.; Golombek, P.; Kuballa, T.; Lachenmeier, D.W. A quantitative1h nmr method for screening cannabinoids in cbd oils. *Toxics* **2021**, *9*, 136. [CrossRef] [PubMed]
76. Araneda, J.F.; Chu, T.; Leclerc, M.C.; Riegel, S.D.; Spingarn, N. Quantitative analysis of cannabinoids using benchtop NMR instruments. *Anal. Methods* **2020**, *12*, 4853–4857. [CrossRef]
77. Mannina, L.; Sobolev, A.P.; Capitani, D.; Iaffaldano, N.; Rosato, M.P.; Ragni, P.; Reale, A.; Sorrentino, E.; D'Amico, I.; Coppola, R. NMR metabolic profiling of organic and aqueous sea bass extracts: Implications in the discrimination of wild and cultured sea bass. *Talanta* **2008**, *77*, 433–444. [CrossRef]
78. Ingallina, C.; Cerreto, A.; Mannina, L.; Circi, S.; Vista, S.; Capitani, D.; Spano, M.; Sobolev, A.P.; Marini, F. Extra-virgin olive oils from nine italian regions: An 1H NMR-chemometric characterization. *Metabolites* **2019**, *9*, 65. [CrossRef]
79. Agiomyrgianaki, A.; Petrakis, P.V.; Dais, P. Influence of harvest year, cultivar and geographical origin on Greek extra virgin olive oils composition: A study by NMR spectroscopy and biometric analysis. *Food Chem.* **2012**, *135*, 2561–2568. [CrossRef] [PubMed]
80. Papadia, P.; Del Coco, L.; Muzzalupo, I.; Rizzi, M.; Perri, E.; Cesari, G.; Simeone, V.; Mondelli, D.; Schena, F.P.; Fanizzi, F.P. Multivariate analysis of 1H-NMR spectra of genetically characterized extra virgin olive oils and growth soil correlations. *JAOCS J. Am. Oil Chem. Soc.* **2011**, *88*, 1463–1475. [CrossRef]
81. Brescia, M.A.; Košir, I.J.; Caldarola, V.; Kidrič, J.; Sacco, A. Chemometric classification of Apulian and Slovenian wines using 1H NMR and ICP-OES together with HPICE data. *J. Agric. Food Chem.* **2003**, *51*, 21–26. [CrossRef] [PubMed]
82. Gougeon, L.; da Costa, G.; Guyon, F.; Richard, T. 1H NMR metabolomics applied to Bordeaux red wines. *Food Chem.* **2019**, *301*, 125257. [CrossRef]
83. Papotti, G.; Bertelli, D.; Graziosi, R.; Silvestri, M.; Bertacchini, L.; Durante, C.; Plessi, M. Application of one- and two-dimensional NMR spectroscopy for the characterization of protected designation of Origin Lambrusco wines of modena. *J. Agric. Food Chem.* **2013**, *61*, 1741–1746. [CrossRef]
84. Mannina, L.; Marini, F.; Gobbino, M.; Sobolev, A.P.; Capitani, D. NMR and chemometrics in tracing European olive oils: The case study of Ligurian samples. *Talanta* **2010**, *80*, 2141–2148. [CrossRef]
85. Mannina, L.; Patumi, M.; Proietti, N.; Bassi, D.; Segre, A.L. Geographical characterization of Italian extra virgin olive oils using high-field 1H NMR spectroscopy. *J. Agric. Food Chem.* **2001**, *49*, 2687–2696. [CrossRef]
86. Sacchi, R.; Mannina, L.; Fiordiponti, P.; Barone, P.; Paolillo, L.; Patumi, M.; Segre, A. Characterization of Italian Extra Virgin Olive Oils Using 1H-NMR Spectroscopy. *J. Agric. Food Chem.* **1998**, *46*, 3947–3951. [CrossRef]
87. Mannina, L.; Sobolev, A.P.; Di Lorenzo, A.; Vista, S.; Tenore, G.C.; Daglia, M. Chemical Composition of Different Botanical Origin Honeys Produced by Sicilian Black Honeybees (Apis mellifera ssp. sicula). *J. Agric. Food Chem.* **2015**, *63*, 5864–5874. [CrossRef]
88. Ingallina, C.; Maccelli, A.; Spano, M.; Di Matteo, G.; Di Sotto, A.; Giusti, A.M.; Vinci, G.; Di Giacomo, S.; Rapa, M.; Ciano, S.; et al. Chemico-biological characterization of torpedino di fondi® tomato fruits: A comparison with san marzano cultivar at two ripeness stages. *Antioxidants* **2020**, *9*, 1027. [CrossRef]
89. Sorrequieta, A.; Abriata, L.; Boggio, S.; Valle, E. Off-the-Vine Ripening of Tomato Fruit Causes Alteration in the Primary Metabolite Composition. *Metabolites* **2013**, *3*, 967. [CrossRef] [PubMed]

90. Sciubba, F.; Avanzato, D.; Vaccaro, A.; Capuani, G.; Spagnoli, M.; Di Cocco, M.E.; Tzareva, I.N.; Delfini, M. Monitoring of pistachio (Pistacia Vera) ripening by high field nuclear magnetic resonance spectroscopy. *Nat. Prod. Res.* **2017**, *31*, 765–772. [CrossRef] [PubMed]
91. Yuan, Y.; Zhao, Y.; Yang, J.; Jiang, Y.; Lu, F.; Jia, Y.; Yang, B. Metabolomic analyses of banana during postharvest senescence by 1H-high resolution-NMR. *Food Chem.* **2017**, *218*, 406–412. [CrossRef] [PubMed]
92. Palmioli, A.; Alberici, D.; Ciaramelli, C.; Airoldi, C. Metabolomic profiling of beers: Combining 1H NMR spectroscopy and chemometric approaches to discriminate craft and industrial products. *Food Chem.* **2020**, *327*, 127025. [CrossRef] [PubMed]
93. Gougeon, L.; da Costa, G.; Richard, T.; Guyon, F. Wine authenticity by quantitative1H NMR versus multitechnique analysis: A case study. *Food Anal. Methods* **2019**, *12*, 956–965. [CrossRef]
94. Gougeon, L.; Da Costa, G.; Le Mao, I.; Ma, W.; Teissedre, P.L.; Guyon, F.; Richard, T. Wine Analysis and Authenticity Using 1H-NMR Metabolomics Data: Application to Chinese Wines. *Food Anal. Methods* **2018**, *11*, 3425–3434. [CrossRef]
95. Ehlers, M.; Horn, B.; Raeke, J.; Fauhl-Hassek, C.; Hermann, A.; Brockmeyer, J.; Riedl, J. Towards harmonization of non-targeted 1H NMR spectroscopy-based wine authentication: Instrument comparison. *Food Control* **2022**, *132*, 108508. [CrossRef]
96. Spiteri, M.; Jamin, E.; Thomas, F.; Rebours, A.; Lees, M.; Rogers, K.M.; Rutledge, D.N. Fast and global authenticity screening of honey using 1H-NMR profiling. *Food Chem.* **2015**, *189*, 60–66. [CrossRef]
97. Toci, A.T.; de Moura Ribeiro, M.V.; de Toledo, P.R.A.B.; Boralle, N.; Pezza, H.R.; Pezza, L. Fingerprint and authenticity roasted coffees by 1H-NMR: The Brazilian coffee case. *Food Sci. Biotechnol.* **2018**, *27*, 19–26. [CrossRef]
98. Ramakrishnan, V.; Ridge, C.D.; Harnly, J.; Mazzola, E.P.; Luthria, D.L. Spectroscopic analysis of wheat fractions and reconstituted whole wheat mixtures by 1H-NMR and NIR. *Cereal Chem.* **2017**, *94*, 471–479. [CrossRef]
99. Girelli, C.R.; Del Coco, L.; Papadia, P.; De Pascali, S.A.; Fanizzi, F.P. Harvest year effects on apulian EVOOs evaluated by 1H NMR based metabolomics. *PeerJ* **2016**, *4*, e2740. [CrossRef] [PubMed]
100. Del Coco, L.; de Pascali, S.A.; Fanizzi, F. *1H NMR Metabolic Profiling of Apulian EVOOs: Fine Pedoclimatic Influences in Salento Cultivars*; RSC: London, UK, 2015; pp. 154–160.
101. Godelmann, R.; Fang, F.; Humpfer, E.; Schütz, B.; Bansbach, M.; Schäfer, H.; Spraul, M. Targeted and nontargeted wine analysis by 1H NMR spectroscopy combined with multivariate statistical analysis. differentiation of important parameters: Grape variety, geographical origin, year of vintage. *J. Agric. Food Chem.* **2013**, *61*, 5610–5619. [CrossRef] [PubMed]
102. Fan, S.; Zhong, Q.; Fauhl-Hassek, C.; Pfister, M.K.H.; Horn, B.; Huang, Z. Classification of Chinese wine varieties using 1H NMR spectroscopy combined with multivariate statistical analysis. *Food Control* **2018**, *88*, 113–122. [CrossRef]
103. Girelli, C.R.; Del Coco, L.; Zelasco, S.; Salimonti, A.; Conforti, F.L.; Biagianti, A.; Barbini, D.; Fanizzi, F.P. Traceability of "Tuscan PGI" extra virgin olive oils by 1H NMR metabolic profiles collection and analysis. *Metabolites* **2018**, *8*, 60. [CrossRef] [PubMed]
104. Longobardi, F.; Ventrella, A.; Napoli, C.; Humpfer, E.; Schütz, B.; Schäfer, H.; Kontominas, M.G.; Sacco, A. Classification of olive oils according to geographical origin by using 1H NMR fingerprinting combined with multivariate analysis. *Food Chem.* **2012**, *130*, 177–183. [CrossRef]
105. Girelli, C.R.; Calò, F.; Angilè, F.; Mazzi, L.; Barbini, D.; Fanizzi, F.P. 1h nmr spectroscopy to characterize italian extra virgin olive oil blends, using statistical models and databases based on monocultivar reference oils. *Foods* **2020**, *9*, 1797. [CrossRef]
106. Caligiani, A.; Palla, L.; Acquotti, D.; Marseglia, A.; Palla, G. Application of 1H NMR for the characterisation of cocoa beans of different geographical origins and fermentation levels. *Food Chem.* **2014**, *157*, 94–99. [CrossRef]
107. Ordoudi, S.A.; Cagliani, L.R.; Lalou, S.; Naziri, E.; Tsimidou, M.Z.; Consonni, R. 1H NMR-based metabolomics of saffron reveals markers for its quality deterioration. *Food Res. Int.* **2015**, *70*, 1–6. [CrossRef]
108. Klare, J.; Rurik, M.; Rottmann, E.; Bollen, A.; Kohlbacher, O.; Fischer, M.; Hackl, T. Determination of the Geographical Origin of *Asparagus officinalis* L. By 1H NMR Spectroscopy. *J. Agric. Food Chem.* **2020**, *68*, 14353–14363. [CrossRef]
109. Schmitt, C.; Schneider, T.; Rumask, L.; Fischer, M.; Hackl, T. Food Profiling: Determination of the Geographical Origin of Walnuts by 1H NMR Spectroscopy Using the Polar Extract. *J. Agric. Food Chem.* **2020**, *68*, 15526–15534. [CrossRef]
110. Bachmann, R.; Klockmann, S.; Haerdter, J.; Fischer, M.; Hackl, T. 1H NMR Spectroscopy for Determination of the Geographical Origin of Hazelnuts. *J. Agric. Food Chem.* **2018**, *66*, 11873–11879. [CrossRef] [PubMed]
111. Luong, D.V.; Tam, N.Q.; Xuan, D.T.T.; Tai, N.T. NMR based metabolomic approach for evaluation of Vietnamese honey. *Vietnam J. Chem.* **2019**, *57*, 712–716. [CrossRef]
112. Schievano, E.; Peggion, E.; Mammi, S. 1H nuclear magnetic resonance spectra of chloroform extracts of honey for chemometric determination of its botanical origin. *J. Agric. Food Chem.* **2010**, *58*, 57–65. [CrossRef]
113. Santucci, C.; Tenori, L.; Luchinat, C. NMR fingerprinting as a tool to evaluate post-harvest time-related changes of peaches, tomatoes and plums. *Food Res. Int.* **2015**, *75*, 106–114. [CrossRef] [PubMed]
114. Da Silva, L.A.; Flumignan, D.L.; Pezza, H.R.; Pezza, L. 1H NMR spectroscopy combined with multivariate data analysis for differentiation of Brazilian lager beer according to brewery. *Eur. Food Res. Technol.* **2019**, *245*, 2365–2372. [CrossRef]
115. Brigante, F.I.; García, M.E.; López Radcenco, A.; Moyna, G.; Wunderlin, D.A.; Baroni, M.V. Identification of chia, flax and sesame seeds authenticity markers by NMR-based untargeted metabolomics and their validation in bakery products containing them. *Food Chem.* **2022**, *387*, 132925. [CrossRef]
116. Guyader, S.; Thomas, F.; Portaluri, V.; Jamin, E.; Akoka, S.; Silvestre, V.; Remaud, G. Authentication of edible fats and oils by non-targeted 13C INEPT NMR spectroscopy. *Food Control* **2018**, *91*, 216–224. [CrossRef]

117. Da Silva, L.A.; Flumignan, D.L.; Tininis, A.G.; Pezza, H.R.; Pezza, L. Discrimination of Brazilian lager beer by 1H NMR spectroscopy combined with chemometrics. *Food Chem.* **2019**, *272*, 488–493. [CrossRef]
118. Yong, C.H.; Muhammad, S.A.; Aziz, F.A.; Nasir, F.I.; Mustafa, M.Z.; Ibrahim, B.; Kelly, S.D.; Cannavan, A.; Seow, E.K. Detecting adulteration of stingless bee honey using untargeted 1H NMR metabolomics with chemometrics. *Food Chem.* **2022**, *368*, 130808. [CrossRef]
119. Tang, F.; Green, H.S.; Wang, S.C.; Hatzakis, E. Analysis and authentication of avocado oil using high resolution nmr spectroscopy. *Molecules* **2021**, *26*, 310. [CrossRef]
120. Andre, C.M.; Soukoulis, C. Food quality assessed by chemometrics. *Foods* **2020**, *9*, 897. [CrossRef] [PubMed]
121. Jimenez-Carvelo, A.M. Data mining/machine learning methods in foodomics. *Curr. Opin. Food Sci.* **2021**, *37*, 76–82. [CrossRef]
122. Corsaro, C.; Vasi, S.; Neri, F.; Mezzasalma, A.M.; Neri, G.; Fazio, E. NMR in Metabolomics: From Conventional Statistics to Machine Learning and Neural Network Approaches. *Appl. Sci.* **2022**, *12*, 2824. [CrossRef]
123. Picone, G.; Mengucci, C.; Capozzi, F. The NMR added value to the green foodomics perspective: Advances by machine learning to the holistic view on food and nutrition. *Magn. Reson. Chem.* **2022**, *60*, 590–596. [CrossRef] [PubMed]
124. Giberson, J.; Scicluna, J.; Legge, N.; Longstaffe, J. *Developments in Benchtop NMR Spectroscopy 2015–2020*, 1st ed.; Elsevier Ltd.: Amsterdam, The Netherlands, 2021; Volume 102, ISBN 9780128246092.
125. Blümich, B. Low-field and benchtop NMR. *J. Magn. Reson.* **2019**, *306*, 27–35. [CrossRef]
126. Grootveld, M.; Percival, B.; Gibson, M.; Osman, Y.; Edgar, M.; Molinari, M.; Mather, M.L.; Casanova, F.; Wilson, P.B. Progress in low-field benchtop NMR spectroscopy in chemical and biochemical analysis. *Anal. Chim. Acta* **2019**, *1067*, 11–30. [CrossRef]